



Swansea University
Prifysgol Abertawe

Analysis of sterols in Human T Helper cells

Eylan Yutuc

Submitted to Swansea University
in fulfilment of the requirements for the
Degree of Doctor of Philosophy

2016

SUMMARY

Oxysterols are oxidised cholesterol species which can be in the form of one or more hydroxyl, carbonyl, epoxide and carboxylic acid of cholesterol and its precursors. They are intermediates in bile acid and steroid hormone biosynthesis pathway and were initially thought not to have any biological activity but now emerged to have roles in lipid homeostasis, embryonic development and immunity. Specifically, activation of macrophages leads to 25-hydroxycholesterol (25-HC) production which contributes to suppression of viral entry and replication. In addition, 7 α ,25-dihydroxycholesterol (7 α ,25-DiHC) has been identified as a ligand for Epstein-Barr virus-induced gene 2 which influences B-cell migration and function. Key to coordinating effective immune responses are CD4 T cells. However, studies involving these cells and oxysterols are currently limited, especially in human CD4⁺ T cells. Moreover, there are currently no optimised mass spectrometry methods for sterol analysis of T cells. This study was inspired with the identification of autoimmune-associated TH17 cells and sterol ligand-activated ROR γ t as its master regulator, prompting a need for a method in analysing sterols in T cells.

Here, *in vitro* cultures of cells isolated from healthy human donors were utilised to study and profile CD4⁺ T cell sterol production using an enzyme assisted derivatisation method and HPLC-ESI-MSⁿ analysis. The function of the produced sterols and the mechanisms of production were also investigated using inhibitors of cholesterol biosynthetic pathway and downstream T cell receptor signalling. In addition, different subsets of CD4 T cells were also screened for sterols to link sterol production and immune function.

Several oxysterols were detected in activated CD4⁺ T cells, including 25-HC, 7 α ,25-DiHC and 24S,25-epoxycholesterol (24S,25-EC), which increases with time but were absent in resting cells. The production of 25HC was seen to be unaffected by suppression of cholesterol biosynthesis compared to 24S,25-EC. Activation of CD4⁺ T cells stimulates several intracellular signalling pathways, and the PKC and MAPK pathways were found to have most influence in sterol production. However, the relationship between interferon and 25-HC in human CD4⁺ T cells was not observed in the current study. Lastly, differentiation of naïve CD4⁺ T cells towards the Treg-polarising conditions saw increased production of 7 α ,24S,25-trihydroxycholesterol not seen in either TH0- or TH2-polarising conditions.

This study paves the way to progress the field of sterolomics and T cell immunology and to understand further the crosstalk between sterol metabolism and immune function.

DECLARATION

This work has not previously been accepted in substance for any degree and is not being concurrently submitted in candidature for any degree.

Signed (candidate)

Date

STATEMENT 1

This thesis is the result of my own investigations, except where otherwise stated. Where correction services have been used, the extent and nature of the correction is clearly marked in a footnote(s).

Other sources are acknowledged by footnotes giving explicit references. A bibliography is appended.

Signed (candidate)

Date

STATEMENT 2

I hereby give consent for my thesis, if accepted, to be available for photocopying and for inter-library loan, and for the title and summary to be made available to outside organisations.

Signed (candidate)

Date

TABLE OF CONTENTS

SUMMARY	ii
DECLARATION AND STATEMENTS.....	iii
ACKNOWLEDGEMENTS	x
DEDICATION	xi
ABBREVIATIONS	xii
LIST OF TABLES	xvi
LIST OF FIGURES	xvii
CHAPTER 1: General Introduction.....	1
1.1. Cholesterol.....	1
1.1.1. Nomenclature, Biology and Functions.....	1
1.1.2. Sources, Synthesis, and Regulation.....	5
1.2. Oxysterols.....	11
1.2.1. Discovery and Brief History	11
1.2.2. Nomenclature	12
1.2.3. Conversion from cholesterol	14
1.2.4. Roles in Cholesterol Regulation and Feedback Mechanisms	16
1.2.5. Roles as Nuclear Receptor (NR) transcription factor and G-Protein Coupled Receptor (GPCR) ligands.....	16
1.2.6. Roles in Immune Function	17
1.3. Current methods of analysis	18
1.4. Immune System	19
1.4.1. Innate Immunity	19
1.4.2. Adaptive Immunity	20
1.5. T Cell Biology	22
1.5.1. Origin and Development	22
1.5.2. T Cell Types and Subsets	25
1.5.3. CD4 T Cell Activation, Expansion and Differentiation	31
1.5.4. T Cell Receptor Signalling	33
1.6. Mass Spectrometry	41
1.6.1. Ionisation Sources	41

1.6.2. Mass Analysers.....	44
1.6.3. Tandem Mass Spectrometry (MSn)	48
1.6.4. Chromatography MS Coupling	48
1.7. General Thesis Aims.....	56
1.8. References.....	57
CHAPTER 2: Materials and Methods.....	74
2.1. Cell Culture.....	74
2.1.1. Cell Culture Materials	74
2.1.2. Human Blood Donors and Ethical approval for human studies	77
2.1.3. Human Peripheral Blood Mononuclear Cell Isolation	77
2.1.4. Human T Lymphocyte Isolation by MACS®	78
2.1.5. Cell Cryopreservation, Storage and Recovery	80
2.1.6. Human T Lymphocyte Culture Conditions	80
2.1.7. Cell Counting and Cell Viability Assay	82
2.1.8. T Lymphocyte Flow Cytometry Assays.....	83
2.2. Sterol Analysis by Liquid Chromatography Mass Spectrometry	88
2.2.1. Sterol Analysis Materials	88
2.2.2. Sample processing using Enzyme-Assisted Derivatisation for Sterol Analysis (EADSA).....	90
2.2.3. Sample preparation prior to LC-ESI-MSn analysis.	96
2.2.4. Sterol Separation, Analysis and Quantitation by HPLC-ESI-MSn.....	99
2.3. Analysis of T Lymphocyte Gene and Protein Expression.....	110
2.3.1. Molecular Biology Materials.....	110
2.3.2. Relative Gene Expression Analysis by RT-qPCR.	112
2.3.3. Soluble Protein Detection and Quantification by Immunoassay.....	117
2.4. References.....	120
CHAPTER 3: Sterols in culture media	122
3.1. Introduction.....	122
3.2. Materials and Methods	122
3.2.1. Media preparation, sterol extraction and LC-MSn analysis.....	122
3.2.2. Alkali hydrolysis of esterified sterols in X-VIVO-20.....	122

3.3. Results	123
3.3.1. Several sterol species were present in Full media and DL media which were absent in Serum-Free RPMI media.	123
3.3.2. Free and total sterols in X-VIVO-20 media.	126
3.4. Discussion.....	128
3.5. References.....	129
CHAPTER 4: Sterols generated by human CD4 ⁺ T cells in vitro	130
4.1. Introduction.....	130
4.2. Materials and Methods	130
4.2.1. Isolation of naïve CD4 ⁺ T cells.	130
4.2.2. Isolation of total CD4 ⁺ T cells.....	131
4.2.3. Separating naïve, memory and TH2 CD4 ⁺ T cells from total CD4 ⁺ T cells.	131
4.2.4. Purity and activation analysis of naïve CD45RA ⁺ CD4 ⁺ T cells, memory CD45RO ⁺ CD4 ⁺ T cells and total CD4 ⁺ T cells by flow cytometry.	131
4.2.5. Culture conditions for unstimulated naïve CD4 ⁺ T cells in SF and DL media.	132
4.2.6. Culture conditions for CD3/CD28 activated and TH17-polarised naïve CD4 ⁺ T cells in X-VIVO-20 media.	132
4.2.7. Culture conditions and extraction of activated naïve CD4 ⁺ T cells in X-VIVO-20 supplemented with 4µg/mL heptadeuterio cholesterol.	135
4.2.8. Time course culture conditions for activated total CD4 ⁺ T cells.	138
4.2.9. Culture conditions for naïve and memory CD4 ⁺ T cells.....	139
4.2.10. Sample processing and sterol analysis.	140
4.3. Results	141
4.3.1. Isolated naïve CD4 ⁺ T cells by MACS were >96% pure.....	141
4.3.2. Naïve CD4 ⁺ T cells do not produce detectable levels of oxysterols when unstimulated in SF RPMI or DL media even after 6 days in culture.	141
4.3.3. Initial cultures of activated naïve CD4 ⁺ T cells and TH17-polarised conditions revealed induced oxysterol production.	145
4.3.4. Some GP-derivatised sterols elutes at slightly different retention times due to geometric isomerism.	151
4.3.5. Low levels of 24,25-EC were produced by non-activated naïve CD4 ⁺ T cells in X VIVO 20 cultures after 6 days which was independent from IL 2 treatment.....	154

4.3.6. Cultures of activated and non-activated naïve CD4 ⁺ cells with deuterated cholesterol revealed different cholesterol import.	158
4.3.7. Time course investigation of total CD4 ⁺ T cell culture revealed increasing oxysterol production relative to length of activation.....	168
4.3.8. Characterising the oxysterols generated by naïve and memory CD4 ⁺ T cells.....	180
4.4. Discussions	188
4.5. References.....	191
CHAPTER 5: Investigating the link between the generation of 24(S)25-EC, 25 HC and 7 α ,25-diHC with induced cholesterol biosynthesis upon CD4 ⁺ T cell activation	193
5.1. Introduction.....	193
5.2. Materials and Methods	194
5.2.1. Preparation of simvastatin.	194
5.2.2. Monitoring cell proliferation by flow cytometry.	194
5.2.3. Monitoring cell death by flow cytometry.....	199
5.2.4. THP-1 cultures and test for simvastatin cytotoxicity.	199
5.2.5. Total CD4 ⁺ T cell cultures with simvastatin.....	200
5.2.6. Monitoring cell activation by flow cytometry.....	200
5.3. Results.....	200
5.3.1. Higher concentrations of simvastatin induce cell death and inhibits proliferation in THP-1 cultures	200
5.3.2. Simvastatin induces cell death and inhibits activation and proliferation in human total CD4 ⁺ T cell cultures	203
5.3.3. Simvastatin inhibits 24(S),25-EC production but not 25-HC and 7 α ,25-diHC.	211
5.3.4. Simvastatin inhibits activation-induced intracellular cholesterol and cholesterol precursor levels.....	212
5.4. Discussion.....	217
5.5. References.....	220
CHAPTER 6: Investigating the relationship between CH25H, 25-HC, IFNG and IFN- γ in CD4 ⁺ T cells.....	222
6.1. Introduction.....	222
6.2. Materials and Methods	223
6.2.1. Total CD4 ⁺ T cell isolation	223

6.2.2. Small interfering RNAs and vectors	223
6.2.3. RNA interference and Cell culture	224
6.2.4. Cytokine treatments in T cell cultures.....	225
6.2.5. Sterol content analysis.....	225
6.2.6. Gene expression and protein secretion analysis	225
6.3. Results	226
6.3.1. Cholesterol 25-hydroxylase silencing led to reduced CH25H mRNA expression and 25-HC production in activated CD4 ⁺ T cells while not affecting cell viability and CD25 expression.	226
6.3.2. Down regulation of CH25H expression and reduced 25-HC does not affect the IFNG mRNA expression and IFN- γ cytokine production	230
6.3.3. 4D-Nucleofection ‘high efficiency’ programme led to reduced cell viability but comparable CH25H silencing to ‘high functionality’ programme.....	230
6.3.4. IFN- γ does not affect CD25 expression or 25-HC production in activated total CD4 ⁺ T cells	232
6.4. Discussion.....	239
6.5. References.....	241
CHAPTER 7: Investigating T cell receptor signalling pathways influencing the generation of 24(S),25-EC, 25-HC and 7 α ,25-DiHC.	243
7.1. Introduction.....	243
7.2. Materials and Methods	245
7.2.1. Preparation of pharmacological inhibitors and activators	245
7.2.2. Total CD4 ⁺ T cell isolation from PBMCs	245
7.2.3. Treatment conditions and activation of total CD4 ⁺ T cells	245
7.2.4. Cell viability and activation assay by flow cytometry	246
7.2.5. Flow cytometric phosphorylation assay of S6 and 4E-BP1 intracellular proteins	246
7.2.6. Measurement of relative SREBP2 and HMGCR mRNA expression levels .	246
7.2.7. Sample processing and sterol analysis	247
7.2.8. Statistical analysis	247
7.3. Results	247
7.3.1. CD3 or CD28 stimulation alone do not fully induce the expression of CD25 and the production of oxysterols, 24(S),25-EC and 25-HC.	247

7.3.2. Increased concentrations of NF-κB signalling inhibitor, BAY-11-7082 induced cell death of activated T cells	251
7.3.3. Other kinase inhibitors and activator treatments did not lead to increased cell death after 48 hours.	251
7.3.4. BAY-11-7082 does not affect oxysterol generation of activated total CD4 ⁺ T cells at sub-toxic concentrations.....	252
7.3.5. U0126 inhibits CD25 expression but induces the production of 24(S),25 EC whereas SB203580 had an opposite effect.....	261
7.3.6. 25-HC production was reduced with U0126 treatment but was increased with SB203580.	261
7.3.7. PMA induces greater production of 25-HC and 7α,25-DiHC than CD3/CD28 stimulation but does not fully induce CD25 expression or cholesterol biosynthesis	264
7.3.8. Gö6983 prevents the activation of CD3/CD28 stimulated total CD4 ⁺ T cells and accumulates intracellular desmosterol.....	264
7.3.9. Treatment with PI3K inhibitor, LY294002, with CD3/CD28-stimulation had no effect on CD25 expression and sterol production.	267
7.3.10. Rapamycin inhibition of mTORC1 in activated had no effect in CD25 expression and sterol production.....	270
7.3.11. Phosphorylation of ribosomal S6 was reduced with Rapamycin and LY294002 but was not significant.....	270
7.3.12. Dual mTORC inhibition by Ku63794 dose-dependently reduced CD25 expression together with pS6, p4E-BP1 and 25-HC but not 24(S),25-EC.....	270
7.3.13. Ku63794 and Rapamycin treatment augmented HMGCR mRNA expression but not SREBP2 in activated total CD4 ⁺ T cells	271
7.4. Discussions	274
7.5. References.....	280
CHAPTER 8: Lipidomic analysis of naïve CD4 ⁺ T cells in TH0- TH2- and Treg polarising conditions.	285
8.1. Introduction.....	285
8.2. Materials and Methods	287
8.2.1. Naïve CD4 ⁺ T cell Isolation from PBMC.....	287
8.2.2. Polarisation cytokines and reagents	287
8.2.3. TH0, TH2 and Treg polarisation culture of naïve CD4 ⁺ T cells	288
8.2.4. Relative gene expression analysis by RT-PCR	288

8.2.5. Purity, cell activation, viability analysis and intracellular protein expression analysis by flow cytometry	291
8.2.6. Analysis of sterol content in culture media	291
8.3. Results	291
8.3.1. Isolated naïve CD4 ⁺ T cells were ≥94% CD4 ⁺ CD45RA ⁺ cells prior to culture.....	291
8.3.2. Reduced T cell viability in TH2 polarising conditions compared to TH0 and Treg.	292
8.3.3. CD25 surface expression was higher in Treg polarised conditions.	292
8.3.4. RT-PCR analysis and flow cytometry confirmed TH2 and Treg polarisation by IL4 and FOXP3 mRNA expression and intracellular protein staining.	296
8.3.5. RORC, FOXP3, and CYP7B1 mRNA expressions were higher in Treg conditions compared to TH0/TH2, follow a similar trend and slightly enhanced with increased IL-2 treatment.....	297
8.3.6. Increased CYP7B1 expression did not reflect an increased RORA expression.....	301
8.3.7. TH2-polarised cells produced the least amount of sterols, with Treg polarised cells producing the most, compared to TH0.....	301
8.3.8. The detected oxysterol, 7 α ,24S,25-TriHC, was produced the most specifically by Treg-polarised cells detected mainly later in culture.	303
8.3.9. Human CD4 ⁺ naïve T cell activation in vitro requires IL-2.....	304
8.3.10. Optimal FOXP3, RORC and CYP7B1 gene expression required a certain concentration range of TGF- β	307
8.3.11. Only the sterol, 7 α ,24S,25-TriHC and its metabolite, 3 oxo,7 α ,24S,25-TriHC follows a trend similar to CYP7B1 and RORC gene expression.	307
8.4. Discussions	311
8.5. References.....	315
CHAPTER 9: General Discussions.....	319
APPENDIX: Published Papers	327

ACKNOWLEDGEMENTS

I would like to express my gratitude to both my supervisors for the opportunity and privilege to study and work with experts in the field of sterols and mass spectrometry. Specifically, to Dr Yuqin Wang who has been a great mentor throughout my project. I owe her my sincere thankfulness for always having an open door, for being thorough, for remembering things that I forgot and supporting me throughout my PhD study. To Professor William J. Griffiths for the informative discussions, highly interesting projects and constant encouragements that were crucial confidence boosts.

I would also like to thank the Griffiths-Wang group members, both past and present, for their advice and contributions, namely: Dr Peter Crick, Dr Jennifer Aponte, Dr Zuzka Simova, Dr Anna Meljon, Dr Katarina Rigdova and Dr Monika Seidel. Specifically, I am thankful for the company of Dr Jonas Abdel-Khalik for being there in those weekend experiments and for the regular constructive debates. Dr Alwena Morgan for her help in starting up the T cell study and acting as my guide in the initial stages of my PhD. And, Dr Tom Hearn for his valuable assistance in gene expression and T cell polarisation studies.

To my sister and brother, who have no idea what I do, but nevertheless supported me emotionally. And finally, to my mother, for all her comforting reassurance and positive reinforcements that kept me going.

DEDICATION

To my wife Hazel, for the unwavering love, support and being the pillar that helps me remain grounded and moving forward. To my son Daryl Zian, this and whatever comes after, are all for you.

ABBREVIATIONS

24S,25-EC	24S,25-epoxycholesterol
25-HC	25-hydroxycholesterol
7-AAD	7-Aminoactinomycin D
7 α ,25-DiHC	7 α ,25-dihydroxycholesterol
ABCA1	ATP-binding cassette A1
ABCG1	ATP-binding cassette G1
AP-1	Activator protein 1
pAPC	Antigen presenting cell (professional)
APC	Allophycocyanin
API	Atmospheric pressure ionisation
ATP	Adenosine triphosphate
BSA	Bovine serum albumin
CA	Cholestenoic Acid
CCL	Chemokine (C-C motif) ligand
CCR	C-C chemokine receptor
CCR	Chemokine (C-C motif) receptor
CD	Cluster of Differentiation
CH25H	Cholesterol 25-hydroxylase
CI	Chemical ionisation
CID	Collision induced dissociation
CLP	Common lymphoid progenitor
Ct	Cycle threshold
CTL	Cytotoxic T lymphocytes
CYP	Cytochrome P450
CYP27A1	Sterol 27-hydroxylase
CYP46A1	Cholesterol 24-hydroxylase
CYP7A1	Cholesterol 7 α -hydroxylase
CYP7B1	Oxysterol 7 α -hydroxylase
DAG	Diacylglycerol
DC	Dendritic cells
DHCR24	24-Dehydrocholesterol reductase
DL	Delipidated
DMSO	Dimethyl sulfoxide
EADSA	Enzyme-assisted derivatisation for steroid analysis
EBI-2	Epstein-Barr virus-induced gene 2
EC	Epoxycholesterol
EI	Electron ionisation
ELISA	Enzyme-linked immunosorbent assay
ER	Endoplasmic reticulum
ERK	extracellular signal regulated kinase
ESI	Electrospray ionisation
EtOH	Ethanol
eV	Electron volts
FA	Fatty acids
FACS	Fluorescence-activated cell sorting
FBS	Fetal bovine serum
FITC	Fluorescein isothiocyanate
FOXP3	Forkhead Box P3
FSC	Forward scatter
FT	Fourier transform
GC	Gas chromatography
GP	Girard's Reagent P
GPCR	G-protein coupled receptor
HC	Hydroxycholesterol
HDL	High density lipoproteins
HESI	Heated electrospray ionisation

HLB	Hyrophobic-lipiphilic balanced
HMG-CoA	3-hydroxy-3-methylglutaryl-CoA
HMGCR	HMG-CoA reductase
HPLC	High performance liquid chromatography
HSD3B7	3 β -hydroxy- Δ 5-C27 steroid oxidoreductase
IFN γ	Interferon gamma
Ig(s)	Immunoglobulin(s)
IL	Interleukin
INSIG1	Insulin-induced gene 1
IPA	Isopropyl alcohol
iPrOH	Propan-2-ol
iSTD	Internal standard
KC	Ketocholesterol
KOH	Potassium Hydroxide
kV	Kilovolts
LC	Liquid chromatography
LDL	Low density lipoproteins
LIT	Linear Ion trap
LPS	Lipopolysaccharide
LTQ	Linear trap quadrupole
LXR	Liver X receptor
<i>m/z</i>	mass-to-charge ratio
MACS	Magnetic-activated Cell Sorting
MALDI	Matrix-assisted laser desorption ionisation
MAPK	Mitogen-activated protein kinase
mCD4	Memory CD4
MeCN	Acetonitrile
MEK1	Mitogen-activated protein kinase kinase 1
MeOH	Methanol
MFI	Median fluorescence intensity
MHC	Major histocompatibility complex
mL	Millilitre
mRNA	Messenger ribonucleic acid
MS	Mass spectrometry
MSn	Multi-stage tandem mass spectrometry
mTORC	Mammalian target of rapamycin complex
M ϕ	Macrophages
nCD4	Naïve CD4
NFAT	Nuclear factor of activated T cells
NF κ B	Nuclear factor kappa-B
NKT	Natural Killer T cells
NP	Normal phase
NR	Nuclear receptor
PAMP	Pathogen-associated molecular pattern
PBMC	Peripheral Blood Mononuclear Cells
PBS	Phosphate Buffered Saline
PE	Phycocerythrin
pg	Picogram
PI3K	Phosphoinositide 3-kinase
PKB	Protein kinase B
PKC	Protein kinase C
PTFE	Polytetrafluoroethylene
PVDF	Polyvinylidene fluoride
RF	Radio frequency
RIC	Reconstructed ion chromatogram
ROR γ t	Retinoic acid receptor-related orphan receptor gamma t
ROS	Reactive oxygen species
RP	Reversed phase
RPMI	Roswell Park Memorial Institute Medium 1640
RPS18	Ribosomal Protein S18

RT	Room Temperature
RXR	Retinoid X receptor
S1P	Sphingosine-1-phosphate
SCAP	SREBP cleavage and activating protein
SF	Serum Free
SMAC	Supramolecular activation complex
SMAC	Supramolecular activation cluster
SMV	Simvastatin
SPE	Solid phase extraction
SREBP	Sterol regulatory element binding protein
SSC	Side Scatter
TCM	Central memory T cells
TCR	T cell receptor
TEC	Thymic epithelial cells
TEM	Effector memory T cells
TFH	Follicular T helper cells
TG	Triglycerides
TGF	Tumour growth factor
TH	T Helper
TIC	Total ion chromatogram
TLC	Thin layer chromatography
TLR	Toll-like receptor
TNF	Tumour necrosis factor
Treg	Regulatory T helper cells
TSA	Tissue specific antigen
VLDL	Very low density lipoproteins
μM	Micromolar

LIST OF TABLES

Table 1.1. Common sterol-metabolism related enzymes.	15
Table 1.2. List of characterised T cell types and subsets with main functions.	26
Table 1.3. List of characterised CD4 ⁺ T helper subsets with differentiation cytokines, transcriptional master regulators and main effector cytokines.....	27
Table 2.1. List of cell culture reagents, cytokines and kits	75
Table 2.2. Culture plate sizes to use according to cell dilution and density for seeding activated CD4 ⁺ T cells.	80
Table 2.3. List of reagents, buffers, materials and kits used for flow cytometric analysis.	84
Table 2.4. List of monoclonal antibodies used for flow cytometry.	85
Table 2.5. List of reagents and materials used for sterol analysis.....	88
Table 2.6. List of sterols monitored and identified using EADSA.	104
Table 2.7. List of reagents, instruments and kits for gene and protein expression analysis.	110
Table 2.8. List of primers and gene targets used for qPCR.	111
Table 3.1. Quantification table for sterols detected in serum-free, full and delipidated media.	125
Table 3.2. Quantification table for sterols detected in X-Vivo-20 with and without hydrolysis in KOH	127
Table 4.1. Cell numbers seeded and end point analysis for naïve CD4 ⁺ pilot cultures in X-VIVO-20.	134
Table 4.2. Culture conditions for TH17-polarised and non-polarised activated (TH0) naïve CD4 ⁺ T cells in X VIVO-20 media.....	134
Table 4.3. Cell numbers seeded and end point analysis for naïve CD4 ⁺ cultures in X-VIVO-20 with 4µg/mL Cholesterol-D7.....	136
Table 4.4. Cell numbers seeded and end point analysis for time course experiments on total CD4 ⁺ cultures in X-VIVO-20.	138
Table 4.5. Cell numbers seeded and end point analysis for comparing naïve and memory CD4 ⁺ cultures in X-VIVO-20.	139
Table 4.6. Sterols detected and quantified from activated CD4 ⁺ T cell culture media fraction extracts after 6 days in X-VIVO-20.....	147
Table 4.7. Sterols detected and quantified from activated CD4 ⁺ T cell pellet after 6 days in X-VIVO- 20.....	148
Table 4.8. Sterols quantified in cell fraction extracts after 3 days in X-VIVO-20 supplemented with 4µg/mL cholesterol-D7.	161
Table 4.9. Sterols quantified in media fraction extracts after 3 days in X-VIVO-20 supplemented with 4µg/mL cholesterol-D7.	161
Table 7.1. Compounds used to modulate intracellular signalling pathways in activated total CD4 ⁺ T cells.	245
Table 7.2. Effect of different treatments to the quantified sterols in the conditioned media fractions of total CD4 ⁺ T cells after 48 hours in culture.	253
Table 7.3. Effect of different treatments to the quantified sterols in the cell fractions of total CD4 ⁺ T cells after 48 hours in culture.	254
Table 7.4. Effect of different treatments to the quantified cholesterol and cholesterol precursors in the cell fractions of total CD4 ⁺ T cells after 48 hours in culture.....	255
Table 8.1. Different treatments for polarising activated naïve CD4 ⁺ T cells used for donor 1 and donor 2.....	289
Table 8.2. Different treatments for polarising activated naïve CD4 ⁺ T cells used for donor 3.....	290

LIST OF FIGURES

Figure 1.1. Cholesterol structure.	3
Figure 1.2. Cholesterol roles and functions.	4
Figure 1.3. Mevalonate pathway from acetyl-CoA to lanosterol.	8
Figure 1.4. Cholesterol biosynthesis pathway from lanosterol. Part 1.	9
Figure 1.5. Cholesterol biosynthesis pathway from lanosterol. Part 2.	10
Figure 1.6. Nomenclature of sterol stereoisomers.	13
Figure 1.7. Hematopoietic cell lineage tree.	21
Figure 1.8. Assembly of the full T cell receptor.	35
Figure 1.9. Initial TCR signalling.	36
Figure 1.10. Signalling cascade initiated from PLC- γ	40
Figure 1.11. Electrospray ionisation (ESI) on an LTQ Orbitrap Velos Pro/Elite.	43
Figure 1.12. Orbitrap Velos Pro/Elite mass spectrometer layout schematics.	45
Figure 1.13. Internal schematics of a dual-cell 2D linear ion trap of the Velos Pro.	47
Figure 1.14. Solid phase extraction (SPE) procedure.	51
Figure 1.15. Different sterol modifications for derivatisation.	53
Figure 2.1. Schematic for the sample preparation for sterol analysis by LCMS.	91
Figure 2.2. Charge-tagging of sterols after cholesterol oxidase treatment.	94
Figure 2.3. Sterols derivatised with Girard's reagent P introduces a quaternary nitrogen.	95
Figure 2.4. Series of sample processing breakdown showing the SPE fractions used for LCMS analysis.	97
Figure 2.5. Liquid chromatography multi-step gradients for derivatised sterol separation.	103
Figure 2.6. Representative process of ion isolation, identification and quantification of sterol species analysed by LCMS on Xcalibur Qual Browser.	109
Figure 3.1. Representative reconstructed ion chromatograms for monohydroxycholesterols present in different culture media.	124
Figure 4.1. Brassicasterol as an internal standard.	136
Figure 4.2. Deuterated 22(R)-HC as an internal standard.	136
Figure 4.3. Structures of GP derivatised sterols in natural and side-chain deuterium-substituted forms.	137
Figure 4.4. Representative flow cytometry analysis of naïve CD4 ⁺ T cells after isolation by MACS®.	142
Figure 4.5. Reconstructed ion chromatogram (RIC) of the monohydroxycholesterols at 534.4054 \pm 10ppm in Fraction1As of unstimulated naïve CD4 ⁺ T cells in SF media after 6 days.	143
Figure 4.6. RIC of the monohydroxycholesterols at 534.4054 \pm 10ppm in Fraction1As of unstimulated naïve CD4 ⁺ T cells in DL media after 6 days.	144
Figure 4.7. Donor 1 total ion chromatogram of monohydroxycholesterol [534 \rightarrow 455 \rightarrow] MS3 transition for activated and polarised naïve CD4 ⁺ T cells.	149
Figure 4.8. Donor 1 representative total ion chromatogram of dihydroxycholesterols [550 \rightarrow 471 \rightarrow] MS3 transition for activated and polarised naïve CD4 ⁺ T cells.	150
Figure 4.9. Formation of E-Z isomers (syn and anti) in GP hydrazone derivatised sterols.	152
Figure 4.10. 24(S),25-EC during the EADSA process.	153
Figure 4.11. RIC of the dihydroxycholesterols at 550.4003 \pm 10ppm in Fraction1As of mock SF RPMI and X-VIVO-20 media.	155
Figure 4.12. RIC of the monohydroxycholesterols at 534.4054 \pm 10ppm in Fraction1As of SF RPMI and X-VIVO-20 media.	155
Figure 4.13. RIC of monohydroxycholesterols at 534.4054 \pm 10ppm of non-treated and 10ng/mL IL-2 treated naïve CD4 ⁺ T cells in SF RPMI and X-VIVO-20 media after 6 days.	156
Figure 4.14. RIC of dihydroxycholesterols at 550.4003 \pm 10ppm of non-treated and 10ng/mL IL-2 treated naïve CD4 ⁺ T cells in SF RPMI and X-VIVO-20 media after 6 days.	157

Figure 4.15. Donor 1 RIC of cholesterol and cholesterol-D7 in non-activated naïve CD4 ⁺ T cells after three days.	162
Figure 4.16. Donor 1 RIC of cholesterol and cholesterol-D7 in activated naïve CD4 ⁺ T cells after three days.	162
Figure 4.17. Donor 3 RIC of cholesterol, cholesterol-D7 and brassicasterol internal standard in non activated naïve CD4 ⁺ T cells after three days in 4µg/mL cholesterol-D7.	163
Figure 4.18. Donor 3 RIC of cholesterol, cholesterol-D7 and brassicasterol internal standard in 2-day activated naïve CD4 ⁺ T cells after pre-incubation and three days in 4µg/mL cholesterol-D7.	163
Figure 4.19. RIC for 534.4054 m/z, 540.4431 m/z and 541.4493 m/z to monitor monohydroxycholesterols, monohydroxycholesterol-D6s and monohydroxycholesterol-D7s in mock X-VIVO-20 media.	164
Figure 4.20. RIC for 550.4003 m/z and 556.4380 m/z to monitor dihydroxycholesterols and dihydroxycholesterol-D6s in mock X-VIVO-20 media.	164
Figure 4.21. Donor 1 RIC for 534.4054 m/z, 540.4431 m/z and 541.4493 m/z to monitor monohydroxycholesterols, monohydroxycholesterol-D6s and monohydroxycholesterol-D7s in media and cell fractions of non-activated and activated naïve CD4 ⁺ T cells after three days in X-VIVO-20 with 4µg/mL Cholesterol-D7.	165
Figure 4.22. Monohydroxycholesterol full mass scan RIC, linear ion trap TIC of MS3 [534→455→] and the MS3 fragmentation spectra of 25-monohydroxycholesterol-D0.	166
Figure 4.23. Monohydroxycholesterol-D6 full mass scan RIC, linear ion trap TIC of MS3 [540→461→] and the MS3 fragmentation spectra of 25-monohydroxycholesterol-D6.	166
Figure 4.24. RIC for 550.4003 m/z and 556.4380 m/z to monitor dihydroxycholesterols and dihydroxycholesterol-D6s in media and cell fractions of non activated and activated naïve CD4 ⁺ T cells after three days in X-VIVO-20 with 4µg/mL Cholesterol D7.	167
Figure 4.25. Pseudocolour CD25/CD4 dot plots of time course experiments on total CD4 ⁺ T cells.	170
Figure 4.26. Donor 1 RIC of monohydroxycholesterols at 534.4054m/z ±10ppm and dihydroxycholesterols at 550.4003m/z ±10ppm in the media fraction of the time course study of activated total CD4 ⁺ T cells.	171
Figure 4.27. Donor 1 RIC of cholestenic acid at 548.3847m/z ±10ppm and hydroxycholestenic acids at 564.3796m/z ±10ppm in the media fraction of the time course study of activated total CD4 ⁺ T cells.	172
Figure 4.28. Time course study of the production of 24S-HC found in culture media of non-activated and activated total CD4 ⁺ T cells.	173
Figure 4.29. Time course study of the production of 24R-HC found in conditioned media of non-activated and activated total CD4 ⁺ T cells.	174
Figure 4.30. Time course study of the production of 25-HC found in conditioned media of non-activated and activated total CD4 ⁺ T cells.	175
Figure 4.31. Time course study of the production of 7α,25-DiHC found in conditioned media of non-activated and activated total CD4 ⁺ T cells.	176
Figure 4.32. Time course study of the production of 24(S),25-EC detected in conditioned media of non-activated and activated total CD4 ⁺ T cells.	177
Figure 4.33. Time course study of the production of 25-HC detected intracellularly of non-activated and activated total CD4 ⁺ T cells.	178
Figure 4.34. Time course study of the production of 7α,25-DiHC detected intracellularly of non-activated and activated total CD4 ⁺ T cells.	178
Figure 4.35. Time course study of the production of 24(S),25-DiHC detected intracellularly of non-activated and activated total CD4 ⁺ T cells.	179
Figure 4.36. Time course study intracellular cholesterol contained in non-activated and activated total CD4 ⁺ T cells.	179
Figure 4.37. Magnetic separation process and pre-culture flow cytometry analysis of naïve and memory CD4 ⁺ T cells for donor 1.	184

Figure 4.38. Magnetic separation process and pre-culture flow cytometry analysis of naïve and memory CD4 ⁺ T cells for donor 2.	184
Figure 4.39. Flow cytometry analysis of CD25-APC stained naïve and memory CD4 ⁺ T cells of donor 1.	185
Figure 4.40. Oxysterols detected in the media fraction of 24 hour activated naïve and memory CD4 ⁺ T cells.	186
Figure 4.41. Pre-culture flow cytometry analysis of the positive and negative fractions after CD294 ⁺ TH2 isolation.	187
Figure 5.1. Simplified mevalonate pathway.	196
Figure 5.2. Structures of HMGCR catalytic subunit ligands.	197
Figure 5.3. Representative gating strategy for identifying live cells and exclusion of dead cells using 7AAD Viability Dye staining.	198
Figure 5.4. Simvastatin inhibits THP-1 cell division and induce cell death in a dose-dependent manner.	202
Figure 5.5. Representative ungated forward and side scatter dot plots of the total human CD4 ⁺ T cells cultured for up to 72 hours with and without activation and simvastatin treatments.	206
Figure 5.6. Flow cytometric 7AAD histograms gated from all cells of total human CD4 ⁺ T cells cultured for up to 72 hours with and without activation and simvastatin treatments for all three donors.	207
Figure 5.7. Flow cytometric CD25-APC histograms gated from live cells of total human CD4 ⁺ T cells cultured for up to 72 hours with and without activation and simvastatin treatments for all three donors.	208
Figure 5.8. Graphical representation of the change in CD25-APC median fluorescence intensities (MFI) in CD4 ⁺ T cells with and without simvastatin treatments for the three donors.	209
Figure 5.9. Flow cytometric cell proliferation dye histograms gated from live cells of total human CD4 ⁺ T cells cultured for up to 72 hours with and without activation and simvastatin treatments.	210
Figure 5.10. Quantification for 24(S),25-Epoxycholesterol detected in conditioned media extracts for each donor. Media were harvested at each time point and sterols extracted in ethanol.	213
Figure 5.11. Quantification for 25-Hydroxycholesterol detected in conditioned media extracts for each donor. Media were harvested at each time point and sterols extracted in ethanol.	214
Figure 5.12. Quantification for 7 α ,25-Dihydroxycholesterol detected in conditioned media extracts for each donor. Media were harvested at each time point and sterols extracted in ethanol.	215
Figure 5.13. Quantification for sterols in cell extracts for Donor 2. At the end of each time point, a portion of cells were lysed by ultrasonication and sterols extracted in ethanol.	216
Figure 6.1. RT-PCR analysis for 48-hour cultured siRNA-treated activated total CD4 ⁺ T cells of donor 1 (147).	227
Figure 6.2. Normalised LC-MSn quantification data from siRNA-treated activated total CD4 ⁺ T cells of donor 1 (147).	228
Figure 6.3. Cytokine production of siRNA-treated 48 hour activated total CD4 ⁺ T cells of donor 1 (147).	229
Figure 6.4. Flow cytometry analysis of 48-hour cultured siRNA-treated Neon®-transfected activated total CD4 ⁺ T cells of donor 1 (147)	229
Figure 6.5. Cell viability flow cytometry analysis of activated total CD4 ⁺ T cells before and after 4D Nucleofection.	233
Figure 6.6. IFN- γ secretion of CH25H siRNA-treated total CD4 ⁺ T cells of donor 2 (191) 48 hours after activation as measured by sandwich ELISA.	234
Figure 6.7. RT-PCR analysis for 48-hour cultured siRNA-treated activated total CD4 ⁺ T cells of donor 2 (191).	234
Figure 6.8. RT-PCR analysis for 48-hour cultured siRNA-treated activated total CD4 ⁺ T cells of donor 3 (164).	235
Figure 6.9. Time course analysis of IFN- γ concentration in anti-CD3/CD28 activated total CD4 ⁺ T cells by sandwich ELISA of donor 3 (164).	236

Figure 6.10. Flow cytometry histograms showing the effect of exogenous IFN- γ treatment or neutralising antibody in the expression of CD25 in total CD4 ⁺ T cells of donor 4 (047).	236
Figure 6.11. Sterols detected and quantified from the cell fractions of total CD4 ⁺ T cells after 48 hours of donor 4 (047).	237
Figure 6.12. Sterols detected and quantified from the media fractions of total CD4 ⁺ T cells after 48 hours of donor 4 (047).	237
Figure 6.13. Effect of neutralising anti-IFN- γ antibodies to CH25H and IFNG expression in activated total CD4 ⁺ T cells of donor 1 (147).	238
Figure 7.1. Signalling pathways downstream of TCR/CD28 stimulation in CD4 ⁺ T cells.	244
Figure 7.2. Representative flow cytometry overlays of the CD25 surface expression of untreated, anti-CD3/CD28, anti-CD3 alone and anti-CD28 alone treated total CD4 ⁺ T cells after 48 hours in culture from donor 5.	249
Figure 7.3. Detected sterols in the media and cell fractions of cultured total CD4 ⁺ T cells after 48 hours.	250
Figure 7.4. Cell viability analysis of 48 hour total CD4 ⁺ T cells treated without and with increasing concentrations of the NF- κ B signalling inhibitor, BAY-11-7082.	256
Figure 7.5. Half-offset overlay histograms comparing the viability staining for BAY-11-7082 treated CD4 ⁺ T cells after 48 hours across three donors.	256
Figure 7.6. Cell viability analysis of 48 hour total CD4 ⁺ T cells with and without activation and/or inhibitor treatments.	257
Figure 7.7. Cell viability analysis of pre-culture and 48 hour activated total CD4 ⁺ T cells treated with 1 μ M of the PKC inhibitor, Gö6983 reveals autofluorescence.	258
Figure 7.8. Overlay histograms of the CD25 expression of BAY-11-7082 treated total CD4 ⁺ T cells from five donors.	259
Figure 7.9. Detected sterols in the media and cell fractions of cultured total CD4 ⁺ T cells after 48 hours.	260
Figure 7.10. Overlay histograms of the CD25 expression of U0126 and SB203580 treated total CD4 ⁺ T cells from three donors.	262
Figure 7.11. Detected 24(S),25-EC and intracellular cholesterol of U0126 and SB203580 treated activated total CD4 ⁺ T cells after 48 hours.	262
Figure 7.12. Detected 25-HC in media fractions of U0126 and SB203580 treated activated total CD4 ⁺ T cells after 48 hours.	263
Figure 7.13. Detected sterols in media and cell fractions of PMA and Gö6983 treated total CD4 ⁺ T cells after 48 hours.	265
Figure 7.14. Overlay histograms of the CD25 expression of PMA-stimulated and Gö6983 treated total CD4 ⁺ T cells from three donors.	266
Figure 7.15. Detected cholesterol precursor, desmosterol, in cell fractions of total CD4 ⁺ T cells after 48 hours with different culture conditions.	266
Figure 7.16. Overlay histograms of the CD25 expression of LY294002 and Rapamycin treated total CD4 ⁺ T cells from three donors.	268
Figure 7.17. Overlay histograms of the ribosomal S6 phosphorylation in total CD4 ⁺ T cells after 48 hours.	268
Figure 7.18. Detected sterols in media and cell fractions of Rapamycin and LY294002 treated total CD4 ⁺ T cells after 48 hours.	269
Figure 7.19. Overlay histograms of CD25, pS6 and p4E-BP1 in total CD4 ⁺ T cells treated with rapamycin and Ku63794 after 48 hours for donor 7.	272
Figure 7.20. Detected sterols in media of Rapamycin and Ku63794-treated total CD4 ⁺ T cells after 48 hours of donor 7.	273
Figure 7.21. Real-time PCR analysis of donor 7 48 hour total CD4 ⁺ T cells with mTORC inhibitors. ..	273
Figure 7.22. Forward scatter flow cytometry analysis of 48 hour total CD4 ⁺ T cells with and without activation and/or inhibitor treatments across six different donors.	279
Figure 8.1. Typical workflow for naïve CD4 T cell isolation, culture, polarisation and analysis.	287

Figure 8.2. Day 0 flow cytometry analysis of naïve CD4 ⁺ T cell purity.	293
Figure 8.3. Representative day 0 dual staining purity analysis of donor 3 (305) naïve CD4 ⁺ T cells.	293
Figure 8.4. Viability analysis of day 6 polarised activated naïve CD4 T cells.	294
Figure 8.5. CD25 expression analysis of activated naïve CD4 T cells of donor 1 and 2 after 6 days.	295
Figure 8.6. RT-PCR analysis for 6-day cultured activated naïve CD4 ⁺ T cells of donor 1 (046) comparing TH0, TH2 and Treg polarisations.	298
Figure 8.7. RT-PCR analysis for 6-day cultured activated naïve CD4 ⁺ T cells of donor 2 (283) comparing TH0, TH2 and Treg polarisations.	299
Figure 8.8. Intracellular IL4 staining of 6-day activated CD4 ⁺ T cells.	300
Figure 8.9. Intracellular FOXP3 staining of 6-day activated CD4 ⁺ T cells.	300
Figure 8.10. Sterols from day 3 and day 6 collected media supernatants of Donor 1 (046) and 2 (283) comparing TH0, TH2 and Treg polarisations.	302
Figure 8.11. CD25 expression analysis of activated naïve CD4 T cells of donor 3 after 6 days.	305
Figure 8.12. Flow cytometry analysis of naïve CD4 ⁺ T cells of donor 3 (305).	306
Figure 8.13. RT-PCR analysis for 6-day cultured activated naïve CD4 ⁺ T cells of donor 3 (305) comparing TH0 and Treg polarisations.	309
Figure 8.14. Sterols from day 3 and day 6 collected media supernatants from Donor 3 (305) comparing TH0 and Treg polarisations.	310
Figure 8.15. Proposed schematic pathway of the sterol precursors and products detected.	314

CHAPTER 1: General Introduction

Oxysterols have lately emerged to be involved in macrophage and B cell immune responses. However, studies around how sterols impact human T cell function are still limited. In the last two years, a few studies have been published which suggested cholesterol precursors or oxysterols to be the natural ligands^[1-3] of the nuclear hormone receptor ROR γ t, a transcription factor driving the differentiation of TH17 cells. However, which sterols are ROR γ t endogenous ligands are still under debate. Before systematically tackling the function of sterols in TH17 cells and autoimmunity, the general landscape of oxysterols and CD4⁺ T cells and techniques for analysis must be established first. Therefore, the focus of this thesis was on human CD4⁺ T helper cells and relating oxysterol production to immune function.

1.1. Cholesterol

Cholesterol is a multifunctional lipid essential in most vertebrate systems, not only serving as an integral cell structural and cell trafficking component but also a precursor for several bioactive metabolites implicated in health and disease.

1.1.1. Nomenclature, Biology and Functions

Discovery of cholesterol originated from the study of gallstones, when a French lipid chemist Michel Chevreul in 1816 isolated and named an alcohol-soluble constituent 'cholesterine', which is Greek for bile (*chole*) and solid (*stereos*)^[4-6]. As common to most sterol/steroid molecules, cholesterol is made up of three cyclohexane rings and a pentane ring assembled as cyclo-pentano-perhydro-phenan-threne with three fusion points forming a rigid trans-trans-trans flat asymmetric 3D structure. The four-ring 17-carbon skeleton is 3 β -hydroxylated, methylated at both C10 and C13 positions with a Δ^5 double bond in ring B and an 8-carbon branched side-chain attached to C17, making up to C₂₇H₄₅OH or systematically named as cholest-5-en-3 β -ol (Figure 1.1)^[7,8].

Cholesterol is an amphipathic molecule with a polar 3 β -hydroxyl head group and a non-polar hydrocarbon ring/side-chain. This attribute permits cholesterol to embed

and orientate distinctively in cellular lipid bilayers. Cholesterol content greatly affect lipid bilayer physical and chemical properties specifically in mechanical stability, lipid order, fluidity and permeability^[9]. In addition, cholesterol together with sphingolipids have been associated with lipid rafts in liquid-ordered phases. Lipid rafts are a combination of different lipids and proteins that form tightly packed microdomains on membranes especially responsible for the assembly and compartmentalisation of signalling molecules^[10]. Intracellularly, sorting is also possible through cholesterol. Proteins and lipids made in the endoplasmic reticulum (ER) are processed through the Golgi apparatus and into endosomes and the cell membrane, with each step following an increasing cholesterol gradient^[11,12]. Outside the cell, cholesterol can act as a starting molecule for several bioactive metabolites (Figure 1.2). Such metabolites consist of steroid hormones and bile salts as well as oxysterols, which will be discussed later. Steroid hormones are powerful signalling and regulatory molecules which have organism-wide effects. All five major classes of steroid hormones: progestogens(C21), glucocorticoids(C21), mineralocorticoids(C21), androgens(C19), and oestrogens(C18) can be derived from cholesterol(C27) through isomerisation and side-chain cleavage^[7]. Moreover, bile salts or bile acids produced in the liver and stored in the gall bladder, which functions to aid in solubilising lipids and its absorption in the small intestine, are also made from cholesterol through a series of oxidation steps. In addition, the process of cholesterol synthesis itself provides a source of intermediates like isoprenoids and 7-dehydrocholesterol important for protein prenylation of various signalling proteins and vitamin D3 synthesis, respectively^[7,13,14].

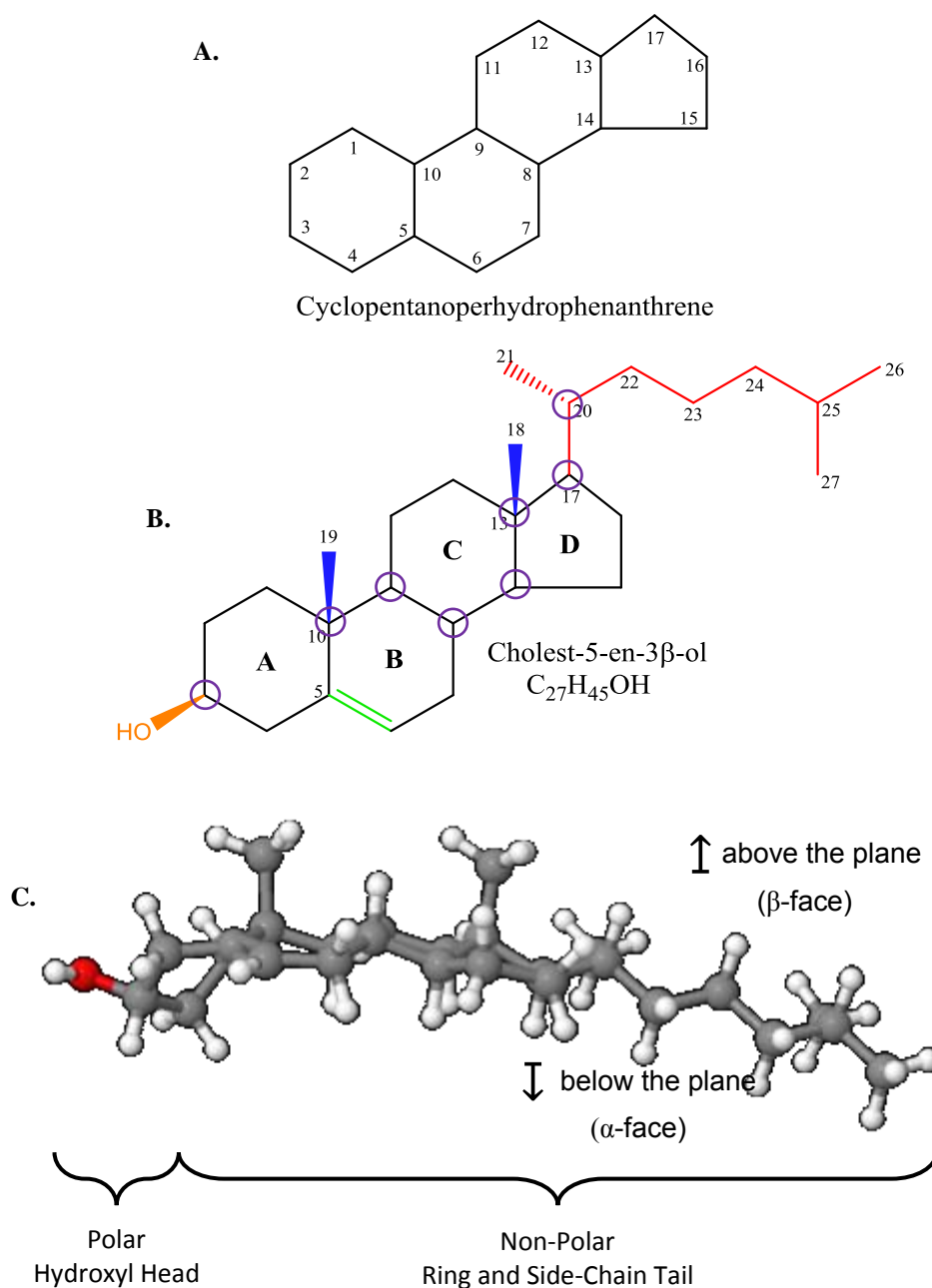


Figure 1.1. Cholesterol structure.

A. The four-ring cyclopentanoperhydrophenanthrene backbone common to sterol and steroid species. B. Cholesterol molecule with its systematic name and molecular formula. It has 8 chiral centres encircled in purple. Modifications of the steroid backbone are the 3 β -hydroxylation (orange), the Δ 5 double bond (green), the two methyl groups at C10 and C13 (blue) and the side-chain attached at C17 (red). C. A ball and stick model of cholesterol showing the rigid planar structure with the two methyl groups above the plane together with the hydroxyl group^[7] [ChemSpider ID 5775].

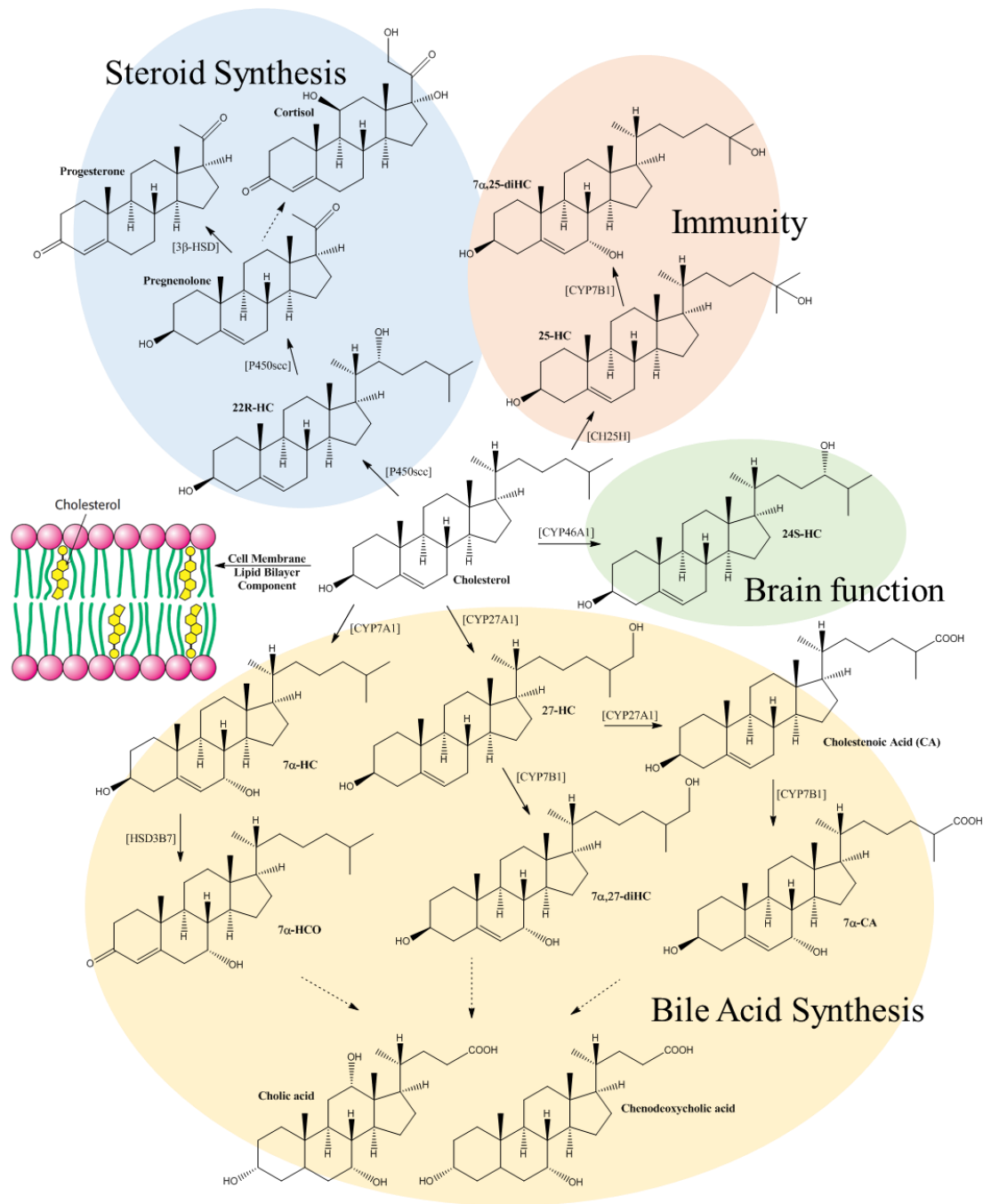


Figure 1.2. Cholesterol roles and functions.

As well as being a vital component of eukaryotic lipid bilayer cell membranes which influences stability, permeability and intracellular signal propagation through lipid raft assembly, cholesterol can act as starting compound of steroid hormones, bile acids/salts^[75], and immunoregulatory oxysterols^[46] as well as influencing neuronal cell health^[35-37]. Lipid bilayer image was taken from Biochemistry 7th edition p.363^[13].

1.1.2. Sources, Synthesis, and Regulation

The two main sources of cholesterol are through diet and by *de novo* cellular synthesis. Around 30% of the body's cholesterol can be of dietary origin but the other 70% are inherently produced by cells. These are typically by hepatocytes in the liver but almost all cholesterol requirements of the brain are made in the central nervous system.

Even with its amphipathic nature, cholesterol is not water-soluble. Consequently, its absorption from diet need a means of transportation through the highly aqueous blood plasma. Lipoproteins like chylomicrons, very low density lipoproteins (VLDL), low density lipoproteins (LDL) and high density lipoproteins (HDL) functions as transient storage and transport of hydrophobic lipids like fatty acids (FA), triglycerides (TG) and cholesterol. Chylomicrons transport these lipids absorbed from the intestine to the liver. Liver cells can then package these lipids in VLDLs to primarily transport FA and TG to the rest of the body like adipose tissue and muscles. Loss of FA and TG results in lipoprotein shrinkage and increase in protein-to-lipid ratio leading to VLDLs transitioning to LDLs as it circulates. LDLs have the highest proportion of cholesterol and serve as the cholesterol delivery mechanism to target cells through LDL receptor mediated endocytosis in the target cell or in the liver. HDLs are the smallest of the lipoproteins made in the liver. Once in circulation, HDL can pick up excess cholesterol in the periphery and return it back into the liver for excretion or metabolism to bile acids. This is essentially known as reverse cholesterol transport mediated by scavenger receptors present in liver cells.

New cholesterol can be made intracellularly through *de novo* synthesis. This biosynthetic pathway, which can be divided into two parts, involves a series of enzyme-catalysed steps starting from the mevalonate pathway to the Bloch pathway (Figure 1.3). This initial pathway occurring in the cytosol utilises acetyl-CoA (2C) produced from other metabolic pathways, and convert it to hydroxy-methylglutaryl-CoA (HMG-CoA 6C). Then, in the ER membrane, the 6C HMG-CoA is reduced to 6C mevalonate by a highly regulated rate-limiting enzyme HMG-CoA reductase (HMGCR). Next, the mevalonate is converted into a 5C isopentenyl pyrophosphate (IPP) through a 3-step phosphorylation with a loss of CO₂. IPP can be isomerised to dimethylallyl pyrophosphate (DMAPP), both of which are combined by a

condensation reaction catalysed by prenyl transferase to a 10C geranyl pyrophosphate (GPP). Via the same enzymatic process, a further 5C IPP is added into the GPP giving rise to a 15C farnesyl pyrophosphate (FPP). Two FPP molecules can subsequently undergo another condensation reaction into a 30C squalene catalysed by squalene synthase. Squalene is then oxidised into 2,3-epoxysqualene or further into 2,3:22,23-diepoxy-squalene by squalene monooxygenase. Next, epoxysqualene can act as substrate to oxidosqualene cyclase or lanosterol synthase, a cyclization step giving rise to the characteristic four-ring steroid nucleus, to produce lanosterol (30C). The formation of lanosterol can feed into the next 18-step Bloch pathway to produce cholesterol (Figure 1.4 and Figure 1.5)^[15,16]. In parallel to this, 24-dehydrocholesterol reductase (DHCR24) can act on lanosterol or on other Bloch pathway intermediates to reduce the double bond at C24 which can feed into another defined cholesterol biosynthetic pathway known as the Kandutsch-Russell pathway. Both pathways proceed in sequence using the same biosynthetic enzymes undergoing a number of oxidation, demethylation, reduction, decarboxylation and isomerisation steps, with multi-step reactions often catalysed by a single enzyme, ultimately losing three carbons species leaving the 27C cholesterol. Another pathway occurs parallel to cholesterol biosynthesis which also uses the same enzymes known as the Shunt pathway. This originates from the repeated oxidation of squalene to 2,3-epoxysqualene to 2,3:22,23-diepoxy-squalene. Consequently, after its cyclization, the same reactions and modifications proceed in the steroid ring system but the epoxide group present in the side chain is preserved giving rise to the production of 24S,25-epoxycholesterol^[17,18].

Each eukaryotic cell is capable of this *de novo* cholesterol biosynthesis using much simpler precursors. As a consequence, cells require a form of regulation to tightly control this biosynthesis. It was initially accepted that cholesterol itself can act as a regulatory molecule to inhibit its synthesis through negative feedback loops. However, more potent regulators, like oxysterols, have been identified^[19]. As the HMGCR acts as the rate-limiting step, this can be the primary method of regulating cholesterol biosynthesis. The HMGCR protein is also regulated through the actions of the sterol regulatory element binding protein 2 (SREBP2) transcription factor^[20] and SREBP cleavage and activating protein (SCAP)^[21]. In cholesterol deprived conditions, SCAP and SREBP2, both normally sequestered in the ER, can bind and co-migrate into the

Golgi apparatus via Coat Protein Complex 2 (COPII) vesicles for modification and activation. There, SCAP gets activated and cleaves SREBP2 and releases the active mature N-terminal transcription factor domain for translocation to the nucleus and initiate transcription of several cholesterol biosynthesis genes including *HMGCR* to drive both cholesterol uptake and *de novo* synthesis^[22]. SCAP contains a sterol-sensing domain which can bind cholesterol^[23], in cholesterol rich conditions. This binding occurs and induces a conformational change in SCAP preventing both its binding to SREBP2 and migration to the Golgi and transcriptional regulation does not occur. In addition, oxysterols like 25-HC, can serve as inhibitory regulators through their interaction with SCAP and another ER resident insulin-induced gene 1 (INSIG1) protein. INSIG1 also contains a sterol-sensing domain of which in the presence of oxysterols, e.g. 25-HC, facilitates INSIG1-SCAP binding, thus restricting both proteins and SREBP2 in the ER and preventing the transcriptional activation of sterol regulatory elements^[24]. Additionally, the ER resident HMGCR enzyme itself contains a sterol-sensing domain in its N-terminal transmembrane domain and when engaged initiates the ubiquitination of the enzyme and subsequent proteolysis^[25,26]. Other forms of control are with kinase phosphorylation or phosphatase dephosphorylation which can deactivate or activate HMGCR, through the actions of glucagon or insulin, respectively^[27]. Apart from its regulation through control of biosynthesis and export, excess cholesterol can also be stored through the addition of fatty acids by acyl-CoA:cholesterol acyltransferase (ACAT) as cholesteryl esters^[28]. When cholesterol is then required the process is reversed by cholesteryl ester hydrolases.

Cholesterol, given its ubiquity in cells, is highly susceptible to oxidation. Such cholesterol oxidation products are known as oxysterols^[29]. Early cholesterol investigations have initially identified oxysterols arising from autoxidation but later studies have identified a variety of enzymes that use cholesterol as its substrate thus producing several biologically active oxysterol species.

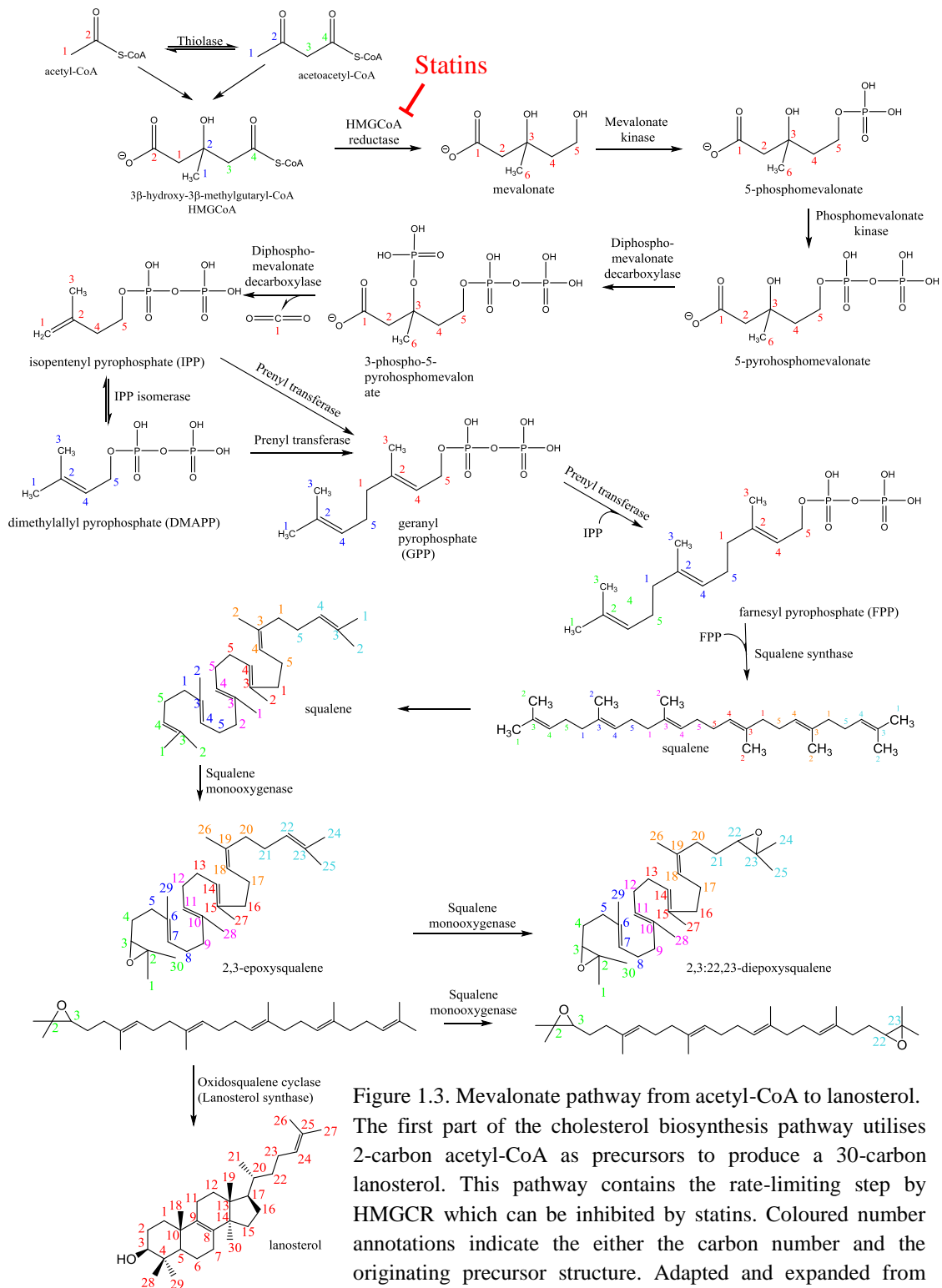


Figure 1.3. Mevalonate pathway from acetyl-CoA to lanosterol. The first part of the cholesterol biosynthesis pathway utilises 2-carbon acetyl-CoA as precursors to produce a 30-carbon lanosterol. This pathway contains the rate-limiting step by HMGCR which can be inhibited by statins. Coloured number annotations indicate the either the carbon number and the originating precursor structure. Adapted and expanded from Mazein et.al^[15].

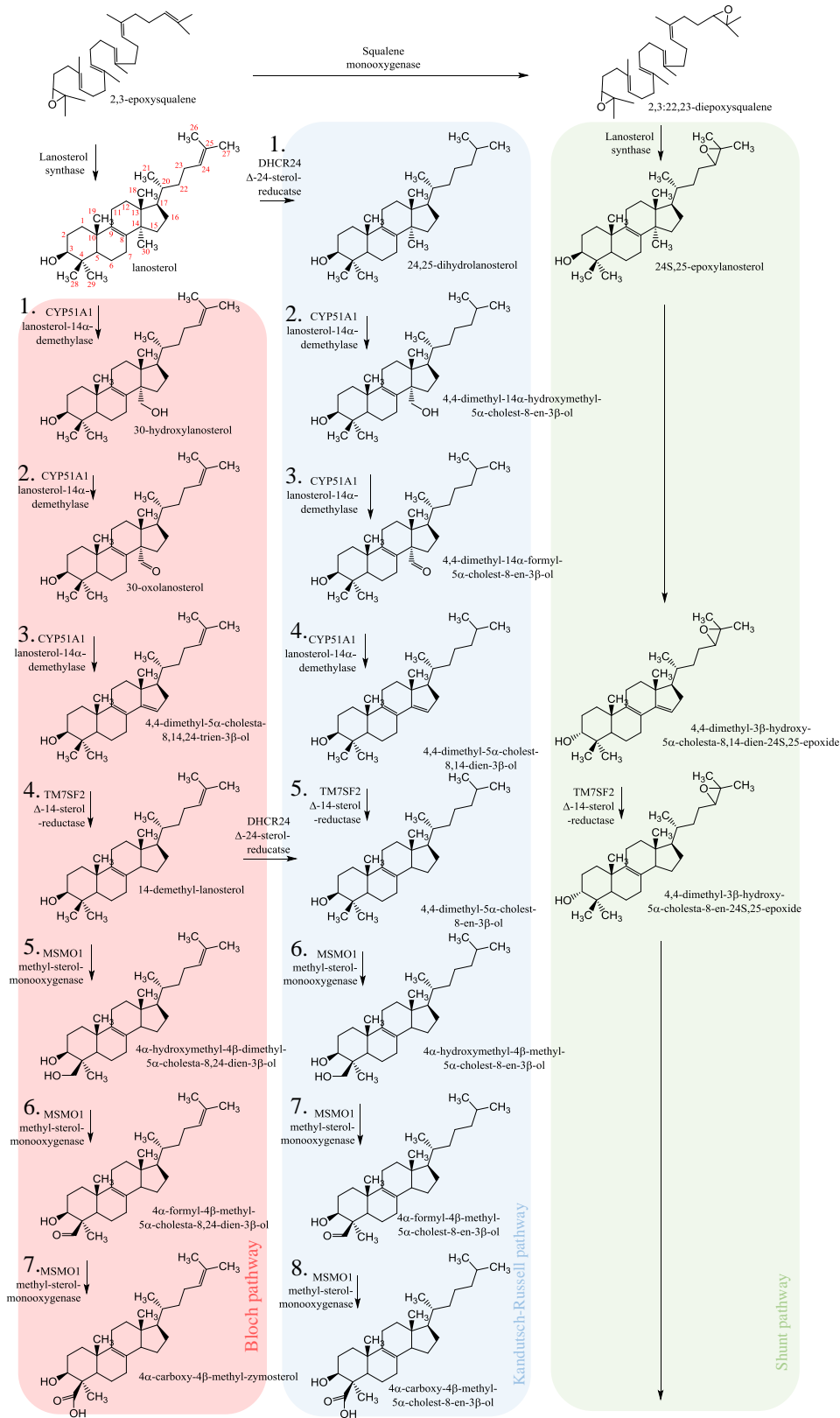


Figure 1.4. Cholesterol biosynthesis pathway from lanosterol. Part 1. After the mevalonate pathway, the 30-carbon squalene is cyclized into lanosterol by lanosterol synthase. The 30-carbon lanosterol can then feed into another 18-step enzyme catalysed reaction to produce cholesterol. Furthermore, the C24 double bond of lanosterol, or at a few intermediates of the Bloch pathway (red) can be reduced by DHCR24 to feed into a parallel Kandutsch-Russell pathway (blue). Adapted from Mazein et.al.^[15].

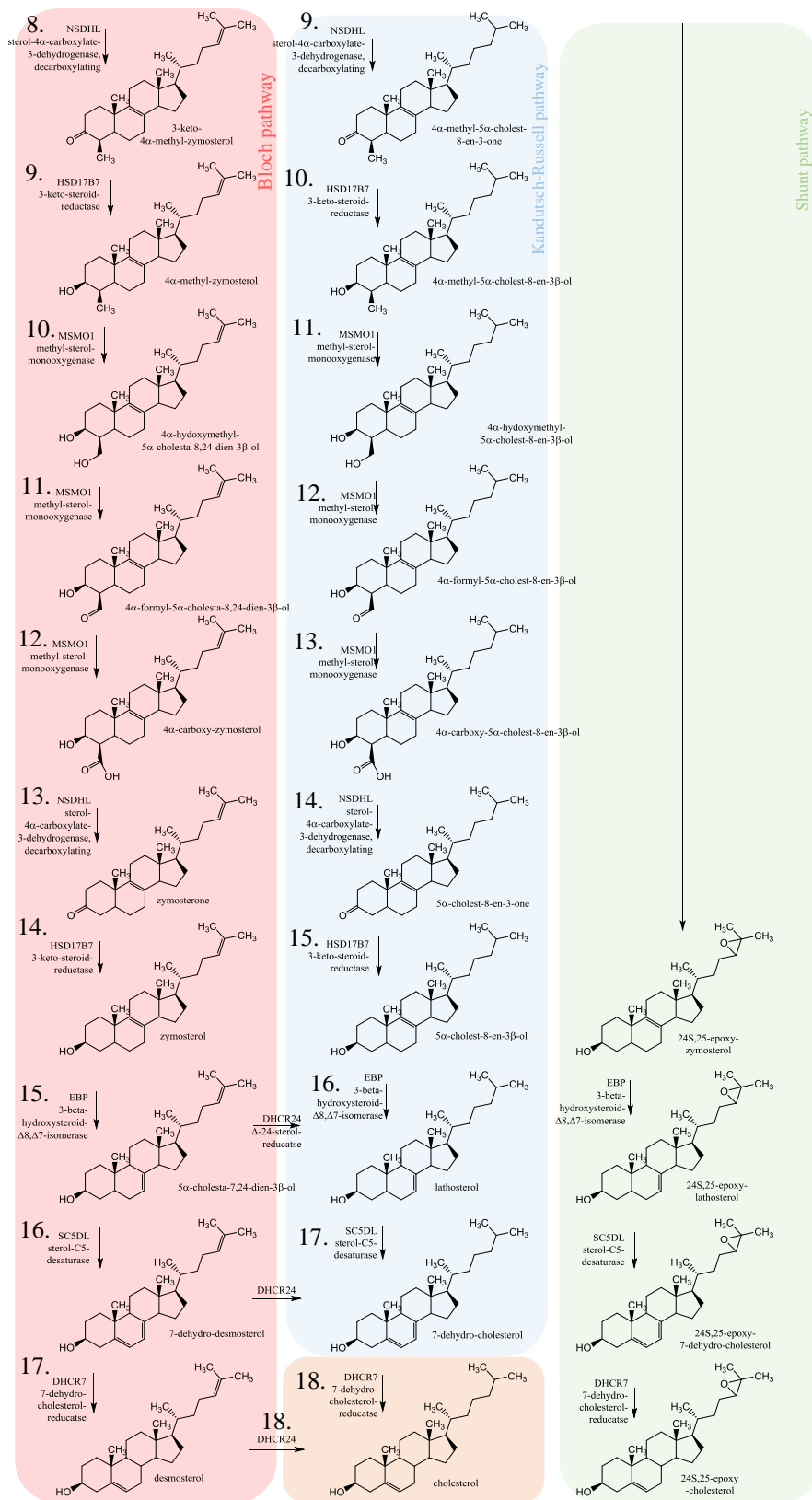


Figure 1.5. Cholesterol biosynthesis pathway from lanosterol. Part 2.

Both of the pathways proceed into a sequential manner utilising the same metabolic enzymes ultimately producing cholesterol from desmosterol through the Bloch pathway or 7-dehydrocholesterol from the Kandutsch-Russell pathway. In addition, a third pathway exists arising from the dual oxidation of squalene to diepoxysqualene before cyclization. This shunt pathway (green) also utilises the same cholesterol biosynthetic enzymes but produces 24S,25-epoxycholesterol instead of cholesterol. Adapted from Mazein et al. [15].

1.2. Oxysterols

Oxysterols are cholesterol derivatives with one or more oxygen containing groups: hydroxyl, keto, hydroperoxy, epoxy, or carboxyl, in addition to the 3 β alcohol group^[30]. These cholesterol intermediates were initially thought to be mere inactive intermediates but expanding knowledge in sterol science have implicated such species in a variety of physiological^[31], metabolic^[32], regulatory^[24,33], cognitive^[34–37], immunogenic^[38–47], and pathological^[1,48–50] roles.

1.2.1. Discovery and Brief History

It was about a century after Chevreul when work by Israel Lifschütz designated monohydroxylated cholesterol derivatives as ‘oxycholesterols’ circa 1906 identified from relatively impure sterol mixtures^[6]. Impure mixtures have pointed a possible issue of cholesterol artefact formation due to reported instability of cholesterol in storage in 1904^[6], to studies in 1914 where heating cholesterol in air yielded oxycholesterol products identified distinctly from cholesterol by colorimetric acid tests^[51]. This made Lifschütz and early investigators question if oxycholesterols were cholesterol metabolites in tissues or mere artefacts formed after isolation by autoxidation. After cholesterol structure was assigned in 1930s^[52], the understanding of cholesterol chemistry increased and its relationships with other sterols, steroid hormones and bile salts were pioneered between 1930s to 1960s^[6,53,54]. Consequently, more oxidised cholesterol species were discovered in the 60s with the application of thin layer chromatography^[55,56]. In the late 60s to 70s, biological roles of oxysterols were confirmed as regulators of cholesterol, when cultured cells demonstrated reduced *de novo* cholesterol biosynthesis in the presence of select oxysterols^[19,57,58]. These studies continue today and so far, oxysterols have been reported to be linked not only to *in vivo* cholesterol homeostasis^[59] but also implicated to have various roles in health and disease^[32].

1.2.2. Nomenclature

Similar to cholesterol (cholest-5-en-3 β -ol), oxysterol species are named and identified from the 27-carbon cholestane^[60]. Positions of distinct modifications such as hydroxylations and/or the presence of unsaturated bonds generally follow the cholesterol numbering system as seen in Figure 1.1B. A few stereodescriptive conventions have arisen historically to identify the orientation and chirality of these additional functional groups in relation to sterol stereochemistry. Most commonly encountered in steroid nomenclature are the α/β anomers and *R/S* axial chirality^[61]. Commonly referenced to ring substituents relative to the steroid plane, substituents below the steroid plane are α anomers denoted by a broken line $\cdots\cdots\cdots$, whereas above the plane are β anomers denoted by a solid line — (Figure 1.6A/B)^[61,62]. Also known as the Cahn-Ingold-Prelog^[63,64] priority rules, the *R/S* chirality nomenclature are conventionally used in substitutions in the sterol side-chain. This establishes the orientation of side chain hydroxyl group, based on a chiral centre with 4 different groups attached. To assign *R/S* to a substituent, all the groups attached to the chiral centre are ranked based on atomic number, if the same number exists, continue along the bonds until there is a difference. Next, the molecule is repositioned at the chiral centre so that the lowest rank is away from the observer. Then, with the remaining three groups in front of the observer, determine the direction of rank order (1st with highest total atomic number to 4th with the least). If the direction is clockwise, the *R*-isomer is assigned; if counter-clockwise, *S*-isomer is assigned (Figure 1.6C/D)^[64,65]. In addition, the *R/S* notation can generally be used for indicating orientation other chiral centres in a sterol structure. For example, the cholest-5-en-3 β -ol can also be cholest-5-en-3(*S*)-ol as the 3 α -OH epimer is a 3(*R*)-OH.

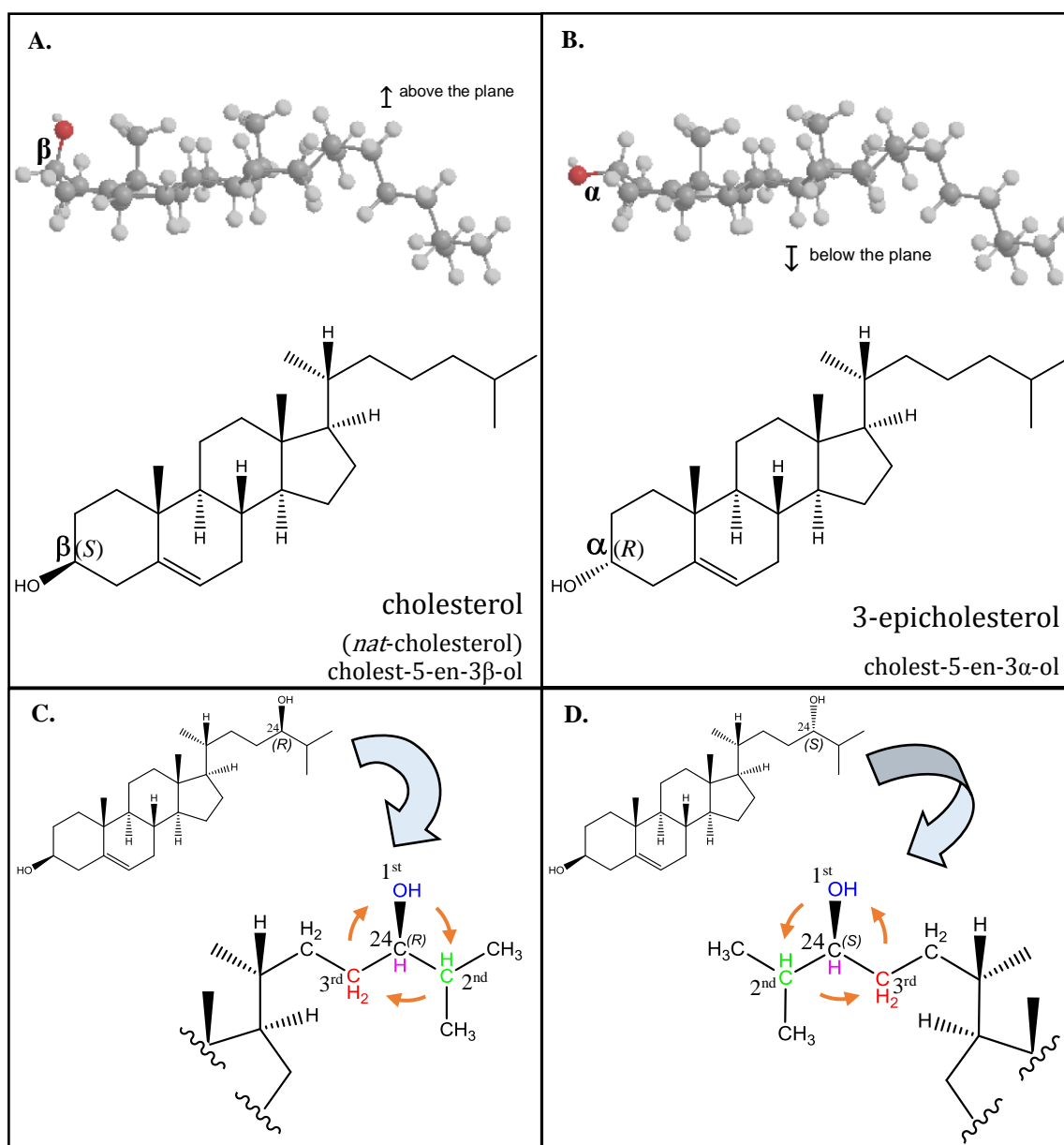


Figure 1.6. Nomenclature of sterol stereoisomers.

Naturally-occurring cholesterol is known as (A) *nat*-cholesterol. Due to cholesterol having several stereo centres, it can also have several isomers like *ent*-cholesterol, where all the stereo centres are reversed relative to *nat*-cholesterol, and (B) 3-epicholesterol where only the 3 β -OH group is isomerised to 3 α -OH^[62]. Another form of notation is the *R/S* notation. This can be assigned to chiral carbon centre and are usually applied to sterol side-chain modification. For example, 24-hydroxycholesterol can either exist as 24R or 24S depending on the orientation of the hydroxyl group at the C24. In 24R-HC, the OH-group (blue) is out of the plane towards the observer and the -H (purple) is away. The ranking goes clockwise with -OH, -CH-CC (green), then -CH₂-C (red) assigning the C24 with the *R* notation. (D) On 24S-HC, the molecule is rotated so that the lowest rank H is away from the observer plane. Here, as the orientation of the OH-group is switched, the ranking goes counter-clockwise assigning C24 with the *S* notation.

1.2.3. Conversion from cholesterol

Compared to the highly abundant cholesterol, oxysterols are present in much lower concentrations typically 1:10³ to 1:10⁶ to that of cholesterol. But even with their low concentrations, they can serve as potent biological regulators or act as intermediates to several sterol-related compounds. Oxysterols can arise from either non-enzymatic or enzymatic means. Non-enzymatic cholesterol oxidation products mostly give rise to ring oxidised species, while enzymatic oxidations are often targeted towards the side-chain.

1.2.3.1. Autoxidation

Due to its structure, cholesterol is easily prone to oxidation. It can be naturally oxidised by exposure to light, heat and air or attack by free radical and reactive oxygen species (ROS)^[66]. Most common cholesterol oxidation products are 7-ketocholesterol, 5,6-epoxycholesterol, 7-hydroxycholesterol, 6-hydroxycholesterol and their structural isomers as well as side-chain oxidised 25-hydroxycholesterol^[6]. These artefacts can occur in cholesterol containing samples as early as its time of collection, to long-term storage, and even more so during manipulation and analysis.

1.2.3.2. Enzymatic

In addition to autoxidation, oxysterols can also be enzymatically derived. This was demonstrated in 1956 when cholesterol was incubated with a subcellular fraction high in mitochondria which led to the formation of 25- and 27-hydroxycholesterols^[67,68]. These side-chain oxidised oxysterols are the ones mostly reported to have biological roles, for example, as inhibitors of sterol biosynthesis^[69,70]. A number of sterol-related enzymes belong to the cytochrome P450 (CYP) family. Other enzymes are also involved in sterol metabolism, which are not CYP. Such enzymes are cholesterol 25-hydroxylase (CH25H) and HSD3B7 which have been linked to immune cell functions^[43]. Table 1.1 lists some of the commonly known enzymes involved in sterol metabolism.

Table 1.1. Common sterol-metabolism related enzymes.

Enzyme	Abbreviation	Notable Function(s)
Cytochrome P450 3A4	CYP3A4	Catabolises cholesterol to 4 β -hydroxycholesterol ^[71] .
Cytochrome P450 7A1	CYP7A1	Involved in the classical bile acid synthesis pathway which converts cholesterol to 7 α -hydroxycholesterol ^[72] .
Cytochrome P450 7B1	CYP7B1	Involved in the hydroxylation of oxysterols at the C7 position ^[73,74] .
Cytochrome P450 8B1	CYP8B1	Adds a hydroxyl group to the sterol C12 position ^[75]
Cytochrome P450 11A1	CYP11A1	Also known as P450scc involved in C21 steroid biosynthesis ^[76] . Catalyses the side-chain cleavage of cholesterol to pregnenolone via two hydroxylations, first as 22R-hydroxycholesterol and then 20 α ,22R-dihydroxycholesterol ^[77] .
Cytochrome P450 27A1	CYP27A1	Involved in the bile acid synthesis. Converts cholesterol to 27-hydroxycholesterol and then to cholestenic acid ^[72]
Cytochrome P450 39A1	CYP39A1	Involved in bile acid metabolism. Converts 24-hydroxycholesterol to 7 α ,24-dihydroxycholesterol ^[78] .
Cytochrome P450 46A1	CYP46A1	Involved in cholesterol homeostasis in brain. Catalyses the conversion of cholesterol to 24S-hydroxycholesterol ^[79] .
Cytochrome P450 51A1 (Lanosterol 14 α -Demethylase)	CYP51A1	Involved in cholesterol biosynthesis in the conversion of lanosterol to 32-hydroxylanosterol ^[15] .
Cholesterol 25-hydroxylase	CH25H	Converts cholesterol to 25-hydroxycholesterol ^[80] .
3 β -Hydroxysteroid Dehydrogenase Type 7	HSD3B7	Has activity against 7 α -hydroxylated sterols. Conversion of cholest-5-ene-3 β ,7 α -diol to 7 α -hydroxycholest-4-en-3-one. ^[81]

1.2.4. Roles in Cholesterol Regulation and Feedback Mechanisms

Oxysterols can act as bioactive mediators. This was demonstrated through their control of cholesterol biosynthesis^[70]. The protein SREBP plays the initiator through the transactivation of cholesterologenic genes^[24]. By the engagement of the sterol-sensing domains, oxysterols can prevent SREBP processing and nuclear migration by INSIG1-mediated retention in the ER^[22,23], as well as controlling the proteolysis of HMGCR, the rate-limiting enzyme of cholesterol biosynthesis^[82]. Furthermore, oxysterols can also exert influence in the efflux of cellular cholesterol through the ATP-binding cassette (ABC) A1 and G1. Genes for these proteins are transcriptionally controlled by liver X receptors (LXR α and LXR β) which are potently activated by certain oxysterol ligands like 24S,25-epoxycholesterol (24S,25-EC)^[83].

1.2.5. Roles as Nuclear Receptor (NR) transcription factor and G-Protein Coupled Receptor (GPCR) ligands

Nuclear receptors are ligand-dependent proteins that are able to influence gene expression by directly binding to DNA^[84]. NRs LXR α/β and retinoid X receptors (RXR) can form heterodimers to initiate transcription. As previously mentioned, oxysterols can serve as potent activating ligands for LXR/RXR^[85] and upon engagement of its oxysterol-binding domain, LXR/RXR upregulates target genes involved in cholesterol efflux such as ABCA1 and ABCG1^[85]. Furthermore, activated LXR also targets a ubiquitin ligase IDOL, which facilitates the degradation of LDL receptors responsible for cholesterol uptake^[86]. Put simply, oxysterol activation of LXRs help the reduction of cellular cholesterol content. In addition, activation of LXR signalling has also been linked with the downregulation of lymphocyte proliferation^[40].

Another group of ligand-modulated NRs are the retinoic acid receptor-related orphan receptors (ROR α , ROR β , ROR γ)^[87]. ROR α and ROR γ have been associated with genes responsible for regulating circadian rhythm, metabolism and immunity^[88–90]. More importantly, certain oxysterols and sterol-derivatives were reported to act as either agonists^[1–3], or inverse agonists^[91,92] for ROR γ t, an isoform of ROR γ which is

essential for thymopoiesis, lymph node development and acts as the master regulating transcription factor for TH17 differentiation^[93,94].

Typically responsive to steroid hormone estradiol, oestrogen receptors (ER) are NRs affecting cellular growth and proliferation^[95,96], which is why they are implicated in cancerous tumour growth^[97]. ER signalling can also be mediated specifically by the oxysterol 27-HC and have thus been linked to breast cancer^[98]. Moreover, 27-HC/ER binding also inhibits nitric oxide production in vascular cells leading to vasoconstriction and increase osteoclast function leading to bone resorption and osteoporosis risk^[99,100].

In contrast to intracellular NRs, GPCRs are cell membrane bound receptors capable of triggering diverse signalling pathways with different functions. The oxysterol 7 α ,25-diHC has been reported to act as a potent ligand for GPR183 or Epstein-Barr virus induced gene 2 receptor (EBI2) which is important for B-cell positioning in lymphoid organs due to its chemoattractive effect^[101,102]. Another GPCR which is receptive to 22R-HC binding is CXC-chemokine receptor 2 (CXCR2) or IL-8R β . It was found that neutrophil migration can be stimulated by tumour-derived 22R-HC gradients but not by its stereoisomer 22S-HC which consequently favour tumour growth and angiogenesis^[103].

1.2.6. Roles in Immune Function

As previously mentioned, oxysterols have been reported to influence a variety of immune functions through ligand-activation of receptors: ROR γ t, EBI2 and LXRs. Furthermore, immune responses can trigger specific oxysterol production. Toll-like receptor (TLR) stimulation revealed an increased expression of cholesterol 25-hydroxylase (CH25H) and 25-HC production in macrophages^[47]. In turn, B-cell exposure to macrophage-derived 25-HC have inhibited B-cell proliferation resulting in immunoglobulin A (IgA) reduction. Conversely, *Ch25h*-deficient mice had elevated levels of IgA^[47]. Further studies found *Ch25h* to be an interferon-inducible gene which have broad roles in viral resistance through either prevention of viral entry or replication^[39,42]. It has been suggested that 25-HC may facilitate this by either the reduction of cellular cholesterol or altering the lipid composition of cell membranes.

Recent studies have reported that *Ch25h* and 25-HC also acts as an amplifier of macrophage immune response in mice by influencing the recruitment and retention of AP-1 transcription factors to their DNA binding sites^[46]. However, the same study has also found that this immune response amplification has a detrimental effect on the host due to inflammation-induced damage in the context of influenza virus clearance. In contrast to this, another study has reported the suppression of inflammasome activity and reduced IL-1 β production of macrophages which demonstrates the anti-inflammatory effects of *Ch25h* and 25-HC exposure in the context of an LPS/bacterial infection in mice^[38].

1.3. Current methods of analysis

With a wide range of possible sterol molecules and dozens currently identified, several methods of analysis have been developed with some still commonly used to this day. Historically, there were simple colorimetric tests like sulfuric acid-chloroform (Salkowski) test, acetic anhydride-sulfuric acid (Liebermann–Burchard) test and acetic acid-sulfuric (Lifschütz) tests^[6]. Then, Bergstrom and Winterstein developed aqueous sodium stearate dispersion which centred on the identification of cholesterol autoxidation products in the 1940s^[104]. Then there was thin-layer chromatography (TLC) in the 1960s which started to realise the complexity of sterol preparations^[105]. This offered a rapid and simple separation useful in predictable synthetic mixtures containing a few components^[106,107] but not as effective in resolving different species in more complex samples like blood extracts. More recently, other analytical methods were subsequently available and developed like gas chromatography and high performance liquid chromatography which are coupled to mass spectrometers^[108]. Recent advancements made in these areas have led the extensive and pioneering studies on oxysterols, especially in mass spectrometry, due to its sensitivity, accuracy and specificity. See *section 1.5.4* for current methods of oxysterol analysis using GC-MS and LC-MS.

1.4. Immune System

The tree of life features a diverse number of phyla, classes and genera. With a wide range of different extant life forms all competing for limited space and resources, organisms have acquired and developed certain characteristics and strategies in order to grow and survive in their environmental niche and ultimately, to reproduce or replicate. These strategies or responses which enable defence against competing organisms can range from simplistic endonuclease cleavage of intruding viral DNA in bacteria^[13] to more complex somatic gene recombination leading to highly diverse but specific identification of pathogen-derived antigens exemplified in mammalian lymphocytes^[109]. These processes are the result of an evolutionary arms race in which single or multicellular organisms adapt to retain or regain an advantage against another organism's antagonistic responses. Collectively, these small adaptations or responses which results to defence and resistance together constitutes an organism's immune system.

We humans, like any other animals in the macroscopic world are in constant struggle, battling off harmful microscopic organisms which can tip the balance between health and disease. Fortunately, our immune system not only have generalised defences against these foreign invaders or pathogens but also can form customised learned resistance on subsequent exposure. These are the innate and the adaptive, the two components of the immune system. Together, these components facilitate four main tasks: firstly, immunological recognition of infectious agents, secondly, control the spread and elimination the infection, thirdly, self-regulation to limit immune-induced collateral damage to host, and lastly, to reform defences for long-term protection against reinfection.

1.4.1. Innate Immunity

Innate immunity is the older of the two components in evolutionary terms, which is present and active in both vertebrates and invertebrates^[110]. Innate responses, either cell-based or non-cell-based are comprised of: anatomical barriers like the tight-knit skin and mucosal surfaces to prevent pathogen entry; secretion of specific enzymes like lysozymes and specialised antimicrobial cationic peptides like defensins which

recognise, digest and disrupt bacterial and fungal cell membranes as well as viral capsids; production of complement system proteins to mark extracellular agents, aid their phagocytosis and recruit other immune cells; responses of leukocytes like natural killer (NK) cells, granular mast cells, neutrophils, basophils and eosinophils (Figure 1.7) by production of cytokines, histamine and other reactive oxygen species to amplify responses or directly kill pathogens; and, actions of phagocytes like monocytes, macrophages and dendritic cells (Figure 1.7) to remove agents, contain them intracellularly for enzymatic degradation and subsequent pathogenic peptide processing and presentation, to act as an innate link to the adaptive immune response.

Once a foreign organism or material has successfully penetrated the hosts physical barriers and consequently initiated cellular damage, these mechanisms are immediately triggered. Most importantly, these responses are fast and wide-ranging across common groups of pathogens. Cell-based innate responses rely on cells mainly derived from myeloid progenitor cells (Figure 1.7) in the bone marrow which develop and mature to possess various receptors. These innate receptors recognise agents via common and highly conserved pathogen-associated molecular patterns (PAMPs) and successful detection can most often result to sufficient control, removal and prevention of large-scale infection and host injury.

1.4.2. Adaptive Immunity

As the innate system relies on general predetermined responses encoded in the germline, it is sometimes not enough to rid the body of all, especially highly adapted, infectious agents. Once the innate system has either been overwhelmed or circumvented and the pathogen continued to thrive and cause damage, this triggers induction of the other immune component, the adaptive immune system which can mount a much more effective response due to its high specificity to the pathogen. The key players in the adaptive arm are the B and T lymphocytes, which have very different but co-operative function in the body. Their efficiency is owed to their ability to produce specific B and T cell antigen receptors, i.e. immunoglobulins (Igs) and T cell receptors (TCRs), achieved through gene recombination.

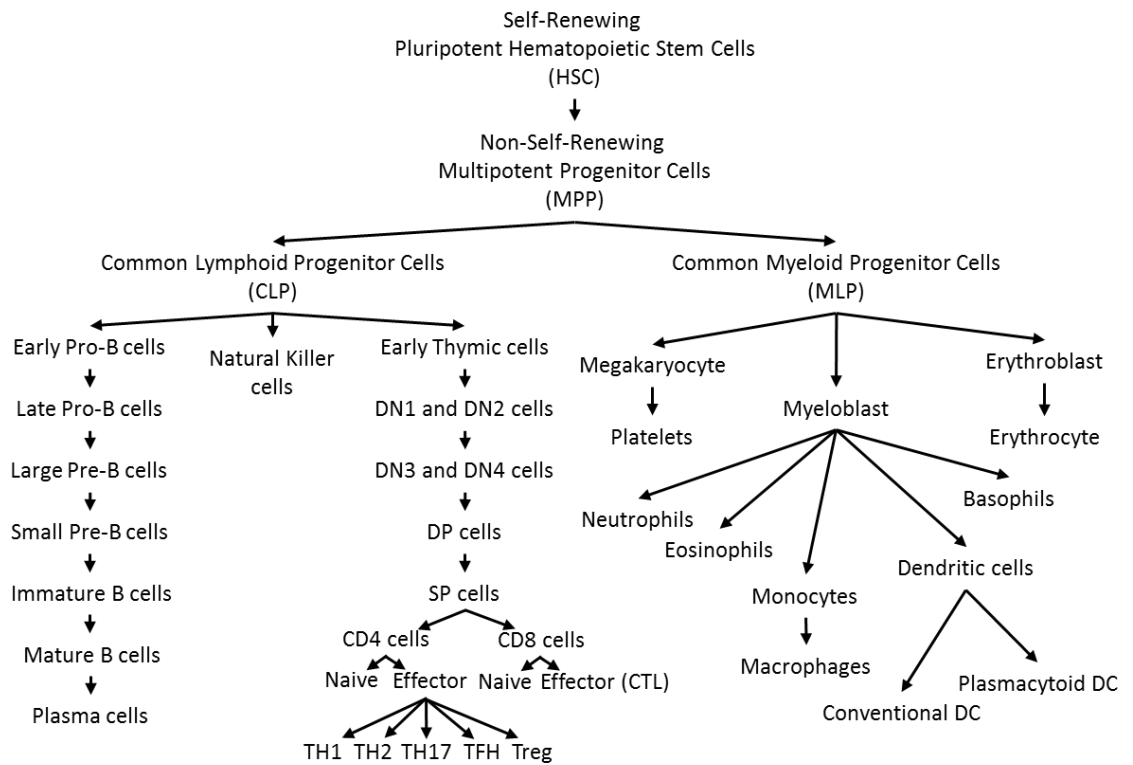


Figure 1.7. Hematopoietic cell lineage tree.

Originating from bone marrow, self-renewing stem cells (HSCs) can develop into non self-renewing progenitor cell giving rise to lymphoid and myeloid lineage. Oxygen-carrying erythrocytes, clotting aid platelets as well innate immune cells: neutrophils, eosinophils, basophils, macrophages and dendritic cells develop from the myeloid progenitor. The lymphoid progenitor gives rise to innate immune natural killer cells, and adaptive immune B and T cells. Adapted from Janeway's Immunobiology and Kuby Immunology^[109,110].

Both B and T lymphocytes arise from lymphoid progenitor cells which are derived from self-renewing pluripotent hematopoietic stem cells in the bone marrow (Figure 1.7). Whereas T cells leave and migrate to the thymus, B cells remain to develop and mature in the bone marrow where developing B cells are exposed to a network of marrow stromal cells which induce growth and differentiation through specific gene expression using cell-to-cell or cytokine-mediated interactions. Developmentally, committed progenitors go through stages of early pro-B cell, late pro-B cell, large pre-B cell, small pre-B cell to immature B cells (Figure 1.7). At each stage, cells lose progenitor markers, start to rearrange antigen receptor genes through the process called V(D)J recombination, transiently divide, undergo further VJ gene rearrangement then express full Igs on their surface. Successful non-autoreactive Ig-bearing B cells known as immature B cells emerge out of the bone marrow and into peripheral lymphoid organs such as the spleen and lymph nodes, where they can fully mature, be activated, proliferate then terminally differentiate into antibody-secreting plasma cells.

1.5. T Cell Biology

T lymphocytes (T cells) play a key role in adaptive immunity mainly to coordinate and regulate other immune responses. In contrast to B cells maturing in the bone marrow, immature T cells continue their development in the thymus. There, thymocytes undergo intensive positive and negative selection process in an antigen-free environment which will balance its self and non-self recognition ability and commit into two distinct types as either CD8-bearing cytotoxic and CD4-bearing helper mature naïve T cells. Mature naïve T cells are released to recirculate around the body via blood and lymph scouting for activated antigen presenting cells (APCs) with the capability for activation, clonal expansion and differentiation to various effector T cell types with the potential for tailored responses specific to an immune challenge.

1.5.1. Origin and Development

T cells originate and develop in a process called thymopoiesis. After leaving the bone marrow, common lymphoid progenitors (CLP) destined to the T cell lineage migrate to the thymus via the blood where these developing T cells are known as thymocytes. These thymocytes express neither mature lymphocyte features nor any antigen

receptors. Developmentally, thymocytes go through different stages based on their surface phenotype from: Early Thymic Progenitors (ETC), Double Negative 1 (DN1) cells, DN2 cells, DN3 cells, DN4 cells, Double Positive (DP) cells to Single Positive (SP) cells subsequently leading to positive then negative selection (Figure 1.7) [111-114]. Over these stages occurring within the thymus, thymocytes interact with resident thymic cells, similar to B cells with marrow stromal cells, both via direct cell-to-cell interactions or cytokine-mediated where thymocytes are also induced to undergo variable, diverse and joining (V(D)J) gene rearrangement^[115,116]. Both B and T cells arise from the same CLP and *in vitro* studies which looked into thymocyte development have revealed a crucial role of Notch1 receptors in either T or B cell lineage commitment^[117]. The thymic microenvironment has sufficient Notch ligands to induce and maintain development of CLPs to T cells. Overexpression or constitutive expression of Notch receptors in progenitors leads to T cell development than B cells in the bone marrow^[118]. Conversely, the knockdown of Notch resulted in heavily biased development of B cells even in the thymus^[119,120].

Once progenitor commitment has been initiated upon entry into the thymus, thymocytes move through distinct locations from the cortical to medullar regions within the thymus which can provide differential interactions and signals from resident thymic epithelial cells (TECs) as well as macrophages (M ϕ s) and dendritic cells (DCs). Specifically, thymocyte maturation and TCR development occurs in the outer cortical region whereas the inner medullar region supports the establishment of T cell self-tolerance. From the blood, lymphoid progenitors enter the thymus through the corticomedullary junction where they are phenotypically named as CD8⁻CD4⁻ DN cells. In addition to lacking either the CD4 or CD8 markers, there are four DN cell stages which differ in the expression of the cell adhesion molecule CD44 and the high affinity IL-2R α CD25, they are namely: CD44⁺CD25⁻ DN1, CD44⁺CD25⁺ DN2, CD44⁻CD25⁺ DN3, and CD44⁻CD25⁻ DN4. On thymic entry, Notch1 receptor-bearing DN1 cells are induced to proliferate by the Notch ligands present in the cortical TECs (cTECs) surface with resulting daughter cells expressing CD25. Some of the DN2 cells then migrate further into the subcapsular cortex where they start simultaneous gene rearrangement of their TCR δ and γ/β chains at chromosome 7 and 14, respectively^[121,122]. Successful expression and signalling strength of both γ and δ chains fully commits the thymocyte to the $\gamma:\delta$ T cell lineage whereas β chain commits

expression to the $\alpha:\beta$ T cell lineage^[115,123,124]. Moreover, some evidence has suggested a role of interleukin-7 receptor (IL-7R) expression in the adoption of $\gamma:\delta$ rather than $\alpha:\beta$ lineage^[125]. Once committed to the $\alpha\beta$ TCR lineage, the immature cells continue to their development through to medullar TECs exposure, ultimately maturing into either CD4⁺ or CD8⁺ $\alpha\beta$ TCR naïve cells.

As $\alpha\beta$ TCR-bearing T cells constitute the majority of the mature T cells compared to $\gamma:\delta$ T cells which offer more diverse roles and developmental branches, $\alpha\beta$ TCR cells will be the sole focus of subsequent sections.

1.5.2. T Cell Types and Subsets

Upon emigration from the thymus to the blood, lymph and lymphatic tissue, the majority of mature T cells with functional TCR fall into either CD8⁺ or CD4⁺ lymphocytes (Figure 1.7). These cells are known as naïve T cells as they still have not encountered their specific antigen and they continually recirculate in the periphery in the hopes of finding it. Naïve T cells are under quiescent state with very low energy requirements and expenditure. Once a naïve T cell binds its TCR to its cognate antigen presented via MHC in an APC surface, they undergo dramatic transformation and genetic reprogramming to eventually become effector T cells. Effector T cells fall into several functional types with each having specific roles, cellular mechanisms and targets. Whereas CD8⁺ T cells are limited to developing into cytotoxic T lymphocytes capable of directly recognising non-self antigens loaded in MHC-I expressed on most nucleated cells. On the other hand, CD4⁺ T cells have the competency to differentiate further into a range of different helper T subsets upon identification of non-self antigens loaded in MHC-II in professional APCs (pAPCs) like M θ , DCs and also B cells. In both cases, productive TCR-antigen-MHC engagement together with appropriate co-stimulatory signals results in T cell activation which subsequently trigger cell survival, growth and clonal expansion of the antigen-specific T cell. Furthermore, given the right microenvironmental signals upon activation, T cell polarisation occurs which leads to T cell differentiation. Currently characterised T cell types/subsets and main functions are listed in Table 1.2.

Table 1.2. List of characterised T cell types and subsets with main functions.

T Lymphocyte Type/Subset	Main functions
CD8 ⁺ Cytotoxic (CTL)	Induce apoptosis on viral and intracellular pathogen infected cells.
CD4 ⁺ Helper 1 (TH1)	Viral and intracellular pathogen defence amplification and support
CD4 ⁺ Helper 2 (TH2)	Parasitic defence, B cell IgE isotype switching
CD4 ⁺ Helper 17 (TH17)	Mucosal barrier immunity, extracellular bacterial and fungal defence, neutrophil recruitment and support
CD4 ⁺ Helper Follicular (TFH)	Support high-affinity antibody production of B cells and isotype switching
CD4 ⁺ Regulatory (Treg)	Downregulation and control of pro-inflammatory responses

Table 1.3. List of characterised CD4 T helper subsets with differentiation cytokines (signal 3), transcriptional master regulators and main effector cytokines.

Human T Helper Lymphocyte Subsets	Human Polarising cytokines	Master regulator/transcription factor	Main effector cytokines/secretions
CD4 ⁺ Helper 1 (TH1)	IL-12 p70, IFN- γ , IL-2, (IL-18) ^[126,127]	T-bet	IFN- γ , TNF- α , IL-2
CD4 ⁺ Helper 2 (TH2)	IL-4, IL-2 ^[128]	GATA3	IL-4, IL-5, IL-10, IL-13
CD4 ⁺ Helper 17 (TH17)	TGF- β , IL-6 ^[129] (IL-1 β , IL-21, IL-23) ^[130]	ROR γ t	IL-17, IL-21, IL-22
CD4 ⁺ Helper Follicular (TFH)	IL-6, IL-21 ^[131]	BCL-6	IL-4, IL-21
CD4 ⁺ Regulatory (Treg)	TGF- β , IL-2	FOXP3 ^[132]	TGF- β , IL-10

Cytotoxic CD8⁺ T lymphocytes (CTLs) are capable of mounting immune responses mainly against internally-infected host cells by direct recognition and apoptosis induction of cells through the production and release of proteolytic enzymes such as perforins and granzymes as well as FAS/FASL interactions. CD8⁺ T cells identify target cells by the recognition of pathogen-derived peptides processed by the infected cells via MHC-I on their cell surface. On the other hand, helper CD4⁺ T cells (TH) mainly reacting to antigens processed and presented on MHC-II on pAPCs, mount an immune response by the characteristic production of soluble protein factors called cytokines which are very effective in augmenting or dampening the responses of other cells. The characteristic and unique cytokine production of TH cells have very close ties to their immune function and thus have been the basis of their identification and classification. Studies made back in 1986 by Mosmann and Coffman characterised different TH subsets initially identifying TH1 and TH2^[133].

Generally, TH1 cells differentiate from activated naïve CD4⁺ T cells exposed to polarising cytokines such as IL-12, interferon- γ (IFN- γ) and IL-18. Signalling through these cytokines leads to the activation of the master regulator transcription factor T-box 21 (TBX21), which drives differentiation of TH1 cells with main functions include immune response against intracellular pathogens as well as boosting the responses of CTLs and phagocytic cells. Conversely, activation plus exposure to IL-4 induces GATA binding protein 3 (GATA3) expression which differentiates the naïve cells into TH2 cells capable of protecting the host against multicellular pathogens like parasitic helminths and supporting eosinophil, basophil, mast cell and B cell effector functions. Successfully polarised TH1 and TH2 cells able to secrete their signature cytokines not only can affect the responses of other cells but also itself and other activated naïve cells in an autocrine or paracrine manner. This in turn acts as a positive feedback loop which amplifies the specific immune response initiated by the pAPC. As a consequence, this enables TH1/TH2 cross regulation, in that TH1 cells can suppress TH2 development by reinforcing their own differentiation while inhibiting the other and vice versa.

This TH1/TH2 dichotomy of CD4⁺ T cells has been widely accepted and applied to explain various immune related disorders until the early 2000s when studies linking IL-12-induced TH1 cells to murine autoimmunity have introduced inconsistencies^[134].

Follow up studies in 2003 identified the disconnect between murine experimental autoimmune encephalitis (EAE) and collagen-induced arthritis (CIA) to TH1 cells^[135–137]. This subsequently led to the identification of a new TH subset distinct from TH1 and TH2 in 2005 by its production of IL-17 family of cytokines^[138]. The aptly named TH17 cells are capable of producing IL-17A, IL-17F, IL-21, and IL-22 which develop from activated naïve CD4⁺ T cells in the presence of TGF- β , IL-6, IL-1 β , IL-22 and IL-23 (in humans) under the control of the transcription factor Retinoic acid receptor-related Orphan Receptor gamma t (ROR γ t)^[93]. Physiologically, TH17 cells have been identified to function mainly as the first adaptive immune responders in mucosal barriers initiating tissue inflammation and neutrophil recruitment in defence against extracellular bacterial and fungal infections. However, uncontrolled TH17 responses have been implicated in various autoimmune disease. The classification of this subset paved a way to the discovery of further functionally different T helper cells.

It was previously mentioned that DP thymocytes in the thymus can develop into another CD4⁺ T cell lineage known as natural regulatory T cells (nTreg). Instead of initiating or amplifying immune responses, these regulatory T cells act to control, block and suppress. This is especially important not only in the inhibition of potentially harmful effector T cells^[139] after pathogen clearance but also to further reinforce self-tolerance on cells that manage to escape negative selection in the thymus which grants essential protection against various autoimmune diseases^[140]. Aside from the “natural” development in the thymus, these immunosuppressive cells can also be “induced” from recirculating naïve CD4 T cells in the periphery known as iTreg^[141]. Both these cells, though developmentally distinct, are phenotypically the same having both CD4 and CD25 surface markers and driven by the presence of TGF- β to express Forkhead Box P3 protein (FOXP3) as their transcriptional regulators^[142]. Treg cells can directly suppress by inducing effector cell apoptosis via TRAIL-DR5 interaction^[143] or indirectly by secretion of anti-inflammatory cytokines such as TGF- β as well as depleting the microenvironment of the IL-2 growth factor^[144] to inhibit T cell proliferation and other effector functions^[145–147].

CD4⁺ T cells which are closely related to B cell antibody responses have been defined as T follicular helper cells (TFH)^[148]. These cells originate from naïve cells which are activated in the presence of IL-21^[131,149,150] and controlled by transcription factor B-

cell lymphoma 6 protein (BCL6)^[151,152]. These cells reside in the germinal centres of secondary lymphoid organs rich in B cells by its unique expression of the CXC chemokine receptor 5 (CXCR5)^[153,154]. There, TFH cells provide vital contact-dependent signals to induce class switch recombination (CSR) of B cells and produce high-affinity antibodies. In all, these differentiated TH cells are characterised based on which polarising cytokines they require, the main transcription factor which regulates their gene expression and their unique cytokine secretion profile; these are listed in Table 1.3. Collectively, TH1 and TH17 cells promote cell-mediated immune responses; TH2 and TFH cells support the humoral and antibody production responses; and Treg functions to mediate and control these pro-inflammatory responses.

So far, we have followed T lymphocytes from development to maturity as quiescent naïve cells, which can be stimulated by a specific pathogen and acquire unique characteristics as effector cells with the ability of clonal expansion and differentiation to mount coordinated immune responses that can clear or control that specific infection. From a very low number of naïve T cells arise numerous antigen-specific effector T cell clones that migrate to the sites of infection. Large numbers are required for effective elimination of pathogens but upon infection resolution, most of the effector population contract and undergo apoptosis. To establish long-term protection, a small proportion of these cells persist and return to resting state but “remember” the distinctive reprogramming they have undergone with the ability to promptly and efficiently react when presented with the same initial antigen^[155]. These long-lived cells are called memory T cells and such formation of immunological memory has become a very important property of the adaptive immune system still under active investigation.

Currently, memory T cells have been generally sub-divided into central memory and effector memory T cell subsets. Central memory T cells (TCM) are phenotypically CD44⁺CD62L⁺CCR7⁺ while effector memory T cells (TEM) are CD44⁺CD62L⁺CCR7⁻^[156]. TCM cells, compared to TEM cells, generally have higher proliferative ability and longer lifespan which continually recirculate but are mostly restricted to secondary lymphoid tissues. Much like naïve cells, TCM cells can activate, proliferate and polarise into different effector subsets depending on microenvironmental stimuli, albeit much easier and faster. Conversely, TEM cells also

recirculate but with a wider area including lung, liver, intestine and skin. These cells have less potential for variable differentiation as they are likely to be committed to one effector subset but faster activation on antigen re-exposure. Although characterisation and roles of memory T cells have been widely studied, scientific evidence are still divided regarding their origins leading to multiple proposed developmental pathway models^[157–159]. Recent studies also reveal a possibility of memory T cells to possess a similar diversity as the effector population^[160].

1.5.3. CD4 T Cell Activation, Expansion and Differentiation

CD4 T cells mainly drive the adaptive immune response and they can do so through interactions via their unique antigen-specific TCRs. Non antigen-experienced naïve T cells continually recirculate through blood, lymph and lymphoid tissues to maximise APC exposure and encounter their cognate antigen. This results in an overwhelming series of cell reprogramming events known as T cell activation.

Pertaining specifically to naïve CD4 helper T cells, their activation is initiated after successful recognition of its TCR-specific antigen loaded in an MHC-II on an activated APC surface with sufficient positive co-stimulation. The contact boundary where surface receptors interact between the T cell and pAPC constitutes an immunological synapse (IS). The IS area widens to form a two tier sequestration of membrane proteins known as the central and peripheral supramolecular activation cluster (cSMAC and pSMAC). Main antigen recognition molecules like the CD4:TCR:MHC-II and CD28:B7 are positioned in the cSMAC while stabilizing adhesion molecules like CD2:CD58 and LFA-1:ICAM-1 surround it in the pSMAC for increased avidity. The cSMAC formation enables sustained T cell:APC interaction and provide two of the three signals required for T cell activation. Signal 1 is delivered by the antigen:MHC-II to the TCR with the CD4 co-receptor further stabilising the binding. This interaction results to signal transduction through CD3 transmembrane complex proteins associated with the TCR. Signal 2 is provided via co-stimulatory CD28 or co-inhibitory CTLA-4 molecules on the T cell via B7 protein ligation on the pAPC. The importance of signal 2 was demonstrated in *in vitro* studies with TCR stimulation in the absence of CD28 co-stimulation resulted to T cell anergy or a state of unresponsiveness even after re-stimulation^[161]. To enable naïve CD4 T cell expansion

and polarisation, stimulated T cells require signal 3. This signal, in the form of cytokines, can be provided by the activated T cell itself, the interacting pAPC or other cells in the immediate local microenvironment. These cytokines bind to the surface of T cells which in itself induce signalling cascades. Different cytokines, as mentioned in previous sections, facilitate the induction of master regulator/transcription factors which direct the progress to different specialized effector subsets. Collectively, signal 1, co-stimulatory signal 2 and polarising signal 3 initiates several intracellular signalling pathways and gene regulation that promote activation, survival and differentiation.

Quiescent naïve T cells have baseline metabolic activity with very low energy requirements by utilising oxidative phosphorylation^[162-164]. Upon activation, intracellular signals initiated in the SMAC direct the T cell to increase their energy requirements and switch to aerobic glycolysis stimulating the expression and membrane trafficking of glucose transporter 1 (GLUT1)^[163,165,166]. This glycolytic switch provides an inefficient energy source but can produce an abundance of biosynthetic precursors^[13,164,167]. These, together with increased transcriptional/translational ability tip the metabolic balance boosting anabolism over catabolism resulting in rapid cell growth and biomass accumulation. Part of this increase in cell mass include the induction of several metabolic processes not only glucose and amino acid uptake but also intrinsic sterol biosynthesis which ensures enough stores of cholesterol, an essential pre-requisite to cell division, are present intracellularly and embedded in the cell membrane^[163,164]. Activated antigen-specific T cells, which formerly arrested at G0 stage, then continue cell cycle progression and undergo multiple rounds of cell division or expansion^[168].

T cell activation not only induces intracellular changes described above but also causes phenotypical and gross morphological changes. Recirculating resting naïve CD4 T cells are typically small and are CD44^{lo}CD45RO^{lo}CD45RA^{hi}CCR7^{hi}CD62L⁺CD69⁻CD25⁻. On the other hand, activated naïve T cells are larger and are CD44^{hi}CD45RO^{hi}CD45RA^{lo}CCR7^{lo}CD62L⁻CD69⁺CD25⁺^[109]. Specifically, the increase in CD44 cell adhesion molecule enables migration of activated cells to peripheral sites of infection^[50,169,170]. CD45RO, the shorter isoform variant of CD45RA, has been reported to provide more sensitive TCR stimulation even at lower

antigen concentrations exemplified by memory T cell populations^[109]. CCR7 in naïve T cells enables homing to secondary lymphoid tissues from the blood as CCR7 ligands CCL19 and CCL21 are present in thymus and lymph nodes^[171–173]. CCR7 down regulation in activated cells is chemotactically complemented by the transient downregulation of sphingosine-1-phosphate receptor (S1PR) to retain proliferating T cells in the lymphoid organ and its re-expression to allow exit of effector cells back out into blood and lymph which are high in S1P lipid, the ligand of S1PR^[174]. L-selectin or CD62L is another cell adhesion marker expressed in naïve T cells which affect migration towards secondary lymphoid organs. CD69 and CD25 are characteristic early and intermediate T cell activation markers expressed mainly for regulation of inflammatory process as the activation inducer molecule and as the high affinity receptor for IL-2, respectively^[175].

1.5.4. T Cell Receptor Signalling

To a large extent, T cell activation is primarily mediated and induced through the TCR. Co-receptors and cytokine-induced effects through signal 2 and 3 are also important but generally necessitates productive TCR engagement as a prerequisite. Non-covalent binding of ligands on these receptors mainly found on the cell surface can cause conformational or biochemical change of the receptor which traverse through the membrane and inside the cell. It is common for even a single ligand-receptor interaction to cause the activation of intracellular signal transduction pathways ultimately resulting in differential gene expressions. Most signal transductions are facilitated via reversible phosphorylation events by enzymes called kinases which can, in turn, be dephosphorylated by phosphatases.

Embedded on the cell membrane, CD4 T cells have a variable α - and β -TCR chains as well as δ -, γ -, ϵ -, and ζ -CD3 chains. Together, these peptide chains form an octameric complex assembled during thymocyte development (Figure 1.8). The α/β part are for antigen recognition whereas the CD3 complex are for intracellular signal transduction. In addition, CD4 association to MHC-II which enhances binding avidity also participates in signalling via lymphocyte-specific protein tyrosine kinase (Lck). Complementary to this, CD28 homodimers expressed on T cells can also be engaged

with a B7 proteins on the APC for additional signalling to further drive T cell activation (Figure 1.9).

The $\alpha\beta$ TCR chains have a short cytoplasmic tails incapable of signalling. However, negatively-charged CD3 dimers can gather around the positively-charged TCR transmembrane domains. These dimers have longer cytoplasmic tails with several immunoreceptor tyrosine-based activation motifs (ITAM). Tyrosine phosphatase CD45 present around the SMAC can activate Lck by dephosphorylation. The TCR-MHC-CD4 interaction brings the CD4-bound active Lck in close proximity to the CD3 ITAMs which allows dual tyrosine phosphorylation. Dual phosphorylated ITAMs can serve as docking site for another kinase, ζ -chain associated protein 70 (ZAP-70), which contains dual phosphate-binding Src homology 2 (SH2) domains. Once docked, Lck can also phosphorylate ZAP-70 which in turn, can phosphorylate both membrane-bound linker of activated T cells (LAT) and 76kDa SH2 containing leukocyte protein (SLP-76). These two adaptor proteins associate via a linker protein known as GADS bringing cytosolic SLP-76 closer to the cell membrane^[176,177]. Formation of this membrane-linked complex recruit phospholipase-C γ (PLC- γ) allowing its activation. From this point, activated PLC- γ has multiple signalling outputs which distally activates three transcription factors: nuclear factor of activated T cells (NFAT), nuclear factor kappa of activated B cells (NF κ B) and activator protein 1 (AP-1), all of which are major player in T cells (Figure 1.9).

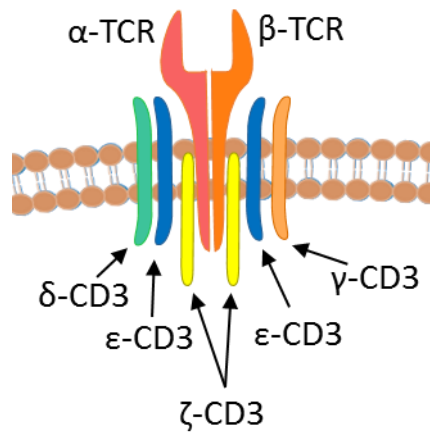


Figure 1.8. Assembly of the full T cell receptor.

The full octameric TCR is composed of the TCR α -chain with the β -chain with associated one δ -, one γ -, two ϵ -, and two ζ -CD3 chains. The negatively charged CD3 dimers associate electrostatically with the positively charged TCR heterodimer.

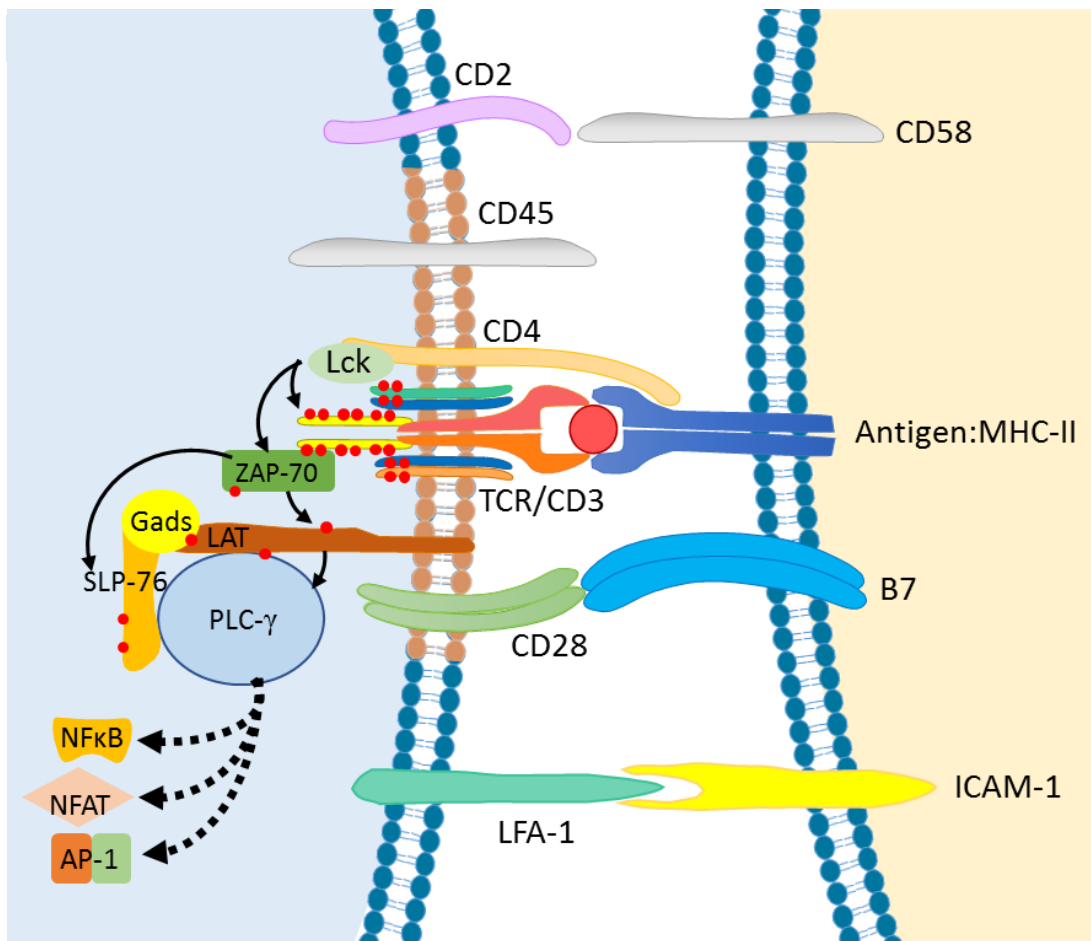


Figure 1.9. Initial TCR signalling.

Antigen inexperienced naïve CD4⁺ initially ‘sweep’ through the cell membranes of pAPCs via cell adhesion molecules LFA-1 and CD2 surface markers. This transient binding allows the presentation of antigens via MHC-II. Upon positive TCR recognition of the antigen and adequate co-signalling via CD28, binding avidity increases in immunological synapse through CD4:MHC-II which permits the migration of further signalling molecules to form the cSMAC. CD4 bound Lck in proximity of CD3 ITAMs allows its phosphorylation as well as ZAP-70 docking. The activated and docked ZAP-70 can further phosphorylate LAT and SLP-76 which is linked together by Gads. The LAT:Gads:SLP-76 complex can recruit PLC-γ near the cell membrane which starts a series of signal propagation to activate transcription factors like NFκB, NFAT and AP-1. Adapted from Janeway’s Immunobiology^[109].

Cell membrane localised PLC- γ can cleave phosphatidylinositol 4,5-bisphosphate (PIP₂) bound in the lipid bilayer. This cleavage leaves diacylglycerol (DAG) in the membrane while releasing inositol-1,4,5-triphosphate (IP₃) in the cytosol. This step serves two purposes: one, DAG serves to recruit further key kinases in the SMAC and two, IP₃ diffusing into the cytosol can bind to its receptor and induce Ca²⁺ cytosolic release from the endoplasmic reticulum (ER) (Figure 1.10C). The increase of intracellular calcium via this ER release together with induced extracellular calcium influx can initiate other signalling proteins like calcium-modulated protein (calmodulin). Calmodulin activation can successively activate calcineurin phosphatase. Inactive NFAT is phosphorylated which blocks it from nuclear entry and retained in the cytosol. This block is released upon NFAT dephosphorylation by calcineurin resulting in its nuclear transport. NFAT can bind to gene regulatory elements of different cytokines and lineage-specific transcription factors which can both positively and negatively regulate the immune responses^[178,179].

Via membrane DAG, protein kinase C θ (PKC- θ) can be recruited near the cell membrane to start another signalling cascade (Figure 1.10B). There, PKC- θ can phosphorylate and activate membrane-bound caspase recruitment domain-containing protein 11 (CARMA1). Multiple activated CARMA1 then complexes with accessory proteins like mucosa-associated lymphoid tissue lymphoma translocation protein 1 (MALT1) and B-cell lymphoma protein 10 (BCL10). This complex next recruits the signal transducer TNF receptor associated factor 6 (TRAF-6) responsible for the activation of transforming growth factor beta-activated kinase 1 (TAK1) via TRAF-6 autoubiquitination^[180]. TAK1 associates with I κ B kinase complex (IKK) via nuclear factor-kappa B essential modulator (NEMO) binding to phosphorylate IKK β . In resting conditions, several NF κ B are sequestered away from the nucleus due the binding of the inhibitor of κ B (I κ B). The activated IKK β can phosphorylate I κ B, resulting in its ubiquitination releasing NF κ B for nuclear translocation. In this way, several NF κ B target genes can be rapidly induced as readily available NF κ B only needs to enter the nucleus, thus eliminating the slower transcription and translation steps of NF κ B proteins as a prerequisite for activation^[181].

Membrane DAG can also bind and recruit RasGRP to activate Ras, a branch of signalling leading to the MAPK/ERK pathway (Figure 1.10A), a relay of mitogen-

activated protein (MAP) kinase phosphorylations which ultimately activate AP-1, crucial for cell growth and division^[182]. In addition, Ras can also be activated via LAT/GADS/SLP-76 recruitment of the adaptor protein growth factor receptor-bound protein 2 (Grb2), which then binds a guanine nucleotide exchange factor, son of sevenless (SOS). SOS activity results in the increase of GTP and decrease of GDP which activated Ras^[183]. Activated Ras starts the phosphorylation of Raf kinase, a MAP kinase kinase kinase (MAP3K). Raf subsequently activates a MAP kinase kinase (MAP2K), MEK1/2, which then proceeds to the last MAP kinase (MAPK), Erk1 or extracellular signal-related kinase. Erk1 phosphorylates a transcription activator Elk which allows its association to a serum response factor leading to the expression of c-Fos, a part of the AP-1 dimer. The other part of AP-1, c-Jun, can be activated via a second parallel MAPK signalling subgroup involving MEKK1, MKK4 and JNK upstream, similar to Raf, MEK1/2 and Erk1.^[184,185] AP-1 can be made up of homo- or heterodimers from either Jun or Fos transcription factor families and distinct combinations permit different gene transcription targets responsible for cell cycle progression and apoptosis^[186].

The third mitogen-activated protein kinase signalling group is the p38 MAPK which normally acts as a cellular stress sensor can also be activated through CD3/CD28 in a non-stress manner^[187,188]. Stress signals like UV radiation, heat, ROS and inflammatory cytokines via TNF/TNFR ligation trigger a signalling cascade from apoptosis signal-regulating kinase 1 (ASK1) to MKK3/6 to p38, as the MAP3K, MAP2K and MAPK, respectively. In activated T cells, an alternative pathway occurs via direct phosphorylation of p38 by ZAP-70 which bypass the MAP3K and MAP2K. ZAP-70 phosphorylates a unique tyrosine site in p38 which induces autophosphorylation of other tyrosine and threonine residues^[189,190]. Generally, MAPK p38 targets a wide array of genes responsible for proteases, cytokines and metabolic regulation^[191].

Co-stimulatory receptors like the CD28 homodimer also participates in signal transduction and gene expression programming upon ligation with APC B7 proteins (Figure 1.9). Upon TCR-MHC engagement, the presence of CD28 co-signal prevents cell anergy and instead enhance CD3 signalling. Due to this, CD28 largely participates synergistically with TCR/CD3, but itself can independently initiate signalling, albeit

to a lesser extent. CD28 features a cytosolic domain with a tyrosine phosphorylation site (YMNM) and proline-rich (PXXP) motifs^[192]. The cytoplasmic phosphorylation site allow the anchored binding and activation, although not exclusively, of phosphatidylinositide 3-kinases (PI3Ks) near the cell membrane^[193]. PI3K sits at the head of the PI3K/AKT/mTOR pathway mainly responsible for inducing protein translation. Consequently, PI3K activation results in the conversion of phosphatidylinositol-phosphate (PIP) to PIP₂ and PIP₃^[194] which can feed into previously mentioned DAG pathways, as well as cascades downstream into protein kinase B (PKB/AKT) activation and then to mammalian target of rapamycin (mTOR)^[195,196]. In addition, adaptor protein VAV interaction with CD28 alone was reported to induce NFκB activity through signalling via Ras-related C3 botulinum toxin substrate 1 (Rac-1) and MEKK1^[197,198].

Chapter 7 explores the effect of some of these signalling pathways in cholesterol-oxysterol metabolism will be looked at.

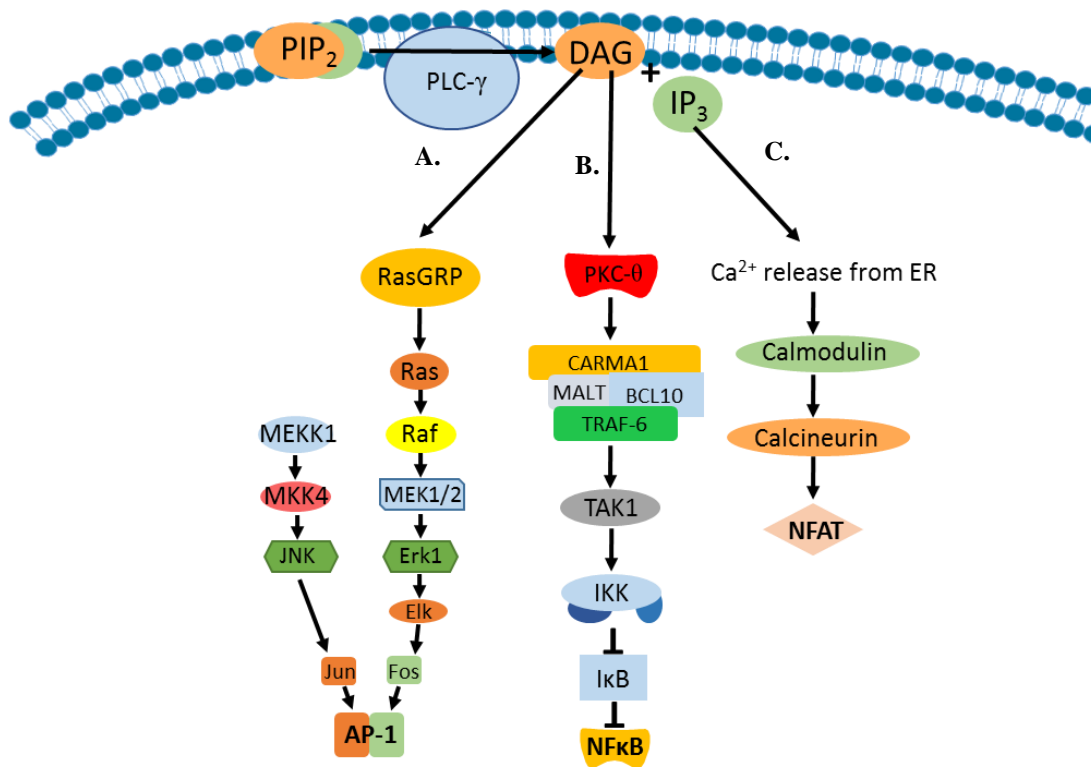


Figure 1.10. Signalling cascade initiated from PLC- γ .

Membrane-associated PIP₂ can be converted to Diacylglycerol (DAG) and IP₃ by activated PLC- γ . The presence of DAG can subsequently recruit and activate (A) RasGRP and (B) PKC- θ to induce the MAPK and PKC pathway resulting to the stimulation and nuclear translocation of AP-1 and NF κ B. The other PIP₂ component, (C) IP₃, can diffuse into the cytoplasm and bind to IP₃ receptors in the endoplasmic reticulum and release stored Ca²⁺ ions. Increase in cytoplasmic calcium in turn activates calmodulin, calcineurin then NFAT. Adapted from Janeway's Immunobiology and Kuby Immunology^[109,110].

1.6. Mass Spectrometry

In simplistic terms, Mass Spectrometry (MS) is an analytical technique which identifies compounds in mixtures based on their mass and charge. It is essentially ion identification and characterisation by means of weighing, but it does so with great sensitivity and accuracy. This technique uses a mass spectrometer which is capable of ionising a sample, sorting the ion mixture by mass and charge then measuring it through a detector. More specifically, there are three main parts of a mass spectrometer: 1) an ionisation source which turns a dried, liquid or gas sample into gas phase ions, and accelerate them towards 2) a mass analyser under high vacuum which can sort and distinguish different constituent ions using electrostatic or electromagnetic fields according to their mass-to-charge ratio (m/z). Then, the sorted ions reach 3) an ion detector which converts single ion currents into amplified electronic signals further processed by a data management system ultimately to create a mass spectrum, a plot of ion abundance against m/z ^[199]. Although these are the two main data provided by mass spectrometers, this data can also be used to gather analyte structural information through fragmentation.

1.6.1. Ionisation Sources

One of the earliest ionisation sources combines electron ionisation (EI) and chemical ionisation (CI). The former utilises volatilisation of the sample under vacuum and its ionisation by high energy electron bombardment yielding extensive fragmentation useful for structural information while the latter uses pre-ionised reagent gases which collide and interact with the analytes thus ionizing them with less fragmentation through proton transfer or as adducts^[200]. Other ionisation methods commonly used for biological analysis are solid-state matrix-assisted laser desorption ionisation (MALDI) and liquid-phase electrospray ionisation (ESI). In MALDI, samples are immobilised on a surface and coated with a matrix which not only holds the sample but also aids its ionisation. A laser pulse is aimed at specific points in the matrix surface causing the generation of gas-phase analyte and matrix plume which are then directed into the mass analyser. Instead of co-crystallizing the sample with matrix, samples can be solubilised in aqueous/solvent mixtures and subjected to ESI.

Electrospray ionisation, which is a concentration-dependent soft ionisation method, uses a stream of liquid passing through a charged heated capillary, creating a spray directed towards a mass analyser under atmospheric pressure^[200–202] (Figure 1.11). The capillary and the sample inlet are at a high potential difference which concentrates charged ions at the tip of the capillary. At the tip, identically charged ions start to accumulate then eventually break off as small droplets once the surface tension is broken^[202–204]. The aerosolised droplets shrink through desolvation leaving ion clusters with decreasing volume and increasing electric charge. Repulsion between the same charged ions further dissociates the droplets through Coulombic fission into bare gas phase ions which are accelerated to the analyser orifice. Ionisation efficiency in ESI is highly dependent on the electric field at the capillary sprayer, its tip diameter and its distance from the sample inlet or counter electrode. This type of ion source often results in generation of quasi-molecular ion with minimal in-source fragmentation^[203]. As ESI is a type of atmospheric pressure ionisation (API) source, liquid-phase solubilised samples pre-separated by liquid chromatography can be readily coupled to it. See *section 1.6.4.2* for its specific application for sterol analysis.

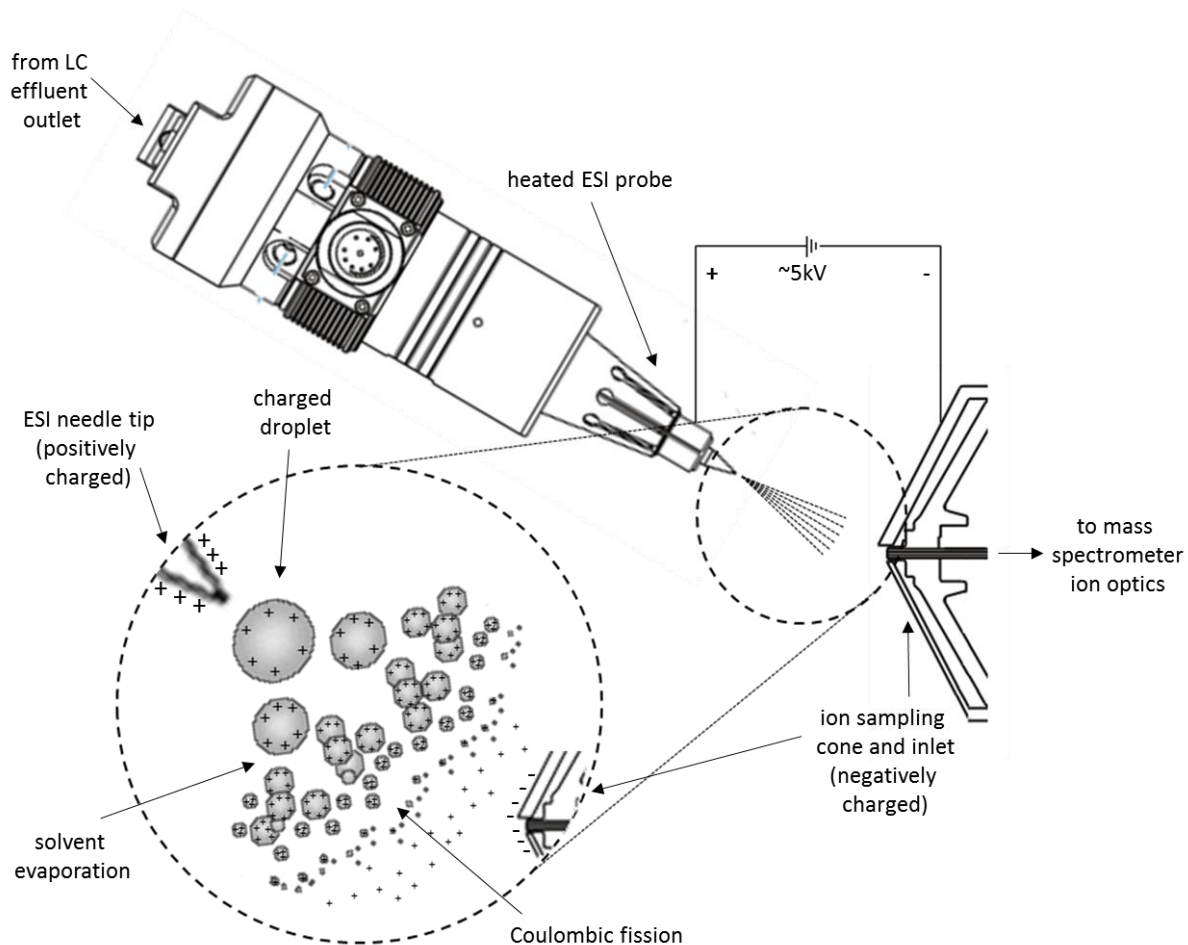


Figure 1.11. Electrospray ionisation (ESI) on an LTQ Orbitrap Velos Pro/Elite. Eluted chemically derivatised sterol species are heated on the HESI-II probe and nebulised by a dry nitrogen sheath/auxilliary gas to form a fine spray with charged droplets. The charge density in each of the droplets increases as the solvent evaporates. At a certain point when the charge density overcomes the surface tension at the surface, the droplet subdivides through Coulombic fission. This process repeats until bare gas phase ions remain which are attracted to the oppositely charged sampling cone/inlet and into the mass spectrometer. Image adapted/modified from Thermo Scientific API source hardware manual^[204].

1.6.2. Mass Analysers

As with different ionisation sources, there are also many types of mass analysers which differ in how ions are sorted before detection. Two of the modern mass analysers used in the current study are listed and described below.

1.6.2.1. Linear Quadrupole Ion Trap (LIT)

Linear quadrupole ion traps are not only operated as mass analysers, they can also act as ion accumulators, ion reaction vessels or as pulsed ion sources^[203]. As the name suggests, a linear quadrupole ion trap consists of four cylindrical electrodes in a square configuration arranged in pairs which are operated with a radio frequency (RF) voltage under vacuum (Figure 1.12A). The alternating potentials of each electrode pair can attract then repel ions of a certain m/z ^[200,205]. Trapping of the ions linearly requires another set of DC electrode segments positioned at either end of the multipoles with higher voltage potentials to reflect the ions back. This trapping also enables a stream of ions to be organised in small ion packets or pulses. Synchronised RF potentials between the four electrodes and end plates can induce ion oscillations with a stable trajectory facilitating ion accumulation, storage, focussing and ejection^[206–208]. This efficient trapping of ions by LITs have been utilised for ion mass analysis. In the case of LTQ Orbitrap Elite with dual-pressure LITs, ions are focussed from the inlet to the first high pressure trap (Figure 1.12B) for storage^[209]. There, it can act as a bridge and eject the stored ions axially to the next trap; act as a mass filter to radially eject ions, retaining only ions with specific m/z ranges; or act as a fragmentation cell where ions can be excited and dissociated by collision with helium gas, known as collision-induced dissociation (CID). From then on, mass filtered ions or fragment ions can be ejected to the low pressure cell (Figure 1.12C) where ion detection can occur. The AC potentials at the quadrupoles are controlled so that ions of specific m/z are resonantly ejected radially via a slit on the middle segment and into electron multipliers (Figure 1.12D). Ions detected at a specific frequency can be amplified by dynodes and converted into an electrical signal^[209]. For more complex analysis or higher mass accuracy detection, ions pulses from the LITs can be axially ejected to the Orbitrap mass analyser with or without prior mass filtering or fragmentation.

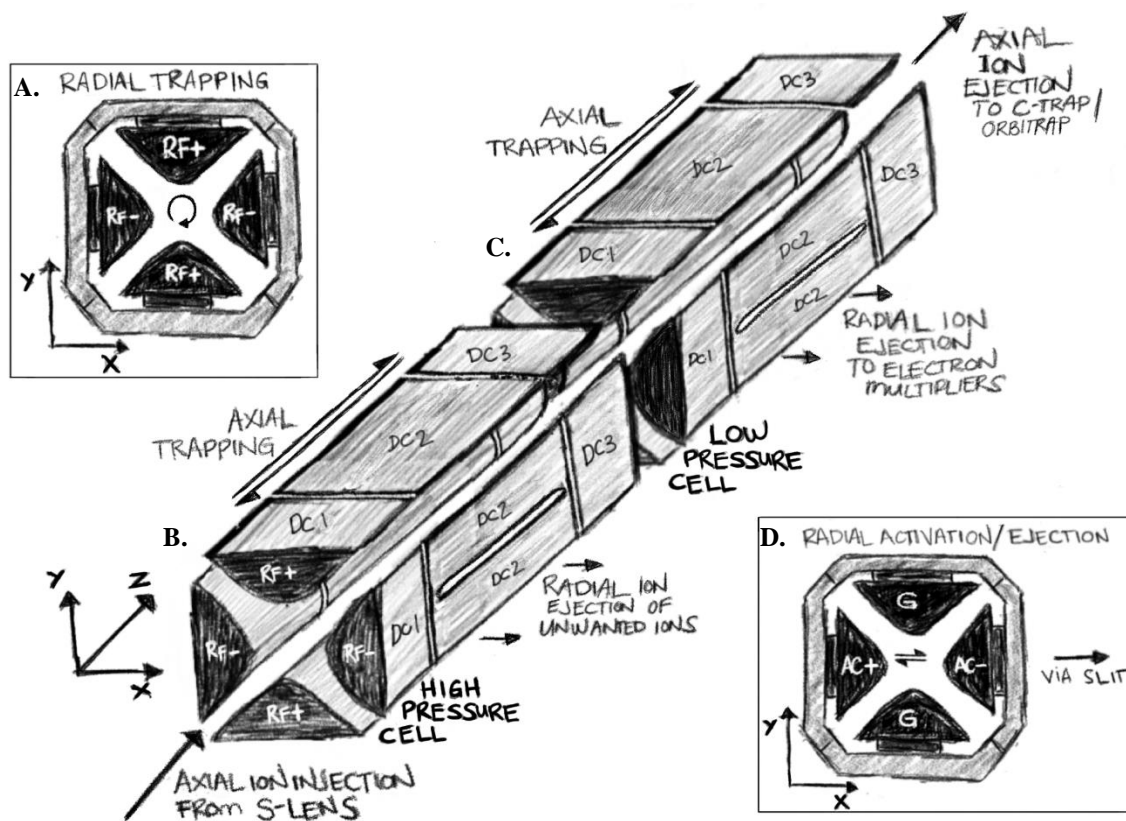


Figure 1.12. Internal schematics of a dual-cell 2D linear ion trap of the Velos Pro.

The Orbitrap Elite is interfaced at the front with a Velos Pro LIT. Ions clusters are contained in the LIT using both axial and radial trapping. A. Upon injection from the S-lens, ions are radially trapped using RF voltages which confines ions between the four quadrupoles. B/C. Ions can be contained axially in the cells using DC voltages applied on the six segments of the quadrupoles. Ion mass filtering, storage and dissociation occurs in the high pressure cell, whereas ion scan-out or detection occurs in the low pressure cell where conversion dynodes/electron multipliers are adjacently placed. D. Trapped ions can be activated or excited with an AC voltage to either act as a mass filter to radially eject ions outside a specific m/z or to eject ions into the detector. Contained ions not for detection in the LIT can be ejected axially into the C-trap/Orbitrap mass analyser.

1.6.2.2. Orbitrap

The Orbitrap features a spindle shaped inner central electrode sandwiched by two outer bell-shaped barrel electrodes at either end. This mass analyser employs the principles of electrical fields for ion trapping like LITs but with a specialised m/z measurement principle. First, the ion pulse ejected from the dual-pressure LITs are transferred into a curved linear trap (C-Trap). Ions arriving in the C-Trap are slowed down through collisions with nitrogen gas present in the trap. The loss of kinetic energy also concentrates the ion packet into a smaller space then RF ramping voltages pushes the ions outwards from the gas-filled C-Trap to the high vacuum Orbitrap^[210] (Figure 1.13). On entry, the ion packet made up of a range of m/z received in the Orbitrap start coherent rotational (around z-axis) and linear (along z-axis) oscillations around the central electrode^[208,211]. The application of increasing DC electrostatic field between the inner and outer electrodes squeezes the rotational oscillating ions away from the outer electrodes and towards the central electrode. Once the ion trajectories are stable, mass detection follows^[212]. In principle, ions with different m/z will have a different linear oscillating frequency along the z-axis, and this linear oscillation can be detected as an alternating frequency sine wave signal (image current) from the two bell-shaped outer electrodes which is then amplified and converted to a digital frequency^[212]. As the Orbitrap can contain several ions of different trajectories, the image current detected can be a combination of several sine wave frequencies. The complex image current output is then deconvoluted into its constituent individual sine waves through a process of Fourier transform (FT)^[208,213,214]. Essentially, this process accurately detects the single ion m/z based on its frequency.

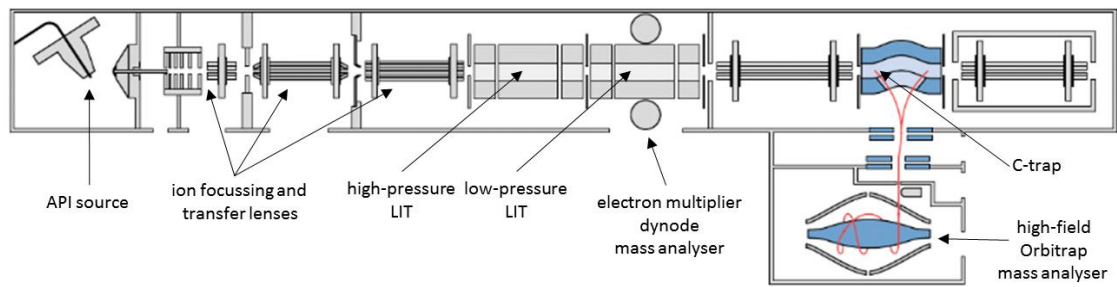


Figure 1.13. Orbitrap Velos Pro/Elite mass spectrometer layout schematics.

A stream of liquid-phase ionised analyte/solvent mix is nebulised into to gas phase ions in the API source and introduced into the mass spectrometer. The ions are accelerated and focussed using a series of ion optics which transfers the ion into the dual-pressure linear ion trap. There, ions can be mass filtered, fragmented, mass analysed or further transferred into the C-trap. Ions entering the C-trap are dampened, slowed down, stored then focussed axially into the high-field Orbitrap mass analyser. Ions take an oscillating trajectory once in the Orbitrap and this unique frequency of oscillation is indicative of its mass-to-charge ratio after Fourier transform processing. Image adapted and modified from <http://planetorbitrap.com/orbitrap-elite>.

1.6.3. Tandem Mass Spectrometry (MSⁿ)

Tandem mass spectrometry is the combination of two or more stages of mass analysis. These can be done in space, where different mass analysers are physically coupled together for distinct analysis events; or in time, where the same instrument can act as an ion storage device and facilitate all mass analysis events^[200].

In this study, targeted tandem MS in time is utilised for structure elucidation using three stages of MS (MS³) using the dual-pressure LITs of an LTQ Orbitrap. For this case, pulsed ionised analytes enter the LITs and are stored. In the first stage of a scan event, the collected ions in the trap are filtered to isolate a specific precursor ion whilst radially ejecting the rest (Figure 1.12B). Collision-induced dissociation (CID) is used to produce precursor-specific daughter fragment ions^[200]. Secondly, a fragment is selected and filtered from the other daughter ions and subsequently fragmented again yielding granddaughter ions. Third and lastly, granddaughter ions are then subjected to mass detection. The work presented in this thesis was largely based on oxysterol mass spectrometric analysis which used the sequential LIT trapping and fragmentation for MS³ analysis while high mass accuracy detection was used in the Orbitrap for MS¹ analysis using a conventional m/z scan.

1.6.4. Chromatography MS Coupling in the analysis of Sterols

1.6.4.1. Gas Chromatography – Mass Spectrometry (GC-MS)

Due to the increasing number of oxysterols and their biological significance, methods of separation and analysis have been developed and optimised. Gas chromatography is an analytical technique in which the separation of analytes in the gaseous state carried by a gas mobile phase relies both on analyte boiling point and reversible interactions with the stationary liquid phase. Thus, samples ideal for GC-MS are low-polarity volatile low-molecular weight compounds. This technique was used extensively in the past for the analysis of cholesterol oxidation products, which branched from steroid and bile acid analysis, from several biological sources like brain and plasma^[215–217]. Several groups have pioneered methods for oxysterols studies by GC-MS and have even extended the analysis to further metabolites like cholestenoic

acids and secosteroid vitamin D derivatives^[215,218,219]. The chemical nature of sterols and requirements for GC-MS warrants an extensive sample preparation prior to analysis. As oxysterols and cholesterol can exist in biofluids as free sterols or as ester conjugates, it was often necessary to hydrolyse these species before extraction. Furthermore, due to the difference in the abundance, isolation of cholesterol from the more polar and less abundant oxysterols were often performed through solid phase extractions (SPE) which also enriches and concentrates the fractions (Figure 1.14). Without the pre-separation, further sample manipulation can lead to formation of cholesterol autoxidation artefacts that can contaminate the oxysterol fraction. Volatility and thermal stability of sterols is often enhanced by derivatisation, most commonly using trimethylsilylation (TMS)^[220] or *tert*-butyldimethylsilylation (TBDMS)^[221]. Derivatisation can reduce the polarity of analyte functional groups, aid GC separation and provide characteristic fragmentation patterns. For quantitative studies, sample preparation can include stable isotope dilution. Samples can then be analysed by GC-MS through monitoring the retention times relative to authentic standards and unique EI fragmentation qualifier ions which can be library matched. Even with the lengthy sample preparation and strict analysis requirements, GC-MS methods for oxysterol analysis are still used today due to its low running cost, ease of use and high chromatographic resolving power.

1.6.4.2. Liquid Chromatography – Mass Spectrometry (LC-MS)

Alongside the development of GC methodologies, the potential of liquid chromatography was also realised, specifically high performance liquid chromatography (HPLC)^[222], for the analysis of sterols which was further expanded to the analysis of sterols in cells and tissues^[223,224]. Compared to GC, sample mixtures for LC are separated in-solution based mainly on functional groups and reversible interactions with the stationary phase. This not only removes the volatility and thermal stability requirement but also offers a wider range of compounds for analysis to include higher molecular weight, ionic and polar analytes. LC-MS methods consist of an analytical column packed with solid or liquid-bound stationary phase and a liquid mobile phase. Reversed phase (RP) LC is commonly used for oxysterol analysis which uses a non-polar hydrophobic stationary phase and a polar mobile phase often containing a pH-adjusted mixture of water and organic solvents. Samples are usually

solvated in similar components as the mobile phases and are injected onto the analytical column for either isocratic or gradient elution. This in-solution analytical separation occurs through the balance between retaining interactions, like van der Waals forces, of the analytes to the stationary phase and the eluting strength of the liquid mobile phase. For reversed phase sterol analysis, more polar hydroxycholesterols are weakly retained in non-polar stationary phase thus elute earlier, whereas less polar cholesterol interacts more strongly with the column and elutes later. Furthermore, sterols like desmosterol also elute slightly earlier than cholesterol due to the presence of an extra double bond. The reverse order of elution is observed with normal phase (NP) chromatography which uses polar-polar interactions of the analyte with the stationary phase.

Even with the volatility and thermal stability issue aside, sterol analysis still requires sample preparation for HPLC-MS analysis similar to GC-MS. Biological sterol extracts will still have a lower abundance of oxysterols than cholesterol with the same problems associated with cholesterol susceptibility for autoxidation, thus necessitating pre-separation by solid phase extraction (Figure 1.14). SPE works by relying on interaction of molecular components with the stationary phase^[225] as in LC columns described above. For RP-SPE, the silica-supported non-polar C18 chains are randomly oriented when dry, thus the column first requires activation through a conditioning step. Exposure of C18 to low polarity solvents organises and increase the surface area of the chains to expose sites where non-polar analytes can interact in the retention step upon sample loading. Column conditioning ensures better binding and recovery^[226,227]. Compounds with no affinity to the stationary phase pass through as the eluate while the rest binds. It is highly likely that other compounds can bind to the column and co-elute with the target compounds. Thus, washing steps are often necessary to rinse out impurities. To desorb the bound analytes of interest at the elution step, solvents like ethanol and methanol can selectively break the retentive van der Waals forces and solubilise sterols back in solution.

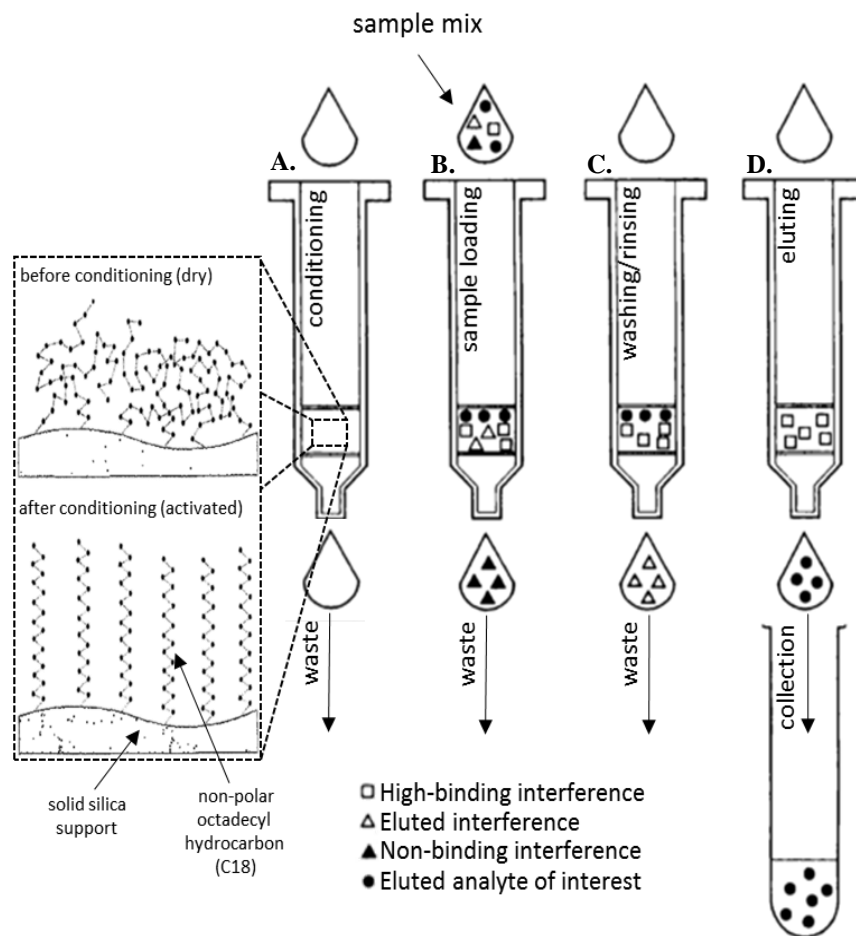


Figure 1.14. Solid phase extraction (SPE) procedure.

A. At the conditioning step, the C18 hydrocarbon moiety bound to a solid silica sorbent support in an SPE cartridge is activated from a random orientation to an ordered orientation which allows the exposure of analyte interaction sites. B. Upon sample loading, analytes and interferences which have an affinity towards the sorbent material will be retained in the column whereas others will pass through as the eluate. C. Retained interfering analytes can further be removed with a washing/rinsing step. D. Finally, analytes of interest can be eluted (eluite) and collected with an appropriate eluent able to break retaining van der Waals forces between sorbent and analyte. Image adapted/modified from Thurman 1998 and Simpson 2000^[225-227].

Sterols, especially free hydroxycholesterols are neutral lipids which are not readily ionised compared to e.g phospholipids, conjugated steroids and bile acids. Due to this, chemical modification by adding a more polar group or a charged moiety through derivatisation is again ideal to improve cholesterol and oxysterol sensitivity upon MS analysis (Figure 1.15). Sterol-related derivatisations which are targeted to the 3-OH position on the steroid nucleus can be as simple as a one-step sulfation used for the quantitation of free cholesterol in cultured cells^[228,229]; lithium methoxyacetylation used in the lipid analysis of mouse dorsal root ganglia^[230]; or after conversion to ketones, conversion to sterol-oximes used for rat neuronal sterols^[231,232]. Alternatively, oxysterols have also been derivatised as picolinyl/nicotinyl esters^[233], *N,N*-dimethylglycine (DMG) esters^[234] or Girard P/T hydrazones^[235,236] for ESI sources. Particularly, the use of Girard P hydrazine as an oxysterol derivatisation reagent has been used on the work presented in this thesis. Girard hydrazines contain a positively charged quaternary nitrogen group that can tag on a sterol molecule containing an oxo group to form the hydrazone. An oxo group would have to be introduced to oxysterol species not having it through an oxidation step facilitated by a cholesterol oxidase enzyme. Differentiation of sterols naturally possessing an oxo group from the ones without can be done by excluding the oxidation step in a repeat derivatisation. There are several advantages which arise from this type of charge-tagging, namely: it introduces specificity to analysis of sterols with oxo groups, it enhances the solubility of the tagged sterols in solvents used in RP chromatography, it improves the formation of gas-phase ions in ESI for increased sensitivity, it produces a prominent neutral loss of 79Da upon MS² CID, and, the resulting [M-79]⁺ ion can further provide unique structure informative fragments upon MS³ CID valuable for sterol fingerprinting^[237]. The use of oxysterol Girard P hydrazones been largely used for ESI^[238–242] but have also been used for MALDI with an α -cyano-4-hydroxycinnamic acid matrix^[243].

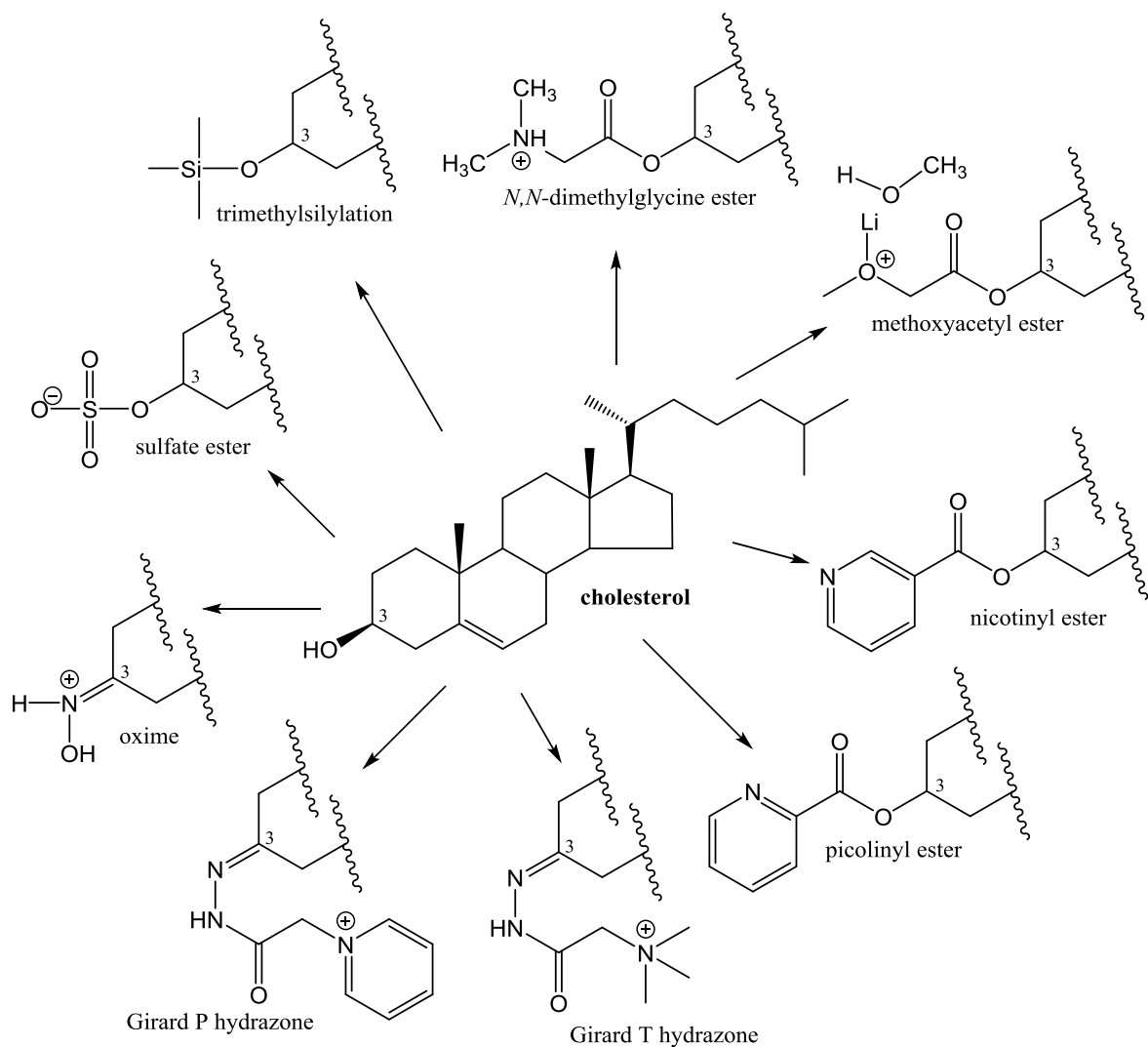


Figure 1.15. Different sterol modifications for derivatisation.

As neutral compounds, it is ideal for sterol species to be chemically modified to aid its mass spectrometry analysis. Such modifications like sulfation^[228], DMG esterification^[234], lithiated methoxyacetyl esterification^[230], oxime formation^[231,232], picolinylnyl/nicotinylnyl esterification^[233] and hydrazone^[235,236] formation help increase ionisation efficiency, sensitivity in API sources and often provide unique fragmentation patterns useful for structural identification.

Nevertheless, some LC-MS methodologies for sterol analysis can and do skip derivatisation steps^[224], especially when interfaced with another API source called atmospheric pressure chemical ionisation (APCI)^[223,244–247]. Unlike in ESI, gas phase ions form in APCI through a series of reactions initiated by electrons from a heated corona discharge needle energetic enough to ionise the atmospheric gasses around it. Dissolved analytes in solvents are first vaporised by a heated nebulising gas which is directed to the corona tip. Ionised atmospheric gasses like N_2^+ , O_2^+ , H_2O^+ , H_3O^+ and NO^+ made in the corona discharge region further react and ionise the vaporised solvent acting as the reagent gas which further ionises the analytes as adducts.

As previously mentioned, LC can be readily interfaced with atmospheric pressure ionisation sources such as electrospray ionisation (ESI) and heated electrospray ionisation (HESI). Specifically, GP-derivatised sterols in solution separated on an LC analytical column are directed to an Ion Max source equipped with an HESI-II probe attached to the front of an LTQ Orbitrap Velos Pro/Elite. The 200 $\mu\text{L}/\text{min}$ column effluent is heated as it passes on the HESI-II probe to help with solvent evaporation and a high potential of around 5kV on the probe needle tip together with the solvent flow induces the formation of a fine mist of droplets that are electrically charged. As the solvent evaporates, the electrical charge density of the droplets increases due to decreasing volume. These eventually break into smaller droplets once they pass a critical point of greater electrostatic repulsion than droplet surface tension. These processes of desolvation and coulombic fission continues to break droplets into even smaller ones until bare gas phase ions are formed which enter the sample inlet of the mass spectrometer. Endogenous and internal standard sterols derivatised with the charged quaternary nitrogen-containing tag are observed as $[\text{M}]^+$ ions. In the mass spectrometer, the focussed ions are transferred to the LIT for fragmentation and mass scanning events or further into the high-field Orbitrap for high mass accuracy scanning events. For a sterol identification scan, the LIT is used. In this scan event, the ions are received, slowed down, and stored in the LIT. The $[\text{M}]^+$ precursor ion is then selected and other ions ejected. With the aid of the distinctive loss of the pyridine ring upon CID at MS^2 in the LIT, the abundant $[\text{M}-79]^+$ ion can be further fragmented by CID at MS^3 for m/z analysis at the LIT detector providing structural information. For a high mass accuracy scan, the high-field Orbitrap is used. In this scan event, an ion cluster passing through the LIT is then slowed down and stored in the C-trap without

scanning, filtering or fragmentation. The $[M]^+$ ions in the C-trap are ejected out and focussed into the high-field Orbitrap. There, ions are stored and subjected to electrostatic potential which induces axial, radial and rotational oscillations. Both the radial and rotational oscillations are affected by the ion entry velocity but not the axial oscillation which is proportional to the ion m/z . This axial oscillation of ions can be detected as an image current frequency using the outer Orbitrap electrodes which are processed via Fourier transform for m/z determination. Together, both tandem LIT MS³ and high-mass accuracy Orbitrap events can identify and quantify sterol species in a fast and effective manner.

In all, HPLC-ESI-MSⁿ described here was exclusively used in the analysis of solubilised sterols for this thesis.

1.7. General Thesis Aims

The overall aim of this PhD study was to profile the oxysterols generated by cultured T helper cells and to relate the oxysterols to their function. Chapters 3 and 4 will profile the oxysterol generation of human CD4⁺ T cells. Chapter 5 will investigate the consequence of inhibiting cholesterol biosynthesis in oxysterol production. Chapter 6 will tackle the effects of the silencing of oxysterol genes in T helper cytokine production. Chapter 7 will identify the signalling pathways associated in the production of oxysterols. And chapter 8 will explore the specific oxysterols generated by differentiated/polarised CD4⁺ T cells.

1.8. References

- [1] P. Soroosh, J. Wu, X. Xue, J. Song, S.W. Sutton, M. Sablad, et al., (2014) Oxysterols are agonist ligands of ROR γ t and drive Th17 cell differentiation., *Proc. Natl. Acad. Sci. U. S. A.* 2–7. doi:10.1073/pnas.1322807111.
- [2] X. Hu, Y. Wang, L.-Y. Hao, X. Liu, C. a Lesch, B.M. Sanchez, et al., (2015) Sterol metabolism controls TH17 differentiation by generating endogenous ROR γ agonists, *Nat. Chem. Biol.* 11 141–147. doi:10.1038/nchembio.1714.
- [3] F.R. Santori, P. Huang, S.A. van de Pavert, E.F. Douglass, D.J. Leaver, B.A. Haubrich, et al., (2015) Identification of Natural ROR γ Ligands that Regulate the Development of Lymphoid Cells, *Cell Metab.* 21 286–297. doi:10.1016/j.cmet.2015.01.004.
- [4] R.P. Cook, *Cholesterol; chemistry, biochemistry, and pathology.*, Academic Press, New York, 1958.
- [5] M.E. Chevreul, (1816) Examen des graisses d’homme, de mouton, de boeuf, de jaguar et d’oie, *Ann. Chim. Phys.* 2 339–372.
- [6] L.L. Smith, *Cholesterol autoxidation*, Plenum, New York, 1981.
- [7] N.B. Myant, *The biology of cholesterol and related steroids*, Heinemann Medical Books, London, 1981.
- [8] H. Martinez-Seara, T. Róg, M. Karttunen, I. Vattulainen, R. Reigada, (2010) Cholesterol induces specific spatial and orientational order in cholesterol/phospholipid membranes, *PLoS One.* 5. doi:10.1371/journal.pone.0011162.
- [9] B. Alberts, A. Johnson, J. Lewis, M. Raff, K. Roberts, P. Walter, *Molecular biology of the cell*, Garland Science, New York, 2002.
- [10] L. Rajendran, K. Simons, (2005) Lipid rafts and membrane dynamics., *J. Cell Sci.* 118 1099–1102. doi:10.1242/jcs.01681.
- [11] G. van Meer, D.R. Voelker, G.W. Feigenson, (2008) Membrane lipids: where they are and how they behave., *Nat. Rev. Mol. Cell Biol.* 9 112–124. doi:10.1038/nrm2330.
- [12] K. Simons, R. Ehehalt, (2002) Cholesterol, lipid rafts, and disease, *J. Clin. Invest.* 110 597–603. doi:10.1172/JCI16390.
- [13] J.M. Berg, J.L. Tymoczko, L. Stryer, *Biochemistry* 7th edition, W H Freeman, New York, NY, 2012. <http://www.ncbi.nlm.nih.gov/books/NBK22528/>.
- [14] M. Wang, P.J. Casey, (2016) Protein prenylation: unique fats make their mark on biology, *Nat. Rev. Mol. Cell Biol.* 17 110–122. doi:10.1038/nrm.2015.11.
- [15] A. Mazein, S. Watterson, W.Y. Hsieh, W.J. Griffiths, P. Ghazal, (2013) A comprehensive machine-readable view of the mammalian cholesterol biosynthesis pathway, *Biochem. Pharmacol.* 86 56–66. doi:10.1016/j.bcp.2013.03.021.
- [16] W.D. Nes, (2011) Biosynthesis of cholesterol and other sterols, *Chem. Rev.* 111 6423–6451. doi:10.1021/cr200021m.
- [17] J.A. Nelson, S.R. Steckbeck, T.A. Spencer, (1981) 24(S),25-Epoxycholesterol is a natural product of mammalian steroid biosynthesis, *J. Am. Chem. Soc.* 103 6974–6975.

doi:10.1021/ja00413a040.

- [18] J.A. Nelson, S.R. Steckbeck, T.A. Spencer, (1981) Biosynthesis of 24,25- Epoxycholesterol from Squalene 2,3;22,23-Dioxide*, *J. Biol. Chem.* 1067–1068.
- [19] A. Kandutsch, H. Chen, H. Heiniger, (1978) Biological activity of some oxygenated sterols, *Science* (80-). 201 498–501. doi:10.1126/science.663671.
- [20] M.R. Briggs, C. Yokoyama, X. Wang, M.S. Brown, J.L. Goldstein, (1993) Nuclear protein that binds sterol regulatory element of low density lipoprotein receptor promoter. I. Identification of the protein and delineation of its target nucleotide sequence., *J. Biol. Chem.* 268 14490–14496. doi:10.1001/jamaneurol.2015.0606.
- [21] J.L. Goldstein, R.A. DeBose-Boyd, M.S. Brown, (2006) Protein Sensors for Membrane Sterols, *Cell.* 124 35–46. doi:10.1016/j.cell.2005.12.022.
- [22] J.D. Horton, J.L. Goldstein, M.S. Brown, (2002) SREBPs: activators of the complete program of cholesterol and fatty acid synthesis in the liver, *J. Clin. Invest.* 109 1125–1131. doi:10.1172/JCI200215593.Lipid.
- [23] A. Radhakrishnan, Y. Ikeda, H.J. Kwon, M.S. Brown, J.L. Goldstein, (2007) Sterol-regulated transport of SREBPs from endoplasmic reticulum to Golgi: oxysterols block transport by binding to Insig., *Proc. Natl. Acad. Sci. U. S. A.* 104 6511–6518. doi:10.1073/pnas.0700899104.
- [24] V. Howe, L.J. Sharpe, S.J. Alexopoulos, S. V. Kunze, N.K. Chua, D. Li, et al., (2016) Cholesterol homeostasis: How do cells sense sterol excess?, *Chem. Phys. Lipids.* 199 170–178. doi:10.1016/j.chemphyslip.2016.02.011.
- [25] Y. Jo, P.C.W. Lee, P. V. Sguigna, R. a. DeBose-Boyd, (2011) Sterol-induced degradation of HMG CoA reductase depends on interplay of two Insigs and two ubiquitin ligases, gp78 and Trc8, *Proc. Natl. Acad. Sci.* 108 20503–20508. doi:10.1073/pnas.1112831108.
- [26] S. Hwang, I.Z. Hartman, L.N. Calhoun, K. Garland, G.A. Young, M.A. Mitsche, et al., (2016) Contribution of accelerated degradation to feedback regulation of 3-hydroxy-3-methylglutaryl coenzyme A reductase and cholesterol metabolism in the liver, *J. Biol. Chem.* 291 13479–13494. doi:10.1074/jbc.M116.728469.
- [27] G.C. Ness, Z. Zhao, L. Wiggins, (1994) Insulin and glucagon modulate hepatic 3-hydroxy-3-methylglutaryl-coenzyme A reductase activity by affecting immunoreactive protein levels., *J. Biol. Chem.* 269 29168–72. <http://www.ncbi.nlm.nih.gov/pubmed/7961882>.
- [28] K.E. Suckling, E.F. Stange, (1985) Role of acyl-CoA: cholesterol acyltransferase in cellular cholesterol metabolism., *J. Lipid Res.* 26 647–671.
- [29] S. Gill, R. Chow, A.J. Brown, (2008) Sterol regulators of cholesterol homeostasis and beyond: The oxysterol hypothesis revisited and revised, *Prog. Lipid Res.* 47 391–404. doi:10.1016/j.plipres.2008.04.002.
- [30] W. Kulig, L. Cwiklik, P. Jurkiewicz, T. Rog, I. Vattulainen, (2016) Cholesterol oxidation products and their biological importance, *Chem. Phys. Lipids.* 199 144–160. doi:10.1016/j.chemphyslip.2016.03.001.
- [31] B. Batetta, F. Sanna, (2006) Cholesterol metabolism during cell growth: Which role for the

- plasma membrane?, *Eur. J. Lipid Sci. Technol.* 108 687–699. doi:10.1002/ejlt.200600015.
- [32] G.J. Schroefer, (2000) Oxysterols: modulators of cholesterol metabolism and other processes., *Physiol. Rev.* 80 361–554. <http://www.ncbi.nlm.nih.gov/pubmed/10617772>.
- [33] S. Theofilopoulos, W. Griffiths, (2014) Cholestenic acids regulate motor neuron survival via liver X receptors, *JCI.* 124 1–14. doi:10.1172/JCI68506DS1.
- [34] A. Solomon, V. Leoni, M. Kivipelto, A. Besga, A.R. Öksengård, P. Julin, et al., (2009) Plasma levels of 24S-hydroxycholesterol reflect brain volumes in patients without objective cognitive impairment but not in those with Alzheimer’s disease, *Neurosci. Lett.* 462 89–93. doi:10.1016/j.neulet.2009.06.073.
- [35] D. Lütjohann, S. Meichsner, H. Pettersson, (2012) Lipids in Alzheimer’s disease and their potential for therapy, *Clin. Lipidol.* 7 65–78. doi:10.2217/clp.11.74.
- [36] D. Lütjohann, a Papassotiropoulos, I. Björkhem, S. Locatelli, M. Bagli, R.D. Oehring, et al., (2000) Plasma 24S-hydroxycholesterol (cerebrosterol) is increased in Alzheimer and vascular demented patients., *J. Lipid Res.* 41 195–8.
- [37] A. Papassotiropoulos, D. Lutjohann, M. Bagli, S. Locatelli, F. Jessen, M.L. Rao, et al., (2000) Plasma 24S-hydroxycholesterol: a peripheral indicator of neuronal degeneration and potential state marker for Alzheimer’s disease, *Neuroreport.* 11 1959–1962. doi:10.1016/S0197-4580(00)82775-X.
- [38] A. Reboldi, E. V. Dang, J.G. McDonald, G. Liang, D.W. Russell, J.G. Cyster, (2014) 25-Hydroxycholesterol suppresses interleukin-1-driven inflammation downstream of type I interferon, *Science* (80-.). 345 679–684. doi:10.1126/science.1254790.
- [39] M. Blanc, W.Y. Hsieh, K. a. Robertson, K. a. Kropp, T. Forster, G. Shui, et al., (2013) The Transcription Factor STAT-1 Couples Macrophage Synthesis of 25-Hydroxycholesterol to the Interferon Antiviral Response, *Immunity.* 38 106–118. doi:10.1016/j.immuni.2012.11.004.
- [40] S.J. Bensinger, M.N. Bradley, S.B. Joseph, N. Zelcer, E.M. Janssen, M.A. Hausner, et al., (2008) LXR Signaling Couples Sterol Metabolism to Proliferation in the Acquired Immune Response, *Cell.* 134 97–111. doi:10.1016/j.cell.2008.04.052.
- [41] Y. Kidani, H. Elsaesser, M.B. Hock, L. Vergnes, K.J. Williams, J.P. Argus, et al., (2013) Sterol regulatory element-binding proteins are essential for the metabolic programming of effector T cells and adaptive immunity., *Nat. Immunol.* 14 489–99. doi:10.1038/ni.2570.
- [42] S. Liu, R. Aliyari, K. Chikere, G. Li, D. Matthew, J.K. Smith, et al., (2013) Interferon-Inducible Cholesterol-25-Hydroxylase Broadly Inhibits Viral Entry by Production of 25-Hydroxycholesterol, *Immunity.* 38 92–105. doi:10.1016/j.immuni.2012.11.005. Interferon-Inducible.
- [43] N.J. Spann, C.K. Glass, (2013) Sterols and oxysterols in immune cell function, *Nat Immunol.* 14 893–900. doi:10.1038/ni.2681.
- [44] K.A. Robertson, W.Y. Hsieh, T. Forster, M. Blanc, H. Lu, P.J. Crick, et al., (2016) An Interferon Regulated MicroRNA Provides Broad Cell-Intrinsic Antiviral Immunity through Multihit Host-Directed Targeting of the Sterol Pathway, *PLOS Biol.* 14 e1002364. doi:10.1371/journal.pbio.1002364.

- [45] D. Lembo, V. Cagno, A. Civra, G. Poli, (2016) Oxysterols: An emerging class of broad spectrum antiviral effectors, *Mol. Aspects Med.* doi:10.1016/j.mam.2016.04.003.
- [46] E.S. Gold, A.H. Diercks, I. Podolsky, R.L. Podyminogin, P.S. Askovich, P.M. Treuting, et al., (2014) 25-Hydroxycholesterol acts as an amplifier of inflammatory signaling., *Proc. Natl. Acad. Sci. U. S. A.* 1–6. doi:10.1073/pnas.1404271111.
- [47] D.R. Bauman, A.D. Bitmansour, J.G. McDonald, B.M. Thompson, G. Liang, D.W. Russell, (2009) 25-Hydroxycholesterol secreted by macrophages in response to Toll-like receptor activation suppresses immunoglobulin A production., *Proc. Natl. Acad. Sci. U. S. A.* 106 16764–16769. doi:10.1073/pnas.0909142106.
- [48] A.J. Brown, W. Jessup, (1999) Oxysterols and atherosclerosis, *Atherosclerosis.* 142 1–28. doi:10.1016/S0021-9150(98)00196-8.
- [49] P. Gamba, G. Testa, S. Gargiulo, E. Staurengi, G. Poli, G. Leonarduzzi, (2015) Oxidized cholesterol as the driving force behind the development of Alzheimer’s disease, *Front. Aging Neurosci.* 7 1–21. doi:10.3389/fnagi.2015.00119.
- [50] F. Chalmin, V. Rochemont, C. Lippens, A. Clottu, A.W. Sailer, D. Merkler, et al., (2015) Oxysterols regulate encephalitogenic CD4+ T cell trafficking during central nervous system autoimmunity, *J. Autoimmun.* 56 45–55. doi:10.1016/j.jaut.2014.10.001.
- [51] F.W. Lamb, (1914) The Oxidation of Cholesterol, *J. Physiol.* 48 151.
- [52] K. Bloch, (1982) The structure of cholesterol and of the bile acids, *Trends Biochem. Sci.* 7 334–336. doi:10.1016/0968-0004(82)90267-5.
- [53] W.O. Lundberg, *Autoxidation and antioxidants.*, Interscience Publishers, New York, 1961.
- [54] L.F. Fieser, M. Fieser, *Steroids*, Reinhold Publishing Corp., New York, 1959.
- [55] D.C. Malins, H.K. Mangold, (1960) Analysis of complex lipid mixtures by thin-layer chromatography and complementary methods., *J. Am. Oil Chem. Soc.* 37 576–578.
- [56] J. Avigan, D.S. Goodman, D. Steinberg, (1963) Thin-layer chromatography of sterols and steroids., *J. Lipid Res.* 4 100–101.
- [57] J. Martyn Bailey, (1966) Lipid metabolism in cultured cells, *Biochim. Biophys. Acta - Lipids Lipid Metab.* 125 226–236. doi:10.1016/0005-2760(66)90064-6.
- [58] G.H. Rothblat, M.K. Buchko, (1971) Effect of exogenous steroids on sterol synthesis in L-cell mouse fibroblasts., *J. Lipid Res.* 12 647–52. <http://www.ncbi.nlm.nih.gov/pubmed/5124529>.
- [59] M.S. Brown, J.L. Goldstein, (1997) The SREBP pathway: Regulation of cholesterol metabolism by proteolysis of a membrane-bound transcription factor, *Cell.* 89 331–340. doi:10.1016/S0092-8674(00)80213-5.
- [60] R.J. Fakheri, N.B. Javitt, (2012) 27-Hydroxycholesterol, does it exist? On the nomenclature and stereochemistry of 26-hydroxylated sterols, *Steroids.* 77 575–577. doi:10.1016/j.steroids.2012.02.006.
- [61] A.D. McNaught, A. Wilkinson, *IUPAC Compendium of Chemical Terminology*, IUPAC, Research Triangle Park, NC, 1997. doi:10.1351/goldbook.
- [62] E.J. Westover, D.F. Covey, (2004) The enantiomer of cholesterol, *J. Membr. Biol.* 202 61–72. doi:10.1007/s00232-004-0714-7.

- [63] R.S. Cahn, C. Ingold, V. Prelog, (1966) Specification of Molecular Chirality, *Angew. Chemie Int. Ed. English*. 5 385–415. doi:10.1002/anie.196603851.
- [64] M. Smith, *March's advanced organic chemistry : reactions, mechanisms, and structure*. 7th Edition, Wiley, Hoboken, New Jersey, 2013.
- [65] W. Reusch, (2013) Chiral Configurations, .
<https://www2.chemistry.msu.edu/faculty/reusch/virttxtjml/sterism3.htm> (accessed September 27, 2016).
- [66] R.C. Murphy, K.M. Johnson, (2008) Cholesterol, reactive oxygen species, and the formation of biologically active mediators, *J. Biol. Chem.* 283 15521–15525. doi:10.1074/jbc.R700049200.
- [67] D.S. Frederickson, K. Ono, (1956) The in vitro production of 25- and 26-hydroxycholesterol and their in vivo metabolism., *Biochim. Biophys. Acta.* 22 183–4. <http://www.ncbi.nlm.nih.gov/pubmed/13373861>.
- [68] D.W. Russell, (2000) Oxysterol biosynthetic enzymes, *Biochim. Biophys. Acta - Mol. Cell Biol. Lipids.* 1529 126–135. doi:10.1016/S1388-1981(00)00142-6.
- [69] M.S. Brown, J.L. Goldstein, (1974) Suppression of 3-hydroxy-3-methylglutaryl coenzyme A reductase activity and inhibition of growth of human fibroblasts by 7-ketocholesterol, *J. Biol. Chem.* 249 7306–7314. <http://www.ncbi.nlm.nih.gov/pubmed/4436312>.
- [70] A.A. Kandutsch, H.W. Chen, (1974) Inhibition of sterol synthesis in cultured mouse cells by cholesterol derivatives oxygenated in the side chain., *J. Biol. Chem.* 249 6057–61. <http://www.ncbi.nlm.nih.gov/pubmed/4472550>.
- [71] K. Bodin, L. Bretillon, Y. Aden, L. Bertilsson, U. Broomé, C. Einarsson, et al., (2001) Antiepileptic drugs increase plasma levels of 4beta-hydroxycholesterol in humans: evidence for involvement of cytochrome p450 3A4., *J. Biol. Chem.* 276 38685–9. doi:10.1074/jbc.M105127200.
- [72] J.Y.L. Chiang, (2009) Bile acids: regulation of synthesis., *J. Lipid Res.* 50 1955–1966. doi:10.1194/jlr.R900010-JLR200.
- [73] K.O. Martin, A.B. Reiss, R. Lathe, N.B. Javitt, (1997) 7 alpha-hydroxylation of 27-hydroxycholesterol: biologic role in the regulation of cholesterol synthesis., *J. Lipid Res.* 38 1053–8. <http://www.ncbi.nlm.nih.gov/pubmed/9186922>.
- [74] A. V. Yantsevich, Y. V. Dichenko, F. MacKenzie, D. V. Mukha, A. V. Baranovsky, A.A. Gilep, et al., (2014) Human steroid and oxysterol 7 α -hydroxylase CYP7B1: substrate specificity,azole binding and misfolding of clinically relevant mutants, *FEBS J.* 281 1700–1713. doi:10.1111/febs.12733.
- [75] D.W. Russell, (2003) The Enzymes, Regulation, and Genetics of Bile Acid Synthesis, *Annu. Rev. Biochem.* 72 137–174. doi:10.1146/annurev.biochem.72.121801.161712.
- [76] Y. Wang, K.M. Sousa, K. Bodin, S. Theofilopoulos, P. Sacchetti, M. Hornshaw, et al., (2009) Targeted lipidomic analysis of oxysterols in the embryonic central nervous system., *Mol. Biosyst.* 5 529–541. doi:10.1039/b819502a.
- [77] S. Sugano, R. Miura, N. Morishima, (1996) Identification of intermediates in the conversion

- of cholesterol to pregnenolone with a reconstituted cytochrome p-450_{scc} system: accumulation of the intermediate modulated by the adrenodoxin level., *J. Biochem.* 120 780–7. <http://www.ncbi.nlm.nih.gov/pubmed/8947841>.
- [78] J. Li-Hawkins, E.G. Lund, A.D. Bronson, D.W. Russell, (2000) Expression cloning of an oxysterol 7 α -hydroxylase selective for 24-hydroxycholesterol., *J. Biol. Chem.* 275 16543–9. doi:10.1074/jbc.M001810200.
- [79] N. Mast, R. Norcross, U. Andersson, M. Shou, K. Nakayama, I. Bjorkhem, et al., (2003) Broad Substrate Specificity of Human Cytochrome P450 46A1 Which Initiates Cholesterol Degradation in the Brain †, *Biochemistry.* 42 14284–14292. doi:10.1021/bi035512f.
- [80] E.G. Lund, T.A. Kerr, J. Sakai, W.P. Li, D.W. Russell, (1998) cDNA cloning of mouse and human cholesterol 25-hydroxylases, polytopic membrane proteins that synthesize a potent oxysterol regulator of lipid metabolism., *J. Biol. Chem.* 273 34316–27. <http://www.jbc.org/content/273/51/34316.full.pdf>.
- [81] M. Schwarz, a C. Wright, D.L. Davis, H. Nazer, I. Björkhem, D.W. Russell, (2000) The bile acid synthetic gene 3 β -hydroxy-Delta(5)-C(27)-steroid oxidoreductase is mutated in progressive intrahepatic cholestasis., *J. Clin. Invest.* 106 1175–84. doi:10.1172/JCI10902.
- [82] S.E. Gale, E.J. Westover, N. Dudley, K. Krishnan, S. Merlin, D.E. Scherrer, et al., (2009) Side chain oxygenated cholesterol regulates cellular cholesterol homeostasis through direct sterol-membrane interactions, *J. Biol. Chem.* 284 1755–1764. doi:10.1074/jbc.M807210200.
- [83] V.M. Olkkonen, O. Béaslas, E. Nissilä, (2012) Oxysterols and Their Cellular Effectors, *Biomolecules.* 2 76–103. doi:10.3390/biom2010076.
- [84] M. Robinson-Rechavi, H. Escriva, V. Laudet, (2003) The nuclear receptor superfamily., *J. Cell Sci.* 116 585–586. doi:10.1242/jcs.00247.
- [85] B.A. Janowski, P.J. Willy, T.R. Devi, J.R. Falck, D.J. Mangelsdorf, (1996) An oxysterol signalling pathway mediated by the nuclear receptor LXR alpha., *Nature.* 383 728–31. doi:10.1038/383728a0.
- [86] N. Zelcer, C. Hong, R. Boyadjian, P. Tontonoz, (2009) LXR Regulates Cholesterol Uptake Through Idol-Dependent Ubiquitination of the LDL Receptor, *Science* (80-.). 325 100–104. doi:10.1126/science.1168974.
- [87] Y. Zhang, X. Luo, D. Wu, Y. Xu, (2014) ROR nuclear receptors: structures, related diseases, and drug discovery, *Acta Pharmacol. Sin.* 36 71–87. doi:10.1038/aps.2014.120.
- [88] A.M. Jetten, H.S. Kang, Y. Takeda, (2013) Retinoic acid-related orphan receptors α and γ : Key regulators of lipid/glucose metabolism, inflammation, and insulin sensitivity, *Front. Endocrinol. (Lausanne).* 4 1–8. doi:10.3389/fendo.2013.00001.
- [89] C. Crumbley, Y. Wang, D.J. Kojetin, T.P. Burris, (2010) Characterization of the core mammalian clock component, NPAS2, as a REV-ERB β /ROR α target gene, *J. Biol. Chem.* 285 35386–35392. doi:10.1074/jbc.M110.129288.
- [90] Y. Takeda, R. Jothi, V. Birault, A.M. Jetten, (2012) ROR γ directly regulates the circadian expression of clock genes and downstream targets in vivo., *Nucleic Acids Res.* 40 8519–35. doi:10.1093/nar/gks630.

- [91] Y. Wang, N. Kumar, L. a. Solt, T.I. Richardson, L.M. Helvering, C. Crumbley, et al., (2010) Modulation of retinoic acid receptor-related orphan receptor alpha and gamma activity by 7-oxygenated sterol ligands., *J. Biol. Chem.* 285 5013–25. doi:10.1074/jbc.M109.080614.
- [92] Y. Wang, N. Kumar, C. Crumbley, P.R. Griffin, T.P. Burris, (2010) A second class of nuclear receptors for oxysterols: Regulation of RORalpha and RORgamma activity by 24S-hydroxycholesterol (cerebrosterol)., *Biochim. Biophys. Acta.* 1801 917–23. doi:10.1016/j.bbali.2010.02.012.
- [93] I.I. Ivanov, B.S. McKenzie, L. Zhou, C.E. Tadokoro, A. Lepelley, J.J. Lafaille, et al., (2006) The Orphan Nuclear Receptor ROR γ t Directs the Differentiation Program of Proinflammatory IL-17+ T Helper Cells, *Cell.* 126 1121–1133. doi:10.1016/j.cell.2006.07.035.
- [94] X.O. Yang, B.P. Pappu, R. Nurieva, A. Akimzhanov, H.S. Kang, Y. Chung, et al., (2008) T Helper 17 Lineage Differentiation Is Programmed by Orphan Nuclear Receptors ROR α and ROR γ , *Immunity.* 28 29–39. doi:10.1016/j.immuni.2007.11.016.
- [95] N. Heldring, A. Pike, S. Andersson, J. Matthews, G. Cheng, J. Hartman, et al., (2007) Estrogen receptors: how do they signal and what are their targets., *Physiol. Rev.* 87 905–31. doi:10.1152/physrev.00026.2006.
- [96] L. a Helguero, M.H. Faulds, J.-Å. Gustafsson, L.-A. Haldosén, (2005) Estrogen receptors alpha (ER α) and beta (ER β) differentially regulate proliferation and apoptosis of the normal murine mammary epithelial cell line HC11, *Oncogene.* 24 6605–6616. doi:10.1038/sj.onc.1208807.
- [97] J.-M. Renoir, V. Marsaud, G. Lazennec, (2013) Estrogen receptor signaling as a target for novel breast cancer therapeutics., *Biochem. Pharmacol.* 85 449–65. doi:10.1016/j.bcp.2012.10.018.
- [98] C.G. Torres, M.E. Ramírez, P. Cruz, M.J. Epuñan, L.E. Valladares, W.D. Sierralta, (2011) 27-hydroxycholesterol induces the transition of MCF7 cells into a mesenchymal phenotype., *Oncol. Rep.* 26 389–97. doi:10.3892/or.2011.1284.
- [99] M. Umetani, P. Ghosh, T. Ishikawa, J. Umetani, M. Ahmed, C. Mineo, et al., (2014) The cholesterol metabolite 27-hydroxycholesterol promotes atherosclerosis via proinflammatory processes mediated by estrogen receptor alpha, *Cell Metab.* 20 172–182. doi:10.1016/j.cmet.2014.05.013.
- [100] C.D. DuSell, E.R. Nelson, X. Wang, J. Abdo, U.I. Mödder, M. Umetani, et al., (2010) The endogenous selective estrogen receptor modulator 27-hydroxycholesterol is a negative regulator of bone homeostasis, *Endocrinology.* 151 3675–3685. doi:10.1210/en.2010-0080.
- [101] C. Liu, X. V Yang, J. Wu, C. Kuei, N.S. Mani, L. Zhang, et al., (2011) Oxysterols direct B-cell migration through EBI2., *Nature.* 475 519–523. doi:10.1038/nature10226.
- [102] S. Hannedouche, J. Zhang, T. Yi, W. Shen, D. Nguyen, J.P. Pereira, et al., (2011) Oxysterols direct immune cell migration via EBI2., *Nature.* 475 524–527. doi:10.1038/nature10280.
- [103] L. Raccosta, R. Fontana, D. Maggioni, C. Lanterna, E.J. Villablanca, A. Paniccia, et al., (2013) The oxysterol-CXCR2 axis plays a key role in the recruitment of tumor-promoting neutrophils, *J. Exp. Med.* 210 1711–1728. doi:10.1084/jem.20130440.
- [104] S. Bergström, O. Wintersteiner, (1941) Autoxidation of sterols in colloidal aqueous solution,

- J. Biochem. 141. <http://www.jbc.org/content/141/2/597.full.pdf>.
- [105] R.D. Bennett, E. Heftmann, (1962) Thin-Layer Chromatography of Sterols, *J. Chromatogr.* 9 359–362.
- [106] L. Aringer, P. Eneroth, L. Nordström, (1976) Side chain hydroxylation of cholesterol, campesterol and beta-sitosterol in rat liver mitochondria., *J. Lipid Res.* 17 263–72. <http://www.jlr.org/content/17/3/263.full.pdf>.
- [107] L. Aringer, L. Nordström, (1981) Chromatographic properties and mass spectrometric fragmentation of dioxygenated C27-, C28-, C29-steroids, *Biol. Mass Spectrom.* 8 183–203. doi:10.1002/bms.1200080502.
- [108] W.J. Griffiths, Y. Wang, (2011) Analysis of oxysterol metabolomes, *Biochim. Biophys. Acta - Mol. Cell Biol. Lipids.* 1811 784–799. doi:10.1016/j.bbalip.2011.05.012.
- [109] K. Murphy, P. Travers, M. Walport, C. Janeway, *Janeway's immunobiology*, Garland Science, New York, 2012.
- [110] J.A. Owen, J. Punt, S.A. Stranford, P.P. Jones, J. Kuby, *Kuby immunology*, W.H. Freeman, New York, 2013.
- [111] D.I. Godfrey, J. Kennedy, T. Suda, A. Zlotnik, (1993) A developmental pathway involving four phenotypically and functionally distinct subsets of CD3-CD4-CD8- triple-negative adult mouse thymocytes defined by CD44 and CD25 expression., *J. Immunol.* 150 4244–52. <http://www.ncbi.nlm.nih.gov/pubmed/8387091>.
- [112] R. Ceredig, T. Rolink, (2002) Opinion: A positive look at double-negative thymocytes, *Nat. Rev. Immunol.* 2 888–897. doi:10.1038/nri937.
- [113] J.C. Zúñiga-Pflücker, (2004) T-cell development made simple., *Nat. Rev. Immunol.* 4 67–72. doi:10.1038/nri1257.
- [114] A.M. Michie, J.C. Zúñiga-Pflücker, (2002) Regulation of thymocyte differentiation: pre-TCR signals and β -selection, *Semin. Immunol.* 14 311–323. doi:10.1016/S1044-5323(02)00064-7.
- [115] E. Hodges, (2003) Diagnostic role of tests for T cell receptor (TCR) genes, *J. Clin. Pathol.* 56 1–11. doi:10.1136/jcp.56.1.1.
- [116] M.M. Davis, P.J. Bjorkman, (1988) T-cell antigen receptor genes and T-cell recognition, *Nature.* 334 395–402. doi:10.1038/334395a0.
- [117] F. Radtke, H.R. MacDonald, F. Tacchini-Cottier, (2013) Regulation of innate and adaptive immunity by Notch, *Nat. Rev. Immunol.* 13 427–437. doi:10.1038/nri3445.
- [118] J.C. Pui, D. Allman, L. Xu, S. DeRocco, F.G. Karnell, S. Bakkour, et al., (1999) Notch1 Expression in Early Lymphopoiesis Influences B versus T Lineage Determination, *Immunity.* 11 299–308. doi:10.1016/S1074-7613(00)80105-3.
- [119] F. Radtke, A. Wilson, G. Stark, M. Bauer, J. van Meerwijk, H.R. MacDonald, et al., (1999) Deficient T Cell Fate Specification in Mice with an Induced Inactivation of Notch1, *Immunity.* 10 547–558. doi:10.1016/S1074-7613(00)80054-0.
- [120] A. Wilson, H.R. MacDonald, F. Radtke, (2001) Notch 1-Deficient Common Lymphoid Precursors Adopt a B Cell Fate in the Thymus, *J. Exp. Med.* 194 1003–1012. doi:10.1084/jem.194.7.1003.

- [121] H. Griesser, E. Champagne, D. Tkachuk, Y. Takihara, M. Lalande, E. Baillie, et al., (1988) The human T cell receptor alpha-delta locus: a physical map of the variable, joining and constant region genes., *Eur. J. Immunol.* 18 641–4. doi:10.1002/eji.1830180424.
- [122] R.K. Wilson, E. Lai, P. Concannon, R.K. Barth, L.E. Hood, (1988) Structure, Organization and Polymorphism of Murine and Human T-Cell Receptor α and β Chain Gene Families, *Immunol. Rev.* 101 149–172. doi:10.1111/j.1600-065X.1988.tb00736.x.
- [123] M.C. Haks, J.M. Lefebvre, J.P.H. Lauritsen, M. Carleton, M. Rhodes, T. Miyazaki, et al., (2005) Attenuation of $\gamma\delta$ TCR Signaling Efficiently Diverts Thymocytes to the $\alpha\beta$ Lineage, *Immunity.* 22 595–606. doi:10.1016/j.immuni.2005.04.003.
- [124] S.M. Hayes, L. Li, P.E. Love, (2005) TCR signal strength influences α beta/ γ delta lineage fate., *Immunity.* 22 583–93. doi:10.1016/j.immuni.2005.03.014.
- [125] J. Kang, A. Volkmann, D.H. Raulet, (2001) Evidence that γ delta versus α beta T cell fate determination is initiated independently of T cell receptor signaling., *J. Exp. Med.* 193 689–98.
<http://www.ncbi.nlm.nih.gov/pubmed/11257136><http://www.ncbi.nlm.nih.gov/pmc/articles/PMC2193423/pdf/001716.pdf>.
- [126] C.S. Hsieh, S.E. Macatonia, C.S. Tripp, S.F. Wolf, A. O’Garra, K.M. Murphy, (1993) Development of TH1 CD4+ T cells through IL-12 produced by Listeria-induced macrophages., *Science.* 260 547–9. doi:10.1126/science.8097338.
- [127] S.E. Macatonia, N.A. Hosken, M. Litton, P. Vieira, C.S. Hsieh, J.A. Culpepper, et al., (1995) Dendritic cells produce IL-12 and direct the development of Th1 cells from naive CD4+ T cells., *J. Immunol.* 154 5071–9. <http://www.ncbi.nlm.nih.gov/pubmed/7730613>.
- [128] S.L. Swain, A.D. Weinberg, M. English, G. Huston, (1990) IL-4 directs the development of Th2-like helper effectors., *J. Immunol.* 145 3796–806.
<http://www.ncbi.nlm.nih.gov/pubmed/2147202>.
- [129] N. Manel, D. Unutmaz, D.R. Littman, (2008) The differentiation of human TH-17 cells requires transforming growth factor- β and induction of the nuclear receptor ROR γ t, *Nat. Immunol.* 9 641–649. doi:10.1038/ni.1610.
- [130] E. V Acosta-Rodriguez, G. Napolitani, A. Lanzavecchia, F. Sallusto, (2007) Interleukins 1 β and 6 but not transforming growth factor- β are essential for the differentiation of interleukin 17-producing human T helper cells., *Nat. Immunol.* 8 942–949. doi:10.1038/ni1496.
- [131] R.I. Nurieva, Y. Chung, D. Hwang, X.O. Yang, H.S. Kang, L. Ma, et al., (2008) Generation of T Follicular Helper Cells Is Mediated by Interleukin-21 but Independent of T Helper 1, 2, or 17 Cell Lineages, *Immunity.* 29 138–149. doi:10.1016/j.immuni.2008.05.009.
- [132] S. Hori, T. Nomura, Saka, (2003) Control of Regulatory T Cell Development by the Transcription Factor Foxp3, *Science.* 299 1057–1061. doi:10.1126/science.1079490.
- [133] T.R. Mosmann, H. Cherwinski, M.W. Bond, M.A. Giedlin, R.L. Coffman, (1986) Two types of murine helper T cell clone. I. Definition according to profiles of lymphokine activities and secreted proteins., *J. Immunol.* 136 2348–57. <http://www.ncbi.nlm.nih.gov/pubmed/2419430>.

- [134] B. Oppmann, R. Lesley, B. Blom, J.C. Timans, Y. Xu, B. Hunte, et al., (2000) Novel p19 Protein Engages IL-12p40 to Form a Cytokine, IL-23, with Biological Activities Similar as Well as Distinct from IL-12, *Immunity*. 13 715–725. doi:10.1016/S1074-7613(00)00070-4.
- [135] D.J. Cua, J. Sherlock, Y. Chen, C. a Murphy, B. Joyce, B. Seymour, et al., (2003) Interleukin-23 rather than interleukin-12 is the critical cytokine for autoimmune inflammation of the brain., *Nature*. 421 744–8. doi:10.1038/nature01355.
- [136] C. a Murphy, C.L. Langrish, Y. Chen, W. Blumenschein, T. McClanahan, R. a Kastelein, et al., (2003) Divergent Pro- and Antiinflammatory Roles for IL-23 and IL-12 in Joint Autoimmune Inflammation, *J. Exp. Med.* 198 1951–1957. doi:10.1084/jem.20030896.
- [137] S. Aggarwal, N. Ghilardi, M.-H. Xie, F.J. de Sauvage, A.L. Gurney, (2003) Interleukin-23 Promotes a Distinct CD4 T Cell Activation State Characterized by the Production of Interleukin-17, *J. Biol. Chem.* 278 1910–1914. doi:10.1074/jbc.M207577200.
- [138] C.L. Langrish, Y. Chen, W.M. Blumenschein, J. Mattson, B. Basham, J.D. Sedgwick, et al., (2005) IL-23 drives a pathogenic T cell population that induces autoimmune inflammation., *J. Exp. Med.* 201 233–240. doi:10.1084/jem.20041257.
- [139] D.J. Campbell, M.A. Koch, (2011) Phenotypical and functional specialization of FOXP3+ regulatory T cells, *Nat. Rev. Immunol.* 11 119–130. doi:10.1038/nri2916.
- [140] T.M. Brusko, A.L. Putnam, J.A. Bluestone, (2008) Human regulatory T cells: role in autoimmune disease and therapeutic opportunities., *Immunol. Rev.* 223 371–90. doi:10.1111/j.1600-065X.2008.00637.x.
- [141] T.S. Davidson, R.J. DiPaolo, J. Andersson, E.M. Shevach, (2007) Cutting Edge: IL-2 is essential for TGF-beta-mediated induction of Foxp3+ T regulatory cells., *J. Immunol.* (Baltimore, Md 1950). 178 4022–4026. doi:178/7/4022 [pii].
- [142] J.D. Fontenot, J.P. Rasmussen, L.M. Williams, J.L. Dooley, A.G. Farr, A.Y. Rudensky, (2005) Regulatory T Cell Lineage Specification by the Forkhead Transcription Factor Foxp3, *Immunity*. 22 329–341. doi:10.1016/j.immuni.2005.01.016.
- [143] X. Ren, F. Ye, Z. Jiang, Y. Chu, S. Xiong, Y. Wang, (2007) Involvement of cellular death in TRAIL/DR5-dependent suppression induced by CD4(+)CD25(+) regulatory T cells., *Cell Death Differ.* 14 2076–84. doi:10.1038/sj.cdd.4402220.
- [144] T. Chinen, A.K. Kannan, A.G. Levine, X. Fan, U. Klein, Y. Zheng, et al., (2016) An essential role for the IL-2 receptor in Treg cell function, *Nat. Immunol.* 1–14. doi:10.1038/ni.3540.
- [145] D.A.A. Vignali, L.W. Collison, C.J. Workman, (2008) How regulatory T cells work., *Nat. Rev. Immunol.* 8 523–32. doi:10.1038/nri2343.
- [146] A.M. Thornton, E.M. Shevach, (1998) CD4+CD25+ immunoregulatory T cells suppress polyclonal T cell activation in vitro by inhibiting interleukin 2 production., *J. Exp. Med.* 188 287–96. <http://www.ncbi.nlm.nih.gov/pubmed/9670041>.
- [147] M. de la Rosa, S. Rutz, H. Dorninger, A. Scheffold, (2004) Interleukin-2 is essential for CD4+CD25+ regulatory T cell function, *Eur. J. Immunol.* 34 2480–2488. doi:10.1002/eji.200425274.
- [148] H. Qi, (2016) T follicular helper cells in space-time, *Nat. Rev. Immunol.*

doi:10.1038/nri.2016.94.

- [149] A. Vogelzang, H.M. McGuire, D. Yu, J. Sprent, C.R. Mackay, C. King, (2008) A Fundamental Role for Interleukin-21 in the Generation of T Follicular Helper Cells, *Immunity*. 29 127–137. doi:10.1016/j.immuni.2008.06.001.
- [150] F. Eddahri, S. Denanglaire, F. Bureau, R. Spolski, W.J. Leonard, O. Leo, et al., (2009) Interleukin-6/STAT3 signaling regulates the ability of naive T cells to acquire B-cell help capacities, *Blood*. 113 2426–2433. doi:10.1182/blood-2008-04-154682.
- [151] R.J. Johnston, A.C. Poholek, D. DiToro, I. Yusuf, D. Eto, B. Barnett, et al., (2009) Bcl6 and Blimp-1 Are Reciprocal and Antagonistic Regulators of T Follicular Helper Cell Differentiation, *Science* (80-.). 325 1006–1010. doi:10.1126/science.1175870.
- [152] R.I. Nurieva, Y. Chung, G.J. Martinez, X.O. Yang, S. Tanaka, T.D. Matskevitch, et al., (2009) Bcl6 Mediates the Development of T Follicular Helper Cells, *Science* (80-.). 325 1001–1005. doi:10.1126/science.1176676.
- [153] P. Schaerli, K. Willimann, A.B. Lang, M. Lipp, P. Loetscher, B. Moser, (2000) CXC chemokine receptor 5 expression defines follicular homing T cells with B cell helper function., *J. Exp. Med.* 192 1553–62.
<https://www.ncbi.nlm.nih.gov/pmc/articles/PMC2193097/pdf/001362.pdf>.
- [154] D. Breitfeld, L. Ohl, E. Kremmer, J. Ellwart, F. Sallusto, M. Lipp, et al., (2000) Follicular B Helper T Cells Express Cxc Chemokine Receptor 5, Localize to B Cell Follicles, and Support Immunoglobulin Production, *J. Exp. Med.* 192 1545–1552. doi:10.1084/jem.192.11.1545.
- [155] C.A. London, M.P. Lodge, A.K. Abbas, (2000) Functional responses and costimulator dependence of memory CD4+ T cells., *J. Immunol.* 164 265–72.
doi:10.4049/jimmunol.164.1.265.
- [156] F. Sallusto, J. Geginat, A. Lanzavecchia, (2004) Central memory and effector memory T cell subsets: function, generation, and maintenance., *Annu. Rev. Immunol.* 22 745–763.
doi:10.1146/annurev.immunol.22.012703.104702.
- [157] S.C. Jameson, D. Masopust, (2009) Diversity in T Cell Memory: An Embarrassment of Riches, *Immunity*. 31 859–871. doi:10.1016/j.immuni.2009.11.007.
- [158] L. Gattinoni, E. Lugli, Y. Ji, Z. Pos, C.M. Paulos, M.F. Quigley, et al., (2011) A human memory T cell subset with stem cell-like properties, *Nat. Med.* 17 1290–1297.
doi:10.1038/nm.2446.
- [159] N.P. Restifo, L. Gattinoni, (2013) Lineage relationship of effector and memory T cells, *Curr. Opin. Immunol.* 25 556–563. doi:10.1016/j.coi.2013.09.003.
- [160] M. Pepper, M.K. Jenkins, (2011) Origins of CD4+ effector and central memory T cells, *Nat. Immunol.* 131 467–471. doi:10.1038/ni.2038.
- [161] J.R. Lamb, B.J. Skidmore, N. Green, J.M. Chiller, M. Feldmann, (1983) Induction of tolerance in influenza virus-immune T lymphocyte clones with synthetic peptides of influenza hemagglutinin., *J. Exp. Med.* 157 1434–47. doi:10.1084/jem.157.5.1434.
- [162] H. Chen, T. Yang, L. Zhu, Y. Zhao, (2014) Cellular Metabolism on T-Cell Development and Function., *Int. Rev. Immunol.* 185 1–15. doi:10.3109/08830185.2014.902452.

- [163] S. Dimeloe, A.-V. Burgener, J. Graehler, C. Hess, (2016) T cell metabolism governing activation, proliferation and differentiation; a modular view, *Immunology*. 1–10. doi:10.1111/imm.12655.
- [164] M. Thurnher, G. Gruenbacher, (2015) T lymphocyte regulation by mevalonate metabolism, *Sci. Signal*. 8 re4-re4. doi:10.1126/scisignal.2005970.
- [165] H.L. Wieman, J.A. Wofford, J.C. Rathmell, (2007) Cytokine Stimulation Promotes Glucose Uptake via Phosphatidylinositol-3 Kinase/Akt Regulation of Glut1 Activity and Trafficking, *Mol. Biol. Cell*. 18 1437–1446. doi:10.1091/mbc.E06-07-0593.
- [166] G. Cretenet, I. Clerc, M. Matias, S. Loisel, M. Craveiro, L. Oburoglu, et al., (2016) Cell surface Glut1 levels distinguish human CD4 and CD8 T lymphocyte subsets with distinct effector functions, *Sci. Rep.* 6 24129. doi:10.1038/srep24129.
- [167] R.J. DeBerardinis, A. Mancuso, E. Daikhin, I. Nissim, M. Yudkoff, S. Wehrli, et al., (2007) Beyond aerobic glycolysis: transformed cells can engage in glutamine metabolism that exceeds the requirement for protein and nucleotide synthesis., *Proc. Natl. Acad. Sci. U. S. A.* 104 19345–50. doi:10.1073/pnas.0709747104.
- [168] T. Mishima, S. Toda, Y. Ando, T. Matsunaga, M. Inobe, (2014) Rapid proliferation of activated lymph node CD4+ T cells is achieved by greatly curtailing the duration of gap phases in cell cycle progression, *Cell. Mol. Biol. Lett.* 19. doi:10.2478/s11658-014-0219-z.
- [169] S.P. Evanko, S. Potter-Perigo, P.L. Bollyky, G.T. Nepom, T.N. Wight, (2012) Hyaluronan and versican in the control of human T-lymphocyte adhesion and migration, *Matrix Biol.* 31 90–100. doi:10.1016/j.matbio.2011.10.004.
- [170] C.A. de la Motte, V.C. Hascall, A. Calabro, B. Yen-Lieberman, S.A. Strong, (1999) Mononuclear Leukocytes Preferentially Bind via CD44 to Hyaluronan on Human Intestinal Mucosal Smooth Muscle Cells after Virus Infection or Treatment with Poly(I{middle dot}C), *J. Biol. Chem.* 274 30747–30755. doi:10.1074/jbc.274.43.30747.
- [171] Z. Bai, H. Hayasaka, M. Kobayashi, W. Li, Z. Guo, M.H. Jang, et al., (2009) CXC chemokine ligand 12 promotes CCR7-dependent naive T cell trafficking to lymph nodes and Peyer’s patches., *J. Immunol.* 182 1287–95. <http://www.ncbi.nlm.nih.gov/pubmed/19155474>.
- [172] R. Yoshida, (1997) Molecular Cloning of a Novel Human CC Chemokine EBI1-ligand Chemokine That Is a Specific Functional Ligand for EBI1, CCR7, *J. Biol. Chem.* 272 13803–13809. doi:10.1074/jbc.272.21.13803.
- [173] K.M. Veerman, M.J. Williams, K. Uchimura, M.S. Singer, J.S. Merzaban, S. Naus, et al., (2007) Interaction of the selectin ligand PSGL-1 with chemokines CCL21 and CCL19 facilitates efficient homing of T cells to secondary lymphoid organs, *Nat. Immunol.* 8 532–539. doi:10.1038/ni1456.
- [174] C.S. Garris, V.A. Blaho, T. Hla, M.H. Han, (2014) Sphingosine-1-phosphate receptor 1 signalling in T cells: trafficking and beyond, *Immunology*. 142 347–353. doi:10.1111/imm.12272.
- [175] A. Caruso, S. Licenziati, M. Corulli, A.D. Canaris, M.A. De Francesco, S. Fiorentini, et al., (1997) Flow cytometric analysis of activation markers on stimulated T cells and their

- correlation with cell proliferation, *Cytometry*. 27 71–76. doi:10.1002/(SICI)1097-0320(19970101)27:1<71::AID-CYTO9>3.0.CO;2-O.
- [176] J. Yoder, C. Pham, Y.M. Iizuka, O. Kanagawa, S.K. Liu, J. McGlade, et al., (2001) Requirement for the SLP-76 adaptor GADS in T cell development., *Science*. 291 1987–91. doi:10.1126/science.1057176.
- [177] S.K. Liu, D.M. Berry, C.J. McGlade, (2001) The role of Gads in hematopoietic cell signalling., *Oncogene*. 20 6284–90. doi:10.1038/sj.onc.1204771.
- [178] F. Macian, (2005) NFAT proteins: key regulators of T-cell development and function., *Nat. Rev. Immunol.* 5 472–84. doi:10.1038/nri1632.
- [179] P.G. Hogan, P.G. Hogan, L. Chen, L. Chen, (2003) Transcriptional regulation by calcium, calcineurin, NFAT. *Genes Dev.* 17 2205–2232. doi:10.1101/gad.1102703.GENES.
- [180] S. Il Kim, M.E. Choi, (2012) TGF- β -activated kinase-1: New insights into the mechanism of TGF- β signaling and kidney disease, *Kidney Res. Clin. Pract.* 31 94–105. doi:10.1016/j.krcp.2012.04.322.
- [181] R. Fagerlund, L. Kinnunen, M. Köhler, I. Julkunen, K. Melén, (2005) NF- κ B is transported into the nucleus by importin α 3 and importin α 4., *J. Biol. Chem.* 280 15942–51. doi:10.1074/jbc.M500814200.
- [182] M. Karin, (1995) The Regulation of AP-1 Activity by Mitogen-activated Protein Kinases, *J. Biol. Chem.* 270 16483–16486. doi:10.1074/jbc.270.28.16483.
- [183] S. Lu, H. Jang, J. Zhang, R. Nussinov, (2016) Inhibitors of Ras-SOS Interactions., *ChemMedChem*. 11 814–21. doi:10.1002/cmdc.201500481.
- [184] M. Rincón, G. Pedraza-Alva, (2003) JNK and p38 MAP kinases in CD4+ and CD8+ T cells., *Immunol. Rev.* 192 131–142. doi:10.1034/j.1600-065X.2003.00019.x.
- [185] R.J. Davis, (2000) Signal Transduction by the JNK Group of MAP Kinases, *Cell*. 103 239–252. doi:10.1016/S0092-8674(00)00116-1.
- [186] E. Shaulian, M. Karin, (2001) AP-1 in cell proliferation and survival, *Oncogene*. 20 2390–2400. doi:10.1038/sj.onc.1204383.
- [187] P.H. Schafer, L. Wang, S. a Wadsworth, J.E. Davis, J.J. Siekierka, (1999) T cell activation signals up-regulate p38 mitogen-activated protein kinase activity and induce TNF- α production in a manner distinct from LPS activation of monocytes., *J. Immunol.* 162 659–668. <http://www.jimmunol.org/content/162/2/659.full.pdf>.
- [188] J. Zhang, K. V Salojin, J.-X. Gao, M.J. Cameron, I. Bergerot, T.L. Delovitch, (1999) p38 mitogen-activated protein kinase mediates signal integration of TCR/CD28 costimulation in primary murine T cells, *J. Immunol.* <http://www.jimmunol.org/content/162/7/3819.short>.
- [189] C.E. Rudd, (2005) MAPK p38 : alternative and nonstressful in T cells, 6 368–370. doi:10.1038/ni0405-368.
- [190] J.M. Salvador, P.R. Mittelstadt, T. Guszczynski, T.D. Copeland, H. Yamaguchi, E. Appella, et al., (2005) Alternative p38 activation pathway mediated by T cell receptor-proximal tyrosine kinases, *Nat. Immunol.* 6 390–395. doi:10.1038/ni1177.
- [191] C. Zer, G. Sachs, J.M. Shin, (2007) Identification of genomic targets downstream of p38

- mitogen-activated protein kinase pathway mediating tumor necrosis factor-alpha signaling., *Physiol. Genomics*. 31 343–51. doi:10.1152/physiolgenomics.00080.2007.
- [192] S.G. Ward, (1996) CD28: a signalling perspective., *Biochem. J.* 318 (Pt 2 361–77. <http://www.ncbi.nlm.nih.gov/pubmed/8809021>.
- [193] K. Higo, M. Oda, H. Morii, J. Takahashi, Y. Harada, S. Ogawa, et al., (2014) Quantitative analysis by surface plasmon resonance of CD28 interaction with cytoplasmic adaptor molecules Grb2, Gads and p85 PI3K., *Immunol. Invest.* 43 1–14. doi:10.3109/08820139.2013.875039.
- [194] S.G. Ward, D.A. Cantrell, (2001) Phosphoinositide 3-kinases in T lymphocyte activation, *Curr. Opin. Immunol.* 13 332–338. doi:10.1016/S0952-7915(00)00223-5.
- [195] K. Okkenhaug, B. Vanhaesebroeck, (2003) PI3K in lymphocyte development, differentiation and activation., *Nat. Rev. Immunol.* 3 317–30. doi:10.1038/nri1056.
- [196] N. Hay, N. Sonenberg, (2004) Upstream and downstream of mTOR, *Genes Dev.* 18 1926–1945. doi:<http://www.genesdev.org/cgi/doi/10.1101/gad.1212704>.
- [197] B. Marinari, A. Costanzo, A. Viola, F. Michel, G. Mangino, O. Acuto, et al., (2002) Vav cooperates with CD28 to induce NF-kappaB activation via a pathway involving Rac-1 and mitogen-activated kinase kinase 1., *Eur. J. Immunol.* 32 447–56. <http://www.ncbi.nlm.nih.gov/pubmed/11813163>.
- [198] C.E. Rudd, M. Raab, (2003) Independent CD28 signaling via VAV and SLP-76: a model for in trans costimulation., *Immunol. Rev.* 192 32–41. <http://www.ncbi.nlm.nih.gov/pubmed/12670393>.
- [199] G.L. Glish, R.W. Vachet, (2003) The basics of mass spectrometry in the twenty-first century., *Nat. Rev. Drug Discov.* 2 140–150. doi:10.1038/nrd1011.
- [200] E. de Hoffmann, V. Stroobant, *Mass spectrometry : principles and applications*, J. Wiley, Chichester, West Sussex, England; Hoboken, NJ, 2007.
- [201] J.B. Fenn, M. Mann, C.K. Meng, S.F. Wong, C.M. Whitehouse, (1990) Electrospray ionization-principles and practice, *Mass Spectrom. Rev.* 9 37–70. doi:10.1002/mas.1280090103.
- [202] M. Yamashita, J.B. Fenn, (1984) Electrospray ion source. Another variation on the free-jet theme, *J Phys.Chem.* 88 4451–4459. doi:10.1021/j150664a002.
- [203] R.B. Cole, *Electrospray and MALDI mass spectrometry*, 2010. doi:papers3://publication/uuid/D28E8E63-8ED6-496F-A5DD-CC323F36D3A4.
- [204] Thermo Scientific, (2009) *Ion Max and Ion Max-S API Source Hardware manual*, 74. <http://tools.thermofisher.com/content/sfs/manuals/Ion-Max-Ion-Max-S-Hardware.pdf>.
- [205] D.J. Douglas, A.J. Frank, D. Mao, (2005) Linear ion traps in mass spectrometry, *Mass Spectrom. Rev.* 24 1–29. doi:10.1002/mas.20004.
- [206] J.C. Schwartz, M.W. Senko, J.E.P. Syka, (2002) A two-dimensional quadrupole ion trap mass spectrometer., *J. Am. Soc. Mass Spectrom.* 13 659–669. doi:10.1016/S1044-0305(02)00384-7.
- [207] J.W. Hager, (2002) A new linear ion trap mass spectrometer, *Rapid Commun. Mass*

- Spectrom. 16 512–526. doi:10.1002/rcm.607.
- [208] J. Gross, *Mass spectrometry : a textbook*, Springer, Berlin; New York, 2004.
- [209] Thermo Fisher Scientific, (2011) LTQ Series Hardware Manual Rev C.,
<https://tools.thermofisher.com/content/sfs/manuals/LTQ-Series-Start.pdf>.
- [210] Thermo Fisher Scientific, (2011) Orbitrap Elite Hardware Manual.,
<http://planetorbitrap.com/orbitrap-elite>.
- [211] A. Makarov, (2000) Electrostatic axially harmonic orbital trapping: A high-performance technique of mass analysis, *Anal. Chem.* 72 1156–1162. doi:10.1021/ac991131p.
- [212] Q. Hu, R.J. Noll, H. Li, A. Makarov, M. Hardman, R.G. Cooks, (2005) The Orbitrap: A new mass spectrometer, *J. Mass Spectrom.* 40 430–443. doi:10.1002/jms.856.
- [213] T.M. Peters, J.C. Williams, J.H.T. Bates, *The Fourier transform in biomedical engineering*, Birkhouser, Boston, 1998.
- [214] M. Scigelova, M. Hornshaw, A. Giannakopoulos, A. Makarov, (2011) Fourier transform mass spectrometry., *Mol. Cell. Proteomics.* 10 M111.009431. doi:10.1074/mcp.M111.009431.
- [215] M. Axelson, B. Mörk, J. Sjövall, (1988) Occurrence of 3 beta-hydroxy-5-cholestenoic acid, 3 beta,7 alpha-dihydroxy-5-cholestenoic acid, and 7 alpha-hydroxy-3-oxo-4-cholestenoic acid as normal constituents in human blood., *J. Lipid Res.* 29 629–41.
<http://www.ncbi.nlm.nih.gov/pubmed/3411238>.
- [216] D. Lütjohann, O. Breuer, G. Ahlborg, I. Nennesmo, a Sidén, U. Diczfalusy, et al., (1996) Cholesterol homeostasis in human brain: evidence for an age-dependent flux of 24S-hydroxycholesterol from the brain into the circulation., *Proc. Natl. Acad. Sci. U. S. A.* 93 9799–9804. doi:10.1073/pnas.93.18.9799.
- [217] C.J.W. Brooks, W.J. Cole, T.D.V. Lawrie, J. MacLachlan, J.H. Borthwick, G.M. Barrett, (1983) Selective reactions in the analytical characterisation of steroids by gas chromatography—Mass spectrometry, *J. Steroid Biochem.* 19 189–201. doi:10.1016/S0022-4731(83)80025-9.
- [218] S. Dzeletovic, O. Breuer, E. Lund, U. Diczfalusy, (1995) Determination of Cholesterol Oxidation Products in Human Plasma by Isotope Dilution-Mass Spectrometry, *Anal. Biochem.* 225 73–80. doi:10.1006/abio.1995.1110.
- [219] J.I. Pedersen, Y. Hagenfeldt, I. Björkhem, (1988) Assay and properties of 25-hydroxyvitamin D 3 23-hydroxylase. Evidence that 23,25-dihydroxyvitamin D 3 is a major metabolite in 1,25-dihydroxyvitamin D 3 -treated or fasted guinea pigs, *Biochem. J.* 250 527–532.
doi:10.1042/bj2500527.
- [220] C. Schummer, O. Delhomme, B.M.R. Appenzeller, R. Wennig, M. Millet, (2009) Comparison of MTBSTFA and BSTFA in derivatization reactions of polar compounds prior to GC/MS analysis, *Talanta.* 77 1473–1482. doi:10.1016/j.talanta.2008.09.043.
- [221] C. Birkemeyer, A. Kolasa, J. Kopka, (2003) Comprehensive chemical derivatization for gas chromatography-mass spectrometry-based multi-targeted profiling of the major phytohormones, *J. Chromatogr. A.* 993 89–102. doi:10.1016/S0021-9673(03)00356-X.
- [222] J.M. Halket, D. Waterman, A.M. Przyborowska, R.K.P. Patel, P.D. Fraser, P.M. Bramley,

- (2005) Chemical derivatization and mass spectral libraries in metabolic profiling by GC/MS and LC/MS/MS, *J. Exp. Bot.* 56 219–243. doi:10.1093/jxb/eri069.
- [223] J.G. McDonald, D.D. Smith, a. R. Stiles, D.W. Russell, (2012) A comprehensive method for extraction and quantitative analysis of sterols and secosteroids from human plasma, *J. Lipid Res.* 53 1399–1409. doi:10.1194/jlr.D022285.
- [224] J.G. McDonald, B.M. Thompson, E.C. McCrum, D.W. Russell, (2007) Extraction and Analysis of Sterols in Biological Matrices by High Performance Liquid Chromatography Electrospray Ionization Mass Spectrometry, *Methods Enzymol.* 432 145–170. doi:10.1016/S0076-6879(07)32006-5.
- [225] E.M. Thurman, M.S. Mills, (1998) Solid-phase extraction : principles and practice,.
- [226] N.J.K. Simpson, (2000) Solid-phase extraction : principles, techniques, and applications, .
http://www.crcnetbase.com/isbn/9781420056242.
- [227] P.W. Majors, R.E. Carr, (2008) Glossary of HPLC/LC Separation Terms, *LCGC Mag.* 118–168. <http://www.chromatographyonline.com/glossary-hplclc-separation-terms> (accessed October 18, 2016).
- [228] R. Sandhoff, B. Brügger, D. Jeckel, W.D. Lehmann, F.T. Wieland, (1999) Determination of cholesterol at the low picomole level by nano-electrospray ionization tandem mass spectrometry, *J. Lipid Res.* 40 126–132.
- [229] R.B. Duff, (1949) Carbohydrate sulphuric esters. Part V. The demonstration of Walden inversion on hydrolysis of barium 1 : 6-anhydro- β -galactose 2-sulphate, *J. Chem. Soc.* 1597–1600. doi:10.1039/JR9490001597.
- [230] H. Cheng, X. Jiang, X. Han, (2007) Alterations in lipid homeostasis of mouse dorsal root ganglia induced by apolipoprotein E deficiency: A shotgun lipidomics study, *J. Neurochem.* 101 57–76. doi:10.1111/j.1471-4159.2006.04342.x.
- [231] S. Liu, J. Sjövall, W.J. Griffiths, (2003) Neurosteroids in Rat Brain: Extraction, Isolation, and Analysis by Nanoscale Liquid Chromatography-Electrospray Mass Spectrometry, *Anal. Chem.* 75 5835–5846. doi:10.1021/ac0346297.
- [232] S. Liu, J. Sjövall, W.J. Griffiths, (2000) Analysis of oxosteroids by nano-electrospray mass spectrometry of their oximes, *Rapid Commun. Mass Spectrom.* 14 390–400. doi:10.1002/(SICI)1097-0231(20000331)14:6<390::AID-RCM882>3.0.CO;2-7.
- [233] R. Sidhu, H. Jiang, N.Y. Farhat, N. Carrillo-Carrasco, M. Woolery, E. Ottinger, et al., (2015) A validated LC-MS/MS assay for quantification of 24(S)-hydroxycholesterol in plasma and cerebrospinal fluid, *J. Lipid Res.* 56 1222–1233. doi:10.1194/jlr.D058487.
- [234] X. Jiang, D.S. Ory, X. Han, (2007) Characterization of oxysterols by electrospray ionization tandem mass spectrometry after one-step derivatization with dimethylglycine, *Rapid Commun. Mass Spectrom.* 21 141–152. doi:10.1002/rcm.2820.
- [235] K. Karu, M. Hornshaw, G. Woffendin, K. Bodin, M. Hamberg, G. Alvelius, et al., (2007) Liquid chromatography-mass spectrometry utilizing multi-stage fragmentation for the identification of oxysterols., *J. Lipid Res.* 48 976–987. doi:10.1194/jlr.M600497-JLR200.
- [236] H. Roberg-Larsen, K. Lund, T. Vehus, N. Solberg, C. Vesterdal, D. Misaghian, et al., (2014)

- Highly automated nano-LC/MS-based approach for thousand cell-scale quantification of side chain-hydroxylated oxysterols., *J. Lipid Res.* 55 1531–1536. doi:10.1194/jlr.D048801.
- [237] W.J. Griffiths, P.J. Crick, Y. Wang, M. Ogundare, K. Tuschl, A. a. Morris, et al., (2013) Analytical strategies for characterization of oxysterol lipidomes: Liver X receptor ligands in plasma, *Free Radic. Biol. Med.* 59 69–84. doi:10.1016/j.freeradbiomed.2012.07.027.
- [238] M. Ogundare, S. Theofilopoulos, A. Lockhart, L.J. Hall, E. Arenas, J. Sjövall, et al., (2010) Cerebrospinal fluid steroidomics: Are bioactive bile acids present in brain?, *J. Biol. Chem.* 285 4666–4679. doi:10.1074/jbc.M109.086678.
- [239] W.J. Griffiths, M. Ogundare, A. Meljon, Y. Wang, (2012) Mass Spectrometry for Steroid Analysis, *Mass Spectrom. Handb.* 297–337. doi:10.1002/9781118180730.ch14.
- [240] A. Meljon, S. Theofilopoulos, C.H.L. Shackleton, G.L. Watson, N.B. Javitt, H.-J. Knölker, et al., (2012) Analysis of bioactive oxysterols in newborn mouse brain by LC/MS., *J. Lipid Res.* 53 2469–83. doi:10.1194/jlr.D028233.
- [241] Y. Wang, K. Karu, A. Meljon, J. Turton, J.L. Yau, J.R. Seckl, et al., (2014) 24S,25-Epoxycholesterol in mouse and rat brain, *Biochem. Biophys. Res. Commun.* 449 229–234. doi:10.1016/j.bbrc.2014.05.012.
- [242] W.J. Griffiths, Y. Wang, G. Alvelius, S. Liu, K. Bodin, J. Sjövall, (2006) Analysis of oxysterols by electrospray tandem mass spectrometry, *J. Am. Soc. Mass Spectrom.* 17 341–362. doi:10.1016/j.jasms.2005.10.012.
- [243] Y. Wang, M. Hornshaw, G. Alvelius, K. Bodin, S. Liu, J. Sjövall, et al., (2006) Matrix-assisted laser desorption/ionization high-energy collision-induced dissociation of steroids: Analysis of oxysterols in rat brain, *Anal. Chem.* 78 164–173. doi:10.1021/ac051461b.
- [244] I. Burkard, K.M. Rentsch, A. von Eckardstein, (2004) Determination of 24S- and 27-hydroxycholesterol in plasma by high-performance liquid chromatography-mass spectrometry., *J. Lipid Res.* 45 776–81. doi:10.1194/jlr.D300036-JLR200.
- [245] A.E. DeBarber, D. Lütjohann, L. Merckens, R.D. Steiner, (2008) Liquid chromatography-tandem mass spectrometry determination of plasma 24S-hydroxycholesterol with chromatographic separation of 25-hydroxycholesterol, *Anal. Biochem.* 381 151–153. doi:10.1016/j.ab.2008.05.037.
- [246] E. Razzazi-Fazeli, S. Kleineisen, W. Luf, (2000) Determination of cholesterol oxides in processed food using high-performance liquid chromatography-mass spectrometry with atmospheric pressure chemical ionisation, *J. Chromatogr. A.* 896 321–334. doi:10.1016/S0021-9673(00)00719-6.
- [247] K. Raith, C. Brenner, H. Farwanah, G. Müller, K. Eder, R.H.H. Neubert, (2005) A new LC/APCI-MS method for the determination of cholesterol oxidation products in food, *J. Chromatogr. A.* 1067 207–211. doi:10.1016/j.chroma.2004.12.053.

CHAPTER 2: Materials and Methods

2.1. Cell Culture

2.1.1. Cell Culture Materials

2.1.1.1. Culture media and modifications.

Majority of the human CD4⁺ T cell cultures were cultured in X-Vivo-20 Chemically Defined, Serum-free Hematopoietic Cell Medium from Lonza (Cat.no. LZBE04-448Q Scientific Laboratory Supplies, Nottingham UK). X-Vivo-20 media was further supplemented prior to use with 2mM Glutamine, 10 Units/mL Penicillin, and 0.1 mg/mL Streptomycin from Sigma-Aldrich (Cat.no. G1146 Dorset, UK) unless otherwise stated. Other T cell cultures used either Gibco RPMI 1640 Media (Cat.no. 31870-025 Life Technologies, Paisley UK), defined as Serum Free Media (SF Media), or an in-house delipidated Media (DL Media) which was Gibco RPMI 1640 modified with 10% Heat inactivated Charcoal-stripped FBS, both from Invitrogen (Cat.no. 12676-011 Life Technologies). Heat inactivation of the charcoal-stripped FBS was done by heating a 50mL aliquot at 56°C water bath for 30 minutes with regular mixing. Both SF media and DL media were additionally supplemented with 50µM β-mercaptoethanol, 2mM Glutamine, 10 Units/mL Penicillin, and 0.1 mg/mL Streptomycin. THP-1 monocytic cell lines were maintained in Full Media which was 10% Heat-inactivated FBS (Cat.no. 10106-169 Life Technologies) in RPMI 1640 supplied with 2mM Glutamine, 10 Units/mL Penicillin, and 0.1 mg/mL Streptomycin.

2.1.1.2. Cell isolation kits and buffers.

T lymphocytes used in this work were obtained from human peripheral mononuclear cells (PBMCs) which were isolated using magnetic-activated cell sorting (MACS®) technology invented by Miltenyi Biotec. Depending on the cells of interest, different kits were used with an autoMACS® separator: CD4⁺ T Cell Isolation Kit, human (Cat.no.130-096-533); Naïve CD4⁺ T Cell Isolation Kit II, human (Cat.no. 130-094-131); CD45RA MicroBeads, human (Cat.no. 130-045-901). Other autoMACS® separator consumables such as columns (Cat.no. 130-021-101), Running Buffers (Cat.no. 130-091-221) and Rinsing Solutions (Cat.no. 130-091-222) were all bought

from Miltenyi Biotec (Surrey UK). Buffers required for isolation were sterile-filtered 0.5% BSA in PBS prepared in house. Syringe PVDF membrane 0.22µm filters were purchased from Sartorius (Surrey UK), Bovine Serum Albumin (BSA) was purchased from Labtech (Sussex UK) (Cat.no. PM-T1725) and Phosphate Buffered Saline (PBS) 1X without Ca²⁺/Mg²⁺ from Lonza (Cat.no. LZBE17-516F).

2.1.1.3. Culture cytokines, activators and inhibitors.

T cells were studied *in vitro* in different culture conditions using reagents and kits listed in Table 2.1.

Table 2.1. List of cell culture reagents, cytokines and kits

Reagent	Catalogue Number	Manufacturer	Additional information
T Cell Activation/Expansion Kit, human	130-091-441	Miltenyi Biotec (Surrey UK)	Only prepared anti-CD3 and anti-CD28 loaded beads
Phorbol 12-myristate 13-acetate (PMA)	P1585	Sigma-Aldrich (Dorset UK)	Reconstituted in sterile DMSO
Ionomycin, calcium salt	I0634	Sigma-Aldrich (Dorset UK)	Reconstituted in sterile DMSO
Simvastatin	S6196	Sigma-Aldrich (Dorset UK)	Converted to β-hydroxy acid form in 10% EtOH
Gö6983	G1918	Sigma-Aldrich (Dorset UK)	PKC inhibitor
BAY-11-7082	196870	Merck Millipore (Nottingham UK)	NF-κB inhibitor
SB-203580	559389	Merck Millipore (Nottingham UK)	p38 MAPK inhibitor
U0126	662005	Merck Millipore (Nottingham UK)	MEK1/2 inhibitor
Rapamycin	553210	Merck Millipore (Nottingham UK)	mTORC1 inhibitor
LY294002	19-142	Merck Millipore (Nottingham UK)	PI3K inhibitor
Ku-63794	475990	Merck Millipore (Nottingham UK)	dual mTORC inhibitor
Human Interleukin-2	14-8029-63	eBioscience (Hatfield UK)	in 40mM Sodium Acetate, 0.2M NaCl, pH 5 1% BSA (sterile filtered) buffer
Human Interleukin-1β	14-8018-62	eBioscience (Hatfield UK)	in 150mM NaCl, 1% BSA in PBS (sterile filtered) buffer
Human Interleukin-21	14-8219-62	eBioscience (Hatfield UK)	20mM Sodium Phosphate, 0.6M NaCl, pH 7.2, 1% BSA (sterile filtered) buffer
Human Interleukin-23	14-8239-63	eBioscience (Hatfield UK)	20mM Sodium Phosphate, 0.2M NaCl, pH 6, 0.5% BSA (sterile filtered) buffer

Human Interferon Gamma	14-8319-80	eBioscience (Hatfield UK)	20 mM phosphate, 400 mM NaCl, pH 7.2, 0.5% BSA. (sterile filtered)
Human Interleukin-6	206-IL/CF	R&D Systems (Abingdon UK)	in PBS
Human Tumour growth factor- β	240-B-002	R&D Systems (Abingdon UK)	in 1mg/mL BSA 4mM HCl (sterile filtered)buffer
Anti-human Interferon- γ	16-7318-85	eBioscience (Hatfield UK)	in PBS
Anti-human Interleukin-4	16-7048-85	eBioscience (Hatfield UK)	in PBS
GolgiStop™ Protein Transport inhibitor (Monensin)	554724	BD Biosciences (Oxford UK)	
Protein Transport Inhibitor Cocktail (500x)	00-4980-93	eBioscience (Hatfield UK)	
Dimethyl Sulphoxide (Hybri-Max®)	D2650	Sigma-Aldrich (Dorset UK)	Sterile for cell culture use
Phosphate Buffered Saline 1X without Ca ²⁺ /Mg ²⁺ (PBS)	BE17-516F	Lonza (Slough UK)	Sterile for cell culture use

2.1.2. Human Blood Donors and Ethical approval for human studies

Peripheral venous blood was taken from the median cubital vein of healthy human donors recruited into the study “Regulation of immune function by oxysterols” by the Clinical Research Facility at Swansea University. All donors had given informed written consent and the ethical approval obtained from Wales Research Ethics Committee 6 (13/WA/0190). All donors were either Swansea University staff or students aged between 18 to 65 years old. A maximum volume of 108mL of drawn blood was collected per donor in 9mL Lithium Heparin tubes (Cat.no. 455084 Greiner Bio-one Stonehouse UK) and was taken to the lab for processing within 1 hour.

2.1.3. Human Peripheral Blood Mononuclear Cell Isolation

Drawn blood was taken and processed in a Class 2 Biosafety cabinet under sterile conditions at the primary tissue culture lab 2nd floor, Institute of Life Sciences 1, Swansea University. Peripheral blood mononuclear cells were isolated from whole blood using Density Gradient Centrifugation using 50mL Leucosep™ tubes (Cat.no. 227290 Griener Bio-One Stonehouse UK) and Histopaque®-1077 Hybri-Max™ (Cat.no H8889 Sigma-Aldrich). Briefly, pre-warmed 15mL of Histopaque was first pipetted into a 50mL Leucosep™ tube and centrifuged at 1000 xg RT for 30 seconds to move the solution to the bottom of the porous filter ready for separation. Next, 12mL of anti-coagulated blood was diluted by adding 20mL pre-warmed PBS and mixed well. Diluted blood was carefully layered on top of the porous membrane of the Leucosep tube. This process was repeated for all blood collected. Filled Leucosep tubes were centrifuged at 800 xg RT for 15 minutes with no brake to separate blood components based on their relative density to histopaque. The top plasma layer was first pipetted out and discarded leaving about 0.5 cm above the buffy coat layer. The buffy coat layer, containing mostly peripheral blood mononuclear cells (PBMCs), was completely pipetted and transferred into a new 50mL tube. The suspension of cells were washed by adding pre-warmed PBS up to 50mL and centrifuged at 250 xg RT for 10 minutes. PBMCs were further washed twice by resuspension of cells with 25mL. Cell pellets from other tubes were combined, resuspended in 0.5% BSA in PBS and mixed well by pipetting and the total volume noted. An aliquot of cells were taken for cell counting with Trypan Blue.

2.1.4. Human T Lymphocyte Isolation by MACS®

When a specific population of T cells were required, an appropriate MACS kit was used with the washed PBMCs suspended in 0.5% BSA in PBS buffer using manufacturer's instructions on an autoMACS® separator. Pre-cooled buffers and beads added were for maximum of 10^7 cells. Volumes were scaled up accordingly for higher cell numbers. Cells were incubated and kept at 2 to 8°C fridge or ice bath.

2.1.4.1. MACS® Depletion protocol for isolating naïve CD4⁺ T cells.

Naïve T cells were isolated using Naïve CD4⁺ T Cell Isolation Kit II, human following manufacturer's instructions. Briefly, counted cells suspended in 0.5% BSA in PBS buffer was pelleted at 515 xg 4°C for 10 minutes then resuspended in 40µL buffer per 10^7 cells. Then, 10µL of Naive CD4⁺ T Cell Biotin-Antibody Cocktail II was added per 10^7 cells, mixed well and incubated for 5 minutes in the fridge. Afterwards, 30µL of buffer per 10^7 cells was added to the cell suspension plus 20µL per 10^7 cells of Naive CD4⁺ T Cell MicroBead Cocktail II. Suspension was mixed well by pipetting and incubated for a further 10 minutes in the fridge. Cells were then separated magnetically on an autoMACS® separator using the “Depletes” programs. Untouched naïve CD4⁺ T cells were collected on the [neg1] port and the positive fraction on the pos1 port. Both fractions were pelleted at 515 xg 4°C 10 minutes then resuspended at the desired concentration in culture media. The procedure magnetically labels and immobilises CD45RO⁺, CD8⁺, CD14⁺, CD15⁺, CD16⁺, CD19⁺, CD25⁺, CD34⁺, CD36⁺, CD56⁺, CD123⁺, TCRγ/δ⁺, HLA-DR⁺, and CD235a⁺ cells in the magnetic column leaving CD4⁺ and CD45RA⁺ cells as unlabelled to flow through.

2.1.4.2. MACS® Depletion protocol for isolating total CD4⁺ T cells.

Total T cells were isolated using CD4⁺ T Cell Isolation Kit, human following manufacturer's instructions. Briefly, counted cells suspended in 0.5% BSA in PBS buffer was pelleted at 515 xg 4°C for 10 minutes then resuspended in 40µL buffer per 10^7 cells. Then, 10µL of CD4⁺ T Cell Biotin-Antibody Cocktail was added per 10^7 cells, mixed well and incubated for 5 minutes in the fridge. Afterwards, 30µL of buffer per 10^7 cells was added to the cell suspension plus 20µL per 10^7 cells of CD4⁺ T Cell MicroBead Cocktail. Suspension was mixed well by pipetting and incubated for a further 10 minutes in the fridge. Cells were then separated magnetically on an

autoMACS® separator using the “Depletes” programs. Untouched total CD4⁺ T cells were collected on the neg1 port and the positive fraction on the pos1 port. Both fractions were pelleted at 515 xg 4°C 10 minutes then resuspended at the desired concentration and X-Vivo-20 culture media. The procedure magnetically labels and immobilises CD8⁺, CD14⁺, CD15⁺, CD16⁺, CD19⁺, CD36⁺, CD56⁺, CD123⁺, TCRγ/δ⁺, and CD235a⁺ cells in the magnetic column leaving only CD4⁺ cells as unlabelled to flow through.

2.1.4.3. MACS® protocol for separating naïve and memory from total CD4⁺ T cells.

In some experiments requiring memory CD4⁺ T cells, a combination of two MACS kits were used. One method used the protocols from *section 2.1.4.2* followed by the protocol in *section 2.1.4.1*. Using this method, naïve CD45RO^{-ve} cells were collected in the neg1 port and CD45RO^{+ve} memory cells collected in the pos1 port. The second method used a third, CD45RA Microbeads, human kit. Firstly, total CD4⁺ T cells were isolated from PMBC as in *section 2.1.4.2*. Then, without resuspension with culture media, cells were washed and further separated using CD45RA Microbeads, human. Briefly, counted total CD4⁺ T cells suspended in 0.5% BSA in PBS buffer was pelleted at 515 xg 4°C for 10 minutes then resuspended in 80µL buffer per 10⁷ cells plus 20µL CD45RA MicroBeads per 10⁷ cells. Microbeads and cells were mixed well and incubated in the fridge for 15 minutes. Labelled cells were washed by the addition of 2mL of buffer and centrifuged at 515 xg 4°C 10 minutes and supernatant removed. Pelleted cells were resuspended in 500µL of buffer per 10⁸ cells and separated on an autoMACS® using the “Depletes” program. Naïve CD45RA^{+ve} cells were collected in the pos1 port and the memory CD45RA^{-ve} fraction in the neg1 port.

2.1.4.4. Pre-depletion of PBMCs of CD14⁺ cells.

When indicated, some PMBC isolated after density gradient separation were first depleted of CD14⁺ cells using, CD14 microbead kit before proceeding to naïve CD4 T cell isolation. This ensured least possible CD14⁺ presence in CD4⁺ cell isolates and also provide a pure CD14⁺ population for other studies.

2.1.5. Cell Cryopreservation, Storage and Recovery

Surplus cells and cells to be kept for long term storage were first counted then washed with pre-warmed PBS and pelleted at 515 xg RT 10 minutes. Next, cells were resuspended in Heat-inactivated FBS supplied with 10% DMSO at concentration of 10×10^6 cells per mL at RT. Cell suspensions were transferred and sealed in 2ml Cryo.S™ cryovials (Cat.no. 122263 Greiner Bio-one, Stonehouse UK) and pre-incubated in an isopropanol-lined freezing container at RT placed in a -80°C freezer overnight to provide a $-1^\circ\text{C}/\text{min}$ cooling rate. Next day, frozen cells were directly transferred into liquid-phase on a nitrogen cryogenic dewar.

For thawing cells, cryovials were briefly submerged into a 37°C water bath (1 to 2 minutes). Once the frozen block of cells were loose from the walls of the tube, it was transferred into pre-warmed 20mL X-Vivo-20 media and allowed to completely thaw. Then cells were pelleted at 515 xg 10 minutes RT and further washed twice with X Vivo 20. Afterwards, cells were counted and resuspended at the desired concentration prior to cell seeding. Cells were kept at seeded conditions in a humidified 37°C 5%CO₂ incubator for a minimum of 12 to 18 hours prior to further culture

2.1.6. Human T Lymphocyte Culture Conditions

2.1.6.1. Cell culture concentration and density.

All studies with T lymphocytes in this thesis were done *in vitro* in a humidified 37°C incubator maintained at 5% CO₂. In the majority of the cultures involving Activation and Expansion Beads, cells were seeded at 2.5×10^6 cells per mL per cm² in tissue culture plates (Greiner Bio-one) depending on seed volume according to table, unless otherwise stated.

Table 2.2. Culture plate sizes to use according to cell dilution and density for seeding activated CD4⁺ T cells.

Cells to be seeded	Final media volume (max volume allowed)	Culture plate used	Greiner Bio-one Cat.no.
0.75×10^6	0.3mL (0.4mL)	96 well plate	655180
2.5×10^6	1.0ml (1.5mL)	48 well plate	677180
5.0×10^6	2.0ml (3.0mL)	24 well plate	662160
10.0×10^6	4.0ml (5.5mL)	12 well plate	665180
25.0×10^6	10ml	6 well plate	657160

2.1.6.2. Antibody loading of MACSiBeads.

T lymphocytes were stimulated *in vitro* using anti-human CD3 and anti-human CD28 loaded MACSiBeads from the T Cell Activation/Expansion Kit, human. The MACSiBeads were loaded in sterile conditions as follows: Firstly, a loading buffer was prepared as 0.5% BSA in PBS with 2mM EDTA·2Na (Cat.no. E4844 Sigma-Aldrich). Next, on a 2mL centrifuge tube, 100µL of anti-CD3-Biotin and 100µL of anti-CD28-Biotin was combined and mixed well. Then, 500µL of thoroughly resuspended anti-Biotin MACSiBeads particles was added to the antibody mix. The final volume was adjusted to 1mL by the addition of 300µL of loading buffer. Finally, the tube was incubated for 2 hours at 4°C and constantly mixed gently using a tube rotator at 4 to 5 rpm. The activations beads, containing 1×10^8 particles per mL was stored at 4°C fridge for up to 4 months. In some experiments, singly loaded MACSiBeads were also used. These were prepared by adding 100µL of anti-CD3-Biotin or 100µL of anti-CD28-Biotin with 500µL anti-Biotin MACSiBeads and 400µL of loading buffer.

2.1.6.3. Activation of CD4⁺ T cells.

When required, isolated T lymphocytes were activated in culture; this was done using the anti-human CD3 and anti-human CD28 loaded MACSiBeads. T cells were activated at 1:2 bead-to-cell ratio where 5µL of loaded MACSiBeads were used per million of cells to be activated. Briefly, the cell number of cells to be activated were determined and seeded at 100µL less than the final volume and the loaded MACSiBeads thoroughly resuspended by vortex. The appropriate amount of MACSiBeads were transferred into a new centrifuge tube, then 200µL of X-Vivo-20 added and mixed well. The beads were pelleted at 300 xg for 5 minutes, supernatant removed, resuspended in 100µL of X-Vivo-20 then added into the seeded cells and mixed well by pipetting. For controls, seeded cells were kept in culture either with non-loaded MACSiBeads or completely without beads.

2.1.7. Cell Counting and Cell Viability Assay

Cell densities and viability were assessed using Trypan Blue exclusion by microscopy or using 7-Aminoactinomycin D staining by flow cytometry.

2.1.7.1. Cell counting and Trypan blue exclusion by microscopy.

In addition to cell counting using a disposable Neubauer-improved haemocytometer (Cat.no. DHC-N01 Labtech), cell viability was also assessed by the incorporation of Trypan Blue Solution (0.4% for microscopy Cat.no. 93595 Sigma-Adrich). An aliquot of cells was taken and diluted with the trypan blue solution, 10 μ L of which was pipetted and counted on a haemocytometer. Briefly, the central 5x5 counting chamber was framed on the microscope and cells which were inside this grid including ones touching the bottom or right border were counted. The cells present in the central counting chamber were in 1mm x 1mm x 0.1mm or 0.1 μ L, which therefore was expressed as $\times 10^4$ cells per mL multiplied by the dilution factor. In high density cell counts, only 5 out of 25 central squares were counted and multiplied by 5 to obtain $\times 10^4$ per mL. The trypan blue stained cells were divided by the total number of cells multiplied by 100 to obtain the percentage of non-viable cells.

2.1.7.2. 7-Aminoactinomycin D cell viability assay by flow cytometry.

When indicated, cells after MACS isolation and/or after culture were used to assess the proportion of dead cells or non-viable cells. Specific staining procedure and analysis are described in *section 5.2.3*. Briefly, 5 μ L of 7-AAD Viability Staining Solution was added to $\geq 0.1 \times 10^6$ cells suspended in 100 μ L of FACS staining buffer 1, and incubated at 4°C for 10 minutes before analysis. The dye was excited using a 488nm blue laser and emission was detected using the 695nm (PerCP-Cy5.5) channel on a BD FACS Aria system, then analysed using FlowJo software (www.flowjo.com/).

2.1.8. T Lymphocyte Flow Cytometry Assays

2.1.8.1. Instrumentation, data acquisition, and software analysis packages.

All cell analysis using flow cytometry was acquired on a regularly calibrated BD FACS Aria running BD FACSDiva acquisition software version 6.1 (BD Biosciences). To minimise debris acquisition, only events with FSC signal of 5,000 or more were recorded. Raw data exported as FCS version 3.0 files were subsequently analysed using either Kaluza Analysis Software version 1.3 (Beckman Coulter, High Wycombe UK) or FlowJo Software version 10 (FlowJo LLC, Ashland Oregon USA) kindly provided by the College of Medicine, Swansea University.

2.1.8.2. Flow cytometry staining reagents, buffers, materials and kits.

Flow cytometric analysis were conducted using the reagents listed in Table 2.3 below.

Table 2.3. List of reagents, buffers, materials and kits used for flow cytometric analysis.

Reagent/Kit	Catalogue Number	Manufacturer	Additional information
FACS Staining Buffer 1	<i>in house</i>	<i>in house</i>	0.2µm sterile filtered 0.2% BSA in PBS with 0.05% (w/v) NaN ₃
FACS Staining Buffer 2	<i>in house</i>	<i>in house</i>	0.2µm sterile filtered 1% Heat-inactivated FCS in PBS with 0.09% (w/v) NaN ₃
Cytofix/Cytoperm™ Fixation and Permeabilisation Solutions	554714	BD Biosciences (Oxford UK)	Contains ready to use Fix/Perm buffer (554722) and 10X concentrated Perm/Wash buffer (554723)
Cell Fix (10X)	340181	BD Biosciences (Oxford UK)	Diluted to 1X with deionised water before use
Ethylenediaminetetraacetic acid disodium salt	E4844	Sigma Aldrich	EDTA·2Na
7AAD Viability Staining Solution	00-6993-50	eBioscience (Hatfield UK)	Used 5µL per 100µL of cells
Cell Proliferation Dye eFluor®450	65-0842-85	eBioscience (Hatfield UK)	Reconstituted to 10mM stock with 165µL anhydrous DMSO
Minisart® high flow syringe filters, 0.2µm	16532	Sartorius	
FACS Tubes 12x75mm 5mL Polypropylene	391-0000	VWR (Lutterworth UK)	
Mr. Frosty Isopropanol-lined freezing container	C1562	Sigma-Aldrich (Dorset UK)	

2.1.8.3. Flow cytometry fluorochrome-conjugated antibodies.

Monoclonal antibodies used for characterising T cell antigen expressions analysed by flow cytometry are listed in Table 2.4.

Table 2.4. List of monoclonal antibodies used for flow cytometry. * denotes use for intracellular staining and # for surface staining

Anti-human antibody	Fluorochrome	Catalogue number (clone)	Manufacturer	Additional information
CD4 [#]	APC	17-0048-42 (OKT4)	eBioscience (Hatfield UK)	
CD4 [#]	FITC	11-0048-42 (OKT4)	eBioscience (Hatfield UK)	
CD25 [#]	APC	17-0259-42 (BC96)	eBioscience (Hatfield UK)	
CD45RA [#]	PerCP-Cy5.5	45-0458-42 (HI100)	eBioscience (Hatfield UK)	
CD45RA [#]	eFluor®450	48-0458-41 (HI100)	eBioscience (Hatfield UK)	
CD45RO [#]	PE-Cy7	25-0457-42 (UCHL1)	eBioscience (Hatfield UK)	
IL-4 [*]	APC	17-7049-41 (8D4-8)	eBioscience (Hatfield UK)	
FOXP3 [*]	eFluor®450	48-4777-41 (236A/E7)	eBioscience (Hatfield UK)	
IFN γ [*]	FITC	11-7319-41 (4S.B3)	eBioscience (Hatfield UK)	
IL-17A [*]	PE	12-7178-41 (eBio64CAP17)	eBioscience (Hatfield UK)	
phospho-4E-BP1 [*]	eFluor®660	50-9107-41 (V3NTY24)	eBioscience (Hatfield UK)	Specific to phosphorylated T36/T45
phospho-S6 ribosomal [*]	PE	12-9007-4 (cupk43k)	eBioscience (Hatfield UK)	Specific to phosphorylated S235/S236

2.1.8.4. Surface staining for flow cytometric analysis.

When indicated, cells after MACS isolation and/or after culture were used to assess the surface expression of T cell antigens. Briefly, an aliquot of cells, typically $\geq 0.1 \times 10^6$ cells per stain per sample, were taken from PBS washed cells, transferred into round bottom polystyrene FACS tubes and suspended into ice cold FACS staining buffer 1 to a final volume of 100 μ L. Next, fluorochrome-conjugated antibodies were quickly spun and 5 μ l of each stain were added onto the stained samples, pulse vortexed and incubated in the dark on ice for 30 minutes together with the unstained samples. After incubation, unbound antibodies were washed with 3mL FACS buffer 1 and centrifuged at 515g 4°C for 7 minutes. Supernatants were discarded and the cells were suspended in 200 μ L FACS staining buffer 1 per tube then submitted for flow cytometric analysis. Cells were kept in the dark and on ice until analysis on the same day. Cells to be analysed next day were fixed by suspending in 1X Cell Fix, covered with parafilm and stored at 4°C fridge.

2.1.8.5. Intracellular staining for flow cytometric analysis.

When indicated cells after culture were used to assess levels of intracellular protein expression or levels of protein phosphorylation. Cells for intracellular protein and phosphoprotein expression analysis were prepared using Cytotfix/Cytoperm™ Solution Kit according to manufacturer's instructions with few modifications. Briefly, an aliquot of cells, typically $\geq 0.25 \times 10^6$ cells per stain per sample, were transferred to a FACS tube. Cells were pelleted at 515 xg 4°C 10 minutes and the supernatant discarded. Cells were fixed/permeabilised with 250 μ L Fix/Perm solution and incubated in the dark at 4°C for 20 minutes. Afterwards, cells were washed twice with 1ml 1x Perm/Wash buffer, centrifuged at 515g 4°C for 5 minutes, then the supernatant discarded. On the second wash, tubes were incubated at 4°C for 10 minutes before centrifugation. Cells were resuspend in 1x Perm/Wash buffer and equally split into unstained and stained samples to a final volume of 50 μ L per sample. To the stained samples, 2.5 μ L of fluorochrome-conjugated antibodies were added, pulse vortexed then incubated in the dark at 4°C for 30 minutes together with the unstained samples. After incubation, each tube was washed with 1mL 1x Perm/Wash buffer and centrifuged at 515g 4°C for 7 minutes, twice. Cells were resuspended in 200 μ L FACS staining buffer 2 and subjected to flow cytometric analysis.

When intracellular staining was to be done at a later time, cells were pelleted and fixed with 100 μ L 4% paraformaldehyde for 15mins at 4°C and washed twice with 1mL FACS buffer 2. Similar to *section 2.1.5*, cells were then resuspended in heat-inactivated FBS supplied with 10% DMSO in Cryo.S™ cryovials and stored in isopropanol-lined freezing container placed in a -80°C freezer. To continue intracellular staining, cells were thawed in a 37°C water bath then washed twice with 1mL FACS buffer 2, and resuspended in 50 μ L 1x Perm/Wash buffer for staining.

2.2. Sterol Analysis by Liquid Chromatography Mass Spectrometry

2.2.1. Sterol Analysis Materials

2.2.1.1. Solvents.

Solvents required for extraction, chromatography and sample preparation are listed in Table 2.5.

Table 2.5. List of reagents and materials used for sterol analysis

Reagent	Catalogue number	Manufacturer	Additional information
Methanol (MeOH)	M/4056/17	Fisher Scientific (Loughborough UK)	HPLC grade
Acetonitrile (MeCN)	A/0626/17	Fisher Scientific (Loughborough UK)	HPLC grade
Isopropanol (IPA)	P/7507/17	Fisher Scientific (Loughborough UK)	HPLC grade
Ethanol (EtOH)	E/0650DF/17	Fisher Scientific (Loughborough UK)	Absolute, Analytical grade
Water	W/0106/17	Fisher Scientific (Loughborough UK)	HPLC grade
Glacial Acetic Acid	20104.334	VWR (Lutterworth UK)	AnalaR NORMAPUR grade
Formic Acid	20318.297	VWR (Lutterworth UK)	
Hydrochloric Acid	H1757	Sigma-Aldrich (Dorset UK)	
Sodium Hydroxide	S5881	Sigma-Aldrich (Dorset UK)	
Potassium Hydroxide	P5958	Sigma-Aldrich (Dorset UK)	
Potassium phosphate monobasic (for molecular biology)	P9791	Sigma-Aldrich (Dorset UK)	50mM KH ₂ PO ₄ was made with HPLC Water adjusted to pH 7 with 1M NaOH
Cholesterol Oxidase	C8649	Sigma-Aldrich (Dorset UK)	From <i>Streptomyces sp.</i> lyophilized powder, ≥20 units/mg protein
Girard's Reagent P (GP)	G0030	Tokyo Chemical Industry Europe (Oxford UK)	[1-(Carboxymethyl)-pyridinium chloride hydrazide]
Sep-Pak® Cert tC18 200mg 3cc	186004618	Waters (Elstree UK)	Used for SPE1
OASIS® HLB 60mg 3cc	WAT094226	Waters (Elstree UK)	Used for SPE2
Hypersil GOLD RP column	25002-052130	Thermo Fisher Scientific (Loughborough UK)	1.9µm particle size, 50x2.1 mm
1.5-mL centrifuge tube	S1615-5500	STARLAB (Milton Keynes UK)	
2.0-mL centrifuge tube	10038760	Fisher Scientific (Loughborough UK)	

12-mL round-bottom tubes, polypropylene	163270	Greiner Bio-one, Stonehouse UK	
15-mL centrifuge tube	10431013	Fisher Scientific (Loughborough UK)	
50-mL centrifuge tube	10038980	Fisher Scientific (Loughborough UK)	
5mL Luer-Lock syringes	11364881	Fisher Scientific (Loughborough UK)	
20-port vacuum extraction manifold	5982-9120	Agilent (Cheshire UK)	Vacuum manifold for 16mm x 100mm tubes
300µL Polypropylene HPLC Vials	186002639	Waters (Elstree UK)	12x32mm screwneck with PTFE/Si pre-slit cap
LTQ ESI Positive calibration solution	11340360	Fisher Scientific (Loughborough UK)	
UltiMate 3000 HPLC system	-----	Dionex	
Orbitrap Velos Pro	IQLAA-EGAAPFADBMAZV	ThermoFisher	
Orbitrap Elite	IQLAA-EGAAPFADBMAZQ	ThermoFisher	

2.2.1.2. Materials for sample preparation and chromatographic separation.

Consumables such as enzyme, solid phase extraction cartridges, polypropylene plasticware, and derivatisation reagents are listed in Table 2.5.

2.2.1.3. Authentic sterol standards and preparation.

Stable isotope dilution in combination with LCMS was used to determine relative quantities of endogenous sterols. The authentic deuterium labelled sterol standards used were namely: 24(R/S)-[26,26,26,27,27,27-²H₆] hydroxycholesterol (Cat.no. 700049P), 22R-[25,26,26,26,27,27,27-²H₇] hydroxycholesterol (Cat.no. 700052P), [25,26,26,26,27,27,27-²H₇] Cholesterol (Cat.no. 700041P) were bought from Avanti Polar Lipids, Inc. (Alabaster, Alabama USA). The [²H₇]-Cholest-5-ene-3β,22(R)-diol was enzymatically oxidised to [²H₇]-Cholest-4-ene-3-oxo,22(R)-ol in house at a stock concentration of 5ng/µL in IPA using the protocol in similar to *section 2.2.2.4* (without proceeding with derivatisation). Then, a combined stock containing 1µg/mL 24(R/S)-HC(D6), 1µg/mL 22(R),3-oxo-HC(D7), and 200µg/mL Cholesterol(D7) in EtOH was made. Prior to sterol extraction, the combined stock was diluted 1:500 with EtOH of which 1mL was added per sample.

2.2.2. Sample processing using Enzyme-Assisted Derivatisation for Sterol Analysis (EADSA)

On cell harvest, cells were resuspended in culture plates by pipetting and transferred into appropriate tubes then centrifuged at 515 xg RT 10 minutes. Media was transferred to a separate tube and pelleted cells were washed with pre-warmed PBS twice then counted. A schematic for the subsequent sample processing adapted from Griffiths et al. 2013 and Griffiths et al. 2008 is outlined in Figure 2.1.

2.2.2.1. Extraction of endogenous sterols from cell fractions.

When available, counted cells in PBS were pelleted again and the supernatant removed. Tubes were flicked to dislodge the pellet and placed on an ultrasonic bath. To each sample, 1mL of EtOH containing 2ng 24(R/S)-HC(D6), 2ng 22(R),3-oxo-HC(D7), and 400ng Cholesterol(D7) was added drop-wise. An additional 50µL of EtOH was added to samples and sonicated for a further 5 minutes then centrifuged at 17,000 xg 4°C for 30 minutes. The 1.05mL EtOH supernatant was transferred to a fresh tube for solid phase extraction and the pellet containing cell debris was stored at -20°C.

2.2.2.2. Extraction of endogenous sterols from media fractions.

Sterols present in culture media was also extracted. Different volumes of media was extracted to maximum of 3mL. A 15ml tube with 1mL of EtOH containing 2ng 24(R/S)-HC(D6), 2ng 22(R),3-oxo-HC(D7), and 400ng Cholesterol(D7) was placed in an ultrasonic bath. To this, an appropriate volume of EtOH, dependent on the media volume to be extracted, was pre-calculated and added to give a final EtOH concentration of 70%. Media were added drop-wise to the sterol standard/EtOH mix and sonicated for a further 5 minutes then centrifuged at 4,500 xg 4°C for 1 hour. The EtOH supernatant was transferred to a fresh tube for solid phase extraction and the pellet containing cell debris was stored at -20°C.

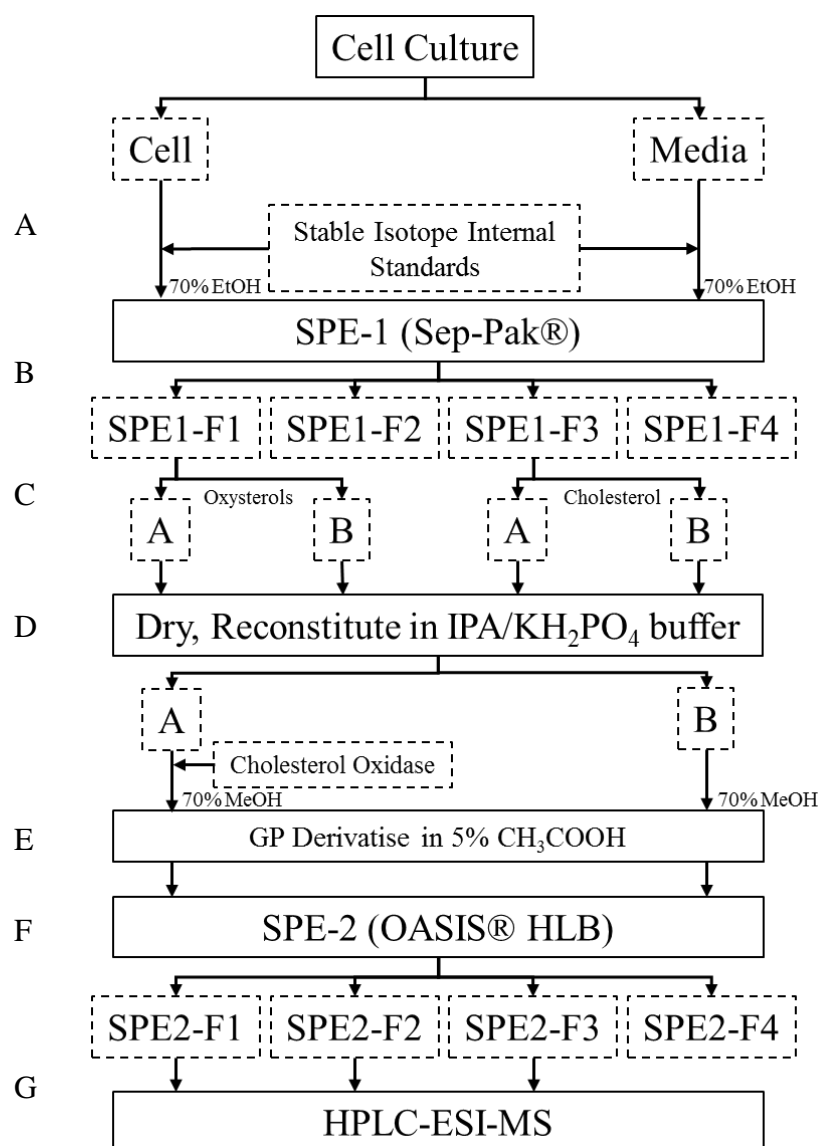


Figure 2.1. Schematic for the sample preparation for sterol analysis by LCMS.

Briefly, after cell culture, cells and media were separated (A). Next, each sample was extracted for sterols in an ultrasonic bath with EtOH containing stable isotope internal standards (B). Each extracts were diluted to 70% EtOH and subjected to a solid phase extraction where cholesterol and oxysterols were separated as fractions 1 and 3 (C). Each fractions were split equally to A and B, dried and reconstituted in IPA/ KH_2PO_4 buffer (D). Then, to each of the A fractions, cholesterol oxidase were added while B fractions were left untreated. Both fractions were incubated at 37°C waterbath for 1 hour (E). Oxidation reactions were stopped by adding and diluting the reaction solution to 70% MeOH. Each sample were derivatised with Girard's Reagent P with 5% acetic acid overnight at RT (F). The excess derivatisation reagent was removed by subjecting the samples to a second solid phase extraction where derivatised sterols were eluted in four fractions (G). Finally, fractions 1 to 3 were subjected to HPLC-ESI-MSⁿ. Modified from Karu et al. 2007^[3].

2.2.2.3. First solid phase extraction (SPE-1) to separate cholesterol and oxysterols.

Since free cholesterol is highly prone to autoxidation and typically present at 1000-fold more than oxysterols, it was necessary to separate these groups to prevent further cholesterol autoxidation which can misrepresent oxysterol levels and also to enrich the oxysterols for analysis without overloading the LC-MS system with excess cholesterol. Cholesterol and more polar oxysterols were separated with a reversed phase SPE procedure. Briefly, Sep-Pak® Cert tC18 cartridge 200mg 3cc were securely placed on a vacuum manifold and the sorbent beds conditioned and solvated with 4mL absolute EtOH followed by 6mL 70% EtOH at a flow rate of ~0.25mL/min or ≤ 2 drops/sec. Flow rate was maintained either using a 5mL Luer-Lock syringe applying positive pressure or a vacuum pump through the manifold. Cell extracts in 1.05mL absolute EtOH were diluted to 70% by the addition of 350 μ L water prior to loading on the conditioned Sep-Pak cartridges; while media extracts already at 70% EtOH were applied straight. Polar sterols were collected from the cell extracts in the first flow through plus a column wash of 5.5mL 70% EtOH as SPE1-Fraction-1 (Fr1) on 12mL tubes. With media extracts, eluent was collected plus a column wash of 1mL 70% EtOH. A further column wash was collected by adding 4mL of 70% EtOH as SPE1-Fraction-2 (Fr2). Cholesterol was eluted with 2mL of absolute EtOH as SPE1-Fraction-3 (Fr3) then a further 2mL absolute EtOH column wash collected as SPE1-Fraction-4 (Fr4). Fr1 and Fr3 were subsequently equally split into SPE1-Fraction-1-A (Fr1A), SPE1-Fraction-1-B (Fr1B), SPE1-Fraction-3-A (Fr3A) and SPE1-Fraction-3-B (Fr3B) into new 12mL tubes and dried overnight in a Scanspeed Vacuum Concentrator (Labogene Lynge DK).

2.2.2.4. Cholesterol oxidase treatment and charge tagging of free sterols with Girard's Reagent P.

The dried fractions: Fr1A, Fr1B, Fr3A and Fr3B, were reconstituted in 100 μ L IPA with 1mL 50mM KH₂PO₄ pH 7 and mixed well by vortex. To the A fractions only, 3 μ L of Cholesterol oxidase (containing 2 μ g/ μ l of protein) was added while B fractions were left untreated. Both reconstituted fractions were mixed well and incubated on a 37°C water bath for 1 hour to oxidise the sterol 3 β -OH-5-ene group to 3-oxo-4-ene group. The reaction was stopped by the addition of 2mL 100% MeOH. Afterwards, 150 μ L of glacial acetic acid was added to all the fractions followed by 150mg of

Girard's reagent P. Both fractions, ~3.25mL at 70% MeOH, were incubated at RT overnight protected from light. The conversion of the sterol 3 β -OH group to a 3-OXO group will permit the reaction of the GP hydrazine to the sterol 3C forming sterol-GP-hydrazones. Derivatisation with GP introduces a quaternary nitrogen which will give the whole molecule a positive charge (Figure 2.2 and Figure 2.3). This increases the ionisation efficiency and also sensitivity in mass spectrometric analysis. At the end of the process, 'A' fractions will contain derivatised sterols which were both 3 β -OH and 3-oxo endogenously; 'B' fractions will only contain derivatised sterols which was endogenously 3-oxo and sterols with 3 β -OH underivatised.

2.2.2.5. Second solid phase extraction (SPE-2) to remove excess derivatisation reagent and sample clean up.

Charge-tagging of sterols with GP required an excess amount of derivatisation reagent to drive the forward reaction. This excess reagent, along with other impurities, were cleaned up using a second reversed phase SPE. Firstly, Oasis® HLB 60mg 3cc cartridges were secured on vacuum manifold and the sorbent beds conditioned/solvated with 6mL 100% MeOH, followed by 6mL 10% MeOH then 4mL 70% MeOH at the same flow rate as SPE-1. Next, the ~3.25mL samples from the previous derivatisation step in *section 2.2.2.4* were applied onto the columns and the flow through collected. Column washes of 1mL 70% MeOH followed by 1mL 35% MeOH was also collected. Then, to the ~5mL flow through, 4mL of HPLC Water was added, mixed well and the applied again, as a first recycle, onto the column and the flow through collected. Column was washed with 1mL 17.5% MeOH and collected. After that, to the ~10mL of collected flow though, 9mL of HPLC water was added and mixed well on a 50mL centrifuge tube. Finally, the ~19mL was applied once more onto the column for a last recycle, and the flow through discarded. Column was finally washed with 6mL of 10% MeOH and also discarded. Bound sterols on the column were eluted in three 1mL 100% MeOH eluates (i.e. Fr1A1, Fr1A2 and Fr1A3) and one 1mL absolute EtOH eluate (Fr1A4) collected in 1.5mL centrifuge tubes. Same procedure was done for Fr1B, Fr3A and Fr3B. Samples were stored in -20°C.

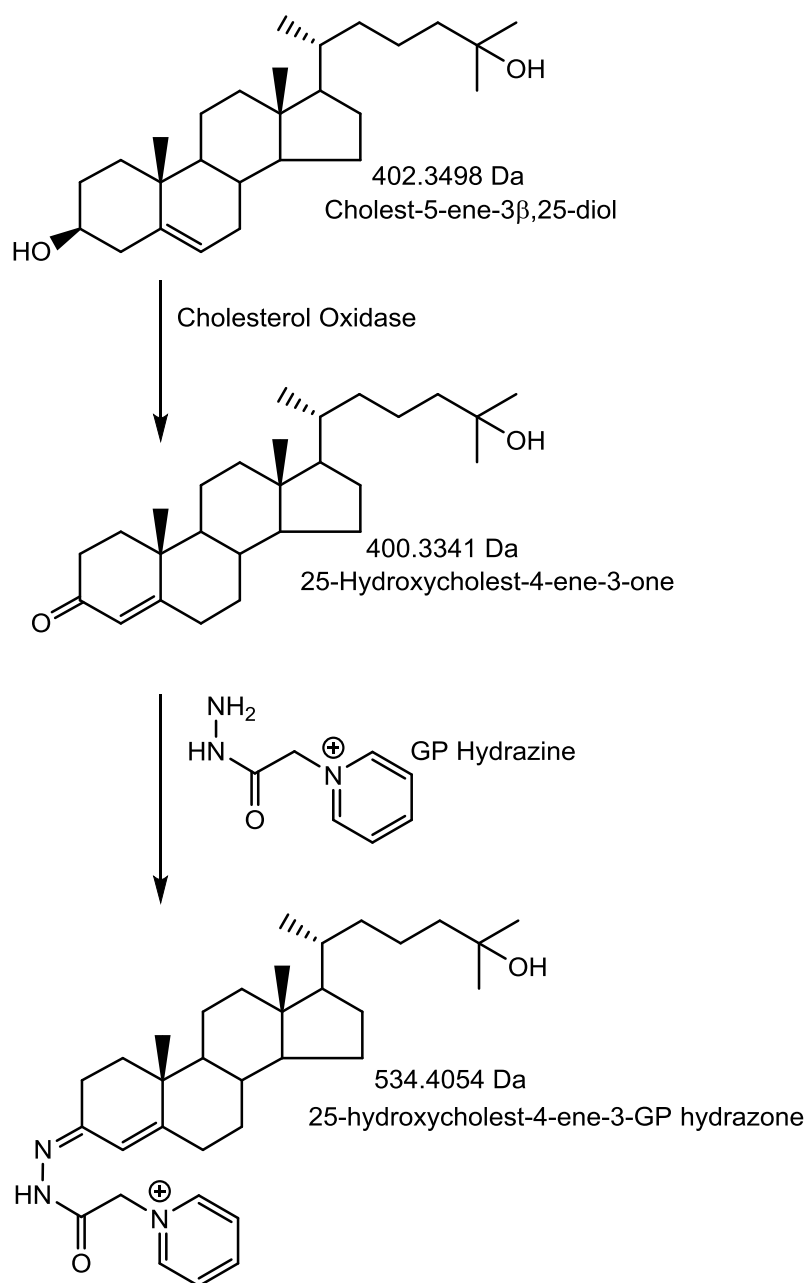


Figure 2.2. Charge-tagging of sterols after cholesterol oxidase treatment.

Sterols in 'A' fraction were treated with cholesterol oxidase to convert the 3 β -hydroxy-5-ene group to a 3-oxo-4-ene group. Subsequently, the 3-oxo group was derivatised with Girard's reagent P hydrazine to GP hydrazone. Sterols already containing 3-oxo groups endogenously were GP derivatised readily without cholesterol oxidase treatment as 'B' fractions. As an example, 25 hydroxycholesterol, with a mass of 402.3498 m/z , was oxidised then GP derivatised to have a $[M]^+$ of 534.4054 m/z [3,16].

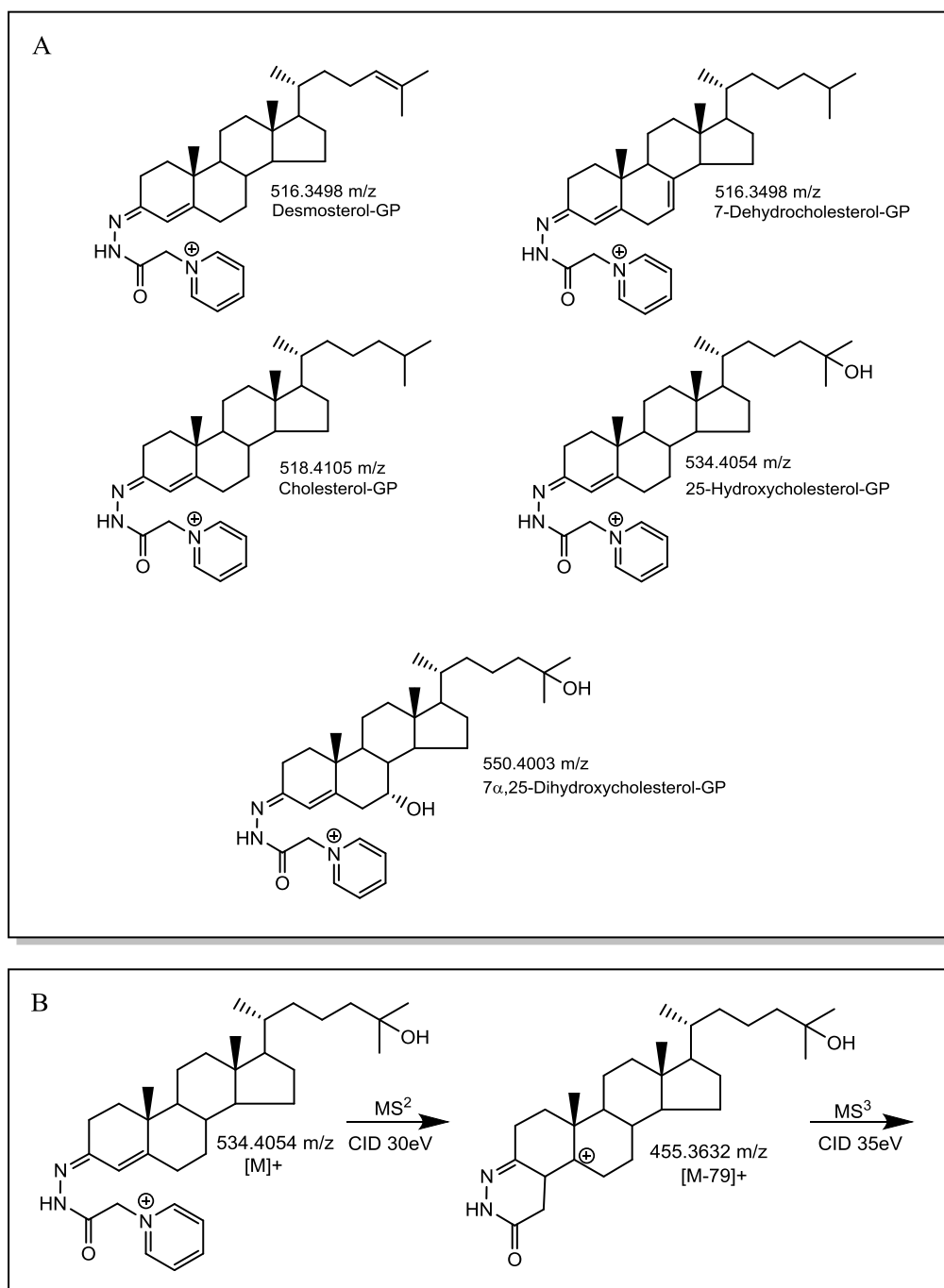


Figure 2.3. Sterols derivatised with Girard's reagent P introduces a quaternary nitrogen.

(A) Structures of some detected GP-derivatised sterols and their [M]⁺ ions masses as detected in the mass spectrometer. The quaternary nitrogen present in the GP increases the sterol ionisation efficiency and sensitivity in the mass spectrometer but also improves selectivity to sterols possessing an oxo group. (B) The [M]⁺ ion for each sterol was the precursor ion selected for MS² fragmentation in the linear ion trap and subsequent MS³ was done for the [M-79]⁺ daughter ion to give a structurally unique MS³ spectra.

2.2.3. Sample preparation prior to LC-ESI-MSⁿ analysis.

Eluted fractions from SPE-2 in *section 2.2.2.5* was prepared before submitting for LC-MSⁿ analysis. As shown in Figure 2.1.D, oxysterols were analysed from Fr1A/B, while cholesterol and cholesterol precursors were analysed from Fr3A/B. Cholesterol oxidase-treated 'A' fractions will contain GP derivatised sterols which endogenously had a 3 β -hydroxy-5-ene group or a 3-oxo-4-ene group. To distinguish sterols which endogenously only contain 3-oxo-4-ene group, 'B' fractions were analysed (Figure 2.1 and Figure 2.4). Upon quantification, the measured sterol in 'B' was taken away from 'A' to provide the amount of sterols which originally contained a 3 β -hydroxy-5-ene group.

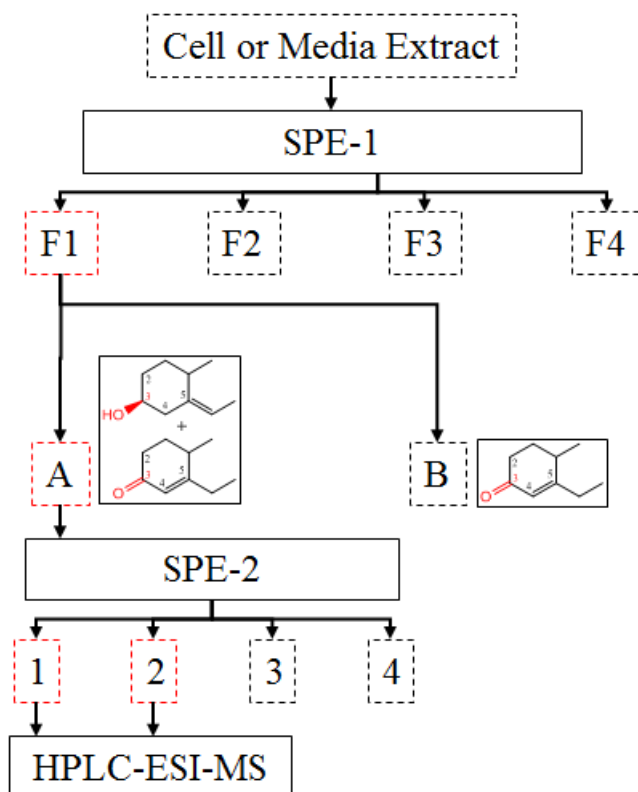


Figure 2.4. Series of sample processing breakdown showing the SPE fractions used for LCMS analysis. From each cell or media extract, oxysterols which endogenously contained a 3 β -hydroxy-5-ene or 3-oxo-4-ene were analysed from diluted Fraction-1-A-1 and Fraction-1-A-2 (red dotted) while cholesterol and cholesterol precursors were analysed from diluted Fraction-3-A-1, Fraction-3-A-2 and Fraction-3-A-3. To analyse sterols which endogenously only have a 3-oxo-4-ene group, corresponding B fractions were used.

2.2.3.1. Oxysterol fraction sample preparation for LCMS.

Oxysterols from either cell or media was analysed by LCMS neat from the SPE2 fractions. Firstly, SPE2-Fractions-1 and 2 (e.g. Fr1A1 and Fr1A2) were centrifuged at 17,000 xg 4°C for 30 minutes to pellet any insoluble particles. Next, a volume of 90µL each from Fr1A1 and Fr1A2 were taken from the top and mixed well in a 1.5mL centrifuge tube. The 180µL was diluted to 60% MeOH by adding 120µL of HPLC water to a final volume of 300µL and mixed well by vortex. From this, 270µL was transferred into 300µL HPLC vials.

2.2.3.2. Cholesterol and cholesterol precursor fraction sample preparation for HPLC-ESI-MSⁿ.

Cholesterol and cholesterol precursors from either cell or media was analysed by LCMS at 1:10 dilution from the SPE2 fractions. Firstly, Fr3A1, Fr3A2 and Fr3A3 were centrifuged at 17,000 xg 4°C for 30 minutes to pellet any insoluble particles. Next, a volume of 10µL each from SPE2-Fractions-1, 2 and 3 were taken from the top and mixed well in a 1.5mL centrifuge tube. From the 30µL, 20µL was taken and diluted 1:10 with 180µL of 100% MeOH. From the 200µL, 180µL was taken and diluted to 60% MeOH by adding 120µL of HPLC water to a final volume of 300µL and mixed well by vortex. From this, 270µL was transferred into 300µL HPLC vials.

2.2.4. Sterol Separation, Analysis and Quantitation by HPLC-ESI-MSⁿ

2.2.4.1. Orbitrap calibration.

Both the Orbitrap Elite and the Orbitrap Velos was regularly maintained and externally calibrated to a mass accuracy of <5ppm with an LTQ ESI Positive calibration solution using the semi-automatic calibration in ThermoTunePlus software.

2.2.4.2. HPLC-ESI-MSⁿ sterol analysis.

Samples in 270µL in HPLC vials prepared from sections 2.2.3.1 or 2.2.3.2 were subjected to chromatographic separation on an UltiMate 3000 HPLC system with a Hypersil GOLD RP column thermostated at 25°C. Samples were loaded and maintained at 4°C on an autosampler and 90µL was injected to the column per run. The separation utilised a gradient with two mobile phases of consisting of 33.3% MeOH, 16.7% MeCN, 50% Water, 0.1% formic acid for mobile phase A; and 63.3% MeOH, 31.7% MeCN, 5% Water, 0.1% formic acid for mobile phase B. Separation was achieved using two experimental LC methods. The 17-minute LC method (Figure 2.5.A) was maintained at 200µL/minute starting at 20% B for 1 minute, then proportion of B was increased linearly to 80% B for 7 minutes. Afterwards, 80% B was sustained for 5 minutes then, equilibrated back to 20% B within 6 seconds and sustained for 3.9 minutes. The 26-minute LC method (Figure 2.5.B) was also maintained at 200µL/minute starting at 20% B increased linearly to 50% B for 10 minutes and was sustained at 50% B for 6 minutes. Afterwards, 50% B was increased linearly to 80% B for 3 minutes then sustained at 80% B for 3 minutes. Gradient was equilibrated back to 20% B within 6 seconds and sustained at 20% B for 3.9 minutes. In both methods the eluate from the column was directed to the electrospray ionisation source of either an Orbitrap Velos or an Orbitrap Elite mass spectrometer running in positive ion mode. Each sample was injected 2 to 3 times as technical replicates and a set of scan events were done for each injection.

2.2.4.3. Scan events and parameters for MS and MS³ in the Orbitrap.

The first recorded scan involved a full MS scan in profile mode on the Orbitrap analyser with a range from 400-610 m/z at 120,000 resolution for the Orbitrap Elite or 30,000 for the Orbitrap Velos. The subsequent multi-stage fragmentation scans in centroid mode were done on the linear ion trap which isolated monoisotopic precursor

ions $[M]^+$ specific to each mass of the GP-derivatised sterols (Figure 2.3.A and Table 2.6). Each precursor ion was fragmented at 30 eV CID collision energy as the first fragmentation event, MS^2 . When daughter ions contained a predicted neutral loss of pyridine ring at $79m/z$, another isolation and fragmentation was done. The $[M-79]^+$ ions were isolated in the linear ion trap and further fragmented at 35 eV CID collision energy as the second fragmentation event, MS^3 . MS^3 fragments after this transition was then detected and recorded using the LIT dynodes^[3]. Afterwards, another set of isolation and subsequent multi-stage CID fragmentation occurs in the LIT for another precursor ion. The instrument method was optimised to execute two to six LIT and fragmentation scans while the Orbitrap analyser records a full accurate mass scan per cycle.

2.2.4.4. Identification and quantification of chromatographically separated sterol species.

By utilising the linear ion trap (LIT) for MS^3 fragmentation, analysis of GP-derivatised sterols became selective and provided a fragmentation pattern characteristic to a particular sterol. Previous members of the group analysed authentic sterol standards, subjected to EADSA and HPLC-ESI- MS^n analysis, which was then compiled to a library with expected chromatographic retention times and specific MS^3 spectra for each authentic sterol. Table 2.6 lists the sterols we monitor and able to identify. This library was used together with the high mass accuracy full mass scan of the Orbitrap analyser to manually isolate, identify, integrate and extract peak areas using a Thermo Xcalibur Qual Browser software version 3.0. Analysis and identification of sterols were performed for each data file acquired per injection. Briefly, a reconstructed ion chromatogram (RIC) with a mass window of 10ppm was done on the full MS scan to isolate the $[M]^+$ ion detected on the Orbitrap analyser, this step isolates all ions detected in the chromatographic run which have the same accurate mass as the sterol of interest (Figure 2.6.A). Next, a total ion chromatogram (TIC) was done on another panel specific for each sterol MS^3 fragmentation performed and detected on the LIT, this step selectively isolates the $[M]^+$ ions which lost $79m/z$ upon MS^2 , $[M-79]^+$ (Figure 2.6.B), which also provide a distinct MS^3 fragmentation pattern which can be cross-referenced with the authentic sterol standards library (Figure 2.6.C). Peaks plotted in

both the full mass RIC and MS³ TIC were considered “sterol-like” and MS³ fragments were compared to the library. Upon proper identification, each full MS peak was integrated and the peak area exported to Microsoft Excel. This identification and subsequent peak area extraction was done for both the internal deuterated sterol standards and the endogenous sterols. The relative quantities of each endogenous sterol was calculated using the formula in Equation 2.1.

2.2.4.5. Normalisation of relative endogenous sterol quantities.

Sterols in media extracts which were quantified using stable isotope dilution mass spectrometry were normalised based on the number of T cells initially seeded in culture. On the other hand, sterols detected in cell extracts were normalised to number of cells that were extracted on the day of harvest. All quantifications were expressed as picograms per million cells (pg/million cells), unless otherwise stated.

Equation 2.1. Formula for calculating the relative endogenous sterol quantity (Q_E) by stable isotope dilution. Legend: $[A_E]$ = Peak area of endogenous sterol; $[A_{iSTD}]$ = Peak area of added internal sterol standard upon extraction; $[Q_{iSTD}]$ = Quantity of added internal sterol standard upon extraction.

$$[Q_E] = \frac{[A_E]}{[A_{iSTD}]} \times [Q_{iSTD}]$$

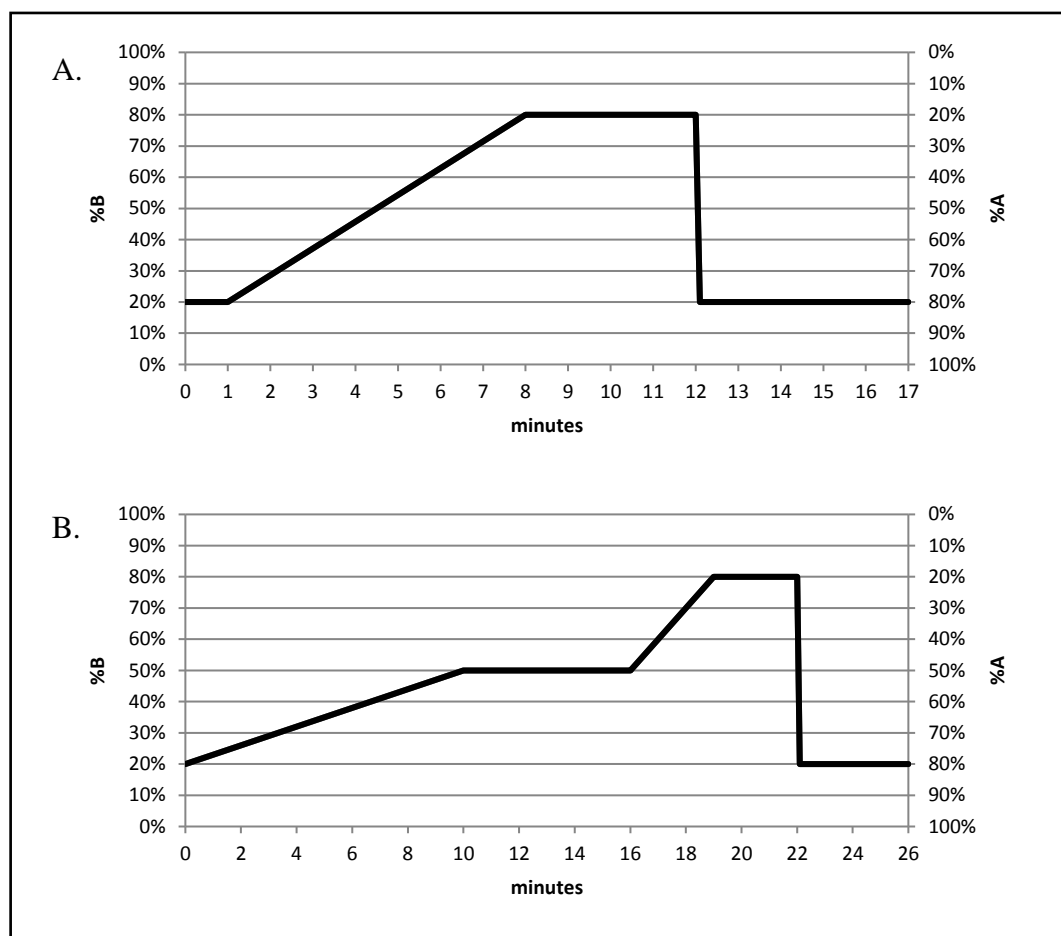
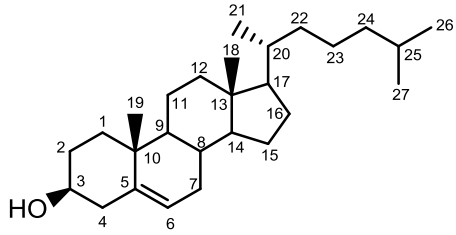
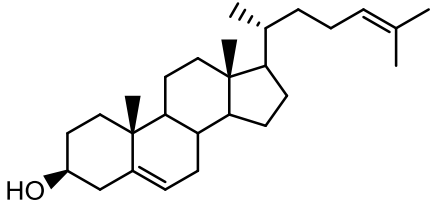
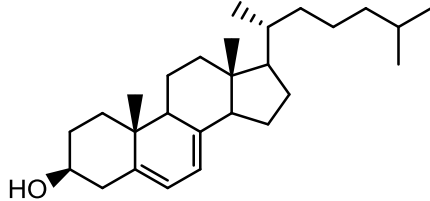
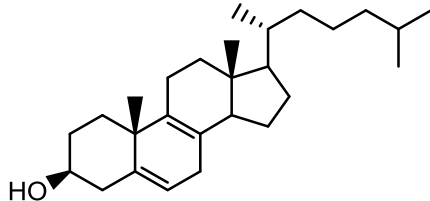
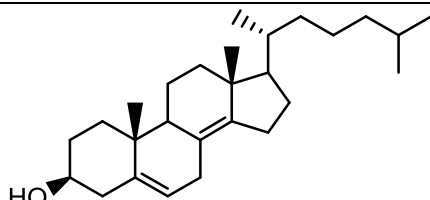
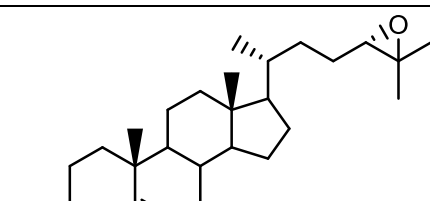


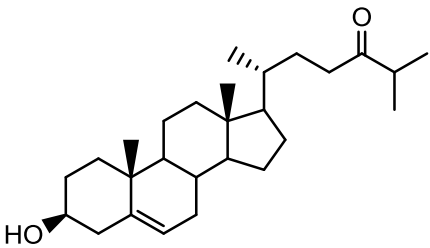
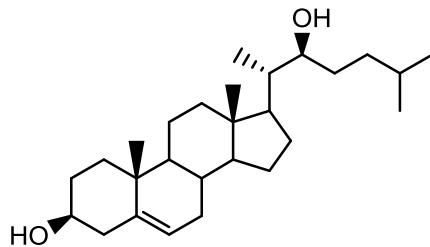
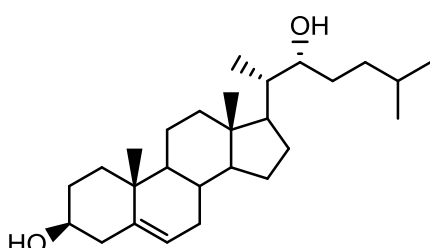
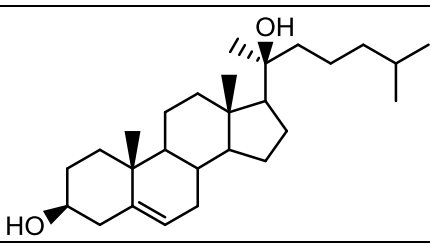
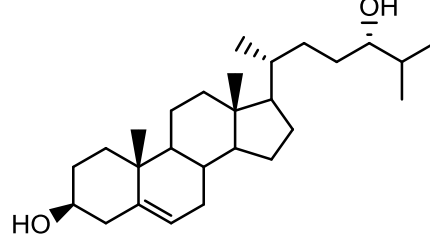
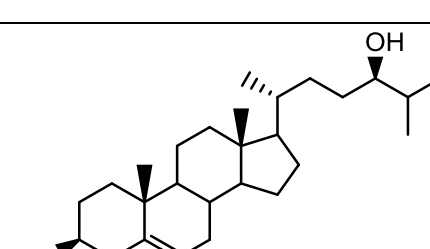
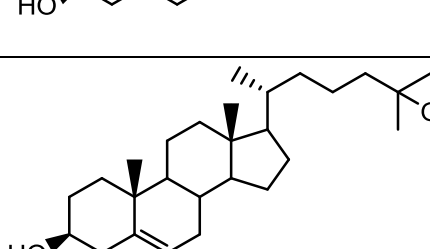
Figure 2.5. Liquid chromatography multi-step gradients for derivatised sterol separation.

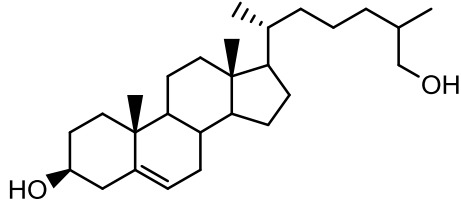
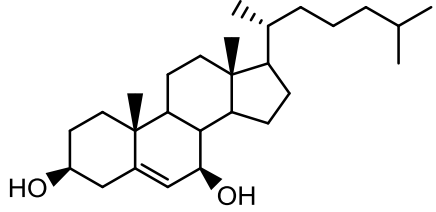
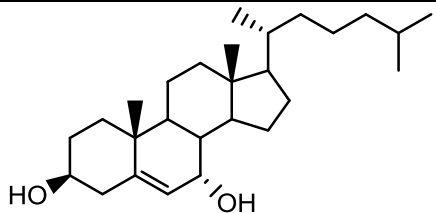
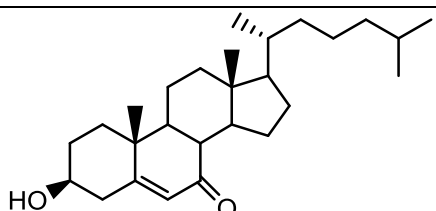
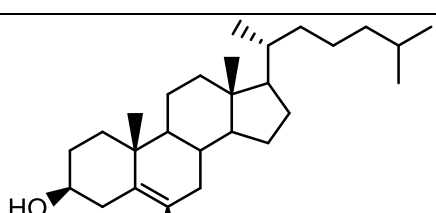
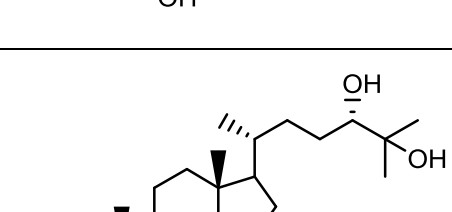
Two LC methods were used to chromatographically separate sterols of the same m/z using two mobile phases. Mobile phases maintained at $200\mu\text{L}/\text{min}$ were degassed and mixed at different proportions at different time points. A. The 17-minute gradient, described by Griffiths et al. 2008, was used early in the study. In general, this provided good separation of sterols but structurally similar monohydroxycholesterols like 24(S)-HC, 25-HC, 24(R)-HC and 27-HC were not easily distinguished due to co-elutions. B. The method was extended to 26 minutes, with emphasis to the time range where the monohydroxycholesterols elute from the column. This broadened the peak shapes and lengthened the total LC run time but gave better separation.

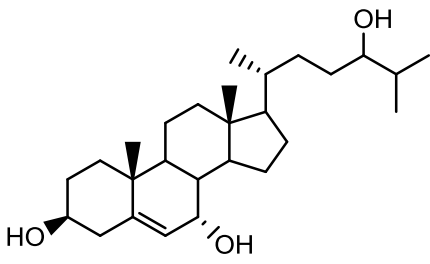
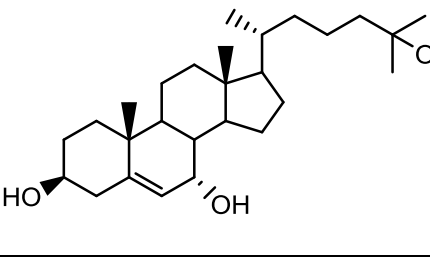
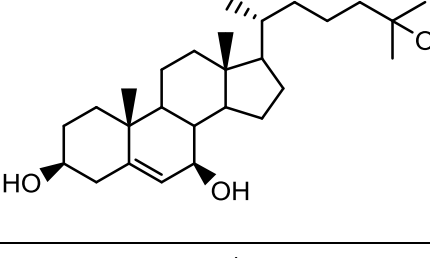
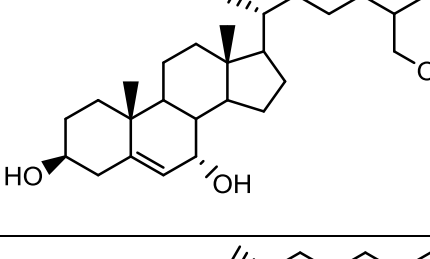
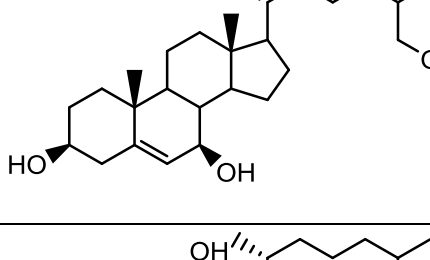
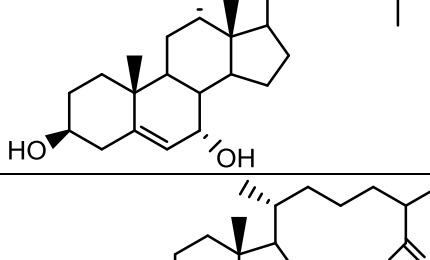
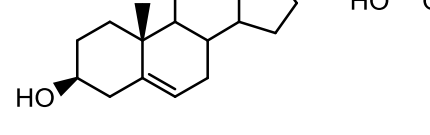
Table 2.6. List of sterols monitored and identified using EADSA.

This is not an exhaustive list and only includes sterols commonly or expected to be detected, some of which may not be derived from authentic sterol standards.

	Common name [Systematic name] "Short name"	Structure	Originating Structure Mass (m/z)	Mass of GP derivative after EADSA [M]⁺ (m/z)
1	Cholesterol [Cholest-5-en-3 β -ol]		386.3549	518.4105
2	Desmosterol [Cholest-5,24-dien-3 β -ol]		384.3392	516.3948
3	7-Dehydro-cholesterol [Cholest-5,7-dien-3 β -ol]		384.3392	516.3948
4	8(9)-Dehydro-cholesterol [Cholest-5,8(9)-dien-3 β -ol]		384.3392	516.3948
5	8(14)-Dehydro-cholesterol [Cholest-5,8(14)-dien-3 β -ol]		384.3392	516.3948
6	24(S),25-Epoxy-cholesterol [24(S),25-Epoxycholest-5-ene-3 β -ol] "24(S),25-EC"		400.3341	532.3898

7	24-Ketocholesterol [24-Ketocholest-5-ene-3 β -ol] "24-KC"		400.3341	532.3898
8	22(S)-Hydroxycholesterol [Cholest-5-ene-3 β ,22S-diol] "22R-HC"		402.3498	534.4054
9	22(R)-Hydroxycholesterol [Cholest-5-ene-3 β ,24R-diol] "22S-HC"		402.3498	534.4054
10	20(S)-Hydroxycholesterol [Cholest-5-ene-3 β ,20S-diol] "20S-HC"		402.3498	534.4054
11	24(S)-Hydroxycholesterol [Cholest-5-ene-3 β ,24S-diol] "24S-HC"		402.3498	534.4054
12	24(R)-Hydroxycholesterol [Cholest-5-ene-3 β ,24R-diol] "24R-HC"		402.3498	534.4054
13	25-Hydroxycholesterol [Cholest-5-ene-3 β ,25-diol] "25-HC"		402.3498	534.4054

14	27-Hydroxy-cholesterol [Cholest-5-ene-3 β ,26-diol] "27-HC"		402.3498	534.4054
15	7 β -Hydroxy-cholesterol [Cholest-5-ene-3 β ,7 β -diol] "7 β -HC"		402.3498	534.4054
16	7 α -Hydroxy-cholesterol [Cholest-5-ene-3 β ,7 α -diol] "7 α -HC"		402.3498	534.4054
17	7-Keto-cholesterol [3 β -Hydroxycholest-5-en-7-one] "7-KC"		402.3498	534.4054
18	6 β -Hydroxy-cholesterol [Cholest-5-ene-3 β ,6 β -diol] "6 β -HC"		402.3498	534.4054
19	24(S),25-Dihydroxy-cholesterol [Cholest-5-ene-3 β ,24(S),25-triol] "24(S),25-DiHC"		418.3447	550.4003

20	7 α ,24-Dihydroxy-cholesterol [Cholest-5-ene-3 β ,7 α ,24-triol] "7 α ,24-DiHC"		418.3447	550.4003
21	7 α ,25-Dihydroxy-cholesterol [Cholest-5-ene-3 β ,7 α ,25-triol] "7 α ,25-DiHC"		418.3447	550.4003
22	7 β ,25-Dihydroxy-cholesterol [Cholest-5-ene-3 β ,7 β ,25-triol] "7 β ,25-DiHC"		418.3447	550.4003
23	7 α ,27-Dihydroxy-cholesterol [Cholest-5-ene-3 β ,7 α ,27-triol] "7 α ,27-DiHC"		418.3447	550.4003
24	7 β ,27-Dihydroxy-cholesterol [Cholest-5-ene-3 β ,7 β ,27-triol] "7 β ,27-DiHC"		418.3447	550.4003
25	7 α ,12 α -Dihydroxy-cholesterol [Cholest-5-ene-3 β ,7 α ,12 α -triol] "7 α ,12 α -DiHC"		418.3447	550.4003
26	Cholestenic acid [3 β -Hydroxycholest-5-en-27-oic acid] "CA"		416.3290	548.3847

27	7 β -Cholestenic acid [3 β ,7 β -Dihydroxycholest-5-en-27-oic acid] “7 β -CA”		432.3240	564.3796
28	7 α -Cholestenic acid [3 β ,7 α -Dihydroxycholest-5-en-27-oic acid] “7 α -CA”		432.3240	564.3796
29	24(S),25-O-Me-Hydroxy-cholesterol		432.3603	564.4160
30	7 α ,24(S),25-Trihydroxy-cholesterol [Cholest-5-ene-3 β ,7 α ,24(S),25-tetrol] “7 α ,24(S),25-TriHC”		434.3396	566.3952
31	7-dehydro, 24(S),25-Dihydroxy-cholesterol [7-Dehydrocholest-5-ene-3 β ,24(S),25-triol] “7D,24(S),25-DiHC”		416.3290	548.3847

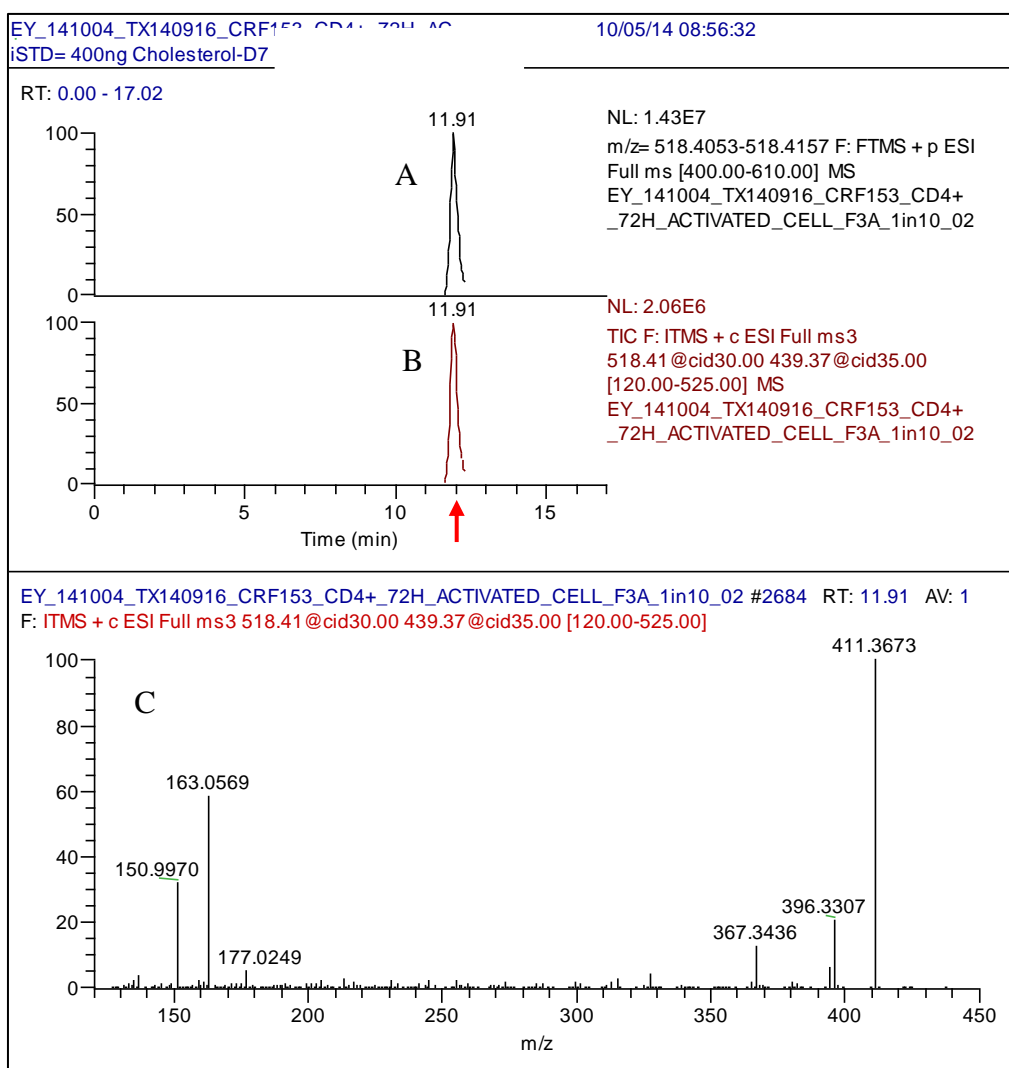


Figure 2.6. Representative process of ion isolation, identification and quantification of sterol species analysed by LCMS on Xcalibur Qual Browser.

(A) Using Cholesterol as an example, a reconstructed ion chromatogram (RIC) was opened on the full MS scan to isolate the cholesterol $[M]^+$ ion, $518.4105 m/z$, detected on the Orbitrap analyser. (B) Next, a total ion chromatogram (TIC) was opened for the MS^3 transition $518 \rightarrow 439 \rightarrow$ in the linear ion trap. (C) Then, the peak apex at 11.91min on the TIC was selected to confirm the fragmentation pattern with the authentic cholesterol standard. Once confirmed, the peak in the full MS scan (A) was integrated and the peak area was exported to Microsoft Excel. This was also done for the internal standard Cholesterol-D7 with a $[M]^+$ ion, $525.4544 m/z$ and MS^3 multi-stage transition of $525 \rightarrow 446 \rightarrow$.

2.3. Analysis of T Lymphocyte Gene and Protein Expression.

2.3.1. Molecular Biology Materials.

2.3.1.1. Reagents, instruments and kits.

Materials used for measuring relative mRNA expression by qPCR and soluble protein expression in culture media by ELISA are listed in Table 2.7.

Table 2.7. List of reagents, instruments and kits for gene and protein expression analysis.

Reagent/Kit	Catalogue Number	Manufacturer	Additional information
RNeasy Mini Kit	74104	Qiagen (Manchester UK)	
QuantiTect Reverse Transcription Kit	205313	Qiagen (Manchester UK)	
SYBR Green PCR Kit	204056	Qiagen (Manchester UK)	
TURBO DNA-free™ Kit	AM1907	Thermo Fisher Scientific (Loughborough UK)	
Tris-EDTA buffer	93283	Sigma-Aldrich	
200µL PCR reaction tubes	732-0548	VWR	
96-well PCR plates	MLL9601	Bio-Rad	
21G 1.5” Needle	12339299	Fisher Scientific	
1mL Luer tip syringe	10142104	Fisher Scientific	
Microseal® ‘B’ Adhesive seals	MSB1001	Bio-Rad	
Tween® 20	P7949	Sigma-Adlrich	
Phosphoric Acid (H ₃ PO ₄)	345245	Sigma-Adlrich	
96-well half-area ELISA plates	675061	Greiner Bio-one (Stonehouse UK)	
96-well Bio-Plex® pro flat bottom black plates	171025001	Bio-Rad (Hemel Hempstead UK)	Used for Luminex assay with Bio-Plex® Handheld Magnetic Washer
Bio-Plex® Calibration Kit	171203060	Bio-Rad (Hemel Hempstead UK)	
Human IFN gamma ELISA Ready-Set-Go!®	88-7316-22	eBioscience (Hatfield UK)	
Luminex® Screening Human Magnetic Assay	LXSAHM	R&D Systems	Multiplex of TNF-α, IFN-γ, IL-17A, IL-6, IL-4 and IL-12p70
4D-Nucleofector™ System	AAF-1002B	Lonza Biologics (Slough UK)	
T100™ Thermal Cycler	1861096	Bio-Rad (Hemel Hempstead UK)	

CFX Connect™ Real-Time PCR Detection System	1855200	Bio-Rad (Hemel Hempstead UK)	
NanoDrop 8000 Spectrophotometer	-----	Thermo Scientific (Loughborough UK)	
POLARStar OMEGA Plate Reader	-----	BMG Labtech (Aylesbury UK)	With 450nm and 570nm filters
Bio-Plex® 200 System	171000205	Bio-Rad (Hemel Hempstead UK)	Equipped with high-throughput fluidics
Bio-Plex® Handheld Magnetic Washer	171020100	Bio-Rad (Hemel Hempstead UK)	

2.3.1.2. Oligonucleotide primers.

The primers used to monitor gene expression are listed in Table 2.8.

Table 2.8. List of primers and gene targets used for qPCR.

Target Gene	Forward and reverse Sequence	Supplier	Reference
Human <i>RPS18</i>	F-5'-GGACAGGATTGACAGATTGAT-3' R-5'-AGTCTCGTTCGTTATCGGAAT-3'	Sigma- Aldrich (Dorset UK)	[4]
Human <i>CH25H</i>	F-5'-TCCCTTGGTCCACTCACAGACT-3' R-5'-TGTGTAAGTACGGAGCGAAGTTG-3'	Sigma- Aldrich	[5]
Human <i>CYP7B1</i>	F-5'-GTCCTACATGGTGACCCTGA-3' R-5'-CATTGCTGGTCCAGTTCC-3'	Sigma- Aldrich	[6]
Human <i>IFNG</i>	F-5'-GGCTTTTCAGCTCTGCATCG-3' R-5'-TCTGTCCTCTCTTTCCAA-3'	Sigma- Aldrich	[7]
Human <i>FOXP3</i>	F-5'-TGACCAAGGCTTCATCTGTG-3' R-5'-GAGGAACTCTGGGAATGTGC-3'	Sigma- Aldrich	[8]
Human <i>IL10</i>	F-5'-GGCGCTGTCATCGATTTCTT-3' R-5'-GGCTTGTAGATGCCTTCTCTTG-3'	Sigma- Aldrich	[9]
Human <i>IL4</i>	F-5'-AACAGCCTCACAGAGCAGAAGAC-3' R-5'-GCCCTGCAGAAGGTTTCCTT-3'	Sigma- Aldrich	[10]
Human <i>IL17A</i>	F-5'-ACCAATCCAAAAGGTCCTC-3' R-5'-GGGGACAGAGTTCATGTGGT-3'	Sigma- Aldrich	[11]
Human <i>SRPBF2</i>	F-5'-CCCTTCAGTGCAACGGTCATTCAC-3' R-5'-TGCCATTGGCCGTTTGTGTC-3'	Sigma- Aldrich	[12]
Human <i>HMGCR</i>	F-5'-GACGTGAACCTATGCTGGTCAG-3' R-5'-GGTATCTGTTTCAGCCACTAAGG-3'	Sigma- Aldrich	[13]
Human <i>RORC</i>	F-5'-TTTTCCGAGGATGAGATTGC-3' R-5'-CTTCCACATGCTGGCTACA-3'	Sigma- Aldrich	[11]
Human <i>RORA</i>	F-5'-TCATGGCTGCAAGAAAAGGT-3' R-5'-GAGGAAAATGAAGTCGCACAA-3'	Sigma- Aldrich	[14]

2.3.2. Relative Gene Expression Analysis by RT-qPCR.

2.3.2.1. Isolation of total RNA from T Lymphocytes.

Total RNA was extracted from T cells using RNeasy Mini Kit following manufacturer's guidelines and instructions. All plasticware and buffers were RNase free. Briefly, after culture, cells were washed in PBS were counted then pelleted at 515 xg RT for 10 minutes and the supernatant removed. Then, 350µL of RLT lysis buffer was added and mixed well. Cells were homogenised to a reduced viscosity using a 21G needle attached to a 1mL syringe by drawing through the needle at least 10 times. Next, 350µL of 70% EtOH was added and mixed well. The 700µL cell lysate was transferred to an RNeasy spin column placed on a 2mL collection tube. The spin column was centrifuged at 8000 xg RT for 15 seconds, flow through discarded, and the spin column placed back on the 2mL collection tube. Spin column was washed with 700µL RW1 buffer then 500µL RPE buffer both at 8000 xg RT for 15 seconds and flow through discarded. Column was washed again with 500µL RPE buffer and centrifuged at 8000 xg RT for 2 minutes, flow through discarded and placed on a new 2mL collection tube. The empty column was further centrifuged at 17,000 xg RT for 1 minute to remove remaining RPE buffer. Finally, bound RNA was eluted with 40µL of RNase-free water pipetted directly at the membrane and centrifuged at 8000 xg RT for 1 minute. Eluted RNA was kept in ice or stored long term in a -80°C freezer.

Nucleic acid concentration and quality was estimated using a NanoDrop 8000 Spectrophotometer.

2.3.2.2. Elimination of genomic DNA by DNase digestion.

When indicated, presence of contaminating DNA from the RNA extract was eliminated using a TURBO DNA-free™ Kit, following manufacturer's instructions, prior to reverse transcription. In brief, 1 to 4µg of RNA was diluted with a final volume of 20µL of RNase-free water in PCR reaction tubes. 2µL of TURBO DNase buffer (10X) was added to each reaction tube followed by 1µL of TURBO DNase then mixed well. Tubes were incubated at 37°C for 30 minutes. To inactivate the DNase, 2µL of thoroughly resuspended DNase inactivation reagent was added and incubated at 22 to 26°C for 5 minutes. The tubes were centrifuged at 10,000 xg for 2 minutes to pellet

the inactivation reagent and the supernatant, containing TURBO DNase treated RNA, transferred to a new RNase-free tube.

2.3.2.3. Complementary DNA synthesis.

When indicated, complementary DNA was synthesised either from the RNA extract in *section 2.3.2.1* or TURBO DNase-treated RNA from *section 2.3.2.2*.

2.3.2.3.1. cDNA synthesis from RNA.

A QuantiTect Reverse Transcription Kit was used following manufacturer's instructions. Briefly, on a 200µL PCR reaction tube, 1 to 3µg of template RNA was diluted to a final volume of 12µL with RNase-free water, then 2µL 7x gDNA Wipeout buffer was added, mixed and incubated at 42°C for 5 minutes. A second set of tubes were setup for 'noRT' samples, when required. An 'RT' mastermix was made containing 4µL RT buffer, 1µL Primer mix, and 1µL RT per sample as well as a 'noRT' mastermix containing 4µL RT buffer, 1µL Primer mix and 1µL RNase-free water per sample, then mixed well. To each of the 'RT' samples, 6µL of 'RT' mastermix was added to final volume of 20µL. Similarly for 'noRT' samples, 6µL of 'noRT' mastermix was added and mixed well. All reaction tubes were incubated at 42°C for 15 minutes followed by 95°C for 3 minutes on a T100™ Thermal Cycler. Synthesised cDNA was stored at -20°C.

2.3.2.3.2. cDNA synthesis from TURBO DNase-treated RNA.

A QuantiTect Reverse Transcription Kit was also used to synthesise cDNA from TURBO DNase-treated RNA. Briefly, on a 200µL PCR reaction tube, 4µL of template RNA was diluted with 8µL RNase-free water, then 2µL 7x gDNA Wipeout buffer was added and incubated at 42°C for 5 minutes. A second set of tubes were setup for noRT samples, when required. An 'RT' mastermix was made containing 4µL RT buffer, 1µL Primer mix, and 1µL RT per sample as well as a 'noRT' mastermix containing 4µL RT buffer, 1µL Primer mix and 1µL RNase free water per sample, then mixed well. To each of the 'RT' samples, 6µL of 'RT' mastermix was added to final volume of 20µL. Similarly for 'noRT' samples, 6µL of 'noRT' mastermix was added and mixed well. All reaction tubes were incubated for 42°C for 15 minutes followed by 95°C for 3 minutes on a T100™ Thermal Cycler. Synthesised cDNA from TURBO DNase-treated RNA was stored at -20°C. Following manufacturer's guidelines, a

maximum of 4 μ L of template TURBO DNase-treated RNA was used per 20 μ L RT reaction volume as components from the DNase step such as the TURBO DNase buffer and DNase Inactivation Reagent could interfere with RT-PCR reactions if proportions exceed 20%. As a consequence, this has reduced the maximum amount of RNA for cDNA synthesis.

2.3.2.4. Primer reconstitution and preparation.

Oligonucleotides were resuspended in Tris-EDTA (TE) buffer for a final concentration of 100 μ M as per supplier's instructions. Aliquots of both forward and reverse primers were diluted 1:1 for a combined stock containing 50 μ M forward and 50 μ M reverse primer mix. The 50 μ M combined stock was then used for RT-PCR reaction diluted 1:50 to give a final primer concentration of 1 μ M. All reconstituted primers were stored at -20°C in a DNase-free/RNase-free tubes.

2.3.2.5. Real Time Quantitative Polymerase Chain Reaction.

Relative gene expression of cultured T lymphocytes were analysed by RT-qPCR using SYBR Green PCR kit. Briefly, after cDNA synthesis, cDNA was diluted from 1:5 to 1:20, determined empirically, with RNase-free water to a final volume of 5 μ L per PCR reaction, mixed well by vortex and centrifuged briefly. A mastermix was prepared for each gene of interest containing 12.5 μ L SYBR Green, 7 μ L RNase-free water, and 0.5 μ L of 50 μ M combined primers per PCR reaction, mixed well by vortex and centrifuged briefly. Next, diluted cDNA was aliquoted at 5 μ L per well in triplicate on a 96-well PCR plate. Then, 20 μ L of mastermix for the gene of interest were added to each well containing cDNA. Afterwards, the plate was sealed using Microseal® B adhesive seal and centrifuged at 1000 xg RT for 1 minute then submitted for qPCR analysis on a CFX Connect™ Real-Time PCR Detection System. The PCR protocol that was followed were: Initial activation step for 5 minutes at 95°C and denature step for 10 seconds at 95°C, next, annealing/extension step at 60°C then the plate was read for SYBR Green fluorescence. The denature and annealing/extension steps were repeated 44 times before a melt curve analysis was done by cooling to 55°C for 5 seconds and temperature steadily ramped up to 95°C at 0.5°C increments every 5 seconds with plate read at each increment.

2.3.2.6. Quantitative PCR Analysis.

Data acquired from the CFX Connect™ Real-Time PCR Detection System was analysed either using Bio-Rad CFX Manager version 3.1 or manually by Microsoft Excel 2013 using the $2^{-\Delta\Delta Ct}$ method ^[15] after exporting triplicate cycle threshold (Ct) values for the control and target genes per sample. After outliers were omitted, the difference in cycle threshold (ΔCt) between the target gene Ct and the housekeeping gene Ct was measured using the mean value calculated from the replicates as in Equation 2.2. Then, the difference between the mean control sample ΔCt and mean treatment sample ΔCt was measured as $\Delta\Delta Ct$ using Equation 2.3. Finally, the relative gene expression level for each target gene for control and treated samples were calculated using Equation 2.4. Comparison of gene expression between control and treated samples were expressed as fold change relative to control samples. Outliers were omitted using the melt curve analysis done after the qPCR run using the CFX Manager.

Equation 2.2. Formula used to measure the cycle threshold difference (ΔCt) of the target gene from the housekeeping gene for each sample.

$$\Delta Ct = \textit{average target gene Ct} - \textit{average housekeeping gene Ct}$$

Equation 2.3. Formula used to measure the cycle threshold difference between treatment ΔCt and control ΔCt samples.

$$\Delta\Delta Ct = \textit{treatment sample } \Delta Ct - \textit{control sample } \Delta Ct$$

Equation 2.4. Formula used for manual determination relative expression of target genes expressed as fold change

$$\textit{fold change} = 2^{-(\Delta\Delta Ct)}$$

2.3.3. Soluble Protein Detection and Quantification by Immunoassay.

Measurement of protein expression was analysed either by flow cytometry for intracellular protein in *section 2.1.8.5* or plate based for soluble protein production. Plate based analysis included the quantification of human Interferon gamma contained in culture media samples by sandwich enzyme-linked immunosorbent assay or multiple analytes (hTNF- α , hIFN γ , hIL-17, hIL-6, hIL-4, and hIL-12p70) by Luminex® magnetic-bead multiplex assays.

2.3.3.1. Measurement of soluble Interferon gamma produced by CD4⁺ T cells by sandwich ELISA.

To measure the production of soluble IFN- γ by T cells, a Human IFN gamma ELISA Ready-Set-Go!® Kit was used according to manufacturer's instructions with few modifications. The sandwich immunoassays were done using half area plates which used half of the reagents manufacturers have suggested. Briefly, the 10X coating buffer was diluted to 1x using distilled water. Then, the 250X capture antibody was diluted to 1x with the 1x coating buffer. A 96-well half-area plate was coated with 50 μ L of 1x capture antibody per well, covered with a plate sealer and incubated in the fridge at 4°C overnight. Following this, plate was washed three times with 200 μ L 0.05% Tween® 20 in PBS wash buffer then blotted dry upside down on an absorbent paper. A 1X assay diluent was diluted from 5X using distilled water. The coated wells were subsequently blocked by adding 100 μ L 1X assay diluent per well, covered with a plate sealer, and incubated at RT for 1 hour on an 800rpm plate shaker. During incubation, the IFN- γ standard was reconstituted with distilled water as per manufacturer certificate of analysis and then afterwards to 15ng/mL using 1X assay diluent. Using the 15ng/mL stock, a 500pg/mL was prepared as the top standard. Next, an 8-point 2-fold serial dilution was done to have a 250, 125, 62.5, 31.25, 15.6, 7.8ng/mL and a blank using the assay diluent. When necessary, media samples were also diluted from neat to 1:400, determined empirically. After the blocking step, plate was washed three times then blotted dry. Standards and samples were added to the plate at 50 μ L per well in duplicate then covered with a plate sealer and incubated at RT for 2 hour on an 800rpm plate shaker. During incubation, 250X detection antibody was diluted to 1x with the assay diluent. After incubation, plate was washed five times then blotted dry. Then, 50 μ L of 1X detection antibody was added to each well, covered

with a plate sealer and incubated at RT for 1 hour on an 800rpm plate shaker. During incubation, 250X avidin-HRP was diluted to 1x with the assay diluent. After incubation, plate was washed five times then blotted dry. Then, 50 μ L of 1X avidin-HRP was added to each well, covered with a plate sealer and incubated at RT for 30 minutes on an 800rpm plate shaker. Afterwards, plate was washed seven times and blotted dry. Using a multichannel pipette, colour was developed by adding 50 μ L of 1X Tetramethylbenzidine (TMB) solution per well then incubated at RT for 30 minutes in the dark. The reaction was stopped using 1M H₃PO₄ added at 25 μ L per well using a multichannel pipette. Finally, the plate was read on a POLARStar OMEGA Plate Reader at 450nm and 570nm.

2.3.3.2. Data analysis for sandwich ELISA.

Optical density (OD) values from 450nm and 570nm were analysed using MARS Data Analysis software from BMG-LABTECH or raw data exported to Microsoft Excel for manual linear regression analysis. Briefly, 570nm OD values subtracted from 450nm OD values, averaged between the duplicates and the average OD of the blanks were subtracted from the sample and standard average ODs. The blank-subtracted OD of the standards were then fitted on a linear regression curve against the standard concentrations to generate a linear equation. The slope and intercept of the equation were used to calculate the concentration of IFN- γ in the samples expressed in ng/mL.

2.3.3.3. Measurement of multiple soluble cytokines produced by CD4⁺ T cells by xMAP® technology.

When indicated, multiple cytokine production by activated CD4⁺ T cells were also analysed using a 6-plex Luminex® Screening Multiplex assay kit from R&D Systems following manufacturer's instructions. The production of TNF- α , IFN- γ , IL-17A, IL-6, IL-4 and IL-12p70 was monitored from media of activated human T cells *in vitro* which were treated with silencing RNA for *CH25H* (as discussed in *section 6.3.2*). Briefly, the samples were first diluted at 1:10 and the lyophilised standards reconstituted based on the certificate of analysis and further prepared a 6-point 3-fold serial dilution using the calibrator diluent. Also, the magnetic human pre-mixed microparticle cocktail was diluted with the diluent at 1:11. Using a 96-well Bio-Plex pro flat bottom plate, 50 μ L of the diluted magnetic human pre-mixed microparticle cocktail was added per well followed by 50 μ L of the diluted samples, 6-point serial

diluted standards and a diluent blank in duplicates. Plate was covered with a foil and incubated on an 800rpm shaker for 2 hours at RT. During incubation, the Bio-Plex® 200 system was calibrated using the MCV plate and Bio-Plex® Calibration kit as per manufacturer instruction. Also, the pre-mixed biotin antibody cocktail was diluted at 1:11. After incubation, the magnetic beads were washed using 100µL 1X wash buffer on a Bio-Plex® Handheld Magnetic Washer three times then gently blotted dry on an absorbent paper. Then, 50µL of the diluted pre-mixed biotin antibody cocktail was added to each well and incubated on an 800rpm shaker for 1 hour at RT. During incubation, streptavidin-PE was diluted at 1:25 using the 1X wash buffer. The plate was washed afterwards and blotted dry then 50µL of diluted streptavidin-PE was added per well, covered with foil then incubated on an 800rpm shaker for 30 minutes at RT. Subsequently, the plate was washed three times and resuspended the magnetic microparticles in 100µL 1X wash buffer. Finally, the plate was momentarily incubated on an 800rpm shaker for 2 minutes at RT then read on a Bio-Plex® 200 System using the correct microbead region as indicated in the certificate of analysis.

2.3.3.4. Data analysis for Luminex® multiplex assay on Bio-Plex Manager™ software.

All data acquisition and analysis were done using the Bio-Plex Manager™ software which fitted a five parameter logistic (5-PL) curve for each analyte and calculated the observed concentration from the blank subtracted PE fluorescence of the 3-fold diluted standard concentrations. Using the curve, concentration of TNF α , IFN- γ , IL-17A, IL-6, IL-4 and IL-12p70 was calculated based on the blank subtracted PE fluorescence multiplied by the dilution factor. In addition, the % coefficient of variation and standard deviation was also calculated from the duplicates.

2.4. References:

- [1] W.J. Griffiths, P.J. Crick, Y. Wang, M. Ogundare, K. Tuschl, A. a. Morris, et al., (2013) Analytical strategies for characterization of oxysterol lipidomes: Liver X receptor ligands in plasma, *Free Radic. Biol. Med.* 59 69–84. doi:10.1016/j.freeradbiomed.2012.07.027.
- [2] W.J. Griffiths, M. Hornshaw, G. Woffendin, S.F. Baker, A. Lockhart, S. Heidelberger, et al., (2008) Discovering oxysterols in plasma: A window on the metabolome, *J. Proteome Res.* 7 3602–3612. doi:10.1021/pr8001639.
- [3] K. Karu, M. Hornshaw, G. Woffendin, K. Bodin, M. Hamberg, G. Alvelius, et al., (2007) Liquid chromatography-mass spectrometry utilizing multi-stage fragmentation for the identification of oxysterols., *J. Lipid Res.* 48 976–987. doi:10.1194/jlr.M600497-JLR200.
- [4] D. Studer, S. Lischer, W. Jochum, M. Ehrbar, M. Zenobi-Wong, K. Maniura-Weber, (2012) Ribosomal protein l13a as a reference gene for human bone marrow-derived mesenchymal stromal cells during expansion, adipo-, chondro-, and osteogenesis., *Tissue Eng. Part C. Methods.* 18 761–71. doi:10.1089/ten.TEC.2012.0081.
- [5] H. Sugiura, A. Koarai, T. Ichikawa, Y. Minakata, K. Matsunaga, T. Hirano, et al., (2012) Increased 25-hydroxycholesterol concentrations in the lungs of patients with chronic obstructive pulmonary disease., *Respirology.* 17 533–40. doi:10.1111/j.1440-1843.2012.02136.x.
- [6] S. Steckelbroeck, M. Watzka, D. Lütjohann, P. Makiola, A. Nassen, V.H.J. Hans, et al., (2002) Characterization of the dehydroepiandrosterone (DHEA) metabolism via oxysterol 7 α -hydroxylase and 17-ketosteroid reductase activity in the human brain, *J. Neurochem.* 83 713–726. doi:10.1046/j.1471-4159.2002.01187.x.
- [7] Y. Shi, X. Fan, W. Meng, H. Deng, N. Zhang, Z. An, (2014) Engagement of immune effector cells by trastuzumab induces HER2/ERBB2 downregulation in cancer cells through STAT1 activation., *Breast Cancer Res.* 16 R33. doi:10.1186/bcr3637.
- [8] C. Huang, S. Martin, C. Pflieger, J. Du, J.H. Buckner, J. a Bluestone, et al., (2013) Cutting Edge: a novel, human-specific interacting protein couples FOXP3 to a chromatin-remodeling complex that contains KAP1/TRIM28., *J. Immunol.* 190 4470–3. doi:10.4049/jimmunol.1203561.
- [9] M. François, R. Romieu-Mourez, M. Li, J. Galipeau, (2012) Human MSC Suppression Correlates With Cytokine Induction of Indoleamine 2,3-Dioxygenase and Bystander M2 Macrophage Differentiation, *Mol. Ther.* 20 187–195. doi:10.1038/mt.2011.189.
- [10] P. Boeuf, I. Vigan-Womas, D. Jublot, S. Loizon, J.-C. Barale, B.D. Akanmori, et al., (2005) CyProQuant-PCR: a real time RT-PCR technique for profiling human cytokines, based on external RNA standards, readily automatable for clinical use., *BMC Immunol.* 6 5. doi:10.1186/1471-2172-6-5.
- [11] N. Manel, D. Unutmaz, D.R. Littman, (2008) The differentiation of human TH-17 cells requires transforming growth factor- β and induction of the nuclear receptor ROR γ t, *Nat. Immunol.* 9 641–649. doi:10.1038/ni.1610.

- [12] F. Caballero, A. Fernández, A.M. De Lacy, J.C. Fernández-Checa, J. Caballería, C. García-Ruiz, (2009) Enhanced free cholesterol, SREBP-2 and StAR expression in human NASH., *J. Hepatol.* 50 789–96. doi:10.1016/j.jhep.2008.12.016.
- [13] K. Cai, N.C. Lucki, M.B. Sewer, (2014) Silencing diacylglycerol kinase-theta expression reduces steroid hormone biosynthesis and cholesterol metabolism in human adrenocortical cells., *Biochim. Biophys. Acta.* 1841 552–62. doi:10.1016/j.bbailip.2013.12.005.
- [14] T. Sarachana, V.W. Hu, (2013) Genome-wide identification of transcriptional targets of RORA reveals direct regulation of multiple genes associated with autism spectrum disorder., *Mol. Autism.* 4 14. doi:10.1186/2040-2392-4-14.
- [15] K.J. Livak, T.D. Schmittgen, (2001) Analysis of relative gene expression data using real-time quantitative PCR and the $2^{-\Delta\Delta C(T)}$ Method., *Methods.* 25 402–8. doi:10.1006/meth.2001.1262.
- [16] W.J. Griffiths, J. Abdel-Khalik, P.J. Crick, E. Yutuc, Y. Wang, (2016) New methods for analysis of oxysterols and related compounds by LC–MS, *J. Steroid Biochem. Mol. Biol.* 162 4–26. doi:10.1016/j.jsbmb.2015.11.017.

CHAPTER 3: Sterols in culture media

3.1. Introduction

In initial stages of the project, different types of culture media and modifications were used to optimise human CD4⁺ T lymphocyte maintenance, growth, activation and sterol metabolism. As cellular sterols produced can either be retained in the cell or exported out to the culture media, it was important to establish a baseline sterol profile for cell-free mock media. This chapter will focus on the detection of free sterols which were naturally present in commercially available culture media as quantified by stable isotope dilution liquid chromatography mass spectrometry. In addition, as sterols can be in 3 β -esterified form or free form^[1], these proportions were also compared in select media.

3.2. Materials and Methods

3.2.1. Media preparation, sterol extraction and LC-MSⁿ analysis.

One to two millilitres of Serum-Free, Delipidated, and Full media with modifications described in *section 2.1.1.1* were extracted in EtOH containing internal sterol standards as described in *section 2.2.2*. Media extracts were subjected to EADSA processing and analysis by HPLC-ESI-MSⁿ on either an Orbitrap Velos or Orbitrap Elite for quantification.

3.2.2. Alkali hydrolysis of esterified sterols in X-VIVO-20.

Deuterated internal sterol standards were diluted in ethanol with 0.35M KOH. Next, 3mL of X-Vivo-20 media was added dropwise to 7mL of 0.35M ethanolic KOH containing 2ng 24(R/S)-HC(D6), 2ng 22(R),3-oxo-HC(D7), and 40ng Cholesterol(D7), ultrasonicated for 5 minutes and incubated at RT for 2 hours protected from light. Afterwards, the sample was ultrasonicated again for 5 minutes and neutralised to pH 7 with 140 μ L glacial acetic acid. Another 3mL of X-VIVO-20 was also done in parallel but in ethanol only, without KOH and acetic acid

neutralisation to represent the free sterols. Both samples were further processed the same way as in *section 2.2.2* then analysed for sterol content by HPLC-ESI-MSⁿ.

3.3. Results

3.3.1. Several sterol species were present in Full media and DL media which were absent in Serum-Free RPMI media.

Table 3.1 lists the detected sterols which were identified using the EASDA method described in *section 2.2.2*. RPMI 1640 modified to only contain β -mercaptoethanol, penicillin, streptomycin and glutamine without foetal bovine serum (Serum-free media) did not contain detectable free sterols except for cholesterol autoxidation artefacts 7α -HC and 6β -HC (Figure 3.1A). These artefacts are likely formed from low levels of contaminating cholesterol during sample preparation exposed in ambient air.

The supplementation of the serum-free media with 10% FBS (Full media) revealed several detectable sterol species. Namely, cholestenic acid and 7α -CA were detected between 350 to 544 pg/mL levels similar to cholesterol autoxidation products 7β -HC, 7α -HC and 6β -HC. Other monohydroxycholesterols like $24(S)$ -HC, $24(R)$ -HC, 25 -HC and 27 -HC were quantified between 45 to 170 pg/mL of media (Figure 3.1B).

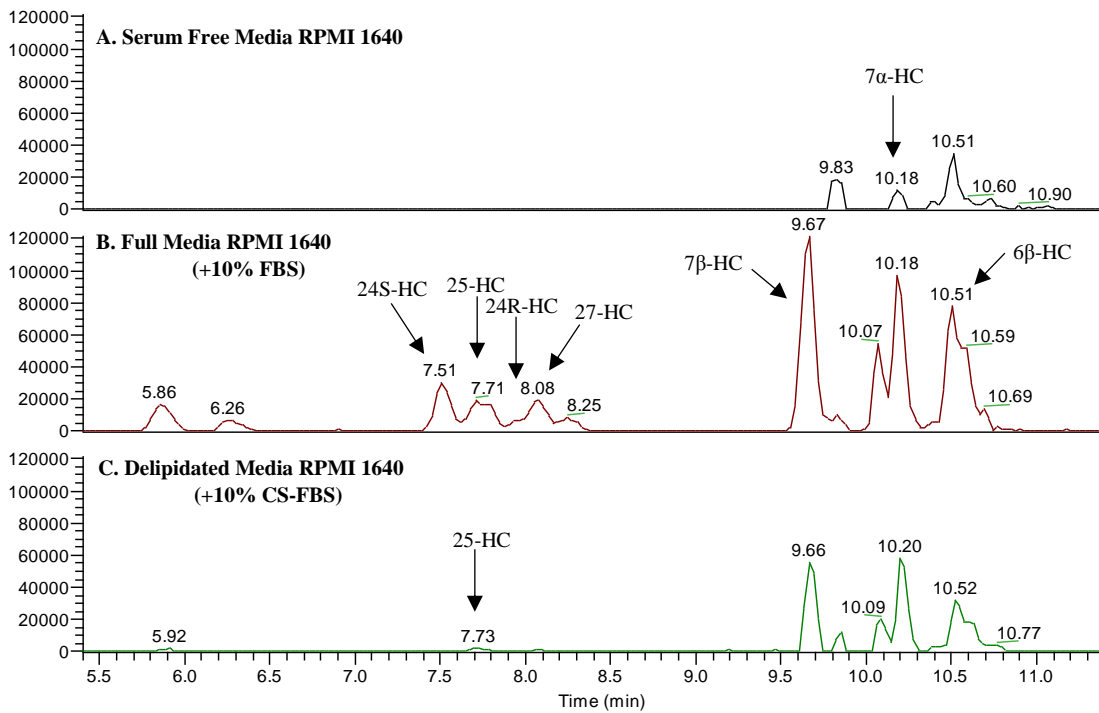


Figure 3.1. Representative reconstructed ion chromatograms for monohydroxycholesterols present in different culture media.

Sterols from (A) 1mL serum free RPMI, (B) 2mL full media RPMI and (C) 1mL delipidated RPMI were extracted using the EADSA method and subjected to analysis by HPLC-ESI-MSⁿ. An abundance of different sterols were detected in full media (with 10% FBS) which were not present or at minimal levels in serum free media. However, modification of RPMI 1640 using 10% charcoal-stripped FBS, as Delipidated media, detected reduced presence of sterols.

Table 3.1. Quantification table for sterols detected in serum-free, full and delipidated media. Values were normalised to the volume of media extracted. n=3 of different extractions.(n.d. = not detected)

Sterol	Quantification (pg/mL \pm SD)		
	Serum-Free RPMI 1640	Full (+10% FBS)	DL (+10% CS-FBS)
24S-HC	n.d.	177.26 \pm 21.39	n.d.
24R-HC	n.d.	46.51 \pm 9.37	n.d.
25-HC	n.d.	59.35 \pm 18.97	40.961 \pm 23.69
27-HC	n.d.	129.37 \pm 15.22	n.d.
7 β -HC	n.d.	523.68 \pm 174.41	139.61 \pm 130.32
7 α -HC	189.13 \pm 109.19	389.73 \pm 146.45	328.97 \pm 72.74
6 β -HC	590.71 \pm 267.13	336.11 \pm 202.63	627.96 \pm 550.38
7 α ,25-DiHC	n.d.	18.55 \pm 2.60	n.d.
7 α ,27-DiHC	n.d.	19.15 \pm 5.60	n.d.
CA	n.d.	544.07 \pm 82.68	256.53 \pm 116.08
7 β -CA	n.d.	54.96 \pm 14.95	n.d.
7 α -CA	n.d.	473.05 \pm 67.51	n.d.

To appropriately study the effects and interactions of sterols in immunity, sterols would have to be removed from serum and this can be accomplished by charcoal-stripping (CS). Charcoal stripping of serum can eliminate non-polar compounds such as steroid hormones, growth factors and lipids but retains salts, glucose and amino acids^[2]. This process can also deplete cholesterol and cholesterol-related compounds in serum. The supplementation of serum-free media with 10% CS-FBS revealed absence of detectable sterols, namely 24S-HC, 24R-HC, 27-HC, 7 α ,25-DiHC, 7 α ,27-DiHC, 7 β -CA and 7 α -CA previously found in Full media (Figure 3.1C). Still, some sterols such as cholestenic acid, 25-HC, 7 β -HC, 7 α -HC and 6 β -HC were detected, albeit at reduced concentrations compared to Full media.

In terms of sterols not present in the tested media, dihydroxycholesterols such as 7 β ,25-DiHC, 7 β ,27-DiHC, 7 α ,12 α -DiHC or 24(S),25-DiHC were not detected, although 7 α ,25-DiHC, 7 α ,27-DiHC were present at trace levels in Full media.

3.3.2. Free and total sterols in X-VIVO-20 media.

Sterols can either exist as unconjugated free sterols or as esterified conjugated forms^[1]. Due to this, an additional alkali hydrolysis step using ethanolic potassium hydroxide was done during sample extraction to cleave any ester modifications and represent total sterols. Table 3.2 lists the quantified levels of free and total sterols detected in X-Vivo-20.

Although X-Vivo-20 was marketed as serum-free, mass spectrometric analysis detected cholesterol and CA at ng/mL levels; and 27-HC, 7 β -CA and 7 α -CA at sub-ng/mL levels, all of which as unconjugated free sterols. Upon extraction in alkaline conditions, it was found that X-Vivo-20 contained similar proportions of cholesterol esters and free cholesterol; plus, 24(S)-HC and 25-HC were detected which suggests that these were present in media as some form of sterol ester. However, CA, 7 β -CA and 7 α -HC were seen to decrease by ~50% due to the possible dehydration of the 7-hydroxyl group to form a 6-ene during the alkali extraction process.

Table 3.2. Quantification table for sterols detected in X-Vivo-20 with and without hydrolysis in KOH Table represents free and total sterols, respectively. Values were normalised to the volume of media/water extracted. n=3. (n.d. = not detected)

Sterol	Quantification (pg/mL \pm SD)			
	Serum-Free X-Vivo-20	Serum-Free X-Vivo-20 (with hydrolysis)	Water blank	Water blank (with hydrolysis)
24S-HC	n.d.	30.32 \pm 0.22	n.d.	n.d.
24R-HC	n.d.	n.d.	n.d.	n.d.
25-HC	n.d.	5.12 \pm 0.37	n.d.	n.d.
27-HC	67.99 \pm 4.03	58.59 \pm 0.67	n.d.	n.d.
7 β -HC	6.73 \pm 1.82	96.44 \pm 3.77	n.d.	n.d.
7 α -HC	3.80 \pm 2.47	41.94 \pm 0.96	n.d.	n.d.
6 β -HC	52.01 \pm 7.18	37.34 \pm 4.12	40.54 \pm 5.67	22.74 \pm 1.22
7 α ,25-DiHC	n.d.	n.d.	n.d.	n.d.
7 α ,27-DiHC	n.d.	n.d.	n.d.	n.d.
CA	5,162.37 \pm 73.63	2,227.26 \pm 25.35	n.d.	n.d.
7 β -CA	217.13 \pm 18.88	96.44 \pm 3.77	n.d.	n.d.
7 α -CA	889.11 \pm 9.04	412.43 \pm 0.63	n.d.	n.d.
Cholesterol	3,478.10 \pm 5.73	10,079.34 \pm 284.29	239.01 \pm 5.51	209.89 \pm 5.20

3.4. Discussion

Analysing mock media established a baseline for the presence of sterols and provided indication for possible interactions of these sterols with cells in culture. Also, the use of different supplemented media can possibly influence the growth, survival and activity of T cells in culture due to their altered sterol content. The subsequent chapters will describe the sterols generated by pure T cell populations mostly cultured in X-Vivo-20 media.

3.5. References

- [1] W.J. Griffiths, P.J. Crick, Y. Wang, (2013) Methods for oxysterol analysis: Past, present and future, *Biochem. Pharmacol.* 86 3–14. doi:10.1016/j.bcp.2013.01.027.
- [2] Z. Cao, C. West, C.S. Norton-Wenzel, R. Rej, F.B. Davis, P.J. Davis, et al., (2009) Effects of resin or charcoal treatment on fetal bovine serum and bovine calf serum., *Endocr. Res.* 34 101–108. doi:10.3109/07435800903204082.

CHAPTER 4: Sterols generated by human CD4⁺ T cells

4.1. Introduction

Quiescent T cells, which are known to have very low metabolism and energy requirements^[1], continuously recirculate between the blood and lymph after maturation and selection in the thymus and other central lymphoid organs. At this stage, their ultimate function is to encounter cognate antigen presented by activated dendritic cells (DC) with proper co-stimulatory signals and cytokines in order to proceed to the next phase of development. This DC interaction triggers the activation of T cells which induces retention in peripheral lymphoid organs prior to clonal expansion and differentiation into effector T cells. A proportion of the effector T cells can then leave the lymphoid organ returning to the circulation to migrate to the site of infection. During these different stages, T cells undergo drastic and dramatic metabolic changes^[2]. Such metabolic changes include cholesterol homeostasis where the expression of the mevalonate pathway rate-limiting enzyme, 3-hydroxy-3-methylglutaryl-Coenzyme A reductase (HMGCR) is induced in stimulated human T cells^[3] resulting in increased cholesterol biosynthesis. However, if any immune-oxysterols such as 25-HC and 7 α ,25-DiHC are generated by T cells has yet to be studied.

Aims:

1. Establish and optimise human CD4⁺ T cell purification and activation methods.
2. Identification and quantification of oxysterols in activated human CD4⁺ T cells.

4.2. Materials and Methods

4.2.1. Isolation of naïve CD4⁺ T cells.

Naïve CD45RA⁺ CD4⁺ T Cells were isolated from human peripheral blood by density gradient centrifugation and MACS® technology as described in *section 2.1.3* and *section*

2.1.4.1. In the experiments, CD14⁺ cells were first removed from the PBMCs before proceeding to naïve CD4⁺ T cells isolation described in *section 2.1.4.4*.

4.2.2. Isolation of total CD4⁺ T cells.

Similar to naïve cell isolations, total CD4⁺ T Cells were isolated from human peripheral blood as above. However, to maximise the recovery and minimise losses associated with repeated magnetic isolations, the CD14⁺ cell depletion was omitted and total CD4⁺ T cells were obtained straight from PBMCs using only one kit described in *section 2.1.4.2*.

4.2.3. Separating naïve, memory and T_H2 CD4⁺ T cells from total CD4⁺ T cells.

In certain experiments, oxysterol production was compared between naïve and memory CD4⁺ T cells. When indicated, these two populations were isolated from total CD4⁺ T cells using two methods described in *section 2.1.4.3*.

In addition, magnetic isolation of CD294⁺ T_H2 cells from total CD4⁺ T cells were attempted to characterise specific oxysterol production when activated. Total CD4⁺ T cells were first isolated from PBMCs using the methods mentioned previously, then a CD294 (CRTH2) Microbead kit was used to positively select for T_H2 cells.

4.2.4. Purity and activation analysis of naïve CD45RA⁺ CD4⁺ T cells, memory CD45RO⁺ CD4⁺ T cells and total CD4⁺ T cells by flow cytometry.

After each isolation for each donor, an aliquot of either naïve to total CD4⁺ T cells were stained with anti-CD45RA and/or anti-CD4 antibodies and analysed by flow cytometry as described in *section 2.1.8.4*. When indicated, the level of activation of CD4⁺ T cells were also assessed at each end point by staining an aliquot of cells stained with anti-CD25 APC antibody and analysed by flow cytometry.

4.2.5. Culture conditions for unstimulated naïve CD4⁺ T cells in SF and DL media.

Isolated naïve CD4⁺ T cells were seeded at 2.5 to 2.8x10⁶ cells in 1 mL in either SF RPMI media or DL media and cultured for four to six days on a 24-well plate at 37°C 5%CO₂ incubator without any further treatments. As reference, mock SF RPMI and DL media were also seeded and processed in parallel with the cell and media fractions. Experiments were done at least twice using different donors.

4.2.6. Culture conditions for CD3/CD28 activated and T_H17-polarised naïve CD4⁺ T cells in X-VIVO-20 media.

Methods for cell culture, activation and polarisation were adapted from Manel et al. 2008. Briefly, naïve CD45RA⁺ CD4⁺ T cells were isolated from healthy human donors (Table 4.1) as in previous experiments and purity was assessed by flow cytometry. Cells were cultured at a density of 2.5x10⁶ cells/mL/cm², activated with anti-CD3- and anti-CD28-loaded microbeads in an X-Vivo-20 hematopoietic media in both non-polarising and T_H17-polarising conditions. At day three cells were split equally, treated with the IL-2 and media topped up. On day six, cells were stimulated with PMA and Ionomycin for 6 hours before harvest. Table 4.2 lists the culture conditions used to activate and polarise the naïve CD4⁺ T cells. Media fractions were extracted for oxysterols for EADSA processing and LCMS analysis. Cells were also extracted for oxysterols when available. Cells were used for RNA extraction and subsequent gene expression analysis performed by Dr Alwena Morgan. Experiments were done using peripheral blood from two different healthy donors. Due to donor cell number variability, isolated number of T cells from donor 1 was low and only 818,000 cells were cultured and all cells harvested were extracted for RNA thus oxysterols in cell fractions were not available. For donor 2, enough cells were isolated for two separate sets. Set 1 cells were all extracted for RNA. Both cell and media fractions were analysed of oxysterol content in Set 2, although the number of cells cultured were not equal. Activated/non-polarised cell counts were 2.5x10⁶ cells while activated/T_H17-polarised cell counts were 5x10⁶ cells. Although normalised by cells number, sterol data quantification would be more comparable if cultured cells were equal. Additional

experiments using donor 3 were conducted to investigate the effect of IL-2 treatment in the induction of oxysterol production in naïve CD4⁺ T cells.

Table 4.1. Cell numbers seeded and end point analysis for naïve CD4⁺ pilot cultures in X-VIVO-20.

Donor	Culture conditions	Number of cells seeded (10 ⁶ cells)	Analysis at Day 6
1 (EY)	T _H 0 in X-VIVO-20	0.818	Cells for RNA, Media for Sterols
	T _H 17 in X-VIVO-20	0.818	Cells for RNA, Media for Sterols
2 (Set 1) (KQ)	T _H 0 in X-VIVO-20	5	Cells for RNA, Media for Sterols
	T _H 17 in X-VIVO-20	5	Cells for RNA, Media for Sterols
2 (Set 2) (KQ)	T _H 0 in X-VIVO-20	2.5	Cells for Sterols, Media for Sterols
	T _H 17 in X-VIVO-20	5	Cells for Sterols, Media for Sterols
3 (GH)	No IL-2 in SF RPMI	0.588	Cells for Sterols, Media for Sterols
	10U/mL IL-2 in SF	0.588	Cells for Sterols, Media for Sterols
	No IL-2 in X-VIVO-20	0.588	Cells for Sterols, Media for Sterols
	10U/mL IL-2 in XV	0.588	Cells for Sterols, Media for Sterols

Table 4.2. Culture conditions for T_H17-polarised and non-polarised activated (T_H0) naïve CD4⁺ T cells in X-VIVO-20 media.

Treatment	Time of treatment	Non-Polarised – T_H0 (final concentration in culture)	T_H17 Polarised (final concentration in culture)
Anti-CD3/CD28-loaded MACSiBeads	Day 0	1:2 bead to cell ratio	1:2 bead to cell ratio
Human IL-2 (eBioscience 14-8029)	Day 0 and 3	10U/mL	10U/mL
Human IL-1β (eBioscience 14-8018)	Day 0 and 3	blank buffer only	10ng/mL
Human IL-6 (R&D 206/IL/CF)	Day 0 and 3	none	10ng/mL
Human IL-21 (eBioscience 14-8219)	Day 0 and 3	blank buffer only	10ng/mL
Human IL-23 (eBioscience 14-8239)	Day 0 and 3	blank buffer only	10ng/mL
Human TGF-β1 (R&D 240-B-002)	Day 0 and 3	blank buffer only	10ng/mL
Anti human IL-4 (neutralising) (eBioscience 16-7048 clone:MP4-25D2)	Day 0 and 3	none	10µg/mL
Anti human IFN-γ (neutralising) (eBioscience 16-7318 clone:NIB42)	Day 0 and 3	none	10µg/mL
Phorbol myristate acetate (PMA)	Day 6	50ng/mL	50ng/mL
Ionomycin	Day 6	500ng/mL	500ng/mL

4.2.7. Culture conditions and extraction of activated naïve CD4⁺ T cells in X-VIVO-20 supplemented with 4µg/mL heptadeuterio cholesterol.

As before, naïve CD4⁺ T cells were isolated by MACS from the CD14⁻ fraction of PBMCs after CD14⁺ cell depletion. Cells were cultured for 3 days at a seeding concentration of 2.5×10^6 cells/mL/cm² in X-VIVO-20 media supplemented with 10µM (4µg/mL) Cholesterol-D7 in either non-activating or CD3/CD28-activating conditions. Experiment was done with three donors with details listed in Table 4.3. Experiments with donor 1 and 2 were not quantified for intracellular cholesterol content due to a lack of internal standard. A third experiment was additionally done to quantify the intracellular cholesterol and cholesterol-D7 in naïve CD4⁺ cells using a plant sterol, brassicasterol as the internal standard (Figure 4.1). Similar culture conditions were used as in donor 1 and 2 but donor 3 naïve CD4⁺ T cells were first incubated in 4µg/mL cholesterol-D7 for 24 hours, then activated and cultured for a further two days and harvested at day three.

As it is possible that the 24(S)-HC, 24(R)-HC and 25-HC can be generated enzymatically from imported Cholesterol-D7 to form 24(S)-HC-D7, 24(R)-HC-D7 and 25-HC-D6, the current internal sterol standard, 24R/S-HC-D6 cannot be used. Instead, 22(R)-HC-D7 was used as the internal standard at 2ng per sample added upon sterol extraction. As previous naïve CD4⁺ T cell cultures did not show any 22(R)-HC production, 22(R)-HC-D7 was considered a good alternative. Figure 4.3 lists the predicted GP-derivatised structures and [M]⁺ precursor ion masses of oxysterols if they were metabolised from Cholesterol-D7.

Table 4.3. Cell numbers seeded and end point analysis for naïve CD4⁺ cultures in X-VIVO-20 with 4µg/mL Cholesterol-D7.

Donor	Culture condition in X-VIVO-20	Number of cells seeded (10 ⁶ cells)	Analysis at Day 3
1 (081)	Non-activated	1.32	Cells for Sterols, Media for Sterols
	Activated for 3 days	1.32	Cells for Sterols, Media for Sterols
2 (083)	Non-activated	6.0	Cells for RNA, Media for Sterols
	Activated for 3 days	6.0	Cells for RNA, Media for Sterols
3 (092)	Non-activated	1.05	Cells for Sterols, Media for Sterols
	Activated for 2 days	1.05	Cells for Sterols, Media for Sterols

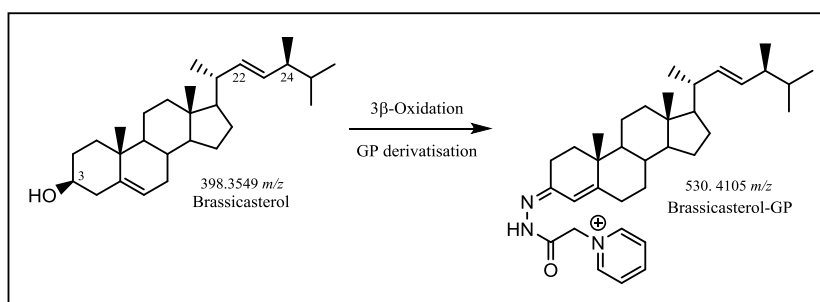


Figure 4.1. Brassicasterol as an internal standard.

The plant sterol, brassicasterol or 24β-methyl cholest-5,22-dien-3β-ol, was used as internal standard added to samples upon sterol extraction to quantify intracellular cholesterol and cholesterol-D7 proportions.

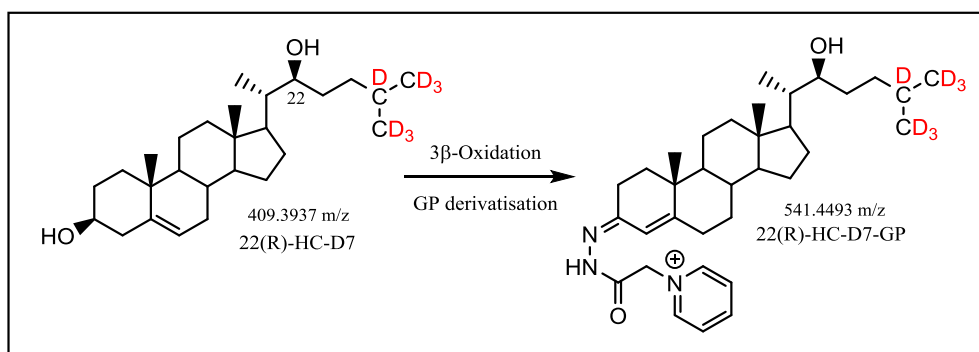


Figure 4.2. Deuterated 22(R)-HC as an internal standard.

The alternative 22(R)-HC-D7 internal sterol standard added at 2ng per sample upon sterol extraction to replace 24(R/S)-HC-D6.

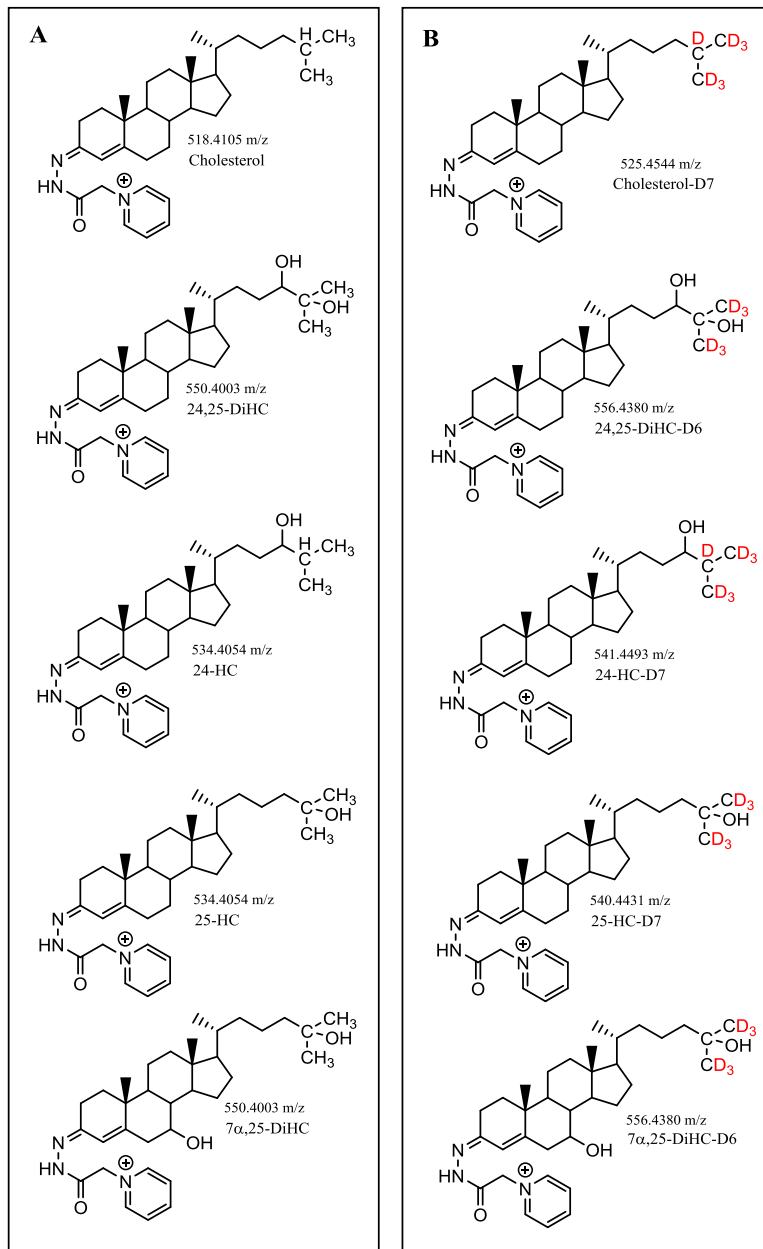


Figure 4.3. Structures of GP derivatised sterols in natural and side-chain deuterium-substituted forms. A. GP-derivatised sterol structures and precursor ion masses of Cholesterol, 24,25-DiHC, 24-HC, 25-HC and 7 α ,25-DiHC. B. Predicted structures and GP-derivatised precursor ion masses of sterols if metabolised from the Cholesterol-D7. Positions of deuterium substitutions are highlighted in red.

4.2.8. Time course culture conditions for activated total CD4⁺ T cells.

Total CD4⁺ T cells magnetically isolated directly from PBMCs were cultured in X-VIVO-20 at a seeding concentration of 2.5x10⁶ cells/mL/cm². Total CD4⁺ T cells were seeded in different wells and activated at the same time. Each well were then extracted at different time points: pre-culture, 1 hour, 4 hours, 16 hours, 24 hours and 48 hours in culture. Parallel to the activated cells corresponding non-activated cells were also seeded and extracted at the same time together with mock X-VIVO-20. Experiments were done with five different donors with details listed in Table 4.4. The level of activation based on CD25 expression was analysed before culture and after 24 to 48 hours. Sterol content was monitored in media fraction extracts from all donors and cell fraction extracts, when available. All of donor 5 cell extracts were used for sterol analysis while for donor 1, 1x10⁶ cell were extracted. All cells of donor 2, 3 and 4 were used for RNA extraction and gene expression analysis conducted by Dr Alwena Morgan.

Table 4.4. Cell numbers seeded and end point analysis for time course experiments on total CD4⁺ cultures in X-VIVO-20.

Donor	Culture condition in X-VIVO-20	Number of cells seeded (10 ⁶ cells) per time point and fraction extracted for sterol analysis at each time point (C=cell; M=media) or flow cytometry analysis (F)					
		0h	1h	4h	16h	24h	48h
1 (007)	Non-activated	(F)	5 (M)	---	---	6.5 (C/M/F)	6.5 (C/M/F)
	Activated		5 (M)	5 (M)	5(M)	6.5 (C/M/F)	6.5 (C/M/F)
2 (124)	Non-activated	(F)	2.8 (M)	---	---	4 (M/F)	---
	Activated		2.8 (M)	2.8 (M)	2.8 (M)	4 (M/F)	---
3 (127)	Non-activated	(F)	---	5 (M)	5 (M)	5 (M)	5 (M/F)
	Activated		---	5 (M)	5 (M)	5 (M)	5 (M/F)
4 (074)	Non-activated	(F)	1.37 (M)	1.37 (M)	1.37 (M)	1.37 (M)	1.37 (M)
	Activated		1.37 (M)	1.37 (M)	1.37 (M)	1.37 (M)	1.37 (M)
5 (010)	Non-activated	3 (C/M/F)	---	---	---	3 (C/M/F)	3.2 (C/M/F)
	Activated		---	---	---	3 (C/M/F)	3.2 (C/M/F)

4.2.9. Culture conditions for naïve and memory CD4⁺ T cells.

Isolated naïve and memory CD4⁺ T cells were cultured at a seeding concentration of 2.5×10^6 cells/mL/cm² in X-VIVO-20. Cells were either activated or left untreated for 24 to 48 hours. Experiment was done with two donors with details in Table 4.5. After 24 or 48 hours, the production of oxysterols in media extracts were compared between the two populations.

Table 4.5. Cell numbers seeded and end point analysis for comparing naïve and memory CD4⁺ cultures in X-VIVO-20.

Donor	CD4 ⁺ T cell culture condition in X-VIVO-20	Number of cells seeded (10^6 cells) per time point and fraction extracted for sterol analysis at each time point (C=cell; M=media) or when flow cytometry analysis was done (F)		
		0h	24h	48h
1 (038)	Naïve Non-activated	(F)	1.26 (M/F)	---
	Naïve Activated		1.26 (M/F)	---
	Memory Non-Activated	(F)	3.18 (C/M/F)	3.18 (C/M/F)
	Memory Activated		3.18 (C/M/F)	3.18 (C/M/F)
2 (092)	Naïve Non-activated	(F)	3.13 (C/M)	---
	Naïve Activated		3.13 (C/M)	3.2 (C/M)
	Memory Non-Activated	(F)	3.13 (C/M)	---
	Memory Activated		3.13 (C/M)	---

In addition, magnetic isolation of CD294⁺ T_H2 cells from total CD4⁺ T cells were attempted twice to characterise specific oxysterol production when activated. Total CD4⁺ T cells were first isolated from PBMCs using the methods mentioned earlier, then a CD294 (CRTH2) Microbead kit was used to positively select for T_H2 cells expressing CD294.

4.2.10. Sample processing and sterol analysis.

At each indicated end point, cells and the media fraction, when available, were extracted for oxysterols as described in *section 2.2.2*. Extracts were processed and subsequently analysed for oxysterol content by LC-ESI-MSⁿ. Sterols were identified and quantified using the method outlined in *section 2.2.4*. In general, only enzymatically-derived oxysterols were monitored. Cholesterol B-ring autoxidation products, which can be produced during the sample preparation and sterols already present in mock media samples were largely considered artefacts and not quantified.

4.3. Results

4.3.1. Isolated naïve CD4⁺ T cells by MACS were >96% pure.

Single stain flow cytometry analysis of cells isolated by MACS were >98% CD45RA⁺ and >97% CD4⁺ cells. Double staining of the cells confirmed >96% to be double positive to CD45RA⁺ CD4⁺. Figure 4.4 shows a representative purity of the CD45RA⁺CD4⁺ cells analysed by flow cytometry prior to culture.

4.3.2. Naïve CD4⁺ T cells do not produce detectable levels of oxysterols when unstimulated in SF RPMI or DL media even after 6 days in culture.

After EADSA and HPLC-ESI-MSⁿ analysis it was found that resting naïve CD4 T cells in culture does not produce detectable levels of enzymatically-derived sterols even after six days in SF RPMI conditions in either cell or conditioned media. Similar to the mock media, only B-ring oxidised sterols, 7 β -HC, 7 α -HC, 6 β -HC were detected (Figure 4.5) and were considered artefacts originating from sample processing. Naïve CD4⁺ T cells were also cultured with DL media. Similar to serum-free cultures, naïve CD4⁺ T cells were not observed to produce detectable levels enzymatically-derived sterols in DL media. Other sterols like 25-HC were detected at trace levels in culture media samples but were not considered to originate from the naïve CD4⁺ T cells as this oxysterol was also present in mock DL media at similar quantities (Figure 4.6).

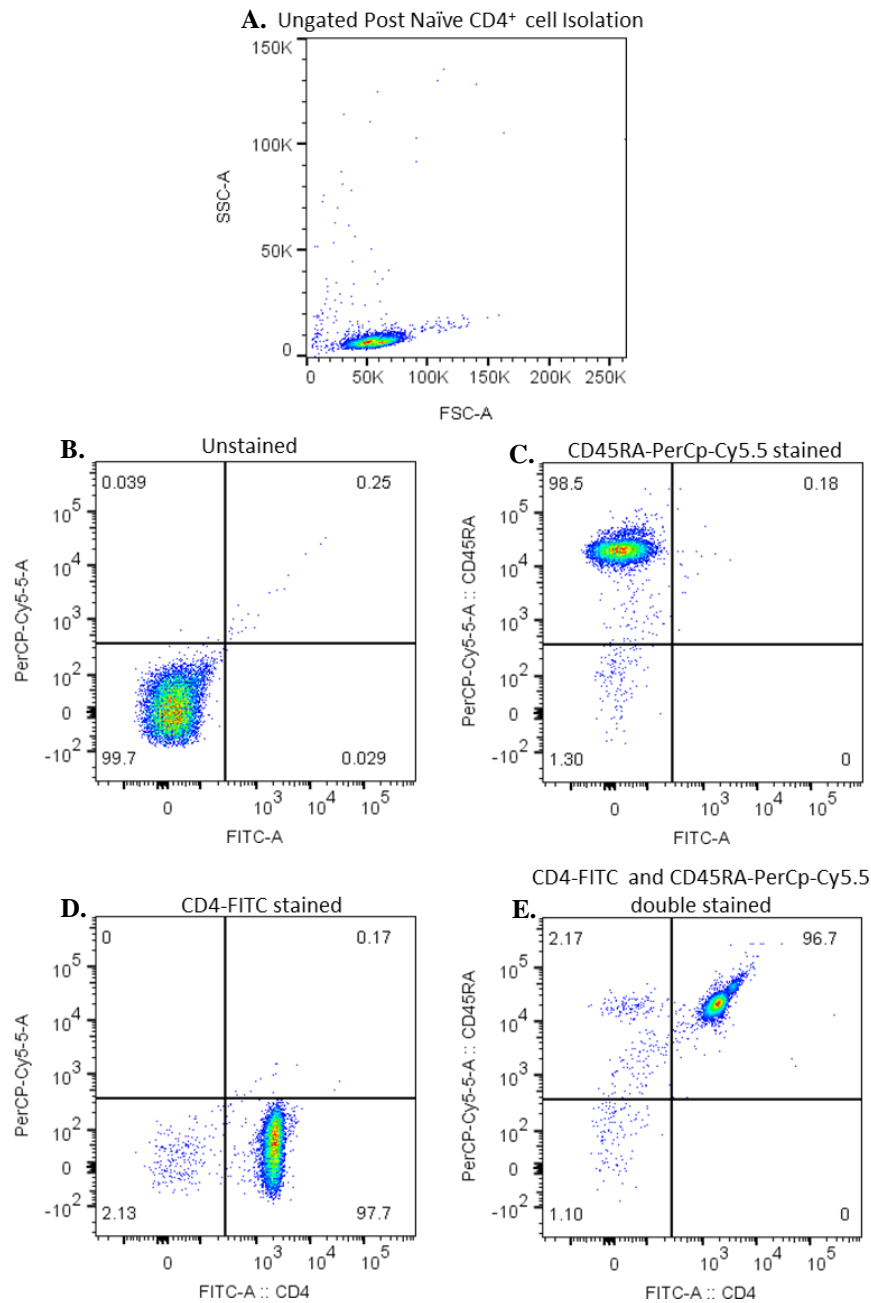


Figure 4.4. Representative flow cytometry analysis of naïve CD4⁺ T cells after isolation by MACS®. (A) Ungated FSC and SSC pseudocolour dot plots showing the naïve CD4⁺ T cells having low granularity and small size. These cells were stained either individually with (C) anti-human CD45RA-PerCp-Cy5.5 or (D) anti-human CD4-FITC or (E) both. 96.7% of the cells were CD45RA⁺/CD4⁺.

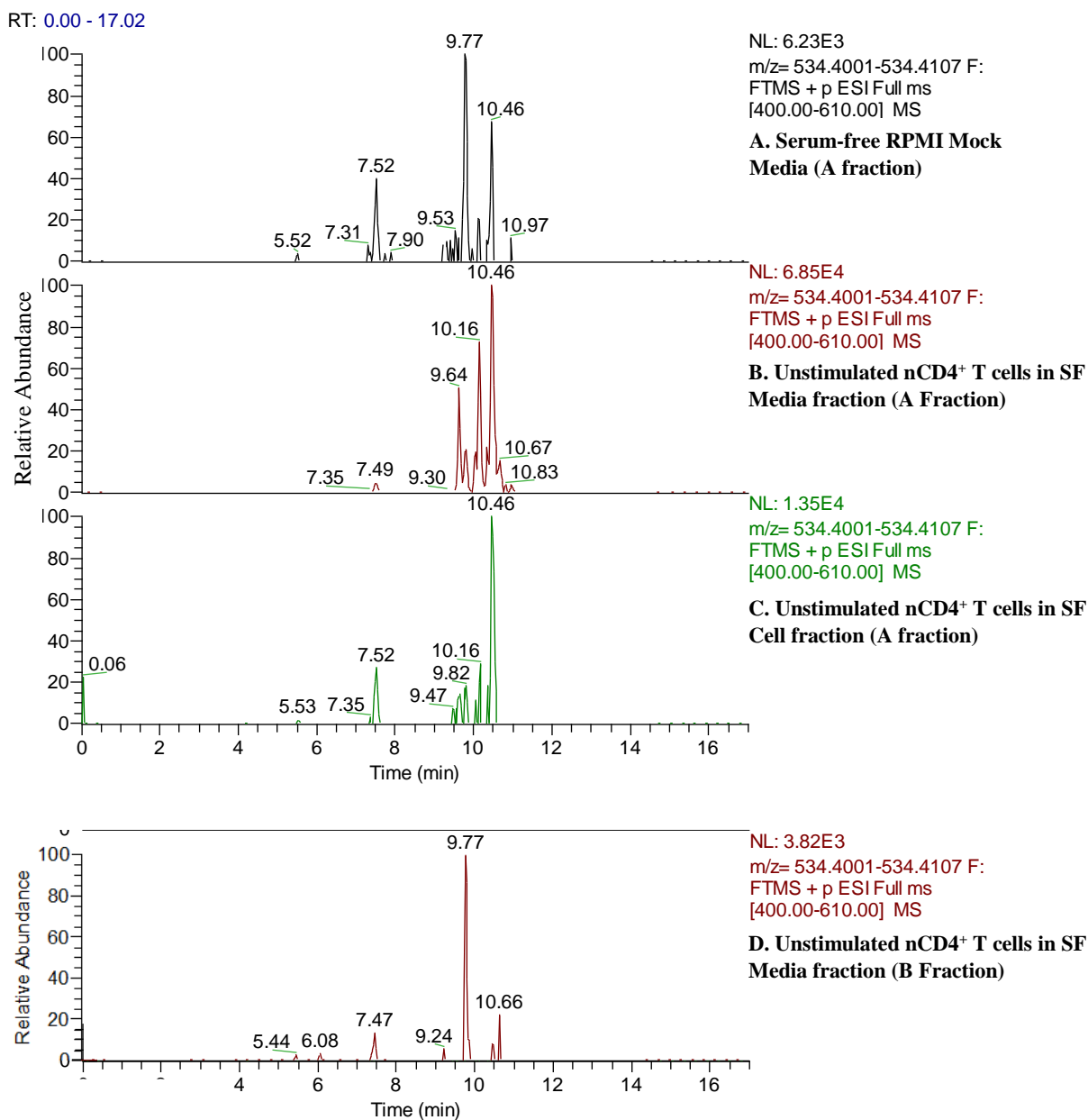


Figure 4.5. Reconstructed ion chromatogram (RIC) of the monohydroxycholesterols at 534.4054 ± 10 ppm in Fraction 1As of unstimulated naïve CD4⁺ T cells in SF media after 6 days.

A,B,C. Naïve CD4⁺ T cells in SF culture did not show detectable levels of enzymatically-derived monohydroxycholesterols in either cell or media fraction. A peak at ~7.5min was present in all samples having the same accurate mass but non-matched MS3 fragmentation. Peaks eluting between 9min to 11min products were identified as B-ring autoxidation products; namely, 9.64min as 7 β -HC, 9.77min as 7-KC, 10.16min as 7 α -HC and 10.46min as 6 β -HC. D. Analysis of Fraction 1Bs only revealed 7-KC at 9.77min.

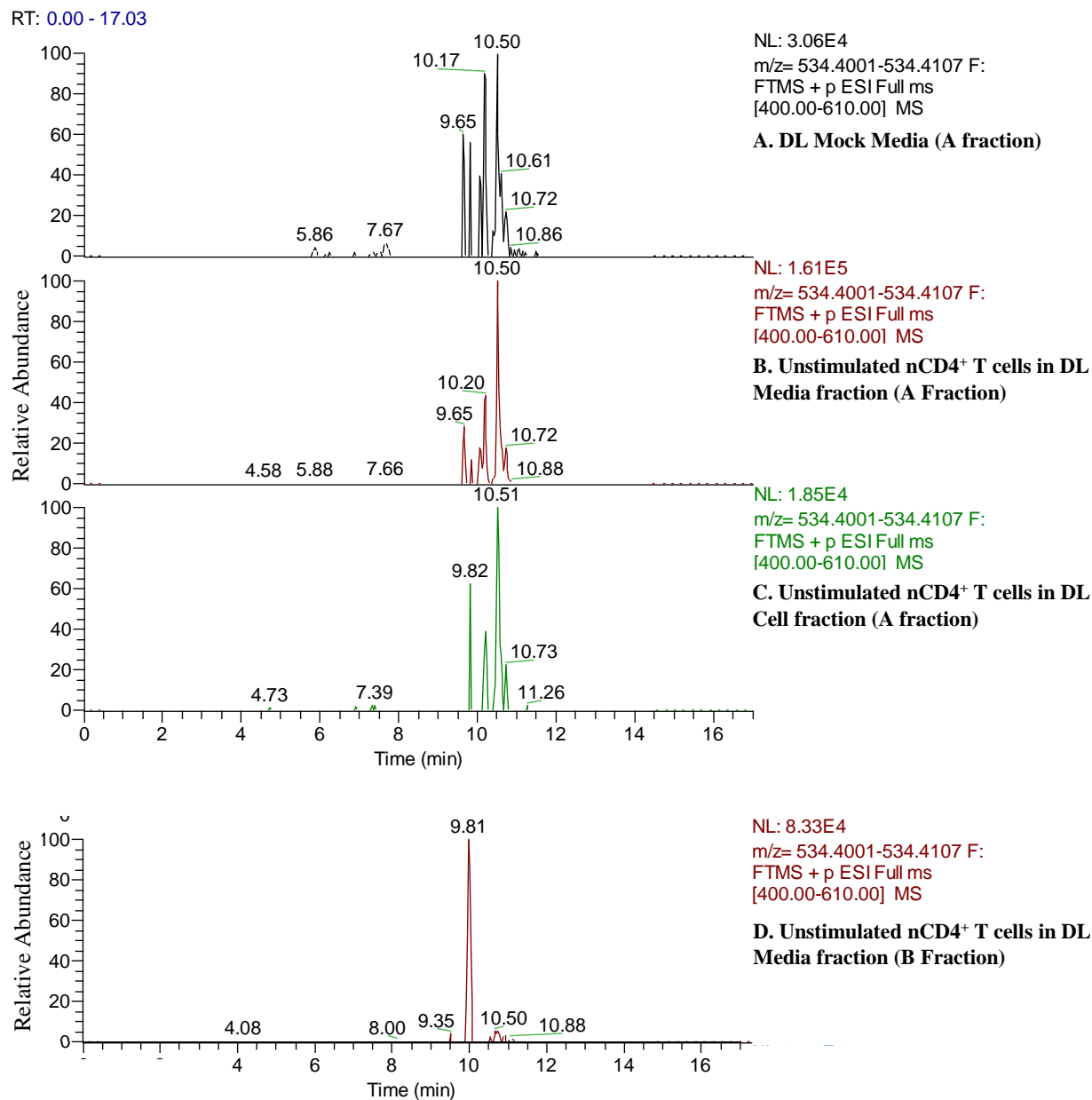


Figure 4.6. RIC of the monohydroxycholesterols at 534.4054 ± 10 ppm in Fraction1As of unstimulated naïve CD4⁺ T cells in DL media after 6 days.

A,B,C. Naïve CD4⁺ T cells in DL also did not produce detectable enzymatically-derived monohydroxycholesterols. Similar to when cultured in SF media, B-ring autoxidation were identified: 9.65min as 7 β -HC, 9.81 as 7-KC, 10.20min as 7 α -HC and 10.50min as 6 β -HC. D. Analysis of Fraction1Bs only revealed 7-KC seen in all chromatograms

4.3.3. Initial cultures of activated naïve CD4⁺ T cells and TH17-polarised conditions revealed induced oxysterol production.

Next, the oxysterol production of naïve CD4⁺ T cells was checked in both activating conditions and polarised towards TH17 subtype. It was found that both activated naïve CD4⁺ T cells and under TH17-polarising conditions produce enzymatically-derived side-chain oxidised monohydroxycholesterols such as 24(S)-HC, 24(R)-HC, and 25-HC at 534.4054*m/z*, which were not present in mock X-VIVO-20 media (Figure 4.7). In addition, 24(S),25-EC, hydrolysed as 24,25-DiHC at 550.4003*m/z* was also detected at substantially higher quantities (Figure 4.8) and its downstream metabolite 7 α -hydroxy-24(S),25-EC detected at 566.3952*m/z*.

Analysis of fraction B for these samples revealed that all of the monohydroxycholesterols detected were the 3 β -hydroxy form and not the 3-oxo form except the cholesterol autoxidation product 7-KC.

The total 24(S),25-EC was obtained by combining the values from 24,25-DiHC, 24-KC and 24-hydroxycholesterol-25-methylether when detected. As seen in Figure 4.10, 24(S),25-EC contains an epoxide group which is labile in acidic solvents used in the derivatisation step in the EADSA process. In previous studies, the epoxide was found to be isomerised to 24-KC, hydrolysed to 24,25-DiHC or methanolized to the 24-hydroxycholesterol-25-methylether and/or 25-hydroxycholesterol-24-methylether^[5,6]. However, in these set of experiments, only the hydrolysed dihydroxycholesterol was predominantly detected.

Table 4.6 and Table 4.7 summarises the quantified sterols in each culture condition per donor.

Other oxysterols like CA, 7 β -CA and 7 α -CA, naturally present in X-VIVO-20 were also monitored and detected but was not observed to be substantially changed between mock

and naïve CD4⁺ T cell conditioned media. Additionally, analysis of cell fraction extracts did not indicate that the cholestenic acids were taken up or produced intracellularly. Figure 4.7 shows a representative MS³ TIC of 534.41→455.36*m/z* for monohydroxycholesterols and Figure 4.8 for the MS³ TIC of dihydroxycholesterols at 550.40→471.36*m/z* using the 17-minute gradient. Other monohydroxycholesterols which were cholesterol B-ring autoxidation products such as 7-KC, 7β-HC, 7α-HC and 6β-HC were also detected but excluded in quantification as these were also detected in mock X-VIVO-20 media similar to 27-HC.

There were a few comparable differences observed between the oxysterols generated by non-polarised and cells under TH17-polarised condition. Non-polarised cells were seen to produce more 25-HC than TH17-polarised cells. Conversely, 7α,24(S),25-TriHC were observed to be more abundant in TH17-polarised conditions than non-polarised. Nevertheless, the biggest change was the actual production of these oxysterols in stimulated conditions compared to their absence in unstimulated conditions. This change in cholesterol metabolism will be the focus of the subsequent sections in this chapter.

Table 4.6. Sterols detected and quantified from activated CD4⁺ T cell culture media fraction extracts after 6 days in X-VIVO-20. Values were normalised to the number of cells initially seeded.

Sterols in Conditioned Media		Activated naïve CD4 T cells +IL-2 (pg/million cells)	
		Non-Polarised (T _H 0) Anti-CD3/CD28 beads +IL-2	T _H 17-Polarised Anti-CD3/CD28 beads +IL-2 +IL-1 β +IL-6 + IL-21 + IL-23 +TGF- β 1 +anti-IL-4 +anti-IFN γ
Donor 1	24(S)-HC	129.6	131.4
	24(R)-HC	18.7	16.1
	25-HC	37.6	23.2
	27-HC	7.9	8.0
	24(S),25-EC	6,013.3	6,239.8
	7 α ,25-DiHC	---	---
	7 α ,24,25-TriHC	100.1	161.9
Donor 2 (Set 1)	24(S)-HC	80.4	43.3
	24(R)-HC	21.9	28.0
	25-HC	172.5	49.4
	27-HC	36.4	19.3
	24(S),25-EC	18,021.2	2,904.4
	7 α ,25-DiHC	---	21.5
	7 α ,24,25-TriHC	193.9	605.1
Donor 2 (Set 2)	24(S)-HC	52.2	43.0
	24(R)-HC	15.0	28.5
	25-HC	91.9	53.6
	27-HC	15.0	18.3
	24(S),25-EC	12,751.2	2,785.7
	7 α ,25-DiHC	---	20.8
	7 α ,24,25-TriHC	144.4	689.4

Table 4.7. Sterols detected and quantified from activated CD4⁺ T cell pellet after 6 days in X-VIVO-20. Values were normalised to the number of cells initially seeded.

Sterols in Cell Pellet		Activated naïve CD4 T cells +IL-2 (pg/million cells)	
		Non-Polarised (T _H 0)	Th17-Polarised
Donor 2 (Set 2)	24(S)-HC	67.6	45.1
	24(R)-HC	---	12.2
	25-HC	21.5	10.7
	27-HC	---	---
	24(S),25-EC	2,105.0	204.3
	7 α ,25-DiHC	---	7.6
	7 α ,24,25-TriHC	---	41.8
	Cholesterol	294,486.5	174,977.6
	Desmosterol	835.6	730.7
	Dehydrocholesterol	510.6	513.6

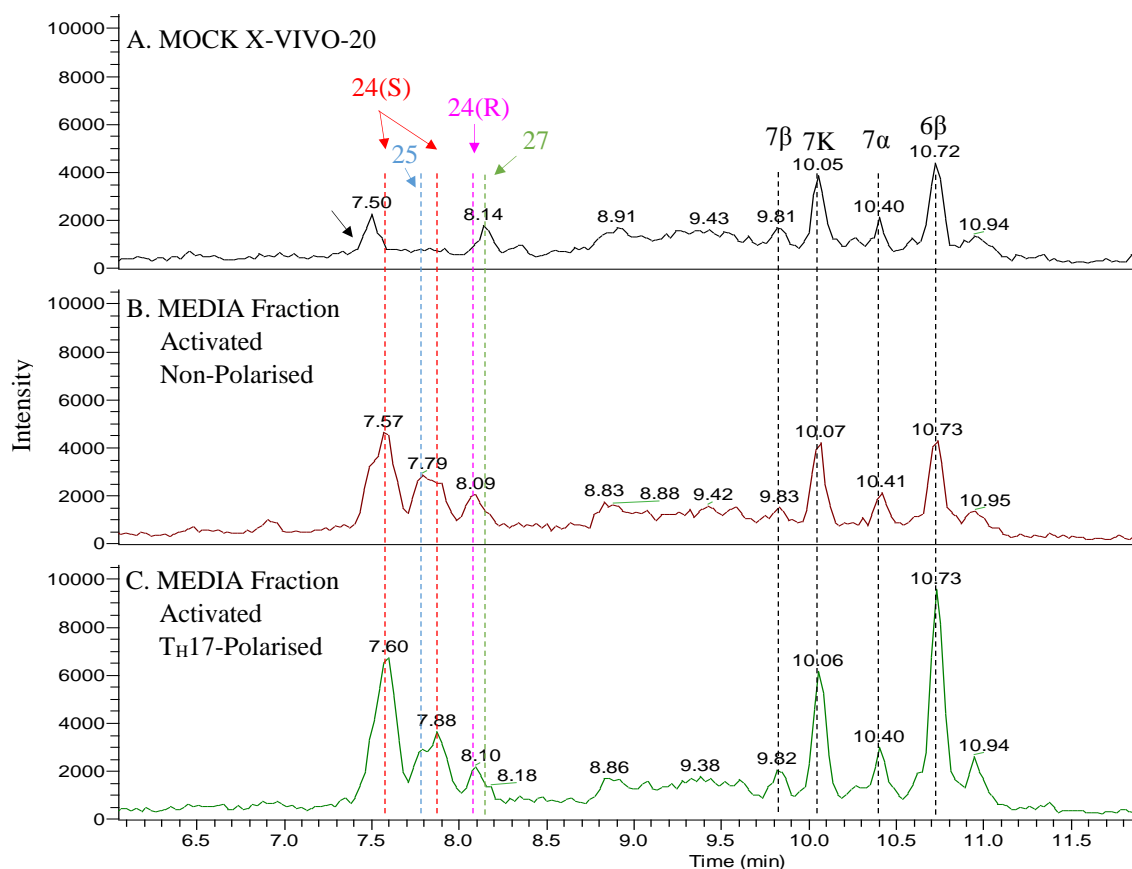


Figure 4.7. Donor 1 total ion chromatogram of monohydroxycholesterol [534→455→] MS³ transition for activated and polarised naïve CD4⁺ T cells.

After 6 days in activating and T_H17-polarising conditions, oxysterols were extracted from the culture media and processed for LCMS analysis. All chromatograms show the presence of cholesterol autoxidation products 7 β -HC, 7-KC, 7 α -HC and 6 β -HC as later eluting peaks. A. Mock X-VIVO-20 was also extracted as background/reference. The peak at 7.50min (black arrow) was detected but was not 24(S)-HC based from its MS³ spectra, it can also be seen as a left shoulder of the 24(S)-HC peak in panel B. Also, the ~8.14min peak was identified as 27-HC to be naturally present in the X-Vivo-20 mock. B. Media extract from activated non-polarised naïve CD4⁺ T cells showed the presence of additional peaks at ~7.59 and ~7.88 identified as 24(S)-HC (red), ~7.79min as 25-HC (blue), ~8.10min as 24(R)-HC (purple) and 27-HC. C. The same peaks were also detected and identified in the media fraction of activated T_H17-polarised naïve CD4⁺ T cells.

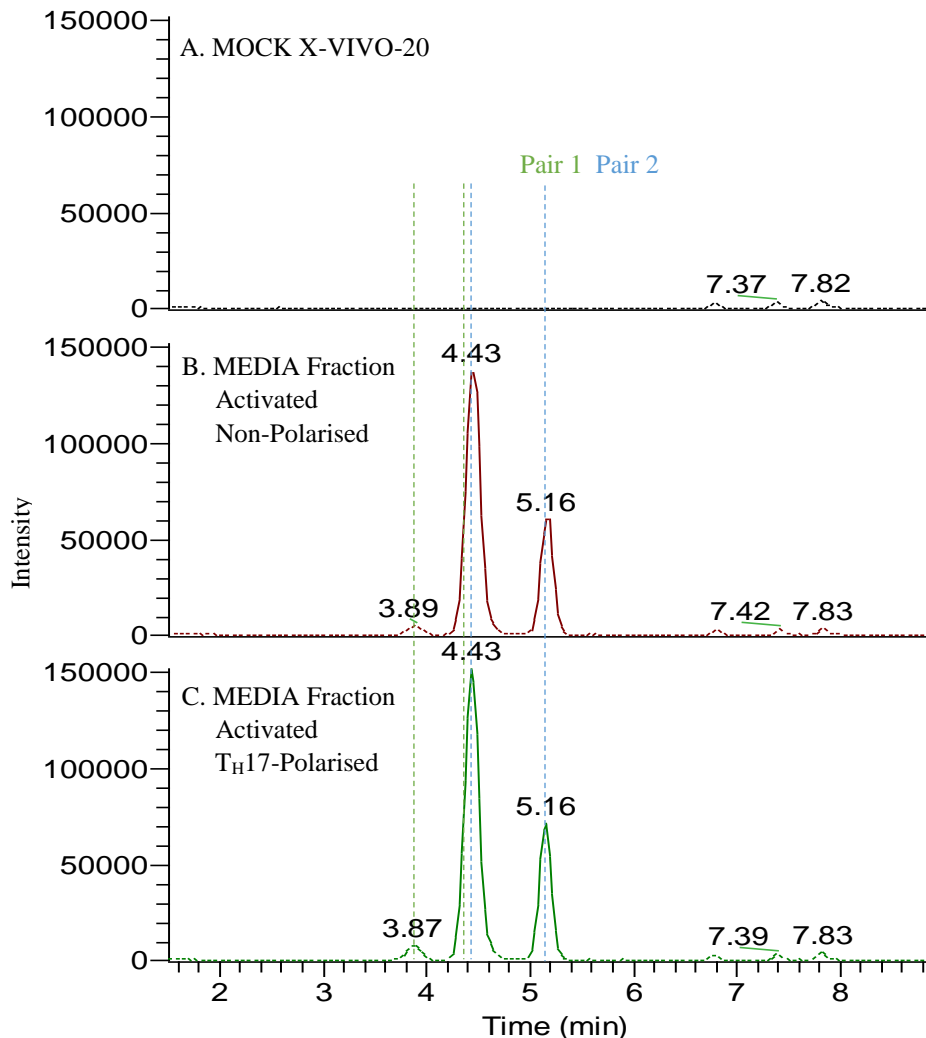


Figure 4.8. Donor 1 representative total ion chromatogram of dihydroxycholesterols [550→471→] MS³ transition for activated and polarised naïve CD4⁺ T cells.

A. No identifiable dihydroxycholesterol peaks were detected in the mock X-VIVO-20 fraction. Three background peaks eluted later at 6.81min, 7.40 and 7.83min were detected but was present in all chromatograms. B/C. The peaks at 4.43min and 5.16min were identified as 24,25-dihydroxycholesterol based from its exact mass and MS³ fragmentation spectra. These set of peaks were only present in conditioned media of the activated naïve CD4⁺ T cells in X-VIVO-20. The 3.87min peak was also identified to have the same fragmentation spectra as the other two peaks. We speculate that this peak is still 24,25-DiHC and that it is present as a pair of peaks (green) but its second peak elutes at the same time as the first peak of the more abundant second pair (blue) at 4.43min. The two sets of two peaks may arise as stereoisomers in the sterol carbon-3 position as *Z*- and *E*- conformations of the GP tag corresponding to two peaks of pair 2 and at the 24-hydroxyl group position as 24(R),25 and 24(S),25 conformations corresponding to pair 1 and 2.

4.3.4. Some GP-derivatised sterols elutes at slightly different retention times due to geometric isomerism.

Some oxysterols like 24(S)-HC and 24,25-DiHC were detected as two peaks in the chromatogram (Figure 4.7 and Figure 4.8). The two peaks were the same sterol that exists as *Z*- and *E*- geometric isomers which can naturally form during Girard's reagent P derivatisation (Figure 4.9). Once injected into the column these derivatised sterols of marginally different conformations can interact differently with the C18 stationary phase resulting to slightly different retention times. This effect can also be observed with the difference in retention times of 24(S)-HC-D6 and 24(R)-HC-D6 internal standards which were chromatographically resolved even with such subtle changes in structure.

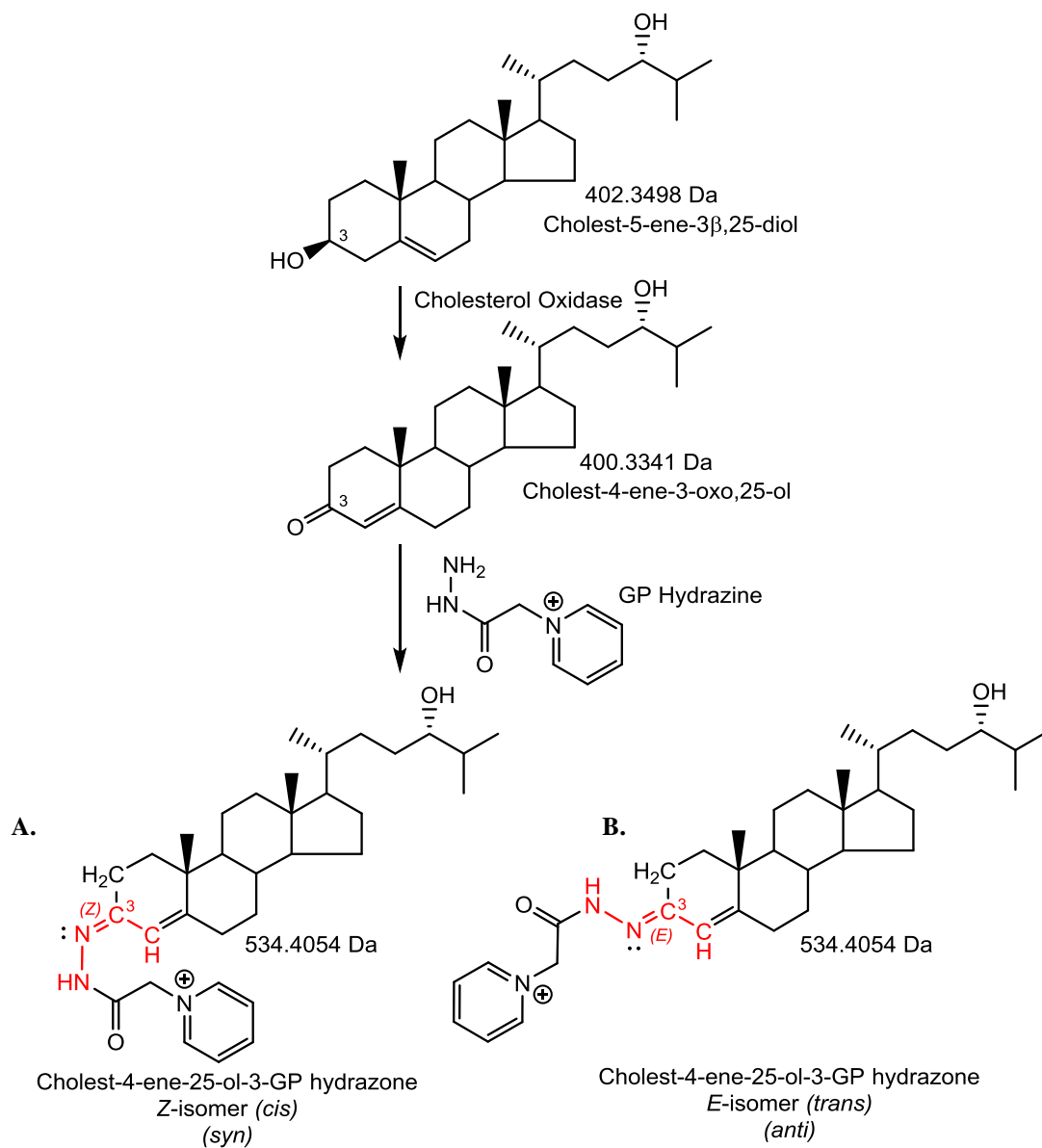


Figure 4.9. Formation of E-Z isomers (*syn* and *anti*) in GP hydrazone derivatised sterols.

As an example, 24(S)-HC forms both Z and E isomers due to the double bond in $^3\text{C}=\text{N}$ (red). The [CH=] on the ^3C side of the double bond acts as the higher priority and the [CH₂] as the lower priority; on the N side of the double bond, the [-NH] acts as the higher priority and the nitrogen lone pair as the lower priority. A. The Z-isomer forms as the “higher” priority [$^3\text{C}-\text{CH}=\text{N}-\text{NH}$] is on the same side as the [N-NH-] of the double bond. B. Conversely, the E-isomer forms as the [N-NH-] is on the opposite side of the double bond. The structural difference between the two isomers in GP-sterols can sometimes be separated by our liquid chromatography method [6,18].

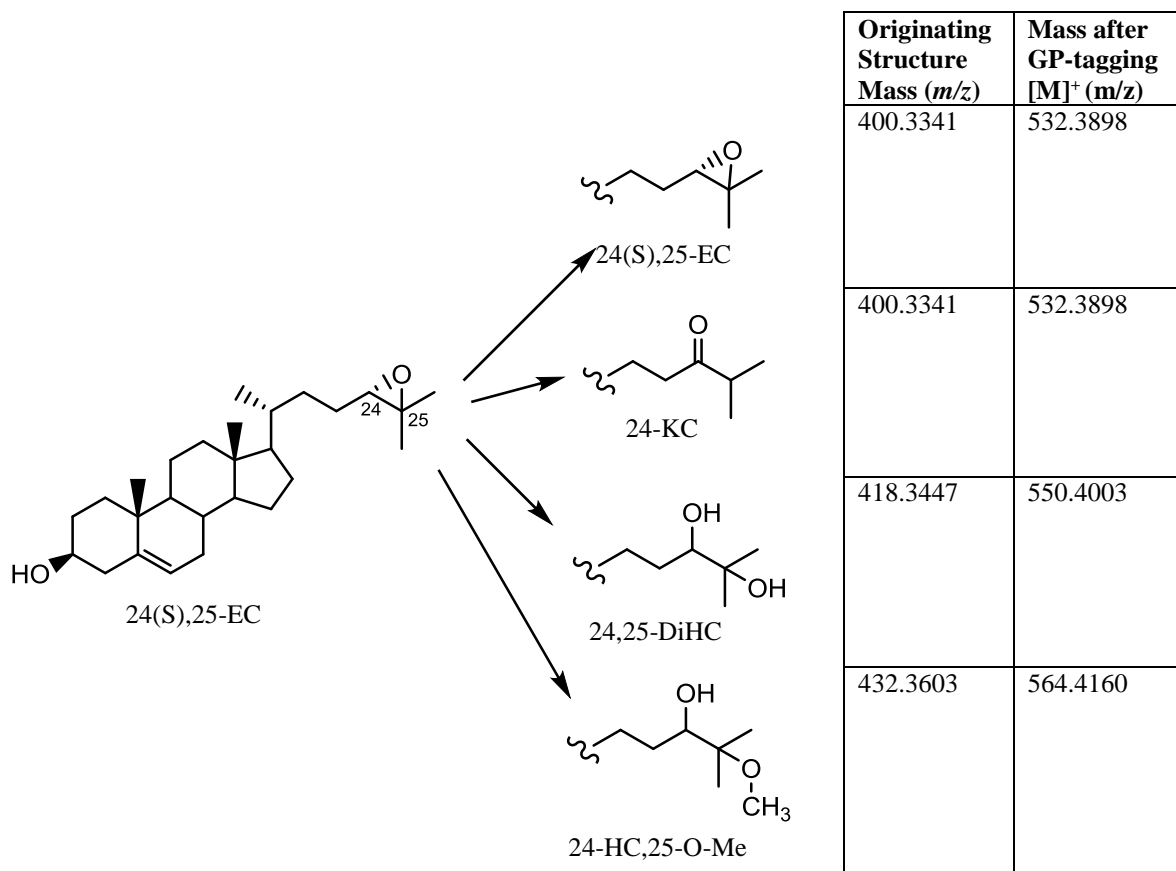


Figure 4.10. 24(S),25-EC during the EADSA process.

Labile epoxide group-containing 24(S),25-EC can be isomerised, hydrolysed or methanolized as [3 β -Hydroxycholest-5-ene-3,24-dione], [Cholest-5-en-3 β ,24,25-triol], or [3 β ,24-Dihydroxycholest-5-ene-25-methoxide], respectively, in acidic solvents thus changing its [M]⁺ ion. The total of these four sterols, when detected, were combined to obtain the total quantity of 24(S),25-EC in the sample^[10,18].

4.3.5. Low levels of 24,25-EC were produced by non-activated naïve CD4⁺ T cells in X-VIVO-20 cultures after 6 days which was independent from IL-2 treatment.

Naïve CD4⁺ cultures in unstimulated SF RPMI or X-VIVO-20 conditions did not reveal any induced monohydroxycholesterol generation in either media or cell fraction. Moreover, IL-2 known to stimulate the growth of T cells, also did not show any effect in the monohydroxycholesterol production (Figure 4.13) which was also similar to mock media extracts (Figure 4.11).

However, low levels of 24,25-DiHC was detected in only X-VIVO-20 cultures in both with or without IL-2 treatment. This oxysterol was not seen when cultured in SF RPMI media (Figure 4.14) or in mock media extracts (Figure 4.12).

Then again, even though 24,25-DiHC was detected, levels of 120 to 195 pg/million cells were low in comparison to the >2,000 pg/million cells detected when cells were activated using anti-CD3/CD28-loaded beads while using the same media. This suggests that oxysterol production was largely induced by the treatment with anti-CD3/CD28-loaded beads and not by the IL-2 growth factor.

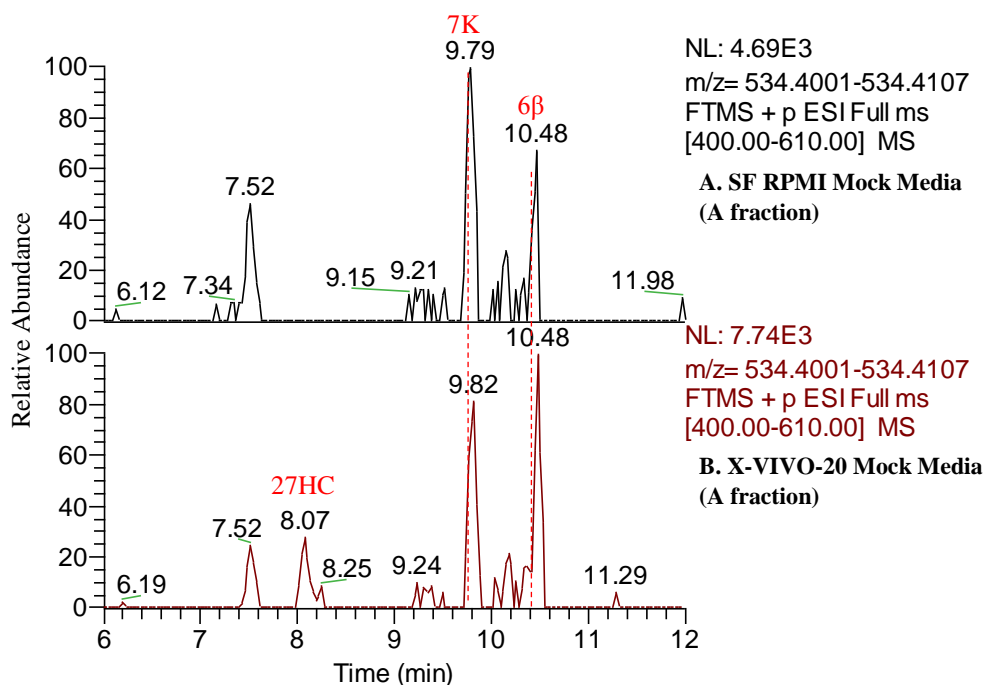


Figure 4.11. RIC of the monohydroxycholesterols at 534.4054 ±10ppm in Fraction1As of SF RPMI and X-VIVO-20 media.

LCMS analysis of both media revealed similar B-ring oxidised sterols: 7-KC at 9.80min and 6β-HC at 10.48min. The background peak at 7.52min were also present. Only the presence of 27-HC at 8.07min was different from the two chromatograms.

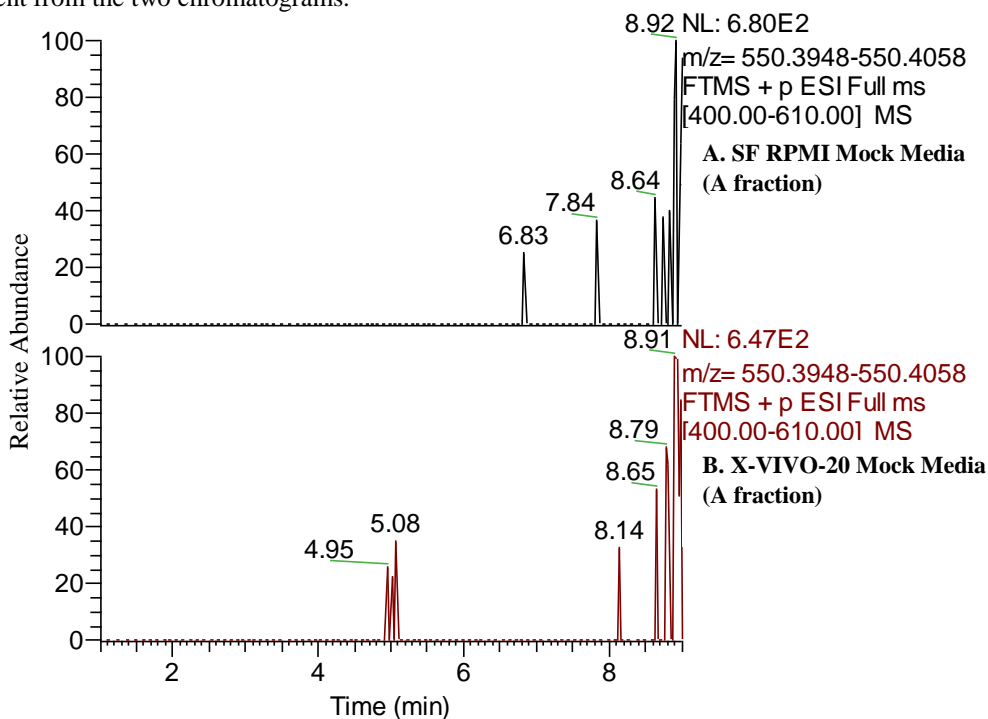


Figure 4.12. RIC of the dihydroxycholesterols at 550.4003 ±10ppm in Fraction1As of mock SF RPMI and X-VIVO-20 media.

No dihydroxycholesterols were detected in either mock media.

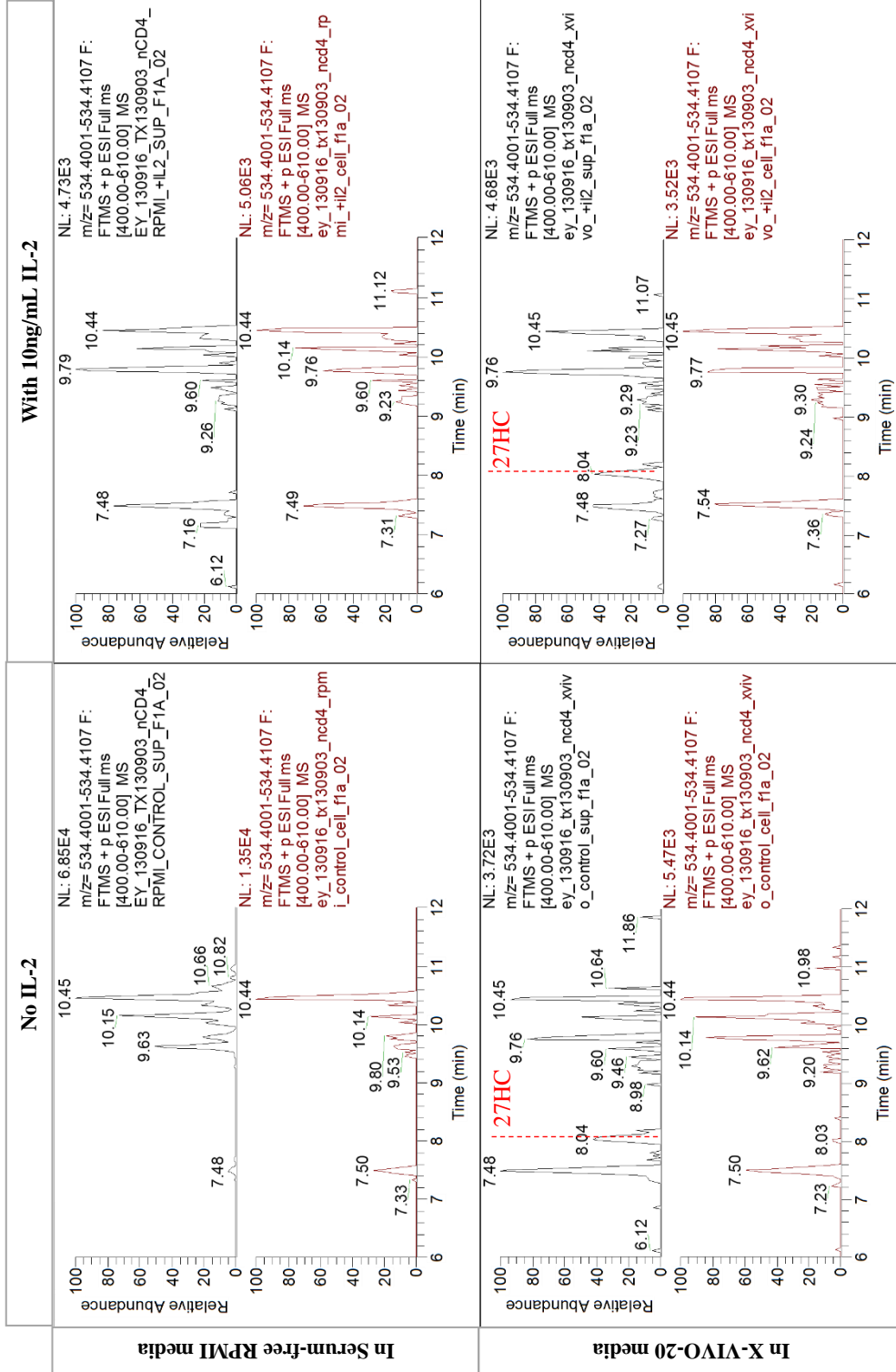


Figure 4.13. RIC of monohydroxycholesterols at 534.4054 ± 10ppm of non-treated and 10ng/mL IL-2 treated naïve CD4⁺ T cells in SF RPMI and X-VIVO-20 media after 6 days. Cultures using either media was not observed to generate enzymatically derived monohydroxycholesterols such as 24(S)-HC, 24(R)-HC and 25-HC. B-ring autoxidation products, from 9.20min to 10.46min, were common in all the samples in either media or cell fraction. 27-HC was only detected (black dashed line) in X-VIVO-20 cultures in the media fraction which is naturally present in the X-VIVO-20 mock media.

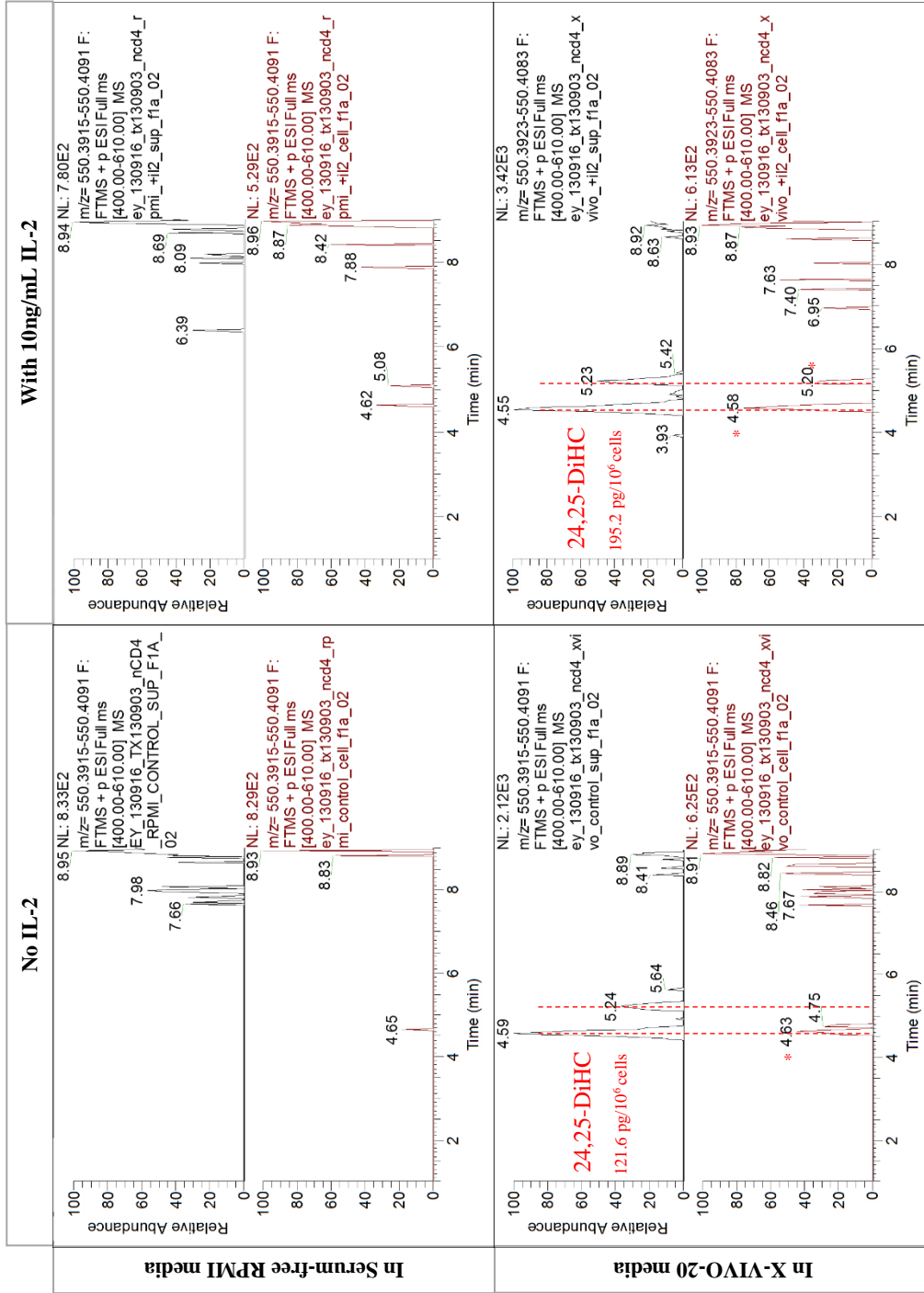


Figure 4.14. RIC of dihydroxycholesterols at 550.4003 ± 10ppm of non-treated and 10ng/mL IL-2 treated naive CD4⁺ T cells in SF RPMI and X-VIVO-20 media after 6 days.

Cultures using X-VIVO-20 media was observed to induce the production of 24,25-DiHC detected in the media fraction (two red dashed lines). Peaks were also found on the correct retention times in cell fractions but the level were too low for proper identification by MS³ fragmentation as indicated by *. Inset numbers indicate the concentration of the peaks at ~4.57min and ~5.23min.

4.3.6. Cultures of activated and non-activated naïve CD4⁺ cells with deuterated cholesterol revealed different cholesterol import.

The most abundant oxysterol detected from activated human naïve CD4⁺ T cells was 24,25-DiHC. It has been suggested that 24,25-DiHC was derived from 24S25-EC generated from the shunt pathway during cholesterol biosynthesis^[7,8], but it is also possible that cholesterol may be oxidised at position 24 and 25 giving rise to 24,25-DiHC. To confirm the origin of 24,25-DiHC, CD4⁺ T cells were activated in the presence of deuterated cholesterol. Since, X-VIVO-20 was found to contain free cholesterol at ~4ng/mL, we treated the naïve CD4⁺ T cells with 1000-fold more heptadeuteriocholesterol at 4µg/mL.

4.3.6.1. Resting naïve CD4⁺ T cells contains more imported deuterated cholesterol than endogenous cholesterol.

As there were no internal standards to quantify the endogenous and deuterated cholesterols in cell fraction extracts for donor 1, relative peak area ratios of non-deuterated-to-deuterated cholesterols were used instead for comparison. Figure 4.15 shows a higher proportion of cholesterol-D7 at 525.4544m/z than cholesterol-D0 at 518.4105m/z in non-activated naïve CD4⁺ T cells of donor 1 with a ratio of 0.26 (Cholesterol D0/D7) after three days incubation. Using donor 3 cells extracted with brassicasterol as the internal standard also confirms the same trend in non-activated naïve CD4⁺ T cells where cholesterol-D0 was quantified at 199 ng/10⁶ cells and cholesterol-D7 at 316 ng/10⁶ cells (Figure 4.17).

4.3.6.2. Activated naïve CD4⁺ T cells contain more endogenous cholesterol than deuterated.

In contrast to non-activated naïve CD4⁺ T cells, cholesterol-D0 was found to be more abundant in activated naïve CD4⁺ T cells than imported deuterated cholesterol with a ratio of 1.40 for donor 1 (Figure 4.16). Furthermore, quantified intracellular cholesterol-D0 of 501 ng/10⁶ cells and cholesterol-D7 of 342 ng/10⁶ cells in donor 3 revealed a similar ratio of 1.46 (Figure 4.18).

Moreover, activated cells were also observed to have a higher total intracellular cholesterol content compared to non-activated. In total, non-activated naïve CD4⁺ T cells were found to contain 515 ng/10⁶ cells of intracellular cholesterol which increased 1.6 times to 843 ng/10⁶ cells when activated for two days. This suggests that activating conditions accumulate intracellular cholesterol by mainly inducing *de novo* cholesterol biosynthesis but only affect cholesterol import slightly.

4.3.6.3. 25-HC was generated from both *de novo* cholesterol and imported cholesterol.

As in previous activated naïve CD4⁺ T cell cultures in X-VIVO-20, enzymatically-derived monohydroxycholesterols such as 24(S)-HC, 24(R)-HC and 25-HC were detected in the media fraction (Figure 4.21.B) while none were present in non-activated media fraction after three days (Figure 4.21.A). As deuterium-labelled cholesterol metabolites, no 24(S)-HC-D7 or 24(R)-HC-D7 were detected at 541.4493*m/z* despite the appreciable amounts produced from endogenous cholesterol-D0. As a reference, none of the monohydroxycholesterols or dihydroxycholesterols were detected in the mock X-VIVO-20 extracted in parallel to the samples (Figure 4.19 and Figure 4.20).

On the contrary, a deuterated cholesterol-D7 metabolite, 25-HC-D6 was found to be produced and exported to the media by activated naïve CD4⁺ T cells (Figure 4.21.B. middle panel). Autoxidation at 25-position of cholesterol-D7 in the media was ruled out as there were no peaks of similar retention time detected in the media fraction of non-activated naïve CD4⁺ T cells (Figure 4.21.A. middle panel). Although, detected at a low level, MS³ fragmentation pattern confirms that both compounds are 25-HC, with daughter ions having 6 Da difference (Figure 4.22 and Figure 4.23). This might suggest a particular role of 25-HC production during the T cell activation process as it is actively produced from either the endogenous cholesterol or imported cholesterol as its precursor.

Table 4.8 and Table 4.9 shows the quantifications of the sterols in all three experiments in cell and media fractions.

4.3.6.4. The 24,25-DiHC detected were not derived from cholesterol.

Analysis of dihydroxycholesterols to monitor deuterated dihydroxycholesterol metabolites with mass $556.3953m/z$ did not reveal any 24,25-DiHC-D6 or 7 α ,25-DiHC-D6. All of the 24,25-DiHC produced were detected on $550.4003m/z$ (Figure 4.24.B/D) suggesting that its production does not come downstream of cholesterol and likely to be from hydrolysed 24(S),25-EC produced via the shunt pathway of the mevalonate pathway^[7,8].

Between the donors 1 and 2, production of 24(S),25-EC was at similar levels of 2,119.6 and 1,697.2 pg/10⁶ cells whilst donor 3 was only 846.8 pg/10⁶cells 9 (Table 4.9). This could be expected as donor 3 cells were only activated for two days compared to three days for donors 1 and 2. Comparison of cell and media fractions revealed the epoxycholesterol to be more abundant in the media fraction than the cell fraction after two to three days of activation. For non-activated cells, there were no 24,25-DiHC detected either cell or media. This could be due to the shorter three-day incubation time making the baseline levels produced to be below the detection limit. This might also apply to 24(S)-HC and 24(R)-HC not detected in donor 3 activated media fraction.

Table 4.8. Sterols quantified in cell fraction extracts after 3 days in X-VIVO-20 supplemented with 4µg/mL cholesterol-D7. Values were normalised to the number of cells extracted on harvest as pg/million cells.

Donor	Culture condition in X-VIVO-20	24(S)-HC		24(R)-HC		25-HC		24(S),25-EC	
		D0	D7	D0	D7	D0	D6	D0	D6
1	Non-activated	---	---	---	---	---	---	---	---
	Activated (3-day)	---	---	---	---	29.3	---	863.4	---
2	Non-activated								
	Activated (3-day)								
3	Non-activated	---	---	---	---	---	---	---	---
	Activated (2-day)	---	---	---	---	24.3	---	462.7	

Table 4.9. Sterols quantified in media fraction extracts after 3 days in X-VIVO-20 supplemented with 4µg/mL cholesterol-D7. Values were normalised to the number of cells initially seeded as pg/million cells.

Donor	Culture condition in X-VIVO-20	24(S)-HC		24(R)-HC		25-HC		24(S),25-EC	
		D0	D7	D0	D7	D0	D6	D0	D6
1	Non-activated	---	---	---	---	---	---	---	---
	Activated (3-day)	48.3	---	10.0	---	92.6	32.4	2,119.6	---
2	Non-activated	---	---	---	---	---	---	---	---
	Activated (3-day)	11.7	---	7.7	---	76.3	8.2	1,697.2	---
3	Non-activated	---	---	---	---	---	---	---	---
	Activated (2-day)	---	---	---	---	65.6	16.0	846.8	---

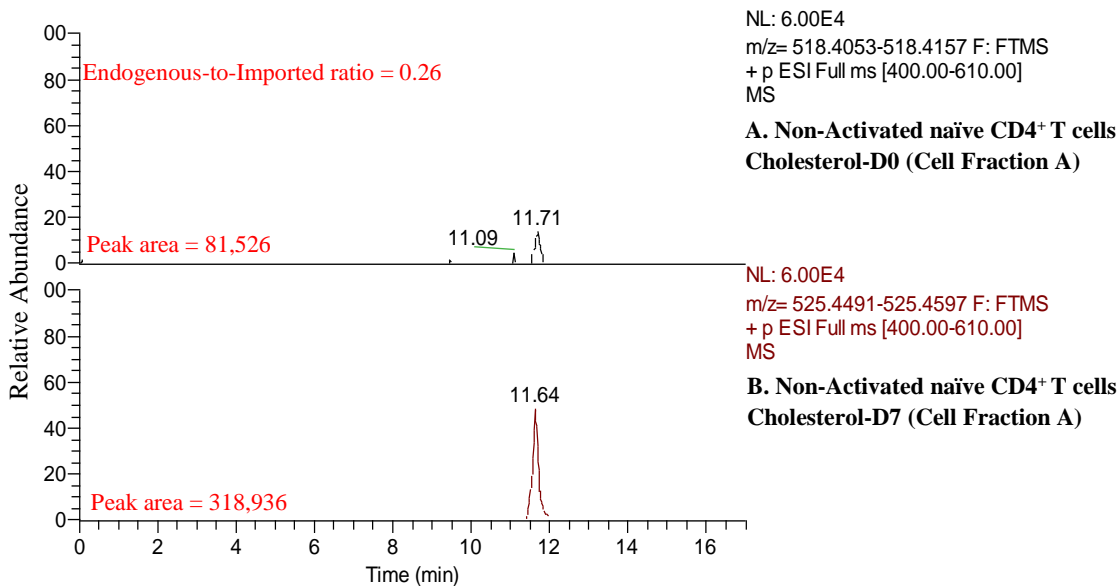


Figure 4.15. Donor 1 RIC of cholesterol and cholesterol-D7 in non-activated naïve CD4⁺ T cells after three days.

A. Cholesterol 11.71min peak identified at 518.4105m/z \pm 10ppm. B. Cholesterol-D7 11.64min peak identified at 525.4544m/z \pm 10ppm. In non-activated naïve CD4⁺ T cells, intracellular cholesterol was mainly media imported cholesterol-D7 with an endogenous-to-imported ratio of 0.26. Deuterium labelled sterols were observed to elute slightly earlier than non-deuterated sterols.

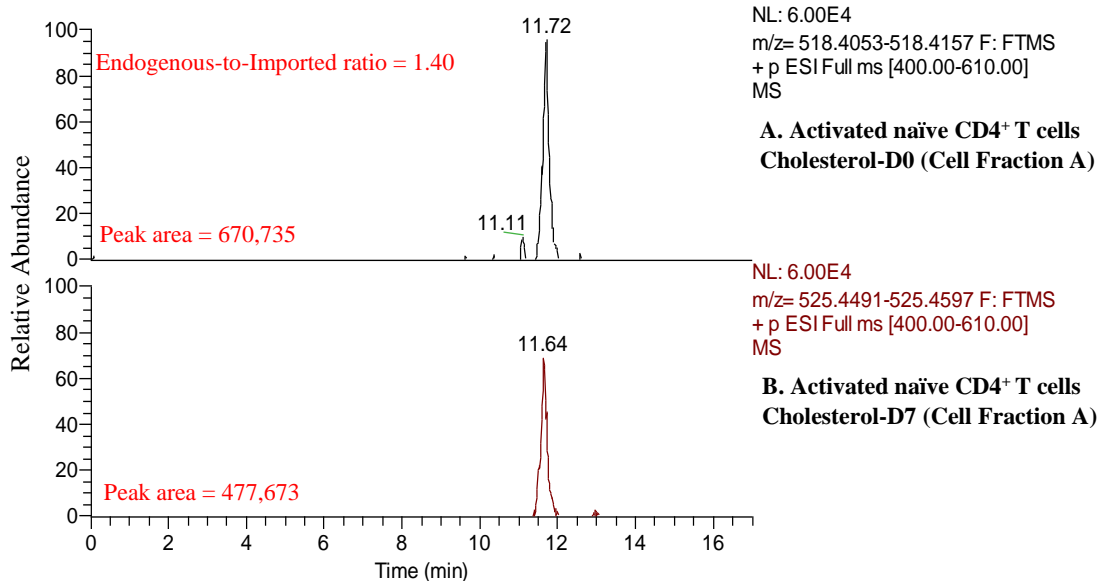


Figure 4.16. Donor 1 RIC of cholesterol and cholesterol-D7 in activated naïve CD4⁺ T cells after three days.

A. Cholesterol chromatogram at 518.4105m/z \pm 10ppm. B. Cholesterol-D7 chromatogram at 525.4544m/z \pm 10ppm. In non-activated naïve CD4⁺ T cells, intracellular cholesterol was mainly media imported cholesterol-D7. In activated naïve CD4⁺ T cells, intracellular cholesterol was mainly *de novo* cholesterol-D0 with an endogenous-to-imported ratio of 1.40. Deuterium labelled sterols were observed to elute slightly earlier than non-deuterated sterols.

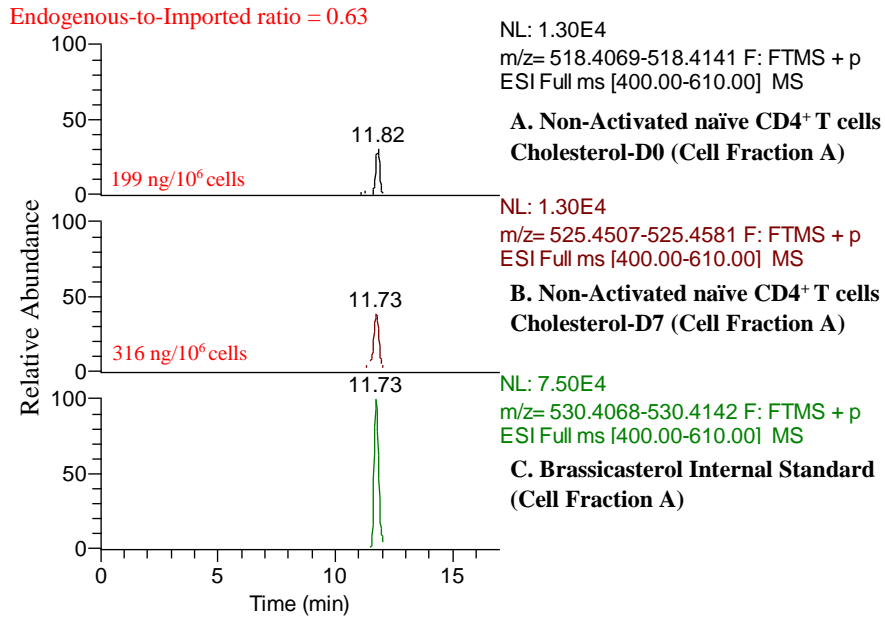


Figure 4.17. Donor 3 RIC of cholesterol, cholesterol-D7 and brassicasterol internal standard in non-activated naïve CD4⁺ T cells after three days in 4µg/mL cholesterol-D7. Proportionally, cholesterol-D7 imported from the media by non-activated naïve CD4⁺ T cells were more abundant than endogenous cholesterol-D0.

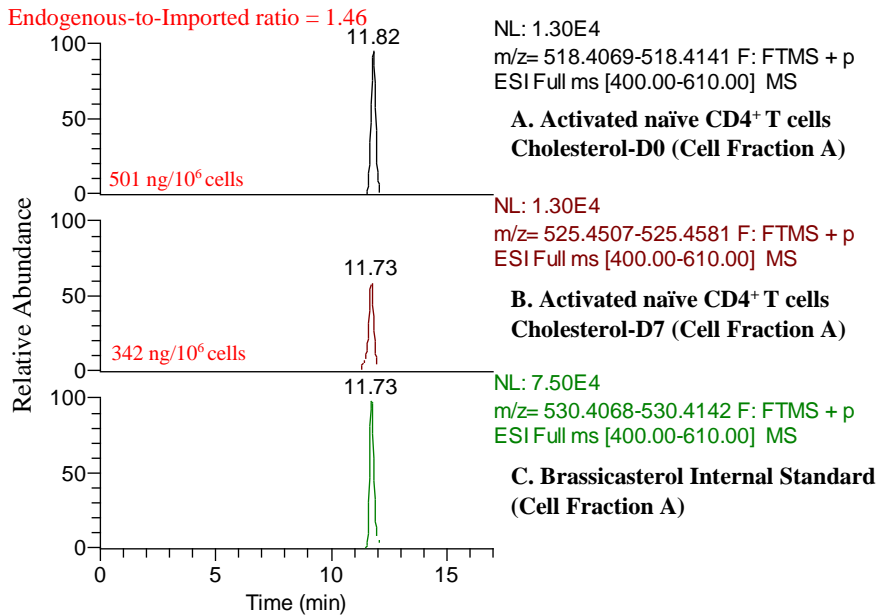


Figure 4.18. Donor 3 RIC of cholesterol, cholesterol-D7 and brassicasterol internal standard in 2-day activated naïve CD4⁺ T cells after pre-incubation and three days in 4µg/mL cholesterol-D7. When activated after 2 days, naïve CD4⁺ T cells were observed to increase in intracellular cholesterol mainly by *de novo* cholesterol synthesis.

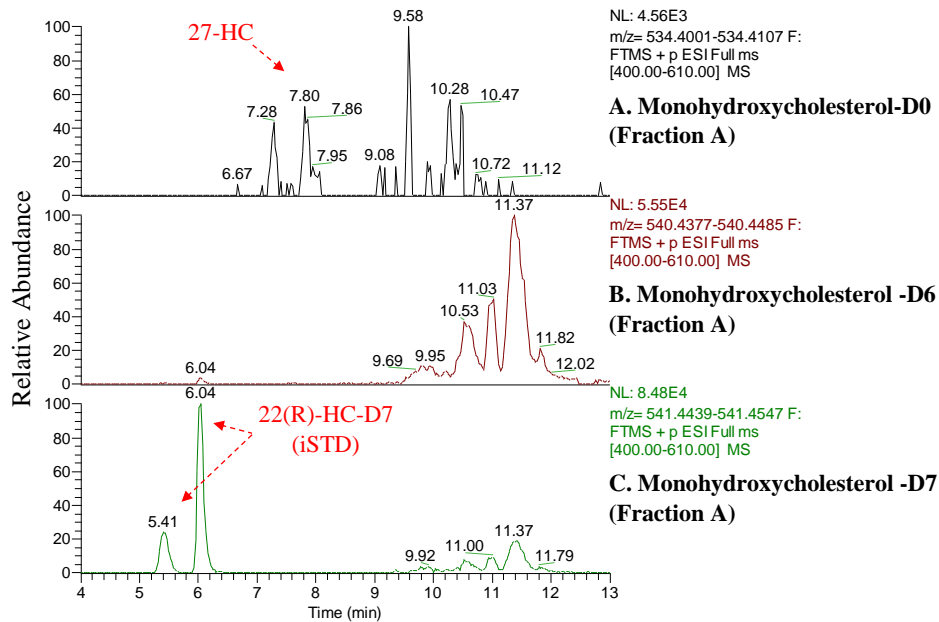


Figure 4.19. RIC for 534.4054 m/z , 540.4431 m/z and 541.4493 m/z to monitor monohydroxycholesterols, monohydroxycholesterol-D6s and monohydroxycholesterol-D7s in mock X-VIVO-20 media. A. Only the background peak at 7.28min and 27-HC at 7.80min were detected in mock media. B. No deuterated monohydroxycholesterols were detected. Peaks from 9.69min to 11.82min were found in all samples and considered as background. C. Only the 22R-HC-D7 internal standard at 5.41min and 6.04min were detected at 541.4493 m/z .

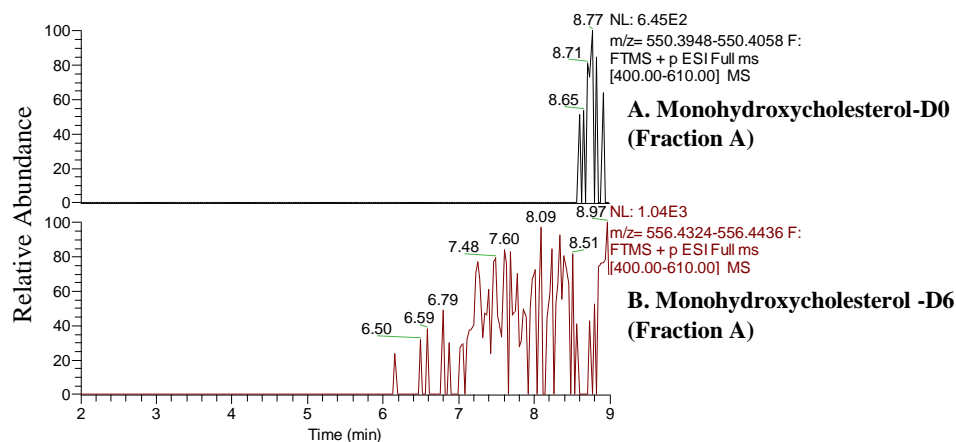


Figure 4.20. RIC for 550.4003 m/z and 556.4380 m/z to monitor dihydroxycholesterols and dihydroxycholesterol-D6s in mock X-VIVO-20 media. A/B. No dihydroxycholesterols were detected in X-VIVO-20.

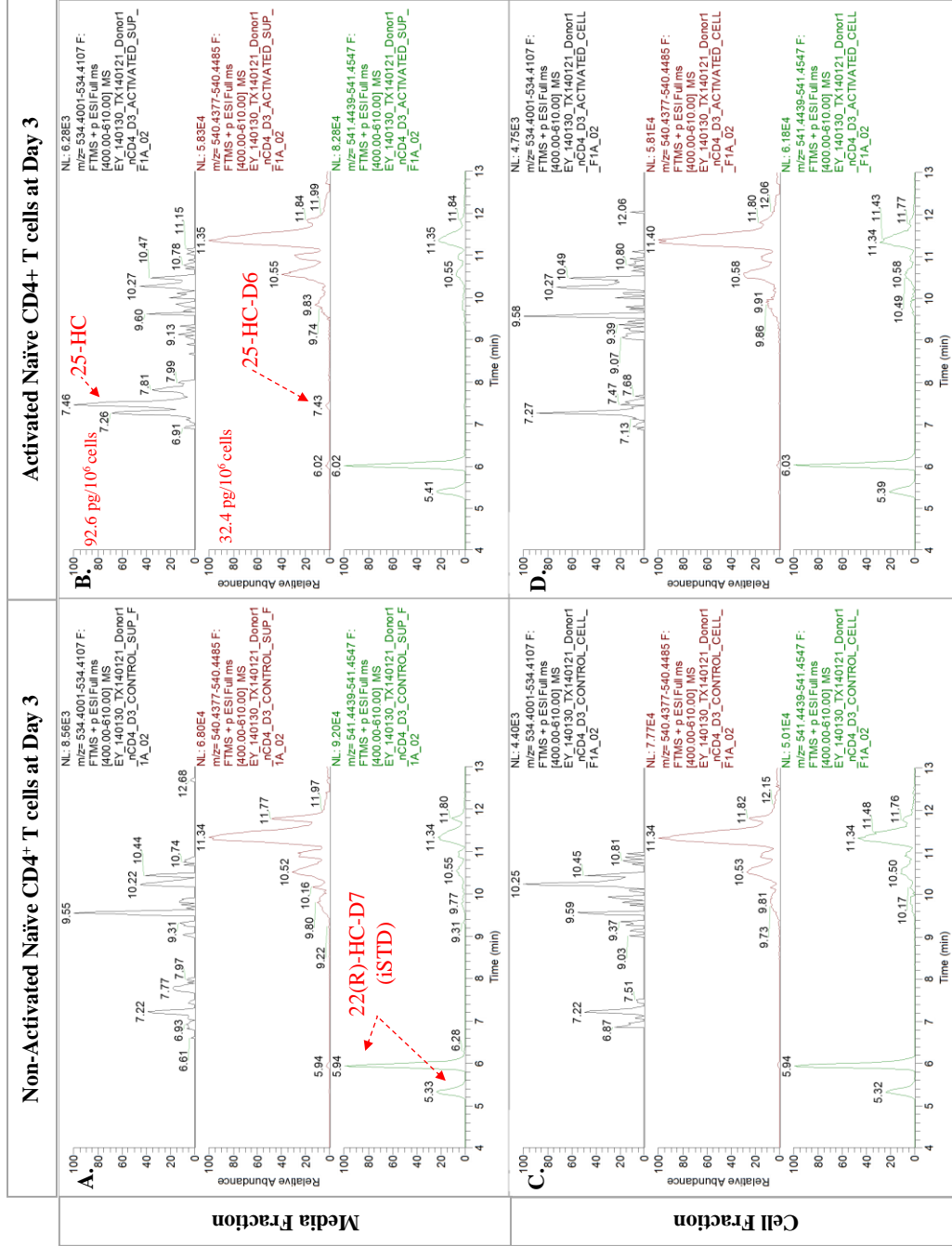


Figure 4.21. Donor 1 RIC for 534.4054 m/z, 540.4431 m/z and 541.4493 m/z to monitor monohydroxycholesterols, monohydroxycholesterol-D6s and monohydroxycholesterol-D7s in media and cell fractions of non-activated and activated naïve CD4⁺ T cells after three days in X-VIVO-20 with 4µg/mL Cholesterol-D7. Monohydroxycholesterols 24(S)-HC, 24(R)-HC, and 25-HC were detected in activated media samples but not in non-activated. There were no 24(S)-HC-D7 or 24(R)-HC-D7 seen on 541.4493m/z in the activated media fractions, although 25-HC-D6 was detected at 7.43min on 540.4431m/z. None of the oxysterols seen in media were detected in cell fractions except the 22(R)-HC-D7 internal standard present in all samples on 541.4493m/z. Inset numbers are the quantified concentration of 25-HC against the 22(R)-HC-D7 internal standard.

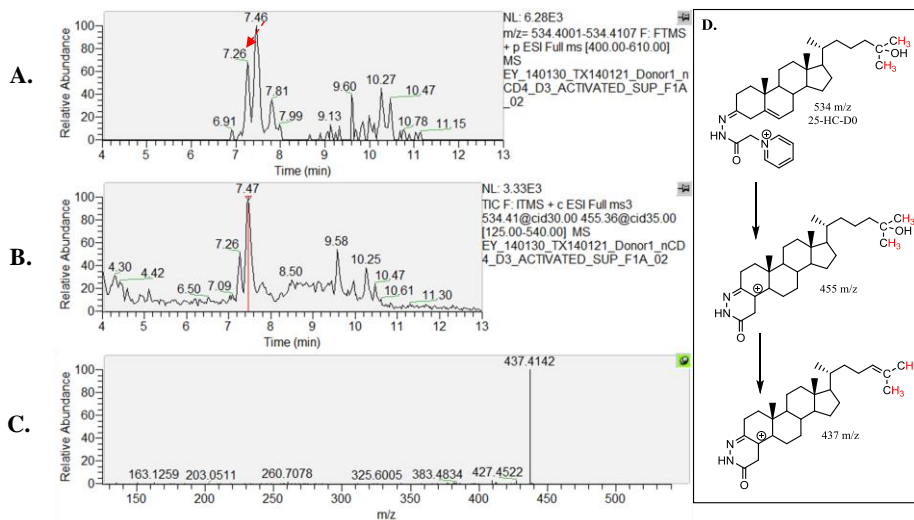


Figure 4.22. Monohydroxycholesterol full mass scan RIC, linear ion trap TIC of MS³ [534→455→] and the MS³ fragmentation spectra of 25-monohydroxycholesterol-D0.

A. Chromatogram of 534.4054 $m/z \pm 10$ ppm showing 25-HC at 7.26 min. B. Corresponding MS³ spectra to identify the 7.46 min peak which confirms that the peak has the correct mass has a neutral loss of 79 m/z upon MS². C. MS³ fragmentation spectra of the 7.47 min peak (red line in B.), with a characteristic base peak of 437.4 m/z , same as the authentic 25-HC reference standard. D. Structures of [M]⁺ precursor ion, [M-79]⁺ after MS², and the [M-79-18]⁺ fragment after MS³.

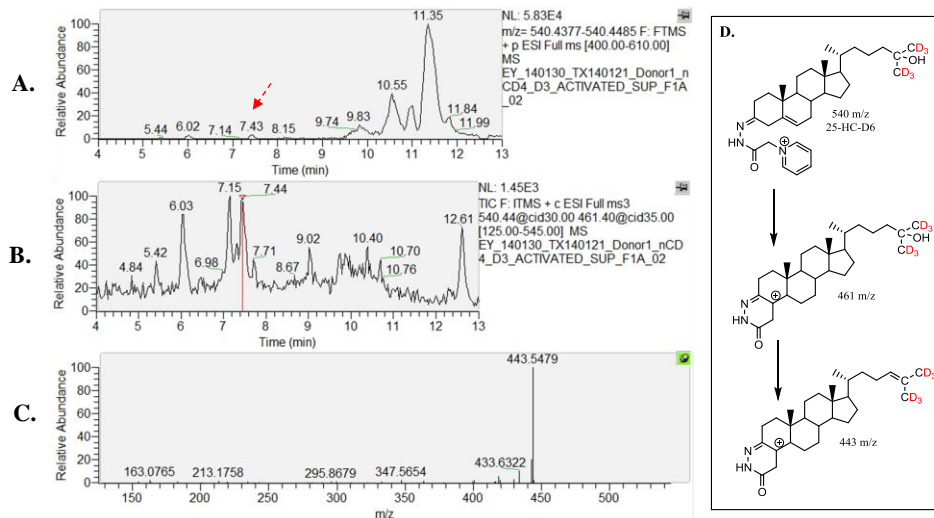


Figure 4.23. Monohydroxycholesterol-D6 full mass scan RIC, linear ion trap TIC of MS³ [540→461→] and the MS³ fragmentation spectra of 25-monohydroxycholesterol-D6.

A. Chromatogram of 540.4431 $m/z \pm 10$ ppm showing only 25-HC-D6 at 7.43 min. B. Corresponding MS³ spectra to identify the 7.43 min peak which confirms that the peak has the correct mass and loses 79 m/z upon MS². C. MS³ fragmentation spectra of 25-HC-D6 which has a similar pattern to the endogenous 25-HC with a base peak 6 Da heavier (437 + 6 = 443). D. Structures of [M]⁺ precursor ion, [M-79]⁺ fragment after MS², and the [M-79-18]⁺ fragment after MS³.

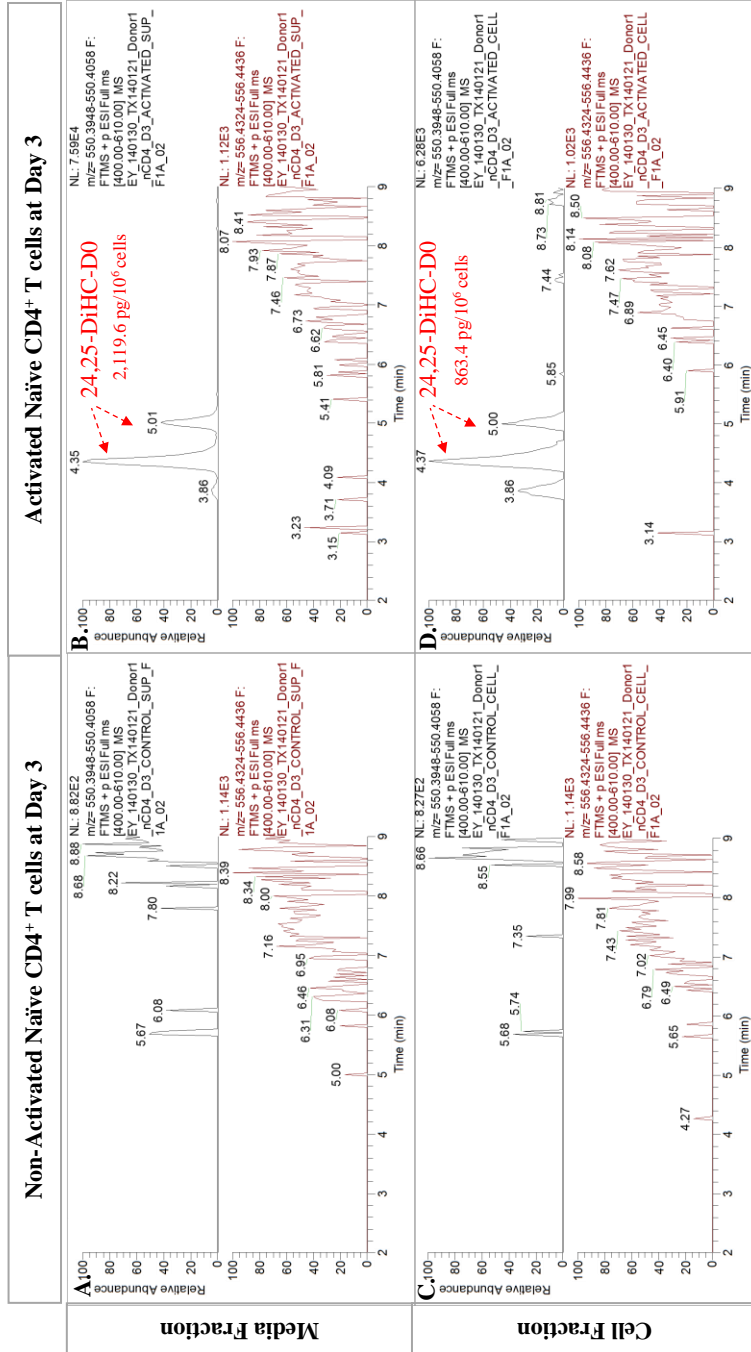


Figure 4.24. RIC for 550.4003 *m/z* and 556.4380 *m/z* to monitor dihydroxycholesterols and dihydroxycholesterol-D6s in media and cell fractions of non-activated and activated naïve CD4⁺ T cells after three days in X-VIVO-20 with 4μg/mL Cholesterol-D7. A/C. No 24,25-DiHC was detected in non-activated cultures after three days in either cell or media fractions. B/D. 24,25-DiHC was only detected in activated naïve CD4⁺ T cells and media fraction. No traces of 24,25-DiHC-D6 were seen to be produced at 556.4380 *m/z* suggesting that the dihydroxycholesterol were not metabolised from imported cholesterol-D7.

4.3.7. Time course investigation of total CD4⁺ T cell culture revealed increasing oxysterol production relative to length of activation.

After observing the increased oxysterols produced between different time points of activated naïve CD4⁺ T cells, the kinetics of oxysterol generation was next investigated. As there were usually limited naïve CD4⁺ T cells available from one donor, total CD4⁺ T cells were used instead in these experiments which include both naïve and memory cells. Also, cultured cells were stained with a marker of CD4⁺ T cell activation, CD25, at different time points.

4.3.7.1. Expression of the CD25 on total CD4⁺ T cell surface increases in activated cells and decreases in non-activated cells.

Flow cytometry analysis at 24 and 48 hour activated total CD4⁺ T cells revealed the increased expression of the IL-2 receptor alpha, CD25 on the T cell surface. For two donors analysed at 24 hours, the percentage of CD25 positive cells was increased from ~47% to ~94%, then up to ~97% at 48 hours (Figure 4.25) parallel to the increased levels of CD25 expression. On the other hand, the proportion of CD25⁺ cells were marginally reduced after 24 to 48 hours in non-activating conditions.

4.3.7.2. 25-HC was first detected in the media fraction 16 hours after activation which continued to increase up to 48 hours.

LC-MSⁿ analysis of oxysterols exported to the media showed increasing levels of 25-HC produced and exported to the media starting after 16 hours of CD3/CD28 stimulation (Figure 4.26.A) which were similar in trend across different donors (Figure 4.30). In contrast, 25-HC in cell fractions of donor 1 and 5 were only detected at 48 hours, levels of which were three to four times lower compared to 25-HC present in media (Figure 4.33).

In addition, 24(S)-HC was detected at low levels from 24 hours post activation (Figure 4.26.A). The 27-HC present in mock X-VIVO-20 media remained constant throughout

the time course suggesting this oxysterol was not produced nor imported by total CD4⁺ T cells. Analysis of non-activated cells did not detect the presence of 25-HC even after 48 hours with exception of donor 1 where low levels were detected.

4.3.7.3. 7 α ,25-DiHC generally follows the same trend as 25-HC.

The production of the downstream metabolite of 25-HC was seen to follow the trend of its precursor, detectable levels of which were generally present more in the media than in cell fractions (Figure 4.34). 7 α ,25-DiHC present in the media was mostly detected at four to seven times lower abundance than 25-HC. Across the different donors, the trend from 4 hour to 24 hours post activation were similar but there was a wide disparity in the normalised values at 48 hours (Figure 4.31). In particular, the dihydroxycholesterol was not detected at all in activated cells of donor 4.

4.3.7.4. 24(S),25-EC production and export to media was also time dependent after CD3/CD28 stimulation.

Production and export of 24(S),25-EC was observed on all activated total CD4⁺ T cells across all donors which was proportionally more observed in the media (Figure 4.32) than the cell fraction (Figure 4.35). The increased levels of this oxysterol in the media suggest that it was actively exported out of the cell. Rate of increase in the detected epoxycholesterol was higher in comparison to the detected levels of 25-HC and 7 α ,25-DiHC. This has made the levels of the epoxycholesterol much higher than other oxysterols at the end of the time course at 48 hours averaging at 690 pg/million cells across four different donors. This increase can be related to the induced cholesterol biosynthesis in in activated cells as intracellular cholesterol levels were also increased.

4.3.7.5. Activated total CD4⁺ T cells accumulate intracellular cholesterol.

Analysis of the cholesterol present in the cell fractions of donor 1 and 5 revealed the build-up of cholesterol only when in activated conditions (Figure 4.36) where as non-activated cells were observed to remain at the same levels. Specifically, 24 hour activated total CD4⁺ cells were seen to accumulate cholesterol 1.5 times more than non-activated cells.

This increase continues to more than double the amount after 48 hours compared to non-activated cells.

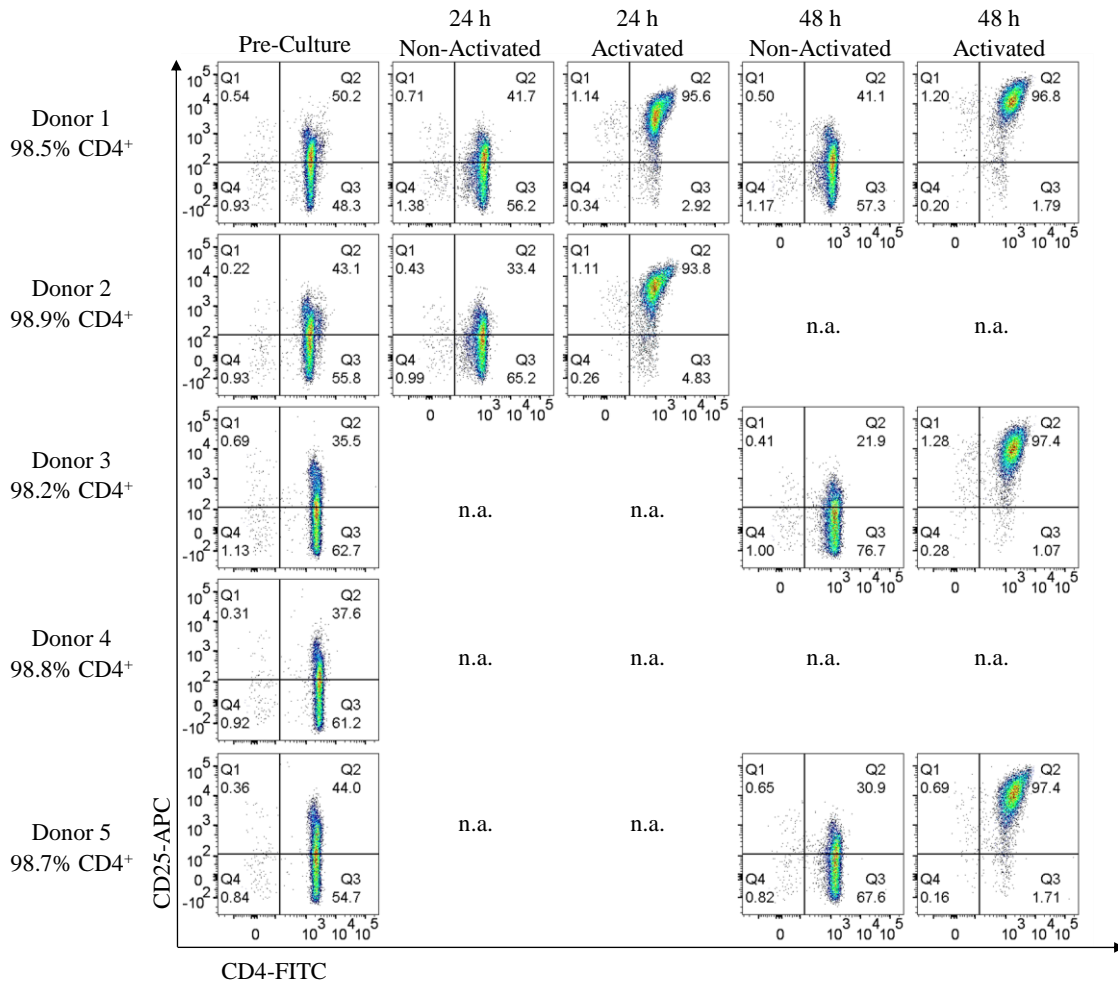


Figure 4.25. Pseudocolour CD25/CD4 dot plots of time course experiments on total CD4⁺ T cells. After total CD4⁺ T cells isolation by MACS, an aliquot was double stained with anti-CD25-APC and anti-CD4-FITC fluorescent antibodies and analysed by flow cytometry. All cells were >98.2% CD4⁺ and cultured either in activated or non-activated conditions. At 24 hour and 48 hour time point, an aliquot was taken and stained again to monitor the change in expression of CD25. Before culture, total CD4⁺ T cells contained between 35% and 50% CD25⁺ cells. This proportion was observed to drop at after 24 to 48 hours when not activated. Conversely, the expression of CD25 in total CD4⁺ T cells were seen to increase to >93.8% after 24 hours and further to 96.8% after 48 hours when treated with anti-CD3/CD28-loaded beads. (n.a. indicates data was not available)

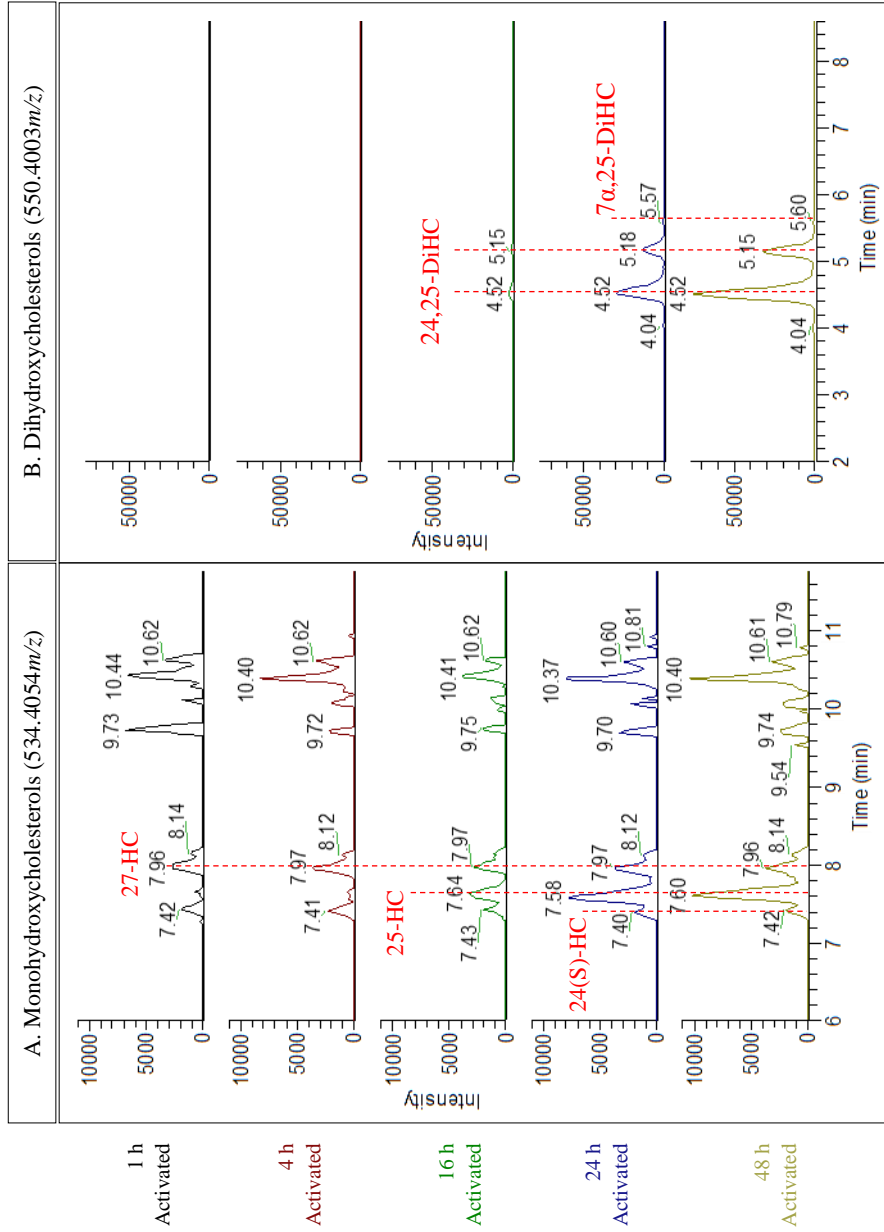


Figure 4.26. Donor 1 RIC of monohydroxycholesterols at 534.4054 $m/z \pm 10$ ppm and dihydroxycholesterols at 550.4003 $m/z \pm 10$ ppm in the media fraction of the time course study of activated total CD4⁺ T cells. During the time course, 27-HC which was naturally present in mock X-VIVO-20 was observed to be consistent whilst 25-HC was detected to be produced from 16 hours post activation and continually increased after 48 hours. Trace levels of 24(S)-HC was detected at 24 to 48 hours. Similar to 25-HC, 24,25-DiHC was first detected 16 hours after activation which continued to increase from 24 to 48 hours.

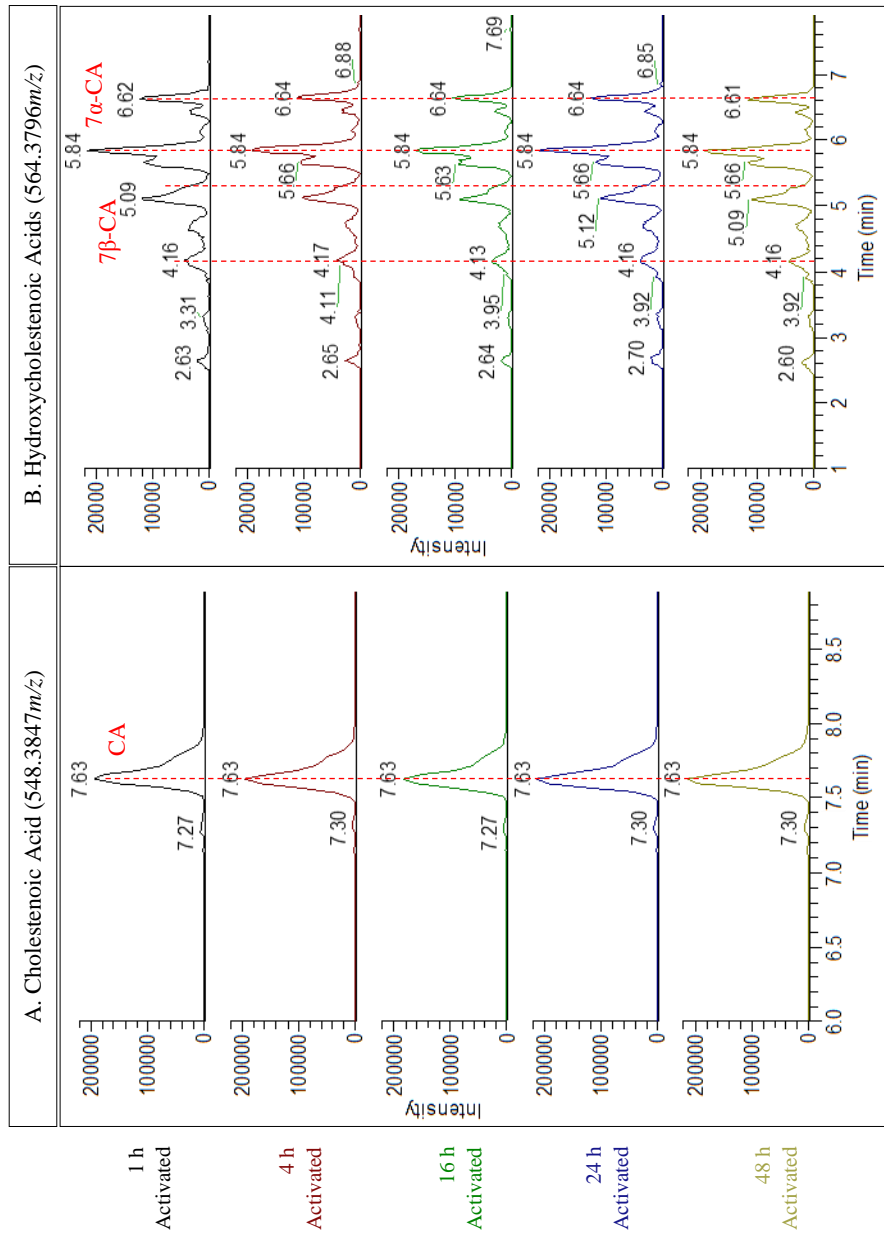


Figure 4.27. Donor 1 RIC of cholestenic acid at 548.3847 $m/z \pm 10$ ppm and hydroxycholestenic acids at 564.3796 $m/z \pm 10$ ppm in the media fraction of the time course study of activated total CD4⁺ T cells. During the time course, CA which was naturally present in X-VIVO-20 was not observed to increase or decrease in intensity. A similar trend was observed with 7 β -CA and 7 α -CA. Analysis of non-activated total CD4⁺ T cells did not indicate any changes as well.

Normalised 24S-hydroxycholesterol in total CD4⁺ T cells – Media fraction

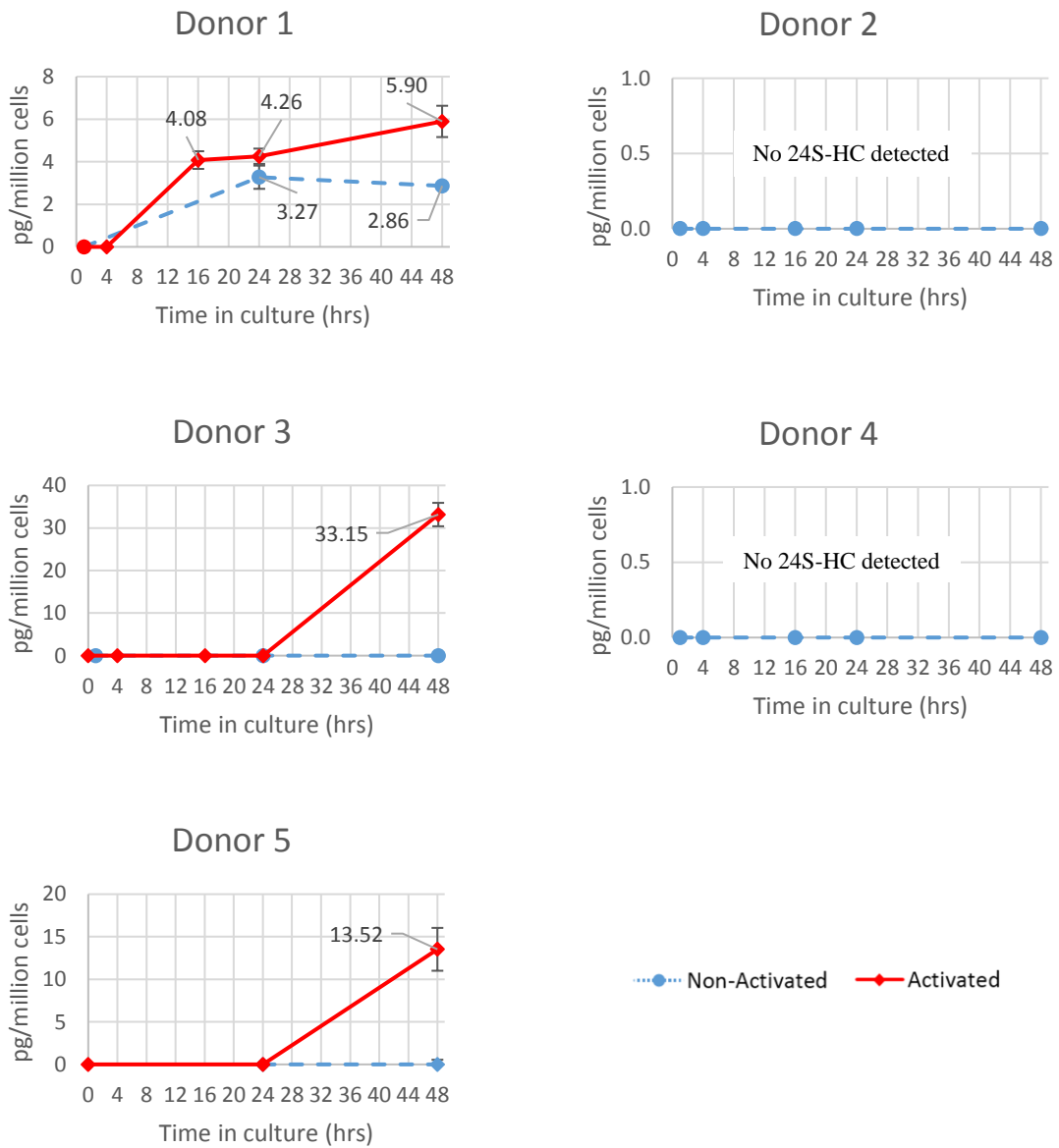


Figure 4.28. Time course study of the production of 24S-HC found in culture media of non-activated and activated total CD4⁺ T cells. Minimal 24S-HC were generally identifiable by MS3 fragmentation which are mostly detected at 48 hours. Quantified data was normalised to the number of cells initially seeded. Error bars indicate the SD of three individual LCMS injections.

Normalised 24R-hydroxycholesterol in total CD4⁺ T cells – Media fraction

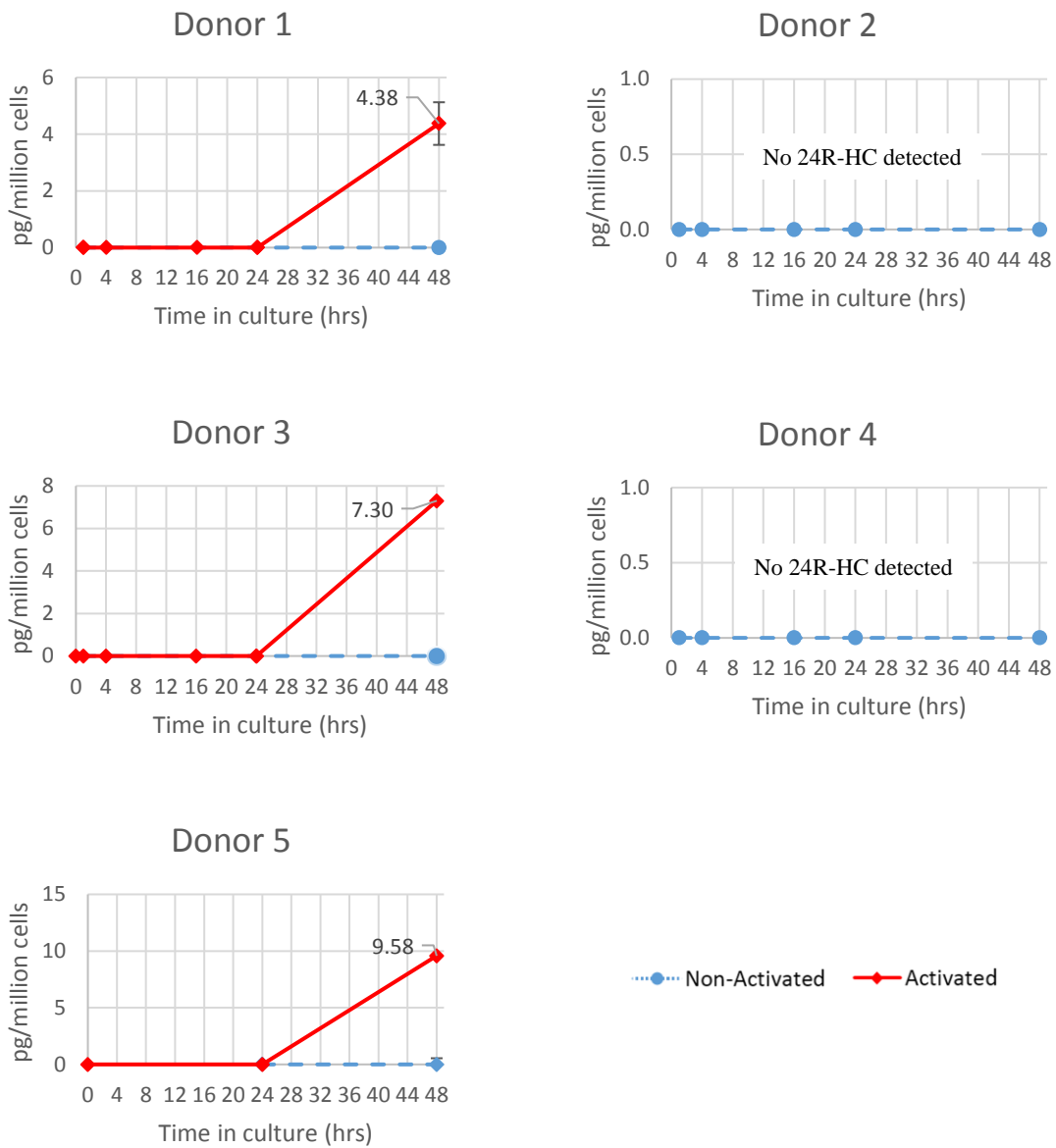


Figure 4.29. Time course study of the production of 24R-HC found in conditioned media of non-activated and activated total CD4⁺ T cells.

There were generally minimal amounts of 24R-HC which are mostly detectable only at 48 hours. Quantified data was normalised to the number of cells initially seeded. Error bars indicate the SD of three individual LCMS injections.

Normalised 25-hydroxycholesterol in total CD4⁺ T cells – Media fraction

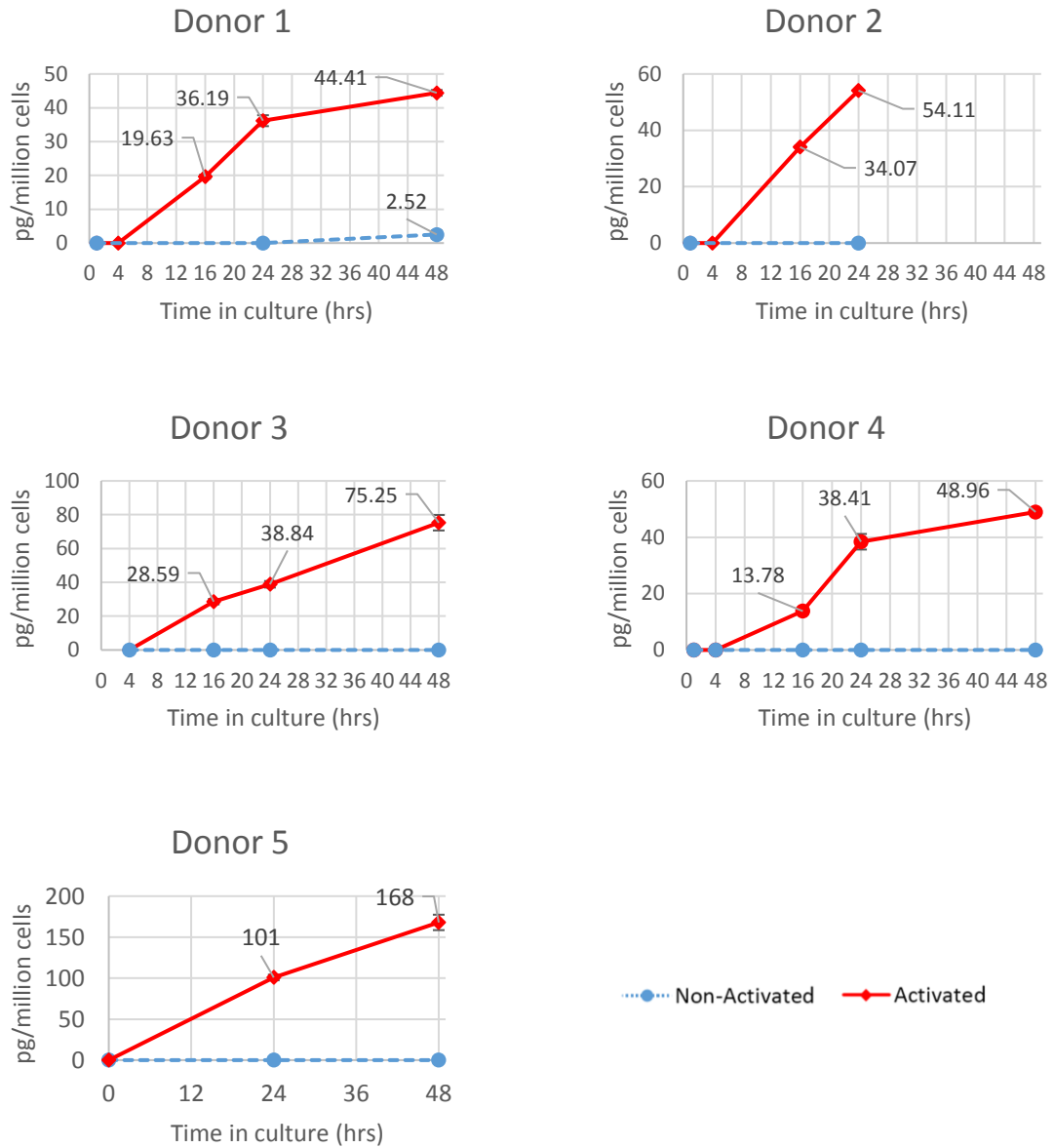


Figure 4.30. Time course study of the production of 25-HC found in conditioned media of non-activated and activated total CD4⁺ T cells.

A general increase in the production of 25-HC was observed across five different donors in activated conditions. Quantified data was normalised to the number of cells initially seeded. Error bars indicate the SD of three individual LCMS injections.

Normalised $7\alpha,25$ -dihydroxycholesterol in total CD4⁺ T cells – Media fraction

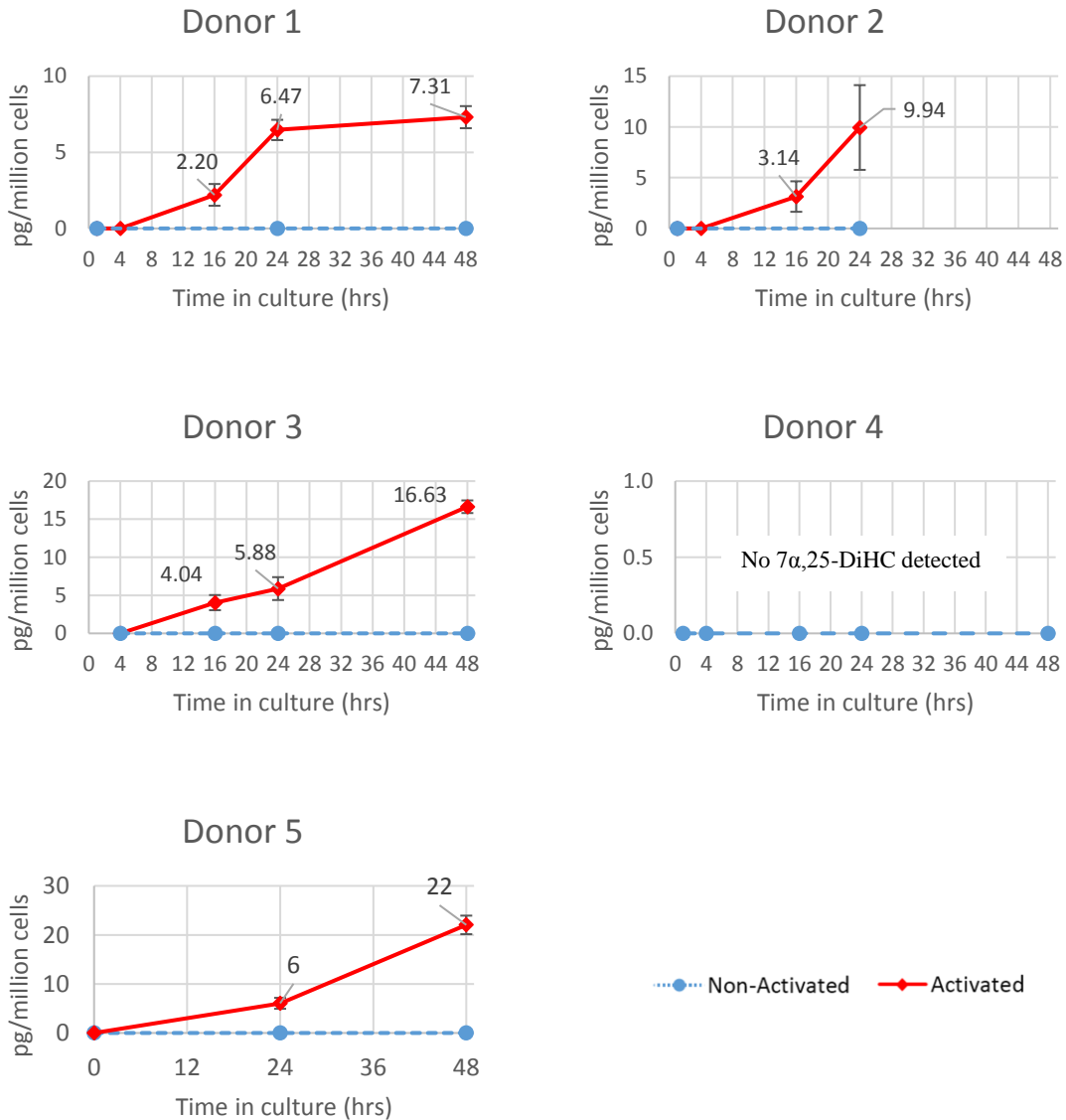


Figure 4.31. Time course study of the production of $7\alpha,25$ -DiHC found in conditioned media of non-activated and activated total CD4⁺ T cells.

A general increase in the production of $7\alpha,25$ -DiHC was observed across four different donors in activated conditions. Donor 4 activated cells were not observed to produce any $7\alpha,25$ -DiHC. Quantified data was normalised to the number of cells initially seeded. Error bars indicate the SD of three individual LCMS injections.

Normalised 24(S),25-epoxycholesterol in total CD4⁺ T cells – Media fraction

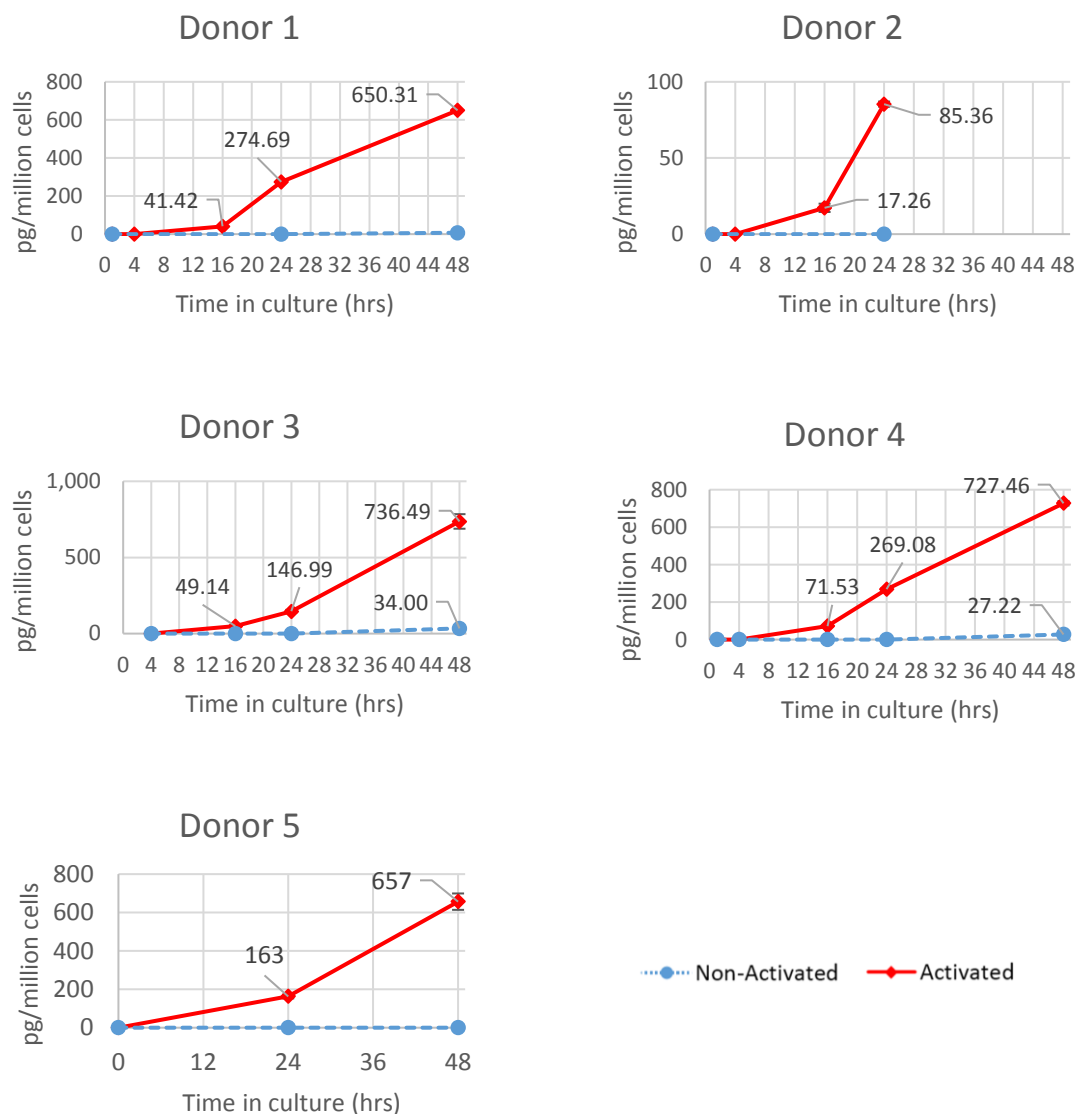


Figure 4.32. Time course study of the production of 24(S),25-EC detected in conditioned media of non-activated and activated total CD4⁺ T cells.

A general increase in the production of 24(S),25-EC was observed across five different donors in activated conditions. Quantified data was normalised to the number of cells initially seeded. Error bars indicate the SD of three individual LCMS injections.

Normalised 25-hydroxycholesterol in total CD4⁺ T cells – Cell fraction

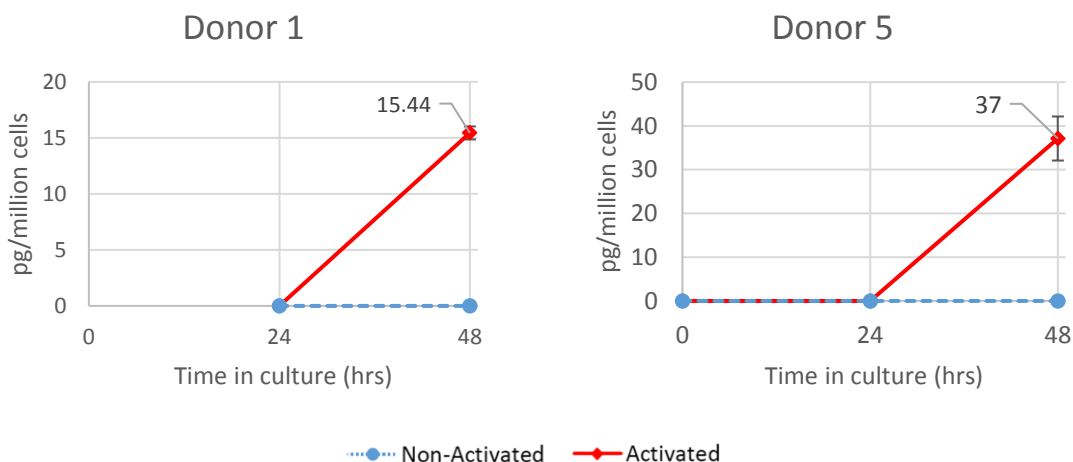


Figure 4.33. Time course study of the production of 25-HC detected intracellularly of non-activated and activated total CD4⁺ T cells.

Intracellular 25-HC was only detected after 48 hours of activation from two donors. Quantified data was normalised to the number of cells extracted at each time point. Error bars indicate the SD of three individual LCMS injections.

Normalised 7 α ,25-dihydroxycholesterol in total CD4⁺ T cells – Cell fraction

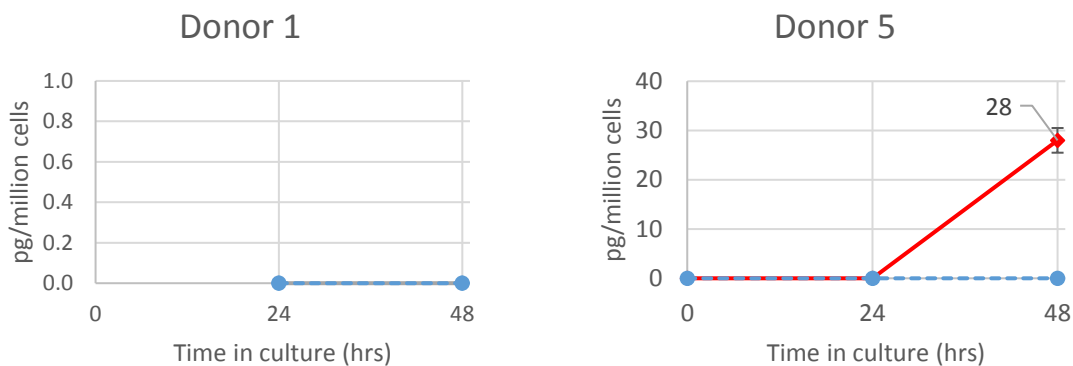


Figure 4.34. Time course study of the production of 7 α ,25-DiHC detected intracellularly of non-activated and activated total CD4⁺ T cells.

Intracellular 7 α ,25-DiHC was detected after 48 hours for donor 5 only. Quantified data was normalised to the number of cells extracted at each time point. Error bars indicate the SD of three individual LCMS injections.

Normalised 24(S),25-epoxycholesterol in total CD4⁺ T cells – Cell fraction

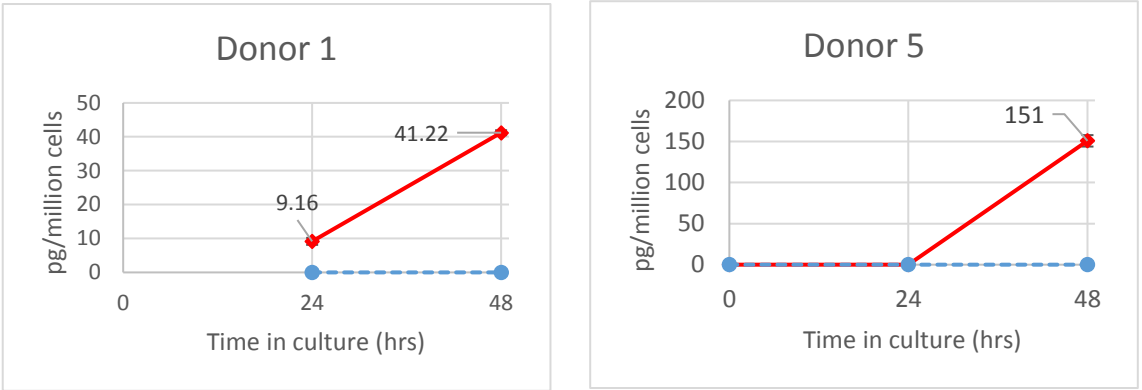


Figure 4.35. Time course study of the production of 24(S),25-DiHC detected intracellularly of non-activated and activated total CD4⁺ T cells.

Most intracellular 24(S),25-DiHC was detected after 48 hours post activation between the two donors. No epoxycholesterol was detected in the non-activated cells. Quantified data was normalised to the number of cells extracted at each time point. Error bars indicate the SD of three individual LCMS injections.

Normalised Cholesterol in total CD4⁺ T cells – Cell fraction

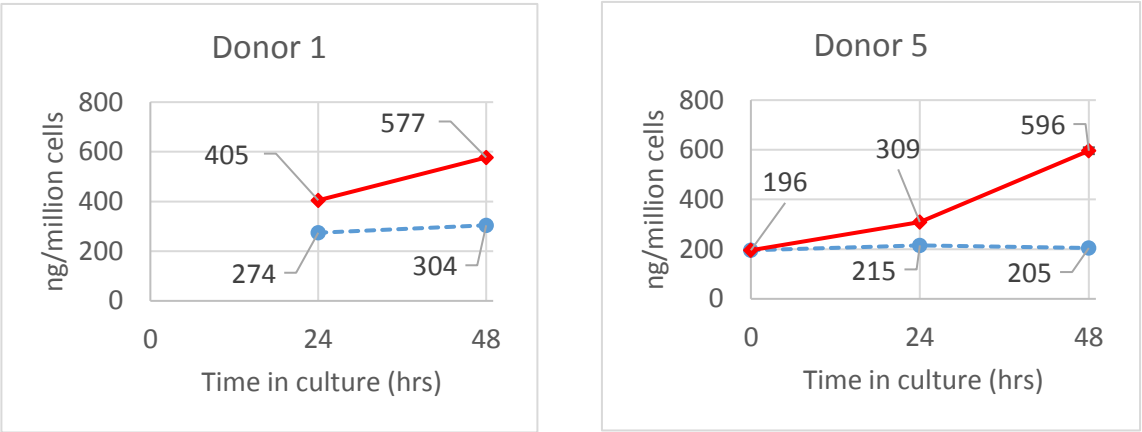


Figure 4.36. Time course study intracellular cholesterol contained in non-activated and activated total CD4⁺ T cells.

Non-activated cells were observed to have a constant concentration of intracellular cholesterol whilst in activated cells, intracellular cholesterol increased two-fold after 24 hour then three-fold after 48 hours. Quantified data was averaged between two LCMS injections and normalised to the number of cells extracted at each time point.

4.3.8. Characterising the oxysterols generated by naïve and memory CD4⁺ T cells.

So far, oxysterol production from both activated naïve and total CD4⁺ have been analysed. Since total CD4⁺ T cells constitutes both naïve and memory populations, we extended the investigation to see how much memory CD4⁺ T cells contribute to the oxysterol levels by isolating each population and culturing them in activating conditions.

4.3.8.1. Comparing the methods for memory CD4⁺ T cell isolation.

Two different methods of memory CD4 T cell isolations were compared (see *section 2.1.4.3*). The first method of isolation provided purer naïve cells than the memory fraction (Figure 4.37). However, the second method provided a purer memory cells but less than naïve population (Figure 4.38). The purity of memory CD4⁺ T cell population were at 95.8% to 99.3% CD45RO^{bright}, respectively.

More specifically, using the naïve CD4⁺ T cell isolation kit after CD4⁺ T cell isolation kit in the first method led to 99% CD45RA^{bright} naïve cells, although these cells were also found to be 49.9% CD45RO^{dim}. Conversely, the memory population of donor 1 also contained 41.8% CD45RA^{dim} cells. On the other hand, using the CD45RA Microbead kit in the second method gave less contaminating CD45RA⁺ cells (13.8%) in the memory fraction thus getting 99.3% CD45RO^{bright} cells. The disadvantage of the second method was the very low purity of isolated naïve cells (73.4% CD45RA⁺) which was even 96.9% CD45RO^{bright}. This was unfortunate but the second method provides a more reliable oxysterol profile for memory CD4⁺ T cells as it contains minimal CD45RA⁺ cells.

4.3.8.2. Memory CD4⁺ T cells contained slightly more CD25⁺ cells than naïve cells.

On both donor isolations, the expression of CD25 was observed to be proportionally higher in the memory fraction than the naïve fraction (Figure 4.37 and Figure 4.38 blue boxes). Donor 1 memory CD4⁺ T cells were found to be 43.1% CD25^{dim} (MFI:136) whilst naïve cells were 10.6% (MFI:27). A similar trend was seen in donor 2 cells where 64.7% (MFI:209) of the memory cells were CD25⁺ whereas the naïve population was 46.8%

(MFI:109). Given that donor 2 naïve CD4⁺ T cells was not purely CD45RA⁺, it can be assumed that the higher CD25⁺ cells were from contaminating CD45RO⁺ cells.

The 24-hour activation of donor 1 cells also showed a slightly higher CD25⁺ expression increase in naïve cells than memory CD4⁺ cells. From 13.7% (MFI:40) CD25⁺ before culture, activated naïve cells were observed to induce CD25 expression on 90.2% (MFI:2,076) of cells whereas memory cells only rose from 43.1% (MFI:136) to 84.9% (MFI:4,544) at 24 hours (Figure 4.39). Furthermore, the extended 48-hour activation of donor 1 memory CD4⁺ T cells saw an increase to 90.3% (MFI:14,109) CD25 expression.

4.3.8.3. No oxysterols were detected in non-activated memory CD4⁺ T cells after 24 hours in culture.

Pure populations of CD45RO⁺ CD4⁺ memory T cells were not observed to produce oxysterols in non-activating conditions after 24 hours in culture. This was not unexpected as previously neither naïve nor total CD4⁺ T cell non-activated cultures were seen to produce any at an early time point of 24 hours.

4.3.8.4. Greater 24(S),25-EC was produced by activated naïve than memory CD4⁺ T cells after 24 hours on both donors.

Oxysterol analysis of the media fractions from both donors revealed that 24 hour activated naïve CD4⁺ T cells produced three times more 24(S),25-EC than memory cells. The activated naïve CD4⁺ T cells of donor 1 was observed to produce 336 pg/million cells of 24(S),25-EC whilst the memory fraction was only 176 pg/million cells (Figure 4.40.A).

Compared to donor 1, activated cells of donor 2 were observed to generally have lower production of 24(S),25-EC. Naïve cells produced 69 pg/million cells of the epoxycholesterol which was still 3.5 times more than the 20 pg/million cells detected in the activated memory cells.

4.3.8.5. Both naïve and memory CD4⁺ T cells produce 25-HC.

The production of 25-HC was detected in both 24 hour activated naïve and memory CD4⁺ T cells. The memory cells of donor 1 was seen to produce 3 times more 25-HC at 150pg/million cells than naïve cells at 53 pg/million cells. For donor 2, the reverse was observed (Figure 4.40.B). 25-HC was the only enzyme-derived monohydroxycholesterol produced by both naïve and memory cells and other oxysterols like 24(S)-HC or 24(R)-HC were not detected.

4.3.8.6. Production of 7 α ,25-DiHC was detected in activated CD45RO^{bright}-containing CD4⁺ T cells at 24 hours.

The activated naïve CD45RA^{bright} and CD45RO^{dim} population from donor 1 were observed to produce both 25-HC and 24S,25-EC but not 7 α ,25-DiHC. However, both of donor 2 naïve and memory CD4⁺ T cells, analysed by flow cytometry to contain CD45RO^{bright} cells (Figure 4.38) were observed to produce 7 α ,25-DiHC in activating conditions within 24 hours which was the same in donor 1 memory CD45RO^{bright} population (Figure 4.40.C). This suggests that production of 7 α ,25-DiHC in donor 2 naïve CD4⁺ population maybe due to the presence of CD45RO⁺ cells. Furthermore, fraction B analysis of donor 1 naïve cells revealed the presence of 3-oxo-7 α ,25-DiHC, the downstream metabolite of HSD3B7 from 7 α ,25-DiHC, at 13.28 pg/million cells leaving the 3 β -hydroxy form of 7 α ,25-DiHC at 35.61 pg/million cells. In contrast, all the detected 7 α ,25-DiHC from both naïve and memory populations of donor two were all as the 3 β -hydroxy form and no 3-oxo-7 α ,25-DiHC.

4.3.8.7. Isolation of CD294⁺ T_H2 from total CD4⁺ cells provided insufficient and impure population for oxysterol profiling.

CD294⁺ cells were isolated from total CD4⁺ T cells of two separate donors. Very low cell numbers, 0.45x10⁶ and 0.76x10⁶, were acquired from 44.28x10⁶ and 37.90x10⁶ total CD4⁺ T cells after positive selection using anti-CD294 microbeads, respectively. This suggests that T_H2 cells in these donors constitute about 1-2% of total CD4⁺ T cells. This goes in line with published reports of 2% average IL4⁺ T_H2 cells present in the CD4⁺ T cell populations [9]. However, flow cytometric analysis of the positive and negative fractions

revealed an accumulation of impurities in the CD249⁺ fraction, possibly due to non-specific binding of the anti-CD294 antibody (Figure 4.41.B/C). Pre-separation of total CD4⁺ T cells stained with anti-CD294-PE antibody already revealed a very low percentage of CD294⁺ cells (Figure 4.41.A). Continuing with the magnetic separation only introduced impurities/debris in the positive fractions on both donors indicated by the D1 gates. This on the other hand removed debris in the negative fractions. Donor 1 positive fraction cells provided 16% CD294⁺ cells whilst donor 2 cells were 54.4%. This implies that the low cell counts isolated after the magnetic separation were mixed with non-T_H2 cells which will not provide specific oxysterol production for T_H2 cells.

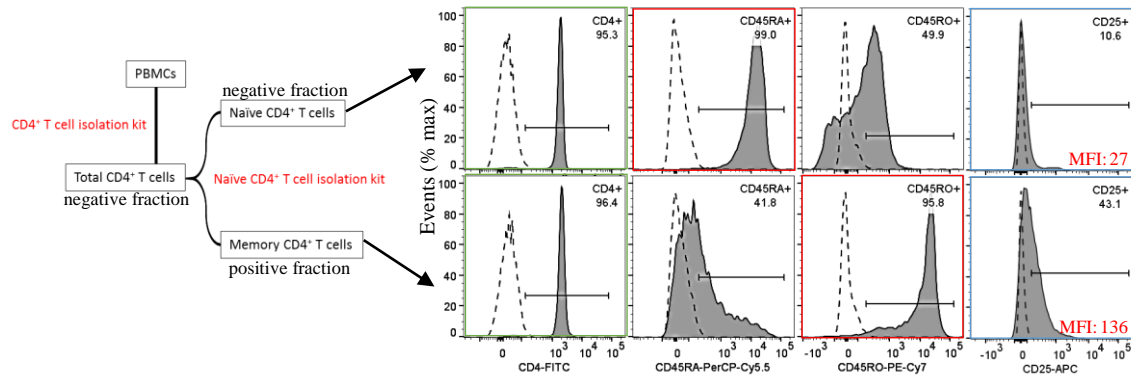


Figure 4.37. Magnetic separation process and pre-culture flow cytometry analysis of naïve and memory CD4⁺ T cells for donor 1.

Both populations were isolated from total CD4⁺ T cells using a Naïve CD4⁺ T cells isolation kit by a depletion process. This provided very good purity of 99% CD45RA^{bright} naïve cells and 95% CD45RO^{bright} memory cells (red boxed). There were observed co-expression of CD45RA and CD45RO in both isolated populations. In addition, both populations were confirmed to be >95.3% CD4⁺ cells (green boxed). Memory CD4⁺ T cells were observed to have more CD25⁺ cells than naïve (blue boxed). Gates were determined using the background fluorescence of unstained samples (1%) indicated by the dotted histograms.

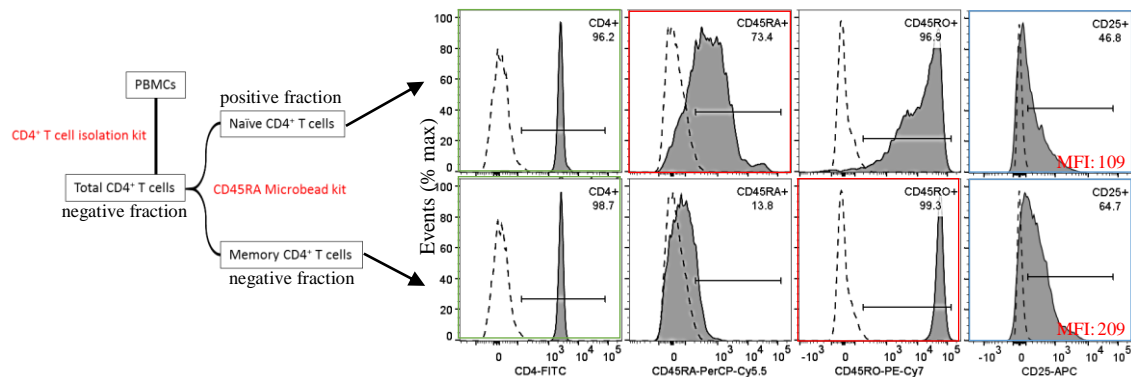


Figure 4.38. Magnetic separation process and pre-culture flow cytometry analysis of naïve and memory CD4⁺ T cells for donor 2.

Both populations were isolated from total CD4⁺ T cells using a CD45RA Microbead kit by a depletion process. This provided lower 73% CD45RA⁺ naïve cells but purer 99% CD45RO^{bright} memory cells (red boxed). In addition, both populations were confirmed to be >96.2% CD4⁺ cells (green boxed). Similar to donor 1, memory CD4⁺ T cells were observed to have more CD25⁺ cells than naïve (blue boxed), although the higher expression of CD25 detected in naïve cells might be due to the CD45RO⁺ memory cells. Moreover, naïve cells using this method of isolation generated a high proportion of CD45RO⁺ cells. Gates were determined using the background fluorescence of unstained (1%) samples indicated by the dotted histograms.

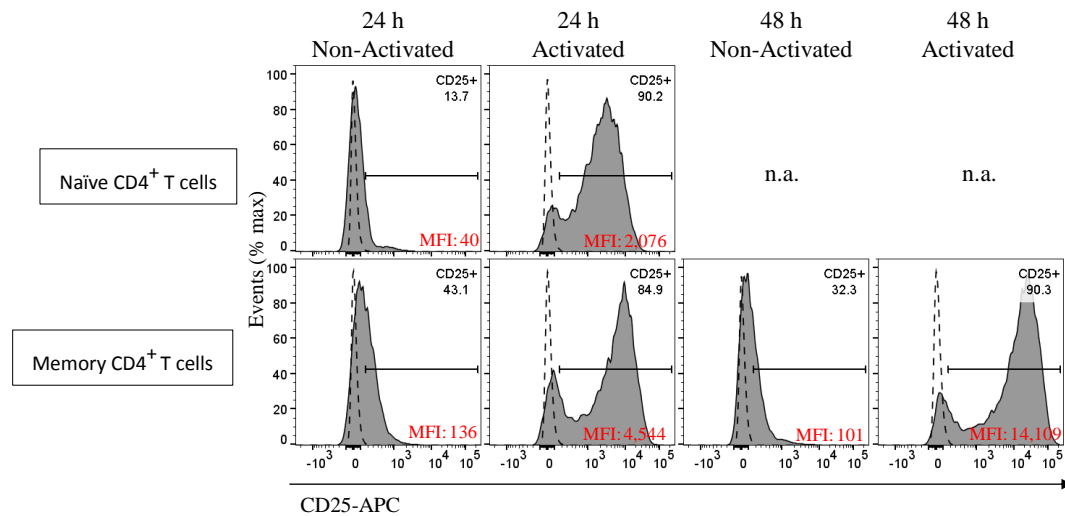


Figure 4.39. Flow cytometry analysis of CD25-APC stained naïve and memory CD4⁺ T cells of donor 1. An aliquot of cells was single stained with anti-CD25-APC of both non-activated and activated naïve and memory CD4⁺ T cells after 24 or 48 hours. At 24 hours, 90.2% (MFI:2,076) of naïve cells were expressing CD25, whilst memory cells were only observed to have 84.9% (MFI:4,544). This expression in memory CD4⁺ T cells increased further to 90.3% (MFI:14,109) after 48 hours. Gates were determined using the background fluorescence of unstained samples (1%) indicated by the dotted histograms.

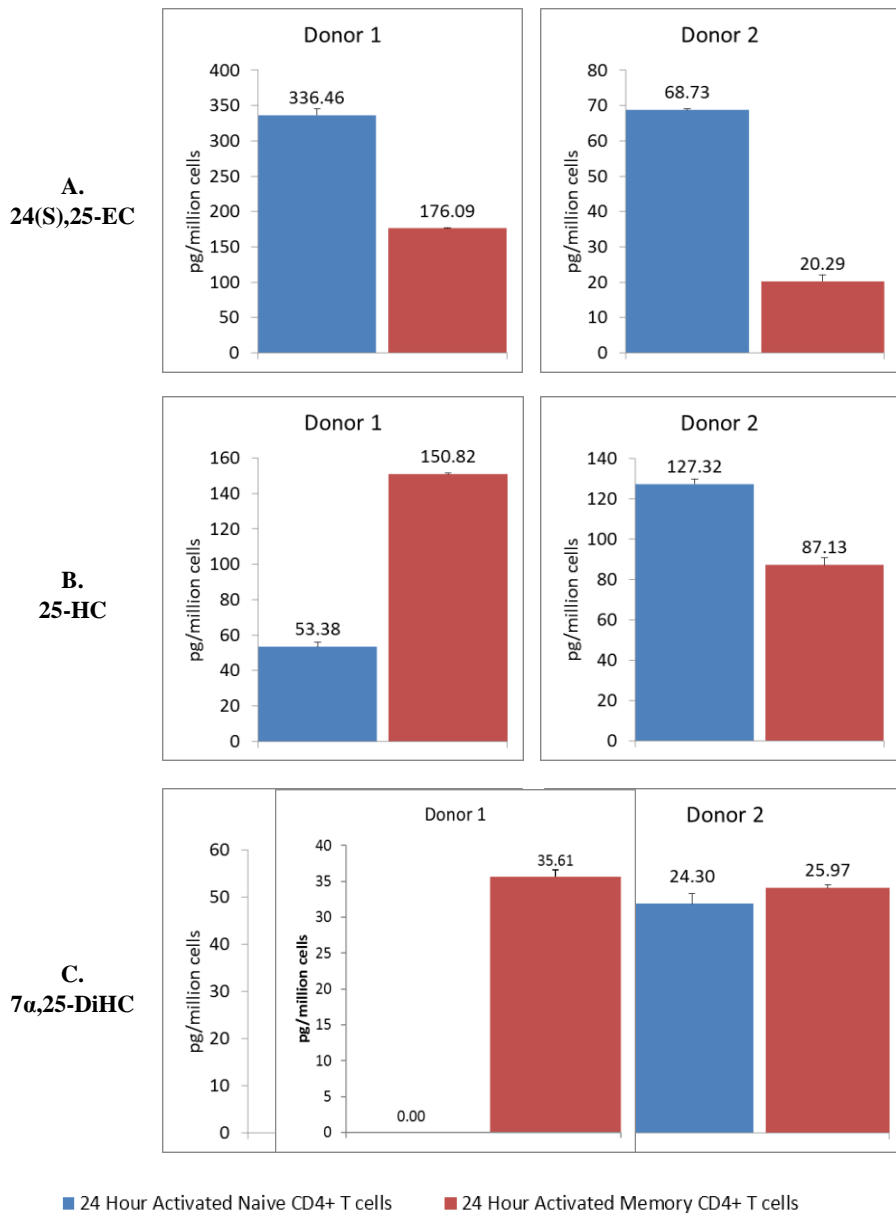


Figure 4.40. Oxysterols detected in the media fraction of 24 hour activated naïve and memory CD4⁺ T cells. A. Comparison of detected 24(S),25-EC between two donors show that naïve cells produce three time more epoxycholesterol than memory cells. B/C. No trend was seen in the production of 25-HC and 7 α ,25-diHC between the two donors. Quantified values were normalised to the number of cells initially seeded and the error bars indicate the SD of three different LCMS injections.

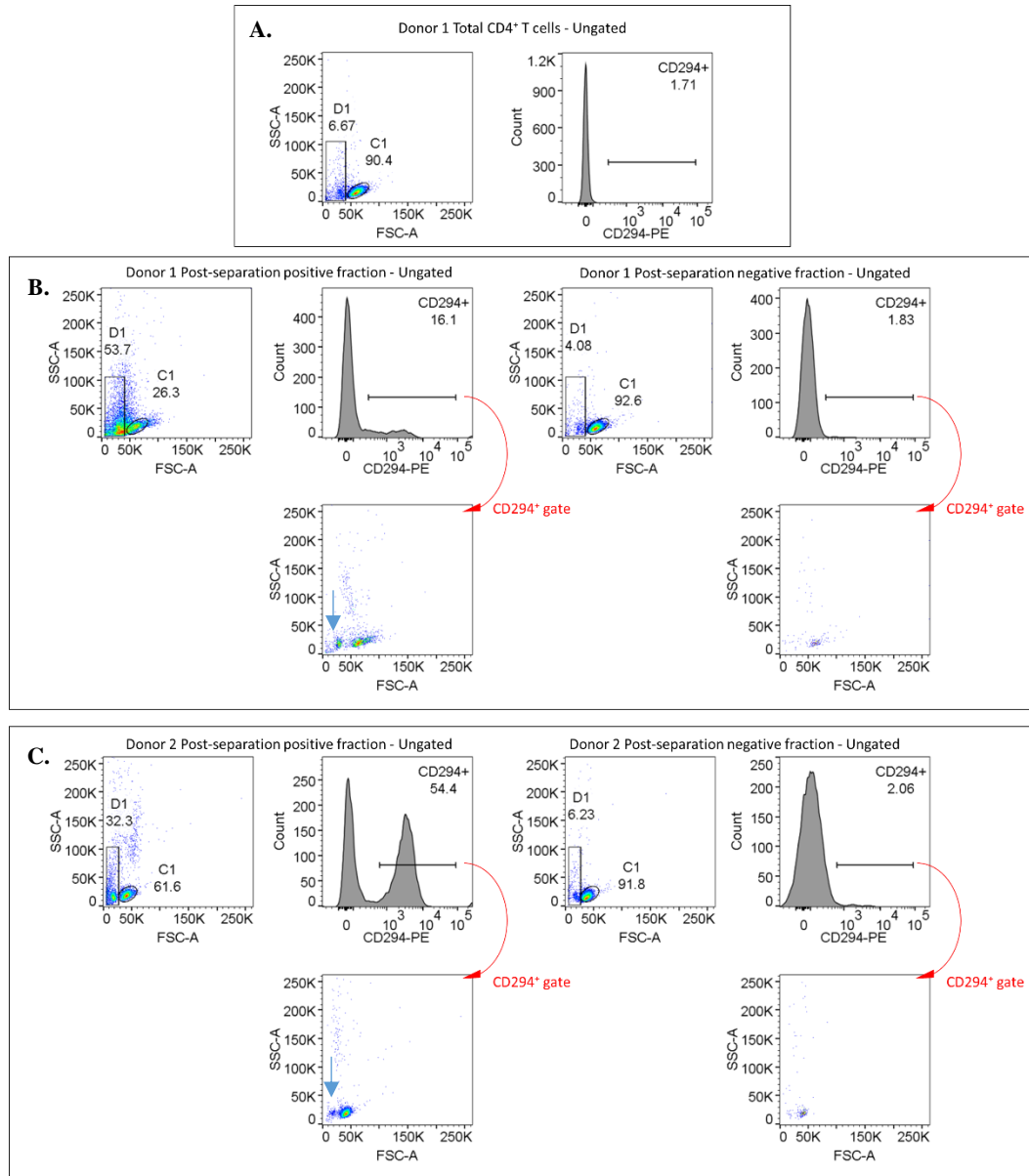


Figure 4.41. Pre-culture flow cytometry analysis of the positive and negative fractions after CD294⁺ T_H2 isolation.

A. Flow cytometry analysis of donor 1 total CD4⁺ T cells prior to magnetic separation indicated a very low proportion of cells which were CD294⁺. B/C. Donor 1 and donor 2 cells after CD294 positive selection. The positive fractions revealed an accumulation of debris indicated by the D1 gates. Of all the events recorded, only 16.1% and 54.4% were CD294⁺ cells. Within the CD294⁺ gate, some still gave FSC/SSC signals similar to debris (blue arrow). This confirms that the isolated cells, even if cultured in activating conditions will not provide reliable production of oxysterols specific to T_H2 cells.

4.4. Discussions

The production of oxysterols by CD4⁺ T cells in culture were explored in this chapter. Different culture media was used for optimal maintenance of the T cells and found that the commercially available serum-free hematopoietic X-VIVO-20 cell media was most suitable. Using this media, it was found that resting CD4⁺ T cells, whether naïve, memory or in co-culture, do not produce detectable levels of cholesterol metabolites. These cells remain in this quiescent state based on the minimal expression of the IL-2R α (CD25), for up to 6 days in culture. However, once stimulated via its T cell receptor and co-activator receptors using anti-CD3 and anti-CD28-loaded microbeads, the CD4⁺ T cells were observed to rapidly upregulate CD25 within 24 hours in addition to the detectable production of downstream cholesterol metabolites. Most notably, measurable levels of 25-HC and 7 α ,25-DiHC were produced as early as 16 hours post-stimulation. A higher proportion of these oxysterols were detected in the conditioned media rather than the cell pellet which in a time-dependent manner accumulate in the conditioned media. This suggests that both these oxysterols were metabolised from cholesterol and exported out. In addition, extended cultures of up to six days resulted in the detection of 24(S)-HC, reported as the main cholesterol metabolite in the brain ^[10]. In contrast, no 27-HC was observed to be produced by human CD4⁺ T cells.

The experiments which included exogenous deuterium-labelled cholesterol revealed a noteworthy result where cholesterol, either *de novo* synthesised or imported from the media, was metabolised to 25-HC upon activation. This was not observed to be the case for other oxysterols like 24(S)-HC and 24(R)-HC which was seen to be produced at similar levels. This might suggest a possible role of 25-HC production during the activation of CD4⁺ T cells. Furthermore, import of the deuterated cholesterol was observed in both activated and non-activated cells, although once activated, majority of the accumulated cholesterol was newly synthesised.

The other oxysterol seen to be produced in higher amounts than 25-HC and 7 α ,25-DiHC was 24(S),25-EC. This oxysterol, however is not derived from the downstream

metabolism of cholesterol but is produced *de novo* parallel to it. T cells were previously reported to have induced the mevalonate pathway to synthesise new cholesterol upon activation, relating it as a checkpoint prior to DNA synthesis and in preparation of building new cell membranes for cell division^[3,11]. T cells have been reported to switch their metabolic activity from oxidative phosphorylation to aerobic glycolysis once stimulated^[12]. This switch gives rise to the production of biosynthetic precursors like acetyl-CoA which can then feed into other anabolic pathways including cholesterol biosynthesis. The generation of 24(S),25-EC could be attributed to the cells' cholesterol biosynthesis being induced in stimulated conditions. As there was limited cholesterol available for uptake in the serum-free X-VIVO-20 media, it was necessary for the cell to produce and accumulate new cholesterol which results in 24(S),25-EC being produced via the shunt pathway^[7,8]. As the majority of the 24(S),25-EC detected was mainly in the media, it is suggestive that it is actively exported by the cells or passively diffuses out of the cells but is prevented from diffusing back in. Epoxycholesterol has been known to be an inhibitor of SPEBP-2 processing and a potent LXR activator^[13,14] and increased presence of this oxysterol intracellularly can lead to decreased expression of cholesterol biosynthesis genes and increased cholesterol export, respectively, which may hinder the activation process.

Isolating and activating the sub-populations of total CD4⁺ T cells gave an indication of the specific oxysterols produced between naïve and memory cells. 7 α ,25-DiHC was not observed to be produced in activated pure cultures of naïve CD4⁺ T cells within 24 hours whereas the presence of activated memory cells in culture results in its detection. The specificity of 7 α ,25-DiHC to the memory population may implicate its role as an EBI2 ligand^[15]. The EBI2 GPCR is expressed in B cells and has been reported to be important in the guiding of B-cells towards a concentration gradient of the oxysterol produced by stromal cells within lymphoid tissues^[16]. Additionally, EBI-2 was reported to be expressed in CD4⁺ DCs and had a role in its distribution within the bridging channels of lymphoid organs to promote its interaction with blood-borne antigens^[17]. The production of this ligand by activated memory T cells, albeit at low concentrations, can be another way of how T cells influence B cell and DC-mediated immune responses.

In general, CD4⁺ T cell activation via CD3/CD28 induces the synthesis and import of cholesterol. This activation also results in the production and accumulation of certain oxysterols which follows the trend of accumulated intracellular cholesterol. It can then be assumed that these cholesterol metabolites, especially 25-HC, were only produced as a consequence of increased substrate availability and may not have any other roles in T cell function compared to other studies in macrophages and B cells. It is therefore worthy to investigate and uncouple the generation of these oxysterols to the induction of cholesterol biosynthesis upon CD4⁺ T cell activation.

4.5. References

- [1] M. Thurnher, G. Gruenbacher, (2015) T lymphocyte regulation by mevalonate metabolism, *Sci. Signal.* 8 re4-re4. doi:10.1126/scisignal.2005970.
- [2] J. a. Maciolek, J. Alex Pasternak, H.L. Wilson, (2014) Metabolism of activated T lymphocytes, *Curr. Opin. Immunol.* 27 60–74. doi:10.1016/j.coi.2014.01.006.
- [3] R. Chakrabarti, E.G. Engleman, (1991) Interrelationships between mevalonate metabolism and the mitogenic signaling pathway in T lymphocyte proliferation, *J. Biol. Chem.* 266 12216–12222. <http://www.jbc.org/content/266/19/12216.full.pdf>.
- [4] N. Manel, D. Unutmaz, D.R. Littman, (2008) The differentiation of human TH-17 cells requires transforming growth factor- β and induction of the nuclear receptor ROR γ t, *Nat. Immunol.* 9 641–649. doi:10.1038/ni.1610.
- [5] Y. Wang, K.M. Sousa, K. Bodin, S. Theofilopoulos, P. Sacchetti, M. Hornshaw, et al., (2009) Targeted lipidomic analysis of oxysterols in the embryonic central nervous system., *Mol. Biosyst.* 5 529–541. doi:10.1039/b819502a.
- [6] W.J. Griffiths, P.J. Crick, Y. Wang, M. Ogundare, K. Tuschl, A. a. Morris, et al., (2013) Analytical strategies for characterization of oxysterol lipidomes: Liver X receptor ligands in plasma, *Free Radic. Biol. Med.* 59 69–84. doi:10.1016/j.freeradbiomed.2012.07.027.
- [7] J.A. Nelson, S.R. Steckbeck, T.A. Spencer, (1981) 24(S),25-Epoxycholesterol is a natural product of mammalian steroid biosynthesis, *J. Am. Chem. Soc.* 103 6974–6975. doi:10.1021/ja00413a040.
- [8] J.A. Nelson, S.R. Steckbeck, T.A. Spencer, (1981) Biosynthesis of 24,25- Epoxycholesterol from Squalene 2,3;22,23-Dioxide*, *J. Biol. Chem.* 1067–1068.
- [9] S. Saito, M. Sakai, Y. Sasaki, K. Tanebe, H. Tsuda, T. Michimata, (1999) Quantitative analysis of peripheral blood Th0, Th1, Th2 and the Th1:Th2 cell ratio during normal human pregnancy and preeclampsia., *Clin. Exp. Immunol.* 117 550–5. <http://www.pubmedcentral.nih.gov/articlerender.fcgi?artid=1905376&tool=pmcentrez&rendertype=abstract> (accessed February 3, 2016).
- [10] A. Meljon, Y. Wang, W.J. Griffiths, (2014) Oxysterols in the brain of the cholesterol 24-hydroxylase knockout mouse, *Biochem. Biophys. Res. Commun.* 1–7. doi:10.1016/j.bbrc.2014.01.153.
- [11] H. Chen, H. Heiniger, A. Kandutsch, (1975) Relationship Between Sterol Synthesis and DNA Synthesis in Phytohemagglutinin-Stimulated Mouse Lymphocytes, *Proc. Natl. Acad. Sci.* 72 1950–1954. doi:10.1177/154405910408300507.
- [12] V.A. Gerriets, J.C. Rathmell, (2012) Metabolic pathways in T cell fate and function, *Trends Immunol.* 33 168–172. doi:10.1016/j.it.2012.01.010.
- [13] B.A. Janowski, M.J. Grogan, S.A. Jones, G.B. Wisely, S.A. Kliewer, E.J. Corey, et al., (1999) Structural requirements of ligands for the oxysterol liver X receptors LXR α and LXR β .,

Proc. Natl. Acad. Sci. U. S. A. 96 266–271. doi:10.1073/pnas.96.1.266.

- [14] A. Radhakrishnan, Y. Ikeda, H.J. Kwon, M.S. Brown, J.L. Goldstein, (2007) Sterol-regulated transport of SREBPs from endoplasmic reticulum to Golgi: oxysterols block transport by binding to Insig., Proc. Natl. Acad. Sci. U. S. A. 104 6511–6518. doi:10.1073/pnas.0700899104.
- [15] S. Hannedouche, J. Zhang, T. Yi, W. Shen, D. Nguyen, J.P. Pereira, et al., (2011) Oxysterols direct immune cell migration via EBI2., Nature. 475 524–527. doi:10.1038/nature10280.
- [16] T. Yi, X. Wang, L.M. Kelly, J. An, Y. Xu, A.W. Sailer, et al., (2012) Oxysterol Gradient Generation by Lymphoid Stromal Cells Guides Activated B Cell Movement during Humoral Responses, Immunity. 37 535–548. doi:10.1016/j.immuni.2012.06.015.
- [17] D. Jarrossay, M. Thelen, (2013) Immune response: steroids drive dendritic cells., Nat. Publ. Gr. 14 424–426. doi:10.1038/ni.2589.
- [18] Y. Wang, K. Karu, A. Meljon, J. Turton, J.L. Yau, J.R. Seckl, et al., (2014) 24S,25-Epoxycholesterol in mouse and rat brain, Biochem. Biophys. Res. Commun. 449 229–234. doi:10.1016/j.bbrc.2014.05.012.

CHAPTER 5: Investigating the link between the generation of 24(S)25-EC, 25-HC and 7 α ,25-diHC with induced cholesterol biosynthesis upon CD4⁺ T cell activation

5.1. Introduction

Cholesterol is an important molecule both at the local cellular level and systemic multicellular level. Cholesterol and cholesterol derivatives are found to be embedded in eukaryotic cell membranes which affects membrane integrity, fluidity and permeability^[1-4]. This sterol also acts as precursor to steroid hormones and bile acids which control systemic functions. Studies also link cholesterol to immune functions as acute infections result in increased cellular incorporation of ³H-mevalonic acid into free cholesterol^[5] and individuals with low total cholesterol were seen to also have lower circulating white blood cells^[6]. Recently it has been shown that oxysterols, e.g. 25-HC and 7 α ,25-diHC play important roles in innate and adaptive immunity.

In the previous chapter, we found that oxysterols are produced in activated human CD4⁺ T cells. The objectives of this chapter were to investigate whether these oxysterols were produced specifically in response to TCR activation or just downstream consequence of induced cholesterol biosynthesis and accumulation intracellularly. The effects of the inhibition of cholesterol biosynthesis on the oxysterols produced by activated total CD4⁺ T cells will be investigated, as well as T cell activation and proliferation. Downregulation of cholesterol biosynthesis was carried out by inhibiting the activity of 3-hydroxy-3methylglutaryl-coenzyme A reductase (HMGCR) the enzyme responsible for the rate-limiting step in the mevalonate pathway (Figure 5.1).

Statins are a group of medicines that help lower cholesterol levels in circulation. Since the discovery of mevastatin in the early 1970's, various other derivatives have been discovered to occur naturally or were synthesised such as simvastatin and fluvastatin (Figure 5.2.D & B). At the cellular level, these molecules act to inhibit HMGCR as they share a similar structure to the native substrate 3-hydroxy-3methylglutaryl-coenzyme A, HMG-CoA (Figure 5.2.C). These drugs compete with HMG-CoA for the

binding to HMGCR and ultimately affect downstream reactions of cholesterol synthesis. Figure 5.1 shows a simplified mevalonate pathway and where statins act.

This study builds on chapter 4 which showed that CD4⁺ T cells produce detectable 25-HC, 7 α ,25-diHC and 24(S),25-EC within 16 hours of being stimulated via CD3/CD28. As activated CD4⁺ T cells induce *de novo* generation of cholesterol^[7] then proceed with cell division and clonal expansion, it is possible that the increase in oxysterols were only an outcome of increased precursors and that metabolising cholesterol was a method of elimination of excess precursors. Total CD4⁺ T cells were used in this study to obtain a general impression for helper T cells irrespective of the differences in naïve and memory populations.

5.2. Materials and Methods

5.2.1. Preparation of simvastatin.

Simvastatin (Sigma-Aldrich) was converted to its active form by treatment with NaOH in EtOH. Briefly, 5mg of simvastatin was dissolved in 100 μ L of 100% EtOH, pH was increased by the addition of 150 μ L of 0.1M NaOH. The solution was incubated at 50°C in a dry heating block for two hours, then, pH was neutralised to 7.0 by the addition of 0.1M HCl. Final volume was adjusted to 1ml with water for a 12mM stock solution ^[8–11].

5.2.2. Monitoring cell proliferation by flow cytometry.

CD4⁺ T cell clonal expansion was monitored by flow cytometry using Cell Proliferation Dye eFluor®450 purchased from eBioscience (Hatfield, UK). The dye was reconstituted as a 10mM stock with anhydrous DMSO. Aliquots of 10 μ L were protected from light and moisture then stored at -20°C for later use. This was used as a 405nm violet laser alternative to the more common carboxyfluorescein diacetate succinimidyl ester (CFDA-SE) which is excited via 488nm blue laser detected in the FITC channel. The cell permeable proliferation dye is non-fluorescent until it covalently binds to cellular primary amine-containing proteins. Then, as the cell undergoes cell division, the amount of fluorescent dye is diluted in each progeny which

can be measured by flow cytometry^[12,13]. Cells were stained with the proliferation dye prior to a 72-hour cell culture based on manufacturer instructions. In brief, freshly isolated cells were resuspended at 10×10^6 cells per mL in PBS and added with equal volume of 20 μ M Cell Proliferation Dye eFluor®450 in PBS. The cell-stain suspension was immediately mixed in a vortex mixer then incubated for 20 minutes at room temperature protected from light. Labelling was stopped by adding 4 volumes of 10% BSA in X-Vivo-20 and incubated for 5 minutes on ice. Cells were pelleted at 515 xg for 10 minutes 20°C and further washed twice with X-Vivo-20 before seeding in culture. At the end of each time point, cells were harvested and aliquots were analysed on a BD FACS Aria. Proliferation dye fluorescence was excited using the 405nm violet laser and emission was detected on the Pacific Blue channel with a 450/40nm band pass filter. Data was analysed using FlowJo software and since other fluorochrome-conjugated antibodies utilised either the 488nm blue laser or the 635nm red laser, no compensation was done during or post data acquisition.

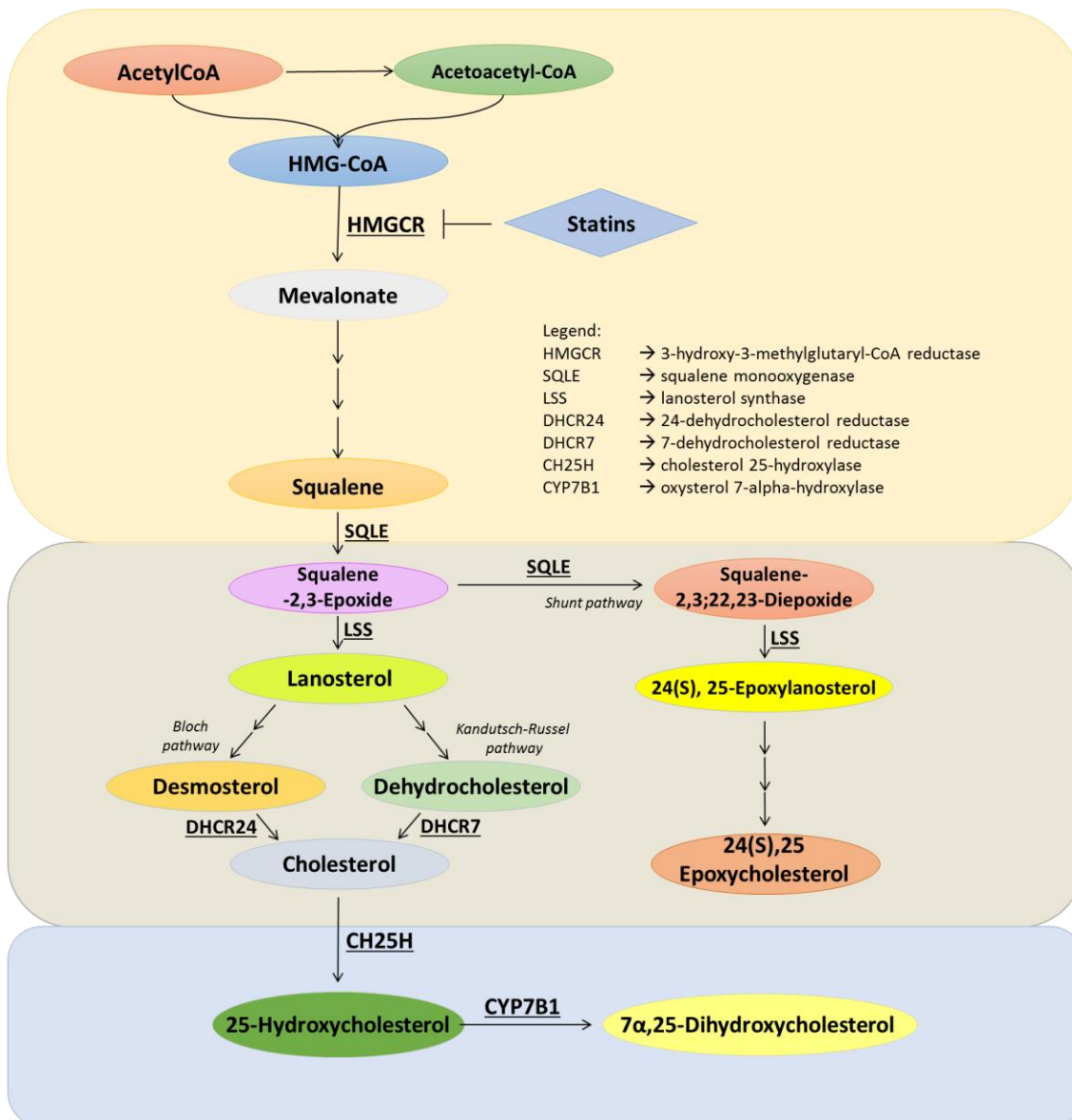


Figure 5.1. Simplified mevalonate pathway.

Mevalonate pathway produces cholesterol and oxysterols: 24(S),25-EC, 25-HC and 7 α ,25-diHC. HMG-CoA is the endogenous substrate of HMGCR to form mevalonate. Statins inhibit this process by competing in the HMGCR active site. Adapted from ^[14].

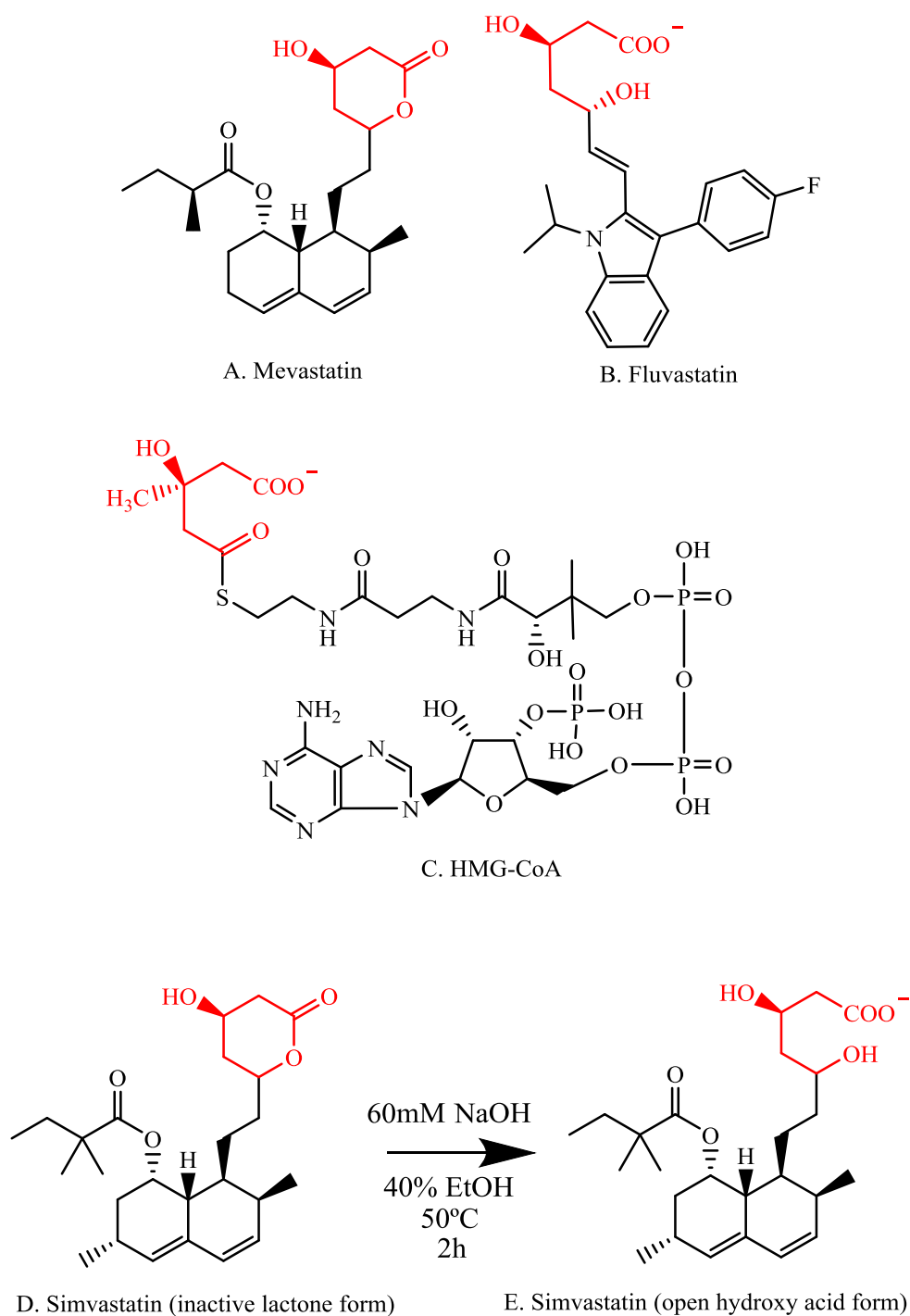
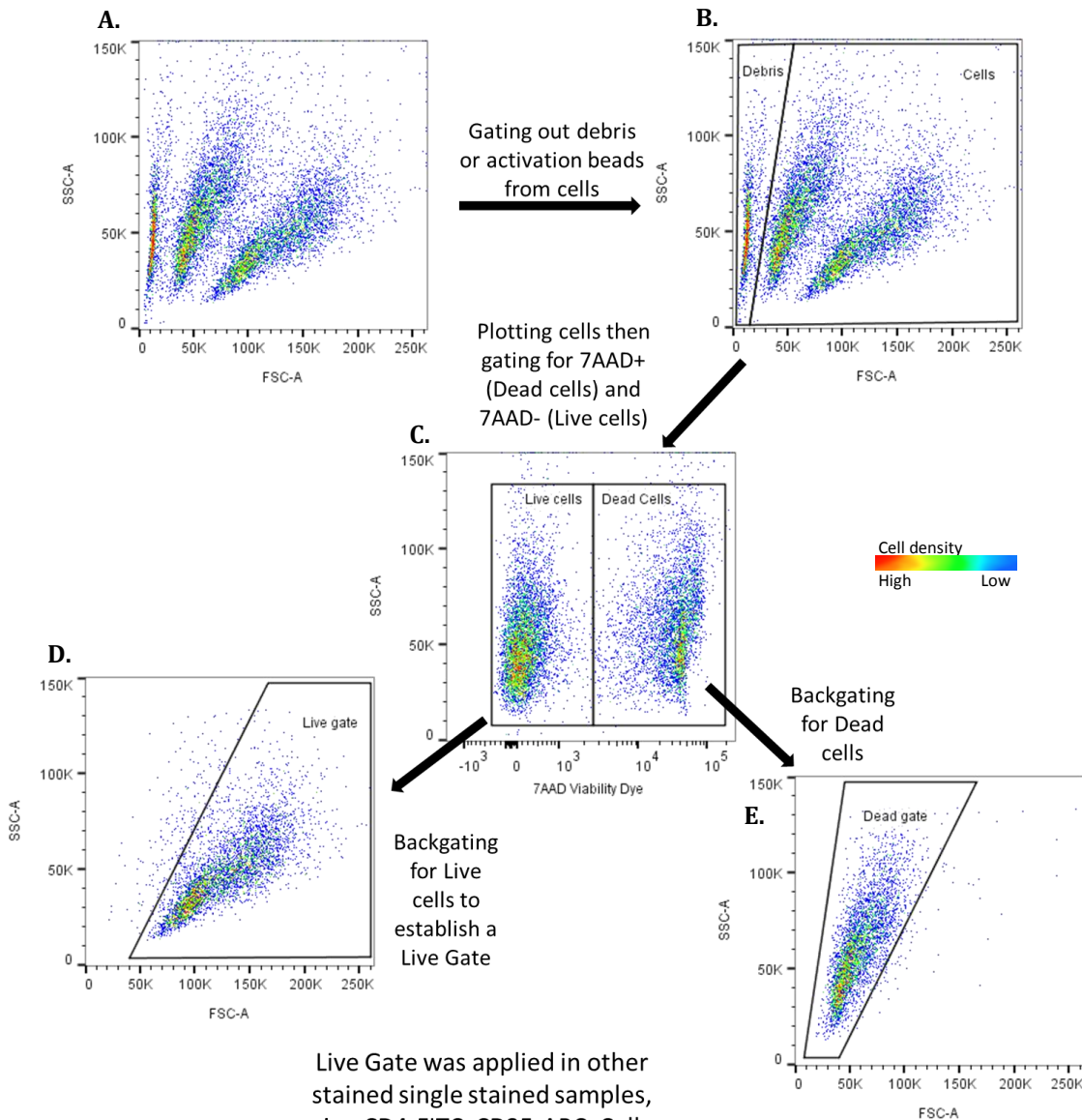


Figure 5.2. Structures of HMGCR catalytic subunit ligands.

Naturally occurring Mevastatin (A), synthetic Fluvastatin (B), the natural HMGCR substrate HMG-CoA (C), the lactone form (D) and open acid form of Simvastatin (E) showing similar hydroxyglutaric acid moieties highlighted in red making the statins an effective competitive inhibitors for HMGCR. Simvastatin was hydrolysed to its active acid form prior to cell culture (D,E.). Adapted from ^[15].



Live Gate was applied in other stained single stained samples, i.e. CD4-FITC, CD25-APC, Cell Proliferation Dye staining, to exclude dead cells and debris from analysis.

Figure 5.3. Representative gating strategy for identifying live cells and exclusion of dead cells using 7AAD Viability Dye staining.

All flow cytometry samples were single stained and were not fixed prior to BD FACS Aria analysis. An aliquot of cells was used for 7-AAD Viability staining. (A) Upon FlowJo analysis, all events were first plotted on a FSC/SSC to gate only cells and (B) exclude debris which have very low FSC. (C) Next, cells were plotted on a 7-AAD/SSC to identify dead/apoptotic cells by stain incorporation. 7-AAD binds to double stranded DNA upon entering cells with compromised cell membranes. Viable cells with intact membrane will not stain with the DNA dye and will have low fluorescence. Dimly and brightly stained events were gated and plotted again on an FSC/SSC. (D,E) Events showing on this plot were gated as live and dead. The live gate was then applied to other single stained aliquots of the same sample.

5.2.3. Monitoring cell death by flow cytometry.

The cellular stress of certain treatments which cause irreparable damage and eventual cell senescence will likely cause processes that may lead to cell death. A typical characteristic of dying cells are compromised cell membranes making them more permeable. In this chapter, this characteristic was used to characterise viable and non-viable cells. In addition to observed reduction in FSC and increased SSC signals, the incorporation of 7-amino-actinomycin D, purchased from eBioscience, was used as an indicator for dead cells. 7-amino-actinomycin D, 7-AAD, first described by ^[16] is a DNA intercalator that binds to GC rich regions which can be excited by a 488nm blue laser and fluoresce at the far red 650nm wavelength. At each analysis time point, an aliquot of non-fixed 0.1×10^6 cells were washed in PBS and resuspended in 100 μ L staining buffer 1 on a 5ml FACS tube. Then, 5 μ L of 7-AAD was added to the cell suspension, mixed and incubated for 10 minutes at 4°C away from light before submitting for flow cytometry analysis. 7-AAD fluorescence was detected on the PerCP-Cy5.5 channel with a 695/40nm band pass filter on a BD FACS Aria. Data was analysed using FlowJo software. Figure 5.3 shows a representative gating strategy used to gate out cell debris and activation beads.

5.2.4. THP-1 cultures and test for simvastatin cytotoxicity.

Before using primary CD4 T cells, the effects of simvastatin were first tested by the use of a THP-1 monocytic cell line maintained and passaged in Full Media. Cells were washed in PBS, stained with Cell Proliferation Dye eFluor®450, washed again then 0.8×10^6 cells were seeded in 2mL or 0.2×10^6 cells/mL in X-Vivo-20 on a 24 well plate. Four different (100x) stocks of 10mM, 1mM, 0.1mM and 0.01mM at 8.6% EtOH were prepared and diluted with X-Vivo-20 from the 12mM stock. A vehicle with 8.6% EtOH in X-Vivo-20 was also prepared. Then, 20 μ L of the diluted stocks and vehicle were added to the 2mL cultures for final simvastatin concentrations of vehicle, 100, 10, 1 and 0.1 μ M, at 0.086% EtOH. Cells were kept for 72 hours in a humidified 37°C incubator at 5% CO₂. After the three-day culture, proliferation and cell death was analysed on a BD FACS Aria.

5.2.5. Total CD4⁺ T cell culture treatment with simvastatin.

For primary cell cultures, freshly isolated total CD4⁺ T cells were split. Some cells were left non-stained and some were stained with the cell proliferation dye. Two 100X X-Vivo-20 diluted stocks, 100 μ M and 10 μ M, was prepared and were added at 1 μ L per 100 μ l of cell culture. Cells were either pre-treated with simvastatin or vehicle for 30 minutes then activated with the addition of anti-CD3/anti-CD28-loaded activation microbeads at 2:1 bead-to-cell ratio or left non-activated to a final density of 2.5x10⁶ cells/mL/cm² in X-Vivo-20. At each time point, cells were harvested then analysed by flow cytometry and sterols from either cells, when available, and media were extracted in ethanol and subjected to EADSA for mass spectrometric analysis. Sterols quantified from the media were normalised to the number of cells initially seeded and sterols present in cells were normalised to the number of cells extracted on the day.

5.2.6. Monitoring cell activation by flow cytometry.

The surface expression of CD25 on CD4⁺ T cells as a marker for activation was also measured by flow cytometry using an anti-human CD25-APC (clone BC96) from eBioscience. Data was acquired on a BD FACS Aria using the 633nm red laser at the APC channel with a 660/20 band pass filter and analysed using FlowJo software. Cells analysed for CD25 expression were gated on live cells to exclude the likely non-specific binding of the antibody to dead or dying cells. Figure 5.3 shows the gating strategy used.

5.3. Results

5.3.1. Higher concentrations of simvastatin induce cell death and inhibit proliferation in THP-1 cultures

Simvastatin was initially evaluated for its cytotoxicity using a THP-1 monocytic cell line where concentrations of 0.1 μ M to 100 μ M was used. Figure 5.4.A shows the cell division of THP-1 in culture was inhibited by simvastatin at concentrations higher than 0.1 μ M. Relative to the 72 hour untreated culture which have undergone two cell divisions indicated by a shoulder on the major peak, the proportion of the generation

2 cells decreases as the concentration of simvastatin increases. Moreover, 10 μ M and 100 μ M simvastatin treated cells only divided once. More importantly, the higher concentrations of simvastatin ($\geq 10\mu\text{M}$) show considerable cell death ($>37\%$) measured by the incorporation of the DNA dye (Figure 5.4.B).

As primary T cells are normally more sensitive than cell lines to chemical treatment, this study showed that simvastatin at 10 μ M and 100 μ M concentrations may also result to non-viable primary cells. Therefore, subsequent cultures with CD4⁺ T cells used simvastatin at 0.1 μ M and 1 μ M concentrations.

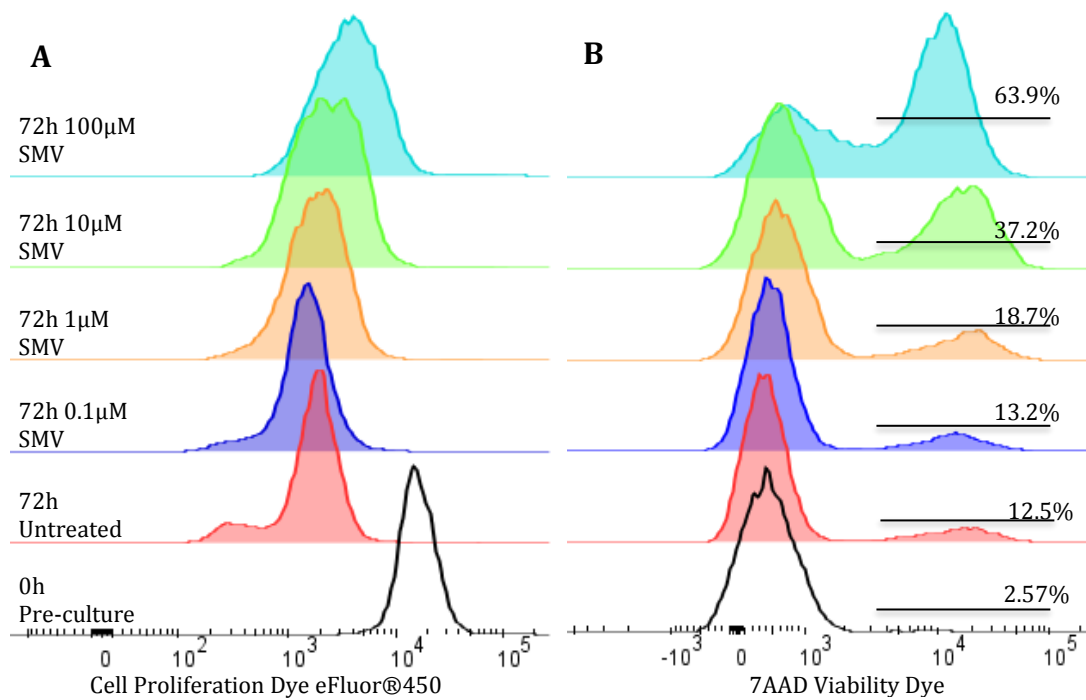


Figure 5.4. Simvastatin inhibits THP-1 cell division and induces cell death in a dose-dependent manner. Flow cytometric histograms showing overlay plots of pre-culture (open histogram) and 72 hour THP-1 cells cultures (filled histograms). A. THP-1 cells were pre-stained with Cell Proliferation Dye® eFluoro450 then cultured with and without different concentrations of simvastatin. At day 3, cell were harvested and assessed for cell proliferation, cells displayed are from 7-AAD- (live) cells. B. At day 3, cells were harvested and stained with 7-AAD Viability Dye. 7-AAD, which can enter membranes of non-viable cells and form DNA complexes resulting to excitable fluorescence. Inset numbers indicate positively staining cells which were dead.

5.3.2. Simvastatin induces cell death and inhibits activation and proliferation in human total CD4⁺ T cell cultures

Isolated total CD4⁺ T cells from peripheral blood were labelled with cell proliferation dye then activated in culture for up to three days in the presence or absence of simvastatin. Analysis by flow cytometry monitored the activation state of the T cells by the surface expression of CD25, cell viability by incorporation of 7-AAD staining, and cell division by the cell proliferation dye fluorescence dilution (Figure 5.5).

The FSC and SSC profiles of the different conditions were first assessed. Non-activated cells were seen to remain homogenous in size and have a low SSC signal from 24 hour to 72 hour in culture similar to pre-culture flow analysis. Activated cells on the other hand immediately displayed a change in cell size and granularity indicated by the increase in both FSC and SSC. At 72 hour, activated cells forms a heterogeneous mixture of different cells sizes. This variation in size was also seen in the simvastatin treated cells, although not as pronounced. Representative plots are shown in Figure 5.5.

The cell viability assay in Figure 5.6 using 7-AAD shows consistently higher proportion of dead cells in simvastatin treated CD4⁺ T cells at 72 hours across all three donors relative to non-statin treated cells. Activated cells were seen to have more dead cells compared to non-activated cells in two of the three donors. Detectable 7-AAD⁺ cells were readily seen at 24 hours albeit at very low proportions and the effect of simvastatin treatments appeared to be non-evident. However, analysis of Donor 2 cells after 48 hours exhibit differences in dead cell proportion in simvastatin treated cells relative to non-statin treated cells. More than 30% of the cells were 7-AAD⁺ and appeared to be independent of the concentration of simvastatin used. In contrast, this effect was not seen in Donor 1 cells at 48 hours, which surprisingly had less dead cells compared to its 24-hour analysis. 7-AAD⁺ cells at 72 hours was observed to have two distinct peaks at different fluorescence intensities and the frequency of the higher intensity peak was relatively greater at 1 μ M simvastatin than 0.1 μ M across all 72 hour donors. This two-peak profile was also more distinguishable in Donor 3 activated cells even without simvastatin. The general trend in this cell viability assay saw an

increased cell death proportional to the length of time in culture and that simvastatin further induced the rate of cell death.

Similar with previous chapters, cell activation assay by flow cytometry in this experiment showed that CD25 expression does not change in non-stimulated human CD4⁺ T cells even after 72 hours in X-Vivo-20 (Figure 5.7 and Figure 5.8). Different donors have different proportions of initial CD25⁺ cells but these numbers stay relatively consistent throughout the three-day time course in non-activated cells as shown by the low median fluorescence intensities (MFI). However, upon stimulation using the anti-CD3/CD28-loaded activation beads, the expression of CD25 were induced at 24 hours and reaching its peak at 48 hours. However, with all three donors, the expression of CD25 was inhibited upon simvastatin treatment in a dose-dependent manner (Figure 5.8). That said, donor variation can still be observed in this cell activation assay which resulted in different responses to the same treatments of simvastatin. In general, the proportion of live cells which were expressing CD25 was only affected slightly by simvastatin treatments but the relative intensity of the staining decreases in higher statin concentrations.

Cells analysed for proliferation (Figure 5.9) included only live cells which were gated on the FSC/SSC in addition to be 7-AAD⁻ (Figure 5.3.C and Figure 5.5). No cell division was detected at 24 hours irrespective of different culture conditions. Moreover, non-activated cells were not observed to divide even after 72 hours. A lower fluorescence intensity peak at the left of the parent peak were observed at 48 hours post activation where about 5% have divided once. In non-simvastatin treated activated cells, proliferation can be clearly observed after 72 hours post activation. More than 50% cells of each donor have undergone up to three cell divisions, where Donor 3 displayed more proliferation than Donor 2. These results indicated that some cells have divided twice within 72 hours. As expected, less activated cells will consequently have less proliferative capacity. The cell proliferation assay showed a negative effect of the HMGCR inhibitor on the proliferative expansion of the activated CD4⁺ T cells. The effect of simvastatin did not appear to manifest at 48 hours as simvastatin-treated cells were comparable to non-treated cells with very minimal cells dividing. With 0.1µM simvastatin treatment at 72 hours, the proliferation was

strikingly affected with less number of cells undergoing cell division but up to three cell divisions was still observed Donors 1 and 3. Relative to the other donors, Donor 2 exhibited less proliferation with 0.1 μ M simvastatin. Treatments with 1 μ M simvastatin further reduced the number of cells that proliferated. It can be seen that 1 μ M prevents the proliferation of majority of the cells at 72 hours across all experiments. But between donors, Donor 3 exhibited more proliferated cells than the other two with a small proportion to have divided twice even at 1 μ M simvastatin. In general, treatment of simvastatin at both concentration inhibits activated CD4⁺ T cell proliferation.

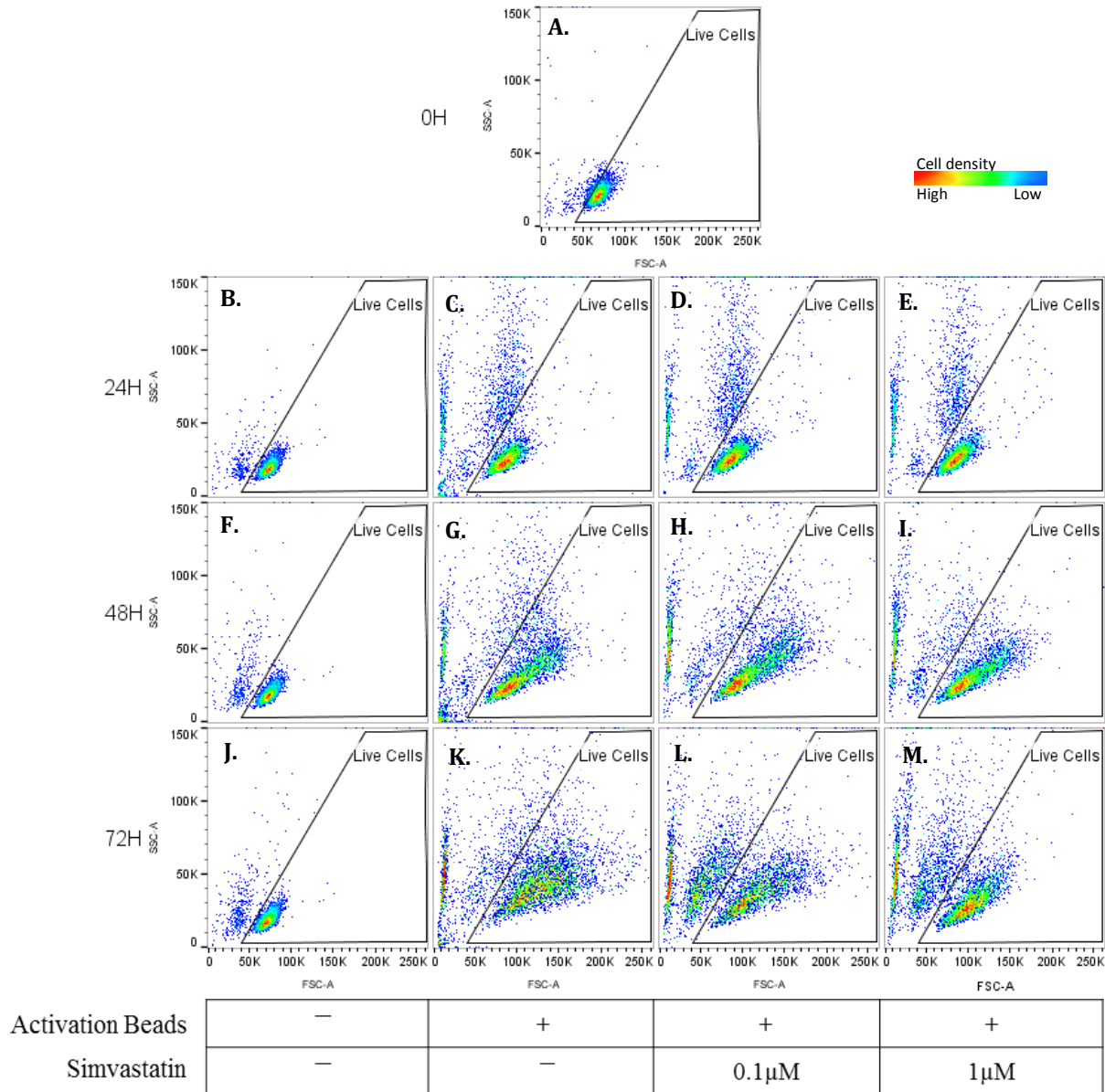


Figure 5.5. Representative ungated forward and side scatter dot plots of the total human CD4⁺ T cells cultured for up to 72 hours with and without activation and simvastatin treatments.

Plots show live gates established using 7-AAD negative cells. (A) Pre-culture plot of freshly MACS®-purified cells using human CD4⁺ T cell Isolation Kit. (B,F,J) Non-activated/untreated cells does not change in its FSC/SSC profile even after three days in culture. However, in the presence of activation beads, cells were observed to change with higher FSC/SSC with longer incubation times. This change was observed to be affected by the treatment of simvastatin.

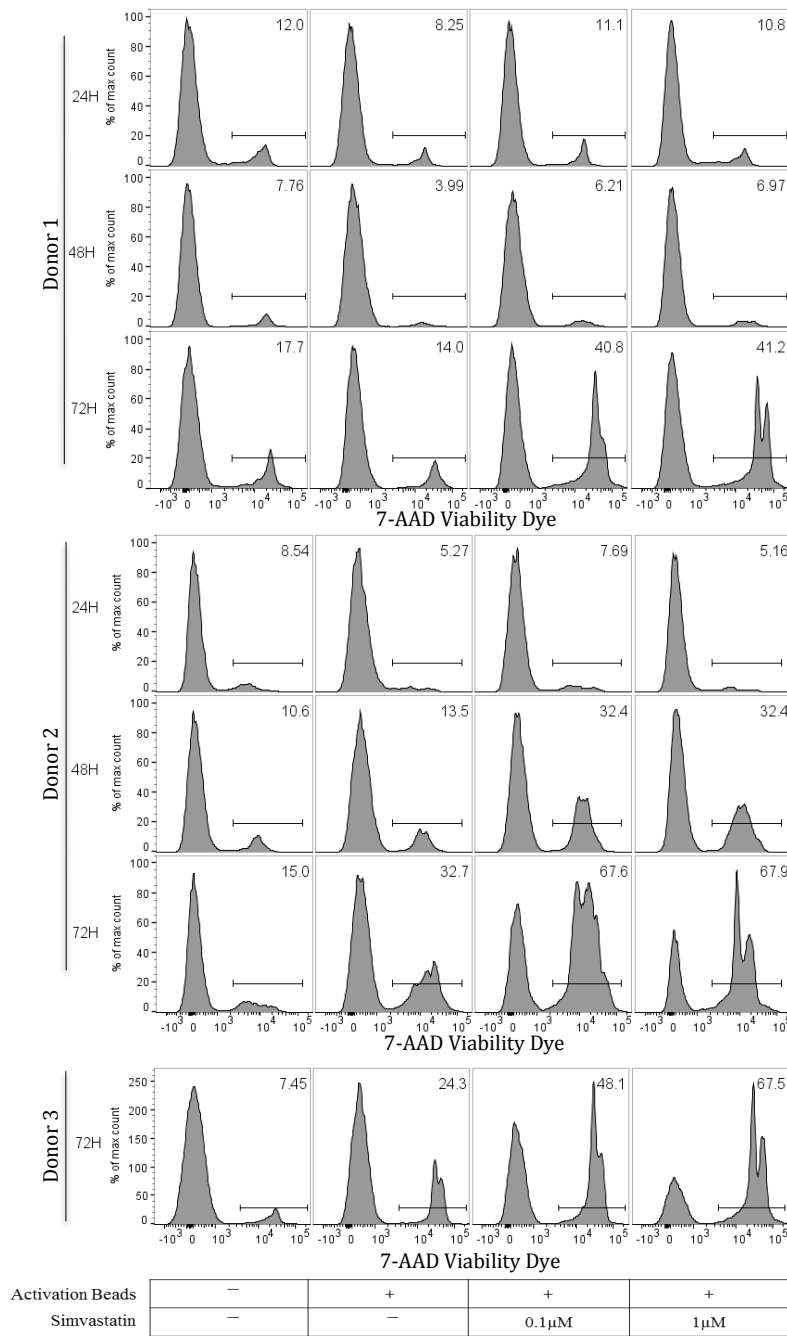


Figure 5.6. Flow cytometric 7-AAD histograms gated from all cells of total human CD4⁺ T cells cultured for up to 72 hours with and without activation and simvastatin treatments for all three donors. An aliquot of harvested cells per condition at each time point were stained with 7-AAD assessed for cell death. The number of dead cells increased relative to the length of time in culture. However, T cells which were treated with simvastatin were observed to have more dead cells than non-simvastatin treated at 72 hours which were similar between three donors. Inset numbers represent the % dead/apoptotic cells (7-AAD⁺).

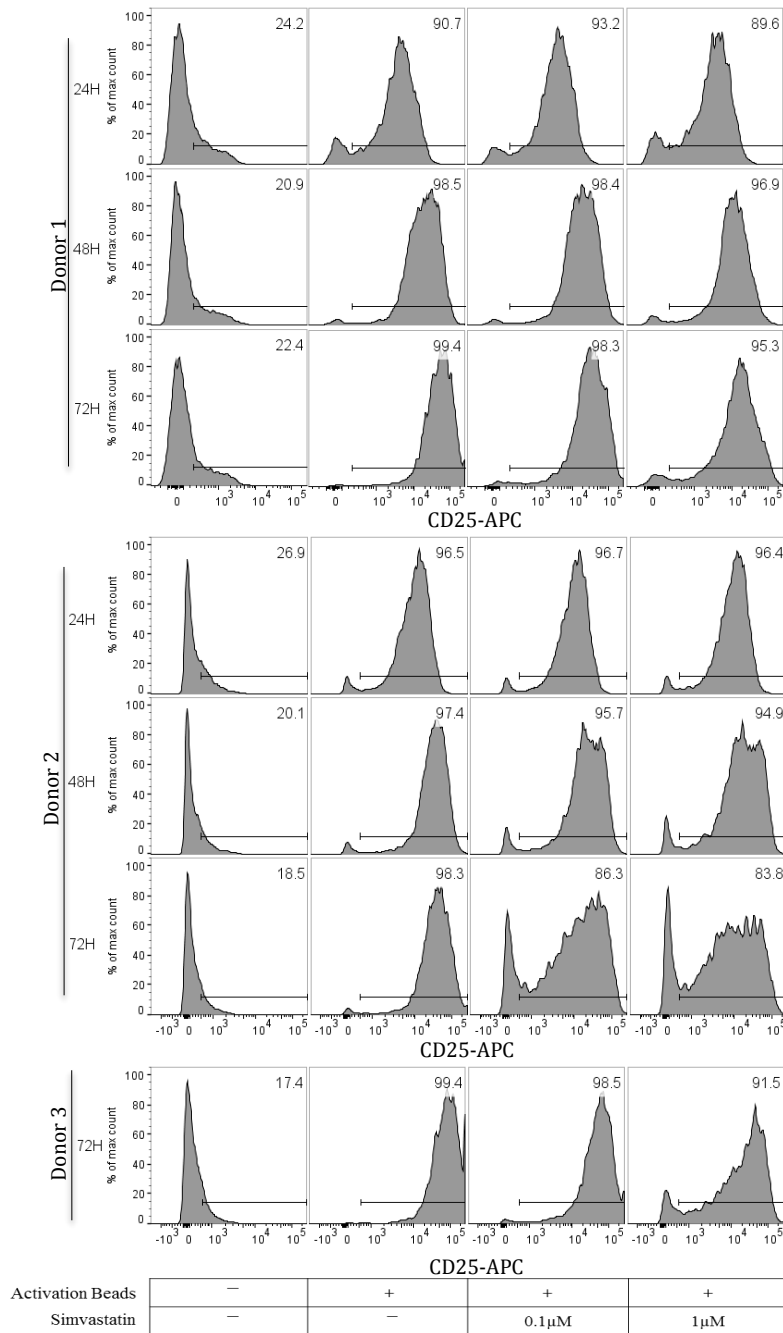


Figure 5.7. Flow cytometric CD25-APC histograms gated from live cells of total human CD4⁺ T cells cultured for up to 72 hours with and without activation and simvastatin treatments for all three donors. As total CD4⁺ T cells isolated from PBMC may contain CD25⁺ cells, i.e. from regulatory T cells, gates cannot be established using non-activated samples. The CD25⁺ gate was determined gating out 99% of the cells in the unstained sample and intensities above this threshold was considered a positively-staining cell. Inset numbers represent the % CD25⁺ cells. Corresponding median fluorescence intensity (MFI) for the CD25⁺ cells are shown in .

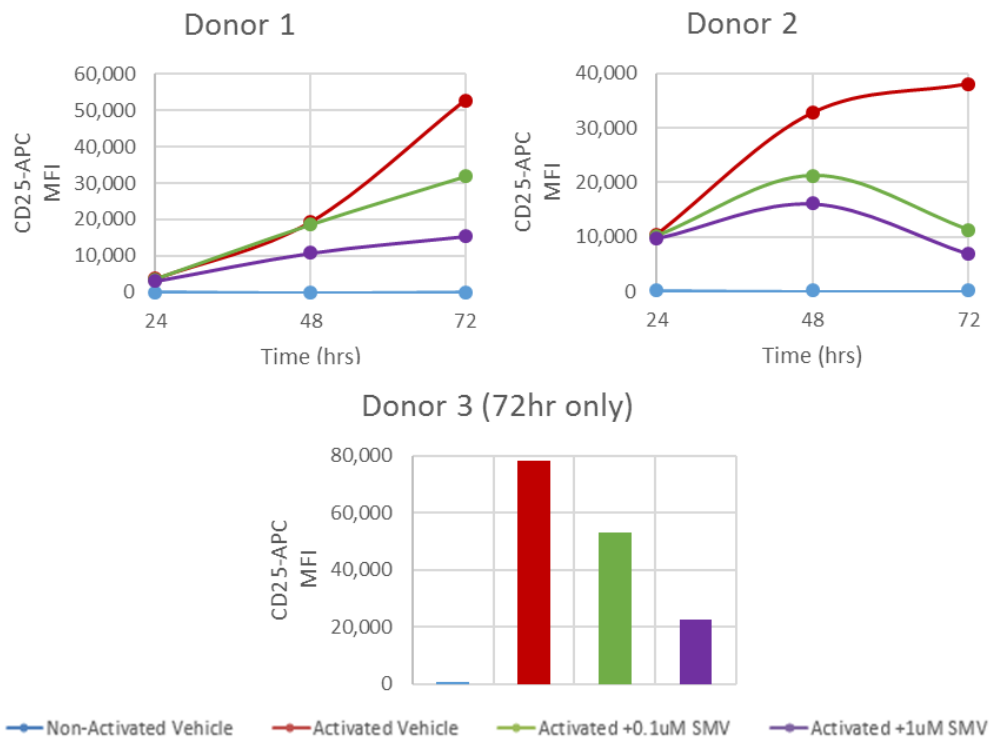


Figure 5.8. Graphical representation of the change in CD25-APC median fluorescence intensities (MFI) in CD4⁺ T cells with and without simvastatin treatments for the three donors. Expression of CD25 generally increased with time in culture. However, simvastatin was observed to affect this level of expression in a dose-dependent manner.

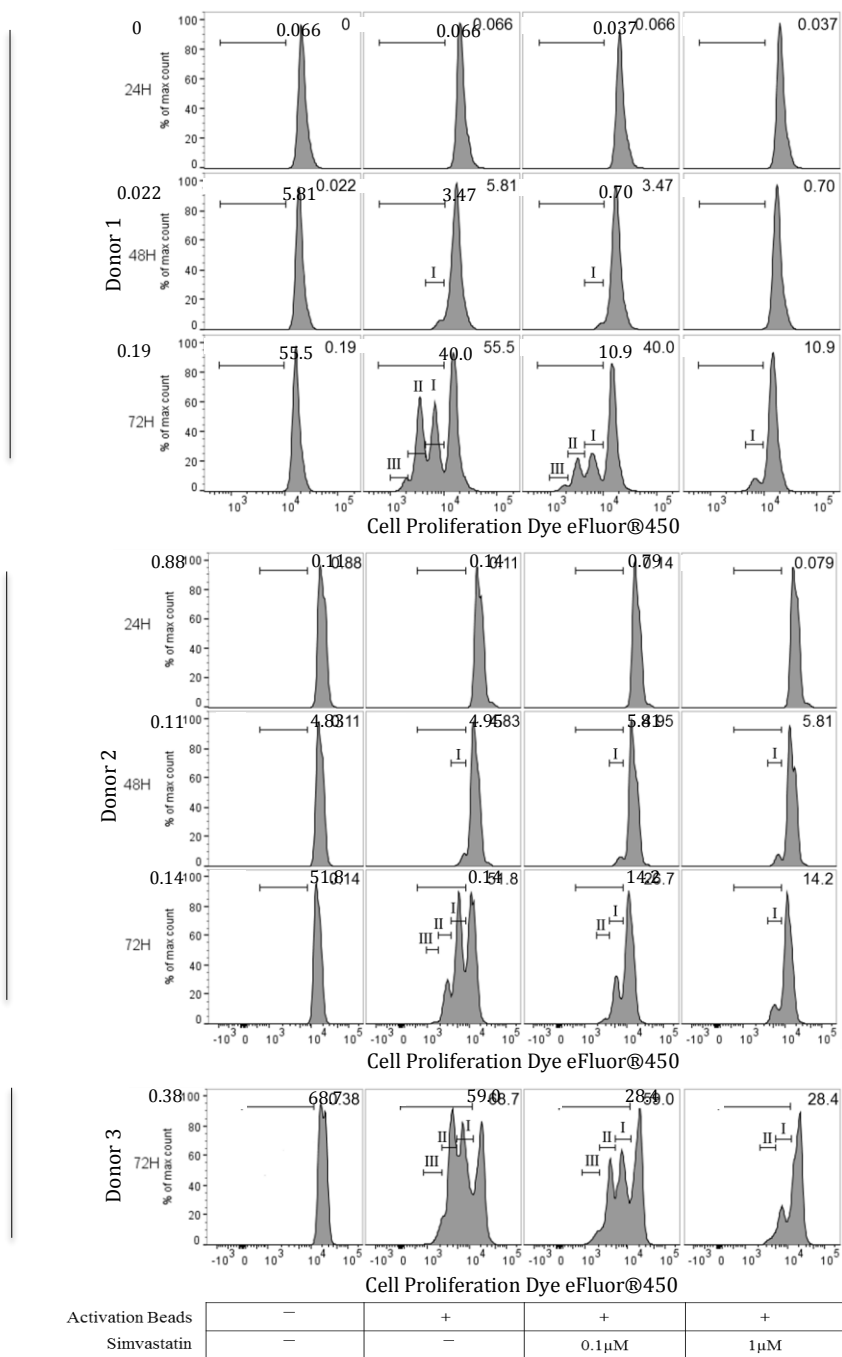


Figure 5.9. Flow cytometric cell proliferation dye histograms gated from live cells of total human CD4⁺ T cells cultured for up to 72 hours with and without activation and simvastatin treatments. Inset numbers represent the % proliferated cells and roman numerals indicate the number of proposed population divisions the cells have undergone. Gates for the % proliferated cells were established by gating out the parent population which has the highest intensity signal at the 450nm detection channel.

5.3.3. Simvastatin inhibits 24(S),25-EC production but not 25-HC and 7 α ,25-diHC.

Cell cultures was harvested at each 24-hour time point for up to 72 hours. Media and cells were separated by centrifugation. On two donors, majority of cells were analysed by flow cytometry leaving insufficient cells to be extracted in EtOH for sterol analysis. Only Donor 2 had enough cells for both analysis. Sterols present in conditioned media were extracted and analysed in all donors and conditions.

Without simvastatin treatments, sterol quantification data showed similar results to previous chapters. The production and export of 24(S),25-EC by activated CD4⁺ T cells were observed to increase proportional to the time after stimulation by the activation beads and in non-activated cells, only trace levels of the epoxycholesterol was detected even at the latest 72 hour time point. Surprisingly, the detected 24(S),25-EC was higher in 0.1 μ M simvastatin treated activated cells seen in Donor 1 and Donor 3 (Figure 5.10.A/C). Donor 2 had the expected effect of simvastatin in terms of CD25 expression and proliferation but was still seen to have similar levels of 24(S),25-EC compared to activation alone (Figure 5.10.B). However, simvastatin at 1 μ M considerably inhibited 24(S),25-EC production despite still having high proportions of CD25 expressing cells. In addition, pre-staining CD4⁺ T cells with Cell Proliferation Dye eFluro®450, did not affect the sterol production (Figure 5.10.C). Data from Donor 3 shows similar quantities of 24(S),25-EC in all treatments. There was a big variation in absolute quantities of 24(S),25-EC produced by three donors. Donor 3, identified earlier to have more than 60% proliferating cells, reported the highest amount of 24(S),25-EC at 3.1 ng/million cells while donor 1 and 2 only had 1.5 and 1.3ng/million cells, respectively. For Donors 1 and 3, this was seen to similarly increase 1.4 fold to 2.2 and 4.5 ng/million cells, respectively, upon treatment with 0.1 μ M simvastatin.

In contrast to the 24(S),25-EC data, the generation of 25-HC by activated cells was not affected by the treatments of simvastatin at either concentration and was more in accordance between donors. Time course graphs of Donor 1 and 2 in Figure 5.11.A/B showed an increased 25-HC exported to the media with very little variation, at 72 hours all activated cells were seen to have generated 150 to 180 pg/million cells. Donor 3 data also displays that proliferation dye staining does not affect the production of 25-

HC. Trace amounts of 25-HC was detected at 25pg/million cells from donor 3 non-activated cells while nothing was detected with the other donors. Similar to 25-HC, the production of downstream metabolites 7 α ,25-diHC was not inhibited by simvastatin. The quantities of 7 α ,25-diHC varied across three donors (Figure 5.12) ranging from 25 to 60 pg/million cells. In general, the trend for 7 α ,25-DiHC production and export follows the 25-HC trend but at 3-fold less abundance.

5.3.4. Simvastatin inhibits activation-induced intracellular cholesterol and cholesterol precursor levels.

Intracellular sterol data was only obtainable from Donor 2 due to limited cell numbers harvested after each time point from the other donors. As before, 24(S), 25-EC, 25-HC and 7 α ,25-DiHC were monitored in addition to cholesterol and two cholesterol precursors. Desmosterol and dehydrocholesterol are formed later in the mevalonate pathway situated at a single reaction step prior to reduction to cholesterol catalysed by two different enzymes, DHCR24 and DHCR7, respectively (Figure 5.1). There was a noticeable effect of simvastatin on cholesterol, desmosterol and dehydrocholesterol where both concentrations have inhibited the production of these sterols to baseline levels similar to non-activated cells (Figure 5.13.D,E,F). In contrast to this, in the absence of simvastatin, activated cells at 72 hours were seen to have intracellular cholesterol doubled from 250 to 500ng/million cells relative to non-activated cells (Figure 5.13.D). Desmosterol and dehydrocholesterol was also observed to be consistently more than 2-fold higher in activated cells from 24 hours until 72 hours.

In all samples extracted at 24 hours, no 24(S),25-EC, 25-HC and 25-HC and 7 α ,25-diHC were detected. At later time points, 24(S),25-EC in activated cells was produced more in 0.1 μ M simvastatin conditions than non-treated cells but was undetectable in 1 μ M conditions (Figure 5.13.A). For cellular 25-HC, simvastatin did not show an effect at 48 hours but was reduced at 72 hours with simvastatin while non-treated cells continued to increase. With regards to 7 α ,25-diHC production, detected levels in the cell were similar to the levels in the media. 7 α ,25-diHC was seen to be higher with increased simvastatin concentrations at 72 hours.

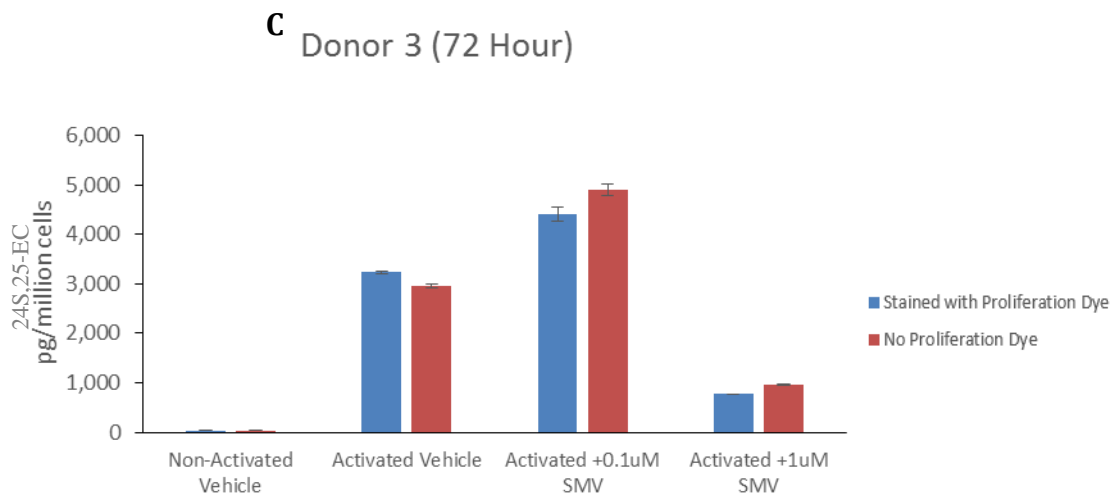
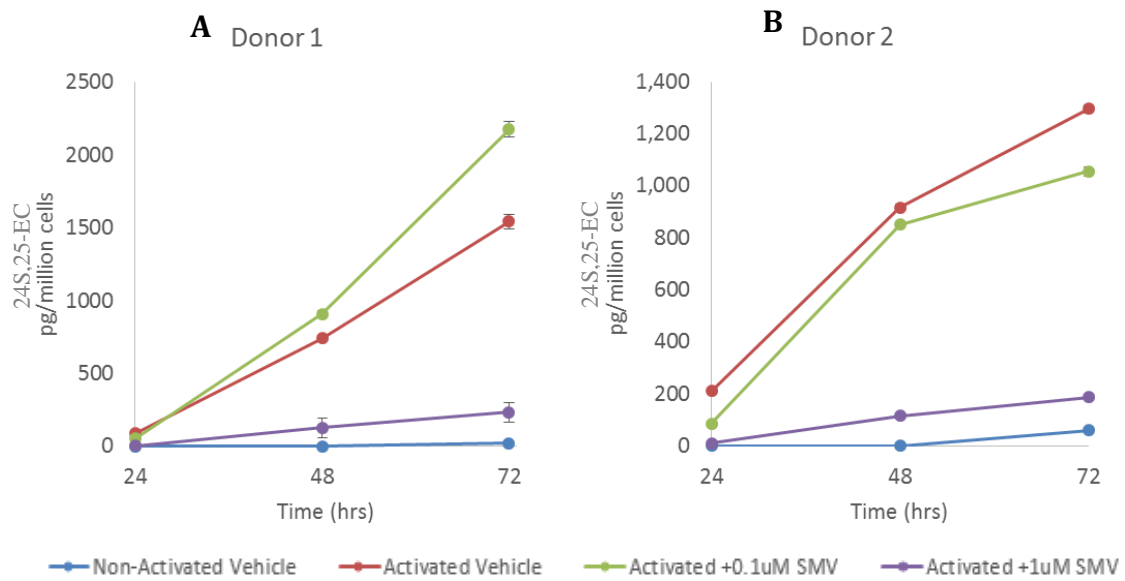


Figure 5.10. Quantification for 24(S),25-Epoxycholesterol detected in conditioned media extracts for each donor. Media were harvested at each time point and sterols extracted in ethanol.

The samples were subjected to EADSA and quantification was performed from reconstructed ion chromatograms by reference to deuterated internal standards. As sterols which have epoxide groups are labile in acidic solvents used in EADSA, data reported were combined quantities of: 24S,25-epoxycholesterol, 24-Ketocholesterol, 24,25-Dihydroxycholesterol, and 25-methyl ether-24-hydroxycholesterol. Error bars indicate SD from three LCMS runs.

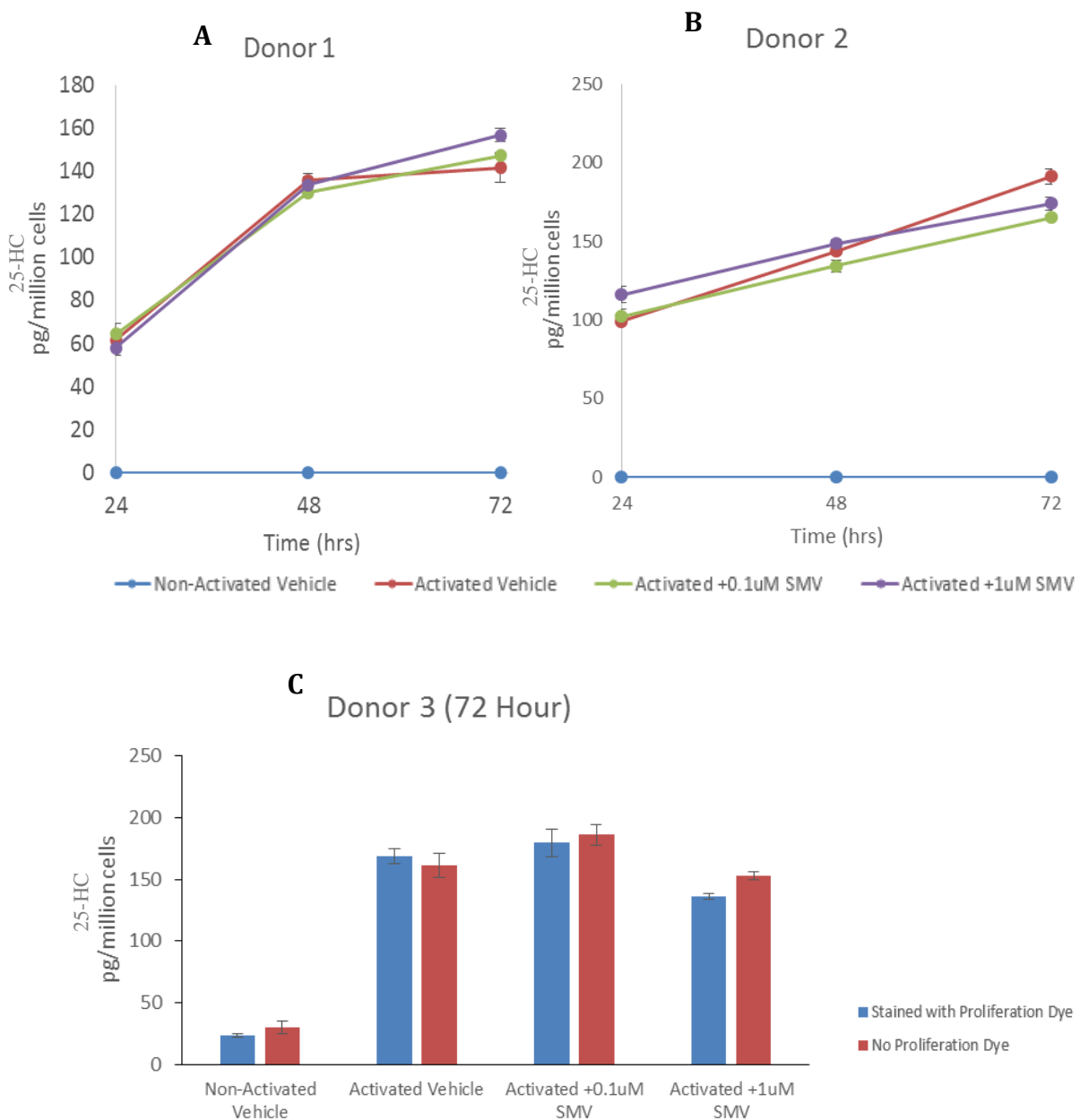


Figure 5.11. Quantification for 25-Hydroxycholesterol detected in conditioned media extracts for each donor. Media were harvested at each time point and sterols extracted in ethanol. The samples were subjected to EADSA and quantification was performed from reconstructed ion chromatograms by reference to deuterated internal standards. Data presented are normalised to the number of cells seeded at the beginning of the experiment. Error bars indicate SD from three LCMS runs.

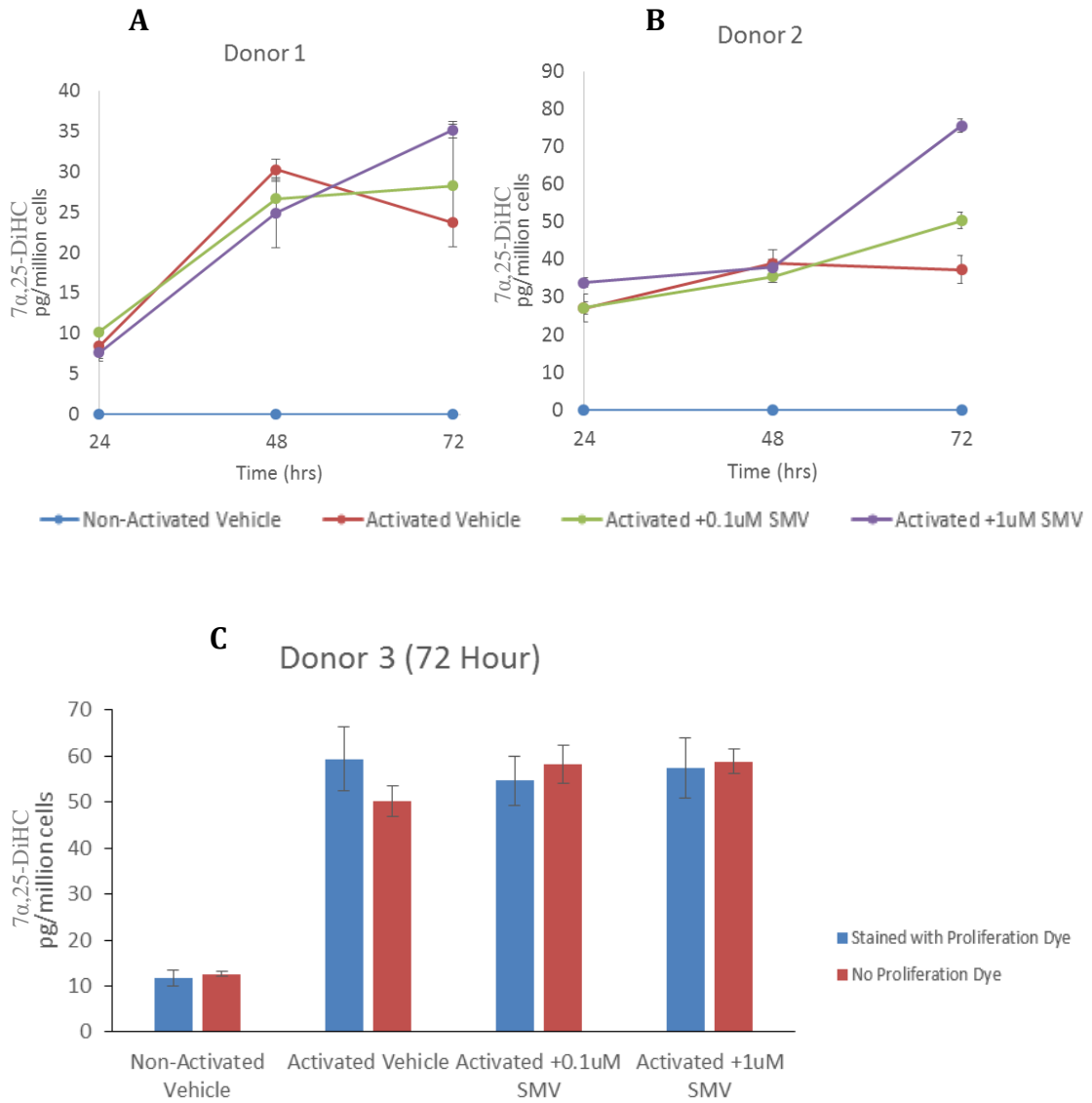


Figure 5.12. Quantification for $7\alpha,25$ -Dihydroxycholesterol detected in conditioned media extracts for each donor. Media were harvested at each time point and sterols extracted in ethanol. The samples were subjected to EADSA and quantification was performed from reconstructed ion chromatograms by reference to deuterated internal standards. Error bars indicate SD from three LCMS runs.

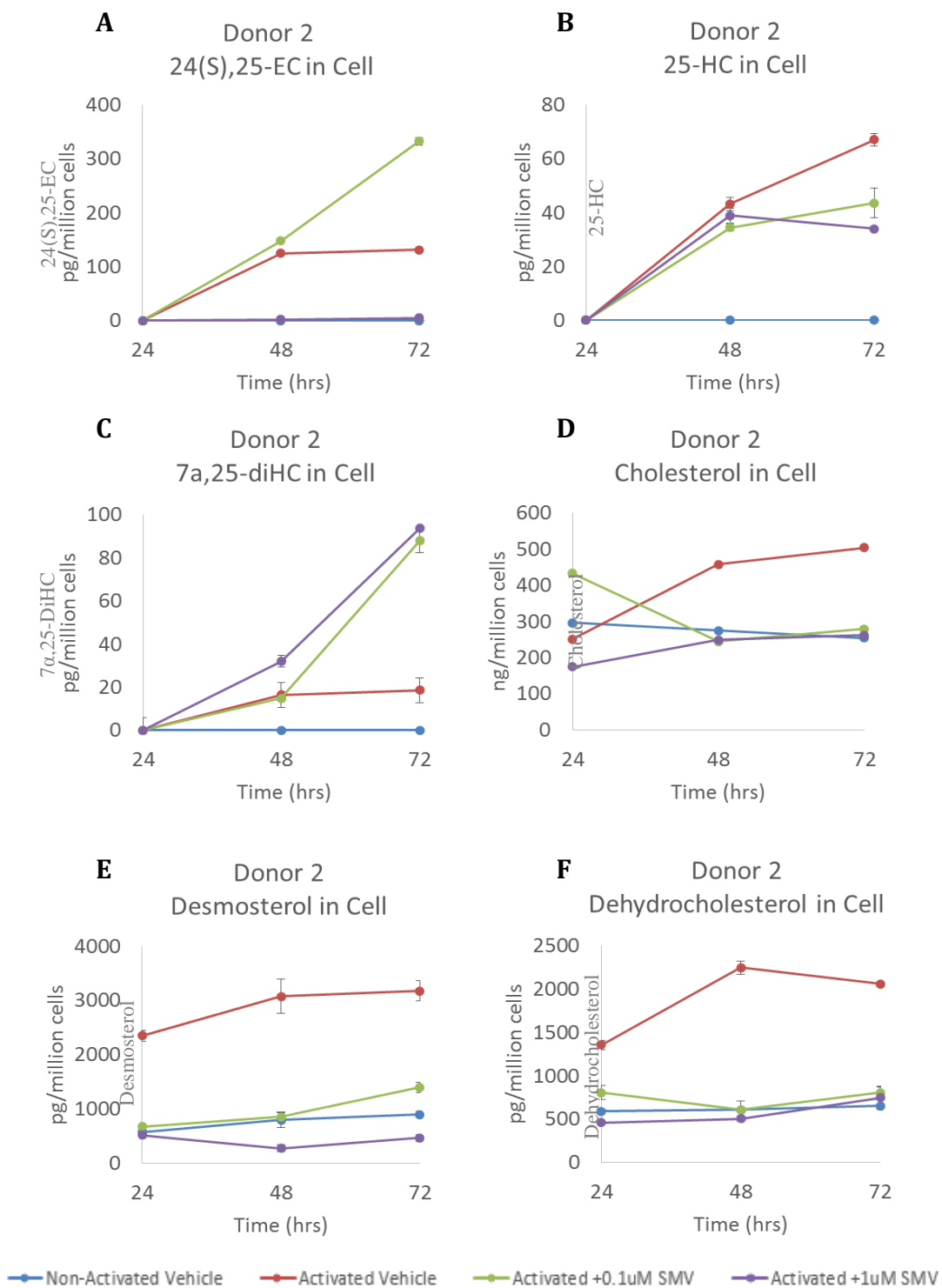


Figure 5.13. Quantification for sterols in cell extracts for Donor 2. At the end of each time point, a portion of cells were lysed by ultrasonication and sterols extracted in ethanol. The samples were subjected to EADSA and quantification was performed from reconstructed ion chromatograms by reference to deuterated internal standards. Error bars indicate SD from three LCMS runs.

5.4. Discussion

The discovery and widespread use of statins in general has marked a medical development in the treatment and management of hypercholesterolemia for reducing the risk of coronary heart disease^[17]. Although statins are effective in reducing circulating cholesterol, their use also reported negative consequences in immune cells and the ability to mount an immune responses^[18–20]. In addition to epidemiological studies by Muldoon et al^[6] where men with hypocholesterolaemia were observed to have lower white blood cells, Kwak et al^[21], demonstrated that statins decrease the IFN γ -induced MHC-II expression in monocyte derived macrophages. Without a full expression of MHC-II, antigens cannot be easily presented to activate CD4⁺ T cells.

The initial experiment using THP-1 cell line cultures indicated the effects of inhibiting cholesterol biosynthesis *in vitro*. Simvastatin not only inhibited the proliferation of THP-1 cells but was also seen to be toxic at higher concentrations (1 μ M). It is possible that simvastatin concentrations >1 μ M can effectively shutdown cholesterol biosynthesis making the cell non-viable. The same outcome was then assumed to occur when used with primary cells. The aim for CD4⁺ T cell culture was to inhibit HMGCR without inducing cytotoxicity, hence 0.1 μ M and 1 μ M concentrations were used.

As different individuals will be exposed to different immune challenges in their lifetime, it can be expected that each donor's CD4⁺ cells will be unique and may respond to the same treatments in different ways. Also, each donor's naïve and memory population proportions vary and may influence the rates at which cells proliferate and express activation markers. For this reason, it was not practical to combine sterol data from the three different donors.

Similar to the work by Ghittoni et al. and Coward et al.^[9,20], this chapter highlighted that statins, even at low 0.1 μ M concentrations, can suppress the activation and proliferation of CD4⁺ T cells in CD3/CD28-stimulating conditions, in addition to its cytotoxic effects. HPLC-MSⁿ data of cholesterol in cells was evidently reduced to baseline levels from 48 hours upon treatment with simvastatin. The same was also true for cholesterol precursors: desmosterol and dehydrocholesterol. It was found that the inhibition of cholesterol biosynthesis at its rate-limiting step, using the active hydroxyl-acid form of simvastatin, has caused a downregulation of the whole pathway

which affected the levels of desmosterol, dehydrocholesterol, cholesterol and the shunt pathway product, 24(S)25-EC (Figure 5.1).

In the present study, the treatment of activated cells with 0.1 μ M simvastatin was found to have induced slightly greater generation of 24(S)25-EC seen in two donors. This epoxycholesterol is generated via a multi-step process parallel to cholesterol synthesis involving the same enzymes. As cholesterol is vital to cellular processes and membrane integrity, its cellular levels are tightly regulated and its differential regulation will likely reflect in the production of 24(S)25-EC. This may suggest that the initial treatment with low concentrations of simvastatin may have reduced cholesterol which consequently drove T cells to upregulate the mevalonate pathway to compensate. It may be likely that at 0.1 μ M concentration, the cells can inactivate simvastatin. It is then possible that the activation and proliferation of activated CD4⁺ T cells were delayed and that response from non-simvastatin treated cells at 72 hours will be achieved by 0.1 μ M simvastatin treated cells at a later time point. At ten-fold higher concentration however, simvastatin may not be easily degraded and its effects, especially cytotoxicity, carry on to deprive cells of precursors needed to survive and proliferate successfully.

The previous chapters showed that the production of 24(S)25-EC, 25-HC and 7 α ,25-DiHC were induced by CD4⁺ T cell activation compared to resting CD4⁺ T cells. Moreover, since they are activation-induced, these sterols may have roles in T cell effector functions. On the other hand, since 24(S)25-EC is linked to increased cholesterol biosynthesis, 25-HC and 7 α ,25-diHC may only be a result of abundant precursors and generation of 25-HC was a way for cells to remove excess cholesterol.

Most unexpectedly, the generation of 25-HC and to a lesser extent 7 α ,25-diHC, was not affected by the downregulation of available precursor, cholesterol. Cellular cholesterol in simvastatin treated cells were found to be at similar levels to non-activated cells but the production of 25-HC and 7 α ,25-diHC was still being generated and exported to the media. Furthermore, 25-HC detected in media constantly increased and at similar levels among different donors. This may suggest that generation of 24(S)25-EC and 25-HC are regulated by different pathways but both originate from

CD3/CD28 stimulation and that the production of 25-HC is not dictated by the availability of intracellular cholesterol.

The cholesterol conversion to 25-HC can be catalysed by the enzyme CH25H (Figure 5.1). Liu et al. and Blanc et al.^[22,23] reported that CH25H was inducible in murine macrophages upon viral challenge or IFN γ treatment via STAT1. They showed that 25-HC was produced upon stimulation and that this oxysterol acts in a paracrine and also autocrine manner. This prompted the investigation of whether this association of CH25H/25-HC to IFN γ was also present in human CD4⁺ T cells.

5.5. References

- [1] V.M. Olkkonen, R. Hynynen, (2009) Interactions of oxysterols with membranes and proteins, *Mol. Aspects Med.* 30 123–133. doi:10.1016/j.mam.2009.02.004.
- [2] J.B. Massey, H.J. Pownall, (2006) Structures of biologically active oxysterols determine their differential effects on phospholipid membranes, *Biochemistry.* 45 10747–10758. doi:10.1021/bi060540u.
- [3] J.M. Kauffman, P.W. Westerman, M.C. Carey, (2000) Fluorocholesterols, in contrast to hydroxycholesterols, exhibit interfacial properties similar to cholesterol., *J. Lipid Res.* 41 991–1003.
- [4] J.B. Massey, H.J. Pownall, (2005) The polar nature of 7-ketocholesterol determines its location within membrane domains and the kinetics of membrane microsolvubilization by apolipoprotein A-I, *Biochemistry.* 44 10423–10433. doi:10.1021/bi0506425.
- [5] R.H. Fiser, J.C. Denniston, R.B. Rindsig, W.R. Beisel, (1971) Effects of Acute Infection on Cholesterogenesis in the Rhesus Monkey, *Exp. Biol. Med.* 138 605–609. doi:10.3181/00379727-138-35951.
- [6] M.F. Muldoon, A. Marsland, J.D. Flory, B.S. Rabin, T.L. Whiteside, S.B. Manuck, (1997) Immune system differences in men with hypo- or hypercholesterolemia., *Clin. Immunol. Immunopathol.* 84 145–9. <http://www.ncbi.nlm.nih.gov/pubmed/9245545> (accessed January 17, 2016).
- [7] J.A. Cuthbert, P.E. Lipsky, (1987) Regulation of lymphocyte proliferation by cholesterol: the role of endogenous sterol metabolism and low density lipoprotein receptors., *Int. J. Tissue React.* 9 447–57. <http://www.ncbi.nlm.nih.gov/pubmed/3448024> (accessed November 27, 2015).
- [8] A. Corsini, S. Bellosta, R. Baetta, R. Fumagalli, R. Paoletti, F. Bernini, (1999) New insights into the pharmacodynamic and pharmacokinetic properties of statins, *Pharmacol. Ther.* 84 413–428. doi:10.1016/S0163-7258(99)00045-5.
- [9] R. Ghittoni, L. Patrussi, K. Pirozzi, M. Pellegrini, P.E. Lazzerini, P.L. Capecchi, et al., (2005) Simvastatin inhibits T-cell activation by selectively impairing the function of Ras superfamily GTPases., *FASEB J.* 19 605–607. doi:10.1096/fj.04-2702fje.
- [10] T. Saito, M. Tsuchida, S. Umehara, T. Kohno, H. Yamamoto, J. Hayashi, (2011) Reduction of spinal cord ischemia/reperfusion injury with simvastatin in rats, *Anesth Analg.* 113 565–571. doi:ANE.0b013e318224ac35 [pii]\r10.1213/ANE.0b013e318224ac35.
- [11] M.M. Sadeghi, M. Collinge, R. Pardi, J.R. Bender, (2000) Simvastatin modulates cytokine-mediated endothelial cell adhesion molecule induction: involvement of an inhibitory G protein., *J. Immunol.* 165 2712–2718.
- [12] A.B. Lyons, (1999) Divided we stand: tracking cell proliferation with carboxyfluorescein diacetate succinimidyl ester., *Immunol. Cell Biol.* 77 509–515. doi:10.1046/j.1440-1711.1999.00864.x.
- [13] B.J.C. Quah, C.R. Parish, (2010) The use of carboxyfluorescein diacetate succinimidyl ester

- (CFSE) to monitor lymphocyte proliferation., *J. Vis. Exp.* doi:10.3791/2259.
- [14] A. Mazein, S. Watterson, W.Y. Hsieh, W.J. Griffiths, P. Ghazal, (2013) A comprehensive machine-readable view of the mammalian cholesterol biosynthesis pathway, *Biochem. Pharmacol.* 86 56–66. doi:10.1016/j.bcp.2013.03.021.
- [15] E.S. Istvan, (2001) Structural Mechanism for Statin Inhibition of HMG-CoA Reductase, *Science* (80-.). 292 1160–1164. doi:10.1126/science.1059344.
- [16] I. Schmid, W.J. Krall, C.H. Uittenbogaart, J. Braun, J. V Giorgi, (1992) Dead cell discrimination with 7-amino-actinomycin D in combination with dual color immunofluorescence in single laser flow cytometry., *Cytometry.* 13 204–8. doi:10.1002/cyto.990130216.
- [17] D.J. Maron, S. Fazio, M.F. Linton, (2000) Current perspectives on statins., *Circulation.* 101 207–13. <http://www.ncbi.nlm.nih.gov/pubmed/10637210> (accessed January 21, 2016).
- [18] B.P. Leung, N. Sattar, A. Crilly, M. Prach, D.W. McCarey, H. Payne, et al., (2003) A novel anti-inflammatory role for simvastatin in inflammatory arthritis., *J. Immunol.* 170 1524–1530. doi:10.4049/jimmunol.170.3.1524.
- [19] O. Aktas, S. Waiczies, A. Smorodchenko, J. Dorr, B. Seeger, T. Prozorovski, et al., (2003) Treatment of relapsing paralysis in experimental encephalomyelitis by targeting Th1 cells through atorvastatin., *J. Exp. Med.* 197 725–33. doi:10.1084/jem.20021425.
- [20] W. Coward, S.C. Chow, (2006) Effect of atorvastatin on TH1 and TH2 cytokine secreting cells during T cell activation and differentiation, *Atherosclerosis.* 186 302–309. doi:10.1016/j.atherosclerosis.2005.08.013.
- [21] B. Kwak, F. Mulhaupt, S. Myit, F. Mach, (2000) Statins as a newly recognized type of immunomodulator., *Nat. Med.* 6 1399–1402. doi:10.1038/82219.
- [22] S. Liu, R. Aliyari, K. Chikere, G. Li, D. Matthew, J.K. Smith, et al., (2013) Interferon-Inducible Cholesterol-25-Hydroxylase Broadly Inhibits Viral Entry by Production of 25-Hydroxycholesterol, *Immunity.* 38 92–105. doi:10.1016/j.immuni.2012.11.005. Interferon-Inducible.
- [23] M. Blanc, W.Y. Hsieh, K. a. Robertson, K. a. Kropp, T. Forster, G. Shui, et al., (2013) The Transcription Factor STAT-1 Couples Macrophage Synthesis of 25-Hydroxycholesterol to the Interferon Antiviral Response, *Immunity.* 38 106–118. doi:10.1016/j.immuni.2012.11.004.

CHAPTER 6: Investigating the relationship between *CH25H*, 25-HC, *IFNG* and *IFN-γ* in Human CD4⁺ T cells.

6.1. Introduction

The sterol 25-hydroxycholesterol (25-HC) has been recently reported to be involved in various immune-related processes in addition to its ability to modulate cholesterol biosynthesis^[1,2]. In 2009, bone marrow derived mouse macrophages were shown to have increased expression of cholesterol-25-hydroxylase (*Ch25h*) and 25-HC production following lipopolysaccharide (LPS) treatment *in vitro*^[3]. Consequently, the same study found increased 25-HC was present in the blood plasma of healthy human volunteers 4 hours after *E.coli* LPS administration which suggested that 25-HC may be involved in endotoxaemia and sepsis. Within the same year, another study found that LPS elicits the increased *Ch25h* expression and 25-HC production via the activation of Toll-like receptors (TLR), mainly TLR-4 in mice both *in vitro* with cultured macrophages and in tissues containing resident macrophages like liver, lungs and brain *in vivo*^[4]. Furthermore, they found augmented immunoglobulin A (IgA) expression in serum, alveoli and intestinal mucosa in *Ch25h*^{-/-} mice via B cell class switch recombination, whereas 25-HC treatment of cytokine-stimulated B cells led to inhibited IgA production.

During 2012 and 2013, two independent groups identified macrophage *Ch25h* in mice as an interferon-induced gene^[5] and linked its actions through STAT1 in inhibiting both viral entry and replication^[6,7]. In 2014, 25-HC was described to have pro-inflammatory signalling actions leading to an amplified immune response when macrophages were treated with the sterol prior to viral and bacterial antigens^[8]. The authors have noted exacerbated morbidity in wild-type compared to *Ch25h*^{-/-} mice after an influenza infection, suggesting that 25-HC contributes to greater immune-mediated damage from increased expression of pro-inflammatory genes like *Il6* and *Csf-1*. In the same year, 25-HC was also published to have anti-inflammatory effects by dampening the macrophage inflammasome pathway activation and suppressing IL-1β expression^[9]. This was demonstrated in the study where *Ch25h*^{-/-} mice were more susceptible to exacerbated

myelin oligodendrocytes glycoprotein-induced experimental autoimmune encephalomyelitis (MOG-induced EAE) with increased IL-17⁺ cells and succumb sooner to LPS-induced death than wild-type controls.

In all, *Ch25h* and 25-HC have been widely described to have roles in macrophages and B cells of mice. However, studies with T cells, which are key in modulating immune responses *in vivo*, are currently limited. This chapter will explore the possible interactions between the *CH25H* gene and the sterol metabolite 25-HC to both interferon- γ gene and cytokine expression in human primary CD4⁺ T cells.

6.2. Materials and Methods

6.2.1. Total CD4⁺ T cell isolation

Total CD4⁺ T cells were negatively selected from the PBMCs of healthy human donors after density gradient centrifugation as described in *section 2.1.2*, *section 2.1.3* and *section 2.1.4.2*.

6.2.2. Small interfering RNAs and vectors

Pre-designed *Silencer*® Select small interfering RNAs (siRNA) were purchased from Thermo Fisher Scientific (Paisley UK) specific to human CH25H (siRNA ID: s17194 Cat.no. 4392420) and human GAPDH (Cat.no. 430849) for positive control together with a non-targeting siRNA (Cat.no. 4390843) as negative control. In other experiments, kit-supplied pmax GFP vector was used as a positive transfection control for electroporation cell viability testing.

6.2.3. RNA interference and Cell culture

RNA interference were conducted by Dr Tom Hearn using either a Neon[®] Transfection system (Thermo Fisher Scientific) or a 4D-Nucleofector[™] System (Lonza Biologics).

The Neon Transfection system was used with a 100 μ L Neon[®] Kit (Cat.no. MPK10025) containing proprietary Neon[®] transfection buffers, tubes and tips from Thermo Fisher Scientific following manufacturer's instructions. Cells were cultured using X-VIVO-20 as described in *section 2.1.1.1* without glutamine, penicillin and streptomycin supplements. Briefly, after magnetic isolation, 2×10^6 total CD4⁺ T cells were pelleted and resuspended in 117 μ L Buffer T. Next, 13 μ L of 10 pmol/ μ L siRNA was added to the cell suspension and mixed well by pipetting. Then, 100 μ L of the cell-siRNA mix was aspirated into a 100 μ L Neon[®] tip and inserted into a Neon[®] tube containing 3 mL of Buffer E2 nested on the Neon[®] Pipette station. Cells inside the tip were electroporated with one pulse of 2150V pulse voltage and 20ms pulse width. Afterwards, cells were pipetted out into a 12-well culture plate containing pre-warmed 1.9 mL of supplement-free X-VIVO-20 and gently rocked to distribute cells. The 1.5×10^6 cells treated with 100 pmol siRNA cultured in 2 mL (50 nM) were incubated for 2 hours at 37°C 5% CO₂ post-transfection before activating using anti-CD3/CD28-loaded microbeads at 1:2 bead to cell ratio by Dr Tom Hearn. Cells were harvested after 48 hours of incubation.

The 4D-Nucleofector[™] System (Core and X Units) was used with a P3 Primary Cell Nucleofector[™] kit containing buffers and 16-well 20 μ L Nucleovette[™] Strips from Lonza Biologics (Slough UK) following manufacturer's instructions. Briefly, after magnetic isolation, 4.5×10^6 total CD4⁺ T cells were pelleted then resuspended in 42 μ L of supplemented P3 buffer and added with 4 μ L of 3 pmol/ μ L of siRNA on a centrifuge tube then mixed well. For each siRNA treatment, 22 μ L of cell suspension was aliquoted carefully avoiding air bubbles, directly at the bottom of each well of the Nucleovette[™] Strip in duplicate, then loaded on the 4D-Nucleofector[™] System and electroporated using either the pre-set high efficiency (FI-115) programme or high functionality (EO-115) programme. Afterwards, 80 μ L of supplement-free X-VIVO-20 was added in each well

then 100µL was transferred to 800µL of pre-warmed X-VIVO-20 on a 24-well plate. Cells remaining in the Nucleovette™ strip were rinsed with 100µL X-VIVO-20 which was added again into the culture plate. The 2×10^6 cells treated with 6pmol siRNA cultured in 1mL (6nM) were incubated for 5 hours at 37°C 5%CO₂ post-Nucleofection before activating with anti-CD3/CD28-loaded microbeads at 1:2 bead to cell ratio by Dr Tom Hearn. Cells were harvested after 48 hours of incubation.

6.2.4. Cytokine treatments in T cell cultures

The IFN- γ production of total CD4⁺ T cells were initially measured at 24, 48 and 72 hours after activation. To investigate a possible effect of IFN- γ cytokine on *CH25H* expression and 25-HC production of CD4⁺ T cells, human recombinant IFN- γ was added or neutralised with anti-IFN γ antibody (eBioscience cat.no. 16-7318 clone:NIB42) in total CD4⁺ T cell cultures seeded at 2.5×10^6 cells/mL/cm² in either activating and non-activating conditions. After 48 hours, cells and media were harvested and analysed for *CH25H* and *IFNG* gene expression by RT-PCR and sterol production by LC-MSⁿ. In other experiments, 10ng/mL of human recombinant IL-1 β was added in culture in either activating or non-activating conditions.

6.2.5. Sterol content analysis

Sterols contained in either the cells and culture media of total CD4⁺ T cells were subjected to EADSA as described in *section 2.2.2* and submitted for LC-MSⁿ analysis for separation, identification and quantification as described in *section 2.2.3* and *2.2.4*.

6.2.6. Gene expression and protein secretion analysis

Messenger RNA expression of *CH25H*, *IFNG*, and *GAPDH* were analysed by qPCR as described in *section 2.3.2*. Raw C_t values normalized against *RPI8S* were used to calculate the relative expression levels in the samples using the $2^{-\Delta\Delta C_t}$ method^[10] performed by Dr Tom Hearn. Additionally, the IFN- γ secreted by the cultured cells into

the media were measured by sandwich ELISA as described in *section 2.3.3.1 and 2.3.3.2* or screened for TNF- α , IL-12p70, IL-4, IL-6 and IL-17 by multiplex assay described in *section 2.3.3.3 and section 2.3.3.4*.

6.3. Results

6.3.1. Cholesterol 25-hydroxylase silencing led to reduced CH25H mRNA expression and 25-HC production in activated CD4⁺ T cells while not affecting cell viability and CD25 expression.

In order to find out what role 25-HC plays in T cell function, the production of 25-HC was blocked using siRNA of *CH25H*. After 48 hours post-transfection of si*CH25H*, conditioned media were collected to measure sterols by LC-MSⁿ and cytokine production by ELISA. Cells were analysed for flow cytometry at end points. Some cells were also extracted for RNA to confirm gene knockdowns and measure *IFNG* mRNA expression which was conducted by Dr Tom Hearn.

Using the Neon[®] Transfection system, *CH25H* expression was knocked down to 32-39% compared to non-targeting (NT) siRNA treatment (Figure 6.1.A/B.). Expectedly, 25-HC in the media was reduced to 14-23% in *CH25H* siRNA-treated cells compared to NT or *GAPDH* siRNA-treated cells whereas 24S,25-EC were similar on targeted siRNA conditions (Figure 6.2). Comparison of CD25 expression levels and 7-AAD staining between non-targeting siRNA-treated and si*CH25H*-treated cells after 48 hours were also comparable (Figure 6.3) which may suggest that a down-regulation of *CH25H* and reduced 25-HC production does not affect the activation-induced CD25 expression or influence the viability of the activated cells.

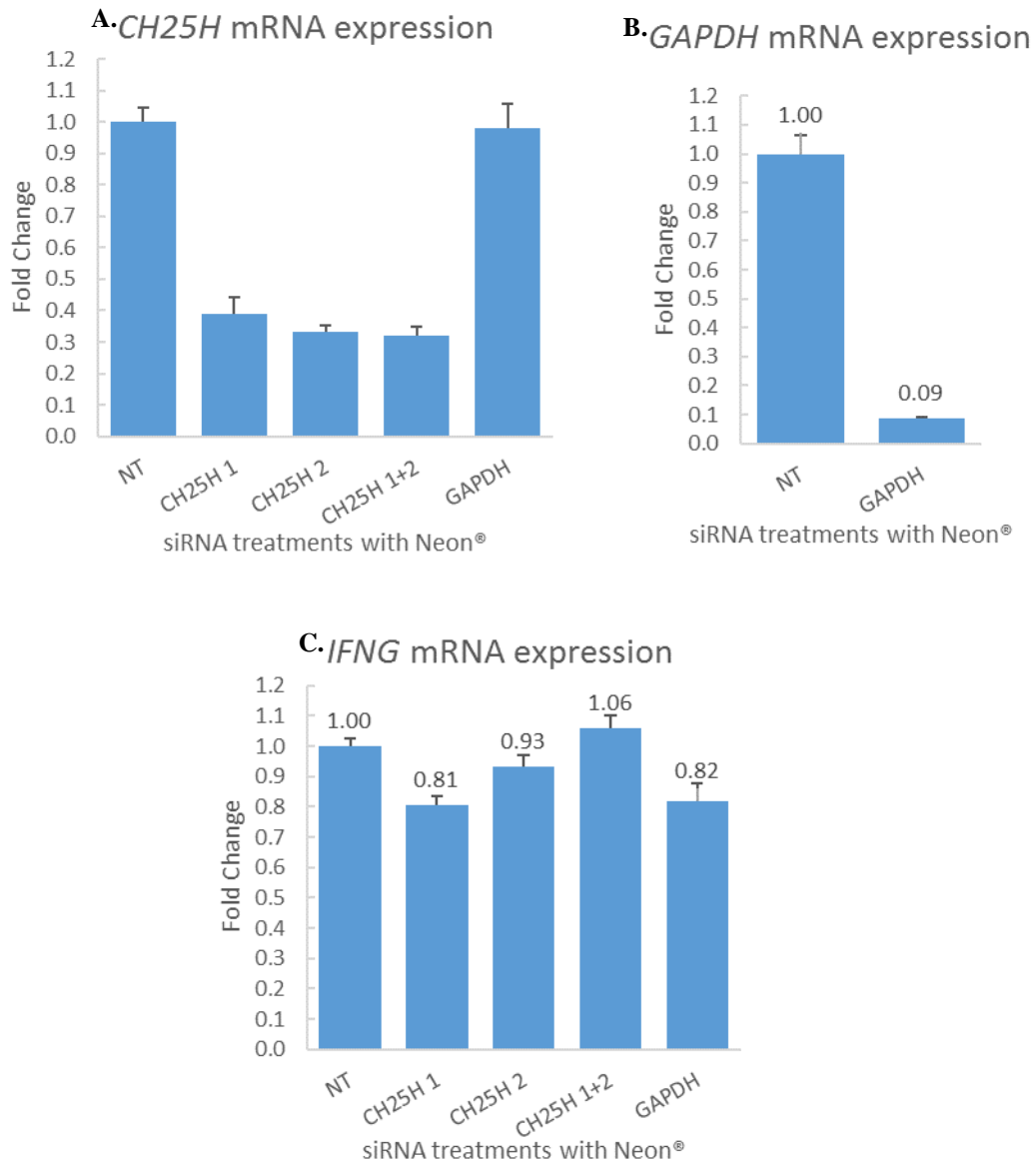


Figure 6.1. RT-PCR analysis for 48-hour cultured siRNA-treated activated total CD4⁺ T cells of donor 1 (147).

A. *CH25H* expression of the *CH25H* siRNA-treated cells were downregulated by 61-68% compared to the non-targeting (NT) negative or the *GAPDH* positive control. B. *GAPDH* expression was also measured which showed a 90% downregulation compared to non-targeting control. C. *IFNG* expression was only downregulated by 20% with *CH25H 1* treatment similar to *GAPDH*, whereas *CH25H 2* and *1+2* was comparable to NT. Pre-designed *CH25H* siRNA included two siRNA labelled '1' and '2' transfected separately at 50nM; 'CH25H 1+2' was a combination of both at 25nM each. Error bars indicate s.e.m. of technical triplicates. Data obtained with permission from Dr Tom Hearn, n=1.

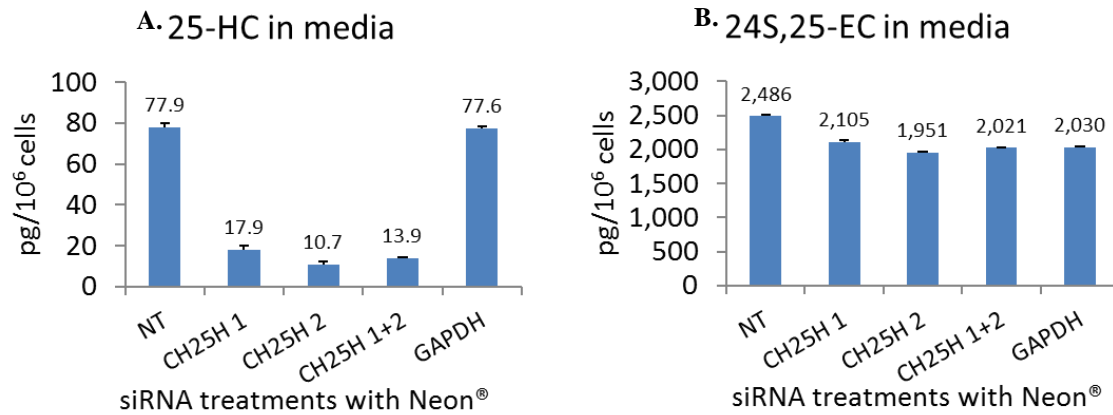


Figure 6.2. Normalised LC-MSⁿ quantification data from siRNA-treated activated total CD4⁺ T cells of donor 1 (147).

A. 25-HC production of *CH25H* siRNA-treated activated cells were reduced by 77-86% compared to when treated with non-targeting siRNA or GAPDH siRNA comparable to the mRNA downregulation. B. Activation-induced 24S,25-EC production on the other hand was only seen to be reduced by 16-22% with *CH25H* or GAPDH siRNA treatment compared to NT siRNA treatment. Data was normalised against number of cells initially seeded. Error bars indicate the s.e.m. of triplicate LC-MSⁿ injections, n=1.

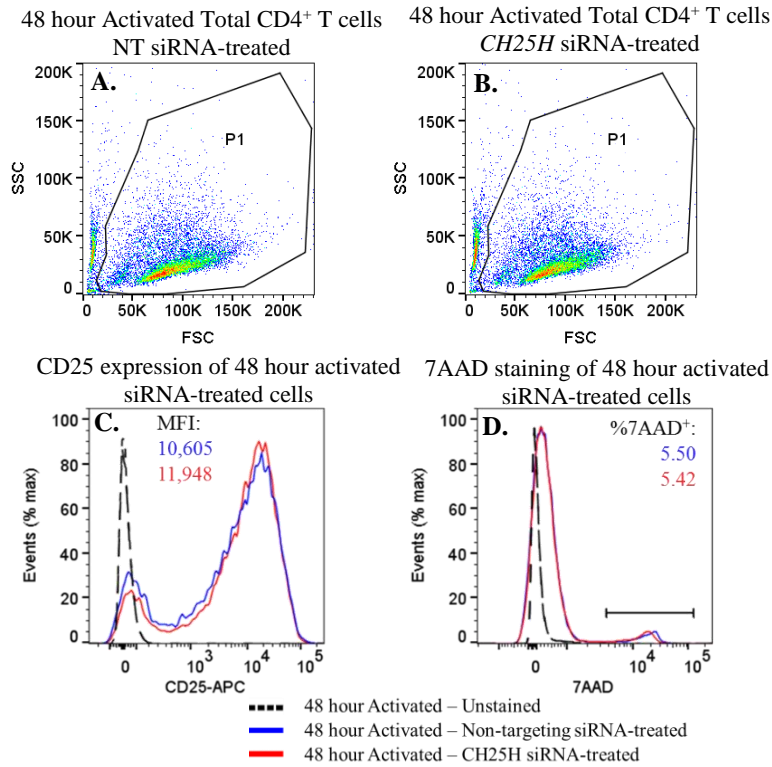


Figure 6.3. Flow cytometry analysis of 48-hour cultured siRNA-treated Neon®-transfected activated total CD4⁺ T cells of donor 1 (147)

A/B. Pseudocolour dot plots of cells showing nearly identical FSC/SSC profiles of negative control and CH25H-silenced cells. C. Overlay histograms showing the CD25-expression of siRNA-treated cells from the 'P1' gate. D. Overlay histograms showing the 7AAD viability dye incorporation of siRNA-treated cells from the 'P1' gate. Coloured inset numbers indicate the CD25 mean fluorescence intensities (MFI) and gated % 7AAD⁺ cells.

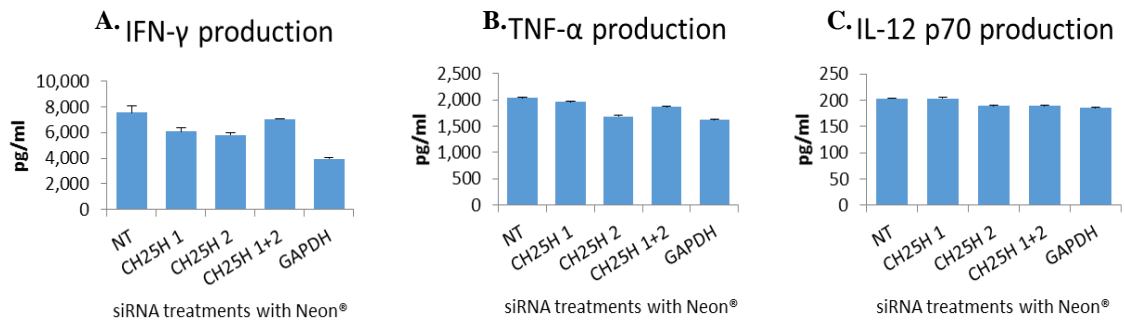


Figure 6.4. Cytokine production of siRNA-treated 48 hour activated total CD4⁺ T cells of donor 1 (147).

A. IFN- γ concentrations in the media of CH25H and GAPDH silenced cells quantified by sandwich ELISA. B/C. TNF- α and IL-12p70 cytokine levels as measured by Luminex® multiplex assay. Other cytokines monitored but undetected were IL-4, IL-17 and IL-6. 1.5×10^6 in 2mL (0.75×10^6 cells/mL) were cultured in a 12-well plate and were activated in all conditions with anti-CD3/CD28-loaded microbeads at 1:2 bead-to-cell ratio. Error bars denote \pm SD from duplicate wells, n=1.

6.3.2. Down regulation of CH25H expression and reduced 25-HC does not affect the IFNG mRNA expression and IFN- γ cytokine production

Activated cells with downregulated *CH25H* expression were observed to have comparable levels of *IFNG* mRNA expression. Furthermore, the results were consistent when *CH25H* siRNA were either used separately or together (Figure 6.1.C). Similarly, the activation-induced IFN- γ production of *CH25H* siRNA-treated total CD4⁺ T cells were also comparable to the NT siRNA treatment as measured by ELISA (Figure 6.4.A).

Additionally, the same culture media samples were subjected to Luminex® multiplex screening which found similar levels of TNF- α and IL-12 p70 (Figure 6.4.B/C) across all siRNA treatments and undetectable levels of IL-17, IL-6 and IL-4.

6.3.3. 4D-Nucleofection ‘high efficiency’ programme led to reduced cell viability but comparable CH25H silencing to ‘high functionality’ programme

To find out if siRNA knockdown efficiency could be improved, RNA interference was further investigated with a 4D-Nucleofector™ transfection system was tested which offered different settings for optimised cell electroporation by Dr Tom Hearn. CD4⁺ T cell viability was initially tested using the different programmes by transfecting a GFP vector as a positive control. Transfections using either electroporation programme resulted in progressive cell death with increased time in culture which was not observed in non-electroporated (no programme) cells (Figure 6.5). However, the high functionality programme resulted in less 7AAD⁺ cells, though lower GFP⁺ cells, compared to the high efficiency programme.

Using the *CH25H* siRNA, both programmes resulted in similar gene silencing (50-56%) after 48 hours when normalised to non-targeting (NT) siRNA (Figure 6.6.A/B). The high functionality programme showed better cell viability which may have led to slightly higher expression of activation-induced *IFNG* gene (Figure 6.6.E) and IFN- γ cytokine production (Figure 6.7) compared to using the high efficiency programme.

The experiment was repeated with another donor using the two *CH25H* siRNAs either separately or together but only with the 4D high functionality programme. RT-PCR analysis of *CH25H* gene silencing was similar to the Neon® transfection experiments and confirmed to be 58-61% compared to NT siRNA controls with no evident effect on the levels of *IFNG* mRNA expression (Figure 6.8).

6.3.4. IFN- γ does not affect CD25 expression or 25-HC production in activated total CD4⁺ T cells

Interferon treatment was reported to induce *Ch25h* expression and 25-HC production in mice bone marrow-derived macrophages. To see if this effect also extends to human CD4⁺ T cells, cells were either treated with recombinant human IFN- γ or with neutralising anti-IFN- γ antibodies in both activating and non-activating conditions and the sterol production measured after 48 hours. Initially, the amount of IFN- γ produced by cultured total CD4⁺ T cells activated via anti-CD3/CD28-loaded microbeads were measured and was found to be around 100ng/mL after 48 hours post-activation (Figure 6.9).

LC-MSⁿ analysis revealed cholesterol and oxysterol production were not changed in the presence of exogenous 100ng/mL recombinant human IFN- γ (Figure 6.11 & Figure 6.12). The sterol content was only observed to increase in activated conditions compared to non-activated cultures. Additionally, there were no considerable effect of IFN- γ treatment in the level of CD25 expression of both non-activated and activated cells (Figure 6.10).

Next, the effect of blocking the endogenous IFN- γ in activated cultures was also investigated. The IFN- γ produced by activated total CD4⁺ T cells were neutralised with 10 μ g/mL anti-IFN- γ and was found to have no clear effect in the production of sterols monitored (Figure 6.11 & Figure 6.12). Furthermore, CD25 expression (Figure 6.10.C) or *CH25H* and *IFNG* mRNA expression (Figure 6.13) were also not observed to be affected by the blocking of endogenous IFN- γ .

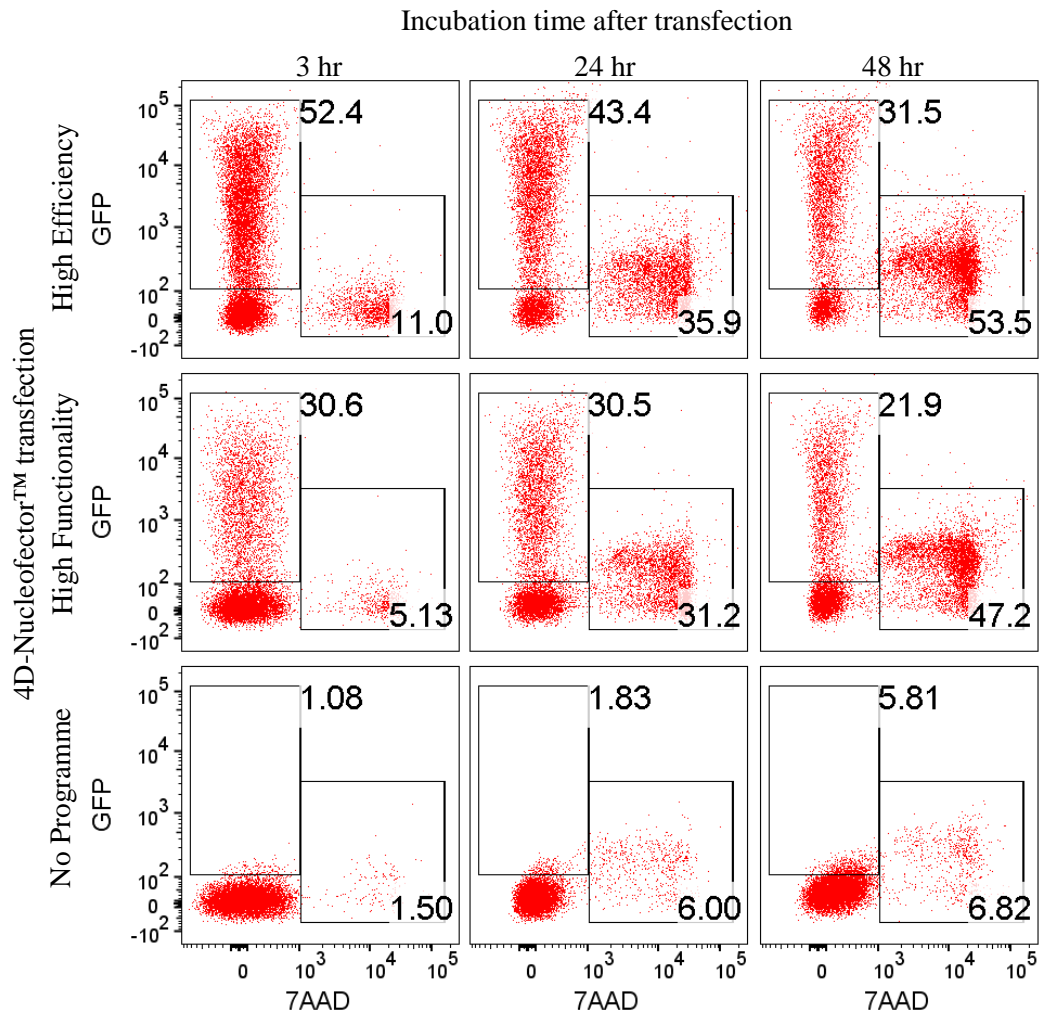


Figure 6.5. Cell viability flow cytometry analysis of activated total CD4⁺ T cells before and after 4D-Nucleofection.

Dot plots show of % of gated GFP⁺ cells and 7AAD⁺ cells (inset numbers) at different incubation times post-nucleofection using the two electroporation programmes and one with no programme. Cells were transfected with pmaxGFP vector as a transfection control, seeded at 2.5x10⁶ cells/mL and activated after 5 hours. Events include all cells but excludes activation microbeads which have very low FSC/SSC. Inset numbers indicate percentage of gated events.

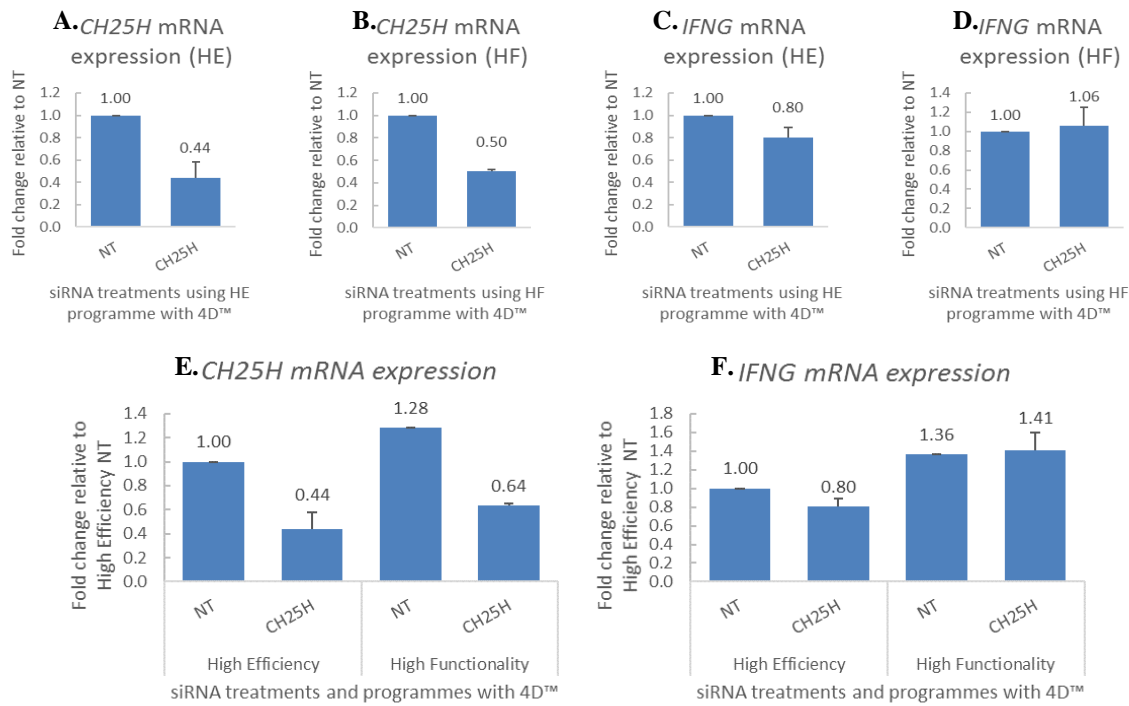


Figure 6.6. RT-PCR analysis for 48-hour cultured siRNA-treated activated total CD4⁺ T cells of donor 2 (191).

A/B. Similar levels of *CH25H* silencing were observed using either high efficiency (HE) or high functionality (HF) when compared to non-targeting (NT) controls. C/D. *IFNG* expression did not reflect the down regulation of *CH25H* expression. E/F. Transfections using the high functionality programme resulted to slightly higher mRNA expression compared to high efficiency. Data obtained with permission from Dr Tom Hearn. Error bars denote \pm SD from duplicate transfections/cultures of one donor, n=1.

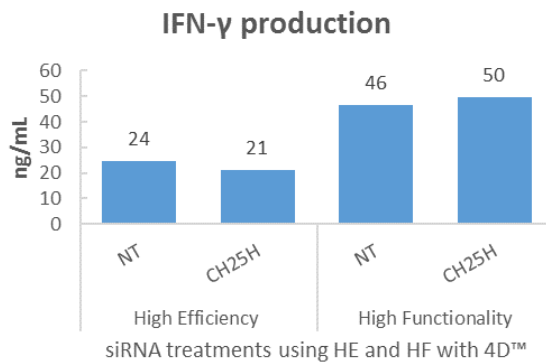


Figure 6.7. IFN- γ secretion of *CH25H* siRNA-treated total CD4⁺ T cells of donor 2 (191) 48 hours after activation as measured by sandwich ELISA.

Similar IFN- γ levels were detected in either *CH25H* or NT siRNA treated cells. Comparing the two transfection programmes, the high functionality was observed to have more IFN- γ production than high efficiency. This trend mirrors the *IFNG* mRNA expression in Figure 6.6.F. Cultured in a 96-well plate, 5×10^5 cells in $200 \mu\text{L}$ (2.5×10^6 cells/mL) were activated in all conditions with anti-CD3/CD28-loaded microbeads at 1:2 bead-to-cell ratio, n=1.

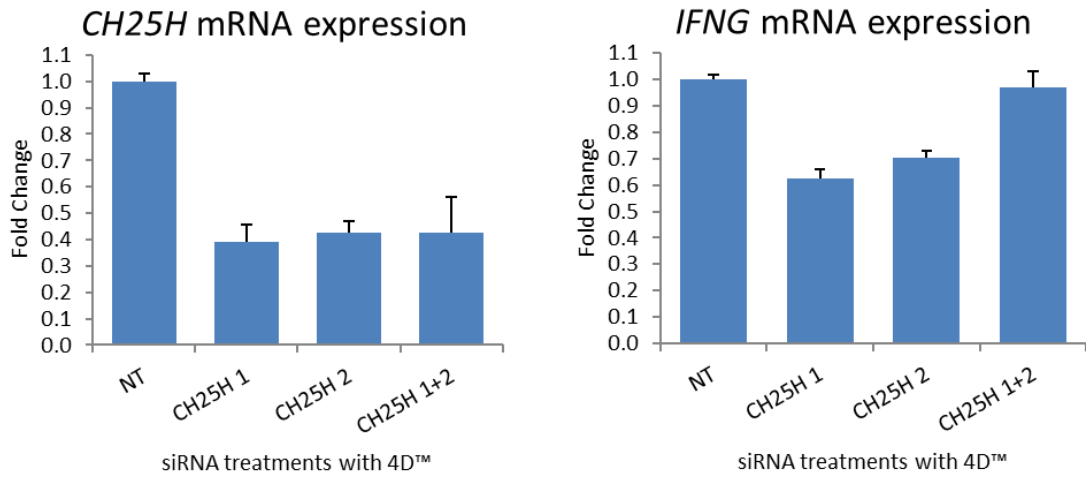


Figure 6.8. RT-PCR analysis for 48-hour cultured siRNA-treated activated total CD4⁺ T cells of donor 3 (164).

A. *CH25H* expression of the *CH25H* siRNA-treated cells were downregulated by 58-61% compared to the NT control. B. *IFNG* expression was downregulated by 30-35% with *CH25H* 1 and 2 when used separately but was comparable to NT control when used together. Pre-designed *CH25H* siRNA ‘1’ and ‘2’ was transfected separately at 6nM; ‘CH25H 1+2’ was a combination of both at 3nM each. Error bars indicate s.e.m. of technical triplicates, n=1.

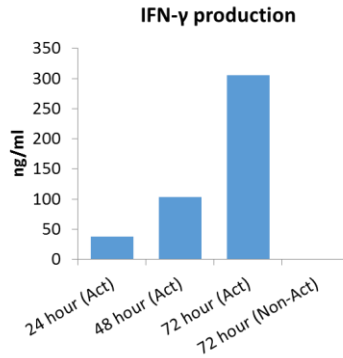


Figure 6.9. Time course analysis of IFN- γ concentration in anti-CD3/CD28 activated total CD4⁺ T cells by sandwich ELISA of donor 3 (164). 0.75x10⁶ cells total CD4⁺ T cells were cultured in 300 μ L X-VIVO-20 media on a 96-well plate (2.5x10⁶ cells/mL/cm²) in either non-activating or activating conditions with anti-CD3/CD8-loaded microbeads at 1:2 bead-to-cell ratio. Non-activated cells did not produce detectable levels of IFN- γ even after 72 hours in culture compared to activated cells, n=1.

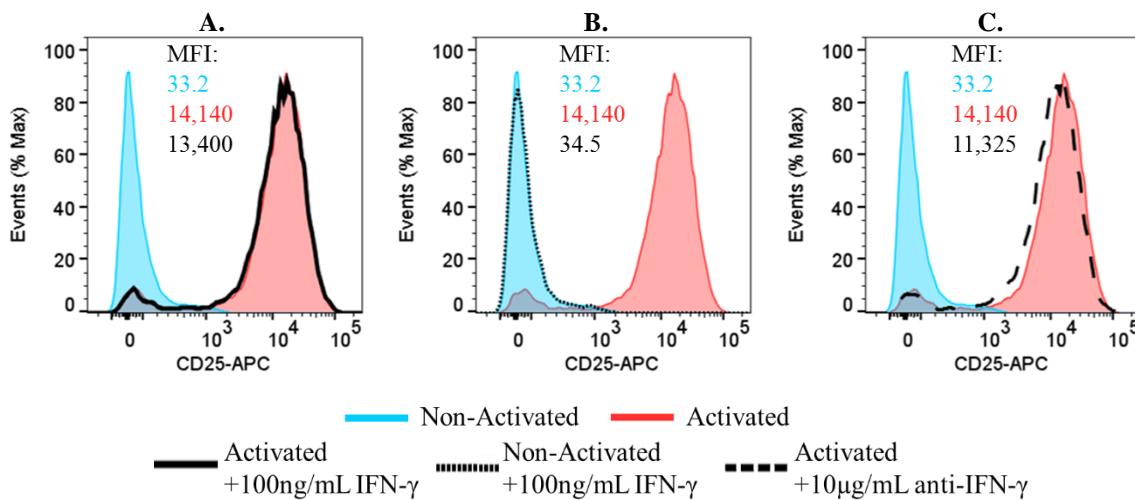


Figure 6.10. Flow cytometry histograms showing the effect of exogenous IFN- γ treatment or neutralising antibody in the expression of CD25 in total CD4⁺ T cells of donor 4 (047). Expression of CD25 was dependent only to activation via CD3/CD28 and IFN- γ at 100ng/mL was not observed to influence CD25 expression in either activating (A) or non-activating conditions (B). In addition, the neutralisation of endogenous IFN- γ produced by activated cells only slightly reduced the activation-induced CD25 expression. Events were gated from all cells to exclude activation microbeads which have low FSC/SSC. Coloured inset numbers indicate the CD25 mean fluorescence intensities (MFI), n=1.

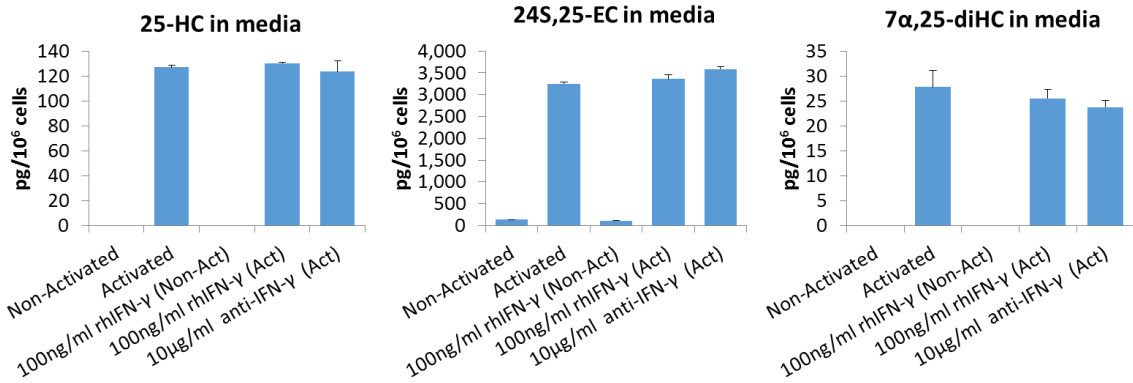


Figure 6.11. Sterols detected and quantified from the media fractions of total CD4⁺ T cells after 48 hours of donor 4 (047).

Mass spectrometry analysis revealed comparable sterol production across all activated cells, irrespective of the addition of recombinant human IFN- γ or neutralisation of IFN- γ . 3×10^6 cells were cultured in 1.2mL on a 48 well plate (2.5×10^6 cells/mL/cm²). Data was normalised to the number of cells initially seeded. Error bars denote \pm SD of triplicate LC-MSⁿ injections, n=1.

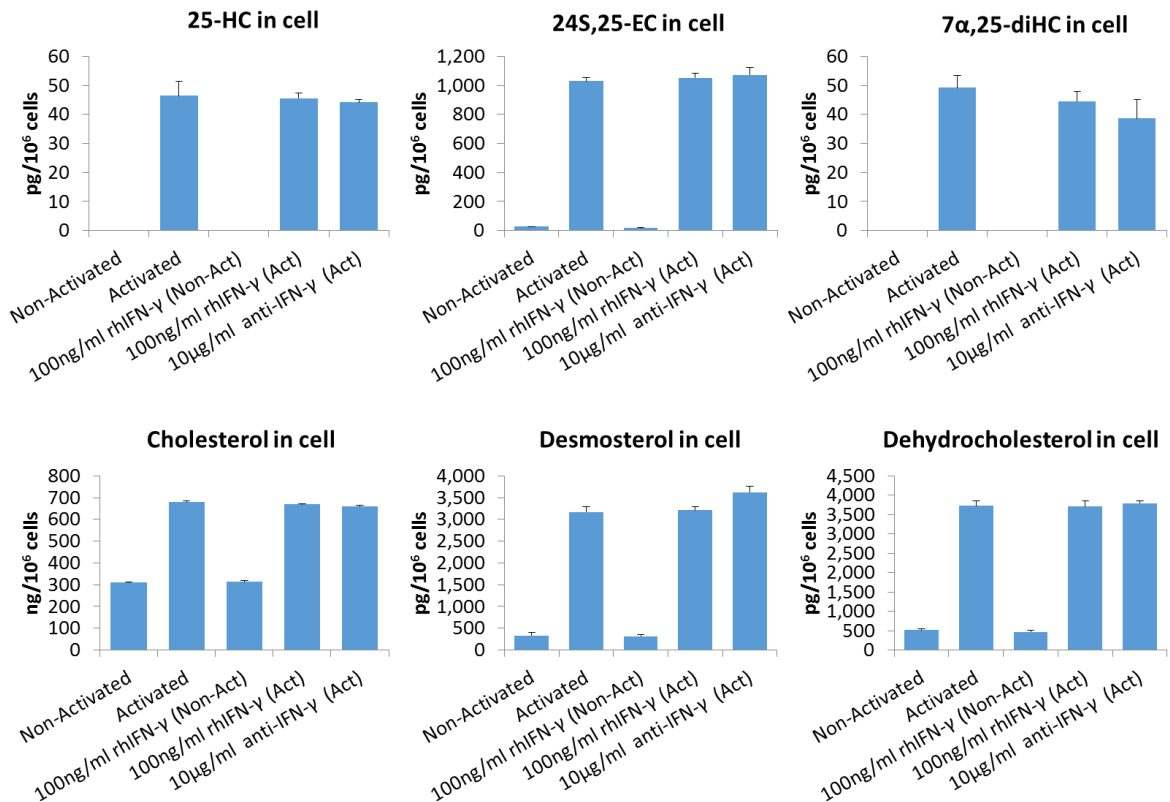


Figure 6.12. Sterols detected and quantified from the cell fractions of total CD4⁺ T cells after 48 hours of donor 4 (047).

Mass spectrometry analysis revealed comparable sterol production across all activated cells, irrespective of the addition of recombinant human IFN- γ or neutralisation with anti-IFN- γ . 3×10^6 cells were cultured in 1.2mL on a 48 well plate (2.5×10^6 cells/mL/cm²). Data was normalised to the number of cells extracted upon harvest. Error bars denote \pm SD of triplicate LC-MSⁿ injections, n=1.

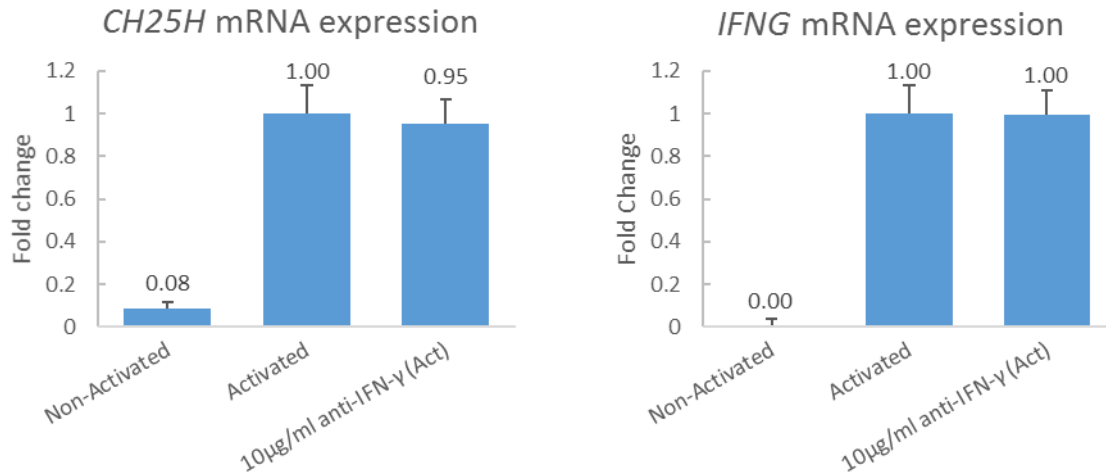


Figure 6.13. Effect of neutralising anti-IFN- γ antibodies to *CH25H* and *IFNG* expression in activated total CD4⁺ T cells of donor 1 (147). Depletion of secreted soluble IFN- γ produced by activated T cells were not seen to have an effect in either *CH25H* or *IFNG* expression. Data obtained with permission from Dr Tom Hearn. Treatment with anti-IFN- γ antibodies was in addition to CD3/CD28 activating conditions and error bars denote s.e.m of triplicates from one donor, n=1

6.4. Discussion

Within the last few years the involvement oxysterols, other than modulating cholesterol metabolism and bile acid intermediates, have been described especially in the context of immunity. Of the oxysterols, 25-HC was identified to have both pro- and anti-inflammatory effects through interferon-associated pathways in murine macrophage models and more recently in B-cells. To date, roles of these oxysterols are less reported in T cells and this chapter have attempted to establish this link using RNA interference and cytokine treatments in a human *in vitro* model.

Gene silencing attempts using siRNA were effective in downregulating *CH25H* expression although the process of electroporation itself led to reduced CD4⁺ T cell viability. RT-PCR analysis of siRNA-treated cells using two electroporation methods have observed a lack of correlation between the *CH25H* silencing and *IFNG* expression. This result was anticipated as *CH25H* was reported as an interferon-stimulated gene in macrophages^[5,9] and not the reverse.

As T cells coordinate immune responses by producing a wide range of cytokines, differential secretion was screened in the culture media of *CH25H*-silenced cells. It was shown that activated total CD4⁺ T cells produce IFN- γ , TNF α and IL-12p70 but unremarkably, there were no observable correlation in the production of TNF α and IL-12p70 with or without *CH25H* down regulation (Figure 6.4.B/C). In addition, the activated total CD4⁺ T cells were not observed to produce detectable amounts of either IL-4 or IL-17, suggesting *CH25H* may not play a part in the production of these T cell cytokines, especially when not under polarising conditions. In contrast, GAPDH silencing led to a slight reduction of IFN- γ production of activated cells (Figure 6.4.A). This effect was unexpected as it has been previously reported that the GAPDH protein can interact with the 3'-untranslated region of IFN- γ mRNA where its binding can limit the translation of the cytokine, implying that GAPDH loss should have increased IFN- γ production^[11,12].

In summary, T cells upregulate *CH25H* leading to increased 25-HC production upon activation but also express *IFNG* and produce ample amounts of IFN- γ . Although both are triggered by activation, results in this chapter shown that expression of these two genes were separate and maybe regulated by distinct pathways in CD4⁺ T cells. Moreover, the results of activated T cell cultures here were unable to define a role of IFN- γ in the production of sterols or activation level. However, the effects of IFN- γ and CH25H were only measured up to 48 hours after activation. This is short considering T cells may take days to weeks for full activation and manifest effector functions^[13]. It is therefore possible that such treatments like increased IFN- γ or lack of *CH25H* expression may exhibit an effect in the later stages of T cell activation. The variation in available IFN- γ could direct the balance in either a TH1^[14] or TH2-like response which may have a knock-on effects in the production of sterols.

This opened the curiosity in questioning the presence of changes in sterol metabolism among the different subsets of CD4⁺ T cells which will be described in chapter 8. But before differentiation to different subsets, T cell activation occurs first which stimulates a multitude of intracellular signalling pathways. Which pathways are involved in directing specific sterol production may then provide clues to understand function.

6.5. References

- [1] C.M. Adams, J. Reitz, J.K. De Brabander, J.D. Feramisco, L. Li, M.S. Brown, et al., (2004) Cholesterol and 25-hydroxycholesterol inhibit activation of SREBPs by different mechanisms, both involving SCAP and insigs, *J. Biol. Chem.* 279 52772–52780. doi:10.1074/jbc.M410302200.
- [2] A. Radhakrishnan, Y. Ikeda, H.J. Kwon, M.S. Brown, J.L. Goldstein, (2007) Sterol-regulated transport of SREBPs from endoplasmic reticulum to Golgi: oxysterols block transport by binding to Insig., *Proc. Natl. Acad. Sci. U. S. A.* 104 6511–6518. doi:10.1073/pnas.0700899104.
- [3] U. Diczfalusy, K.E. Olofsson, A.-M. Carlsson, M. Gong, D.T. Golenbock, O. Rooyackers, et al., (2009) Marked upregulation of cholesterol 25-hydroxylase expression by lipopolysaccharide., *J. Lipid Res.* 50 2258–2264. doi:10.1194/jlr.M900107-JLR200.
- [4] D.R. Bauman, A.D. Bitmansour, J.G. McDonald, B.M. Thompson, G. Liang, D.W. Russell, (2009) 25-Hydroxycholesterol secreted by macrophages in response to Toll-like receptor activation suppresses immunoglobulin A production., *Proc. Natl. Acad. Sci. U. S. A.* 106 16764–16769. doi:10.1073/pnas.0909142106.
- [5] S.-Y. Liu, D.J. Sanchez, R. Aliyari, S. Lu, G. Cheng, (2012) Systematic identification of type I and type II interferon-induced antiviral factors., *Proc. Natl. Acad. Sci. U. S. A.* 109 4239–44. doi:10.1073/pnas.1114981109.
- [6] M. Blanc, W.Y. Hsieh, K. a. Robertson, K. a. Kropp, T. Forster, G. Shui, et al., (2013) The Transcription Factor STAT-1 Couples Macrophage Synthesis of 25-Hydroxycholesterol to the Interferon Antiviral Response, *Immunity.* 38 106–118. doi:10.1016/j.immuni.2012.11.004.
- [7] S. Liu, R. Aliyari, K. Chikere, G. Li, D. Matthew, J.K. Smith, et al., (2013) Interferon-Inducible Cholesterol-25-Hydroxylase Broadly Inhibits Viral Entry by Production of 25-Hydroxycholesterol, *Immunity.* 38 92–105. doi:10.1016/j.immuni.2012.11.005.
- [8] E.S. Gold, A.H. Diercks, I. Podolsky, R.L. Podyminogin, P.S. Askovich, P.M. Treuting, et al., (2014) 25-Hydroxycholesterol acts as an amplifier of inflammatory signaling., *Proc. Natl. Acad. Sci. U. S. A.* 1–6. doi:10.1073/pnas.1404271111.
- [9] A. Reboldi, E. V. Dang, J.G. McDonald, G. Liang, D.W. Russell, J.G. Cyster, (2014) 25-Hydroxycholesterol suppresses interleukin-1-driven inflammation downstream of type I interferon, *Science (80-.).* 345 679–684. doi:10.1126/science.1254790.
- [10] K.J. Livak, T.D. Schmittgen, (2001) Analysis of relative gene expression data using real-time quantitative PCR and the 2(-Delta Delta C(T)) Method., *Methods.* 25 402–8. doi:10.1006/meth.2001.1262.
- [11] E. Nagy, W.F.C. Rigby, (1995) Glyceraldehyde-3-phosphate Dehydrogenase Selectively Binds AU-rich RNA in the NAD⁺-binding Region (Rossmann Fold), *J. Biol. Chem.* 270 2755–2763. doi:10.1074/jbc.270.6.2755.

- [12] C.-H. Chang, J.D. Curtis, L.B. Maggi, B. Faubert, A. V. Villarino, D. O'Sullivan, et al., (2013) Posttranscriptional control of T cell effector function by aerobic glycolysis., *Cell*. 153 1239–51. doi:10.1016/j.cell.2013.05.016.
- [13] K. Murphy, P. Travers, M. Walport, C. Janeway, *Janeway's immunobiology*, Garland Science, New York, 2012.
- [14] A.E. Wakil, Z.-E. Wang, J.C. Ryan, D.J. Fowell, R.M. Locksley, (1998) Interferon γ Derived from CD4 + T Cells Is Sufficient to Mediate T Helper Cell Type 1 Development, *J. Exp. Med.* 188 1651–1656. doi:10.1084/jem.188.9.1651.

CHAPTER 7: Investigating T cell receptor signalling pathways influencing the generation of 24(S),25-EC, 25-HC and 7 α ,25-DiHC.

7.1. Introduction

It has been previously reported that cholesterol biosynthesis and its intracellular accumulation is important for membrane formation and as a checkpoint in cell cycle^[1,2]. Previous chapters have also established the production of certain oxysterols in response to CD4⁺ T cell activation and investigated the consequence of inhibited cholesterol biosynthesis in T cell activation, proliferation and oxysterol production using simvastatin treatments.

As mentioned in *section 1.5.4*, activation of T cells via CD3/CD28-stimulation can ultimately lead to the activation of transcription factors such as NF- κ B, NFAT and AP-1 which direct gene expression leading to enhanced CD4⁺ T cell survival, proliferation and differentiation^[3]. Between the external stimuli provided by TCR/CD28 engagement in the membrane and these transcription factors in the nucleus, several interconnected signal transduction pathways are activated which are mostly conveyed via phosphorylation events initiated by protein kinases.

After TCR/CD28 engagement, several phosphorylation events occur which eventually recruit phospholipase C γ (PLC γ) near the membrane of the immunological synapse (Figure 7.1). There, PLC γ can stimulate the activation of nuclear factor of activated T cells (NFAT) via increasing cytosolic calcium concentrations, activate PKC signalling and MAPK pathways to activate NF κ B and AP-1 transcription factors, respectively, to turn on pro-survival genes (Figure 7.1). In addition, the mTORC1 pathway can be triggered via activation of PI3K^[4] or through mTORC2 via AKT^[5] which promotes protein translation. In all, the stimulation of these pathways contributes to proper and effective T cell activation.

However, studies specifically linking these protein kinase signalling pathways with sterol metabolism in activated primary human T cells *in vitro* are currently limited.

This chapter aims to determine which pathways are involved in the regulation of cholesterol metabolism in activated human CD4⁺ T cells, specifically, to distinguish which pathways influence the production of 25-HC, 7 α ,25-diHC, 24(S),25-EC, cholesterol and its precursors by the use of pharmacological inhibitors and activators.

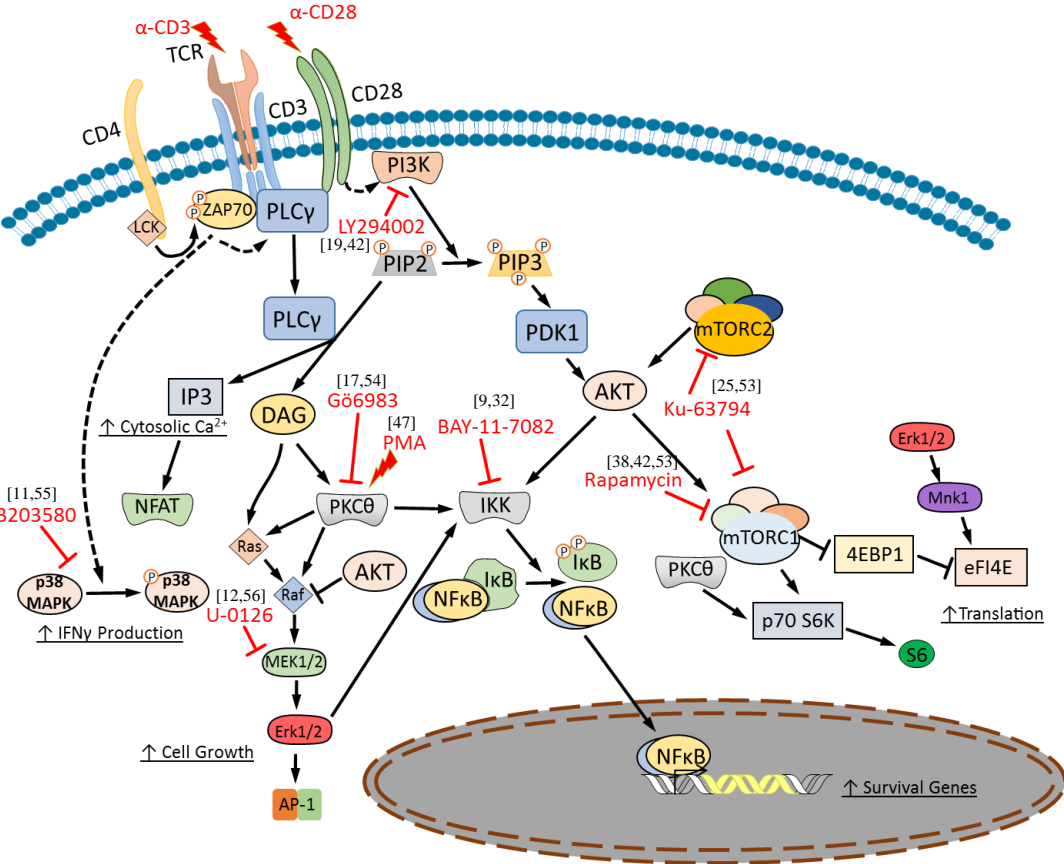


Figure 7.1. Signalling pathways downstream of TCR/CD28 stimulation in CD4⁺ T cells. Several interconnected signalling pathways stem from the initial engagement of TCR and CD28, with all leading to the activation of transcription factors which promote T cell activation and survival. This chapter will look into the effect of inhibiting select pathways using pharmacological inhibitors (red) in the sterol production of total CD4⁺ T cells in activating conditions, as well as CD25 expression and viability.

7.2. Materials and Methods

7.2.1. Preparation of pharmacological inhibitors and activators

Inhibitors specific to certain signalling pathway kinases were commercially bought as lyophilised solid and reconstituted as stock concentrations under sterile conditions using 100% sterile dimethyl sulfoxide (DMSO). Table 7.1 lists the compounds with their target kinases

Table 7.1. Compounds used to modulate intracellular signalling pathways in activated total CD4⁺ T cells.

Compound	Target Kinase	CAS number	Manufacturer
BAY-11-7082	IKK (NF- κ B) inhibitor	19542-67-7	Merck Millipore
Gö6983	pan-PKC inhibitor	133053-19-7	Sigma-Aldrich
SB-203580	p38 MAPK inhibitor	152121-47-6	Merck Millipore
U0126	MEK1/2 (ERK1/2) inhibitor	109511-58-2	Merck Millipore
Rapamycin	mTORC1 inhibitor	53123-88-9	Merck Millipore
LY294002	PI3K inhibitor	154447-36-6	Merck Millipore
Ku-63794	mTORC1/2 inhibitor	938440-64-3	Merck Millipore
PMA	pan-PKC activator	16561-29-8	Sigma-Aldrich

7.2.2. Total CD4⁺ T cell isolation from PBMCs

Total CD4⁺ T cells were negatively selected from the PMBCs of 7 healthy human donors after density gradient centrifugation as described in *section 2.1.2*, *section 2.1.3* and *section 2.1.4.2*. Purity was confirmed by flow cytometry to be >95% CD4⁺ cells.

7.2.3. Treatment conditions and activation of total CD4⁺ T cells

Isolated total CD4⁺ T cells were first seeded at 2.5×10^6 cells/ml/cm² using X-VIVO-20 on an appropriate tissue culture plate as in *section 2.1.6.1*. Next, diluted stocks were made with X-VIVO-20 as 100x of the desired final concentration in 10% DMSO. The diluted stocks were added at 10 μ L per mL of cell culture. Cells were pre-incubated with the pharmacological compounds for 30 minutes at 37°C 5% CO₂ humidified

incubator before activation by adding anti-CD3/anti-CD28 loaded microbeads at 1:2 bead-to-cell ratio and cultured for 48 hours. A non-activated negative control and an anti-CD3/CD28 activated positive control were also included treated only with DMSO vehicle for reference sterol production. Moreover, the effect of stimulating CD3 or CD28 alone were explored by treating the cells with microbeads singly loaded with either anti-CD3 or anti-CD28 at 1:2 bead-to-cell ratio. The final DMSO content in all treated and non-treated wells were at 0.1%.

7.2.4. Cell viability and activation assay by flow cytometry

After 48 hours in culture, an aliquot of the treated cells was stained with 7-AAD Viability Staining Solution to estimate the cell death and analysed by flow cytometry as described in *section 2.1.7.2*. Additionally, the level of T cell activation was measured as the expression of CD25 surface marker. An aliquot of cells was stained with anti-human CD25-APC and analysed by flow cytometry as described in *section 2.1.8.4*. All data acquisition was done on a BD FACS Aria and analysed using FlowJo software.

7.2.5. Flow cytometric phosphorylation assay of S6 and 4E-BP1 intracellular proteins

In some experiments, phosphorylation status of the 40S ribosomal S6 protein (pS6) at S235/S236 and eukaryotic translation initiation factor eIF4E-binding protein 1 (p4E-BP1) at T36/T45 were monitored in activated conditions in the presence or absence of select inhibitors using fluorochrome-conjugated antibodies as listed in *section 2.1.8.3* Table 2.4.

7.2.6. Measurement of relative SREBP2 and HMGCR mRNA expression levels

Cells from donor 7 were extracted for total RNA and was subjected to RT-PCR analysis as described in *section 2.3.2* using the $2^{-\Delta\Delta C_t}$ method to measure the relative

SREBP2 and HMGCR expression normalised to *RPI8S* in activated CD4⁺ T cells in the presence or absence of certain kinase inhibitors.

7.2.7. Sample processing and sterol analysis

After culture, remaining cells and media were harvested, extracted, and analysed for sterol content using HPLC-ESI-MSⁿ. 25-HC, 7 α ,25-DiHC and 24(S),25-EC were monitored and quantified in the media and cell fraction. Additionally, cholesterol, desmosterol, dehydrocholesterol and dehydrodesmosterol were monitored and quantified in the cell fractions. Quantified sterols by stable isotope dilution MS in media and cell fractions were normalised to the number of cells initially seeded and number of cells extracted at 48 hours, respectively. As the absolute sterols produced can vary depending on donors, all treatments were normalised and expressed as % relative to the positive control, anti-CD3/CD28 activated CD4⁺ T cells.

7.2.8. Statistical analysis

When indicated, differences in mean sterol quantities normalised at pg/million cells and flow cytometric assays with median fluorescence intensities (MFI) were tested for statistical significance using Microsoft Excel Analysis Toolpak two-tailed unpaired T tests where *p* values of 0.05 or less were considered statistically significant.

7.3. Results

7.3.1. CD3 or CD28 stimulation alone do not fully induce the expression of CD25 and the production of oxysterols, 24(S),25-EC and 25-HC.

The expression of CD25 did not change in either untreated cells or anti-CD28 after 48 hours in culture. An increase in CD25 expression was observed when CD4⁺ T cells were treated with anti-CD3 loaded microbead where 69.7% of the cells are CD25⁺ but full activation (>99%) was only seen when the cells were treated with anti-CD3/CD28 loaded microbeads (Figure 7.2). This suggests that effective T cell activation requires dual stimulation and the TCR signalling pathway can be partially triggered through

CD3 stimulation but must be complemented with CD28 stimulation for full activation (Figure 7.1).

The oxysterol production was measured and compared to cells with anti-CD3/CD28. In agreement with their level of activation, anti-CD3 treated cells were seen to produce about 55% of the 24(S),25-EC compared to activated cells whereas the untreated and anti-CD28 treated cells were only 5% and 8% respectively (Figure 7.3A). As in previous chapters, 25-HC was detected in activated cells but not in non-activated cells after 48 hours. Moreover, 25-HC was undetected in the media of CD4⁺ T cells treated with anti-CD3 loaded microbeads or anti-CD28 loaded microbeads (Figure 7.3B). This trend was also seen with 7 α ,25-DiHC (Figure 7.3C). Analysis of these oxysterols in the cell fraction revealed 24(S),25-EC to be of similar trend to the media fraction whereas 25-HC and 7 α ,25-DiHC were undetected.

Intracellular cholesterol content in activated total CD4⁺ T cells has been previously shown to double compared to non-activated cells after 48 hours. Stimulation by anti-CD3 or anti-CD28 alone however does not accumulate intracellular cholesterol with levels not significantly different from non-activated cells (Figure 7.3D).

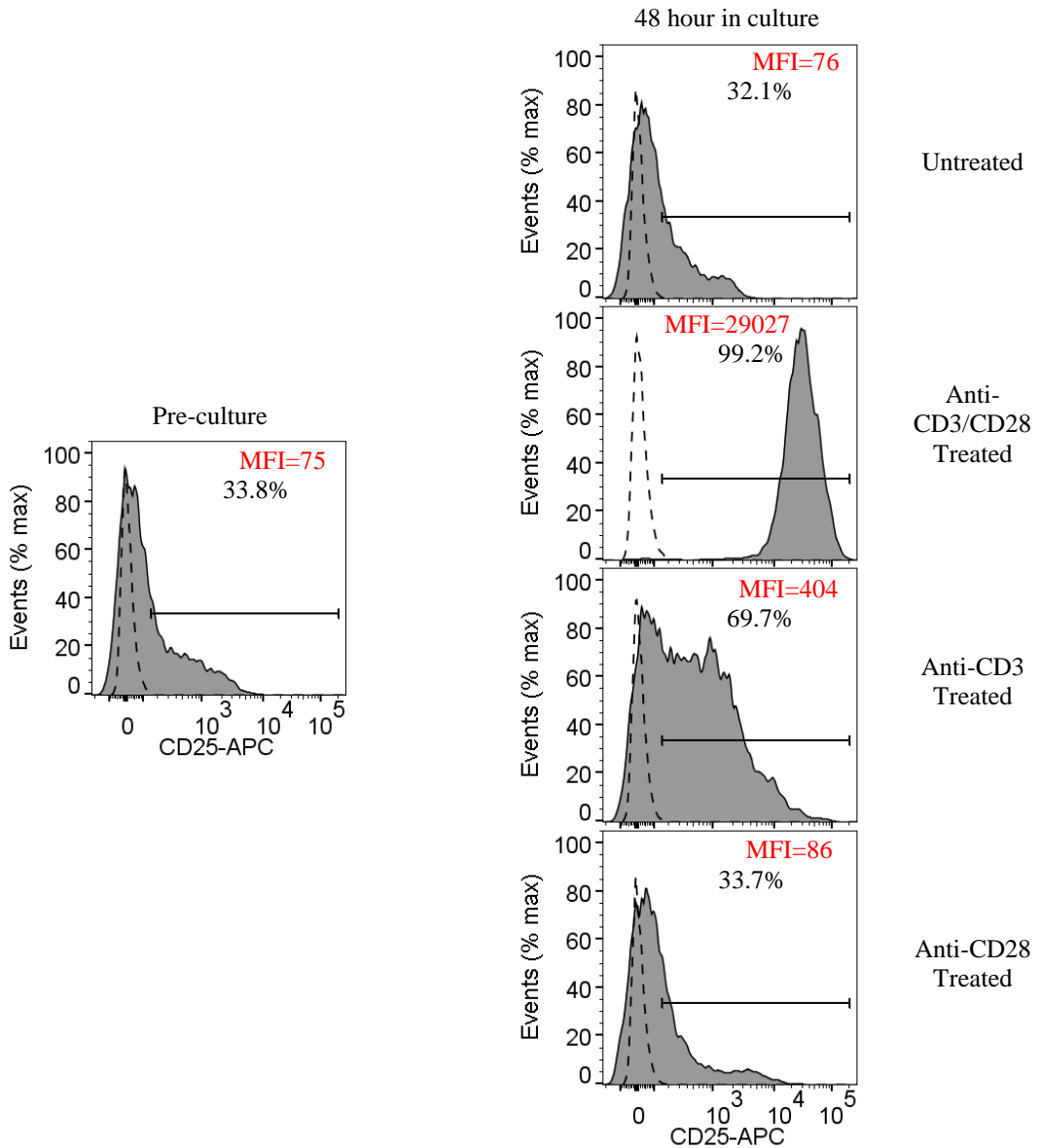
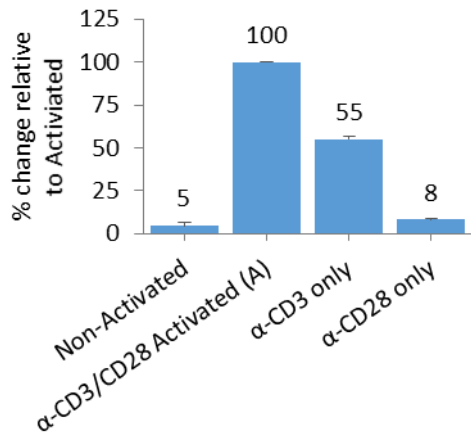


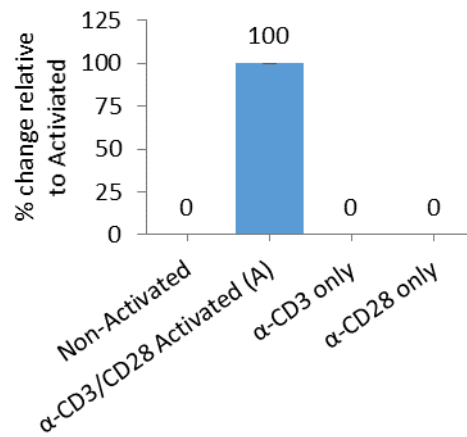
Figure 7.2. Representative flow cytometry overlays of the CD25 surface expression of untreated, anti-CD3/CD28, anti-CD3 alone and anti-CD28 alone treated total CD4⁺ T cells after 48 hours in culture from donor 5.

Full activation based on the expression of CD25 was exhibited only upon stimulation of both CD3 and CD28 but not alone. Some increase in CD25 expression was observed in the CD3-only treated cells but the CD28-only treatment was similar to the untreated and pre-culture. All analysis were gated from the live lymphocytes based on the FSC/SSC profile. Filled histograms indicate the CD25-stained samples and dashed histograms as unstained. Red inset numbers indicate the median fluorescence intensity (MFI) of the CD25-stained cells and black inset numbers indicate the % gated CD25⁺ cells.

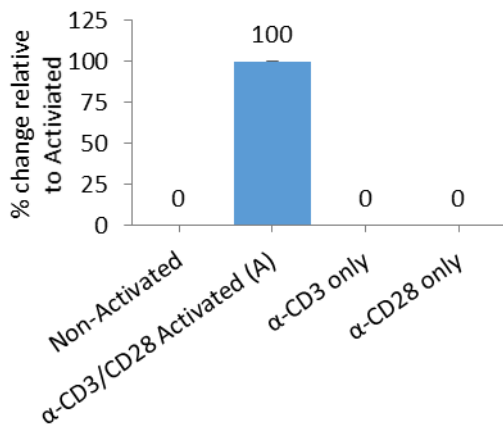
A. 24(S),25-EC in Media fractions



B. 25-HC in Media fractions



C. 7α,25-DiHC in Media fractions



D. Cholesterol in Cell fractions

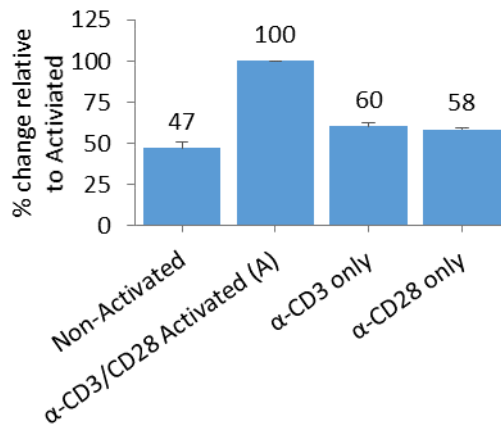


Figure 7.3. Detected sterols in the media and cell fractions of cultured total CD4⁺ T cells after 48 hours. A. 24(S),25-EC was observed to be minimally produced in untreated and CD28-stimulating conditions while treatment in CD3-stimulating conditions produced half of what was produced in CD3/CD28-stimulating conditions. B/C. No 25-HC and 7α,25-DiHC was detected in untreated, CD3-stimulating or CD28-stimulating conditions. D. The amount of intracellular cholesterol doubles in CD3/CD28 activating conditions by 48 hours compared to non-activated. Intracellular cholesterol in T cells which were CD3-stimulated or CD28-stimulated alone were similar non-activated cells. Percentage values were relative to the quantified sterols in CD3/CD28 activated conditions and averaged for each donor taken from Table 7.2 and Table 7.4. Error bars denote s.e.m; all plots at n=3, except α-CD3 in cell fraction which is n=2.

7.3.2. Increased concentrations of NF- κ B signalling inhibitor, BAY-11-7082 induced cell death of activated T cells

NF- κ B signalling has been reported to be activated in stimulated T cells [6]. In resting cells, NF- κ B is associated with I κ B- α in the cytoplasm which prevents its translocation to the nucleus. Upon the need for NF κ B signalling, I κ B- α is phosphorylated by IKK α for degradation which releases NF- κ B migration to the nucleus and rapidly activates its target genes^[7,8] (Figure 7.1). BAY-11-7082 blocks the activity of IKK α leading to reduced I κ B- α phosphorylation and subsequent NF- κ B signalling^[9].

Initial tests with different concentrations (5 μ M, 2 μ M and 1 μ M) of BAY-11-7082 were used to block the NF- κ B signalling in activated total CD4⁺ T cells. 7-AAD viability staining revealed higher concentrations of BAY-11-7082 induced extensive cytotoxicity and cell death at $\geq 42.3\%$ with $\geq 2\mu$ M treatment (Figure 7.4). This prompted the use of the lowest concentration of 1 μ M for subsequent biological replicates.

7.3.3. Other kinase inhibitors and activator treatments did not lead to increased cell death after 48 hours.

Total CD4⁺ T cells were treated with several inhibitors/activators and cell viability were assessed by 7-AAD incorporation. Flow cytometric analysis after 48 hours revealed most treatments with anti-CD3 microbeads, anti-CD28 microbeads, BAY-11-7082 at 1 μ M, U0126 at 10 μ M, SB203580 at 10 μ M, LY294002 at 10 μ M and Rapamycin at 0.1 μ M of different donors led to varied 7-AAD⁺ cells between 4% to 38% (Figure 7.6). Cells treated with the PKC inhibitor, Gö6983, resulted in autofluorescence at the same channel as 7-AAD (PerCP-Cy5.5) due to the compound naturally having a red-orange colour. This made it difficult to directly assess cell viability of Gö6983-treated cells (Figure 7.7). Therefore, cell viability of Gö6983-treated cells were instead assessed indirectly by a decrease in FSC/SSC signals which normally correspond to dead cells.

7.3.4. BAY-11-7082 does not affect oxysterol generation of activated total CD4⁺ T cells at sub-toxic concentrations.

Activated total CD4⁺ T cells treated with 1 μ M BAY-11-7082 did not have a significant effect in the production of oxysterols 25-HC and 24(S),25-EC compared to untreated cells (Table 7.2 and Table 7.3).

However, the surface expression of CD25 was inconsistent among BAY-11-7082 treated activated cells and untreated activated cells after 48 hours across all five donors. More specifically, CD25 expression of 1 μ M BAY-11-7082-treated cells were similar to non-treated activated cells on three experiments but was dissimilar on two (Figure 7.8).

With the normalised sterol data, BAY-11-7082 treatments with activation revealed 24(S),25-EC and 25-HC production and intracellular cholesterol were similar to non-treated activated cells across donors 1, 2 and 3 (Figure 7.9) with the exception for 7 α ,25-DiHC which was only detected in BAY-11-7082-treated activated cells of donor 2 (at 98% compared to untreated activated cells) but not in donor 1 and 3 (Table 7.2B).

Table 7.2. Effect of different treatments to the quantified sterols in the conditioned media fractions of total CD4⁺ T cells after 48 hours in culture.

A. 25-hydroxycholesterol. B. 7 α ,25-Dihydroxycholesterol. C.24(S),25-Epoxycholesterol. Values were quantified using stable isotope dilution MS averaged over three injections then normalised to the number of cells initially seeded. “+A” indicates inhibitor treatments in anti-CD3/CD28 activating conditions. n.d.=not detected.

A. 25-HC in Media fractions (pg/million cells)

Donor	Non-Activated	α -CD3/CD28 Activated (A)	α -CD3 only	α -CD28 only	50ng/ml PMA	1 μ M Gö6983 + A	1 μ M BAY-11-7082 + A	10 μ M U0126 + A	10 μ M SB203580 + A	0.1 μ M Rapamycin + A	10 μ M LY294002 + A
1 (254)	n.d.	50					55	17	61		50
2 (047)	n.d.	127					133		174		90
3 (009)	n.d.	59		n.d.	252	n.d.	70			63	39
4 (089)	n.d.	69	n.d.	n.d.	261	n.d.		23	82	92	
5 (169)	n.d.	125	n.d.	n.d.		n.d.		20		124	
6 (027)	n.d.	84	n.d.		181			13	98		
7 (118)	n.d.	92								109	

B. 7 α ,25-DiHC in Media fractions (pg/million cells)

Donor	Non-Activated	α -CD3/CD28 Activated (A)	α -CD3 only	α -CD28 only	50ng/ml PMA	1 μ M Gö6983 + A	1 μ M BAY-11-7082 + A	10 μ M U0126 + A	10 μ M SB203580 + A	0.1 μ M Rapamycin + A	10 μ M LY294002 + A
1 (254)	n.d.	17					n.d.	n.d.	22		19
2 (047)	n.d.	28					27		53		19
3 (009)	n.d.	11		n.d.	55	n.d.	n.d.			n.d.	n.d.
4 (089)	n.d.	14	n.d.	n.d.	105	n.d.		n.d.	27	25	
5 (169)	n.d.	51	n.d.	n.d.		n.d.		n.d.		49	
6 (027)	n.d.	16	n.d.		22			n.d.	13		
7 (118)	n.d.	0								n.d.	

C. 24(S),25-EC in Media fractions (pg/million cells)

Donor	Non-Activated	α -CD3/CD28 Activated (A)	α -CD3 only	α -CD28 only	50ng/ml PMA	1 μ M Gö6983 + A	1 μ M BAY-11-7082 + A	10 μ M U0126 + A	10 μ M SB203580 + A	0.1 μ M Rapamycin + A	10 μ M LY294002 + A
1 (254)	66	4,461					7,373	5,625	2,258		4,886
2 (047)	133	3,248					3,023		1,258		3,461
3 (009)	374	3,725		376	1,891	2,991	4,490			4,076	4,111
4 (089)	23	1,318	699	97	350	500		2,006	555	1,558	
5 (169)	10	520	270	38		127		679		506	
6 (027)	12	626	376		473			1,049	370		
7 (118)	430	3,634								5,683	

Table 7.3. Effect of different treatments to the quantified sterols in the cell fractions of total CD4⁺ T cells after 48 hours in culture.

A. 25-hydroxycholesterol. B. 7 α ,25-Dihydroxycholesterol. C.24(S),25-Epoxycholesterol. Values were quantified using stable isotope dilution MS averaged over three injections then normalised to the number of cells extracted on the day of harvest. “+A” indicates inhibitor treatments in anti-CD3/CD28 activating conditions. n.d.=not detected.

A. 25-HC in Cell fractions (pg/million cells)

Donor	Non-Activated	α -CD3/CD28 Activated (A)	α -CD3	α -CD28	50ng/ml PMA	1 μ M G δ 6983 + A	1 μ M BAY-11-7082 + A	10 μ M U0126 + A	10 μ M SB203580 + A	0.1 μ M Rapamycin + A	10 μ M LY294002 + A
1 (254)	n.d.	n.d.					n.d.	n.d.	n.d.		n.d.
2 (047)	n.d.	46					40		42		7
3 (009)	n.d.	29		n.d.	n.d.	n.d.	n.d.			n.d.	n.d.
4 (089)	n.d.	19	n.d.	n.d.	54	n.d.		n.d.	13	17	
5 (169)	n.d.	60	n.d.	n.d.		n.d.		n.d.		45	
6 (027)	n.d.	56									

B. 7 α ,25-DIHC in Cell fractions (pg/million cells)

Donor	Non-Activated	α -CD3/CD28 Activated (A)	α -CD3	α -CD28	50ng/ml PMA	1 μ M G δ 6983 + A	1 μ M BAY-11-7082 + A	10 μ M U0126 + A	10 μ M SB203580 + A	0.1 μ M Rapamycin + A	10 μ M LY294002 + A
1 (254)	n.d.	n.d.					n.d.	n.d.	n.d.		n.d.
2 (047)	n.d.	49					46		85		n.d.
3 (009)	n.d.	n.d.		n.d.	n.d.	n.d.	n.d.			n.d.	n.d.
4 (089)	n.d.	12	n.d.	n.d.	160	n.d.		n.d.	22	29	
5 (169)	n.d.	259	n.d.	n.d.		n.d.		n.d.		339	
6 (027)	n.d.	54									

C. 24(S),25-EC in Cell fractions (pg/million cells)

Donor	Non-Activated	α -CD3/CD28 Activated (A)	α -CD3	α -CD28	50ng/ml PMA	1 μ M G δ 6983 + A	1 μ M BAY-11-7082 + A	10 μ M U0126 + A	10 μ M SB203580 + A	0.1 μ M Rapamycin + A	10 μ M LY294002 + A
1 (254)	n.d.	648					745	660	290		739
2 (047)	26	1,028					870		350		876
3 (009)	n.d.	1,716		n.d.	422	698	1,970			1,349	1,549
4 (089)	n.d.	186	89	n.d.	47	51		431	72	337	
5 (169)	n.d.	403	95	n.d.		41		288		448	
6 (027)	n.d.	306									

Table 7.4. Effect of different treatments to the quantified cholesterol and cholesterol precursors in the cell fractions of total CD4⁺ T cells after 48 hours in culture.

A. Cholesterol. B. Desmosterol. C. Dehydrocholesterol. D. Dehydrodesmosterol. Values were quantified using stable isotope dilution MS averaged over three injections then normalised to the number of cells extracted on day of harvest. “+A” indicates inhibitor treatments in anti-CD3/CD28 activating conditions.

A. Cholesterol in Cell fractions (ng/million cells)

Donor	Non-Activated	α-CD3/CD28 Activated (A)	α-CD3	α-CD28	50ng/ml PMA	1μM G66983 +A	1μM BAY-11-7082 +A	10μM U0126 +A	10μM SB203580 +A	0.1μM Rapamycin +A	10μM LY294002 +A
1 (254)	211	410					307	332	339		369
2 (047)	310	679					671		459		463
3 (009)	259	485		286	314	352	540			459	465
4 (089)	272	494	315	296	370	298		500	358	558	
5 (169)	165	593	336	331		390		438		736	
6 (027)	330	686									

B. Desmosterol in Cell fractions (ng/million cells)

Donor	Non-Activated	α-CD3/CD28 Activated (A)	α-CD3	α-CD28	50ng/ml PMA	1μM G66983 +A	1μM BAY-11-7082 +A	10μM U0126 +A	10μM SB203580 +A	0.1μM Rapamycin +A	10μM LY294002 +A
1 (254)	0.30	1.64					1.05	2.68	1.84		1.43
2 (047)	0.33	3.17					3.18		4.01		1.68
3 (009)	0.54	8.65		0.70	3.93	31.01	7.15			6.63	6.01
4 (089)	0.45	3.16	0.84	0.79	3.86	38.95		7.46	5.08	2.36	
5 (169)	0.30	5.48	1.51	1.05		29.19		5.15		4.52	
6 (027)	0.23	2.01									

C. Dehydrocholesterol in Cell fractions (ng/million cells)

Donor	Non-Activated	α-CD3/CD28 Activated (A)	α-CD3	α-CD28	50ng/ml PMA	1μM G66983 +A	1μM BAY-11-7082 +A	10μM U0126 +A	10μM SB203580 +A	0.1μM Rapamycin +A	10μM LY294002 +A
1 (254)	0.26	2.41					1.53	1.60	1.31		2.11
2 (047)	0.52	3.73					3.73		1.68		2.09
3 (009)	0.32	3.87		0.41	2.24	1.76	4.07			2.60	2.68
4 (089)	0.27	1.97	0.67	0.36	1.93	1.19		1.69	1.11	1.66	
5 (169)	0.17	3.26	1.26	0.53		1.57		1.64		2.83	
6 (027)	0.52	3.33									

D. Dehydrodesmosterol in Cell fractions (ng/million cells)

Donor	Non-Activated	α-CD3/CD28 Activated (A)	α-CD3	α-CD28	50ng/ml PMA	1μM G66983 +A	1μM BAY-11-7082 +A	10μM U0126 +A	10μM SB203580 +A	0.1μM Rapamycin +A	10μM LY294002 +A
1 (254)	0.22	0.63					0.99	0.84	0.34		1.41
2 (047)	0.38	0.35					0.37		0.26		1.24
3 (009)	0.57	1.20		0.88	4.76	2.45	2.66			1.98	2.94
4 (089)	0.22	0.35	0.64	0.38	2.68	0.47		0.44	0.16	0.50	
5 (169)	0.34	1.19	1.52	0.80		1.09		1.42		2.70	
6 (027)	0.42	0.78									

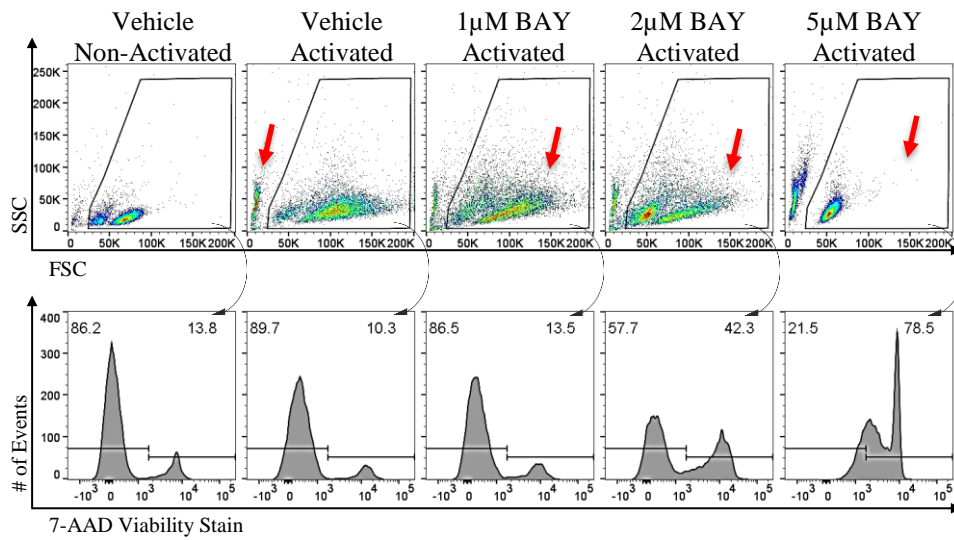


Figure 7.4. Cell viability analysis of 48 hour total CD4⁺ T cells treated without and with increasing concentrations of the NF-κB signalling inhibitor, BAY-11-7082.

Top panel. The FSC/SSC dot plot showing the increasing FSC and SSC signals of activated cells compared to non-activated. 5µM BAY-11-7082 completely prevented the increase in FSC/SSC signals. Bottom panel. 7-AAD⁺ cells after culture increased as the concentrations of treatments increased. 5µM and 2µM of BAY-11-7082 resulted to 78% and 42% 7-AAD⁺ cells, respectively, whilst 1µM were comparable to both non-BAY-11-7082-treated conditions. Events were gated on all cells which excludes activation beads and debris with very low FSC/SSC signals (red arrow).

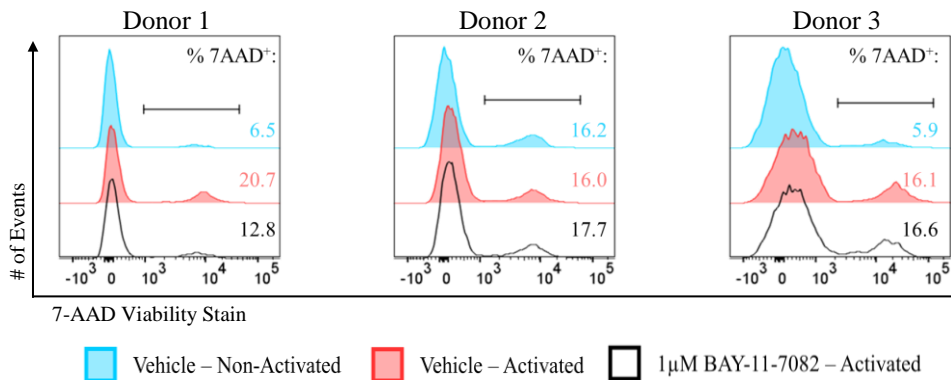


Figure 7.5. Half-offset overlay histograms comparing the viability staining for BAY-11-7082 treated CD4⁺ T cells after 48 hours across three donors.

No considerable cytotoxicity was induced by the treatment of 1µM BAY-11-7082. The level of cell death indicated by the incorporation of the 7-AAD viability stain in 1µM BAY-11-7082 treated activated cells (black open histograms) were similar to untreated cells (blue and red filled histograms). Events were gated on all cells which excludes activation beads and debris with very low FSC/SSC signals.

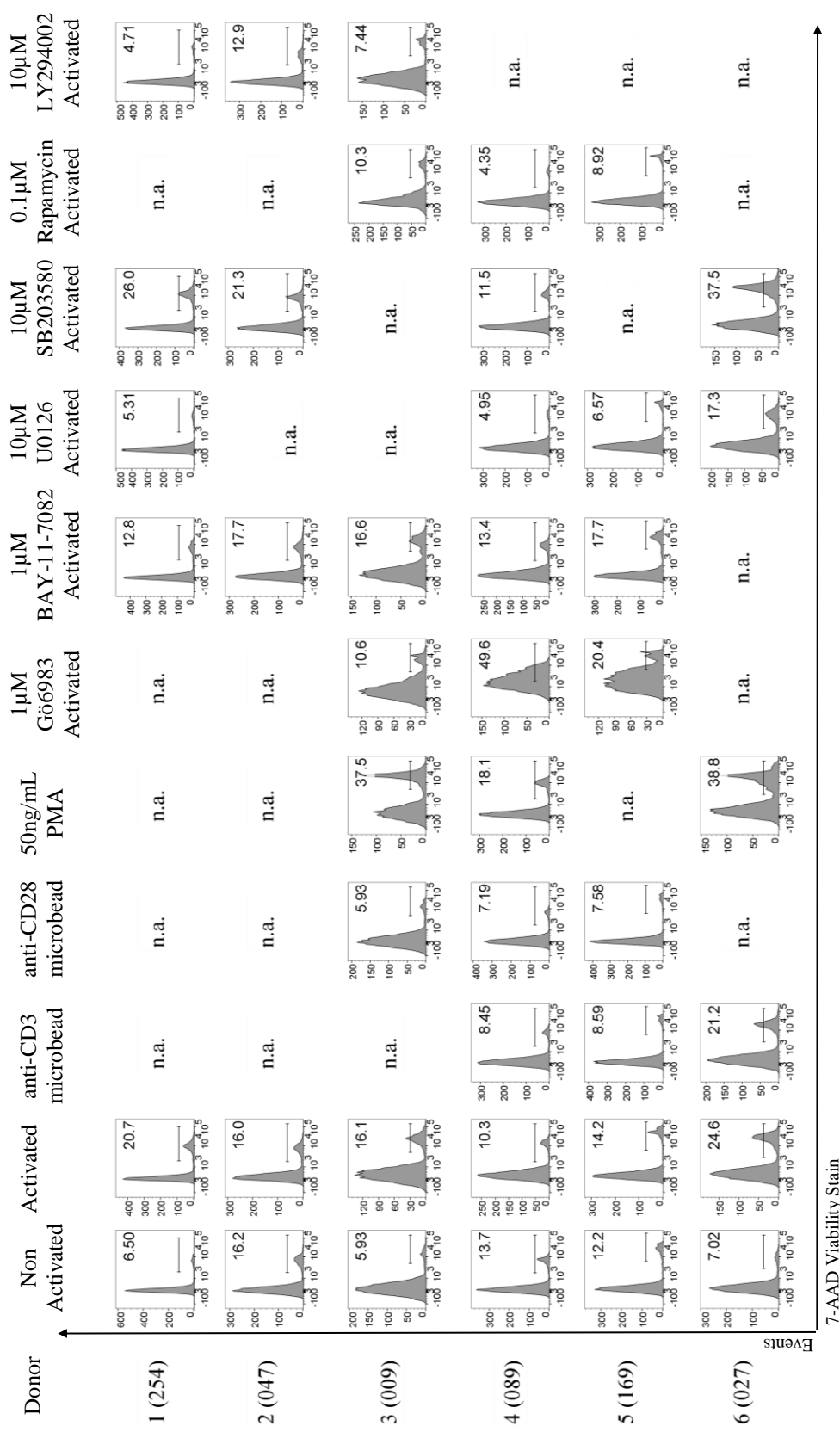


Figure 7.6. Cell viability analysis of 48 hour total CD4⁺ T cells with and without activation and/or inhibitor treatments. Most treatments did not lead to substantial cell death except PMA-stimulated cells. Viability of cells treated with Gö6983 was unquantifiable due to autofluorescence at the PerCP-Cy5.5 channel. Histograms were plotted from all cells which exclude debris and microbeads with very low FSC/SSC signals. Inset numbers inside each plot indicate the percentage of the gated 7-AAD⁺ cells.

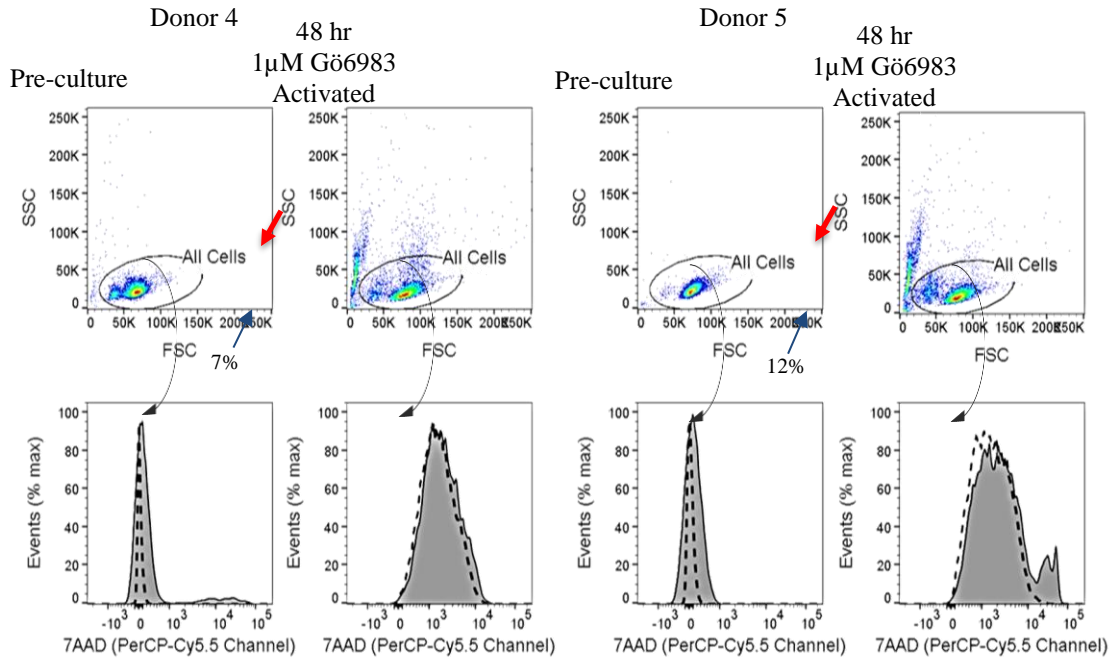


Figure 7.7. Cell viability analysis of pre-culture and 48 hour activated total CD4⁺ T cells treated with 1µM of the PKC inhibitor, Gö6983 reveals autofluorescence.

Top row. Ungated FSC/SSC dot plots of total CD4⁺ T cells before and after 48 hours of activation with Gö6983 treatment revealed a slight increase in cell size. Bottom row. Overlay histograms gated from 'All Cells' of unstained (dashed) and 7-AAD stained cells (filled) before and after 48 hour culture shows the cells acquire autofluorescence at the PerCP-Cy5.5 channel after Gö6983 treatment. Although this makes the quantification of 7-AAD⁺ cells less straightforward, the FSC/SSC plots show minor proportion (7% and 12%) of cells which were smaller in size suggestive of dead cells (left side of 'All Cells' gate - blue arrow). Gating was done to exclude activation microbeads (red arrow) added to the culture which were not removed prior to flow cytometry analysis.

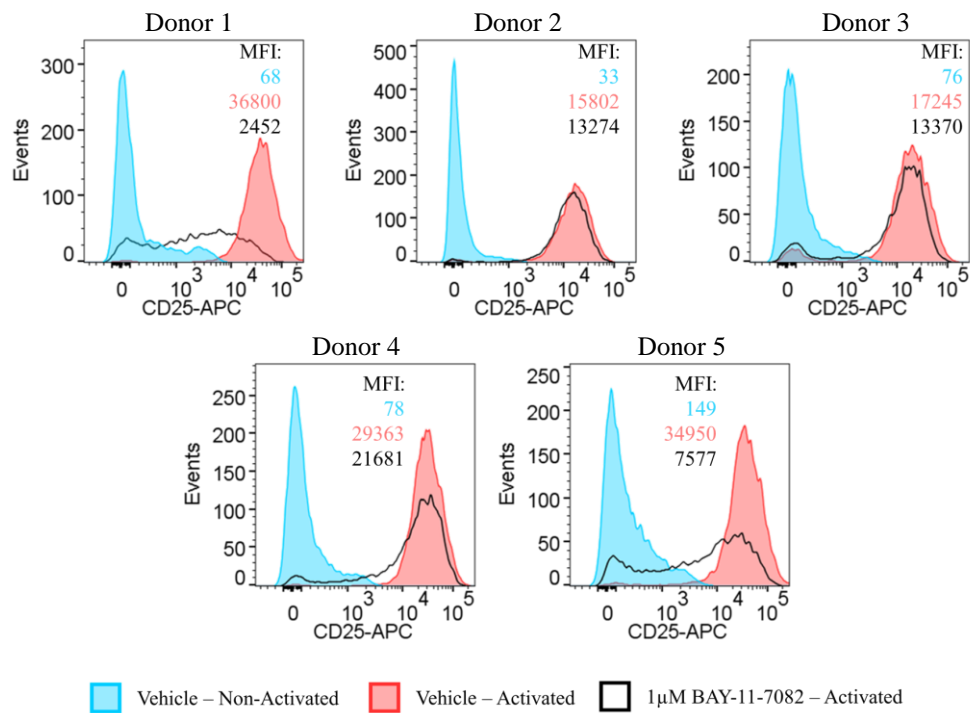


Figure 7.8. Overlay histograms of the CD25 expression of BAY-11-7082 treated total CD4⁺ T cells from five donors.

The effect of 1µM BAY-11-7082 on CD25 expression was inconsistent across five donors. On some donors (2, 3 and 4), CD25 of BAY-11-7082-treated cells (black open histograms) were similar to untreated activated cells (red filled histograms). However, for donors 1 and 5, lower CD25 expression can be evidently observed. Coloured inset numbers indicate the mean fluorescence intensities. Events were gated from live cells based on FSC/SSC signals and 7-AAD⁻ staining.

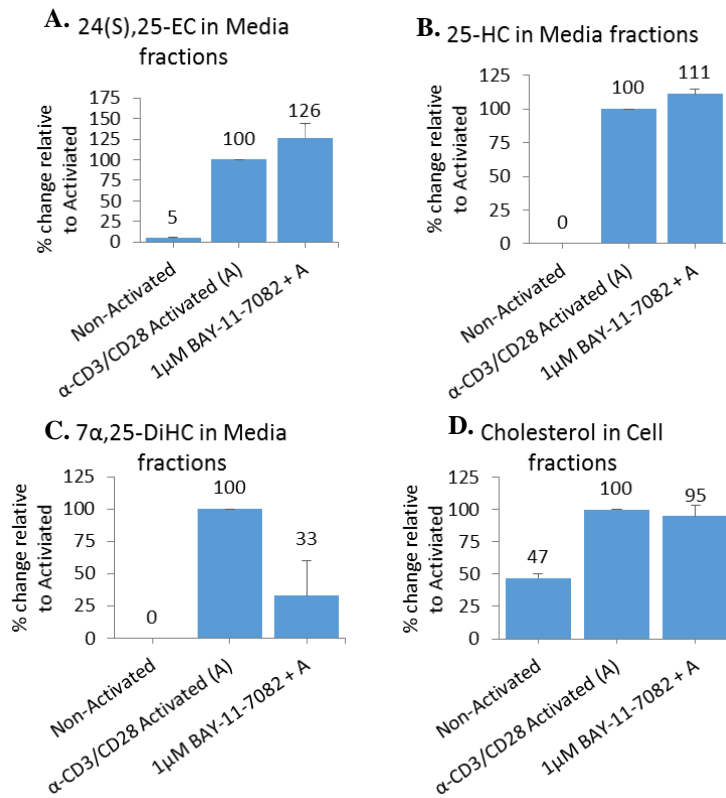


Figure 7.9. Detected sterols in the media and cell fractions of cultured total CD4⁺ T cells after 48 hours. A/B/D. The quantified 24(S)25-EC, 25-HC and intracellular cholesterol was similar between the BAY-11-7082 treated activated cells and untreated activated cells. C. The 7α,25-DiHC however was only detectable in donor 2 and not in donors 1 and 3 which made the average lower. Percentage values were relative to the quantified sterols in CD3/CD28 activated conditions and averaged for each donor taken from Table 7.2 and Table 7.4. Error bars denote s.e.m; n=3

7.3.5. U0126 inhibits CD25 expression but induces the production of 24(S),25-EC whereas SB203580 had an opposite effect.

Mitogen-activated protein (MAP) kinase signalling has been implicated in CD4⁺ T cells with roles from cell survival to proliferation and differentiation [10,11]. The inhibitors U0126 and SB203580 have been both reported to selectively inhibit MAPK kinases MEK1/2 and p38^{MAPK}, respectively [12,13].

Inhibition of MEK1/2 by U0126 treatment resulted in significantly ($p < 0.01$) marked reduction of CD25 expression based on MFI compared to non-treated activated total CD4⁺ T cells (Figure 7.10 top). In addition, U0126 treatment revealed a consistent increase, though not statistically significant, in detected 24(S),25-EC in the both cell and conditioned media fractions.

An opposite effect was observed with the inhibition of p38 MAPK with SB203580 in activated CD4⁺ T cells, where the 24(S),25-EC were reduced, but was not statistically significant, compared to untreated activated cells (Figure 7.11). Although visually similar to non-treated activated cells, the expression of CD25 in SB203580-treated activated cells were significantly lower ($p < 0.05$) than untreated activated cells based on unpaired T-test of CD25 MFI (Figure 7.10 bottom).

Intracellular cholesterol content in both U0126 and SB203580-treated cells were seen to be reduced compared to non-treated activated cells but was also not significant (Table 7.2 and Table 7.4)

7.3.6. 25-HC production was reduced with U0126 treatment but was increased with SB203580.

The production of 25-HC was observed to be significantly ($p < 0.05$) and markedly reduced in U0126-treated activated cells. On the contrary, SB203580-treated activated cells resulted in an increase in 25-HC production detected in the conditioned media fractions, although it did not reach significance (Figure 7.12).

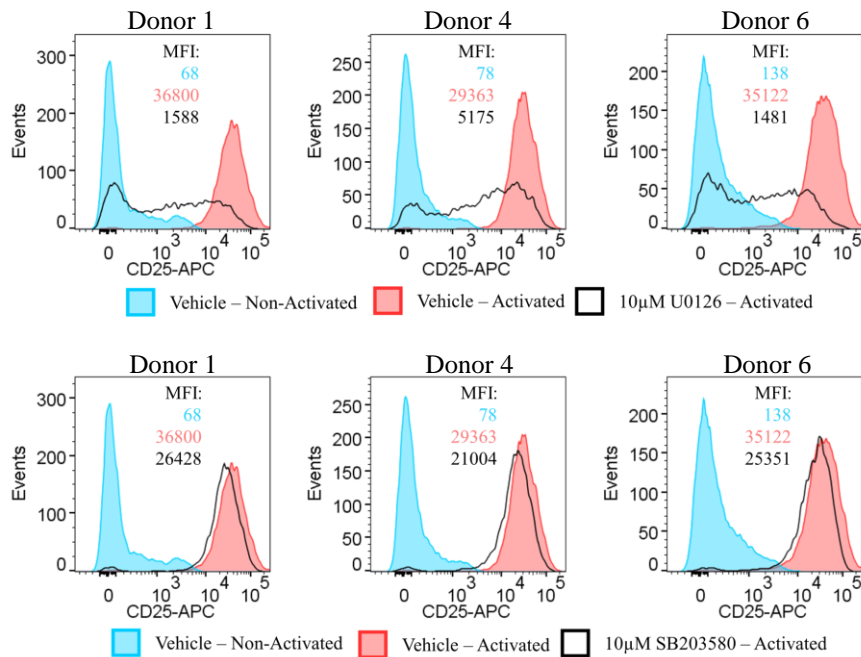


Figure 7.10. Overlay histograms of the CD25 expression of U0126 and SB203580 treated total CD4⁺ T cells from three donors.

Top row. 10µM U0126 treated activated cells (black open histograms) reproducibly had significantly reduced ($p < 0.01$) CD25 expression compared to untreated activated cells (red filled histograms). Bottom row. Treatment with 10µM SB203580 (black open histograms) slightly reduced the expression of CD25 but was still significantly lower ($p < 0.05$) the untreated activated cells (red filled histograms). Coloured inset numbers indicate the mean fluorescence intensities. Events were gated from live cells based on FSC/SSC signals and 7-AAD⁻ staining.

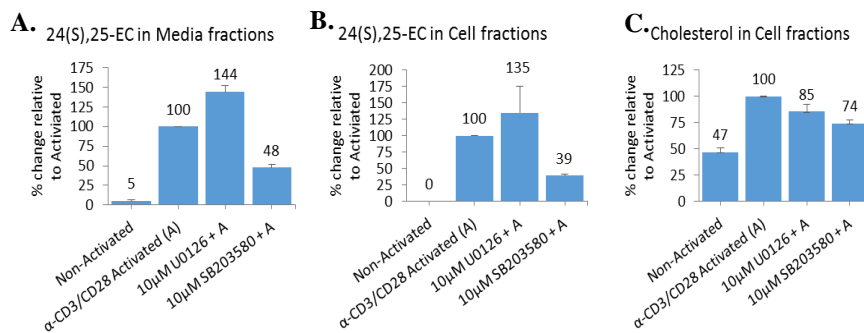


Figure 7.11. Detected 24(S),25-EC and intracellular cholesterol of U0126 and SB203580 treated activated total CD4⁺ T cells after 48 hours.

A/B. Although not statistically significant, activation of total CD4⁺ T cells with the treatment of U0126 saw an increased the production of 24(S),25-EC in both media and cell fractions but was reduced by SB203580. C. Both U0126 and SB203580 showed reduced intracellular cholesterol levels than non-treated activated cells. Percentage values were relative to the quantified sterols in CD3/CD28 activated conditions and averaged for each donor taken from Table 7.2, Table 7.3 and Table 7.4. Error bars denote s.e.m; n=3

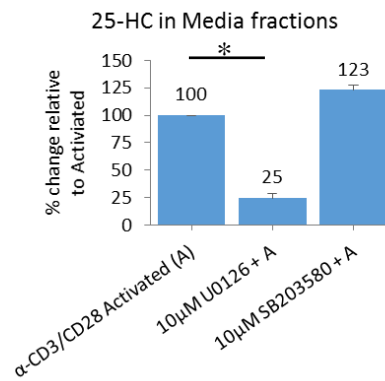


Figure 7.12. Detected 25-HC in media fractions of U0126 and SB203580 treated activated total CD4⁺ T cells after 48 hours.

U0126 treatment lead to significantly reduced production of 25-HC. In contrast, the effect of SB203580 treatment resulted in a slightly higher 25-HC production compared to CD3/CD28 activation alone. Percentage values were relative to the quantified sterols in CD3/CD28 activated conditions and averaged for each donor taken from Table 7.2. Error bars denote s.e.m; n=3. * $p \leq 0.05$

7.3.7. PMA induces greater production of 25-HC and 7 α ,25-DiHC than CD3/CD28 stimulation but does not fully induce CD25 expression or cholesterol biosynthesis

CD3/CD28 stimulation induces downstream signalling pathways that eventually activate Protein Kinase C (PKC). The treatment of PMA bypasses the need for activation signals upstream of PKC by directly inducing its phosphorylation resulting to the induced activation of T cells^[14]. This mode of cell activation resulted in 3.4 times higher production of 25-HC and 4.7 times higher 7 α ,25-DiHC but with less 24(S),25-EC or intracellular cholesterol compared to CD3/CD28-activation (Figure 7.13). However, the PMA stimulated cells revealed a variable but statistically significant ($p < 0.05$) reduction in CD25 expression compared to CD3/CD28 stimulation based on MFI values (Figure 7.14). This suggests that PKC stimulation through PMA does not fully induce cholesterol biosynthesis the same way as with CD3/CD28 stimulation, but can activate pathways leading to 25-HC and 7 α ,25-DiHC production.

7.3.8. Gö6983 prevents the activation of CD3/CD28 stimulated total CD4⁺ T cells and accumulates intracellular desmosterol

In addition to activating PKC signalling directly by PMA and indirectly by CD3/CD28-stimulation, its inhibition was also explored using Gö6983 in CD3/CD28 activating conditions. Gö6983 treatment of CD3/CD28-stimulated CD4⁺ T cells at 1 μ M completely prevented the activation-induced CD25 surface expression (Figure 7.14). Consistent with the failure of cells to activate, 25-HC and 7 α ,25-DiHC were also undetectable which were similar to untreated non-activated cells (Figure 7.13). Less 24(S),25-EC and intracellular cholesterol was observed when compared to CD3/CD28-activated cells, which adds weight to the importance of PKC in T cell activation. In addition, it suggests that activation is required for induced cholesterol biosynthesis. However, treatment with Gö6983 of activated cells led to a significant accumulation of intracellular desmosterol 7 times higher compared to activation alone.

This drastic increase in intracellular desmosterol was specific to PKC inhibition and was not observed with any other inhibitor treatments (Figure 7.15).

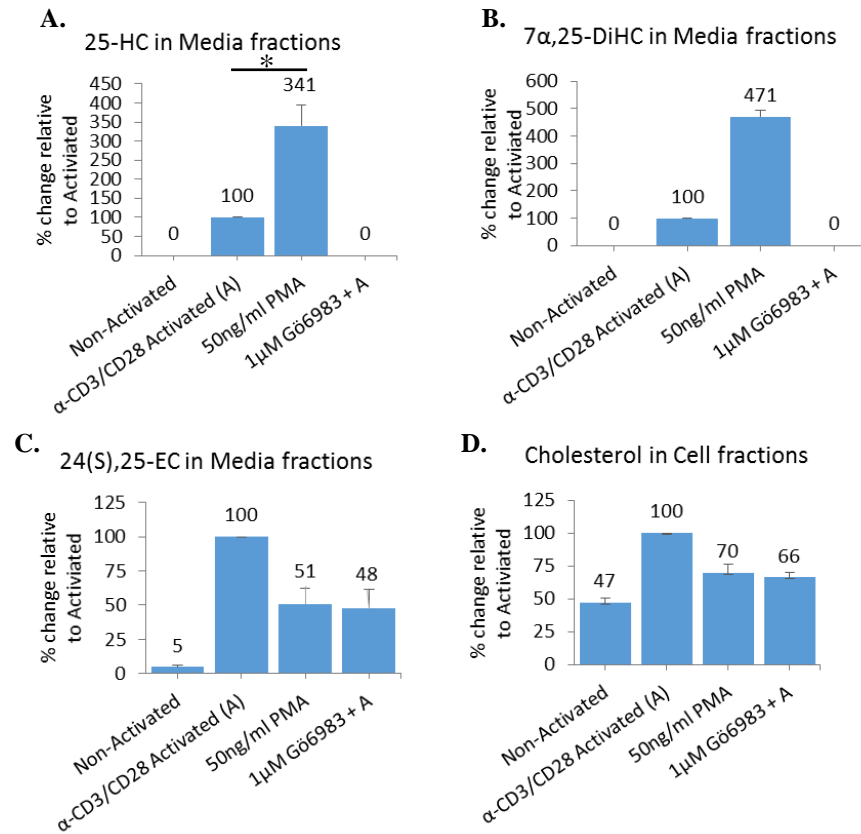


Figure 7.13. Detected sterols in media and cell fractions of PMA and Gö6983 treated total CD4⁺ T cells after 48 hours.

A/B. PMA treatment caused a 3.4x and 4.7x increase in the detected 25-HC and 7 α ,25-DiHC, respectively, in media fractions compared to CD3/CD28-activation. On the other hand, Gö6983 treatment resulted in undetectable levels even with CD3/CD28 stimulation. C/D. The production of 24(S),25-EC was moderately induced with PMA treatment which were reflective of the intracellular cholesterol levels which was similar to Gö6983-treated activated cells. Percentage values were relative to the quantified sterols in CD3/CD28 activated conditions and averaged for each donor. Error bars denote s.e.m; n=3. * $p \leq 0.05$

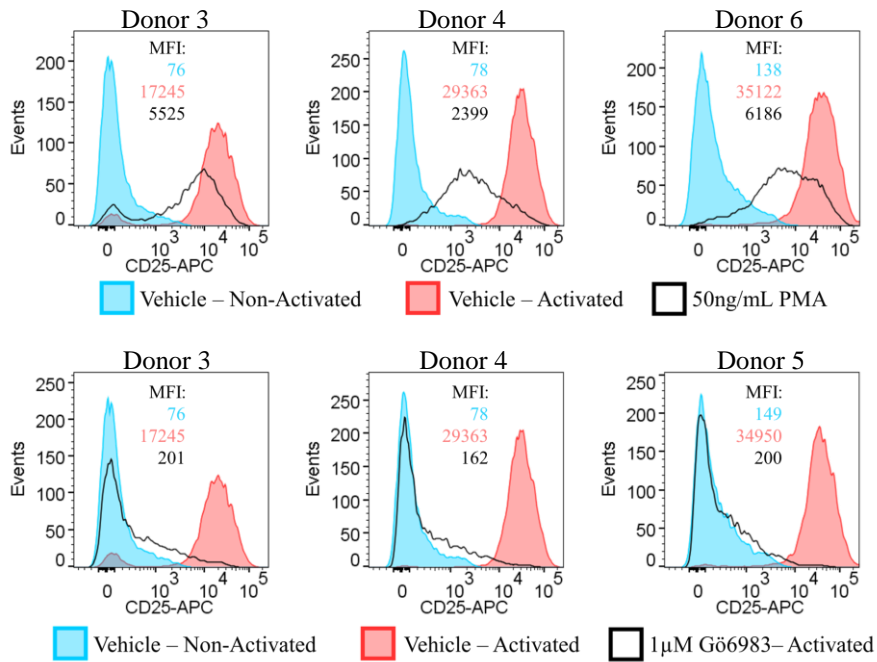


Figure 7.14. Overlay histograms of the CD25 expression of PMA-stimulated and Gö6983 treated total CD4⁺ T cells from three donors.

Top row. T cell stimulation by PMA treatment resulted in variable but significantly lower ($p=0.04$) expression levels of CD25 compared to CD3/CD28 stimulation. Bottom row. CD3/CD28-stimulation in the presence of 1µM Gö6983 consistently prevented the activation-induced expression CD25 leading to levels similar to non-activated cells. Coloured inset numbers indicate the mean fluorescence intensities. Events were gated from live cells based on FSC/SSC signals and 7-AAD⁻ cells.

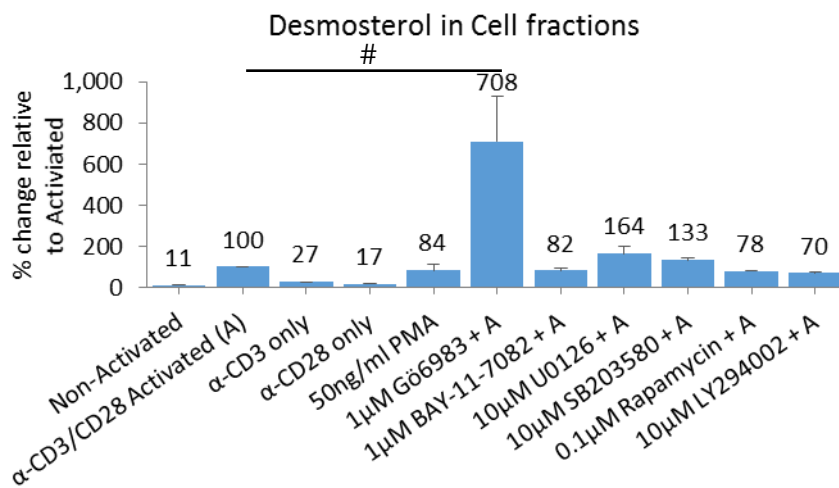


Figure 7.15. Detected cholesterol precursor, desmosterol, in cell fractions of total CD4⁺ T cells after 48 hours with different culture conditions.

Desmosterol was observed to be greatly detected in activated cells with 1µM of Gö6983 compared to activated alone. Marginal increase were observed in treatments with U0126 and SB203580 whereas Rapamycin and LY294002 resulted in a slight decrease relative to activated alone. Percentage values were relative to the quantified sterols in CD3/CD28 activated conditions and averaged for each donor. Error bars denote s.e.m; n=3. # $p \leq 0.01$

7.3.9. Treatment with PI3K inhibitor, LY294002, with CD3/CD28-stimulation had no effect on CD25 expression and sterol production.

PI3K signalling become activated very early upon CD3/CD28 stimulation which initiates the AKT/PKB pathway to promote cell survival and growth^[15]. However, PI3K inhibition in total CD4⁺ T cells by 10 μ M LY294002 in activated conditions did not see a significant reduction in CD25 expression (Figure 7.16), though a tendency for CD25 expression to decrease was observed.

Due to this, the inhibitory activity of LY294002 was tested by assessing the phosphorylation of its downstream target, ribosomal protein S6. LY294002 treatment at 10 μ M of CD4⁺ T cells in activating conditions saw a reduction in phosphorylated-S6 compared to activation alone, although it did not reach significance. (Figure 7.17 top).

In line with this, intracellular cholesterol, 24(S),25-EC, 25-HC and 7 α ,25-DiHC production also did not see any significant change compared to untreated activated cells (Figure 7.18).

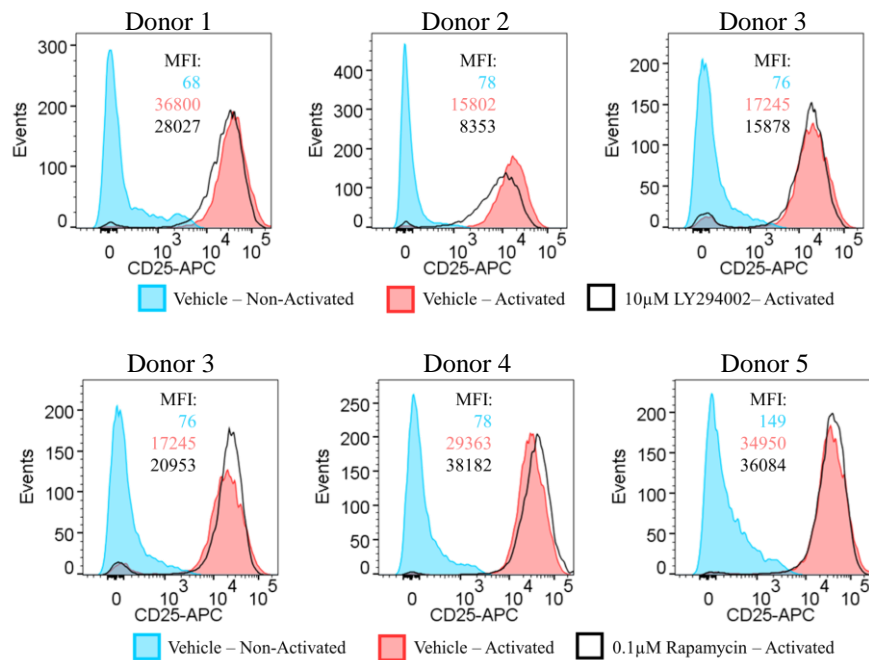


Figure 7.16. Overlay histograms of the CD25 expression of LY294002 and Rapamycin treated total CD4⁺ T cells from three donors.

Top row. Activated cells in the presence of 10µM LY294002 did not see a significant reduction on CD25 expression compared to activated alone based on MFI. Bottom row. Conversely, treatment of 0.1µM Rapamycin in activating conditions also did not see a significant increase in the expression of CD25. Coloured inset numbers indicate the mean fluorescence intensities. Events were gated from live cells based on FSC/SSC signals and 7-AAD⁻ staining.

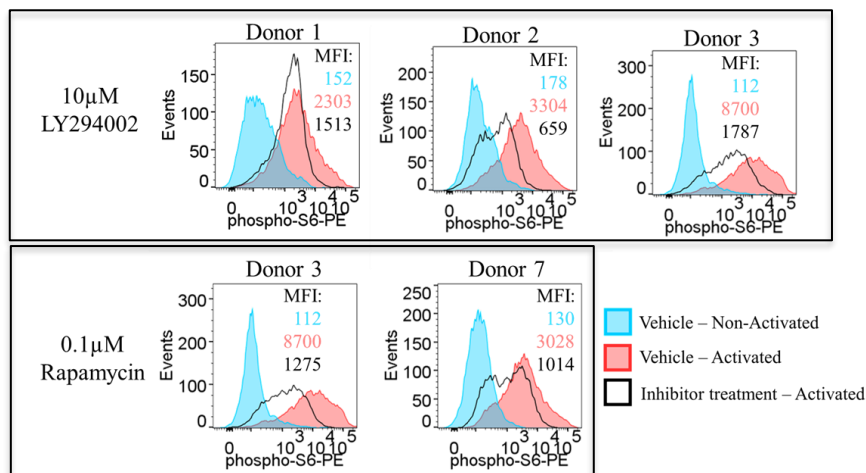


Figure 7.17. Overlay histograms of the ribosomal S6 phosphorylation in total CD4⁺ T cells after 48 hours.

Top row. The phosphorylation of S6 was reduced in the presence of LY294002 compared to activated alone, but did not reach significance. Bottom row. Activated cells treated with 0.1µM Rapamycin revealed a reduction on pS6, although significance cannot be tested due to only two replicates.

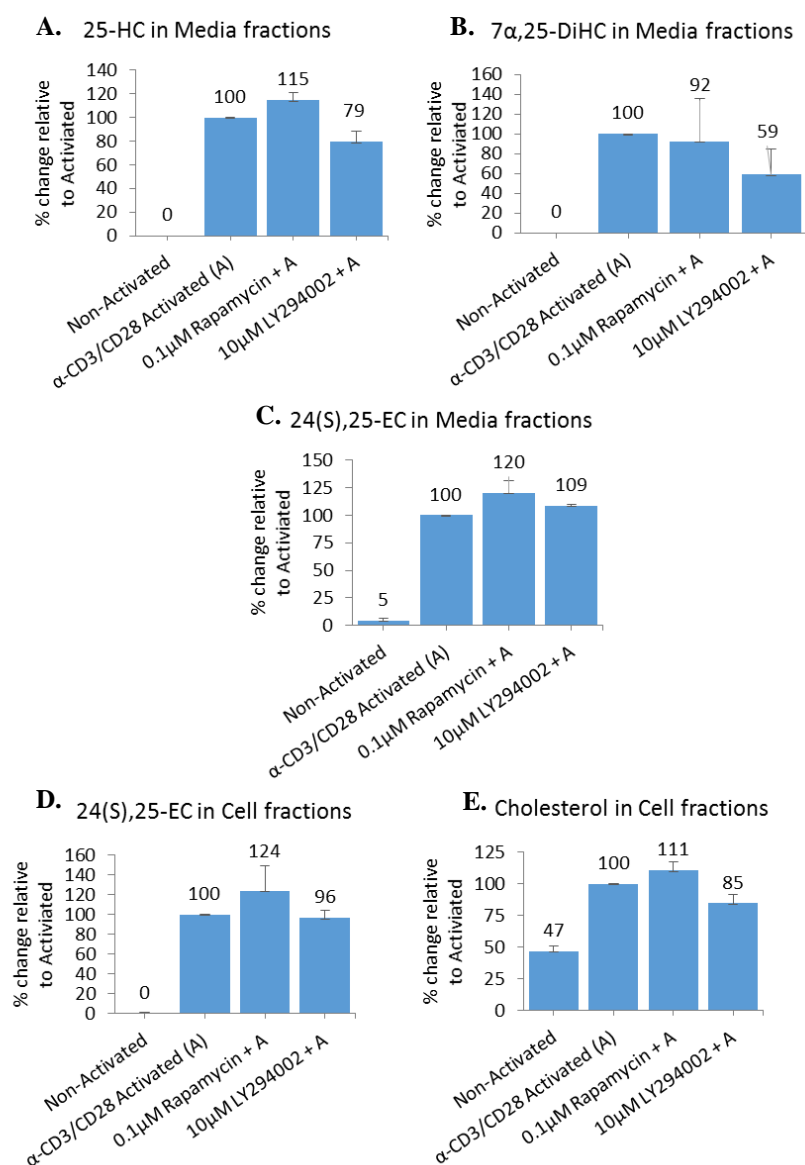


Figure 7.18. Detected sterols in media and cell fractions of Rapamycin and LY294002 treated total CD4⁺ T cells after 48 hours.

A/B. Rapamycin and LY294002 treatment of activated cells did not see any statistically significant change in the production of 25-HC and 7α,25-DiHC compared to activated alone. C/D. The same trend was observed in the generation of 24(S),25-EC between cell and media fractions where rapamycin caused a slight increase but no effect from LY294002. E. Intracellular cholesterol was also seen to be slightly accumulated in rapamycin treated cells but was marginally reduced with LY294002. Percentage values were relative to the quantified sterols in CD3/CD28 activated conditions and averaged for each donor. Error bars denote s.e.m; n=3

7.3.10. Rapamycin inhibition of mTORC1 in CD3/CD28 activated CD4⁺ T cells had no effect in CD25 expression and sterol production.

The mammalian target of rapamycin complex 1 (mTORC1) has been reported to be activated by the PI3K/Akt signalling pathway, which then activate the components of translation machinery to promote protein synthesis^[16] and regulate cholesterol biosynthetic gene expression^[17,18]. Thus, inhibition of the PI3K may also affect mTORC1 targets and inhibition of either should have the similar cellular effects.

Similar to LY294002 treatments, rapamycin at 0.1 μ M did not show a statistically significant change in expression of CD25 compared to activated alone (Figure 7.16), but a contrasting tendency was observed where CD25 expression was increased with rapamycin treatment. In accordance with this, the production of 25-HC, 24(S),25-EC and intracellular cholesterol accumulation in activated cells were also similar to non-treated cells even in the presence of rapamycin after 48 hours (Figure 7.18).

7.3.11. Phosphorylation of ribosomal S6 was reduced with Rapamycin and LY294002 but was not significant.

Some of the main translation-related targets of mTORC1 activation are the S6K/ribosomalS6 and 4E-BP1/eIF4E pathway^[19,20]. The result where rapamycin treatment did not significantly affect cell activation led to the supposition that the inhibitor may not be acting on its target, mTORC1. To assess this, phosphorylation of the ribosomal S6 was monitored in activated total CD4⁺ T cells in the presence or absence of some inhibitors. Similar to a previous study^[21], intracellular staining of 10 μ M LY294002-treated or 0.1 μ M rapamycin-treated activated cells revealed a reduction in phosphorylated S6 protein compared to non-treated activated cells, though statistical significance was not reached or was not tested (n=2), respectively (Figure 7.17 bottom).

7.3.12. Dual mTORC inhibition by Ku63794 dose-dependently reduced CD25 expression together with pS6, p4E-BP1 and 25-HC but not 24(S),25-EC.

The protein kinase mTOR can be assembled as two distinct protein complexes, namely: mTORC1 and mTORC2. In contrast to mTORC1, mTORC2 sits upstream of the AKT pathway where mTORC1 is an indirect downstream target (Figure 7.1). This suggests that mTORC1 may be activated indirectly by mTORC2. Furthermore, whereas mTORC1 is rapamycin-sensitive, mTORC2 has been reported to be insensitive in short-term cultures^[22,23]. For this, the dual mTOR-inhibitor Ku63794 was used to assess the effect of inhibiting both mTOR complexes^[24,25].

The inhibition of both mTORC1 and mTORC2 in activated cells with the use of Ku63794 caused a dose-dependent reduction in phosphorylation of S6 in addition to 4E-BP1 and CD25 expression (Figure 7.19). The production of 25-HC but not of 24(S),25-EC was reduced with 5 μ M Ku63794 (Figure 7.20). This data suggests that the production of 25-HC may be linked to mTORC2 but not mTORC1 and that production of 24(S),25-EC or cholesterol biosynthesis can still be induced without mTORC1 or mTORC2.

7.3.13. Ku63794 and Rapamycin treatment augmented HMGCR mRNA expression but not SREBP2 in activated total CD4⁺ T cells

Cells from donor 7 after culture was extracted for RNA to compare the expression of cholesterol biosynthesis genes, *SREBP2* and *HMGCR*. RT-PCR analysis showed neither Ku63794 nor Rapamycin affected the mRNA expression of *SREBP2* (Figure 7.21). On the other hand, the expression of a downstream SREBP2 target, *HMGCR* was seen to be further induced in activated cells in the presence of rapamycin. This effect was also observed with Ku63794 treatment although at a lesser extent. This result suggests that inhibition of mTOR complexes may result in the activation of another pathway which may affect *HMGCR* mRNA levels.

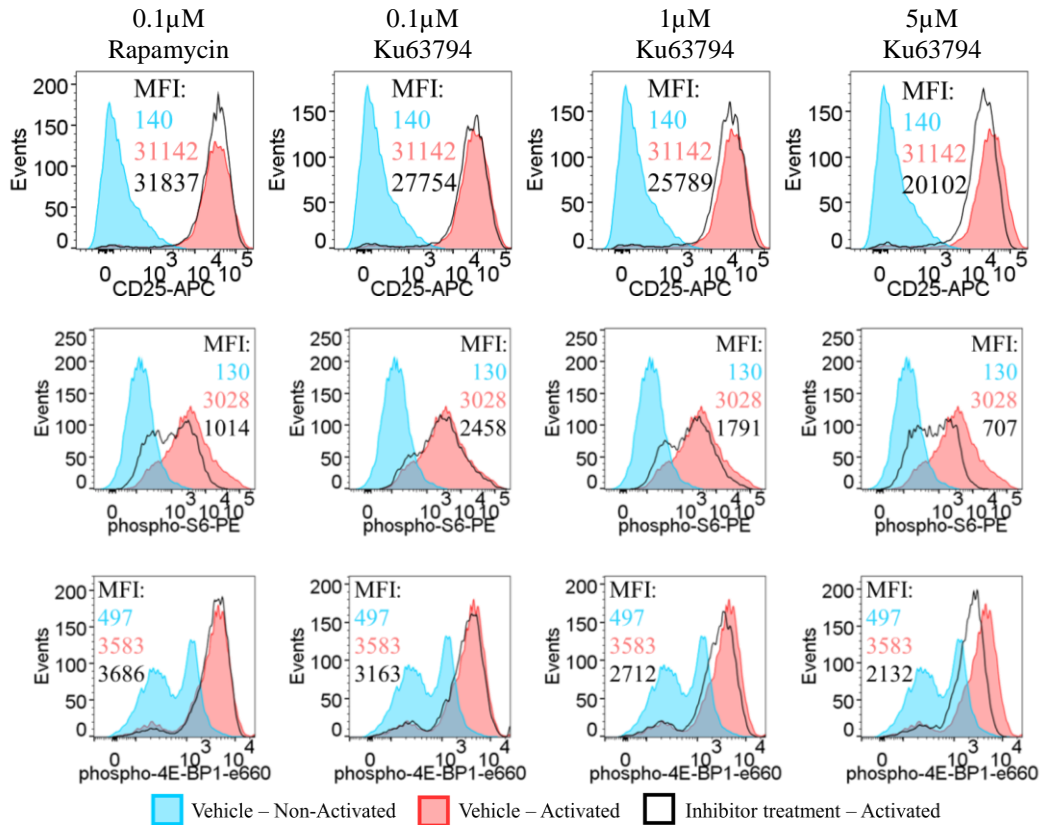


Figure 7.19. Overlay histograms of CD25, pS6 and p4E-BP1 in total CD4+ T cells treated with rapamycin and Ku63794 after 48 hours for donor 7.

Top row. Similar to previous rapamycin-treated activated cells, the CD25 expression was not repressed with mTORC1 inhibition. However, dual mTORC1/2 inhibition by Ku63794 treatment showed a decrease in CD25 in higher (5µM) concentrations. Middle row. As before, phospho-S6 dropped with mTORC1 inhibition with 0.1µM rapamycin. In addition, pS6 also reduced dose-dependently with Ku63794. Bottom row. Non-activated cells were observed to have two levels of 4E-BP1 hypophosphorylated states. Activation of the cells was seen induce hyperphosphorylation of the repressor protein. In contrast to pS6, the phosphorylation state of 4E-BP1 in the presence of 0.1µM rapamycin compared to activated alone was similar. However, Ku63794 dose-dependently reduced p4E-BP1 similar to pS6.

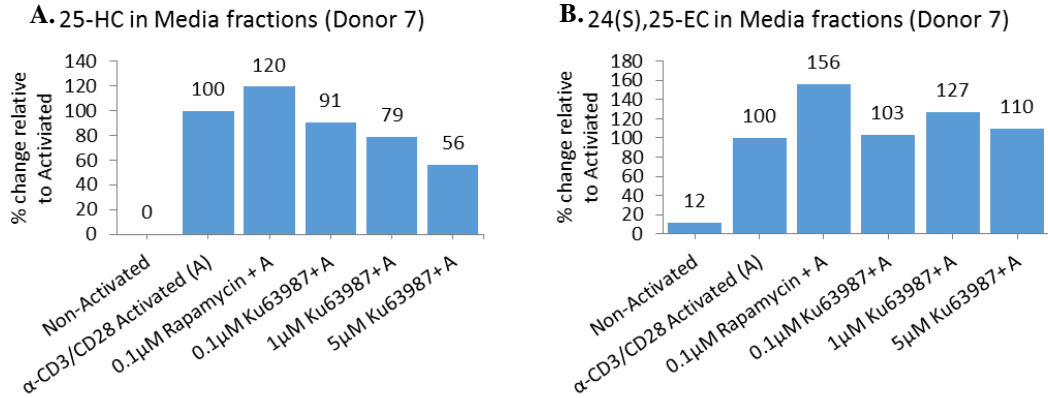


Figure 7.20. Detected sterols in media of Rapamycin and Ku63794-treated total CD4⁺ T cells after 48 hours of donor 7.

Dual mTOR inhibition led to the dose-dependent reduction in 25-HC production (A) of activated cells but not 24(S),25-EC (B) whereas rapamycin-treatment followed the same increased tendency as before compared to activated alone.

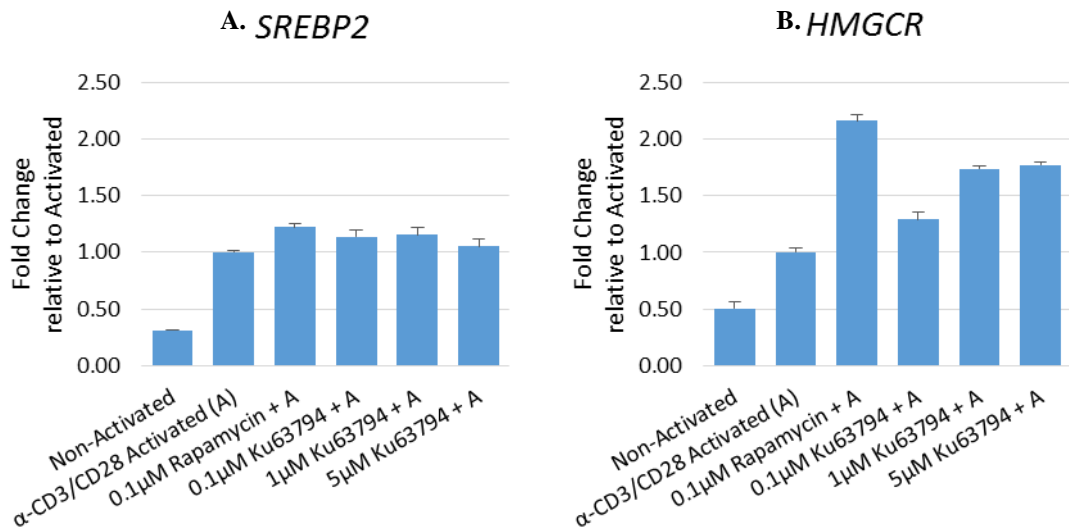


Figure 7.21. Real-time PCR analysis of donor 7 48 hour total CD4⁺ T cells with mTORC inhibitors. A. activated cells showed an increased expression of *SREBP2* compared to non-activated cells whereas treatment of either Rapamycin or Ku63794 did not affect the expression of *SREBP2* compared to activated alone. B. *HMGCR* expression was also increased in activated cells compared to non-activated cells. Treatment of Rapamycin in activating conditions, and to a lesser extent Ku63794, further increased *HMGCR* expression. Error bars denote s.e.m of the technical triplicates.

7.4. Discussions

After engagement of cognate antigens to TCR with proper co-stimulation in T cells, several signalling pathways are activated leading to cell growth, survival and proliferation. In this chapter, the effect of the inhibition of different protein kinases which direct these signalling pathways were investigated in relation to cholesterol metabolism and oxysterol production.

Experiments with sub-optimal stimulation using CD3 or CD28 alone revealed the importance of co-stimulation to initiate ideal T cell activation via CD25 expression, accumulation of intracellular cholesterol and the production of oxysterols. Early studies on the effect of T cell co-stimulation revealed that aggregation of sphingolipid-cholesterol-rich rafts at the TCR contact site were present upon dual stimulation^[26]. Whereas CD28 stimulation alone did not induce any T cell activation or sterol production in the current study, stimulation with CD3 alone did increase the expression of CD25 marker and production of 24(S),25-EC was detectable after 48 hours, although relatively lower compared to dual stimulation. T cells are known to undergo anergy in response to inadequate stimulation, especially when lacking co-stimulation^[27]. CD3 signalling triggers Ca^{2+} influx which induces expression of anergy-associated genes via calcineurin/NF-AT signalling and CD28 stimulation counter acts anergy commitment by also activating NF- κ B and AP-1 transcription factors to promote IL-2 production^[28,29]. Studies have reported NF-AT transcription of IL-2 following anti-CD28 stimulation independent of CD3 ligation^[30]. In contrast, a more recent study using mice splenic T cells reported induction of cholesterol synthesis-related genes to be similar between CD3 stimulation alone and CD3/CD28 co-stimulation^[17]. Although stimulation of anti-CD28-loaded microbeads alone in the current study did not lead to any observable difference compared to non-stimulated cells, stimulation by a mitogenic anti-CD28 antibody without CD3 engagement has been reported to induce PLC γ , PKC θ /NF- κ B signalling and Ca^{2+} flux in rat T cells compared to a conventional anti-CD28 antibody^[31]. In the current experiments, the production of 25-HC, 7 α ,25-diHC and intracellular cholesterol accumulation was

observable only in CD3/CD28 stimulated cells. Collectively, these suggest that primary CD4⁺ T cells may require dual stimulation in inducing intracellular pathways to fully express CD25 and augment cholesterol synthesis and metabolism.

As well as directing a wide range of effector T cell responses^[32], NF- κ B signalling has been implicated in the control of the T cell survival gene Bcl-xL^[33]. Activated T cells rely on sustained NF κ B activity for protection against activation-induced cell death^[34]. The lack of pro-survival signals may explain why increased concentrations of BAY-11-7082 led to considerable cell death in CD3/CD28-stimulated cells after 48 hours (Figure 7.4). Whereas the sub-toxic dose of 1 μ M did not result to extensive T cell death, it also did not have any substantial effect in both CD25 expression and sterol production. This result may suggest that signalling events triggered by anti-CD3/CD28-loaded microbeads can overcome the inhibition by BAY-11-7082 at such low concentrations or that other ways of NF- κ B nuclear translocation were present which bypass BAY-11-7082 actions.

Another pathway triggered downstream of CD3/CD28 is the MAPK signalling cascade which includes MEK/ERK and p38^{MAPK}^[11,35]. Our results indicate that increased CD25 expression and 25-HC production may be regulated by MEK1/2 signalling as these were reduced when MEK1/2 activity was inhibited. It was interesting that even though cells were less activated with U0126 treatment, production of 24(S)25-EC was actually stimulated but only slightly increased the levels of intracellular cholesterol. Although belonging to the same family of MAP kinases, p38 are stress-activated rather than growth factor activated. It was therefore not surprising to see different consequences in their signalling inhibition. As SB203580 did not affect the activation of T cells or 25-HC production but reduced both intracellular cholesterol levels and 24(S),25-EC, this may indicate a role of p38^{MAPK} in cholesterol biosynthesis. This can be considered a further indication that the level of T cell activation correlates with 25-HC production and that these two are regulated separately from cholesterol biosynthesis. It may also be possible that the use of an inhibitor of one pathway leads to the activation of another, where a study using SB203580 treatment on mouse 3T3 and human 293 cells resulted in activation of Raf^[36], an upstream activator

MEK/ERK^[37]. If these effects apply to primary CD4⁺ T cells as well and if MEK1/2 does have influence in 25-HC production, SB203580 may further increase CD3/CD28-induced Raf/MEK/ERK signalling leading to marginal increase in 25-HC compared to activated alone observed in the current study (Figure 7.12).

Inconsistencies between the present study and published literature arose with LY294002 and Rapamycin treatments. Signalling by mTOR complexes (mTORC) has been reported to regulate cholesterol biosynthetic gene expression in cell lines^[38] and differential activation of either mTORC1 or mTORC2 were needed to promote specific T helper subsets^[39]. In primary total CD4⁺ T cells of the current study, both CD25 expression and sterol profiles of rapamycin-treated activated cells were comparable to non-treated activated cells (Figure 7.16Figure 7.18). This suggests that mTORC1 may not important in CD4⁺ T cell CD25 expression or 25-HC production when stimulated via CD3/CD28. Others have demonstrated a differential effect of rapamycin inhibition on CD25 expression when T cells were activated by various stimuli which reported CD25 expression via activated PKC (using PMA) was rapamycin-resistant but the activation via CD3 or ionomycin was rapamycin-sensitive^[40]. Building upon this, it is probable that CD25-expression via CD3/CD28 co-stimulation may also be rapamycin-resistant as co-stimulation can induce stronger TCR signalling and PKC activation. On closer inspection, MFI of CD25 and detected 25-HC was comparable if not even slightly induced in activated T cells in the presence of rapamycin consistently across different donors (Figure 7.16Figure 7.18). This may be attributed to a negative feedback loop triggered by rapamycin-induced mTORC1/S6K inhibition which activates PI3K/AKT signalling reported to be present in cell lines^[41].

Situated higher up the pathway, PI3K activation occurs very early upon CD3/CD28-stimulation and with both PI3K and mTOR belonging to the same family of signalling kinases^[19,42] their activation eventually leads to increased protein translation which is a characteristic of activated and proliferating cells. Multiple groups have demonstrated PI3K induction after CD28 ligation independent from CD3 stimulation^[43-45]. Inhibition of PI3K by LY294002 has been reported to inhibit cell growth and proliferation but does not block the activation-induced upregulation of

CD25 in mice CD8⁺ cells^[46], which agrees with the results of the current study (Figure 7.16). T cell proliferation was not monitored or quantified in the current study but cell size of LY294002-treated activated cells were observed to be slightly smaller compared to non-treated activated cells (Figure 7.22) at the same 48-hour time point.

Rapamycin with along with PI3K inhibitors: wortmannin and LY292002 has been shown to disrupt the phosphorylation of 4E-BP1 in B-cell stimulated T cells^[19]. Although this report does not agree with the results of the current study (Figure 7.19), Freeley et al. showed that rapamycin does not affect the activity of PKC θ induced by either PMA treatment or anti-CD3/CD28 stimulation and further revealed that inhibiting PI3K with LY294002 results in the blockade of PKC θ phosphorylation^[47].

Most signalling pathways induced after CD3/CD28-stimulation appear to also result in the activation of PKCs. PKC isoenzymes have been reported to translocate from the cytosol to the membrane after PMA treatment and influence IL-2 gene activation^[48] although not the expression of high affinity IL-2R^[49] which can contribute to an auto inductive positive feedback loop. Studies with co-cultures identified the theta isoform being specific in T cells which are recruited in the immunological synapse via membrane bound diacylglycerol (DAG)^[50,51]. The result of PMA treatment closely associates activated PKC signalling and its downstream targets in the production of both 25-HC and 7 α ,25-diHC. As the detected 25-HC and 7 α ,25-diHC was higher when PKC was directly induced than indirectly via CD3/CD28, it was apparent that 25-HC may be regulated by PKC. Even with increased 25-HC production, PMA-activated cells had less IL-2R expression and reduced cholesterol biosynthesis compared to CD3/CD28-stimulated cells (Figure 7.13). A similar study reported that constant PMA exposure (>24hrs) resulted in inhibited T cell IL2R expression and diminished proliferative ability^[49]. In addition, PMA treatment was inconsistent with the correlation of increased 25-HC production together with increased levels of CD25 expression seen in Chapter 5. As the current study did not include Ionomycin treatment, PMA stimulation alone should have only activated novel PKC isoenzymes (δ, ϵ, θ) which only require DAG without Ca²⁺ flux and not conventional PKCs (α, β, γ) which needs both. In this sense, 25-HC production may be narrowed down to regulation by novel PKCs in human CD4⁺ T cells. Inhibition by Gö6983 completely blocked 25-HC

production which may be a consequence of either inactive PKC signalling or the failure of the T cells to activate in general; or perhaps there were other non-specific effects of PKC inhibitors like DHCR24 activity downregulation^[52], resulting in desmosterol accumulation. However, it was still apparent that other pathways triggered by CD3/CD28 were still induced which led to a modest increase in 24(S),25-EC and intracellular cholesterol. In all, it was evident that PMA-triggered pathways were strong in inducing 25-HC but weak in cholesterol biosynthesis.

In summary, the CD3/CD28 stimulation of total CD4⁺ T cells and simultaneous inhibition of major signalling pathways have indicated links in TCR signal transduction pathways and cholesterol metabolism. Most interestingly, PKCs may have an important role in the conversion of cholesterol to 25-HC, and also its further metabolism to 7 α ,25-DiHC. In addition, two MAPK signalling cascades differentially influenced sterol metabolism with MEK/ERK appearing to be involved in T cell activation and 25-HC production but not cholesterol biosynthesis whereas p38 MAPK affects cholesterol biosynthesis and not 25-HC.

To confirm these results, activating each of these signalling pathways by specific pharmacological activators independently of CD3/CD28 stimulation and monitoring changes in sterol metabolism may be a good direction to take for further investigation.

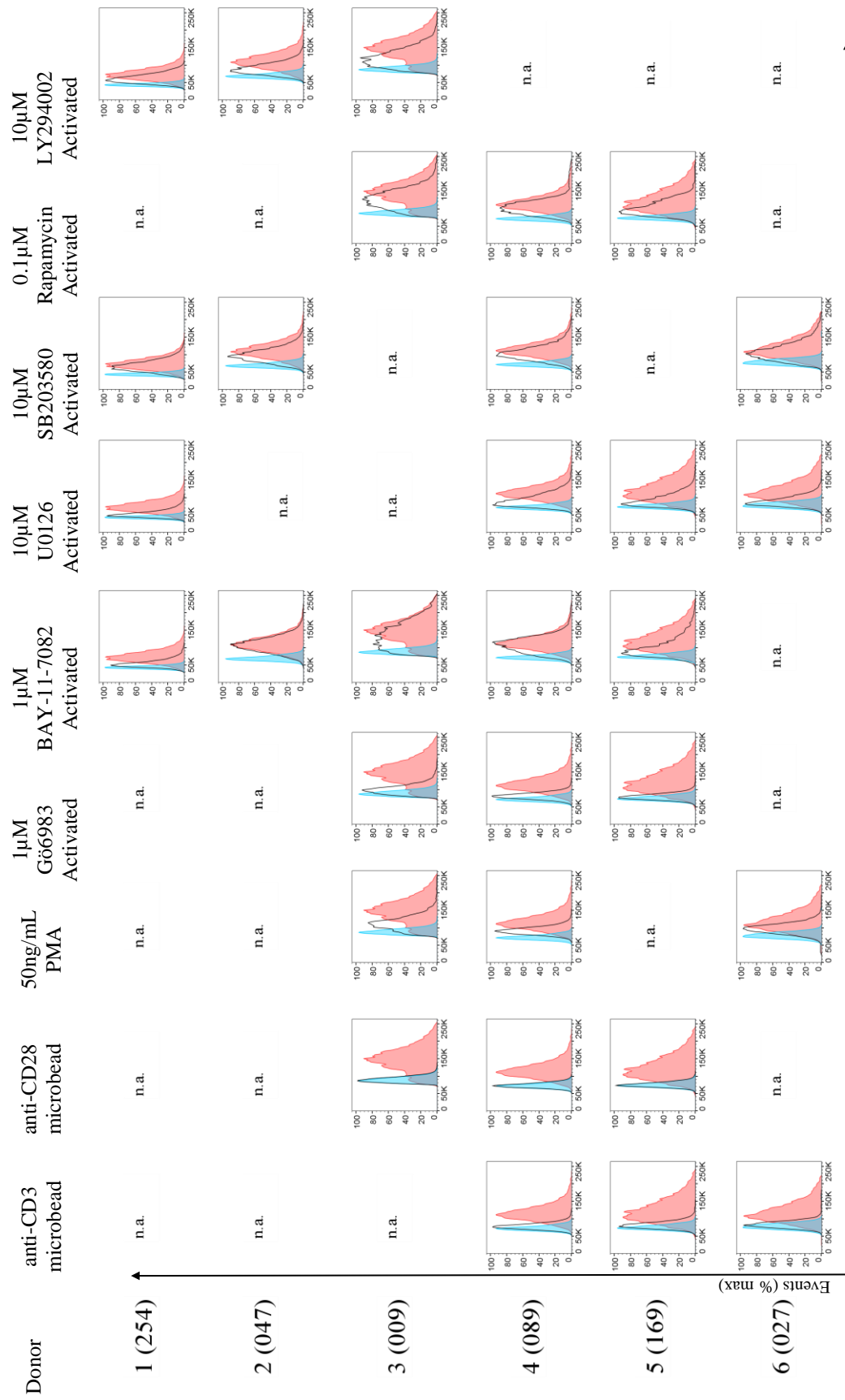


Figure 7.22. Forward scatter flow cytometry analysis of 48 hour total CD4⁺ T cells with and without activation and/or inhibitor treatments across six different donors.

Cells were activated by anti-CD3/CD28 loaded microbeads (red filled histograms) or left untreated (blue filled histograms). Additionally, FSC signals of activated and non-activated cells were compared to anti-CD3 or anti-CD28 stimulation, PMA or different inhibitor treatments in activating conditions.

7.5. References

- [1] H. Chen, H. Heiniger, A. Kandutsch, (1975) Relationship Between Sterol Synthesis and DNA Synthesis in Phytohemagglutinin-Stimulated Mouse Lymphocytes, *Proc. Natl. Acad. Sci.* 72 1950–1954. doi:10.1177/154405910408300507.
- [2] P. Singh, R. Saxena, G. Srinivas, G. Pande, A. Chattopadhyay, (2013) Cholesterol Biosynthesis and Homeostasis in Regulation of the Cell Cycle, *PLoS One.* 8. doi:10.1371/journal.pone.0058833.
- [3] M. Huse, (2009) The T-cell-receptor signaling network., *J. Cell Sci.* 122 1269–1273. doi:10.1242/jcs.042762.
- [4] M.E. Feldman, B. Apsel, A. Uotila, R. Loewith, Z. a. Knight, D. Ruggero, et al., (2009) Active-site inhibitors of mTOR target rapamycin-resistant outputs of mTORC1 and mTORC2, *PLoS Biol.* 7 0371–0383. doi:10.1371/journal.pbio.1000038.
- [5] C. Coquillard, V. Vilchez, F. Marti, R. Gedaly, (2015) mTOR Signaling in Regulatory T Cell Differentiation and Expansion., www.symbiosisonlinepublishing.com.
- [6] S. Paul, B.C. Schaefer, (2013) A new look at T cell receptor signaling to nuclear factor- κ B, *Trends Immunol.* 34 269–281. doi:10.1016/j.it.2013.02.002.
- [7] M. Karin, (1999) The Beginning of the End: κ B Kinase (IKK) and NF- κ B Activation, *J. Biol. Chem.* 274 27339–27342. doi:10.1074/jbc.274.39.27339.
- [8] Y.R. Thaker, C.E. Rudd, (2015) Distinct NF- κ B activation pathways engaged by T-cell receptor and co-receptor CD28 on T-cells, *Inflamm. Cell Signal.* 1–6. doi:10.14800/ics.613.
- [9] J. Lee, M.H. Rhee, E. Kim, J.Y. Cho, (2012) BAY 11-7082 is a broad-spectrum inhibitor with anti-inflammatory activity against multiple targets, *Mediators Inflamm.* 2012. doi:10.1155/2012/416036.
- [10] L. Guo, C. Chen, Q. Liang, M.Z. Karim, M.M. Gorska, R. Alam, (2013) Nuclear translocation of MEK1 triggers a complex T cell response through the corepressor silencing mediator of retinoid and thyroid hormone receptor., *J. Immunol.* 190 159–67. doi:10.4049/jimmunol.1201657.
- [11] M. Rincón, G. Pedraza-Alva, (2003) JNK and p38 MAP kinases in CD4+ and CD8+ T cells., *Immunol. Rev.* 192 131–142. doi:10.1034/j.1600-065X.2003.00019.x.
- [12] M.F. Favata, K.Y. Horiuchi, E.J. Manos, J. Daulerio, D. Stradley, W.S. Feeser, et al., (1998) Identification of a Novel Inhibitor of Mitogen-activated Protein Kinase Kinase, *J. Biol. Chem.* 273 18623–18632. doi:10.1074/jbc.273.29.18623.
- [13] P.H. Schafer, S.A. Wadsworth, L. Wang, J.J. Siekierka, (1999) p38 alpha mitogen-activated protein kinase is activated by CD28-mediated signaling and is required for IL-4 production by human CD4+CD45RO+ T cells and Th2 effector cells., *J. Immunol.* 162 7110–9.
- [14] M. Castagna, Y. Takai, K. Kaibuchi, K. Sano, U. Kikkawa, Y. Nishizuka, (1982) Direct activation of calcium-activated, phospholipid-dependent protein kinase by tumor-promoting phorbol esters., *J. Biol. Chem.* 257 7847–51. <http://www.ncbi.nlm.nih.gov/pubmed/7085651>.

- [15] B. Vanhaesebroeck, D.R. Alessi, (2000) The PI3K-PDK1 connection: more than just a road to PKB., *Biochem. J.* 346 Pt 3 561–76. doi:10.1042/0264-6021:3460561.
- [16] N. Hay, N. Sonenberg, (2004) Upstream and downstream of mTOR, *Genes Dev.* 18 1926–1945. doi:http://www.genesdev.org/cgi/doi/10.1101/gad.1212704.
- [17] Y. Kidani, H. Elsaesser, M.B. Hock, L. Vergnes, K.J. Williams, J.P. Argus, et al., (2013) Sterol regulatory element-binding proteins are essential for the metabolic programming of effector T cells and adaptive immunity., *Nat. Immunol.* 14 489–99. doi:10.1038/ni.2570.
- [18] B.T. Wang, G.S. Ducker, A.J. Barczak, R. Barbeau, D.J. Erle, K.M. Shokat, (2011) The mammalian target of rapamycin regulates cholesterol biosynthetic gene expression and exhibits a rapamycin-resistant transcriptional profile., *Proc. Natl. Acad. Sci. U. S. A.* 108 15201–15206. doi:10.1073/pnas.1103746108.
- [19] G.J. Brunn, J. Williams, C. Sabers, G. Wiederrecht, J.C. Lawrence, R.T. Abraham, (1996) Direct inhibition of the signaling functions of the mammalian target of rapamycin by the phosphoinositide 3-kinase inhibitors, wortmannin and LY294002., *EMBO J.* 15 5256–5267. <http://www.ncbi.nlm.nih.gov/pmc/articles/PMC452270/pdf/emboj00019-0136.pdf>.
- [20] I. Ruvinsky, O. Meyuhas, (2006) Ribosomal protein S6 phosphorylation: from protein synthesis to cell size, *Trends Biochem. Sci.* 31 342–348. doi:10.1016/j.tibs.2006.04.003.
- [21] H. Tang, E. Hornstein, M. Stolovich, G. Levy, M. Livingstone, D. Templeton, et al., (2001) Amino acid-induced translation of TOP mRNAs is fully dependent on phosphatidylinositol 3-kinase-mediated signaling, is partially inhibited by rapamycin, and is independent of S6K1 and rpS6 phosphorylation., *Mol. Cell. Biol.* 21 8671–83. doi:10.1128/MCB.21.24.8671-8683.2001.
- [22] Dos D. Sarbassov, S.M. Ali, D.-H. Kim, D.A. Guertin, R.R. Latek, H. Erdjument-Bromage, et al., (2004) Rictor, a Novel Binding Partner of mTOR, Defines a Rapamycin-Insensitive and Raptor-Independent Pathway that Regulates the Cytoskeleton, *Curr. Biol.* 14 1296–1302. doi:10.1016/j.cub.2004.06.054.
- [23] D.D. Sarbassov, S.M. Ali, S. Sengupta, J.H. Sheen, P.P. Hsu, A.F. Bagley, et al., (2006) Prolonged Rapamycin Treatment Inhibits mTORC2 Assembly and Akt/PKB, *Mol. Cell.* 22 159–168. doi:10.1016/j.molcel.2006.03.029.
- [24] J.M. García-Martínez, J. Moran, R.G. Clarke, A. Gray, S.C. Cosulich, C.M. Chresta, et al., (2009) Ku-0063794 is a specific inhibitor of the mammalian target of rapamycin (mTOR)., *Biochem. J.* 421 29–42. doi:10.1042/BJ20090489.
- [25] K. Malagu, H. Duggan, K. Menear, M. Hummersone, S. Gomez, C. Bailey, et al., (2009) The discovery and optimisation of pyrido[2,3-d]pyrimidine-2,4-diamines as potent and selective inhibitors of mTOR kinase, *Bioorganic Med. Chem. Lett.* 19 5950–5953. doi:10.1016/j.bmcl.2009.08.038.
- [26] A. Viola, S. Schroeder, Y. Sakakibara, A. Lanzavecchia, (1999) T lymphocyte costimulation mediated by reorganization of membrane microdomains., *Science.* 283 680–2. doi:10.1126/science.283.5402.680.

- [27] R.H. Schwartz, (2003) T cell anergy, *Annu. Rev. Immunol.* 21 305–34.
doi:10.1146/annurev.immunol.21.120601.141110.
- [28] F. Macián, S.H. Im, F.J. García-Cózar, A. Rao, (2004) T-cell anergy, *Curr. Opin. Immunol.* 16 209–216. doi:10.1016/j.coi.2004.01.013.
- [29] N. Isakov, A. Altman, (2012) PKC-theta-mediated signal delivery from the TCR/CD28 surface receptors, *Front. Immunol.* 3 1–12. doi:10.3389/fimmu.2012.00273.
- [30] M. Raab, S. Pfister, C.E. Rudd, (2001) CD28 signaling via VAV/SLP-76 adaptors: Regulation of cytokine transcription independent of TCR ligation, *Immunity.* 15 921–933.
doi:10.1016/S1074-7613(01)00248-5.
- [31] K.M. Dennehy, A. Kerstan, A. Bischof, J.H. Park, S.Y. Na, T. H??nig, (2003) Mitogenic signals through CD28 activate the protein kinase C theta- NF-kappaB pathway in primary peripheral T cells, *Int. Immunol.* 15 655–663. doi:10.1093/intimm/dxg063.
- [32] H. Oh, S. Ghosh, (2013) NF-kB: roles and regulation in different CD4 + T-cell subsets, *Immunol. Rev.* 252 41–51. doi:10.1111/imr.12033.
- [33] A. Khoshnan, C. Tindell, I. Laux, D. Bae, B. Bennett, A.E. Nel, (2000) The NF-kappa B cascade is important in Bcl-xL expression and for the anti-apoptotic effects of the CD28 receptor in primary human CD4+ lymphocytes., *J. Immunol.* 165 1743–54.
<http://www.ncbi.nlm.nih.gov/pubmed/10925251>.
- [34] Y.Y. Wan, J. DeGregori, (2003) The survival of antigen-stimulated T cells requires NFkappaB-mediated inhibition of p73 expression, *Immunity.* 18 331–342.
doi:10.1016/S1074-7613(03)00053-0.
- [35] R.L. Kortum, A.K. Rouquette-Jazdanian, L.E. Samelson, (2013) Ras and extracellular signal-regulated kinase signaling in thymocytes and T cells, *Trends Immunol.* 34 259–268.
doi:10.1016/j.it.2013.02.004.
- [36] C.A. Hall-Jackson, P.A. Eyers, P. Cohen, M. Goedert, F.T. Boyle, N. Hewitt, et al., (1999) Paradoxical activation of Raf by a novel Raf inhibitor, *Chem. Biol.* 6 559–568.
doi:10.1016/S1074-5521(99)80088-X.
- [37] F. Chang, L.S. Steelman, J.T. Lee, J.G. Shelton, P.M. Navolanic, W.L. Blalock, et al., (2003) Signal transduction mediated by the Ras/Raf/MEK/ERK pathway from cytokine receptors to transcription factors: potential targeting for therapeutic intervention, *Leukemia.* 17 1263–1293. doi:10.1038/sj.leu.2402945.
- [38] B.T. Wang, G.S. Ducker, A.J. Barczak, R. Barbeau, D.J. Erle, K.M. Shokat, (2011) The mammalian target of rapamycin regulates cholesterol biosynthetic gene expression and exhibits a rapamycin-resistant transcriptional profile., *Proc. Natl. Acad. Sci. U. S. A.* 108 15201–15206. doi:10.1073/pnas.1103746108.
- [39] H. Chi, (2012) Regulation and function of mTOR signalling in T cell fate decisions, *Nat. Rev. Immunol.* 12 325–338. doi:10.1038/nri3198.
- [40] G. Woerly, N. Brooks, B. Ryffel, (1996) Effect of rapamycin on the expression of the IL-2 receptor (CD25)., *Clin. Exp. Immunol.* 103 322–7.

<http://www.pubmedcentral.nih.gov/articlerender.fcgi?artid=2200333&tool=pmcentrez&rendertype=abstract>.

- [41] X. Wan, B. Harkavy, N. Shen, P. Grohar, L.J. Helman, (2007) Rapamycin induces feedback activation of Akt signaling through an IGF-1R-dependent mechanism, *Oncogene*. 26 1932–1940. doi:10.1038/sj.onc.1209990.
- [42] E.M. Breslin, P.C. White, A.M. Shore, M. Clement, P. Brennan, (2005) LY294002 and rapamycin co-operate to inhibit T-cell proliferation., *Br. J. Pharmacol.* 144 791–800. doi:10.1038/sj.bjp.0706061.
- [43] C. Camperio, M. Muscolini, E. Volpe, D. Di Mitri, R. Mechelli, M.C. Buscarinu, et al., (2014) CD28 ligation in the absence of TCR stimulation up-regulates IL-17A and pro-inflammatory cytokines in relapsing-remitting multiple sclerosis T lymphocytes, *Immunol. Lett.* 158 134–142. doi:10.1016/j.imlet.2013.12.020.
- [44] K. V Prasad, Y.C. Cai, M. Raab, B. Duckworth, L. Cantley, S.E. Shoelson, et al., (1994) T-cell antigen CD28 interacts with the lipid kinase phosphatidylinositol 3-kinase by a cytoplasmic Tyr(P)-Met-Xaa-Met motif., *Proc. Natl. Acad. Sci. U. S. A.* 91 2834–8. doi:10.1073/pnas.91.7.2834.
- [45] M. Tacke, G. Hanke, T. Hanke, T. H??nig, (1997) CD28-mediated induction of proliferation in resting T cells in vitro and in vivo without engagement of the T cell receptor: Evidence for functionally distinct forms of CD28, *Eur. J. Immunol.* 27 239–247. doi:10.1002/eji.1830270136.
- [46] P.S. Costello, M. Gallagher, D. Cantrell, (2002) Sustained and dynamic inositol lipid metabolism inside and outside the immunological synapse., *Nat. Immunol.* 3 1082–1089. doi:10.1038/ni848.
- [47] M. Freeley, Y. Volkov, D. Kelleher, A. Long, (2005) Stimulus-induced phosphorylation of PKC theta at the C-terminal hydrophobic-motif in human T lymphocytes, *Biochem. Biophys. Res. Commun.* 334 619–630. doi:10.1016/j.bbrc.2005.06.136.
- [48] G. Baier, G. Baier-Bitterlich, N. Meller, K.M. Coggeshall, L. Giampa, D. Telford, et al., (1994) Expression and biochemical characterization of human protein kinase C-theta., *Eur. J. Biochem.* 225 195–203.
- [49] R.K. Chopra, D.C. Powers, W.H. Adler, J.E. Nagel, (1989) Phorbol myristate acetate and calcium ionophore A23187-stimulated human T cells do not express high-affinity IL-2 receptors., *Immunology*. 66 54–60.
<http://www.pubmedcentral.nih.gov/articlerender.fcgi?artid=1385120&tool=pmcentrez&rendertype=abstract>.
- [50] C.R.F. Monks, H. Kupfer, I. Tamir, A. Barlow, A. Kupfer, (1997) Selective modulation of protein kinase C- θ during T-cell activation, *Nature*. 385 83–86. doi:10.1038/385083a0.
- [51] K.-F. Kong, T. Yokosuka, A.J. Canonigo-Balancio, N. Isakov, T. Saito, A. Altman, (2011) A motif in the V3 domain of the kinase PKC- θ determines its localization in the immunological synapse and functions in T cells via association with CD28, *Nat. Immunol.* 12 1105–1112.

doi:10.1038/ni.2120.

- [52] W. Luu, E.J. Zerenturk, I. Kristiana, M.P. Bucknall, L.J. Sharpe, A.J. Brown, (2014) Signaling regulates activity of DHCR24, the final enzyme in cholesterol synthesis., *J. Lipid Res.* 55 410–20. doi:10.1194/jlr.M043257.
- [53] M. Andrs, J. Korabecny, D. Jun, Z. Hodny, J. Bartek, K. Kuca, (2015) Phosphatidylinositol 3 - Kinase (PI3K) and Phosphatidylinositol 3 - Kinase-Related Kinase (PIKK) Inhibitors: Importance of the Morpholine Ring.,
- [54] S. Thebault, J. Ochoa-Garay, (2004) Characterization of TCR-induced phosphorylation of PKC?? in primary murine lymphocytes, *Mol. Immunol.* 40 931–942. doi:10.1016/j.molimm.2003.10.014.
- [55] J.M. Salvador, P.R. Mittelstadt, T. Guszczynski, T.D. Copeland, H. Yamaguchi, E. Appella, et al., (2005) Alternative p38 activation pathway mediated by T cell receptor-proximal tyrosine kinases, *Nat. Immunol.* 6 390–395. doi:10.1038/ni1177.
- [56] C. Berset, S. Audétat, J. Tietz, T. Gunde, A. Barberis, A. Schumacher, et al., (2005) Protein Kinase Inhibitors, 105 95–105. <http://www.ncbi.nlm.nih.gov/pmc/articles/PMC1221339/pdf/10998351.pdf>.

CHAPTER 8: Sterolomic analysis of naïve CD4⁺ T cells in TH0- TH2- and Treg-polarising conditions.

8.1. Introduction

T lymphocytes, along with B lymphocytes, comprise the adaptive arm of the immune system. They were previously regarded as the second-line of defence once the innate arm has been overwhelmed by invading pathogens^[1] but recent studies have put the adaptive activation alongside the innate. B cells exhibit their humoral immunity functions mainly by establishing immunological memory through production of antibodies whereas T cells, either cytotoxic CD8⁺ or helper CD4⁺ cells, enable cell-mediated killing or help coordinate responses of other immune cells, respectively.

T cells can be classified further into subsets which have specialised functions based on immune challenge. Recent advances in immunology have described more of these subsets in addition to the classical binary TH1 and TH2 identified by Mossman and Coffman in 1986^[2]. Put simply, TH1, TH2 and TH17 subsets mount pro-inflammatory responses against pathogens ranging from intracellular bacteria and viruses to extracellular challenges from parasites and fungi while T regulatory cells (Treg) enable resolution of these inflammatory responses and also mediate tolerance^[3]. T cells can deliver these responses directly by cell-to-cell contact but effective coordination within tissue microenvironments utilises the production of specific chemokines or cytokines^[4,5]. Moreover, Treg cells can develop naturally from the thymus as nTreg or, like other effector T helper cells, can be induced in the periphery from mature naïve T cells as iTreg^[6]. Considerable attention in the last decade have been put into the recently discovered TH17 subset due to its particular production of IL-17 family of cytokines not observed in TH1 and TH2 and its roles in autoimmune pathology^[7].

Much like for other T cell subsets, it did not take long for a master regulator to be identified for TH17 cells. The induction of Retinoic Acid Receptor-related orphan receptor gamma t (ROR γ t) was described to be important in TH17 differentiation and function^[8,9]. Furthermore, ROR activity have been described to be ligand-regulated^[10-12] by cholesterol biosynthesis intermediates^[13] or specific sterols like 7 α ,27-DiHC^[14], 7 β ,27-diHC^[14], and desmosterol^[15]. This and further recent reports linking several

distinct cholesterol metabolites^[16-21] and sterol metabolism^[22,23] to functions of several immune cells creates an opportunity to explore further immunomodulatory effects of these neutral lipids.

In all, T helper cells are a diverse group cells with dynamic roles in host defence. It was determined in previous chapters that there is a dramatic change in T cell cholesterol metabolism upon activation. As activated T cells eventually differentiate into regulatory or effector subsets, this chapter utilises the current methodology and focuses on the identification of sterol profiles specific to polarised activated naïve CD4⁺ T cells with the aim to correlate sterol metabolism to T cell function. Polarisation towards TH2 and iTreg conditions were selected for this study as TH1 and TH17 cells were being investigated by Dr Tom Hearn in parallel. For simplicity, iTreg cells generated *in vitro* in this chapter will be termed as Treg cells.

8.2. Materials and Methods

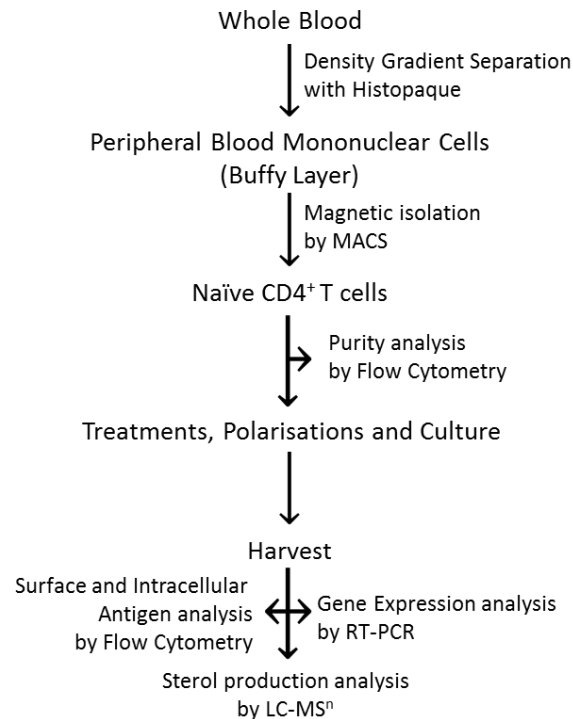


Figure 8.1. Typical workflow for naïve CD4 T cell isolation, culture, polarisation and analysis. High purity naïve CD4⁺ T cells were magnetically isolated from mononuclear cells of peripherally drawn human blood then activated and polarised *in vitro*. At end point, cell viability, activation, protein and gene expression were monitored to confirm presence of differentiated cells for correlation with its sterol production.

8.2.1. Naïve CD4⁺ T cell Isolation from PBMC

Naïve CD4⁺ T cells were negatively selected magnetically from the PMBCs of healthy human donors after density gradient centrifugation as described in *section 2.1.2*, *section 2.1.3* and *section 2.1.4.1*.

8.2.2. Polarisation cytokines and reagents

Recombinant human proteins: IL-2, IL-4 and TGF- β and neutralising antibodies: anti-IFN γ and anti-IL-4 as listed in *section 2.1.1.3* (Table 2.1) were used to polarise the activated naïve CD4⁺ T cells to either TH0, TH2 or induced Treg.

8.2.3. TH0, TH2 and Treg polarisation culture of naïve CD4⁺ T cells

Isolated naïve CD4⁺ T cells were seeded at 1x10⁶ cells/mL in X-VIVO-20 media on a 24-well plate. Alongside, cells were activated using anti-CD3/CD28-loaded MACSiBeads at 1:2 bead-to-cell ratio in the presence of the recombinant proteins and antibodies listed in Table 8.1 (for donor 1 and 2) or Table 8.2 (for donor 3) then incubated at 37°C 5%CO₂, as previously described in *section 2.1.6.3*. After 3 days, majority of the media (~80-85%) above the T cell monolayer at the bottom of the plate were carefully collected. Cell cultures were split when necessary then topped up with X-VIVO-20 to the initial seeding volume containing the same cytokine and antibody treatments as in day 0 but excluding activation beads, then incubated for a further 3 days. On day 6, cell cultures were stimulated transiently with 50ng/mL PMA and 500ng/mL Ionomycin for 1 hour, afterwards treated with BD GolgiStop™ at 1:1500, then further incubated for 5 hours. Subsequently, cell and media were harvested with cells extracted for RNA/gene expression analysis or for flow cytometry and media for sterol analysis.

More specifically, the number of naïve CD4⁺ T cells cultured from donor 1, 2 and 3 were 2.13x10⁶ in 2.13mL, 2.00x10⁶ in 2.00mL, and 1.62x10⁶ in 1.6mL, respectively.

8.2.4. Relative gene expression analysis by RT-PCR

RNA extracts from harvested cells were processed for RT-PCR analysis as described in *section 2.3.2* using select primers listed in *section 2.3.1.2* Table 2.8. When indicated, extracted total RNA were additionally treated with TurboDNase (ThermoFisher) following manufacturer instructions before proceeding to cDNA synthesis using QuantiTect Reverse Transcription Kit (Qiagen) and RT-PCR analysis using SYBR Green PCR Kit (Qiagen). Relative expression was obtained by normalisation against *RP18S*, and calculated using the $2^{-\Delta\Delta Ct}$ method^[28].

Table 8.1. Different treatments for polarising activated naïve CD4⁺ T cells used for donor 1 and donor 2. (B:C, bead-to-cell ratio, 10U IL-2 = 1.75ng IL-2).

Polarisation Condition		Treatments					
		Day 0 only	Day 0 and Day 3				
		Anti-CD3/CD28 beads (B:C)	IL-2 (U/mL)	IL-4 (ng/mL)	TGF-β1 (ng/mL)	Anti-IFN γ (μg/mL)	Anti-IL4 (μg/mL)
1	TH0 (A)	✓ (1:2)	10	---	---	---	---
2	TH2 ^[24]	✓(1:2)	10	25	---	10	---
3	Treg (10/5) ^[25]	✓(1:2)	10	---	5	10	10
4	Treg (50/5) ^[26,27]	✓(1:2)	50	---	5	10	10
5	Non-Activated	---	---	---	---	---	---
6	Non-Activated + IL-2	---	10	---	---	---	---

Table 8.2. Different treatments for polarising activated naïve CD4⁺ T cells used for donor 3. (B:C, bead-to-cell ratio, 10U IL-2 = 1.75ng IL-2).

Polarisation Condition		Treatments					
		Day 0 only	Day 0 and Day 3				
		Anti-CD3/CD28 beads (B:C)	IL-2 (U/mL)	IL-4 (ng/mL)	TGF-β1 (ng/mL)	Anti-IFNγ (μg/mL)	Anti-IL4 (μg/mL)
1	TH0 (A)	✓ (1:2)	10	---	---	---	---
2	TH0 (B)	✓(1:2)	10	---	---	10	10
3	TH0 (C)	✓(1:2)	50	---	---	10	10
4	TH0 (D)	✓(1:2)	---	---	---	10	10
5	Treg (50/5) ^[26,27]	✓(1:2)	50	---	5	10	10
6	Treg (50/10)	✓(1:2)	50	---	10	10	10
7	Treg (50/1)	✓(1:2)	50	---	1	10	10
8	Treg (50/0.2)	✓(1:2)	50	---	0.2	10	10

8.2.5. Purity, cell activation, viability analysis and intracellular protein expression analysis by flow cytometry

At day 0, after magnetic depletion by MACS, an aliquot of cells was stained with anti-CD4-FITC, anti-CD45RA-eFluoro450, anti-CD25-APC and 7-AAD for flow cytometry analysis. On day of harvest, cells were analysed for cell activation and cell viability with anti-CD25-APC and 7-AAD. Additionally, some of the PMA/Ionomycin-stimulated and GolgiStop-treated cells were fixed, permeabilized and stained intracellularly for FOXP3 and IL-4 as described in *section 2.1.8.5*. All data were acquired on a FACS Aria (BD Biosciences) and analysed by FlowJo software (FlowJo, LLC).

8.2.6. Analysis of sterol content in culture media

Collected culture media on day 3 and day 6 were extracted in absolute ethanol added with deuterium-substituted internal sterol standards, which were subsequently processed for sterol identification and content quantification by LC-MSⁿ as described in *section 2.2.2.2*.

8.3. Results

8.3.1. Isolated naïve CD4⁺ T cells were $\geq 94\%$ CD4⁺CD45RA⁺ cells prior to culture.

Post-magnetic isolation of naïve CD4⁺ T cells from PBMCs, an aliquot of cells was stained with fluorochrome-conjugated antibodies and 7-AAD viability dye. Flow cytometric analysis revealed a very high percentage ($\geq 94\%$) of CD4⁺/CD45RA⁺ double positive cells (Figure 8.3) across all independent isolations from three different donors (Figure 8.2). These cells were then seeded, activated and polarised for up to 6 days.

8.3.2. Reduced T cell viability in TH2 polarising conditions compared to TH0 and Treg.

The activation of naïve CD4⁺ T cells with 25ng/mL IL-4 and 10µg/mL anti-IFN γ antibody resulted in a higher proportion of 7-AAD⁺ cells after 6 days on culture. 7-AAD flow analysis of day 6 harvested cells showed a reduced cell viability in cultures polarised to TH2 conditions compared to TH0 and Treg (Figure 8.4).

8.3.3. CD25 surface expression was higher in Treg polarised conditions.

As expected, there was a general increase in CD25 expression in the activated naïve CD4⁺ T cells across different polarisation conditions after 6 days in culture. However, activated cells treated with Treg polarisation cytokine TGF- β in the presence of anti-IL4 and anti-IFN γ neutralising antibodies resulted in a relatively higher surface expression of CD25 compared to TH2 and TH0 based on measured median fluorescence intensities across two donors (Figure 8.5).

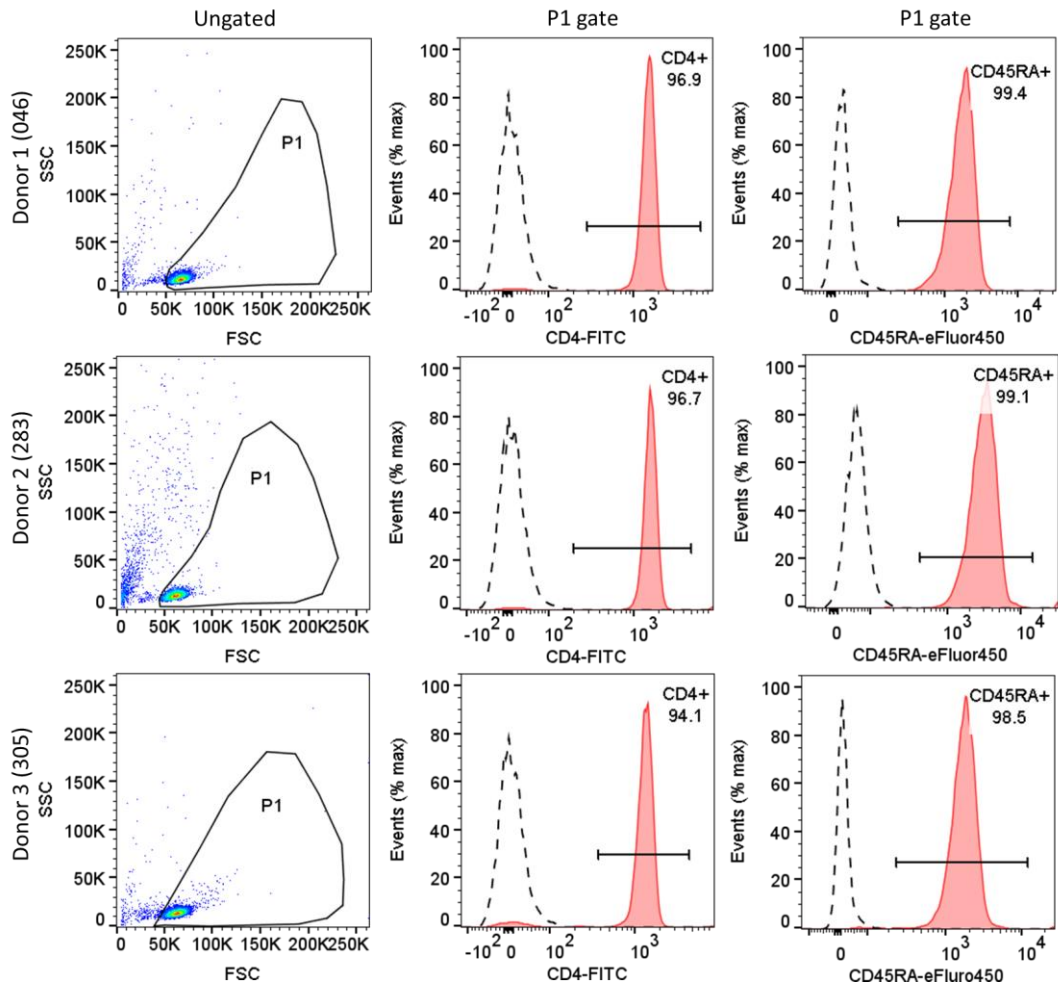


Figure 8.2. Day 0 flow cytometry analysis of naïve CD4⁺ T cell purity. Naïve CD4⁺ T cells isolated by negative selection yielded 94-96% CD4⁺ and 98-99% CD45RA⁺ cells for culture across three independent donors. The isolated cells show a generally homogenous population with P1 gate to exclude debris which have very low FSC/SSC signals. Filled histograms show stained cells and dashed histograms as unstained. Inset numbers indicate percentage gated cells.

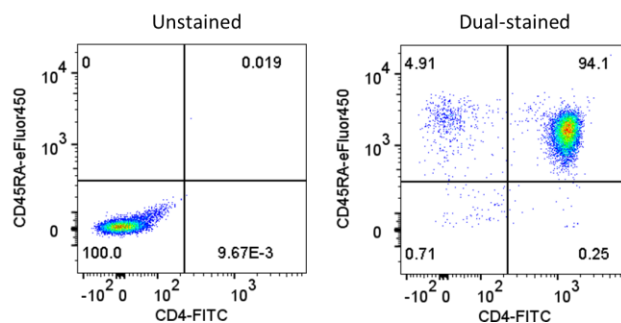


Figure 8.3. Representative day 0 dual staining purity analysis of donor 3 (305) naïve CD4⁺ T cells. Flow cytometry analysis confirmed that cells used for activation and polarisation were 94% CD4⁺ CD45RA⁺ cells prior to culture. Events shown were gated from P1 gate shown in Figure 8.2. Inset numbers indicate percentage cells in each quadrant.

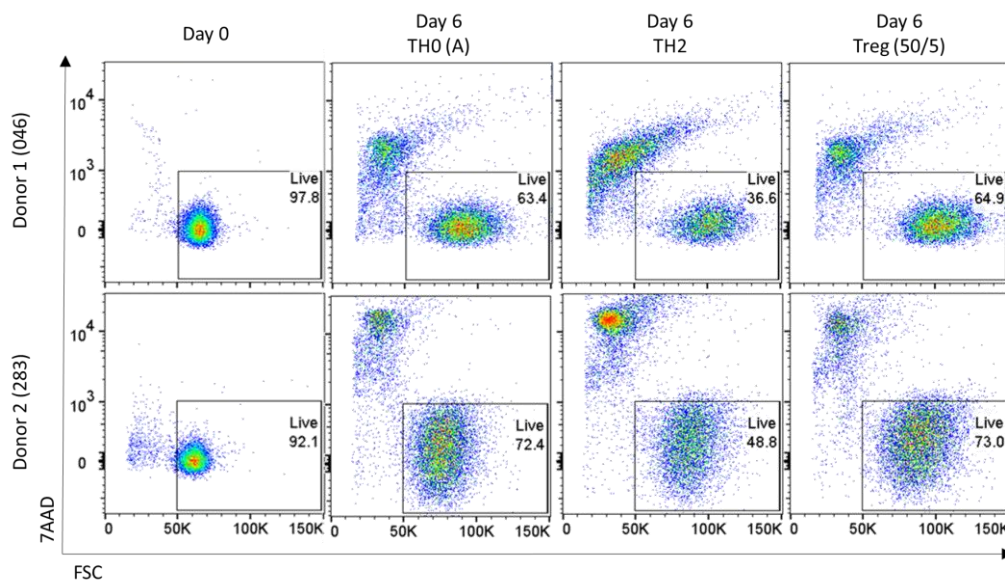


Figure 8.4. Viability analysis of day 6 polarised activated naïve CD4 T cells. Flow cytometry analysis of 7-AAD stained cells revealed proportionately lower cell viability in TH2 polarising conditions containing 36%-48% live cells, compared to TH0 and Treg which had 63%-73% after 6 days in culture. FSC/7-AAD plots exclude activation beads which have very low FSC signals and were 7-AAD negative. Inset numbers indicate percentage of live cells which are 7-AAD negative.

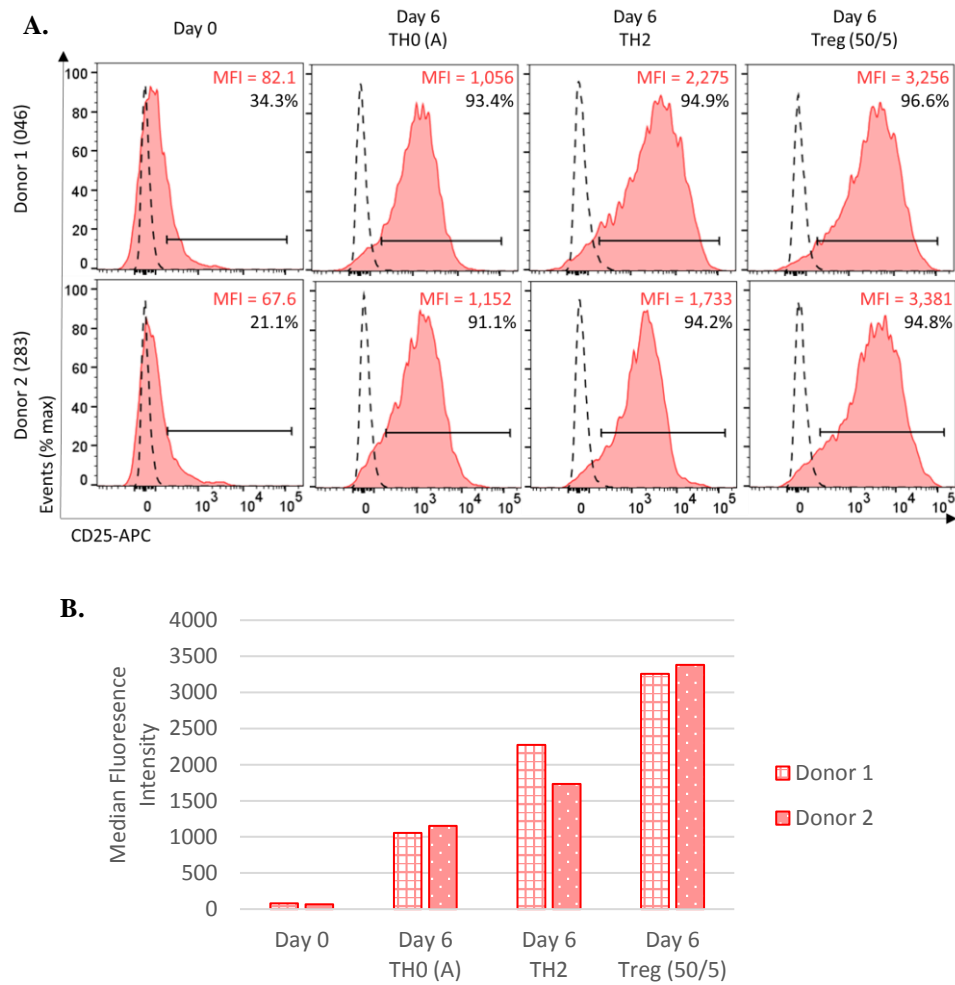


Figure 8.5. CD25 expression analysis of activated naïve CD4 T cells of donor 1 and 2 after 6 days. CD25 expression was relatively higher in Treg polarised cells than TH2 and TH0. A. Flow cytometry filled histograms show the CD25-APC-stained cells and dashed histograms as unstained. Events displayed were of the “Live” gates from Figure 8.4. Gates were set such that 98-99% of events in the unstained samples were excluded. Red and black inset numbers indicate median fluorescence intensities (MFI) and percentage gated cells, respectively. B. MFI were plotted to show the CD25 expression between the two donors and between different polarising conditions.

8.3.4. RT-PCR analysis and flow cytometry confirmed TH2 and Treg polarisation by IL4 and FOXP3 mRNA expression and intracellular protein staining.

An aliquot of cells from each culture condition on day 6 was extracted for RNA and subsequently submitted for cDNA synthesis and relative gene expression analysis for *IL4*, *FOXP3*, *IL17A*, *IL10*, *RORC*, *RORA*, *CH25H* and *CYP7B1* as previously described in *section 2.3.2*.

RT-PCR analysis confirmed TH2 and Treg polarisation by the 10- to 40-fold increase in *IL-4* mRNA and 9- to 18-fold increase in *FOXP3* mRNA expression compared to non-polarised TH0 cultures across two different donors (Figure 8.6A/B & Figure 8.7A/B). Moreover, the increase in *IL4* and *FOXP3* mRNA expressions were reflected by the increased proportion of IL4⁺ and FOXP3⁺ cells in TH2-polarising and Treg-polarising conditions, respectively, as analysed by intracellular staining (Figure 8.8 and Figure 8.9).

Interestingly, *IL-10* was seen upregulated in TH2 conditions but not in Treg conditions, even though Treg cells can produce and mediate regulatory function through IL-10^[29]. This agrees with a study by Cousins et.al 2002 where IL-10 was reported to be produced transiently during TH2 polarisation peaking at day 7 but subsides afterwards^[30]. Moreover, the absence of *IL-10* gene expression in Treg-polarised cells also agrees with the current literature describing *FOXP3* expression does not directly imply *IL-10* expression^[31] and that IL-10-producing Treg cells and FOXP3⁺ cells are developmentally distinct Treg subsets^[32].

8.3.5. RORC, FOXP3, and CYP7B1 mRNA expressions were higher in Treg conditions compared to TH0/TH2.

Expression of *RORC*, *FOXP3*, and *CYP7B1* genes were observed to be specifically induced in culture conditions containing 5ng/mL TGF- β (Figure 8.6B/E/H, Figure 8.7B/E/H). These gene expressions were shown to be further enhanced by the increased IL-2 treatment from 10U/mL to 50U/mL (Treg-10/5 and Treg-50/5). Generally, this matches with studies reporting TGF- β induces both *RORC*^[33] and *FOXP3*^[34] expression. This also provides a link between the described plasticity of Treg and TH17 cells, both requiring TGF- β for development.

The sterol metabolism-related gene *CYP7B1*, which encodes for the microsomal enzyme oxysterol-7 α -hydroxylase to catalyse the 7 α -hydroxylation of an oxysterol, has already been described to be an ROR α target gene in mice^[35], although it is yet to be reported to also be an ROR γ target gene in humans or regulated by TGF- β signalling. In the current study using human T cells, Treg polarisation does not appear to highly induce ROR α (Figure 8.6.F, Figure 8.7.F).

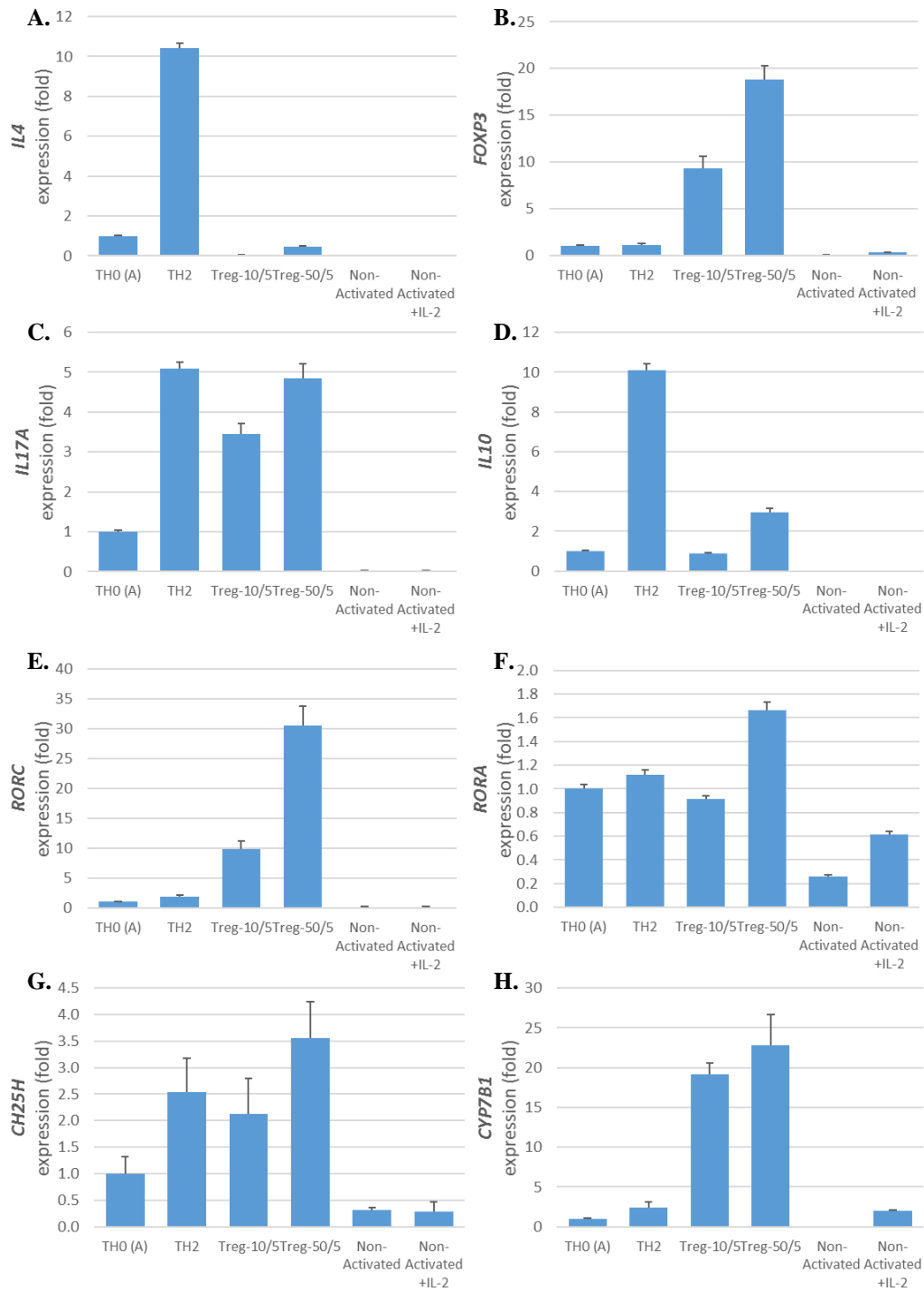


Figure 8.6. RT-PCR analysis for 6-day cultured activated naive CD4⁺ T cells of donor 1 (046) comparing TH0, TH2 and Treg polarisations.

Complementary DNA synthesised from TurboDNase-treated RNA was used for *IL4*, *CH25H* and *CYP7B1* expression analysis whereas cDNA from non-TurboDNase-treated RNA was used for *FOXP3*, *IL10*, *RORA*, *RORC* and *IL17A* which were all normalised to *RP18S* expression. Fold change were relative to TH0. Error bars indicate s.e.m from triplicate wells.

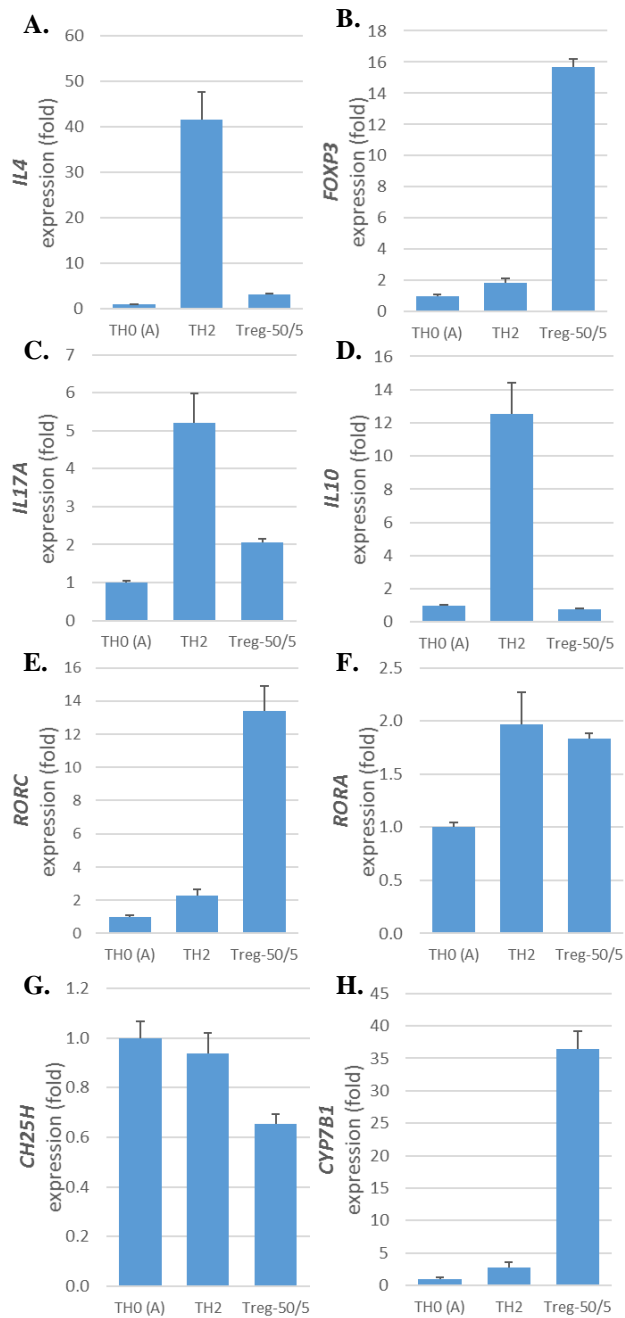


Figure 8.7. RT-PCR analysis for 6-day cultured activated naive CD4⁺ T cells of donor 2 (283) comparing TH0, TH2 and Treg polarisations.

Complementary DNA synthesised from TurboDNase-treated RNA was used for *CH25H* and *CYP7B1* expression analysis whereas cDNA from non-TurboDNase-treated RNA was used for *IL4*, *FOXP3*, *IL10*, *RORA*, *RORC* and *IL17A* which were all normalised to *RP18S* expression. Fold change were relative to TH0. Error bars indicate s.e.m from triplicate wells.

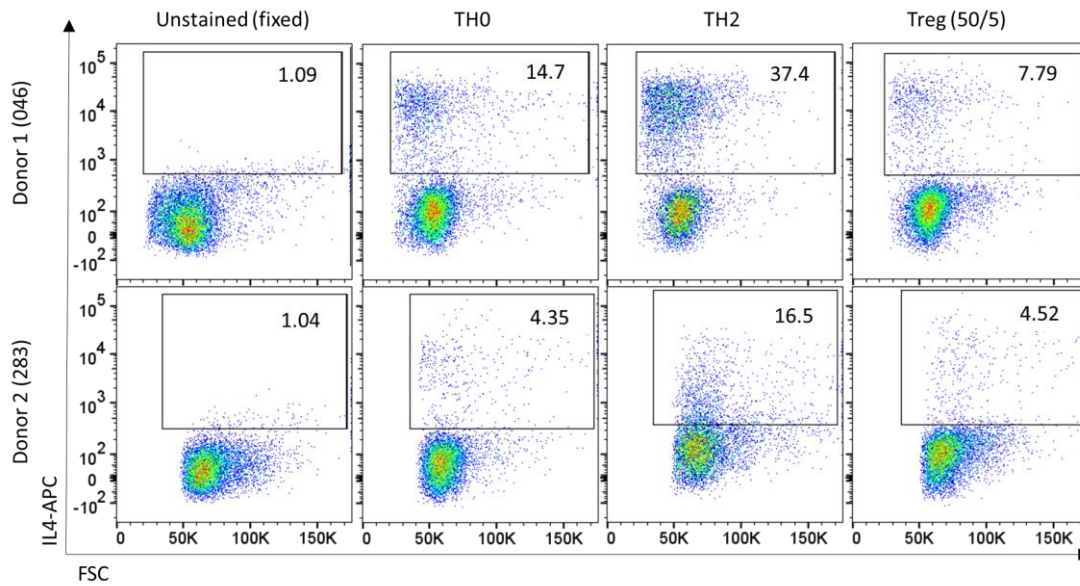


Figure 8.8. Intracellular IL4 staining of 6-day activated CD4⁺ T cells.

Fixation, permeabilization and anti-IL4-APC staining of PMA/Ionomycin/GolgiStop-treated cells confirmed relatively higher IL4⁺ cells in TH2-polarising conditions than TH0 and Treg across both donors. All plots were gated from activation bead-excluded events. Inset numbers indicate the percentage of gated IL4⁺ cells. Unstained (fixed) TH2-polarised cells were used as the negative control to determine the gates.

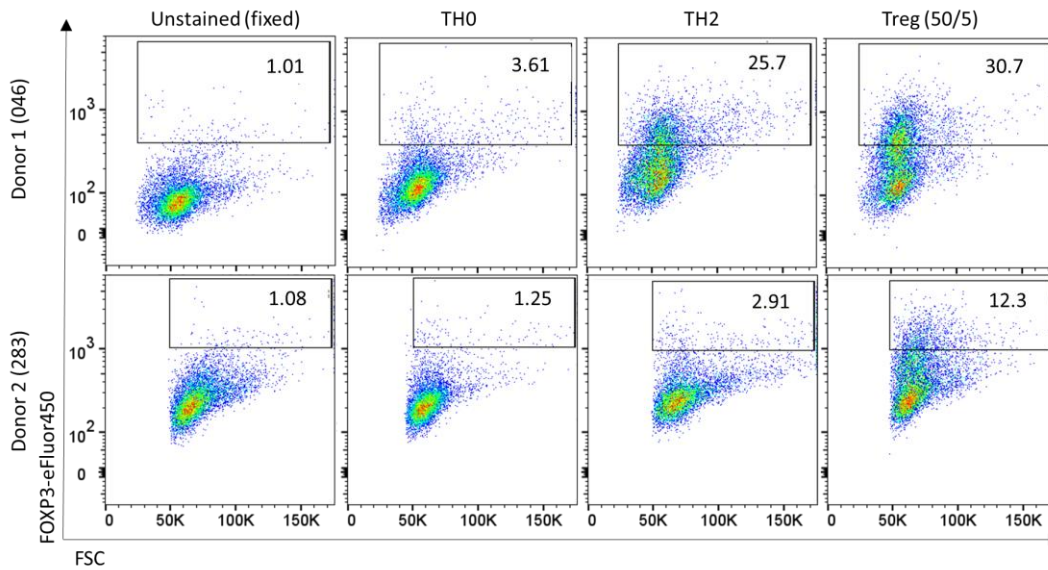


Figure 8.9. Intracellular FOXP3 staining of 6-day activated CD4⁺ T cells.

Fixation, permeabilization and anti-FOXP3-eFluor450 staining of harvested cells confirmed relatively higher FOXP3⁺ cells in Treg-polarising conditions than TH0 and TH2 across both donors. All plots were gated to exclude activation beads with very low FSC signals. Inset numbers indicate the percentage of gated FOXP3⁺ cells. Unstained (fixed) Treg-polarised cells were used as the negative control to determine the gates.

8.3.6. Increased CYP7B1 expression did not reflect an increased RORA expression.

The 20- to 35- fold increase seen in *CYP7B1* expression relative to TH0 was not reflected by *RORA* expression (Figure 8.6.F/H Figure 8.7.F/H). *RORA* expression did not show any obvious trend across different treatments and donors, which also only seen a maximal fold change of 1.8 to 2.0 relative to TH0. This is in contrast to mice studies reported by Wada et.al.^[35], which may suggest a separate or additional regulation of activating the *CYP7B1* gene in human CD4 T cells directly or indirectly from TGF- β stimulation.

8.3.7. TH2-polarised cells produced the least amount of sterols, with Treg-polarised cells producing the most, compared to TH0.

Cells polarised in TH2 conditions were observed to have produced the least sterols in comparison to TH0 and Treg(s) (Figure 8.10) after 6 days in culture. Although quantified sterols were all normalised to the number of cells initially seeded, this may have been directly due to cells in TH2 conditions being slightly less viable (Figure 8.4) than TH0 and Treg cells in culture. Generally, Treg-polarised cells produced more 25-HC, 24S-HC, 24S,25-EC and 7 α ,24S,25-TriHC relative to TH0.

More specifically, monohydroxycholesterol like 25-HC was produced in high abundance early in the culture (day 0 to day 3) after activation whereas reduced production were observed between day 3 and day 6 from both donors (Figure 8.10.B). In contrast to 25-HC, the 24S,25-EC was detected higher later in the culture at day 6 than in day 3 (Figure 8.10.C). These trends on 25-HC and 24S,25-EC were observed to be the similar between the two donors, although only a marginal increase in 24S,25-EC was seen for donor 2 at day 6. Another monohydroxycholesterol, 24S-HC, was seen also to be produced by the activated cells only. 24S-HC followed a similar trend as the 24S,25-EC production (Figure 8.10.A), with the least and most detected from TH2 and Treg, respectively.



Figure 8.10. Sterols from day 3 and day 6 collected media supernatants of Donor 1 (046) and 2 (283) comparing TH0, TH2 and Treg polarisations.

Media supernatants collected from day 3 media refresh and day 6 harvest were extracted for sterols and submitted for LC-MSⁿ analysis and quantification. Minimal to no sterols were detected in non-activated cells with or without 10U/mL rhIL-2 even after 6 days of culture. On activated and polarised cells: A. 24S-Hydroxycholesterol, B. 25-Hydroxycholesterol, C. 24S,25-Epoxycholesterol, D. 7 α ,24S,25-Trihydroxycholesterol and its metabolite, E. 3-oxo,7 α ,24S,25-Trihydroxycholesterol were detected in both day 3 and day 6. All quantifications were normalised to number of cells seeded.

8.3.8. The detected oxysterol, 7 α ,24S,25-TriHC, was produced the most specifically by Treg-polarised cells detected mainly later in culture.

Most notable of the sterols monitored, 7 α ,24S,25-TriHC was found to be produced in substantial amounts specific to Treg-polarised cells. Also, its metabolite via enzyme 3 β -hydroxy- Δ 5-C²⁷-steroid oxidoreductase (HSD3B7) catalysis (Figure 8.15), 3-oxo,7 α ,24S,25-TriHC, was also detected at about 50% of its precursor (Figure 8.10.E cf. Figure 8.10.D). Majority of these sterols were detected at day 6 culture media extracts with minimal levels at day 3. The TH0/TH2/Treg comparison, repeated with donor 2, confirms 7 α ,24S,25-TriHC and 3-oxo,7 α ,24S,25-TriHC production to be specific in Treg-polarised conditions.

The result in which cells in Treg-polarising conditions produce more oxysterols prompted the consideration of the effect of varying concentrations of TGF- β and other treatments like IL-2 and anti-IFN- γ and anti-IL-4 neutralising antibodies. These were explored with CD3/CD28-activated naïve CD4 T cells of donor 3 treated with a range of TGF- β with constant IL-2 (50U/mL) treatment as before (**Error! Reference source not found.**). In addition, since different IL-2 treatments previously slightly affected several gene expressions of Treg-polarised cells, the possible effect of 10U/mL and 50U/mL in isolation was tested using non-polarising TH0(B) and TH0(C) conditions, respectively.

8.3.9. Human CD4⁺ naïve T cell activation *in vitro* requires IL-2.

Comparison of donor 3 activated cells to donor 1 and 2 reveals a generally lower expression of CD25 based on median fluorescence intensities (Figure 8.5 cf. Figure 8.11).

The effect of the lack of exogenous IL-2 in T cells was demonstrated by TH0(D) conditions having much reduced levels of CD25 expression even in activating conditions compared to TH0(C) (Figure 8.12.D&E, middle CD25 row). TH0(D), which were naïve CD4⁺ T cells stimulated with anti-CD3/CD28-loaded beads in anti-IFN- γ and anti-IL-4 neutralising antibodies without additional IL-2, also unexpectedly failed to accumulate cell mass even after 6 days in culture, indicated by a lack of FSC increase (Figure 8.12, top SSC row). For this specific treatment, the results may be attributed to the combination of insufficient IL-2 growth factor in culture.

Specifically looking at IL-2 effect, TH0(D) can be compared with TH0(B) and TH0(C), in which all three had anti-IFN- γ and anti-IL-4 neutralising antibodies but only differ in the amounts of IL-2 concentrations with 0U/mL, 10U/mL and 50U/mL, respectively. Despite the 5 times increase in IL-2, flow cytometry analysis revealed only a minor difference in the proportion of CD25⁺ cells and cell size between TH0(B) and TH0(C) (Figure 8.12.C&D). This suggests that in CD3/CD28-stimulated conditions, the presence of additional IL-2 growth factor may have a role for successful activation progression of human CD4⁺ T cells especially in IFN- γ and IL-4 depleted environments. Gene expression analysis of *CYP7B1*, *RORC*, *FOXP3* and *RORA* also shown minimal change between different TH0 conditions (Figure 8.13). Unfortunately, TH0(D) had to be excluded from gene expression analysis due to insufficient RNA material extracted.

Comparison of TH0(A) and TH0(B) results indicate a minimal impact of the anti-IFN- γ and anti-IL-4 neutralising antibodies to both gene expression (Figure 8.13) and sterol production (Figure 8.14) in the presence of 10U/mL IL-2.

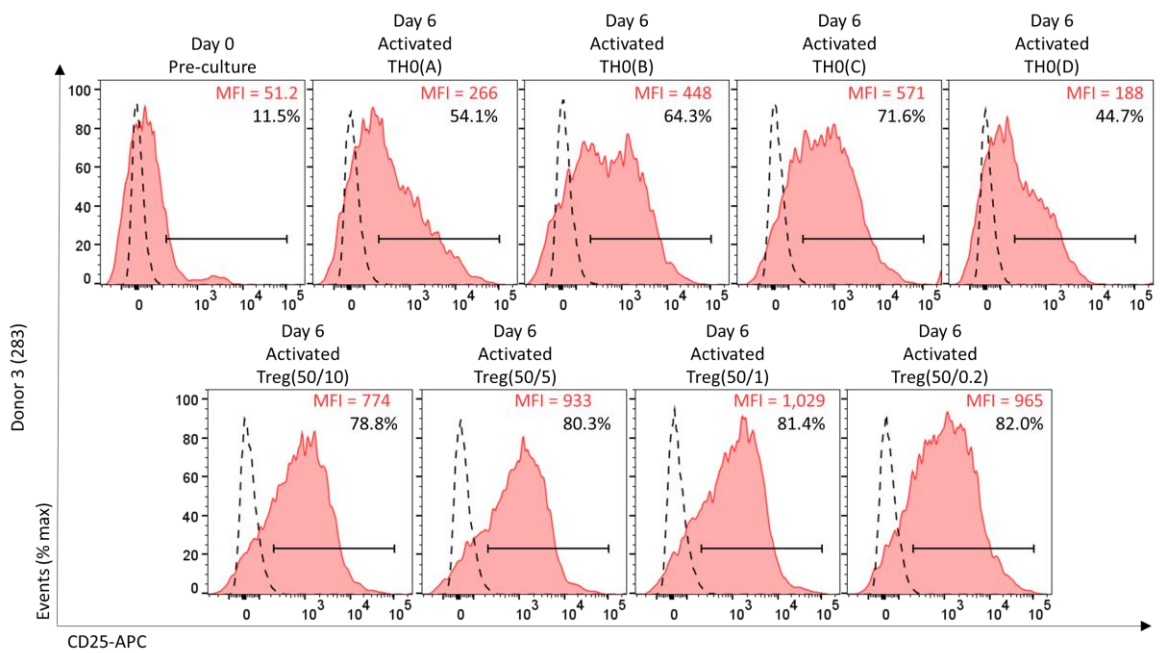


Figure 8.11. CD25 expression analysis of activated naïve CD4 T cells of donor 3 after 6 days. CD25 expression was higher in Treg polarised cells than in non-polarised TH0 conditions. Filled histograms show the CD25-APC-stained cells and dashed histograms as unstained. Events displayed were from live gates similar to Figure 8.4, which excludes activation beads. Gates were set such that 98-99% of events were outside in unstained samples. Red and black inset numbers indicate median fluorescence intensities (MFI) and percentage gated cells, respectively.

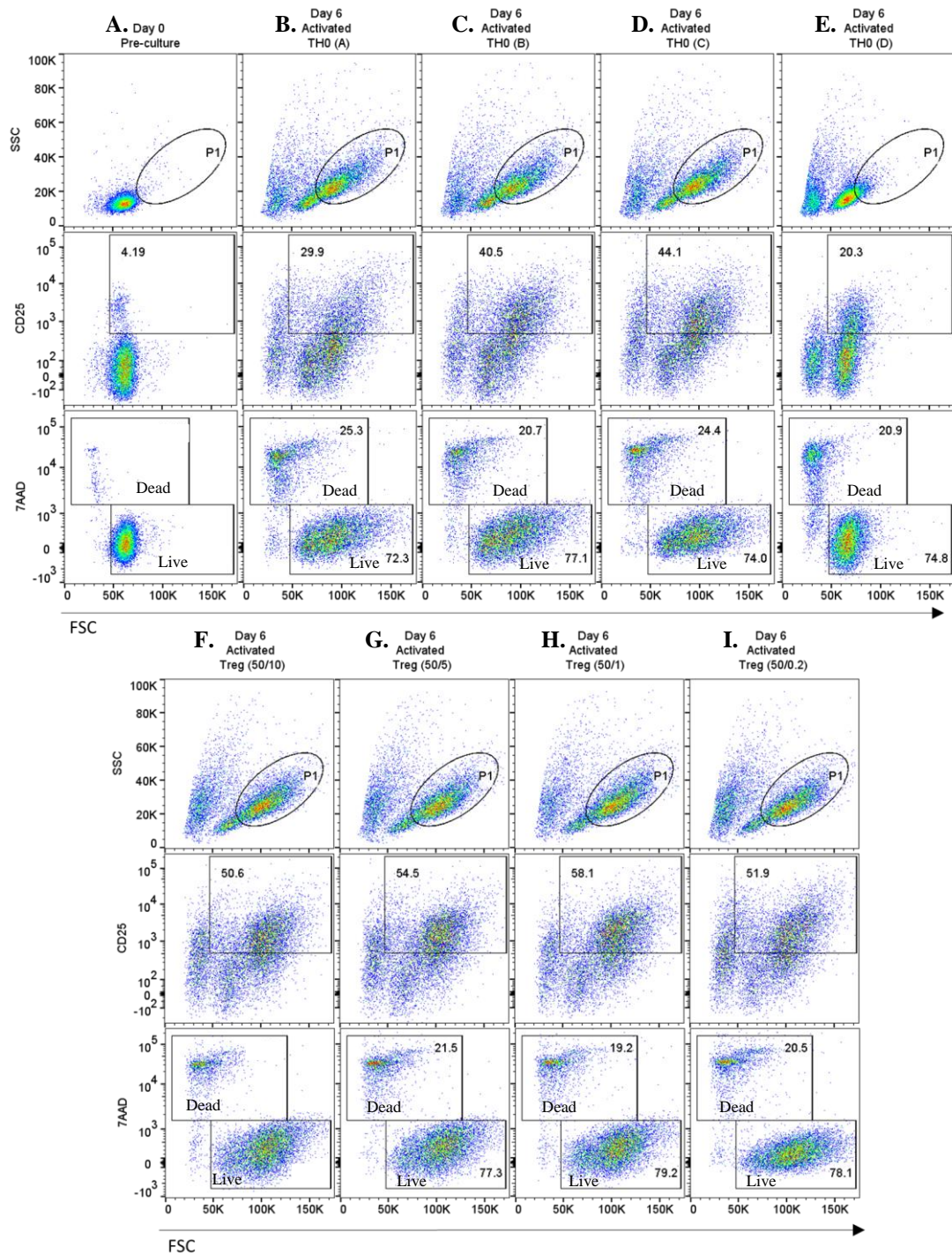


Figure 8.12. Flow cytometry analysis of naive CD4⁺ T cells of donor 3 (305). Aliquot of cells before(A.) and after (B.-I.) the 6-day activated cultures were stained with CD25-APC and 7-AAD to monitor cell size, activation and viability. With reference to day 0 cells, most activated cells at day 6 saw an increase in FSC/SSC signals relating to increase in cells size (P1 gate) and increase in CD25⁺ cells relating to activation level. TH0(D) cells, however, did not follow this trend even though all conditions saw good cell viability. Pseudocolour dot plots show all events excluding activation beads. Black inset numbers indicate the percentage of the gated cells for the corresponding stains.

8.3.10. Optimal FOXP3, RORC and CYP7B1 gene expression required a certain concentration range of TGF- β .

To confirm the effect of TGF- β treatments on the gene expression and sterol production, activated naïve CD4⁺ T cells were treated with a range from 0.2ng/mL to 10ng/mL with the same amount of exogenous IL-2 (50U/mL) and neutralising antibodies to block unwanted TH1 or TH2 polarisation.

Genes *CYP7B1*, *RORC* and *FOXP3* were distinctly upregulated in Treg-polarised conditions compared to all TH0 conditions. More specifically amongst the Treg conditions, treatments with 1ng/mL to 5ng/mL of TGF- β lead to moderately higher levels of *CYP7B1*, *RORC* and *FOXP3* expression relative to 0.2ng/mL (Figure 8.13.A-C). In contrast, *RORA* did not follow this trend showing a minimal 1.3-fold change compared to TH0(C) (Figure 8.13.D) which were similar to results from donor 1 and 2.

Moreover, in terms of T cell activation progression, all Treg-polarised cells were observed to enlarge in size and express higher CD25 compared to TH0 cells (Figure 8.12.F-I), again, a trend similar to donor 1 and 2.

8.3.11. Only the sterol, 7 α ,24S,25-TriHC and its metabolite, 3-oxo,7 α ,24S,25-TriHC follows a trend similar to CYP7B1 and RORC gene expression.

Building upon the results from donor 1 and 2, the same sterols were monitored for donor 3. The activated cells expectedly produced more sterols in Treg-polarised conditions compared to non-polarised TH0 conditions and largely during day 4 to day 6. In contrast, there were no considerable change in 24S-HC, 25-HC and 24S,25-EC production across different Treg conditions in either day 3 or day 6 media (Figure 8.14.A-C). Furthermore, the production of 7 α ,24S,25-TriHC in Treg-conditions on day 6 were observed to follow an optimal curve with maximal production between 1ng/mL to 5ng/mL of TGF- β treatment (Figure 8.14.D), which was also reflected by *CYP7B1* and *RORC* expression (Figure 8.13.A/B). This curve or increased production

was not seen in day 3 media samples suggesting that this is a late-stage sterol triggered by TGF- β signalling after T cell activation.

Donor 3 cells can be seen to have much lower 24S,25-EC and 7 α ,24S,25-TriHC in comparison to sterols quantified from donor 1 and 2. Nevertheless, the production of 7 α ,24S,25-TriHC and 3-oxo,7 α ,24S,25-TriHC are still higher in Treg condition which is correlated to induced gene expression of *CYP7B1* and *RORC*.

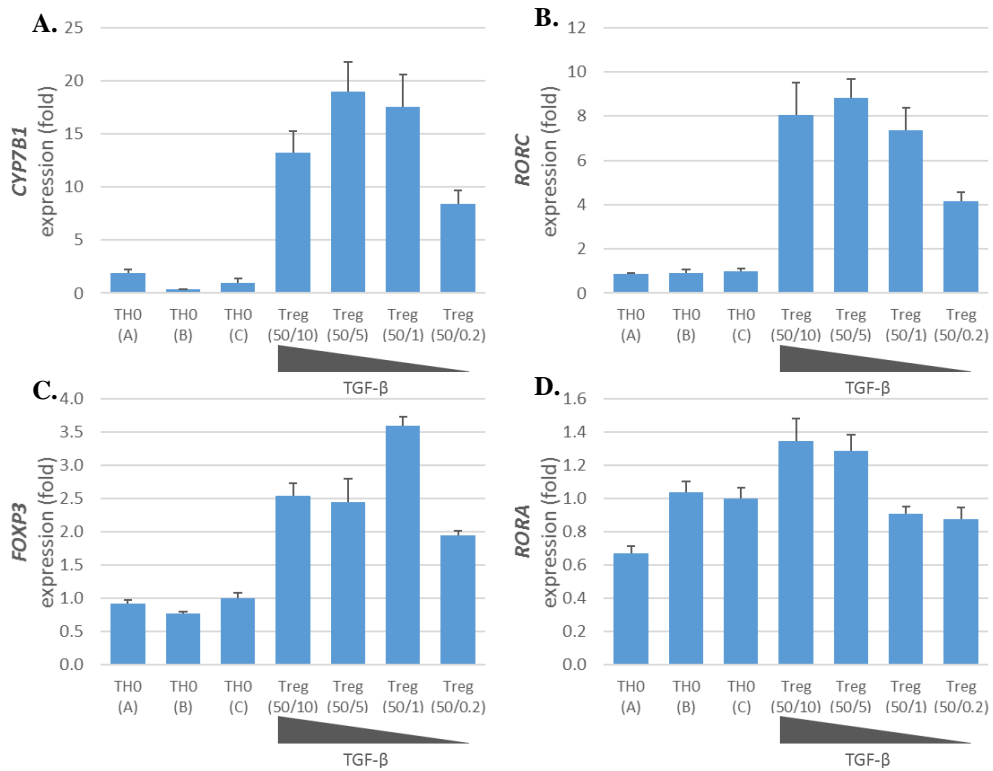


Figure 8.13. RT-PCR analysis for 6-day cultured activated naive CD4⁺ T cells of donor 3 (305) comparing TH0 and Treg polarisations.

Gene expression of *CYP7B1* and *RORC* was only upregulated in TGFβ-treated cells. Maximum expression levels of *CYP7B1* and *RORC* were observed at 5ng/ml. This effect was less evident in the expression of *FOXP3* and *RORA*. Complementary DNA synthesised from TurboDNase-treated RNA was used for *CYP7B1* and *FOXP3* expression analysis whereas cDNA from non-TurboDNase-treated RNA was used for *RORC* and *RORA*, all normalised to RP18S expression. Fold change were relative to TH0(C) which was treated similar to Treg cultures but without TGF-β. Error bars indicate s.e.m from triplicate wells.

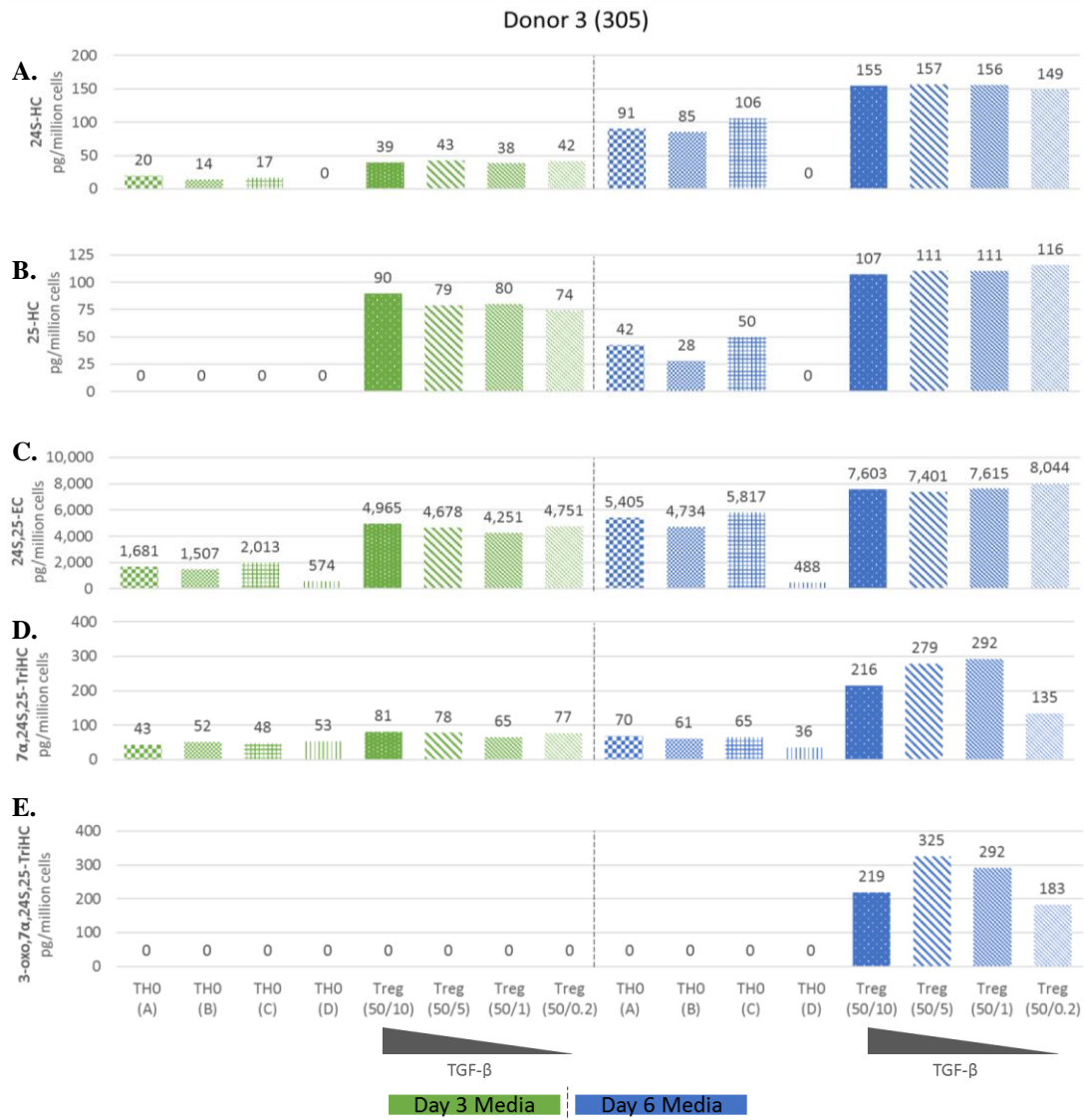


Figure 8.14. Sterols from day 3 and day 6 collected media supernatants from Donor 3 (305) comparing TH0 and Treg polarisations.

As before, media supernatants collected on day 3 and day 6 were extracted for sterols, processed and analysed by LC-MSⁿ. Donor 3 cells generally produced lower 24S,25-EC and 7α,24S,25-TriHC than donor 1 and 2. All quantifications were normalised to number of cells seeded.

8.4. Discussions

As preceding chapters presented sterol results from peripherally isolated total CD4⁺ T cells which were heterogeneous and may contain different subsets at different proportions, this chapter set out to seek sterols which were specific to certain T helper cell subsets once polarised. Due the number of naive CD4⁺ T cells present in peripheral blood were usually limited, only a few subsets were investigated and compared to non-polarised TH0 or non-activated conditions. Polarisation conditions towards TH2 and Treg were selected as TH1 and TH17 conditions were already being investigated by another member of the group.

Treg-polarised cells were generally seen to be more activated based on the increased CD25 expression compared to TH2 and non-polarised TH0. However, expression of CD25 alone cannot be the sole basis of activation status. Other activation markers like early CD69 and late HLA-DR, which are also expressed by activated cells^[36], albeit at different time periods, should be included in measuring T cell activation. The increased CD25 expression of the Treg cells here may be a form of suppressive feature^[4] which can deplete microenvironments of IL-2 required by other subsets for activation. It is then possible that a proportion of polarised cells were differentiated Treg cells which are phenotypically CD4⁺FOXP3⁺CD25⁺ cells be misrepresented as activated cells.

As seen in TH0(D), restricting the cytokine feedback loops with neutralising antibodies without exogenous IL-2, was found not only to be detrimental to the activation-induced CD25 expression and physical cell growth but also for the production of oxysterols and stimulation of transcription. This shows the requirement of IL-2 sourced from other immune cells for proper activation especially of naïve cells but also the likely effect of IL-2 depletion elicited by Treg cells.

In humans, the expression of the transcription factor ROR γ t has largely been the consensus on what regulates TH17 differentiation^[8,33]. Additionally, TH17 cells were reported to have synergistic upregulation of ROR α . We have seen that polarisation towards Treg in this chapter also leads to higher *RORC* expression. That said, Treg polarisation results here only saw *RORC* but no *RORA* upregulation. In mice, both *Foxp3* and *Rorc* have been reported to be co-expressed by TCR-stimulated naïve T

cells exposed to TGF- β , but Foxp3 was also described to antagonise ROR γ t in *IL-17* and *IL-23r* induction^[37]. Moreover, results here identified a lack of *IL-17* gene expression in Treg, thus disregarding high *RORC* expressing cells to be TH17 cells. It can be seen in this chapter that such dual expression pattern also exists in human T cells and that lineage commitment may require further factors like all-trans retinoic acid^[26,34,38] for Treg and IL-1/IL-6/IL-21/IL-23^[24,33,37,39] for TH17 in addition to the expression of their master regulators.

Upon closer inspection of the sterol production between the three donors, experiments with donor 3 generally yielded less sterols compared to 1 and 2. This reduced production may be a consequence of donor 3 cells not being fully activated. This is indicated by the minor increase in CD25 expressions (Figure 8.11 cf. Figure 8.5) across different conditions. Nevertheless, this was consistent in all conditions in donor 3 and differential gene expression was still observed in the presence of variable TGF- β treatment. It is therefore safe to say that TGF- β can dose dependently affect expression of *CYP7B1*, *RORC* and *FOXP3* *in vitro* in the presence of IL-2. As a consequence of altered *CYP7B1* (Figure 8.13.A), its enzymatic sterol product also follows as seen in Figure 8.14.D/E.

In the sterol metabolic pathway, cholesterol can be enzymatically hydroxylated at several positions as intermediates like 24S-HC by CYP46A1 and 25-HC by CH25H. Likewise, the shunt pathway product of cholesterol biosynthesis, 24S,25-EC, can also be modified by hydroxylation. 24S,25-EC have been previously suggested as a substrate to the *CYP7B1*^[40], and the increase in its expression in TGF- β -treated cells coinciding with the specific increase in detected 7 α ,24S,25-TriHC indicates that such a pathway exists in human Treg cells. Furthermore, these intermediates can still be modified by hydroxylation or oxidation at other positions and several of such modified sterol compounds have been described to have distinct biological activities. Studies with 7 α ,25-DiHC, the *CYP7B1* product from 25-HC, specifically identified the 3 β -hydroxy form to have potent biological activity as an EBI2-GPCR high affinity ligand which can be inactivated to the 3-oxo,7 α ,25-DiHC form by HSD3B7^[41].

Despite being able to have polarised cells in culture in all three donors characterised by confirmed differences in mRNA expression and intracellular protein staining, only a few sterols were found to be distinctly produced. The 2- to 4-fold changes in 25-HC,

24S-HC and 24S,25-EC between TH0, TH2 and Treg conditions suggest that these sterols may not be directly subset specific. Furthermore, inconsistencies in the induction *CH25H* (Figure 8.6.G cf. Figure 8.7.G) and 25-HC production between donor 1 and 2 further imply a lack of association of the induction of this sterol to a specific T cell subset. That said, subtle changes were observed for 25-HC as it was detected mostly in the first three days after activation then slows down between 4-6 days. This is in contrast to 24S-HC and 24S,25-EC which continues to be produced increasingly after 3 days. Moreover, as $7\alpha,24S,25$ -TriHC and 3-oxo, $7\alpha,24S,25$ -TriHC were observed to be detected in media mostly after 3 days, there appears to be a delay in its production, which was also dependent on a specific TGF- β treatment. However, this delay may not be with its production but with its release. It possible that this sterol can be initially produced and retained intracellularly then time-dependently secreted. In hindsight, the analysis of sterols in cell samples and *CYP7B1* gene expression analysis at day 3, would reveal if indeed the delay is in secretion than its production. In addition, its further metabolism from the 3β -hydroxy form to the 3-oxo form, likely via *HSD3B7* catalysis^[41,42], may suggest a role specific to TGF- β -treated cells. Together, 25-HC and $7\alpha,24S,25$ -TriHC shows a dynamic nature of sterol metabolism as it also changes as T cells transition through different phases of activation from resting naïve to functional effector/regulatory cells.

Ultimately, it was apparent that activation of naïve CD4⁺ T cells upregulate cholesterol biosynthesis which consequently produces copious amounts of 24S,25-EC. The activation and further polarisation towards Treg or treatment with TGF- β additionally upregulates the expression of *CYP7B1* facilitating the increased production of $3\beta,7\alpha$ -dihydroxycholest-5-en-24S,25-epoxide (detected as $7\alpha,24S,25$ -TriHC) from 24S,25-EC (Figure 8.15). Moreover, differences in the proportion of 3β -hydroxy or 3-oxo forms of the sterol may play a role in its biological activity, if any. Still, the significance of *CYP7B1* and its sterol metabolite in Treg biology remains to be explored which can be a direction for further investigation.

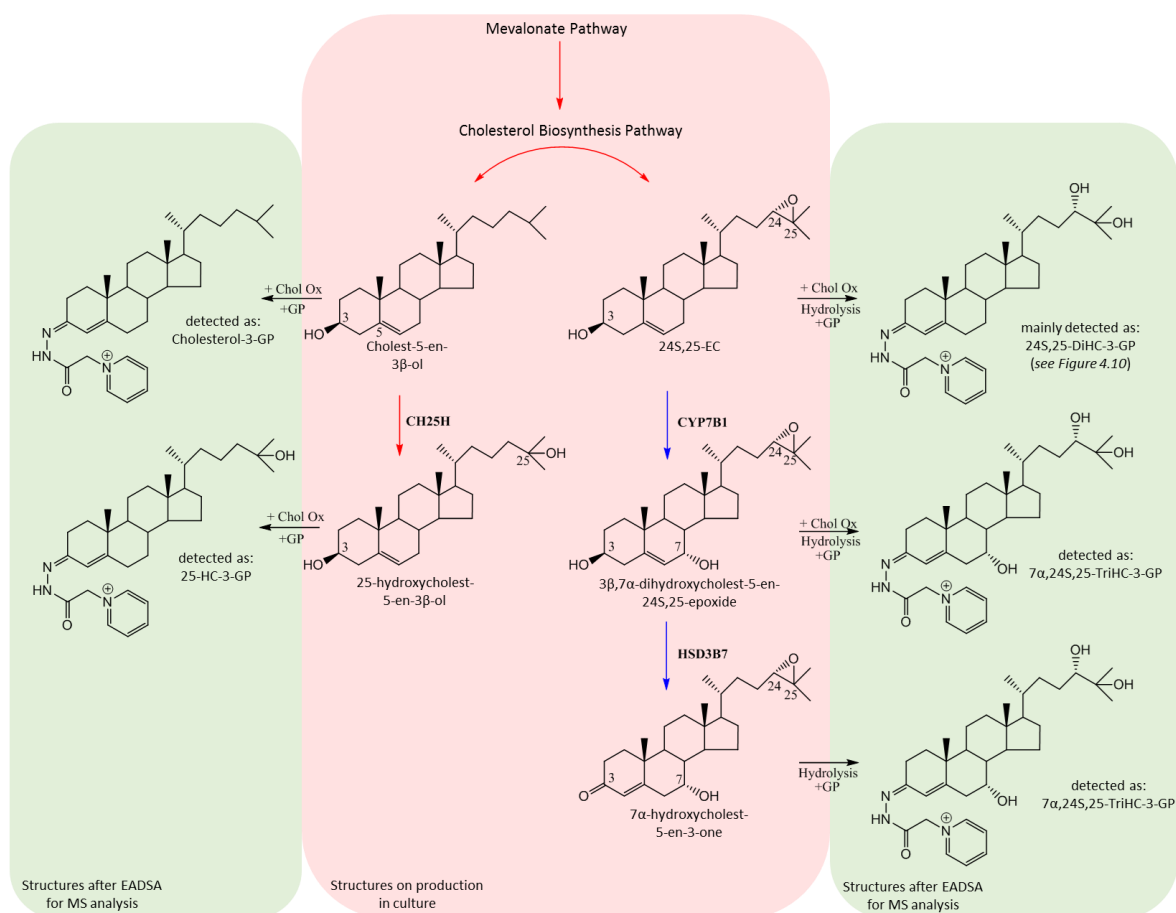


Figure 8.15. Proposed schematic pathway of the sterol precursors and products detected.

Cholesterol and 24S,25-EC are produced in parallel through cholesterol biosynthesis after the mevalonate pathway. From there, cholesterol can be modified by hydroxylation through CH25H or CYP46A1(not shown) to produce 25-HC or 24S-HC, respectively. Likewise, the increased precursor 24S,25-EC and upregulation of CYP7B1 enables the production of 3β,7α-dihydroxycholest-5-en-24S,25-epoxide which can be further metabolised by HSD3B7 to 7α-hydroxycholest-5-en-3-one. Red arrows indicate sterol pathways stimulated in CD3/CD28-activating conditions, while blue arrows indicate sterol pathways upregulated in both activating and Treg-polarising conditions. Structures in pink areas represent pathways and reactions occurring in culture, whereas structures in green areas occur after sample preparation and GP derivatisation as separated and identified by HPLC-MSⁿ. See table 2.6 for a longer list of detectable sterols.

8.5. References

- [1] A.O. Hovden, K. Haldorsen, (2008) The Seventh Edition of the Janeway's Immunobiology, *Scand. J. Immunol.* 68 112–112. doi:10.1111/j.1365-3083.2008.02123.x.
- [2] T.R. Mosmann, H. Cherwinski, M.W. Bond, M.A. Giedlin, R.L. Coffman, (1986) Two types of murine helper T cell clone. I. Definition according to profiles of lymphokine activities and secreted proteins., *J. Immunol.* 136 2348–57. <http://www.ncbi.nlm.nih.gov/pubmed/2419430>.
- [3] J. Zhu, W.E. Paul, (2008) CD4 T cells: fates, functions, and faults., *Blood.* 112 1557–69. doi:10.1182/blood-2008-05-078154.
- [4] D.A.A. Vignali, L.W. Collison, C.J. Workman, (2008) How regulatory T cells work., *Nat. Rev. Immunol.* 8 523–32. doi:10.1038/nri2343.
- [5] E.M. Shevach, (2009) Mechanisms of foxp3+ T regulatory cell-mediated suppression., *Immunity.* 30 636–45. doi:10.1016/j.immuni.2009.04.010.
- [6] J.E. Belizário, W. Brandão, C. Rossato, J.P. Peron, (2016) Thymic and Postthymic Regulation of Naïve CD4 + T-Cell Lineage Fates in Humans and Mice Models, *Mediators Inflamm.* 2016 1–16. doi:10.1155/2016/9523628.
- [7] L.E. Harrington, R.D. Hatton, P.R. Mangan, H. Turner, T.L. Murphy, K.M. Murphy, et al., (2005) Interleukin 17-producing CD4+ effector T cells develop via a lineage distinct from the T helper type 1 and 2 lineages., *Nat. Immunol.* 6 1123–1132. doi:10.1038/ni1254.
- [8] I.I. Ivanov, B.S. McKenzie, L. Zhou, C.E. Tadokoro, A. Lepelley, J.J. Lafaille, et al., (2006) The Orphan Nuclear Receptor ROR γ t Directs the Differentiation Program of Proinflammatory IL-17+ T Helper Cells, *Cell.* 126 1121–1133. doi:10.1016/j.cell.2006.07.035.
- [9] S.Q. Crome, A.Y. Wang, C.Y. Kang, M.K. Levings, (2009) The role of retinoic acid-related orphan receptor variant 2 and IL-17 in the development and function of human CD4+ T cells, *Eur. J. Immunol.* 39 1480–1493. doi:10.1002/eji.200838908.
- [10] L. Jin, D. Martynowski, S. Zheng, T. Wada, W. Xie, Y. Li, (2010) Structural basis for hydroxycholesterols as natural ligands of orphan nuclear receptor ROR γ , *Mol. Endocrinol.* 24 923–929. doi:10.1210/me.2009-0507.
- [11] Y. Wang, N. Kumar, C. Crumbley, P.R. Griffin, T.P. Burris, (2010) A second class of nuclear receptors for oxysterols: Regulation of ROR α and ROR γ activity by 24S-hydroxycholesterol (cerebrosterol), *Biochim. Biophys. Acta.* 1801 917–23. doi:10.1016/j.bbailip.2010.02.012.
- [12] Y. Wang, N. Kumar, L. a. Solt, T.I. Richardson, L.M. Helvering, C. Crumbley, et al., (2010) Modulation of retinoic acid receptor-related orphan receptor alpha and gamma activity by 7-oxygenated sterol ligands., *J. Biol. Chem.* 285 5013–25. doi:10.1074/jbc.M109.080614.
- [13] F.R. Santori, P. Huang, S.A. van de Pavert, E.F. Douglass, D.J. Leaver, B.A. Haubrich, et al., (2015) Identification of Natural ROR γ Ligands that Regulate the Development of Lymphoid Cells, *Cell Metab.* 21 286–297. doi:10.1016/j.cmet.2015.01.004.
- [14] P. Soroosh, J. Wu, X. Xue, J. Song, S.W. Sutton, M. Sablad, et al., (2014) Oxysterols are agonist ligands of ROR γ t and drive Th17 cell differentiation., *Proc. Natl. Acad. Sci. U. S. A.*

- 2–7. doi:10.1073/pnas.1322807111.
- [15] X. Hu, Y. Wang, L.-Y. Hao, X. Liu, C. a Lesch, B.M. Sanchez, et al., (2015) Sterol metabolism controls TH17 differentiation by generating endogenous ROR γ agonists, *Nat. Chem. Biol.* 11 141–147. doi:10.1038/nchembio.1714.
- [16] A. Reboldi, E. V. Dang, J.G. McDonald, G. Liang, D.W. Russell, J.G. Cyster, (2014) 25-Hydroxycholesterol suppresses interleukin-1-driven inflammation downstream of type I interferon, *Science* (80-.). 345 679–684. doi:10.1126/science.1254790.
- [17] M. Blanc, W.Y. Hsieh, K. a. Robertson, K. a. Kropp, T. Forster, G. Shui, et al., (2013) The Transcription Factor STAT-1 Couples Macrophage Synthesis of 25-Hydroxycholesterol to the Interferon Antiviral Response, *Immunity*. 38 106–118. doi:10.1016/j.immuni.2012.11.004.
- [18] S. Liu, R. Aliyari, K. Chikere, G. Li, D. Matthew, J.K. Smith, et al., (2013) Interferon-Inducible Cholesterol-25-Hydroxylase Broadly Inhibits Viral Entry by Production of 25-Hydroxycholesterol, *Immunity*. 38 92–105. doi:10.1016/j.immuni.2012.11.005. Interferon-Inducible.
- [19] D.R. Bauman, A.D. Bitmansour, J.G. McDonald, B.M. Thompson, G. Liang, D.W. Russell, (2009) 25-Hydroxycholesterol secreted by macrophages in response to Toll-like receptor activation suppresses immunoglobulin A production., *Proc. Natl. Acad. Sci. U. S. A.* 106 16764–16769. doi:10.1073/pnas.0909142106.
- [20] S. Hannedouche, J. Zhang, T. Yi, W. Shen, D. Nguyen, J.P. Pereira, et al., (2011) Oxysterols direct immune cell migration via EBI2., *Nature*. 475 524–527. doi:10.1038/nature10280.
- [21] C. Liu, X. V Yang, J. Wu, C. Kuei, N.S. Mani, L. Zhang, et al., (2011) Oxysterols direct B-cell migration through EBI2., *Nature*. 475 519–523. doi:10.1038/nature10226.
- [22] S.J. Bensinger, M.N. Bradley, S.B. Joseph, N. Zelcer, E.M. Janssen, M.A. Hausner, et al., (2008) LXR Signaling Couples Sterol Metabolism to Proliferation in the Acquired Immune Response, *Cell*. 134 97–111. doi:10.1016/j.cell.2008.04.052.
- [23] Y. Kidani, H. Elsaesser, M.B. Hock, L. Vergnes, K.J. Williams, J.P. Argus, et al., (2013) Sterol regulatory element-binding proteins are essential for the metabolic programming of effector T cells and adaptive immunity., *Nat. Immunol.* 14 489–99. doi:10.1038/ni.2570.
- [24] E. Volpe, N. Servant, R. Zollinger, S.I. Bogiatzi, P. Hupé, E. Barillot, et al., (2008) A critical function for transforming growth factor-beta, interleukin 23 and proinflammatory cytokines in driving and modulating human T(H)-17 responses., *Nat. Immunol.* 9 650–657. doi:10.1038/ni.1613.
- [25] G.I. Ellis, M.C. Reneer, A.C. Vélez-Ortega, A. McCool, F. Martí, (2012) Generation of induced regulatory T cells from primary human naïve and memory T cells., *J. Vis. Exp.* 1–6. doi:10.3791/3738.
- [26] J. Wang, T.W.J. Huizinga, R.E.M. Toes, (2009) De novo generation and enhanced suppression of human CD4+CD25+ regulatory T cells by retinoic acid., *J. Immunol.* 183 4119–26. doi:10.4049/jimmunol.0901065.
- [27] D.Q. Tran, H. Ramsey, E.M. Shevach, (2007) Induction of FOXP3 expression in naive human CD4+FOXP3 T cells by T-cell receptor stimulation is transforming growth factor- dependent

- but does not confer a regulatory phenotype, *Blood*. 110 2983–2990. doi:10.1182/blood-2007-06-094656.
- [28] K.J. Livak, T.D. Schmittgen, (2001) Analysis of relative gene expression data using real-time quantitative PCR and the 2(-Delta Delta C(T)) Method., *Methods*. 25 402–8. doi:10.1006/meth.2001.1262.
- [29] K.H. Kang, S.H. Im, (2005) Differential regulation of the IL-10 gene in Th1 and Th2 T cells, *Ann. N. Y. Acad. Sci.* 1050 97–107. doi:10.1196/annals.1313.011.
- [30] D.J. Cousins, T.H. Lee, D.Z. Staynov, (2002) Cytokine coexpression during human Th1/Th2 cell differentiation: direct evidence for coordinated expression of Th2 cytokines., *J. Immunol.* 169 2498–2506. doi:10.4049/jimmunol.169.5.2498.
- [31] C.L. Maynard, L.E. Harrington, K.M. Janowski, J.R. Oliver, C.L. Zindl, A.Y. Rudensky, et al., (2007) Regulatory T cells expressing interleukin 10 develop from Foxp3+ and Foxp3- precursor cells in the absence of interleukin 10., *Nat. Immunol.* 8 931–41. doi:10.1038/ni1504.
- [32] S.E. Allan, R. Broady, S. Gregori, M.E. Himmel, N. Locke, M.G. Roncarolo, et al., (2008) CD4+ T-regulatory cells: Toward therapy for human diseases, *Immunol. Rev.* 223 391–421. doi:10.1111/j.1600-065X.2008.00634.x.
- [33] N. Manel, D. Unutmaz, D.R. Littman, (2008) The differentiation of human TH-17 cells requires transforming growth factor- β and induction of the nuclear receptor ROR γ t, *Nat. Immunol.* 9 641–649. doi:10.1038/ni.1610.
- [34] L. Lu, X. Zhou, J. Wang, S.G. Zheng, D.A. Horwitz, (2010) Characterization of Protective Human CD4+CD25+ FOXP3+ Regulatory T Cells Generated with IL-2, TGF- β and Retinoic Acid, *PLoS One*. 5 e15150. doi:10.1371/journal.pone.0015150.
- [35] T. Wada, H.S. Kang, M. Angers, H. Gong, S. Bhatia, S. Khadem, et al., (2008) Identification of oxysterol 7 α -hydroxylase (Cyp7b1) as a novel retinoid-related orphan receptor alpha (RORalpha) (NR1F1) target gene and a functional cross-talk between RORalpha and liver X receptor (NR1H3)., *Mol. Pharmacol.* 73 891–9. doi:10.1124/mol.107.040741.
- [36] I. Rea, S. McNerlan, H. Alexander, (1999) CD69, CD25, and HLA-DR activation antigen expression on CD3+ lymphocytes and relationship to serum TNF- α , IFN- γ , and sIL-2R levels in aging, *Exp. Gerontol.* 34 79–93. doi:10.1016/S0531-5565(98)00058-8.
- [37] L. Zhou, J.E. Lopes, M.M.W. Chong, I.I. Ivanov, R. Min, G.D. Victora, et al., (2008) TGF-beta-induced Foxp3 inhibits T(H)17 cell differentiation by antagonizing ROR γ function., *Nature*. 453 236–240. doi:10.1038/nature06878.
- [38] A. Schmidt, M. Eriksson, M.M. Shang, H. Weyd, J. Tegnér, (2016) Comparative analysis of protocols to induce human CD4+Foxp3+ regulatory T cells by combinations of IL-2, TGF-beta, retinoic acid, rapamycin and butyrate, *PLoS One*. 11 1–31. doi:10.1371/journal.pone.0148474.
- [39] L. Yang, D.E. Anderson, C. Baecher-Allan, W.D. Hastings, E. Bettelli, M. Oukka, et al., (2008) IL-21 and TGF-beta are required for differentiation of human T(H)17 cells., *Nature*. 454 350–352. doi:10.1038/nature07021.

- [40] Y. Wang, K. Karu, A. Meljon, J. Turton, J.L. Yau, J.R. Seckl, et al., (2014) 24S,25-Epoxycholesterol in mouse and rat brain, *Biochem. Biophys. Res. Commun.* 449 229–234. doi:10.1016/j.bbrc.2014.05.012.
- [41] T. Yi, X. Wang, L.M. Kelly, J. An, Y. Xu, A.W. Sailer, et al., (2012) Oxysterol Gradient Generation by Lymphoid Stromal Cells Guides Activated B Cell Movement during Humoral Responses, *Immunity*. 37 535–548. doi:10.1016/j.immuni.2012.06.015.
- [42] D.W. Russell, (2003) The Enzymes, Regulation, and Genetics of Bile Acid Synthesis, *Annu. Rev. Biochem.* 72 137–174. doi:10.1146/annurev.biochem.72.121801.161712.

CHAPTER 9: General Discussions

With the recent emergence of the biological significance of oxysterols from being mere intermediates of bile acid and steroid biosynthesis to having potent roles in cholesterol homeostasis and neuronal development, it was unsurprising now to find that these oxidised cholesterol metabolites also play a part in immunological responses. The studies described herein investigated the link between sterol metabolism, production of oxysterols and human CD4⁺ T cells. As no method was available to analyse such sterols in *in vitro* cultured T cells, an enzyme-assisted derivatisation method together with high performance liquid chromatography coupled with multi-stage fragmentation mass spectrometry was optimised from previous studies^[1-3].

With this method naturally occurring sterols present in different media used for T cell culture, either in its free form or esterified form, were screened and quantified (Chapter 3). This revealed the base levels of sterols in these media and identified the culture media suitable for this study. It was found that resting human CD4⁺ T cells do not produce detectable levels of endogenous oxysterols which can be attributed to its very low metabolic state. However, several species of oxysterols were detected upon T cell activation both present intracellularly and in the conditioned media (Chapter 4).

Firstly, intracellular cholesterol levels were seen doubled 48 hours after stimulation with anti-CD3/CD28-loaded microbeads. In addition, activated T cells were seen to start proliferation between 48 to 72 hours after being activated (Chapter 5). The increase in intracellular cholesterol goes in line with the requirement of cells to have enough resources to proceed with the cell cycle and cholesterol has been shown to be an essential cellular component. Secondly, an oxysterol which is not derived from cholesterol was also detected in relatively high quantities mostly in the conditioned media of the activated cells and continually increased in the duration of the culture. The oxysterol 24S,25-epoxycholesterol (24S,25-EC) is a by-product of cholesterol biosynthesis through a shunt pathway which utilises the same enzymes used in the 19-step biosynthetic pathway from its common precursor, squalene (Figure 1.4 and 1.5). As

both the cholesterol pathway and shunt pathway use the same enzymes, production of 24S,25-EC can be an indication of an active cholesterol pathway^[4]. This became useful in assessing the activation of cholesterol biosynthesis as measuring cholesterol directly in either cell pellet or conditioned media cannot provide a correct quantification for *de novo* synthesised cholesterol. As cholesterol biosynthesis and metabolism is tightly regulated, its intracellular levels rarely drastically change. In addition, analysis of cholesterol in the media can be affected by several factors including cellular death which can release cellular cholesterol into the media. Its increased proportion found in the conditioned media rather than intracellularly may stem from its biological activity. 24S,25-EC has been reported to act as a potent ligand for Liver X receptors (LXRs)^[5]. LXRs are nuclear receptors which can regulate cholesterol metabolism in which its activation results in the expression of cholesterol efflux genes such as ATP-binding cassette transporters (ABCG1 and ABCA1)^[6] and repression of cholesterol uptake genes^[7]. Due to this, 24S,25-EC may be actively exported into the media to prevent its intracellular accumulation and ligand-dependent activation of LXR. Other effects independent from LXR were reported where 24S,25-EC was found to regulate cholesterol synthesis by interfering with 24-dehydrocholesterol reductase or DHCR24, resulting in the rapid accumulation of the substrate desmosterol, at the expense of cholesterol^[8]. Lastly, 25-hydroxycholesterol (25-HC) was observed to also increase time-dependently in culture after T-cell activation via CD3/CD28 stimulation which was mostly seen in the conditioned media. A further augmented 25-HC production was seen when CD4⁺ T cells were stimulated through PMA, which is a PKC activator (Chapter 7). This suggested that PKC and its downstream signalling may be involved in either cholesterol-25-hydroxylase (CH25H) expression or 25-HC production. Conversely, when PKC was inhibited with Gö6983, T cell activation was completely blocked even in the presence of CD3/CD28 stimulation due to very low CD25 surface expression. This further highlights the role of PKC and its signalling CD4⁺ T cell activation in general. Having said that, it is also possible that the cells were prevented from progressing to an optimal activated state by the Gö6983 off-target effects. It was previously reported that PKC inhibitors affect the activity of DHCR24^[9]. This enzyme sits just above the conversion of desmosterol to cholesterol (Figure 1.5). Consequently, inhibition of

DHCR24 was seen to result in desmosterol accumulation intracellularly. With this blockage, T cells may have also lacked the necessary levels of intracellular cholesterol to proceed with activation and proliferation even if other TCR downstream signalling pathways were functional.

The inhibition of cholesterol biosynthesis using the drug simvastatin at 1 μ M saw a reduction of 24S,25-EC with the lack of cellular proliferation compared to activated cells without simvastatin (Chapter 5). However, 25-HC production of these cells were not seen to be affected even with the simvastatin treatments which continued to increase until that end of culture at 72 hours. Correspondingly, the downstream metabolite of 25-HC via the activity of CYP7B1, 7 α ,25-DiHC was seen to also increase with the duration of culture which was also observed to be unaffected by inhibited cholesterol biosynthesis. Given that 7 α ,25-DiHC was reported to be a potent EBI2 GPCR ligand important in B cell function, this suggested that both 25-HC and 7 α ,25-DiHC may be involved in immune function particularly in the CD4⁺ T cell activation process that is modulated separately from the induction of cholesterol biosynthesis and its production is not just a way of removing excess cholesterol.

Previous reports have highlighted the role of 25-HC in macrophage immune responses. Bauman et.al (2009) demonstrated the induction of *Ch25h* and subsequent increase in 25-HC in TLR-stimulated murine macrophages^[10]. They found that the 25-HC resulted in suppressed B cell proliferation and decreased IgA production. Blanc et.al (2013) and Liu et.al (2013) both confirmed that murine macrophage secretion of 25-HC results from a broad innate immune anti-viral response which was regulated via STAT1 and interferon (IFN) signalling^[11,12]. More recently, Reboldi et.al (2014) reported that the absence of *Ch25h* in mice macrophages leads to increased *Il-1 β* transcription and inflammasome activation. These studies prompted the extrapolation of the IFN–*CH25H*–25-HC relationship to human CD4⁺ T cells. RNA interference in the current study with human CD4⁺ T cells *in vitro* generally revealed a disconnect in this relationship (Chapter 6). Though the downregulation of *CH25H* by the use of small interfering RNA efficiently reduced the expression of *CH25H* mRNA and the oxysterol

product 25-HC, this did not see an observable effect in both the expression of *IFNG* and the production of IFN γ cytokine. Likewise, the production of 25-HC in activated CD4⁺ T cells were unaffected in the presence of additional IFN γ or in anti-IFN γ -neutralised cultures. Furthermore, the exogenous IFN γ in CD4⁺ T cells cultures did not result in increased activation state via CD25 expression, and neither with its depletion using a neutralising antibody. This suggests that the link between IFN and *CH25H*/25-HC may not exist in human CD4⁺ cells in an *in vitro* setting. Having said that, the current study only explored IFN γ which is a type-II interferon. This warrants further investigation with IFN α and IFN β which are type-I interferons^[13–15].

The current study also addressed how oxysterols are modulated downstream of TCR/CD28 signalling (Chapter 7). As several interconnected signalling pathways regulated by protein kinases are activated after CD3/CD28 stimulation, oxysterol production was monitored in activated conditions in the absence or presence of certain pharmacological inhibitors. Pathways involving PKC, NF κ B, MAPK, PI3K, mTORC1 and mTORC2 were considered (Figure 7.1). In all, PI3K and mTORC1 inhibition did not cause significant effect in the production of oxysterols in activated cells. The dual inhibition of mTORC1 and mTORC2 saw a dose-dependent reduction in both CD25 and 25-HC, although this requires further biological replicates to establish significance levels. NF κ B inhibition had inconclusive effects in CD25 activation but also did not significantly affect oxysterol production. On the other hand, modulation of PKC and MAPK pathways generated differences in both CD25 expression and oxysterol production. As mentioned above, PKC activation of CD4⁺ T cells using PMA lead to a significantly increased 25-HC as well as its metabolite 7 α ,25-DiHC whereas its inhibition led to a complete block of T cell activation based on CD25 expression. This also showed that PKC activation through PMA does not fully induce the cholesterol biosynthesis pathway due to less 24S,25-EC detected. Two distinct MAPK pathways were seen to have affected both CD25 expression and oxysterol production with opposite tendencies. MEK/Erk inhibition saw a significant reduction in 25-HC production whereas p38 MAPK inhibition saw no difference. The CD25 expression of both MEK/Erk-inhibited and p38 MAPK-inhibited activated cells saw a reduction, with

MEK/Erk inhibition displaying a greater decrease. This may suggest that MEK/Erk to be involved in T cell activation and 25-HC production and but not p38. Some of these inhibitions have led to consistent trends with regards to increase or decrease in activation level and oxysterol production but do not reach significance. This may be attributed to the different predispositions when studying cells from human donors. Therefore, to determine significance of the changes observed, this inhibitor study demands further biological replicates.

After tackling oxysterol production in total CD4⁺ T cells which may contain varying proportions of naïve and memory cells, the study reverted to inspecting whether any oxysterols are specifically produced in subset effector cells which may indicate the biological function of the molecules. This was carried out by differentiating naïve CD4⁺ T cells into effector cells in the presence of relevant cytokines. Another member of the group was investigating the differences in oxysterol production in TH1- and TH17-polarised conditions. Due to this, differences in TH0-, TH2- and Treg-polarised naïve CD4⁺ T cells were investigated at instead (Chapter 8). Differentiation of naïve CD4⁺ T cells towards either TH2 and Tregs was confirmed by both gene expression analysis and intracellular protein analysis. Treg-polarised naïve CD4⁺ T cells showed in increased mRNA expression of *FOXP3* but surprisingly also had induced *RORC* and *CYP7B1*. It was reported by Wada et.al (2008) that *Cyp7b1* is a gene target of *Rora* in mice^[16]. Genes *RORC* and *RORA* encode the human ROR γ and ROR α nuclear receptors which were implicated to have roles in TH17 differentiation^[17] and the fact that TH17 and Treg have reciprocal and plastic relationship^[18,19], the increased *RORC* in Treg-polarised conditions can be due to TGF β treatment as previously reported by Zhou et.al (2008)^[20]. This ROR γ /Foxp3 co-expression was also described by Yang et.al (2008) to be present in TH17 development in the presence of TGF β and that further polarising cytokines like IL-6 are required to antagonise one transcription factor against the other^[21]. Sterol analysis of the conditioned media of the polarised CD4⁺ T cells showed a similar trend in 25-HC and 24S,25-EC. However, the extended culture of up to 6 days found the majority of the 25-HC produced was detected in the first three days of conditioned media while increased 24S,25-EC were detected from day 4 to day 6. In addition, Treg-

polarised cells were found to have greater 25-HC and 24S,25-EC production than TH0- or TH2-polarised cells. This greater Treg production of 25-HC may be speculated to be indicative of the previously reported anti-inflammatory roles of 25-HC. Moreover, differential polarisation conditions identified the importance of oxysterol 7 α ,24S,25-trihydroxycholesterol and its further metabolite 3-oxo-7 α ,24S,25-trihydroxycholesterol, (via HSD3B7) which were both specifically increased in Treg conditions, but not in TH0 and TH2. Proportions of the 3 β -hydroxy and 3-oxo forms varied in the experiments but more of the 3 β -hydroxy were generally found. Currently, the function of this oxysterol is unknown or if it does have any biological activity. If it does, it may be speculated that the 3-oxo form may be an inactive form whereas the 3 β -hydroxy is the active form, similar to the potent biological activity of the 3 β -hydroxy form of 7 α ,25-DiHC to EBI-2 GPCR but not the metabolite 3-oxo-7 α ,25-DiHC^[22]. Then again, more biological replicates are required to confirm this specific oxysterol production and to shed some light in to its function in CD4⁺ T cells differentiation.

To conclude, the work described here shows a method of analysing sterols in human CD4⁺ T cells and the identification of the oxysterol species can create opportunities for further investigation. In particular, the bioactivity of 7 α ,24S,25-TriHC would be worth pursuing in both Treg and TH17 conditions, as well as the other interactions of PKC and MAPK pathways that may modulate sterol metabolism and vice versa.

References

- [1] K. Karu, M. Hornshaw, G. Woffendin, K. Bodin, M. Hamberg, G. Alvelius, et al., (2007) Liquid chromatography-mass spectrometry utilizing multi-stage fragmentation for the identification of oxysterols., *J. Lipid Res.* 48 976–987. doi:10.1194/jlr.M600497-JLR200.
- [2] W.J. Griffiths, M. Ogundare, A. Meljon, Y. Wang, (2012) Mass Spectrometry for Steroid Analysis, *Mass Spectrom. Handb.* 297–337. doi:10.1002/9781118180730.ch14.
- [3] M. Ogundare, S. Theofilopoulos, A. Lockhart, L.J. Hall, E. Arenas, J. Sjövall, et al., (2010) Cerebrospinal fluid steroidomics: Are bioactive bile acids present in brain?, *J. Biol. Chem.* 285 4666–4679. doi:10.1074/jbc.M109.086678.
- [4] J. Wong, C.M. Quinn, A.J. Brown, (2007) Synthesis of the oxysterol, 24(S), 25-epoxycholesterol, parallels cholesterol production and may protect against cellular accumulation of newly-synthesized cholesterol., *Lipids Health Dis.* 6 10. doi:10.1186/1476-511X-6-10.
- [5] B.A. Janowski, M.J. Grogan, S.A. Jones, G.B. Wisely, S.A. Kliewer, E.J. Corey, et al., (1999) Structural requirements of ligands for the oxysterol liver X receptors LXRalpha and LXRbeta., *Proc. Natl. Acad. Sci. U. S. A.* 96 266–271. doi:10.1073/pnas.96.1.266.
- [6] P. a. Edwards, M. a. Kennedy, P. a. Mak, (2002) LXRs; oxysterol-activated nuclear receptors that regulate genes controlling lipid homeostasis., *Vascul. Pharmacol.* 38 249–56. doi:10.1016/S1537-1891(02)00175-1.
- [7] N. Zelcer, C. Hong, R. Boyadjian, P. Tontonoz, (2009) LXR Regulates Cholesterol Uptake Through Idol-Dependent Ubiquitination of the LDL Receptor, *Science (80-.)*. 325 100–104. doi:10.1126/science.1168974.
- [8] E.J. Zerenturk, I. Kristiana, S. Gill, A.J. Brown, (2012) The endogenous regulator 24(S),25-epoxycholesterol inhibits cholesterol synthesis at DHCR24 (Seladin-1), *Biochim. Biophys. Acta - Mol. Cell Biol. Lipids.* 1821 1269–1277. doi:10.1016/j.bbalip.2011.11.009.
- [9] W. Luu, E.J. Zerenturk, I. Kristiana, M.P. Bucknall, L.J. Sharpe, A.J. Brown, (2014) Signaling regulates activity of DHCR24, the final enzyme in cholesterol synthesis., *J. Lipid Res.* 55 410–20. doi:10.1194/jlr.M043257.
- [10] D.R. Bauman, A.D. Bitmansour, J.G. McDonald, B.M. Thompson, G. Liang, D.W. Russell, (2009) 25-Hydroxycholesterol secreted by macrophages in response to Toll-like receptor activation suppresses immunoglobulin A production., *Proc. Natl. Acad. Sci. U. S. A.* 106 16764–16769. doi:10.1073/pnas.0909142106.
- [11] M. Blanc, W.Y. Hsieh, K. a. Robertson, K. a. Kropp, T. Forster, G. Shui, et al., (2013) The Transcription Factor STAT-1 Couples Macrophage Synthesis of 25-Hydroxycholesterol to the Interferon Antiviral Response, *Immunity.* 38 106–118. doi:10.1016/j.immuni.2012.11.004.
- [12] S. Liu, R. Aliyari, K. Chikere, G. Li, D. Matthew, J.K. Smith, et al., (2013) Interferon-Inducible Cholesterol-25-Hydroxylase Broadly Inhibits Viral Entry by Production of 25-

Hydroxycholesterol, *Immunity*. 38 92–105. doi:10.1016/j.immuni.2012.11.005. Interferon-Inducible.

- [13] D.F. Tough, (2012) Modulation of T-cell function by type I interferon, *Immunol. Cell Biol.* 90 492–497. doi:10.1038/icb.2012.7.
- [14] A. Kaser, S. Nagata, H. Tilg, (1999) Interferon alpha augments activation-induced T cell death by upregulation of Fas (CD95/APO-1) and Fas ligand expression., *Cytokine*. 11 736–43. doi:10.1006/cyto.1998.0484.
- [15] D. Pilling, A.N. Akbar, J. Girdlestone, C.H. Orteu, N.J. Borthwick, N. Amft, et al., (1999) Interferon-beta mediates stromal cell rescue of T cells from apoptosis., *Eur. J. Immunol.* 29 1041–50. doi:10.1002/(SICI)1521-4141(199903)29:03<1041::AID-IMMU1041>3.0.CO;2-# [pii].
- [16] T. Wada, H.S. Kang, M. Angers, H. Gong, S. Bhatia, S. Khadem, et al., (2008) Identification of oxysterol 7 α -hydroxylase (Cyp7b1) as a novel retinoid-related orphan receptor alpha (ROR α) (NR1F1) target gene and a functional cross-talk between ROR α and liver X receptor (NR1H3)., *Mol. Pharmacol.* 73 891–9. doi:10.1124/mol.107.040741.
- [17] X.O. Yang, B.P. Pappu, R. Nurieva, A. Akimzhanov, H.S. Kang, Y. Chung, et al., (2008) T Helper 17 Lineage Differentiation Is Programmed by Orphan Nuclear Receptors ROR α and ROR γ , *Immunity*. 28 29–39. doi:10.1016/j.immuni.2007.11.016.
- [18] E. Bettelli, Y. Carrier, W. Gao, T. Korn, T.B. Strom, M. Oukka, et al., (2006) Reciprocal developmental pathways for the generation of pathogenic effector TH17 and regulatory T cells., *Nature*. 441 235–238. doi:10.1038/nature04753.
- [19] Y.K. Lee, R. Mukasa, R.D. Hatton, C.T. Weaver, (2009) Developmental plasticity of Th17 and Treg cells, *Curr. Opin. Immunol.* 21 274–280. doi:10.1016/j.coi.2009.05.021.
- [20] L. Zhou, J.E. Lopes, M.M.W. Chong, I.I. Ivanov, R. Min, G.D. Vitoria, et al., (2008) TGF- β -induced Foxp3 inhibits T(H)17 cell differentiation by antagonizing ROR γ function., *Nature*. 453 236–240. doi:10.1038/nature06878.
- [21] X.O. Yang, R. Nurieva, G.J. Martinez, H.S. Kang, Y. Chung, B.P. Pappu, et al., (2008) Molecular Antagonism and Plasticity of Regulatory and Inflammatory T Cell Programs, *Immunity*. 29 44–56. doi:10.1016/j.immuni.2008.05.007.
- [22] J.G. Cyster, E. V. Dang, A. Reboldi, T. Yi, (2014) 25-Hydroxycholesterols in innate and adaptive immunity, *Nat. Rev. Immunol.* 14 731–743. doi:10.1038/nri3755.

APPENDIX: Published papers

K.A. Robertson, W.Y. Hsieh, T. Forster, M. Blanc, H. Lu, P.J. Crick, E. Yutuc, et al., (2016) An Interferon Regulated MicroRNA Provides Broad Cell-Intrinsic Antiviral Immunity through Multihit Host-Directed Targeting of the Sterol Pathway, *PLOS Biol.* 14 e1002364. doi:10.1371/journal.pbio.1002364.

J. Abdel-Khalik, E. Yutuc, P.J. Crick, J.-Å. Gustafsson, M. Warner, G. Roman, et al., (2016) Defective cholesterol metabolism in amyotrophic lateral sclerosis, *J. Lipid Res.* 2013 jlr.P071639. doi:10.1194/jlr.P071639.